Oxidative Medicine and Cellular Longevity

Redox Status, Inflammation, and Immunity in Metabolic Disorders and Chronic Autoimmune Inflammatory Diseases

Lead Guest Editor: Ewa Barg
Guest Editors: Helena Moreira, Katarzyna Gębczak, and Jacek Toporski

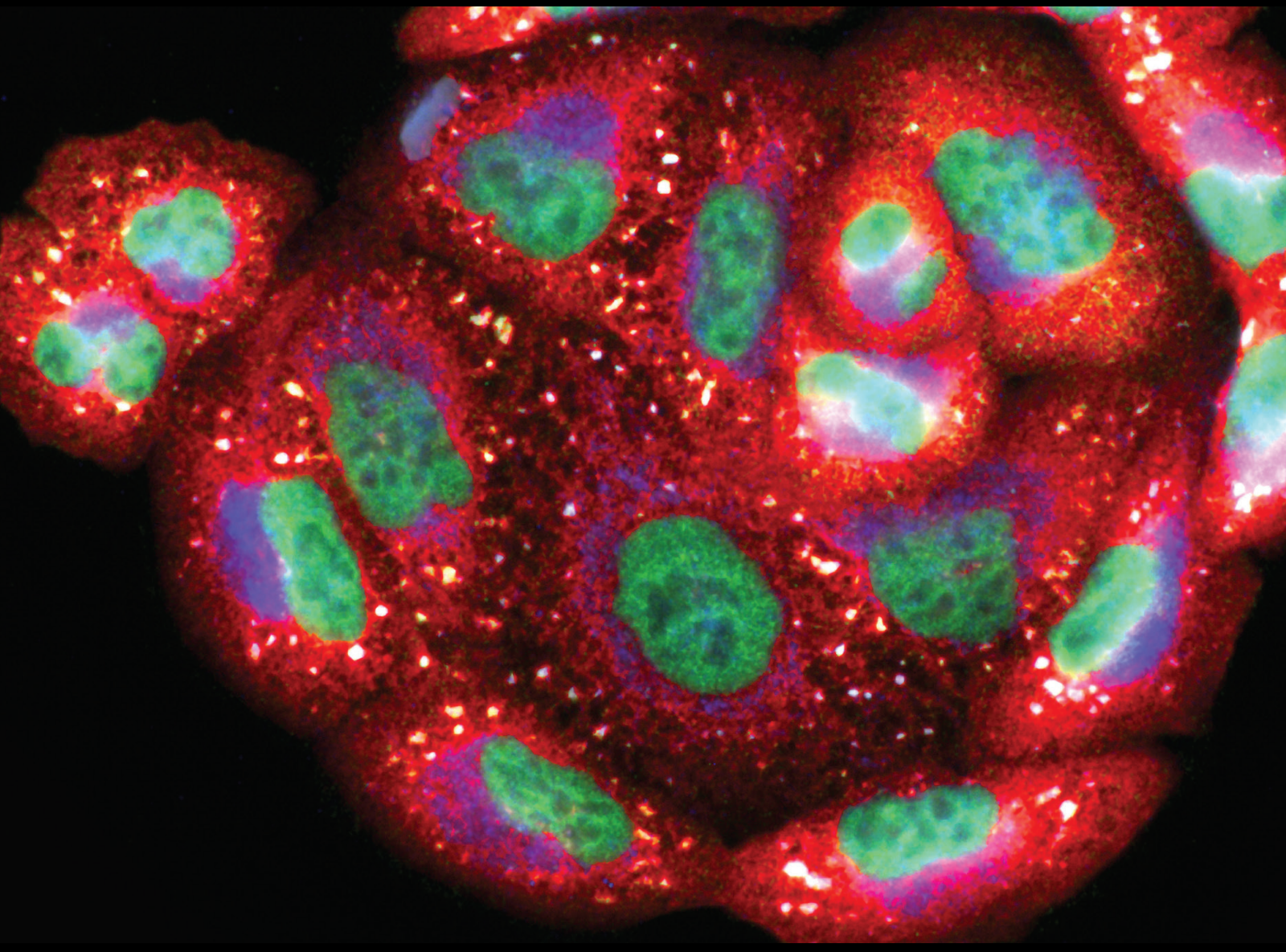

Redox Status, Inflammation, and Immunity in Metabolic Disorders and Chronic Autoimmune Inflammatory Diseases

Oxidative Medicine and Cellular Longevity

Redox Status, Inflammation, and Immunity in Metabolic Disorders and Chronic Autoimmune Inflammatory Diseases

Lead Guest Editor: Ewa Barg
Guest Editors: Helena Moreira, Katarzyna Gębczak, and Jacek Toporski

Contents

Hindawi
Oxidative Medicine and Cellular Longevity
Volume 2023, Article ID 2305163, 11 pages
https://doi.org/10.1155/2023/2305163

Research Article

miR-31-5p as a Potential Circulating Biomarker and Tracer of Clinical Improvement for Chronic Inflammatory Demyelinating Polyneuropathy

Edyta Dziadkowiak,[1] Dagmara Baczyńska,[2] Małgorzata Wieczorek,[3] Mateusz Olbromski,[4] Helena Moreira,[5] Monika Mrozowska,[4] Sławomir Budrewicz,[1] Piotr Dzięgiel,[4] Ewa Barg,[5] and Magdalena Koszewicz[1]

[1]*Department of Neurology, Wroclaw Medical University, Borowska 213, 50-556 Wroclaw, Poland*
[2]*Department of Molecular and Cellular Biology, Wroclaw Medical University, Borowska 211A, Wroclaw, Poland*
[3]*Faculty of Earth Sciences and Environmental Management, University of Wroclaw, Uniwersytecki 1, 50-137 Wroclaw, Poland*
[4]*Department of Histology and Embryology, Wroclaw Medical University, ul. Chałubinskiego 6a, 50-368 Wroclaw, Poland*
[5]*Department of Basic Medical Sciences, Wroclaw Medical University, Borowska 211, 50-556 Wroclaw, Poland*

Correspondence should be addressed to Edyta Dziadkowiak; edbkowal@gmail.com

Received 19 June 2022; Revised 2 September 2022; Accepted 6 October 2022; Published 10 April 2023

Academic Editor: Abdur Rauf

Background. MicroRNAs are endogenous, small noncoding RNA molecules that play a pivotal role in the regulation of gene expression. MicroRNAs are involved in many biological processes such as proliferation, cell differentiation, neovascularization, and apoptosis. Studies on microRNA expression may contribute to a better understanding of the pathomechanism of chronic inflammatory demyelinating polyneuropathy (CIDP) and consequently enable the development of new therapeutic measures using antisense miRNAs (antagomirs). In this study, we evaluated the level of miR-31-5p in the serum of patients with CIDP and its correlation with the miR-31-5p level and clinical presentation and electrophysiological and biochemical parameters. *Methods*. The study group consisted of 48 patients, mean age 61.60 ± 11.76, who fulfilled the diagnostic criteria of a typical variant of CIDP. The expression of miR-31-5p in patient serum probes was investigated by droplet digital PCR. The results were correlated with neurophysiological findings and the patient's clinical and biochemical parameters. *Results*. The mean copy number of miRNA-31 in 100 μl serum was 1288.64 ± 2001.02 in the CIDP group of patients, while in the control group, it was 3743.09 ± 4026.90. There was a significant positive correlation (0.426) between IgIV treatment duration and miR-31-5p expression. Patients without IgIV treatment showed significantly lower levels of miR-31 compared to the treated group (259.44 ± 304.02 vs. 1559.48 ± 2168.45; $p = 0.002$). The group of patients with body weight > 80 kg showed statistically significantly lower levels of miRNA-31-5p than the patients with lower body weight (934.37 ± 1739.66 vs. 1784.62 ± 2271.62, respectively; $p = 0.014$). Similarly, the patients with elevated cerebrospinal fluid (CSF) protein levels had significantly higher miRNA-31-5p expression than those with normal protein levels (1393.93 ± 1932.27 vs. 987.38 ± 2364.10, respectively; $p = 0.044$). *Conclusion*. The results may support the hypothesis that miR-31-5p is strongly involved in the autoimmune process in CIDP. The positive correlation between higher miR-31-5p levels and duration of IVIg treatment may be an additional factor explaining the efficacy of prolonged IVIg therapy in CIDP.

1. Introduction

MicroRNAs (miRNAs) are a family of single-stranded, noncoding gene expression, endogenous regulatory molecules formed from double-stranded precursors. miRNAs are a group of molecules about 21-23 nucleotides in length that posttranscriptionally regulate gene expression and thus contribute to the modulation of numerous complex and disease-

relevant cellular processes, including cell proliferation, cell motility, cell cycle control, neovascularization, apoptosis, and stress response. Their role depends mainly on their complementarity to the 3′UTR regions of targeted miRNAs. The importance of these molecules is demonstrated by the fact that more than one-third of protein-coding genes in human cells are regulated by miRNAs. It was estimated that genes encoding miRNAs account for 1-5% of all genes in humans and animals [1–3]. Previous studies had reported that miR-31-5p plays an essential role in tumor suppression in hepatocellular carcinoma by regulating the cell cycle and epithelia-mesenchymal transition. In addition, the altered expression of miR-31-5p was also confirmed in other tumors such as esophageal squamous cell carcinoma, gastric cancer, colorectal cancer, breast cancer, and cervical cancer [4–6].

On the other hand, together with other miRNAs such as miR-1, miR-133a, miR-133b, and miR-206, miR-31 belongs to dystromirs (Dystromirs as Serum Biomarkers for Monitoring the Disease Severity in Duchenne Muscular Dystrophy) due to the specific expression in muscle cells and roles in skeletal muscle maintenance and regeneration [7]. It has been shown that miR-31 is involved in muscle proliferation and differentiation, as it increases myoblast transformation in myotubes [8]. Furthermore, miR-31 modulates dystrophin expression by targeting the 3′UTR of the dystrophin transcript and repressing its translation. Therefore, miR-31 has been suggested as a suitable target for improving dystrophin recovery in exon skipping therapy in Duchenne muscular dystrophy [7, 9].

The level and effect of miR-31 thus vary by the type of the autoimmune disease [10–12]. miR-31 expression increases in the mice T cells in experimental autoimmune encephalomyelitis (EAE) and keratinocytes of patients with psoriasis, and its activation is associated with exacerbation of both diseases [12–14]. In contrast, patients with systemic lupus erythematosus have decreased expression of miR-31 in T cells, where it plays protective roles [15]. Moreover, miR-31 may also modulate the immune response of neutrophils [12].

The immune system homeostasis is mediated by regulatory T (Treg) cells [10]. miR-31 regulates Treg cells through several mechanisms, including suppression of FOXP3 (forkhead box P3) protein involved in Treg cell differentiation. Furthermore, miR-31 can repress the generation of peripherally derived Treg cells [11], which differentiate into secondary lymphoid organs and tissues to control autoimmune responses under specific inflammatory conditions [12]. Zhang et al. [13] identified a potential FOXP3-binding site within the promoter region of the gene encoding murine miR-31, suggesting that FOXP3 may directly target miR-31. FOXP3+ Treg cells are critical in maintaining immune tolerance and homeostasis of the immune system. The molecular mechanisms underlying the stability, plasticity, and functional activity of Treg cells have been much studied in recent years. Therefore, identifying the molecular mechanisms by which FOXP3 and miR-31 regulate each other and identifying the other downstream target genes in this regulatory network can assist in the development of novel treatments for autoimmune diseases [16, 17].

Chronic inflammatory demyelinating polyneuropathy (CIDP) is an acquired autoimmune neuropathy in which nerve damage occurs by both cellular and humoral mechanisms. The incidence rates varied between 0.15 and 0.70 cases per 100,000 persons per year. This disease occurs in all age groups, but its prevalence increases with age and is more common in men than in women. The median disease duration to diagnosis was ten months (range, 2-64) [18–20].

While various antibodies have been identified, including IgG4 classes directed against proteins of the Ranvier node and the nodal area, the diagnosis of CIDP is still based on clinical and electrophysiological criteria [18, 21, 22]. There is no specific biomarker characteristic for CIDP, which seems to be much-needed. Research on miRNAs appears to be helpful in the search for diagnostic markers and may contribute to the development of potential treatment. The incorrect expression of particular miRNAs may result from genome changes or abnormalities in their biogenesis or may be related to epigenetic factors regulating gene expression. Not only are the structurally determined changes in miRNA expression levels significant, but also their epigenetic regulation. Modulation of miRNA expression by changes in the methylation level of their genes will probably be a future target for new therapies in CIDP.

The aim of this study was to evaluate the expression of miR-31-5p in serum in CIDP patients with the assessment of the correlation between miR-31-5p level and clinical presentation and electrophysiological and biochemical parameters. Electrodiagnostics (nerve conduction studies) are recommended to confirm the clinical diagnosis of typical CIDP, so special attention was paid to the analysis of the correlation of electrophysiological parameters with miR-31-5p levels. In addition, we examined whether diabetes mellitus could influence the level of the miRNA-31 level. CSF analysis should be considered to exclude diagnoses other than CIDP; in particular, elevated protein levels in CSF should be interpreted with caution in the case of diabetes mellitus comorbidity. We also analyzed the relationship between IVIg treatment duration and miRNA expression.

2. Materials and Methods

The study group consisted of 48 patients (female: 8, male: 40), who fulfilled the CIDP diagnostic criteria according to the European Academy of Neurology/Peripheral Nerve Society guideline [18]. The mean age was 61.60 ± 11.76 years. A plasma exchange (5 exchanges over 2 weeks) procedure was performed in 23 patients with CIDP. Chronic immunosuppressive treatment was used in 43 patients, including corticosteroids (prednisolone) in 20 patients, and immunosuppressive drugs in 13 patients (mycophenolate mofetil in 9 patients, azathioprinum in 3 patients, and ciclosporin in 1 patient). In addition, 17 patients had diabetes mellitus type 2, including a history of plasma exchange for the immediate treatment of CIDP, while 9 patients received chronic immunosuppressive therapy (azathioprinum in 4 patients and mycophenolate mofetil

in 5 patients). Hypertension was recognized in 23 patients. Also, 23 patients had degenerative changes of the lumbosacral vertebral column.

Patients with variants of CIDP (distal, multifocal, focal, motor, and sensory), chronic immune sensory polyradiculopathy (CISP), multifocal motor neuropathy (MMN), mononeuritis multiplex, hereditary demyelinating neuropathy, chronic ataxic neuropathy with disialosyl antibodies (CANDA) and chronic ataxic neuropathy, ophthalmoplegia, IgM paraproteinaemia, cold agglutinin and disialosyl antibodies (CANOMAD), cerebellar ataxia, neuropathy, vestibular areflexia syndrome (CANVAS), and POEMS syndrome were excluded from this study. Patients with IgG or IgA monoclonal gammopathy of undetermined significance and IgM monoclonal gammopathy without antibodies to MAG were also excluded. HIV infection, other immunological conditions, and malignancy were also excluded. Amyloidosis, liver and kidney damage, multiple myeloma and osteosclerotic myeloma, venous insufficiency and chronic limb ischaemia, myopathy and neuromuscular junction disease, dorsal column lesions (such as syphilis, paraneoplastic diseases, and copper deficiency) and toxic neuropathies (e.g., due to chemotherapy and vitamin B6 poisoning), and peripheral nerve tumors were excluded.

Vitamin B12 levels in all patients were normal. All patients were negative for tumor markers, antibodies against neuronal antigens, and antibodies characteristic for autoimmune disorders, including connective tissue diseases. All patients showed a good response to the treatment, IVIg in particular.

The control group consisted of 13 subjects. The control group was matched for sex, age, comorbidities, IBM index, and smoking.

2.1. Ethical Standards. All subjects in the patient and control groups were informed in detail about the purpose and procedure of the study and gave written informed consent to participate in the study. The authors had a positive opinion of the Bioethics Committee of the Medical University of Wrocław No. KB-719/2021 on conducting this study.

2.2. Clinical and Biochemical Evaluation. Clinical improvement was defined according to the following scales: INCAT disability scale (the significance was established as ≥1 point), Medical Research Council (MRC) sum score (as ≥2 to 4 points), and grip strength measured by hand dynamometer (+ more than 10% of the output value). The Inflammatory Neuropathy Cause And Treatment (INCAT) disability scale was first used in a clinical trial comparing the efficacy and safety of intravenous immunoglobulin with oral prednisone in patients with CIDP [23]. The scale is a measure of activity limitation by assessing upper and lower limb dysfunction. The INCAT score is inversely related to function, where 0 indicates no functional impairment and 10 indicates an inability to perform any purposeful movement of the limbs [24].

Serum microRNA-31 copy number; immunoglobulin IgG, IgM, IgA and levels; and creatine kinase (CK) activity were estimated. In addition, pleocytosis and protein levels were determined in cerebrospinal fluid.

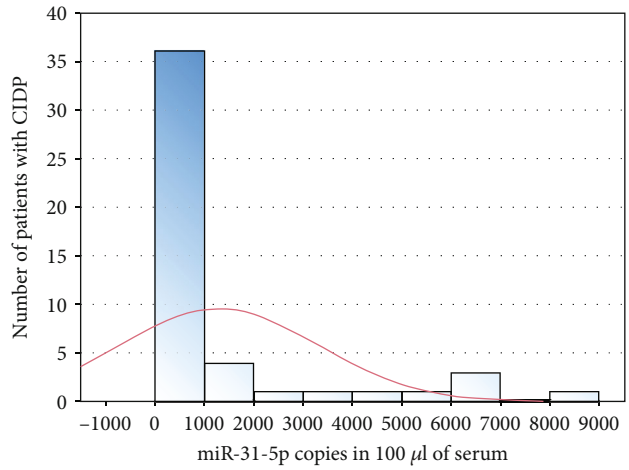

Figure 1: Histogram of miR-31-5p copies in 100 μl of serum in the patient group.

Correlations between miRNA-31 expression and disease duration, clinical parameters (upper limb, lower limb, total INCAT), IgIV treatment time, body weight, and selected biochemical parameters (IgG, IgM, IgA, CK, CSF protein levels, and CSF) were calculated. The group of patients was divided into subgroups based on the disease duration (≤5 years/>5 years), body weight (≤80 kg/> 80 kg), INCAT total (0–4/5–10), the presence of diabetes mellitus type 2 (yes/no), hypertension (yes/no), CK level (normal/above normal), CSF pleocytosis (<5/>5 cells/μl), protein (<50 g/dl/≥50 g/dl), and IgIV treatment (yes/no).

2.3. Electroneurography. The electrophysiological tests were carried out using the Viking Quest version 10.0 device. Motor and sensory nerves were performed using standard methods [25], with the evaluation of latency, amplitude, and conduction velocity. All tests were done under the same conditions. The same distance from the stimulating and active electrodes was used. The room temperature fluctuated between 21 and 23°C, and the temperature of the extremities was not less than 32°C. Compound muscle action potential (CMAP) was determined in the median, ulnar, peroneal, and tibial nerves. F-wave latency was studied for all motor nerves. Sensory nerve action potential (SNAP) was determined in the median, ulnar, and sural nerves.

2.4. Serum Collection and RNA Isolation. Blood samples were collected from CIDP patients and controls. Serum fractions were isolated within 2 hours after blood collection using 10-minute centrifugation at 1900 × g and then at 16,000 × g. For serum miRNA isolation, the miRNeasy Serum/Plasma Advanced Kit (Qiagen, Germany) was used according to the manufacturer's protocol. Then, miRNA samples were frozen and stored at -80°C.

2.5. Reverse Transcription. Reverse transcription reactions (RT) were performed using 2,5 μl of extracted microRNAs,

Table 1: The clinical characteristics of patients without and with diabetes.

		Group of patients without diabetes		Group of patients with diabetes		p value
		Mean	SD	Mean	SD	
miR-31-5p/100 μl of serum		1366.33	2054.54	1146.97	1953.03	0.332
Duration of the CIDP (years)		5.35	3.07	5.24	3.42	0.688
Duration of IgIV treatment (months)		17.16	13.01	12.00	14.90	0.076
Body weight (kg)		87.32	20.27	90.24	20.12	0.726
INCAT upper limbs		1.94	1.00	1.12	0.70	0.005
INCAT lower limbs		1.97	1.17	1.41	0.80	0.086
Serum	CK (IU/l)	279.13	197.57	250.59	194.48	0.698
	IgG (g/l)	10.95	2.87	10.55	1.86	0846
	IgA (g/l)	2.29	0.86	2.65	1.28	0.532
Cerebrospinal fluid	IgM (g/l)	1.18	0.83	0.87	0.63	0.200
	Pleocytosis (cells/μl)	3.43	2.49	4.18	3.70	0.796
	Protein (mg/dl)	72.39	37.20	7741	30.66	0.499
Age (years)		59.23	11.93	65.94	10.40	0.070
ni			31		17	
Gender		F = 8	M = 23	F = 0	M = 17	

Abbreviation: *ni*: number of patients in the group.

TaqMan microRNA Reverse Transcription Kit (Thermo Fisher Scientific, Foster City, CA, USA), and specific RT primers for miR-31-5p in a final volume of 7.5 μl according to manufacturer's recommendation. All RT products were diluted twice with water.

2.6. ddPCR. Droplet digital PCR was applied as a method of miR-31expression analysis due to its high accuracy, reproducibility, and sensitivity [26]. The ddPCR reaction mixtures contained the following: 1.33 μl of RT product, 1 μl of TaqMan miRNA-specific probe (ID 002279, Thermo Fisher Scientific), 7.67 μl of molecular biology-grade water, and 10 μl of 2x ddPCR™ Master Mix for Probes (Bio-Rad). A total of 20 μl of the reaction mixtures was loaded into a plastic cartridge with 70 μl of Droplet Generation Oil for Probes in the QX200 Droplet Generator (all from Bio-Rad). The droplets obtained from each sample were then transferred to a 96-well PCR plate (Eppendorf, Hamburg, Germany). PCR amplifications were carried out in the C1000 Touch Thermal Cycler at 95°C for 10 min, followed by 40 cycles at 95°C for 3 sec and 60°C for 1 min and 1 cycle at 98°C for 10 min ending at room temperature (RT). Finally, the plate was loaded on a Droplet Reader (BioRad) and read automatically. Absolute quantification (AQ) of each miRNA was calculated from the number of positive counts per panel using Poisson distribution. The quantification of the target miRNAs is presented as the number of copies/100 μl of serum.

2.7. Data Analysis. Statistical analyses were performed using Statistica 13.0 software. Normality of distributions was tested using the Shapiro-Wilk test. Due to the lack of normality of distribution for many variables, Spearman's rank correlation coefficient was used to analyze relationships between variables. Due to the same reason, subgroup (based on the disease duration, body weight, INCAT total, etc.) comparisons were made using the Mann–Whitney U. The level of statistical significance for all variables was set at alpha = 0.05.

3. Results

3.1. The Clinical and Electrophysiological Data of the Study Group. The mean duration of CIDP was 5.31 years (SD ± 3.16). A total INCAT score was equal to 3.10 ± 2.14. The INCAT score for the upper limbs was 1.65 ± 0.98, and for the lower limbs, 1.77 ± 1.08. The mean body weight was 88.35 ± 20.05 kg; 28 patients (female: 4, male: 24) had a body weight > 80 kg. Blood tests results were as described: CK 269.02 ± 194.88 IU/l, IgG level 10.81 ± 2.55 g/l, IgA 2.42 ± 1.03 g/l, and IgM 1.07 ± 0.77 g/l. CSF general examination showed a mean pleocytosis amounting to 3.70 ± 2.9 cells/μl, and the protein level was 74.20 ± 34.71 mg/dl. The mean copy number of miR-31-5p in 100 μl serum was 1288.64 ± 2001.02 (Figure 1) in the CIDP group of patients, while in the control group, 3743.09 ± 4026.90.

Seventeen (17) patients had diabetes mellitus, and all of them were men. Table 1 shows the clinical characteristics of patients with and without diabetes. The mean electrophysiological parameters for subjects are shown in Table 2.

The electrophysiological parameters were also compared between patients with and without concomitant diabetes mellitus. A significantly longer latency of the sural nerve SNAP was found in the diabetic group (4.25 ± 0.6 vs. 3.71 ± 0.86; $p = 0.037$). There was no statistical significance between the other parameters in the above groups.

3.2. The Correlations between MicroRNA-31-5p Copy Number and the Data Studied. A significant correlation of

Table 2: The mean electrophysiological parameters of CIDP patients.

Nerve conduction		Electrophysiological parameters	Patients $n = 48$
Motor	Median (wrist-elbow)	Latency (ms)	6.20 ± 3.94
		Amplitude (mV)	5.28 ± 3.75
		CV (m/s)	37.50 ± 18.26
	Ulnar (wrist-elbow)	Latency (ms)	3.60 ± 1.40
		Amplitude (mV)	7.04 ± 3.20
		CV (m/s)	46.48 ± 11.35
	Peroneal (ankle head of fibula)	Latency (ms)	6.16 ± 1.88
		Amplitude (mV)	2.01 ± 1.67
		CV (m/s)	37.19 ± 6.81
	Tibial (ankle popliteal fossa)	Latency (ms)	6.26 ± 1.38
		Amplitude (mV)	3.19 ± 3.13
		CV (m/s)	35.97 ± 7.74
Sensory	Median (digit II)	Latency (ms)	3.64 ± 1.03
		Amplitude (μV)	11.01 ± 7.25
		CV (m/s)	42.08 ± 7.69
	Ulnar (digit V)	Latency (ms)	3.13 ± 0.94
		Amplitude (μV)	10.36 ± 6.69
		CV (m/s)	42.96 ± 8.89
	Sural	Latency (ms)	3.82 ± 0.67
		Amplitude (μV)	5.10 ± 3.92
		CV (m/s)	43.47 ± 9.85
F-wave studies	Median	F-latency (ms)	34.34 ± 6.95
	Ulnar		35.01 ± 7.74
	Peroneal		67.17 ± 8.25
	Tibial		67.62 ± 8.05

Table 3: Correlations of miR-31-5p with clinical and biochemical data in CIDP patients.

Data			Correlations
Clinical Parameters	Disease duration		-0.024
	IgIV treatment time		0.426
	Weight		-0.117
	INCAT	Upper limb	0.186
		Lower limb	0.109
		Total	0.167
Biochemical parameters	Serum	CK	-0.019
		IgG	0.212
		IgA	-0.209
		IgM	0.067
	Cerebrospinal fluid	Protein levels	0.123
		Pleocytosis	0.023

miR-31-5p was noted for the duration of IgIV treatment (0.426) (Table 3, Figure 2). Based on J. Guilford's classification, we showed a low correlation ($0.1 < |r| \leq 0.3$) between microRNA-31-5p levels and IgG (0.212) and IgA (-0.209) levels, peroneal CMAP latency (0.25), tibial CMAP latency (0.24), and SNAP conduction velocity of

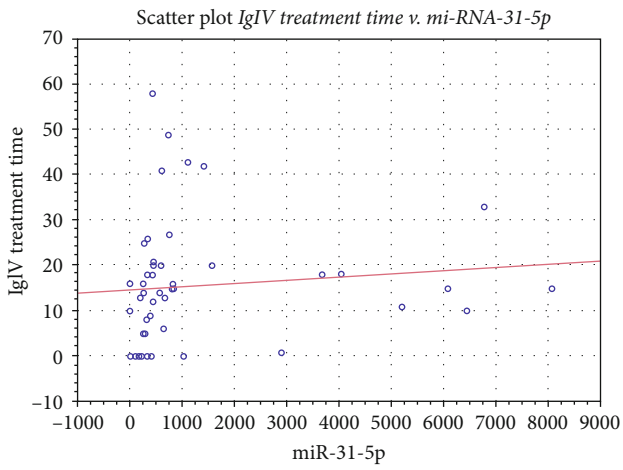

Figure 2: Scatter plot of the correlation between miR-31-5p expression and IgIV treatment time in CIDP patients.

the ulnar nerve (0.26). We did not find any significant correlation between microRNA-31-5p expression and other clinical, biochemical, and electrophysiological parameters (Tables 3 and 4).

The patients with body weight > 80 kg showed significantly lower levels of miRNA-31-5p than those with lower body weight (934.37 ± 1739.66 vs. 1784.62 ± 2271.62, respectively; $p = 0.014$). Conversely, patients with high protein levels in CSF showed significantly higher levels of miRNA-31-5p than those with normal protein levels (1393.93 ± 1932.27 vs. 987.38 ± 2364.10, respectively; $p = 0.044$).

3.3. The Group Characteristics in relation to IgIV Treatment. In the patient group, 38 subjects (female: 6, male: 32) were treated with IgIV. The patients who were not treated with IgIV demonstrated markedly decreased levels of miR-31-5p versus the patients who were treated (259.44 ± 304.02 vs. 1559.48 ± 2168.45, respectively; $p = 0.002$). The copy number of miR-31-5p in the group of patients treated with IgIV compared to the control group was lower but not statistically significant (1559.48 ± 2168.45 vs. 3743.09 ± 4026.90, respectively; $p = 0.157$), while in the group of patients not treated with IgIV compared to the control group, it was significantly lower (259.44 ± 304.02 vs. 3743.09 ± 4026.90, respectively; $p = 0.014$) (Figure 3).

In addition, the group of patients treated with IgIV showed significantly higher protein levels in the cerebrospinal fluid than the group of patients untreated with IgIV (79.59 ± 36.20 vs. 54.29 ± 18.90, respectively; $p = 0.017$). There were no significant statistical differences between IgA, IgG,and IgM levels between the groups of patients treated and untreated with IgIV.

3.4. The Characteristics of Patients with Upregulation of MicroRNA-31-5p Expression. Upregulation of microRNA-31-5p expression, determined as value > mean value + 3SD, was found in 5 patients. The mean copy number of miR-31-5p in 100 μl serum was 6503.76. In this group of patients, the mean electrophysiological parameters were better than the mean values obtained in the entire CIDP group (Table 5). The biochemical parameters in this group of patients showed the following: CK 215.60 U/l, IgG level 9.3 g/l, IgA 2.7 g/l, and IgM 0.62 g/l. CSF general examination showed a mean pleocytosis amounting to 3.60 cell/μl, and the protein level was 60.14 mg/dl. The mean duration of CIDP disease was 5 years, mean IgIV treatment time 16.80 months, and mean weight 96 kg. A total INCAT score was equal to 2.2, and the INCAT score for the upper limbs was 1.00 and for the lower limbs 1.40.

4. Discussion

The most important result of our study is the finding of low miRNA-31 values in CIDP patients. The small copies of microRNA-31 can be attempted to explain the reciprocal dysregulation of the transcription factors in patients with CIDP. Several studies demonstrate that miR-31 can positively regulate cell proliferation, differentiation, and activity by regulating NF-κB, RAS/MAPK, Notch, and some cytokine signalling pathways [12, 14, 27, 28]. The increased miRNA-31 copies in our patients treated with IVIg may be due to the mechanism of action of IVIg. IVIg inactivates, silences, or leads to apoptosis of T cells, while restoring the balance of anti- and proinflammatory cytokines. Additionally, IVIg are thought to interfere with the passage of autoimmune cells across the blood-nerve barrier and to reduce antibody production by B cells, interfere with B cell proliferation through cell surface receptors, and block the activity of certain B cell subtypes. IVIg may also contain numerous anti-idiotypes that neutralise pathogenic antibodies. Finally, it has been shown that IVIg treatment interrupts several steps in the complement activation cascade and affects activity mediated by the Fc receptor [29–31].

The findings of Ripamonti et al. [32] highlighted miRNA-31 as a possible target for modulation of T cell-dependent antibody responses in humans with immune dysregulation. Antibody production by B lymphocytes requires support from follicular helper T (TFH) cells—a specific subgroup of CD4+ T lymphocytes. TFH cell role needs the presence of BCL6 (B cell lymphoma 6), a transcriptional repressor with unclear gene target responsible for helper activity. Combined miRNA analysis with gene expression profiling in human TFH cells, the authors found that the level of miR-31 is upregulated. The authors concluded that their findings highlight miR-31 as a possible target to modulate human T cell-dependent antibody responses in the settings of infection, vaccination, or immune dysregulation. In our study, we were able to confirm the upregulation process only in 5 patients. The patients with a high level of miRNA-31 had better clinical (in INCAT score) and electrophysiological parameters, although due to the small number of subjects, statistical analysis could not be performed. They also showed lower CK activity, lower IgG and IgM levels, as well as lower CSF protein levels.

We demonstrated a low positive correlation between miRNA-31 and serum IgG level. Previous studies have found that patients with Guillain-Barré syndrome (GBS) have high variability in serum immunoglobulin G (IgG)

Table 4: Correlation between the electrophysiological parameters and expression of miRNA31-5p in serum in CIDP patients.

Nerve conduction		Electrophysiological parameters	Correlation miRNA
Motor	Median (wrist-elbow)	Latency	0.05
		Amplitude	-0.12
		CV	-0.08
	Ulnar (wrist-elbow)	Latency	0.02
		Amplitude	-0.04
		CV	-0.13
	Peroneal (ankle head of fibula)	Latency	0.25
		Amplitude	0.12
		CV	-0.01
	Tibial (ankle popliteal fossa)	Latency	0.24
		Amplitude	-0.05
		CV	0.12
Sensory	Median (digit II)	Latency	0.09
		Amplitude	-0.11
		CV	-0.01
	Ulnar (digit V)	Latency	-0.14
		Amplitude	-0.15
		CV	0.26
	Sural	Latency	-0.13
		Amplitude	-0.16
		CV	0.08
F-wave studies	Median	F-latency	-0.08
	Ulnar		0.09
	Peroneal		-0.09
	Tibial		0.01

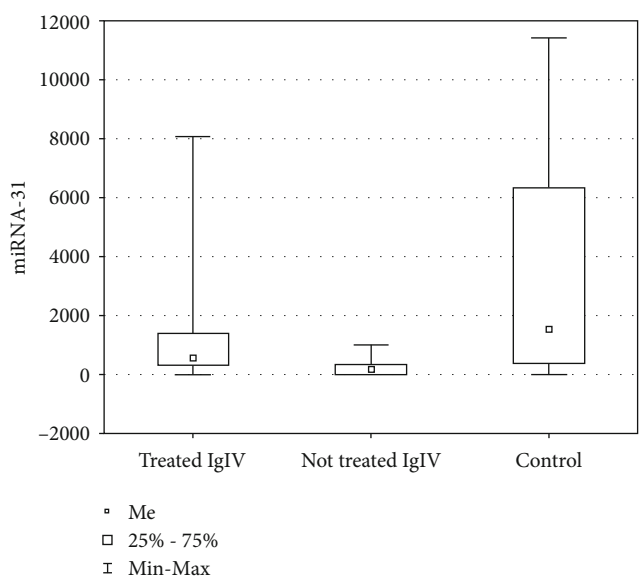

Figure 3: Graph showing the mean copy number of miR-31-5p in the patient group—treated and untreated with IgIV—and in the control group.

levels after standard IVIg treatment and that large increases in serum IgG (ΔIgG) are associated with better treatment outcome. A recent prospective study in CIDP indicated that the increased ΔIgG level after standard IVIg dosage in the continuous treatment was relatively constant within individual patients. This level could differ between patients who were treated with the same stable dosage and with interval of IVIg [33]. In our study, there were no statistically significant differences in IgG levels between treated and untreated IgIV groups, as well as in the patients with miRNA-31 upregulation. In the CIDP patients, we additionally revealed the low negative correlation between IgA and miRNA-31 levels, but no significant differences were found between IgA levels in the patient and healthy groups. In the course of IgA deficiency, the occurrence of autoimmune diseases has been found to be significantly more frequent than in patients with normal levels of this immunoglobulin. The relationships between IgA, IgG, and miRNA-31 in our study group were ambiguous and did not allow drawing clear conclusions.

We found a positive, average correlation between the duration of IVIg treatment and miRNA-31-5p expression. IVIg has been shown to inactivate or lead to T cell apoptosis, while restoring the balance of anti- and proinflammatory cytokines. Additionally, IVIg is thought to interfere

Table 5: The mean electrophysiological parameters of CIDP patients with upregulation of microRNA-31 expression.

Nerve conduction		Electrophysiological parameters	Patients $n = 5$
Motor	Median (wrist-elbow)	Latency (ms)	6.38
		Amplitude (mV)	7.08
		CV (m/s)	47.4
	Ulnar (wrist-elbow)	Latency (ms)	2.96
		Amplitude (mV)	8.78
		CV (m/s)	47.2
	Peroneal (ankle head of fibula)	Latency (ms)	6.28
		Amplitude (mV)	2.12
		CV (m/s)	40.8
	Tibial (ankle popliteal fossa)	Latency (ms)	6.68
		Amplitude (mV)	3.30
		CV (m/s)	38.10
Sensory	Median (digit II)	Latency (ms)	3.52
		Amplitude (μV)	11.30
		CV (m/s)	48.80
	Ulnar (digit V)	Latency (ms)	2.72
		Amplitude (μV)	11.90
		CV (m/s)	44.60
	Sural	Latency (ms)	3.61
		Amplitude (μV)	4.20
		CV (m/s)	44.10
F-wave studies	Median	F-latency (ms)	32.76
	Ulnar		32.48
	Peroneal		68.89
	Tibial		65.76

with the passage of autoimmune cells across the blood-nerve barrier and to reduce antibody production by B cells, interfere with B cell proliferation through cell surface receptors, block the activity of certain B cell subtypes, interrupt several steps in the complement activation cascade, and affect activity mediated by the Fc receptor [31, 34]. The correlations between IVIg treatment effectiveness and miRNA level were described in many studies in different clinical situations [35–38]. IVIg replacement therapy in different immunodeficiency patients is thought to be able to modulate miRNA level. miRNAs seem to be a valid target to develop new therapies and potential biomarkers in different inflammatory diseases. Based on the literature and their original results, the authors proposed an additional hypothesis for the mechanism of miR-31-5p regulation [39–42]. According to the miRDB database, the target of miR-31-5p is the miRNA for the sphingomyelin synthase 1 (SGMS1) gene. Sphingomyelin synthase converts ceramide to sphingomyelin, so the amount of CSF sphingomyelin directly depends on its amount and activity. If in CIDP the level of miR-31-5p decreases (as we observe in our studies, CIDP patients not treated with IgIV have very low levels of this miR compared to control and treated patients), this may directly affect the increase in the level of its target, SGMS1, and consequently sphingomyelin. The application of IgIV therapy improves the condition of patients by, among other things, increasing miR31-5p (in our observations, patients after IgIV therapy have statistically higher levels of miR31-5p), which decreases SGM1A and consequently affects the reduction of sphingomyelin. On this basis, we can conclude that the level of circulating serum miR-31-5p may not only be a helpful diagnostic biomarker in CIDP but also a tracer of clinical improvement in patients with CIDP undergoing IgIV therapy.

We tried to consider other factors influencing the miRNA level in our patients and the results of treatment. The lower levels of miRNA-31 were observed in the patients with high body weight. There are many controversies regarding the importance of obesity in the CIDP patients and its influence on the IVIg treatment. Pharmacokinetic difference in lean and obese patients at higher doses of IVIg were observed, but it seems to be small to influence the IVIg dosage. Sometimes, a very high IgG level is observed in obese patients treated with IVIg [43]. The CIDP patients with and without diabetes mellitus were similar in the clinical and electrophysiological tests; miRNA-31, IgG, Ig A, CK, and CSF protein levels did not differ either. Our results were

similar to other studies in which the differences between patients with and without DM were not seen [44].

Influencing miRNA function may contribute to a better understanding of the CIDP pathogenesis and the selection of an effective type of treatment. It is worth noting that abnormal expression of individual microRNAs may result from changes in the genome or abnormalities in their biogenesis or may be related to epigenetic factors regulating gene expression [45–49]. The work of Vinci et al. [47] highlighted that not only structurally determined changes in miRNA expression levels but also their epigenetic regulation seemed to be important in the CIDP pathogenesis and may become future targets for the development of new therapies modulating miRNA expression through changes in the level of methylation of their genes. Additionally, the interaction between miR-31 and the NF-κB signalling pathway is the subject of many studies. The positive feedback loop formed by miR-31 and NF-κB signalling may bring new ideas for the treatment of some autoimmune conditions [14, 48–52]. In a previous study, the authors demonstrated significantly higher levels of IL-6, IL-2, IL-4, and TNF-α and an increased CD4+/CD8 + ratio in patients with CIDP compared to controls. Electrophysiological parameters in CIDP patients were also found to be closely related to the autoimmune process. All these studies may contribute to a better understanding of the pathomechanism of CIDP [53].

The authors are aware of the study's limitations. Due to the complexity of miRNA roles, the main limitation was the selection of only one miRNA type. The selection was based on the literature and the importance of miRNA-31 related to CIDP issues. Additionally, this study and the control group were rather small. The patient group was not homogeneous in terms of disease duration, type of treatment, and additional medical conditions.

5. Conclusion

In this study, we have shown the reduced level of miRNA-31-5p in the patients with typical CIDP. It was significantly reduced in the patients who were not treated with IVIg. In the treated group, miRNA was approaching the correct level, and in some patients, it was upregulated.

These patients had better clinical and electrophysiological results than other patients with CIDP. We observed a clearly negative impact of the obesity on the clinical and electrophysiological status with a lower miRNA-31 level. All these results could support the thesis that miRNA-31 is highly involved in the autoimmune process in CIDP. The positive relationship between the higher level of miRNA-31 and the duration of IVIg treatment may be an additional factor explaining the effectiveness of the prolonged IVIg therapy in CIDP. The presence of diabetes mellitus does not significantly influence the miRNA-31 level and clinical and electrophysiological status. Further studies are needed to assess whether such miRNAs could represent novel potential biomarkers in the management and therapy of CIDP patients.

Abbreviations

CSF:	Cerebrospinal fluid
CIDP:	Chronic inflammatory demyelinating polyneuropathy
CK:	Creatine kinase
EAE:	Experimental autoimmune encephalomyelitis
FOXP3:	Forkhead box P3
GBSl:	Guillain-Barré syndrome
IgIV treatment:	Immunoglobulin intravenous treatment
miRNAs:	MicroRNAs
miRNA-31-5p:	MicroRNA-31-5p
Nuclear factor kappa B:	Nuclear factor kappa B
SGMS1:	Sphingomyelin synthase 1.

Data Availability

The data sets used and/or analyzed during the current study are available from the corresponding author on reasonable request.

Ethical Approval

The authors had a positive opinion of the Bioethics Committee of the Medical University of Wrocław No. KB-719/2021 to perform the study. The study was conducted in accordance with the Declaration of Helsinki with amendments of 2013.

Consent

The authors informed the patients and control subjects in detail about the planned study and obtained written consent to conduct it.

Conflicts of Interest

The authors declare that they have no conflicts of interest.

Authors' Contributions

E.D. was responsible for the study concept, design, and data analysis and interpretation; D.B was responsible for data analysis and interpretation; M.W. was responsible for the statistical analysis; M.O., H.M., M.M., P.D., and E.B. handled the data collection; S.B. reviewed the manuscript; and M.K. was responsible for the critical revision of the manuscript for important intellectual content. All authors contributed to the article and approved the submitted version manuscript.

Acknowledgments

This research was financially supported by the Ministry of Health Subvention according to number SUBZ.220.22.102 from the IT Simple System of Wroclaw Medical University.

References

[1] B. Liu, J. Li, and M. J. Cairns, "Identifying miRNAs, targets and functions," *Briefings in Bioinformatics*, vol. 15, no. 1, pp. 1–19, 2014.

[2] B. Liu, L. Liu, A. Tsykin, G. J. Goodall, M. J. Cairns, and J. Li, "Discovering functional microRNA-mRNA regulatory modules in heterogeneous data," *Advances in Experimental Medicine and Biology*, vol. 774, pp. 267–290, 2013.

[3] M. M. Akhtar, L. Micolucci, M. S. Islam, F. Olivieri, and A. D. Procopio, "Bioinformatic tools for microRNA dissection," *Nucleic Acids Research*, vol. 44, no. 1, pp. 24–44, 2016.

[4] G. Zhao, C. Han, Z. Zhang, L. Wang, and J. Xu, "Increased expression of microRNA-31-5p inhibits cell proliferation, migration, and invasion via regulating Sp1 transcription factor in HepG2 hepatocellular carcinoma cell line," *Biochemical and Biophysical Research Communications.*, vol. 490, no. 2, pp. 371–377, 2017.

[5] H. S. Kim, K. S. Lee, H. J. Bae et al., "MicroRNA-31 functions as a tumor suppressor by regulating cell cycle and epithislial-mesenchymal transition regulatory proteins in liver cancer," *Oncotarget*, vol. 6, no. 10, pp. 8089–8102, 2015.

[6] W. Zheng, Z. Liu, W. Zhang, and X. Hu, "miR-31 functions as an oncogene in cervical cancer," *Archives of Gynecology and Obstetrics*, vol. 292, no. 5, pp. 1083–1089, 2015.

[7] I. T. Zaharieva, M. Calissano, M. Scoto et al., "Dystromirs as serum biomarkers for monitoring this disease severity in Duchenne muscular dystrophy," *PLoS One*, vol. 25, article e80263, 2013.

[8] V. Pegoraro, A. Merico, and C. Angelini, "Micro-RNAs in ALS muscle: differences in gender, age at onset and disease duration," *Journal of the Neurological Sciences*, vol. 15, pp. 58–63, 2017.

[9] D. Cacchiarelli, T. Incitti, J. Martone et al., "miR-31 modulates dystrophin expression: new implications for Duchenne muscular dystrophy therapy," *EMBO Reports*, vol. 12, no. 2, pp. 136–141, 2011.

[10] X. Li and Y. Zheng, "Regulatory T cell identity: formation and maintenance," *Trends in Immunology*, vol. 36, no. 6, pp. 344–353, 2015.

[11] C. Dhamne, Y. Chung, A. M. Alousi, L. J. Cooper, and D. Q. Tran, "Peripheral and thymic foxp3(+) regulatory T cells in search of origin, distinction, and function," *Frontiers in Immunology*, vol. 27, p. 253, 2013.

[12] N. A. Stepicheva and J. L. Song, "Function and regulation of microRNA-31 in development and disease," *Molecular Reproduction and Development*, vol. 83, no. 8, pp. 654–674, 2016.

[13] L. Zhang, F. Ke, Z. Liu et al., "MicroRNA-31 negatively regulates peripherally derived regulatory T-cell generation by repressing retinoic acid-inducible protein 3," *Nature Communications*, vol. 13, p. 7639, 2015.

[14] S. Yan, Z. Xu, F. Lou et al., "NF-κB-induced microRNA-31 promotes epidermal hyperplasia by repressing protein phosphatase 6 in psoriasis," *Nature Communications*, vol. 3, p. 7652, 2015.

[15] W. Fan, D. Liang, Y. Tang et al., "Identification of microRNA-31 as a novel regulator contributing to impaired interleukin-2 production in T cells from patients with systemic lupus erythematosus," *Arthritis and Rheumatism*, vol. 64, no. 11, pp. 3715–3725, 2012.

[16] R. Rouas, H. Fayyad-Kazan, N. El Zein et al., "Human natural Treg microRNA signature: role of microRNA-31 and microRNA-21 in FOXP3 expression," *European Journal of Immunology*, vol. 36, pp. 1608–1618, 2009.

[17] H. Zhou, F. Lou, J. Bai et al., "A peptide encoded by pri-miRNA-31 represses autoimmunity by promoting Treg differentiation," *EMBO Reports*, vol. 23, article e53475, 2022.

[18] P. Y. Van den Bergh, P. A. van Doorn, R. D. Hadden et al., "European Academy of Neurology/Peripheral Nerve Society guideline on diagnosis and treatment of chronic inflammatory demyelinating polyradiculoneuropathy: report of a joint task force—second revision," *Journal of the Peripheral Nervous System*, vol. 26, no. 3, pp. 242–268, 2021.

[19] M. C. Broers, C. Bunschoten, D. Nieboer, H. F. Lingsma, and B. C. Jacobs, "Incidence and prevalence of chronic inflammatory demyelinating polyradiculoneuropathy: a systematic review and meta-analysis," *Neuroepidemiology*, vol. 52, no. 3-4, pp. 161–172, 2019.

[20] M. Ryan and S. J. Ryan, "Chronic inflammatory demyelinating polyneuropathy: considerations for diagnosis, management, and population health," *The American Journal of Managed Care*, vol. 24, 17 Suppl, pp. S371–S379, 2018.

[21] J. I. Kira, "Anti-neurofascin 155 antibody-positive chronic inflammatory demyelinating polyneuropathy/combined central and peripheral demyelination: strategies for diagnosis and treatment based on the disease mechanism," *Frontiers in Neurology*, vol. 10, article 665136, 2021.

[22] A. Cortese, R. Lombardi, C. Briani et al., "Antibodies to neurofascin, contactin-1, and contactin-associated protein 1 in CIDP: clinical relevance of IgG isotype," *Neurology-Neuroimmunology Neuroinflammation.*, vol. 21, article e639, 2019.

[23] R. Press, F. Hiew, and Y. Rajabally, "Steroids for chronic inflammatory demyelinating polyradiculoneuropathy: evidence base and clinical practice," *Acta Neurologica Scandinavica*, vol. 133, no. 4, pp. 228–238, 2016.

[24] A. Breiner, C. Barnett, and V. Bril, "INCAT disability score: a critical analysis of its measurement properties," *Muscle & Nerve*, vol. 50, no. 2, pp. 164–169, 2014.

[25] A. Morokoff, J. Jones, H. Nguyen et al., "Serum microRNA is a biomarker for post-operative monitoring in glioma," *Journal of Neuro-Oncology*, vol. 149, no. 3, pp. 391–400, 2020.

[26] E. Stålberg, H. van Dijk, B. Falck et al., "Standards for quantification of EMG and neurography," *Clinical Neurophysiology*, vol. 130, no. 9, pp. 1688–1729, 2019.

[27] F. Wang, Y. Gao, Y. Yuan et al., "MicroRNA-31 can positively regulate the proliferation, differentiation and migration of keratinocytes," *Biomed Hub.*, vol. 5, no. 2, pp. 93–104, 2020.

[28] X. Zhou, J. Zhang, Y. Li, L. Cui, K. Wu, and H. Luo, "Astaxanthin inhibits microglia M1 activation against inflammatory injury triggered by lipopolysaccharide through down-regulating miR-31-5p," *Life Sciences*, vol. 15, article 118943, 2021.

[29] H. Orbach, U. Katz, Y. Sherer, and Y. Shoenfeld, "Intravenous immunoglobulin: adverse effects and safe administration," *Clinical Reviews in Allergy and Immunology*, vol. 29, article 173184, 2005.

[30] J. A. Allen, D. F. Gelinas, M. Freimer, M. C. Runken, and G. I. Wolfe, "Immunoglobulin administration for the treatment of CIDP: IVIG or SCIG?," *Journal of the Neurological Sciences*, vol. 15, article 116497, 2020.

[31] J. D. Lünemann, F. Nimmerjahn, and M. C. Dalakas, "Intravenous immunoglobulin in neurology–mode of action and clinical efficacy," *Nature Reviews. Neurology*, vol. 11, no. 2, pp. 80–89, 2015.

[32] A. Ripamonti, E. Provasi, M. Lorenzo et al., "Repression of miR-31 by BCL6 stabilizes the helper function of human follicular helper T cells," *Proceedings of the National Academy of Sciences of the United States of America*, vol. 28, pp. 12797–12802, 2017.

[33] P. A. van Doorn, K. Kuitwaard, and B. C. Jacobs, "Serum IgG levels as biomarkers for optimizing IVIg therapy in CIDP," *Journal of the Peripheral Nervous System*, vol. 16, suppl 1, pp. 38–40, 2011.

[34] H. P. Hartung, "Advances in the understanding of the mechanism of action of IVIg," *Journal of Neurology*, vol. 255, suppl 3, pp. 3–6, 2008.

[35] L. Padet, L. Loubaki, and R. Bazin, "Use of IVIg to identify potential miRNA targets for allograft rejection and GvHD therapy," *Clinical Transplantation*, vol. 29, no. 6, pp. 543–546, 2015.

[36] B. De Felice, E. Nigro, R. Polito et al., "Differently expressed microRNA in response to the first Ig replacement therapy in common variable immunodeficiency patients," *Scientific Reports*, vol. 8, article 21482, 2020.

[37] Y. Wang, C. Li, L. Niu, M. Fu, J. Tian, and X. An, "Difference in serum miRNA expression between immunoglobulin-sensitive and -insensitive incomplete Kawasaki disease patients," *Experimental and Therapeutic Medicine*, vol. 21, p. 162, 2021.

[38] Q. Gao, Y. Ma, D. Yuan, Q. C. Zhang, J. Zeng, and H. Li, "MicroRNA-125b in peripheral blood: a potential biomarker for severity and prognosis of children with viral encephalitis," *Neurological Sciences*, vol. 38, no. 8, pp. 1437–1444, 2017.

[39] G. Capodivento, C. De Michelis, M. Carpo et al., "CSF sphingomyelin: a new biomarker of demyelination in the diagnosis and management of CIDP and GBS," *Journal of Neurology, Neurosurgery, and Psychiatry*, vol. 92, no. 3, pp. 303–310, 2021.

[40] S. Kusunoki, "CSF sphingomyelin: possible biomarker of demyelination," *Journal of Neurology, Neurosurgery, and Psychiatry*, vol. 92, no. 3, p. 232, 2021.

[41] M. Péter, W. Török, A. Petrovics-Balog, L. Vígh, L. Vécsei, and G. Balogh, "Cerebrospinal fluid lipidomic biomarker signatures of demyelination for multiple sclerosis and Guillain-Barré syndrome," *Scientific Reports*, vol. 27, p. 18380, 2020.

[42] W. Shi, F. Dong, Y. Jiang et al., "Construction of prognostic microRNA signature for human invasive breast cancer by integrated analysis," *Oncotargets and Therapy*, vol. 15, pp. 1979–2010, 2019.

[43] J. P. Hodkinson, "Considerations for dosing immunoglobulin in obese patients," *Clinical and Experimental Immunology*, vol. 188, no. 3, pp. 353–362, 2017.

[44] Y. A. Rajabally, M. Stettner, B. C. Kieseier, H. P. Hartung, and R. A. Malik, "CIDP and other inflammatory neuropathies in diabetes – diagnosis and management," *Nature Reviews. Neurology*, vol. 13, no. 10, pp. 599–611, 2017.

[45] M. Gholipour, M. Taheri, J. Mehvari Habibabadi, N. Nazer, A. Sayad, and S. Ghafouri-Fard, "Dysregulation of lncRNAs in autoimmune neuropathies," *Scientific Reports*, vol. 9, p. 16061, 2021.

[46] M. Albanese, Y. F. Chen, C. Hüls et al., "MicroRNAs are minor constituents of extracellular vesicles that are rarely delivered to target cells," *PLoS Genetics*, vol. 6, article e1009951, 2021.

[47] S. Vinci, S. Gelmini, I. Mancini et al., "Genetic and epigenetic factors in regulation of microRNA in colorectal cancers," *Methods*, vol. 59, no. 1, pp. 138–146, 2013.

[48] J. Mattes, M. Yang, and P. S. Foster, "Regulation of microRNA by antagomirs," *American Journal of Respiratory Cell and Molecular Biology*, vol. 36, no. 1, pp. 8–12, 2007.

[49] J. Krützfeldt, N. Rajewsky, R. Braich et al., "Silencing of microRNAs in vivo with 'antagomirs'," *Nature*, vol. 438, no. 7068, pp. 685–689, 2005.

[50] S. G. Tangye, E. K. Deenick, U. Palendira, and C. S. Ma, "T cell–B cell interactions in primary immunodeficiencies," *Annals of the New York Academy of Sciences*, vol. 1250, no. 1, pp. 1–13, 2012.

[51] K. Louis, C. Macedo, and D. Metes, "Targeting T follicular helper cells to control humoral allogeneic immunity," *Transplantation*, vol. 105, no. 11, pp. e168–e180, 2021.

[52] J. Hu, C. Havenar-Daughton, and S. Crotty, "Modulation of SAP dependent T:B cell interactions as a strategy to improve vaccination," *Current Opinion in Virology*, vol. 3, article 363370, 2013.

[53] E. Dziadkowiak, H. Moreira, M. Wieczorek, S. Budrewicz, E. Barg, and M. Koszewicz, "Correlations between electrophysiological parameters, lymphocyte distribution and cytokine levels in patients with chronic demyelinating inflammatory polyneuropathy," *Journal of Personalized Medicine*, vol. 11, no. 8, p. 766, 2021.

Hindawi
Oxidative Medicine and Cellular Longevity
Volume 2023, Article ID 3479688, 11 pages
https://doi.org/10.1155/2023/3479688

Research Article

PW06 Triggered Fas-FADD to Induce Apoptotic Cell Death In Human Pancreatic Carcinoma MIA *PaCa-2* Cells through the Activation of the Caspase-Mediated Pathway

Yi-Ping Huang,[1] Te-Chun Hsia,[2,3] Chun-An Yeh,[1] Yi-Shih Ma,[4,5] Sheng-Yao Hsu,[6,7] Yi-Chung Liu,[8] Ping-Chiang Lyu,[9] Kuang-Chi Lai,[10] Shu-Fen Peng,[11,12] Jin-Cherng Lien,[13] and Wen-Tsong Hsieh[14,15]

[1]*Department of Physiology, School of Medicine, China Medical University, Taichung 404333, Taiwan*
[2]*Department of Medical Research, China Medical University Hospital, Taichung 404333, Taiwan*
[3]*Department of Respiratory Therapy, China Medical University, Taichung 404333, Taiwan*
[4]*School of Chinese Medicine for Post-Baccalaureate, I-Shou University, Kaohsiung 84001, Taiwan*
[5]*Department of Chinese Medicine, E-Da Hospital, Kaohsiung 82385, Taiwan*
[6]*Department of Ophthalmology, An Nan Hospital, China Medical University, Tainan 709, Taiwan*
[7]*Department of Optometry, Chung Hwa University of Medical Technology, Tainan 717302, Taiwan*
[8]*Institute of Population Health Sciences, National Health Research Institutes, Miaoli 350, Taiwan*
[9]*Institute of Bioinformatics and Structural Biology, National Tsing-Hua University, Hsinchu 300044, Taiwan*
[10]*Department of Medical Laboratory Science and Biotechnology, College of Medical Technology, Chung Hwa University of Medical Technology, Tainan, Taiwan*
[11]*Department of Biological Science and Technology, China Medical University, Taichung 406040, Taiwan*
[12]*Department of Internal Medicine, China Medical University Hospital, Taichung 404333, Taiwan*
[13]*School of Pharmacy, China Medical University, Taichung 406040, Taiwan*
[14]*Chinese Medicine Research Center, China Medical University, Taichung 404333, Taiwan*
[15]*Department of Pharmacology, China Medical University, Taichung 404333, Taiwan*

Correspondence should be addressed to Jin-Cherng Lien; jclien@mail.cmu.edu.tw
and Wen-Tsong Hsieh; wthsieh@mail.cmu.edu.tw

Received 20 May 2022; Revised 25 August 2022; Accepted 21 September 2022; Published 11 February 2023

Academic Editor: Helena Moreira

Pancreatic cancer has higher incidence and mortality rates worldwide. PW06 [(E)-3-(9-ethyl-9H-carbazol-3-yl)-1-(2,5-dimethoxyphenyl) prop-2-en-1-one] is a carbazole derivative containing chalcone moiety which was designed for inhibiting tumorigenesis in human pancreatic cancer. This study is aimed at investigating PW06-induced anticancer effects in human pancreatic cancer MIA PaCa-2 cells *in vitro*. The results showed PW06 potent antiproliferative/cytotoxic activities and induced cell morphological changes in a human pancreatic cancer cell line (MIA PaCa-2), and these effects are concentration-dependent (IC_{50} is 0.43 μM). Annexin V and DAPI staining assays indicated that PW06 induced apoptotic cell death and DNA condensation. Western blotting indicated that PW06 increased the proapoptotic proteins such as Bak and Bad but decreased the antiapoptotic protein such as Bcl-2 and Bcl-xL. Moreover, PW06 increased the active form of caspase-8, caspase-9, and caspase-3, PARP, releasing cytochrome c, AIF, and Endo G from mitochondria in MIA PaCa-2 cells. Confocal laser microscopy assay also confirmed that PW06 increased Bak and decreased Bcl-xL. Also, the cells were pretreated with inhibitors of caspase-3, caspase-8, and caspase-9 and then were treated with PW06, resulting in increased viable cell number compared to PW06 treated only. Furthermore, PW06 showed a potent binding ability with hydrophobic interactions in the core site of the

Fas-Fas death domains (FADD). In conclusion, PW06 can potent binding ability to the Fas-FADD which led to antiproliferative, cytotoxic activities, and apoptosis induction accompanied by the caspase-dependent and mitochondria-dependent pathways in human pancreatic cancer MIA PaCa-2 cells.

1. Introduction

Pancreatic cancer is one of the highest mortality rates in the cancer population worldwide. Recently, pancreatic ductal adenocarcinoma accounts for 3% of all new cancer cases and is responsible for 8% of cancer deaths in 2020 [1]. In 2018, it accounted for 458,918 new cases of pancreatic cancer worldwide. However, it caused about 432,242 patients to die [2]. Moreover, pancreatic cancer is often diagnosed in patients with terminal stages that led to difficult-to-curable surgery. Thus, it caused higher patient death [3]. However, the overall five-year survival rate is less than 10% [4]. It has been predicted to become the second leading cause of cancer mortality in developed countries [5]. Currently, the curative treatment for pancreatic cancer patients is surgical resection followed by adjuvant chemotherapy [6]. Nevertheless, the cure rate is still unsatisfactory. Thus, it is urgently needed to develop nonsurgical therapeutic approaches to effectively treat patients with pancreatic cancer.

Apoptosis is programmed cell death and is also referred to as a process of cell suicide. Apoptotic proteins involved in cellular demise by which the body maintains the homeostasis of the internal environment are triggered by a range of internal and external factors of cells [7]. Numerous clinical chemotherapeutic anticancer drugs have been known to induce apoptotic death in cancer cells [8]. Currently, apoptosis can be classified into the death receptor pathway, endoplasmic reticulum stress pathway, and mitochondria pathway [9, 10]. The death receptor pathway, also known as an extrinsic pathway, is triggered by agents via death receptors such as Fas-Fas death domains (FADD), TNF (tumor necrosis factor), and TRAILR 1 (tumor necrosis factor-related apoptosis-inducing ligand receptor 1) [11]. Upon Fas and ligand engagement, which activated the intracellular signaling of triggering the initiator caspase-8 then moves downstream for cell apoptosis [12]. The endoplasmic reticulum stress pathway of apoptosis was developed via the IRE1/apoptosis signal-regulating kinase 1 (ASK1)/JNK pathway, the caspase-12 kinase pathway, and the CCAAT/enhancer-binding protein homologous protein (CHOP)/growth arrest- and DNA damage-inducible gene 153 (GADD153) pathway [13, 14]. The mitochondrial pathway, also known as the intrinsic apoptosis pathway, is triggered by DNA damage and activation of p53, followed by a cascade of events leading to mitochondrial outer membrane permeabilization for releasing apoptosis factors [15].

Caspases are intrinsically involved in the mitochondrial pathway. Caspase-9 is the initiative protein in the caspase family, triggering the activation of caspase-3 leading to apoptosis development [9]. B cell leukemia/lymphoma 2 (Bcl-2) family of proteins has involved the regulation of apoptosis through activities of their proapoptotic proteins (Bak and Bax) and anti-apoptotic proteins (Bcl-2 and Bcl-xL) by operating independently or dependently between internal death signals and the cell's surface for ensuring a balance [16].

Some carbazole alkaloids have been reported to inhibit the motility, migration, and proliferation of human pancreatic cancer cells [17–19]. Moreover, chalcone possesses anticancer in human pancreatic cancer [20, 21]. PW06 [(E)-3-(9-ethyl-9H-carbazol-3-yl)-1-(2,5-dimethoxyphenyl) prop-2-en-1-one] is a carbazole derivative containing chalcone moiety chemical compound that was first designed and synthesized for inhibiting tumorigenesis in human pancreatic cancer. Therefore, in the present study, we aim to investigate the molecular mechanism of PW06-induced apoptosis effects on human pancreatic carcinoma MIA *PaCa-2* cells. Herein, we also have attempted to define the chemotherapeutic and chemosensitizing potential of PW06 on MIA PaCa-2 cells *in vitro*.

2. Materials and Methods

2.1. Chemicals and Reagents. PW06 (Figure 1) was generated by Dr. Jin-Cherng Lien (College of Pharmacy, China Medical University, Taichung, Taiwan). DAPI, propidium iodide (PI), and trypsin-EDTA were purchased from Sigma Chemical Co. (St. Louis, MO, USA). Dulbecco's modified Eagle's medium (DMEM), fetal bovine serum (FBS), L-glutamine, and penicillin-streptomycin were purchased from GIBCO®/Invitrogen Life Technologies (Carlsbad, California, USA). Primary antibodies against -Bid, -Bax, -p53, -Bcl-2, -Bcl-xL,-XIAP, -cytochrome c, -caspase-9, -caspase-3, -caspase-8, -PARP, -Fas, -Endo G, and peroxidase-conjugated secondary antibodies were purchased from Cell Signaling Technology, Inc. (Beverly, MA, USA). Alternatively, primary antibodies against β-actin, Bcl-xL, Bak, and AIF were purchased from Sigma-Aldrich (St. Louis, MO, USA).

2.2. NMR Spectra of PW06. 1H-NMR (CDCl3-d1, 400 MHz) (ppm) *MS (m/z): 385 (M+):* 1.42 (t, J =7.2 Hz, 3H, -CH2CH3), 3.81 (s, 3H, 5'-OCH3), 3.86 (s, 3H, 2'-OCH3), 4.35 (q, J =7.2 Hz, 2H, -CH2CH3), 6.94 (d, J =8.8 Hz, 1H, H-3'), 7.01 (dd, J =8.8, 2.8 Hz, 1H, H-4'), 7.18 (d, J =2.8 Hz, 1H, H-6'), 7.26 (dd, J =7.2, 7.2 Hz, 1H, H-6), 7.36-7.42 (m, 3H, H-1,8, CH=CH-C=O), 7.48 (dd, J =7.6, 7.6 Hz, 1H, H-7), 7.73 (d, J =8.4 Hz, 1H, H-2), 7.83 (d, J =15.6 Hz, 1H, CH=CH-C=O), 8.09 (d, J =7.6 Hz, 1H, H-5), 8.28 (s, 1H, H-4).

2.3. Cell Culture. The human pancreatic carcinoma cell line (MIA *PaCa-2*) was obtained from the Food Industry Research and Development Institute (Hsinchu, Taiwan). The cells were cultured in Dulbecco's modified Eagle's medium (DMEM) supplemented with 10% fetal bovine serum (FBS) (HyClone, Logan, UT, USA), 100 μg/ml streptomycin, 100 units/ml penicillin, and 2 mM L-glutamine,

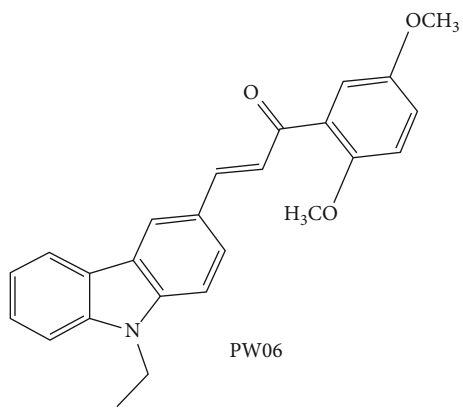

Figure 1: The chemical structure of PW06.

incubated at 37°C in a humidified incubator containing 5% CO_2chamber. The cells were subcultured following the standard protocol.

2.4. Cell Morphology and Viability Assays. MIA *PaCa-2* cells (2×10^5 cells/well) were kept and treated in 12-well plates with DMEM medium with PW06 (0, 0.2, 0.4, 0.6, 0.8, and 1.0 μM) for 24 and 48 h. Cell morphological changes were examined and photographed under phase contrast microscopy at 200×. After cells were photographed, the cells from each treatment were collected for measuring the total viable cell number by MTT assay (viable cells reduce 3-(4,5-dimethylthiazol-2-yl)-5-(3-carboxymethoxyphenyl)-2-(4-sulfophenyl)-2H-tetrazolium (MTS) to a formazan product) as previously [22]. Each condition was tested 3 times.

2.5. Cell Apoptosis Was Measured by Annexin V Staining. Annexin V-FITC apoptosis detection kit examined apoptotic cell death as described previously [16]. Moreover, staining was performed by the method described in the manufacturer's instructions. In brief, MIA PaCa-2 cells (2×10^5 cells/ml) were plated onto 24-well culture plates for 24 h and were incubated with 0, 0.2, 0.4, and 0.8 μM of PW06 for 48 h. The cells from each treatment were collected and resuspended in annexin V binding buffer and were incubated with annexin V-FITC for 15 min in the dark, and apoptotic cell death was analyzed using BD FACS Calibur as described previously [16]. The apoptosis rate was further analyzed using MultiCycle software (Beckman Coulter, Brea, CA, USA).

2.6. DAPI Staining. DAPI staining measured cell nuclear condensation and fragmentation as previously described [23]. In brief, MIA PaCa-2 cells (2×10^5 cells/well) were seeded in the 12-well plates for 24 h and were incubated at 0, 0.2, 0.4, and 0.8 μM of PW06 for 48 h with three replicated wells set in each treatment. The cells were washed with PBS and were fixed in 3% paraformaldehyde in PBS for 20 min at room temperature, washed, collected, spread onto slides, and stained with DAPI solution (2 μg/ml) in the dark for 5 min, and then examined and photographed using a fluorescence microscope.

2.7. Western Blotting Analysis. MIA PaCa-2 cells (1×10^6 cells/well) were plated in a 12-well plate for 24 h and were incubated with PW06 (0, 0.2, 0.4, 0.6, and 0.8 μM) for 48 h, and the cells were collected. Isolated cells were lysed, and total protein was quantitated using a Bio-Rad protein assay kit (Hercules, California, USA) described previously [24]. A 30 μg of protein was electrophoresed on 12% (v/v) SDS-polyacrylamide gel (PAGE) and was then electrotransferred to polyvinylidene difluoride (PVDF) membranes. Membranes were blocked with PBST (PBS, 0.05% Tween-20) containing 5% nonfat dry milk and were probed with primary antibodies such as anti-Bid, -Bak, -Bax, -p53, -Bcl-2, -Bcl-xL, -XIAP, -cytochrome c, -caspase-9, -caspase-3, -caspase-8, -PARP, -Fas, -Endo G, and -AIF or α-tubulin in 0.1% PBST (1 : 1000) for 1 h at room temperature. The membranes were washed three times in TBS containing 0.05% Tween 20. At the end of washing, the appropriate peroxidase-labeled conjugated anti-mouse IgG (Santa Cruz Biotechnology) secondary antibody (1 : 1000) was added to the membrane for 1 h at room temperature. Specific bands (antibody-reactive bands) were enhanced using chemiluminescence signal reagents using ECL detection (Amersham Biosciences ECLTM) and using Bio-Rad ChemiDoc™ System for chemiluminescence western blot detection, and densitometry was performed as described previously [24].

2.8. Cells Were Pretreated with the Inhibitors of Caspase-3, Caspase-8, and Caspase-9 for Measuring Cell Viability. MTT assay measured the total viable cell number in MIA PaCa-2 cells as described previously [25]. In brief, MIA PaCa cells (2×10^5 cells/well) were kept in a 12-well plate and were pretreated with the inhibitors of caspase-8, caspase-9, and caspase-3 (z-IETD-fmk, z-LEHD-fmk, and z-DEVD-fmk, respectively) and then were incubated with or without PW06 for 48 h, and the cells were assayed the total viable cell number by using MTT assay.

2.9. Immunofluorescence Staining. MIA PaCa-2 cells (1.5×10^4 cells/well) were placed on a 6-well plate and treated with 0 and 0.4 μM of PW06 for 48 h; the cells were fixed in 4% formaldehyde in PBS for 15 min and permeabilized for 1 h with 0.3% Triton-X 100 in PBS. After that, the cells were washed and stained with anti-Bcl-xL and -Bak (green fluorescence) followed with FITC-conjugated goat anti-mouse IgG (secondary antibody). The nucleus was stained by DAPI (blue fluorescence) and PI (red fluorescence) for double-check, and Leica TCS SP2 Confocal Spectral Microscope was used to examine photomicrography as described previously [26]. The localization of Bcl-xLor Bak in the cytosol was formed in green color based on blue and red overlapped pixels.

2.10. Protein-Ligand Docking Assay. The molecular docking software PyRx version 0.98 for AutoDock Vina was used for all docking calculations [27]. The ligand structure of PW06 was created from the Reaxys database (Elsevier, NL). The receptor structure, FasL (PDB: 3EZQ), was obtained from the RCSB Protein Data Bank [28]. The AutoDock Vina automatically samples different conformations of

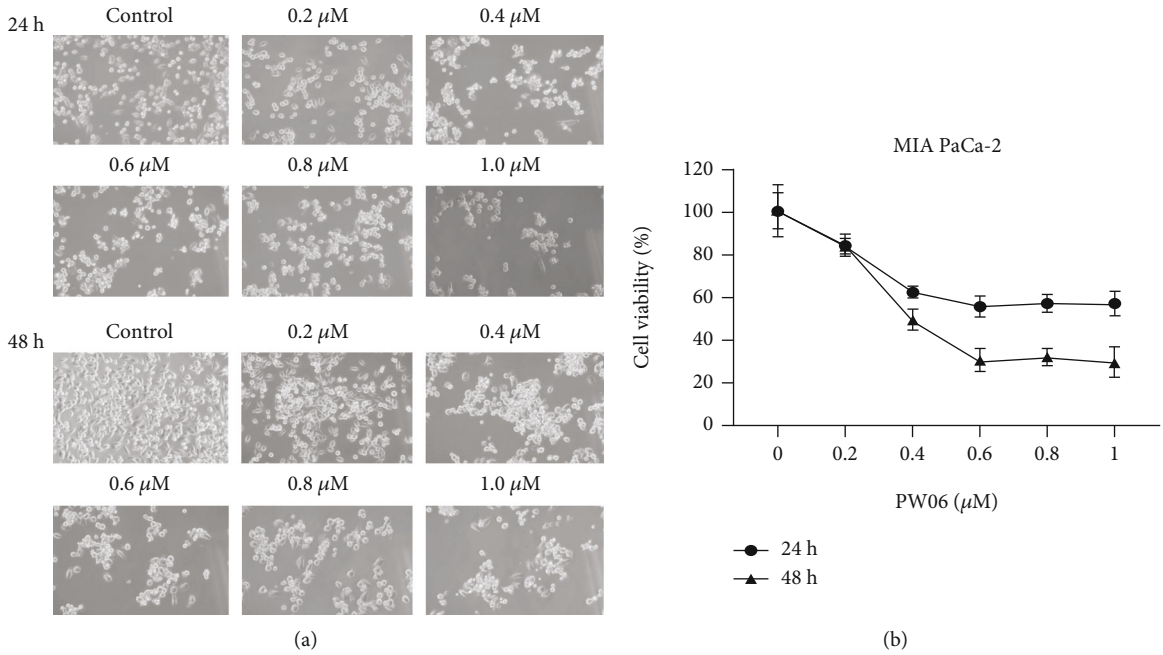

Figure 2: PW06 affected cell morphology and decreased cell viability of MIA PaCa-2 cells. The cells were treated with PW06 (0, 0.2, 0.4, 0.6, 0.8, and 1.0 μM) for 24 and 48 h. Cell morphological changes were examined and photographed under phase contrast microscopy at x400 (a). The cells were collected for measuring the total viable cell number (b) by MTT assay as described in Materials and Methods. The IC_{50} is around 0.43 μM for 48 h.

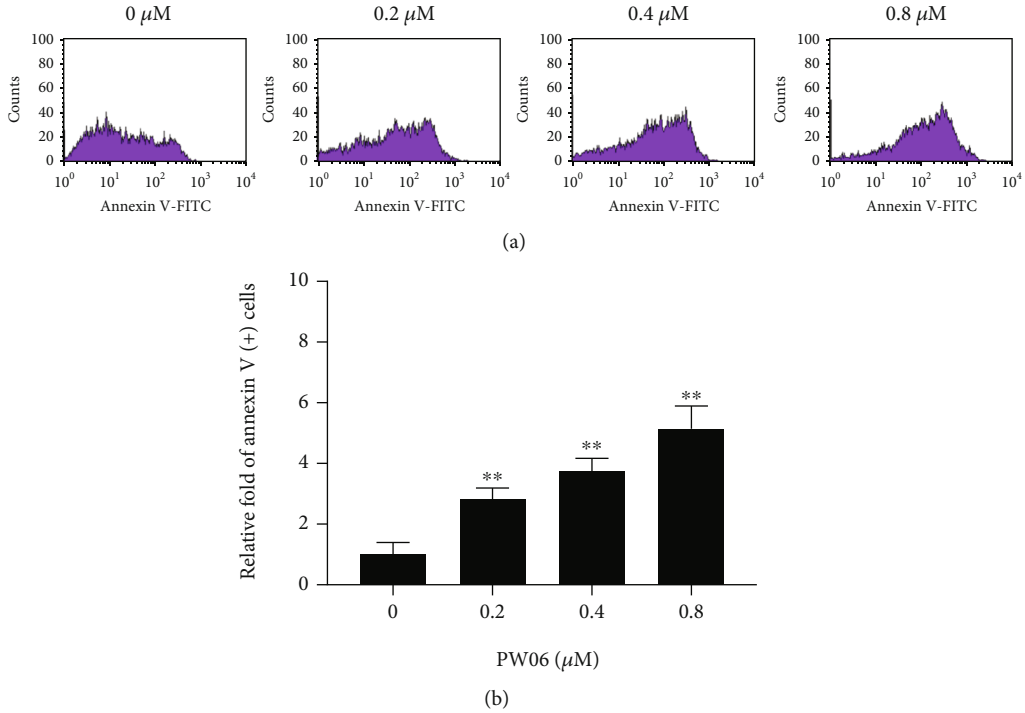

Figure 3: PW06 induces apoptotic cell death in MIA PaCa-2 cells. The cells were treated with PW06 (0, 0.2, 0.4, and 0.8 μM) for 48 h and were measured apoptotic cell death using annexin-V staining as described in Materials and Methods. (a) Profiles of flow cytometric assay. (b) The relative fold of apoptotic cell death. $^{**}p < 0.01$, the significant difference between PW06-treated groups and the control as analyzed by Student's t-test.

the ligands to fit the predicted binding site best. The docking results were analyzed and based on the protein-ligand complex's binding affinity (kcal/mol). Docked complexes were visualized and analyzed using the PyMOL Molecular Graphics System (Ver. 2.4 Schrödinger, Portland, OR, USA) [29]. The interactions between protein and ligand

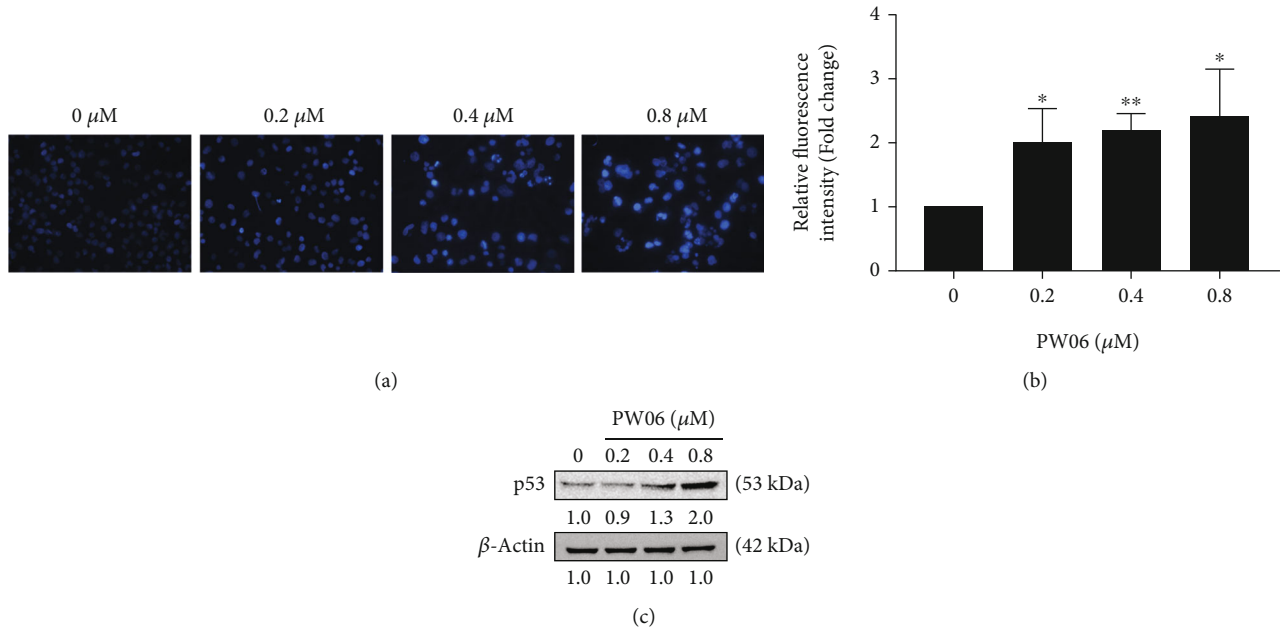

Figure 4: PW06 induces chromatin condensation in MIA PaCa-2 cells. The cells were treated with PW06 (0, 0.2, 0.4, and 0.8 μM) for 48 h and were stained with DAPI. (a) Moreover, photographed using fluorescence microscopy, their intensities of DAPI fluorescence were measured. (b) The relative fluorescence intensity of chromatin condensation. $^{*}p < 0.05$ and $^{**}p < 0.01$, the significant difference between PW06-treated groups and the control as analyzed by Student's t-test. (c) The cells have also measured the expression of p53 as described in Materials and Methods.

were analyzed using the "LIGPLOT" module within the LigPlot+ program (v2.2) [30]. The receptor structure and ligand were prepared, and then, docking was performed into a grid box space with x-, y, and z-axes, and dimensions were adjusted to 73.07 Å × 87.33 Å × 98.34 Å. The docking simulation process with the exhaustiveness parameter is set to 50, and the number of modes is set to 9.

2.11. Statistical Analysis. Each of the experiment and assay was done at least three times, and all data were presented as means ± standard deviation (SD). Student's t-test carried out statistical analysis, with the following significance levels: $^{*}p < 0.05$.

3. Results

3.1. PW06 Induced Cell Morphological Changes and Decreased Cell Viability in MIA PaCa-2 Cells. MIA PaCa-2cells were treated with various concentrations (0, 0.2, 0.4, 0.6, 0.8, and 1.0 μM) for 24 and 48 h. The cells were examined and photographed for morphological changes as shown in Figure 2(a). The total cell viability was further measured, and the results are presented in Figure 2(b). The results showed that PW06 significantly induced cell morphological changes based on reduced cell number, increased cell debris, and developed cells shrunken or aggregated in a concentration-dependent manner presented in Figure 2(a). Moreover, in Figure 2(b) after the calculation of the total viable cell number indicated that PW06 decreased the total viable cell number of MIA PaCa-2 cells around16.4-70.6% for 48 h, these effects are concentration-dependent, and IC_{50} is around 0.43 μM.

3.2. PW06 Induces Apoptotic Cell Death in MIA PaCa-2 Cells. PW06 reduced total cell viability through apoptotic cell death in MIA PaCa-2 cells for further confirmation. The cells were treated with PW06 (0, 0.2, 0.4, and 0.8 μM) for 48 h and were collected to measure the apoptotic cell death using annexin-V staining and further analyzed by flow cytometry; the results are shown in Figure 3. The data indicated that PW06 treatment leads to an increase in the number of apoptotic cell death from 2.85- to 5.16-folds compared to control groups. These effects are concentration-dependent in MIA PaCa-2 cells.

3.3. PW06 Induces the Chromatin Condensation in MIA PaCa-2cells. MIA PaCa-2 cells were treated with PW06 (0, 0.2, 0.4, and 0.8 μM) for 48 h and were stained with DAPI followed by being examined and photographed using fluorescence microscopy and relative fluorescence as shown in Figure 4(a). And the cells were harvested to investigate p53 expression by western blotting, shown in Figure 4(b). The results indicated that the brighter fluorescence and relative fluorescence of MIA PaCa-2 cells after 48 h of PW06 treatment have higher than that of the control; the effects were from 1.97- to 2.41-folds in a concentration-dependent manner (Figure 4(a)). Bright fluorescence meant the presence of nicked DNA (DNA damage) and chromatin condensation. Thus, we further investigated the expression of p53, and the results indicated that PW06-treated cells have a higher expression of p53 than the control (Figure 4). These observations demonstrated that PW06 reduced total viable cell number via the induction of cell DNA damage, condensation, and apoptosis in MIA PaCA-2 cells.

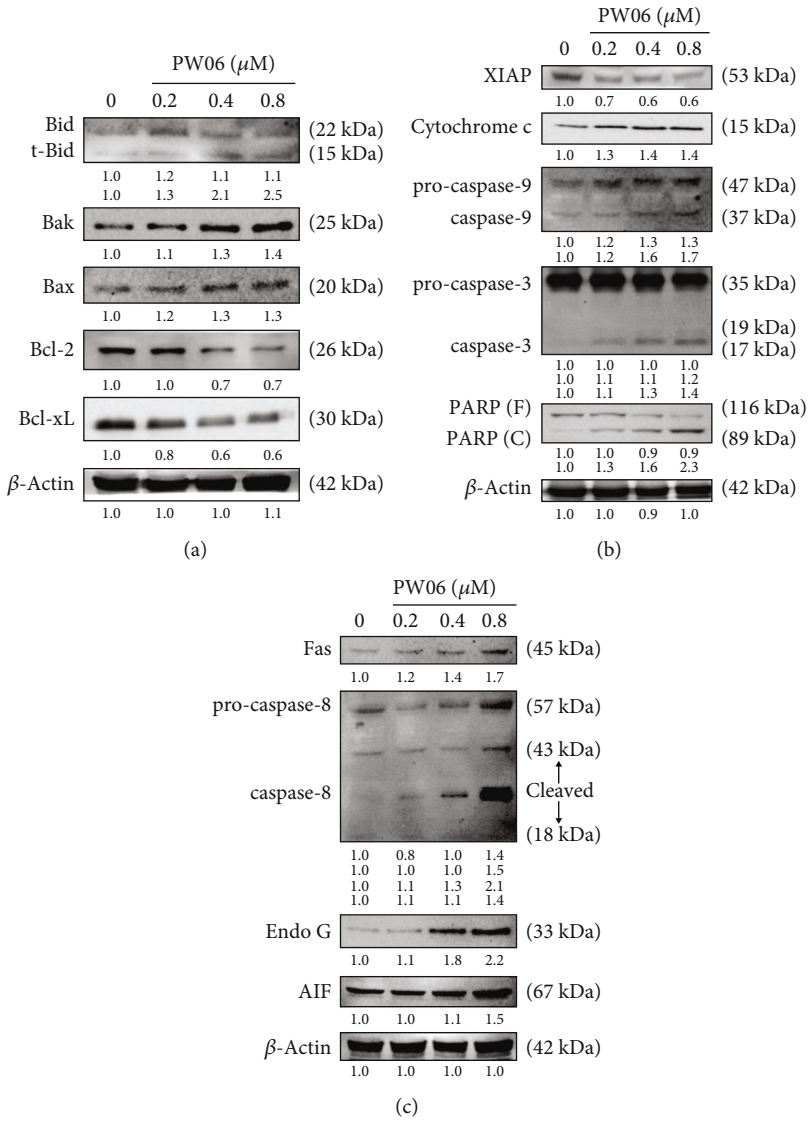

Figure 5: PW06 altered apoptosis-associated protein expression in MIA PaCa-2 cells. The cells were treated with 0, 0.2, 0.4, and 0.8 μM of PW06 for 24 h, and protein expressions were examined by western blotting as described in Materials and Methods. (a) Bid, Bak, Bax, Bcl-2, and Bcl-xL. (b) XIAP, cytochrome c, caspase-9, caspase-3, and PARP. (c). Fas, caspase-8, Endo G, and AIF.

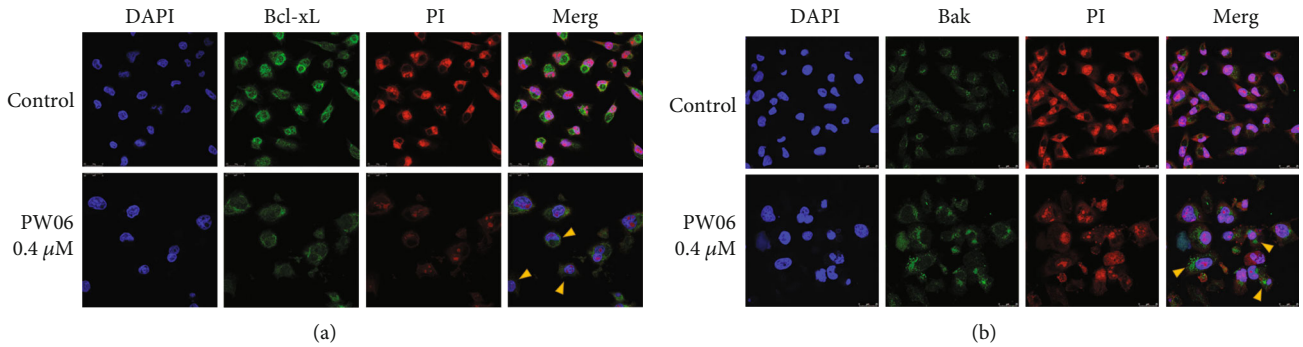

Figure 6: PW06 influenced the expression of Bcl-xL and Bak in MIA PaCa-2 cells. The cells were treated with 0 and 0.4 μM of PW06 for 48 h, and the cells were stained by anti-Bcl-xL (a) and -Bak (b) and then were stained with secondary antibody (FITC-conjugated goat anti-mouse IgG; green fluorescence). All cells were stained by PI (red fluorescence) and DAPI (blue fluorescence) for nucleus double-check examination and were observed under a Leica TCS SP2 Confocal Spectral Microscope as described in Materials and Methods.

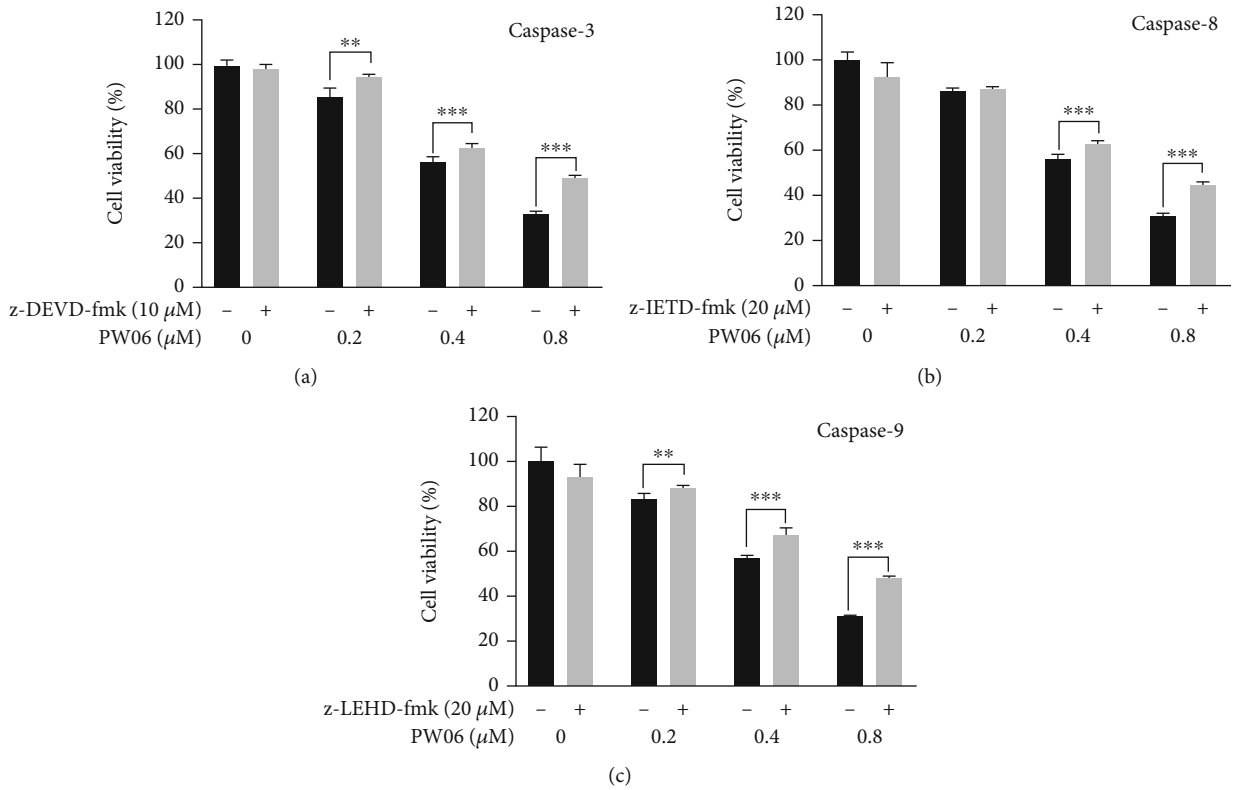

Figure 7: Inhibitors of caspase-3, caspase-8, and caspase-9 affect PW06 and decreased cell viability in MIA PaCa-2 cells. The cells were pretreated with z-DEVD-fmk, z-IETD-fmk, and z-LEHD-fmk and treated with PW06 (0, 0.2, 0.4, and 0.8 μM) for 48 h and were harvested for measuring the cell viability ((a) caspase-3, (b) caspase-9, and (c) caspase-8) using MTT assays as described in Materials and Methods. $^{**}p < 0.01$ and $^{***}p < 0.001$, significant difference between pretreated inhibitor groups and the control as analyzed by Student's t-test.

3.4. PW06 Altered the Apoptosis-Associated Protein Expression in MIA PaCa-2 Cells. To further confirm whether or not PW06-induced apoptotic cell death is involved in the molecular mechanisms in MIA PaCa-2 cells with apoptosis-associated protein expressions, that was examined by western blotting, and the results are shown in Figures 5(a)–5(c). Figure 5(a) indicates that PW06 increased the proapoptotic proteins such as tBid, Bak, and Bax. However, it inhibited antiapoptotic proteins such asBcl-2 and Bcl-xL expression in MIA PaCa-2 cells, thus promoting apoptotic. Moreover, PW06 increased cytochrome c, the active form of caspase-9, caspase-3, and PARP, but decreased XIAP (Figure 5(b)), leading to cell apoptosis. Figure 5(c) indicates that PW06 increased Fas, the active form of caspase-8 that triggers cell apoptosis. Furthermore, it also increased Endo G and AIF for cell apoptosis in MIA PaCa-2 cells (Figure 5(c)). These results indicated that PW06 induced apoptotic cell death in MIA PaCa-2 cells.

3.5. PW06 Influenced the Expression of Bcl-xL and Bak in MIA PaCa-2 Cells. MIA PaCa-2 cells were treated with 0.4 μM of PW06 for 48 h. Then, the expression of Bcl-xL and Bak was examined by confocal laser microscopy, and the results are shown in Figures 6(a) and 6(b). The results indicated that PW06 reduced the expression of Bcl-xL (Figure 6(a)) and increased Bak (Figure 6(b)); both figures indicated that both proteins are involved apoptotic cell death in MIA PaCa-2 cells after being exposed to PW06 *in vitro*.

3.6. Pretreatment of Inhibitors of Caspases Led to Increasing Viable Cells in PW06 Treatment of MIA PaCa-2 Cells. To further confirm whether the caspases were involved or not in PW06-induced cell death, MIA PaCa-2 cells were pretreated with inhibitors of caspase-3, caspase-8, and caspase-9. They then were treated with PW06 0, 0.2, 0.4, and 0.8 μM for 48 h, and the cells were collected for measuring the percentage of viable cells. The results are shown in Figures 7(a)–7(c), which indicated that those inhibitors were pretreated, followed by PW06 treatment which increased the viable cells compared to PW06 treatment only. These results also showed that PW06-induced apoptotic cell death might involve the activations of caspase-3, caspase-8, and caspase-9 in MIA PaCa-2 cells.

3.7. Effects of PW06 on Fas-FADD with Protein-Ligand Docking. To further characterize how PW06 interacts with Fas-FADD, molecular docking analysis was conducted to evaluate potential interaction sites with PyRx. The program proposed two potential models which are shown in Figure 8. Model 1 predicts that the carbazole end of the PW06 may be inserted into the cavity between Fas and FADD and interacts with Ala183, Leu186, Gln187, and Ser190 in FADD and Asn302 and Thr305 in FAS through hydrophobic interactions (Figure 8(a)). Besides, PW06 also

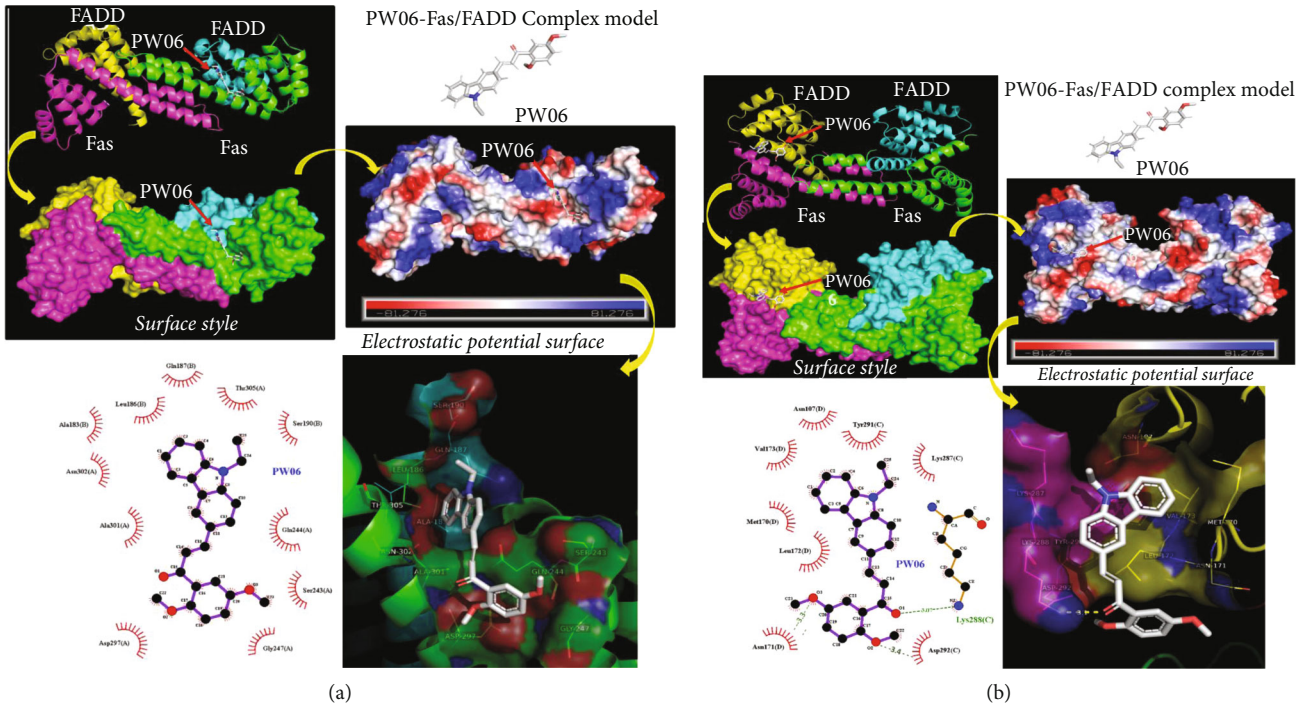

Figure 8: Effects of PW06 on Fas-FADD with protein-ligand docking. There are two types of receptor docking situations of PW06 binding models to Fas-FADD models. (a) and (b) The protein-ligand docking models indicated that PW06 has 2 binding situations models to the tetrameric arrangement of Fas-FADD. The results come through PW06 at least has 6 binding models to tetrameric arrangement of Fas-FADD in two major binding situations, respectively. The binding site was established as a surface model, and the inhibitor was displayed as a ball and stick model. The green-dashed line indicates the hydrogen bond pairing with each other. The red circles identify the residues on each plot that was equivalent. Red or pink eyebrow-like icons illustrate hydrophobic interactions. The details of the experimental preform were described in Materials and Methods.

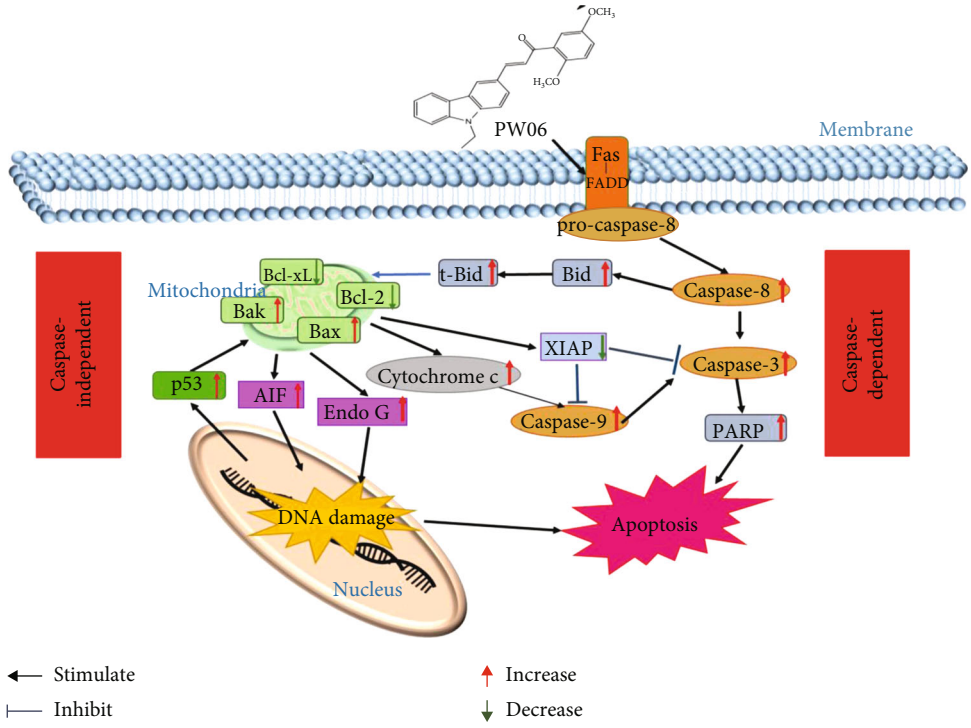

Figure 9: The possible signaling pathways for PW06-induced apoptotic cell death in MIA PaCa-2 cells *in vitro*.

has hydrophobic interactions with Ser243, Gln244, Gly247, Asp297, and Ala301 in FAS. Simulation results indicated that the best binding affinity of PW06 was -7.3 kcal/mol. On the other hand, model 2 predicts that PW06 may be inserted into the groove between Fas and FADD and interacts with Asn107, Met170, Asn171, Leu172, and Val173 in FADD and Lys287, Lys288, Tyr291, and Asp292 in FAS through hydrophobic interactions and forms a hydrogen bond with Lys288 (Figure 8(b)). In this model, the best binding affinity of PW06 was -6.7 kcal/mol.

4. Discussion

Currently, many clinical drugs are obtained from natural products. Moreover, numerous studies also showed that dietary fruits and vegetables, including flavonoids, may be used as potential candidates for developing chemotherapeutic agents [31]. However, many current clinical drugs still induced side effects; thus, selecting clinically used drugs for further synthesis to reduce side effects will increase the efficacy for patients. Therefore, herein, the present study set the synthesized compound (PW06) for investigating whether or not it can induce cell death; thus, the first experiments showed that PW06 decrease in viability observed in the cell line (MIA PaCa-2) could be due to a reduction in cell proliferation or an increase in cell death and senescence; we further analyzed the effect of PW06 on cell apoptosis and further examining associated protein expression in MIA PaCa-2 cells.

In the present study, we found that (1) PW06 induced cell morphological change and decreased total cell viability (Figures 2(a) and 2(b)); (2) induced apoptotic cell death was examined by annexin V staining (Figure 3); (3) induced DNA condensation (Figure 4(a)) and increased p53 (Figure 4(b)); (4) induced proapoptotic proteins expressions such as Bak and Bax but decreased antiapoptotic proteins such as Bcl-2 and Bcl-xL (Figure 5(a)); increased active form of caspase-8, caspase-9, and caspase-3 (Figure 5(b)); and increased Fas, the active form of Endo G, AIF, and PARP (Figure 5(c)); (5) confocal laser microscopy examining indicated that PW06 decreased Bcl-xL and increased Bak (Figures 6(a) and 6(b)) in MIA PaCa-2 cells; and (6) the cells were pretreated with inhibitors of caspase-3, caspase-8, and caspase-9 and treated with PW06 leading to increase viable cells (Figures 7(a)–7 (c)).

The effects of PW06 on MIA PaCa-2 cells were examined through the changes of viable cells and detected the morphological cell charges. Figure 2 indicates that PW06 significantly induced cell morphological changes based on the examined and photographed under phase contrast microscopy. To further investigate, PW06 decreased total cell viability. Thus, annexin V and DAPI staining assays were performed to investigate apoptotic cell death and DNA condensation, respectively, and the results are presented in Figures 3 and 4. Annexin V assay for cell apoptosis and DAPI staining are accepted protocols for investigating cell apoptosis based on the chromatin condensation [32, 33]. Figures 4(a) and 4(b) indicate that PW06 induced chromatin condensation (apoptotic cells) in MIA PaCa-2 cells.

It is well documented that various antiapoptotic (Bcl-2, Bcl-xL, Mcl-1, etc.) and proapoptotic (Bax, Bak, Bim, Bid, etc.) proteins regulate intrinsic/mitochondrial pathways [34, 35]. Therefore, one of the pathways associated with apoptosis factors attended to be targeted for cancer therapy is the antiapoptotic B-cell lymphoma-2 (Bcl-2) family of proteins, including Bcl-w and Bcl-xL Bfl1/A-1, Bcl-2, Mcl-1, and Bcl-B [36]. Bax is a pore-forming and mitochondria-associated protein, a death-promoting member named proapoptotic protein [37]. Mitochondrial dynamics have also been associated with cell death. Bcl-xL, an antiapoptotic protein, was found on the mitochondrial membrane, and it prevents mitochondria-dependent death processes by blocking the oligomerization of prodeath proteins, including Bax and Bak [38, 39]. Based on pieces of literature, they have shown a connection between Bcl-2 family members (Bax, Bak, Bcl-2, and Bcl-xL) and proteins involved in mitochondrial morphogenesis [40, 41]. In this aspect, PW06 might cause cell death through the changes of ratio Bax/Bcl-2 and caspase activation, followed by cell apoptosis in MIA PaCa-2 cells. Therefore, PW06-induced cell apoptosis also involved the Bcl-2 family in MIA PaCa-2 cells *in vitro* (Figure 5(a)). Furthermore, Figure 5(a) also shows that PW06 increased the proapoptotic proteins (tBid, Bak, and Bax) but inhibited antiapoptotic protein (Bcl-2 and Bcl-xL) expression in MIA PaCa-2 cells. Moreover, the confocal laser microscopy system also confirmed that PW06 increased Bak and decreased Bcl-xL in MIA PaCa-2 cells (Figure 6).

Furthermore, the overexpression of Bcl-2 and Bcl-xL will suppress the proapoptotic mitochondria. It could result in cytosolic accumulation of cytochrome c. Moreover, the release of cytochrome c will open the mitochondrial permeability transition pore [42]. Bax has been shown to trigger cytochrome c from isolated mitochondria [43]. The agents reduced the Bax/Bcl-2 ratio but increased the level of XIAP and cleaved caspase-3/caspase-9; and cleaved PARP can induce apoptosis [44]. For further investigation which were the cell apoptosis-associated proteins involved in PW06-induced cell apoptosis in MIA PaCa-2 cells. Thus, western blotting was used to investigate the protein expression, increasing Fas and the active form of caspase-8, caspase-9, and caspase-3 in MIA PaCa-2 cells after exposure to PW06 for 48 h, and the results are presented in Figure 5(b). Therefore, we suggested that PW06 induced apoptotic cell death by activating caspase dependently.

In mitochondria, cytochrome c, Endo G, and AIF were followed by the activation of caspases-9 and caspase-3, and the apoptotic cell death was developed which was named intrinsic pathway apoptosis [45]. Z-VAD-fmk is a pancaspase inhibitor [46], z-IETD-fmk is a caspase-8 inhibitor, and Z-LEHD-fmk is a caspase-9 inhibitor [47] that prevents apoptosis in many different cell types. For further exploration which were the mitochondria-associated proteins were related to PW06-induced cell apoptosis in MIA PaCa-2 cells. Thus, PW06 increased Fas, cytochrome c, Endo G, AIF, and cleaved form of PARP but decreased the XIAP expression in MIA PaCa-2 cells, and the results are presented in Figure 5(c). Thus, Fas are involved in PW06-induced apoptosis *via* the extrinsic pathway of apoptosis.

Activated Fas and FADD can promote procaspase-8 transfer to caspase-8 and activate two apoptotic pathways, the extrinsic and the intrinsic pathways [48]. The Fas-FADD complex consists of two tetrameric assemblies containing four Fas death domains and four FADD death domains in these two asymmetric assembly units [49]. The global docking results showed that PW06 is mainly bound in the gap between the Fas-FADD interface. In two potential binding models, PW06 can form a stable complex with Fas-FADD via hydrophobic interaction and hydrogen bonding (Figures 8(a) and 8(b)). And these simulation results can be combined with the above experimental data to illustrate the binding ability of PW06 to Fas-FADD.

Thus, the apoptosis pathway assumes that PW06 interacted with the Fas-FADD proteins and then activates the caspase-independent apoptotic pathway (mitochondria-related pathway) and the caspase-dependent apoptotic pathway in human pancreatic cancer MIA PaCa-2 cells. Overall, the possible apoptosis signaling pathways of PW06 on MIA PaCa-2 cells are summarized in Figure 9.

Data Availability

The data used to support the findings of this study are included within the article.

Conflicts of Interest

The authors have no conflicts of interest to disclose.

Authors' Contributions

Jin-Cherng Lien and Wen-Tsong Hsieh contributed equally to this work.

Acknowledgments

We appreciate the Structural Proteomics and Pharmaceutical Application Service provided by the BP Bioinformatics Core (http://www.tbi.org.tw/), funded by the National Core Facility for Biopharmaceuticals (NCFB). This research was funded by the Drug Development Center & Chinese Medicine Research Center, China Medical University, from the Featured Areas Research Center Program within the Higher Education Sprout Project framework by the Ministry of Education (MOE) in Taiwan (CMRC-CHM-4, CMU110-TC-04, and CMU103-ASIA-21). Experiments and data analysis were performed using Medical Research Core Facilities, Office of Research & Development, at China Medical University.

References

[1] R. L. Siegel, K. D. Miller, and A. Jemal, "Cancer statistics, 2020," *CA: a Cancer Journal for Clinicians*, vol. 70, no. 1, pp. 7–30, 2020.

[2] P. Rawla, T. Sunkara, and V. Gaduputi, "Epidemiology of pancreatic cancer: global trends, etiology and risk factors," *World Journal of Oncology*, vol. 10, no. 1, pp. 10–27, 2019.

[3] T. Kamisawa, L. D. Wood, T. Itoi, and K. Takaori, "Pancreatic cancer," *The Lancet*, vol. 388, no. 10039, pp. 73–85, 2016.

[4] P. Sarantis, E. Koustas, A. Papadimitropoulou, A. G. Papavassiliou, and M. V. Karamouzis, "Pancreatic ductal adenocarcinoma: treatment hurdles, tumor microenvironment and immunotherapy," *World Journal of Gastrointestinal Oncology*, vol. 12, no. 2, pp. 173–181, 2020.

[5] R. L. Siegel, K. D. Miller, and A. Jemal, "Cancer statistics, 2018," *CA: a Cancer Journal for Clinicians*, vol. 68, no. 1, pp. 7–30, 2018.

[6] B. P. T. Loveday, L. Lipton, and B. N. Thomson, "Pancreatic cancer: an update on diagnosis and management," *Australian Journal of General Practice*, vol. 48, no. 12, pp. 826–831, 2019.

[7] S. Paone, A. A. Baxter, M. D. Hulett, and I. K. H. Poon, "Endothelial cell apoptosis and the role of endothelial cell-derived extracellular vesicles in the progression of atherosclerosis," *Cellular and Molecular Life Sciences*, vol. 76, no. 6, pp. 1093–1106, 2019.

[8] J. Liu, H. Wang, J. Wang et al., "Total flavonoid aglycones extract in *Radix Scutellariae* induces cross- regulation between autophagy and apoptosis in pancreatic cancer cells," *Journal of Ethnopharmacology*, vol. 235, pp. 133–140, 2019.

[9] C. J. Van Noorden, "The history of Z-VAD-FMK, a tool for understanding the significance of caspase inhibition," *Acta Histochemica*, vol. 103, no. 3, pp. 241–251, 2001.

[10] Y. Li, D. Kong, B. Bao, A. Ahmad, and F. H. Sarkar, "Induction of cancer cell death by isoflavone: the role of multiple signaling pathways," *Nutrients*, vol. 3, no. 10, pp. 877–896, 2011.

[11] T. Sessler, S. Healy, A. Samali, and E. Szegezdi, "Structural determinants of DISC function: new insights into death receptor- mediated apoptosis signalling," *Pharmacology & Therapeutics*, vol. 140, no. 2, pp. 186–199, 2013.

[12] J. Wen, N. Ramadevi, D. Nguyen, C. Perkins, E. Worthington, and K. Bhalla, "Antileukemic drugs increase death receptor 5 levels and enhance Apo-2L-induced apoptosis of human acute leukemia cells," *Blood*, vol. 96, no. 12, pp. 3900–3906, 2000.

[13] S. Oyadomari and M. Mori, "Roles of CHOP/GADD153 in endoplasmic reticulum stress," *Cell Death and Differentiation*, vol. 11, no. 4, pp. 381–389, 2004.

[14] C. Hetz, "The unfolded protein response: controlling cell fate decisions under ER stress and beyond," *Nature Reviews Molecular Cell Biology*, vol. 13, no. 2, pp. 89–102, 2012.

[15] G. Kroemer, L. Galluzzi, and C. Brenner, "Mitochondrial membrane permeabilization in cell death," *Physiological Reviews*, vol. 87, no. 1, pp. 99–163, 2007.

[16] Y. C. Hsiao, F. S. Chueh, Y. S. Ma et al., "Genistein enhances the effects of L-asparaginase on inducing cell apoptosis in human leukemia cancer HL-60 cells," *Environmental Toxicology*, vol. 36, no. 5, pp. 764–772, 2021.

[17] C. Pei, Q. He, S. Liang, and X. Gong, "Mahanimbine exerts anticancer effects on human pancreatic cancer cells by triggering cell cycle arrest, apoptosis, and modulation of AKT/mammalian target of rapamycin (mTOR) and signal transducer and activator of transcription 3 (STAT3) signalling pathways," *Medical Science Monitor*, vol. 24, pp. 6975–6983, 2018.

[18] C. Saturnino, C. Palladino, M. Napoli et al., "Synthesis and biological evaluation of new N-alkylcarbazole derivatives as STAT3 inhibitors: preliminary study," *European Journal of Medicinal Chemistry*, vol. 60, pp. 112–119, 2013.

[19] L. S. Tsutsumi, D. Gündisch, and D. Sun, "Carbazole scaffold in medicinal chemistry and natural products: a review from 2010-2015," *Current Topics in Medicinal Chemistry*, vol. 16, no. 11, pp. 1290–1313, 2016.

[20] P. Singh, A. Anand, and V. Kumar, "Recent developments in biological activities of chalcones: a mini review," *European Journal of Medicinal Chemistry*, vol. 85, pp. 758–777, 2014.

[21] W. Jiang, S. Zhao, L. Xu et al., "The inhibitory effects of xanthohumol, a prenylated chalcone derived from hops, on cell growth and tumorigenesis in human pancreatic cancer," *Biomedicine & Pharmacotherapy*, vol. 73, pp. 40–47, 2015.

[22] H. R. Momeni, M. H. Abnosi, and N. Eskandari, "Quantitative evaluation of human sperm viability using MTT assay: a laboratory study," *International Journal of Reproductive BioMedicine (IJRM)*, vol. 18, no. 11, pp. 983–988, 2020.

[23] K.-C. Cheng, C. J. Wang, Y. C. Chang et al., "Mulberry fruits extracts induce apoptosis and autophagy of liver cancer cell and prevent hepatocarcinogenesis in vivo," *Journal of Food and Drug Analysis*, vol. 28, no. 1, pp. 84–93, 2020.

[24] Z. Y. Cheng, Y. T. Hsiao, Y. P. Huang et al., "Casticin induces DNA damage and affects DNA repair associated protein expression in human lung cancer A549 cells (running title: casticin induces DNA damage in lung cancer cells)," *Molecules*, vol. 25, no. 2, 2020.

[25] H. J. Lee, E. K. Lee, Y. E. Seo et al., "Roles of Bcl-2 and caspase-9 and -3 in CD30-induced human eosinophil apoptosis," *Journal of Microbiology, Immunology, and Infection*, vol. 50, no. 2, pp. 145–152, 2017.

[26] A. C. Huang, Y.-D. Cheng, L.-H. Huang et al., "Casticin induces DNA damage and impairs DNA repair in human bladder cancer TSGH-8301 cells," *Anticancer Research*, vol. 39, no. 4, pp. 1839–1847, 2019.

[27] S. Dallakyan and A. J. Olson, "Small-molecule library screening by docking with PyRx," *Methods in Molecular Biology*, vol. 1263, pp. 243–250, 2015.

[28] H. M. Berman, J. Westbrook, Z. Feng et al., "The Protein Data Bank," *Nucleic Acids Research*, vol. 28, no. 1, pp. 235–242, 2000.

[29] Y.-J. Wang, S. C. Lee, C. H. Hsu, Y. H. Kuo, C. C. Yang, and F. J. Lin, "Antcins, triterpenoids from *Antrodia cinnamomea*, as new agonists for peroxisome proliferator-activated receptor α," *Journal of Food and Drug Analysis*, vol. 27, no. 1, pp. 295–304, 2019.

[30] R. A. Laskowski and M. B. Swindells, "LigPlot+: multiple ligand-protein interaction diagrams for drug discovery," *Journal of Chemical Information and Modeling*, vol. 51, no. 10, pp. 2778–2786, 2011.

[31] T. A. Bhat, D. Nambiar, A. Pal, R. Agarwal, and R. P. Singh, "Fisetin inhibits various attributes of angiogenesis in vitro and in vivo–implications for angioprevention," *Carcinogenesis*, vol. 33, no. 2, pp. 385–393, 2012.

[32] C. S. Yu, A. C. Huang, J. S. Yang et al., "Safrole induces G0/G1 phase arrest via inhibition of cyclin E and provokes apoptosis through endoplasmic reticulum stress and mitochondrion-dependent pathways in human leukemia HL-60 cells," *Anticancer Research*, vol. 32, no. 5, pp. 1671–1679, 2012.

[33] S. Patathananone, S. Thammasirirak, J. Daduang, J. G. Chung, Y. Temsiripong, and S. Daduang, "Bioactive compounds from crocodile (Crocodylus siamensis) white blood cells induced apoptotic cell death in hela cells," *Environmental Toxicology*, vol. 31, no. 8, pp. 986–997, 2016.

[34] C. Loreto, G. La Rocca, R. Anzalone et al., "The role of intrinsic pathway in apoptosis activation and progression in Peyronie's disease," *BioMed Research International*, vol. 2014, Article ID 616149, 10 pages, 2014.

[35] R. Caltabiano, R. Leonardi, G. Musumeci et al., "Apoptosis in temporomandibular joint disc with internal derangement involves mitochondrial-dependent pathways. An in vivo study," *Acta Odontologica Scandinavica*, vol. 71, no. 3-4, pp. 577–583, 2013.

[36] M. H. Kang and C. P. Reynolds, "Bcl-2 inhibitors: targeting mitochondrial apoptotic pathways in cancer therapy," *Clinical Cancer Research*, vol. 15, no. 4, pp. 1126–1132, 2009.

[37] S. Gupta, G. E. N. Kass, E. Szegezdi, and B. Joseph, "The mitochondrial death pathway: a promising therapeutic target in diseases," *Journal of Cellular and Molecular Medicine*, vol. 13, no. 6, pp. 1004–1033, 2009.

[38] M. Sanaei and F. Kavoosi, "Effect of valproic acid on the class I histone deacetylase 1, 2 and 3, tumor suppressor genes p21WAF1/CIP1 and p53, and intrinsic mitochondrial apoptotic pathway, pro- (Bax, Bak, and Bim) and anti- (Bcl-2, Bcl-xL, and Mcl-1) apoptotic genes expression, cell viability, and apoptosis induction in hepatocellular carcinoma HepG2 cell line," *Asian Pacific Journal of Cancer Prevention*, vol. 22, no. S1, pp. 89–95, 2021.

[39] S. Dadsena, L. E. King, and A. J. García-Sáez, "Apoptosis regulation at the mitochondria membrane level," *Biochimica et Biophysica Acta (BBA) - Biomembranes*, vol. 2021, no. 12, article 183716, 2021.

[40] J. Yang, X. Liu, K. Bhalla et al., "Prevention of apoptosis by Bcl-2: release of cytochrome c from mitochondria blocked," *Science*, vol. 275, no. 5303, pp. 1129–1132, 1997.

[41] M. M. Cleland, K. L. Norris, M. Karbowski et al., "Bcl-2 family interaction with the mitochondrial morphogenesis machinery," *Cell Death & Differentiation*, vol. 18, no. 2, pp. 235–247, 2011.

[42] P. X. Petit, S. A. Susin, N. Zamzami, B. Mignotte, and G. Kroemer, "Mitochondria and programmed cell death: back to the future," *FEBS Letters*, vol. 396, no. 1, pp. 7–13, 1996.

[43] R. Eskes, B. Antonsson, A. Osen-Sand et al., "Bax-induced cytochrome C release from mitochondria is independent of the permeability transition pore but highly dependent on Mg2+ ions," *The Journal of Cell Biology*, vol. 143, no. 1, pp. 217–224, 1998.

[44] J. Zheng, M. Long, Z. Qin, F. Wang, Z. Chen, and L. Li, "Nicorandil inhibits cardiomyocyte apoptosis and improves cardiac function by suppressing the HtrA2/XIAP/PARP signaling after coronary microembolization in rats," *Pharmacology Research & Perspectives*, vol. 9, no. 1, article e00699, 2021.

[45] I. Jorgensen, M. Rayamajhi, and E. A. Miao, "Programmed cell death as a defence against infection," *Nature Reviews Immunology*, vol. 17, no. 3, pp. 151–164, 2017.

[46] A. Rodríguez-Enfedaque, E. Delmas, A. Guillaume et al., "zVAD-fmk upregulates caspase-9 cleavage and activity in etoposide-induced cell death of mouse embryonic fibroblasts," *Biochimica et Biophysica Acta*, vol. 1823, no. 8, pp. 1343–1352, 2012.

[47] L. McGlorthan, A. Paucarmayta, Y. Casablanca, G. L. Maxwell, and V. Syed, "Progesterone induces apoptosis by activation of caspase-8 and calcitriol via activation of caspase-9 pathways in ovarian and endometrial cancer cells In Vitro," *Apoptosis*, vol. 26, no. 3-4, pp. 184–194, 2021.

[48] D. Sobrido-Cameán and A. Barreiro-Iglesias, "Role of caspase-8 and Fas in cell death after spinal cord injury," *Frontiers in Molecular Neuroscience*, vol. 11, p. 101, 2018.

[49] F. L. Scott, B. Stec, C. Pop et al., "The Fas-FADD death domain complex structure unravels signalling by receptor clustering," *Nature*, vol. 457, no. 7232, pp. 1019–1022, 2009.

Hindawi
Oxidative Medicine and Cellular Longevity
Volume 2022, Article ID 6060677, 20 pages
https://doi.org/10.1155/2022/6060677

Research Article

Integrated Experimental Approach, Phytochemistry, and Network Pharmacology to Explore the Potential Mechanisms of *Cinnamomi Ramulus* for Rheumatoid Arthritis

Jia Liu,[1] Qing Zhang,[1] Yuanyuan Chen,[1] Lingyu Wang,[1] Ting Tao,[1] Qiang Ren,[1,2] Xiuping Chen,[3] and Yunhui Chen[1]

[1]*Chengdu University of Traditional Chinese Medicine, Chengdu 611137, China*
[2]*Hospital of Chengdu University of Traditional Chinese Medicine, Chengdu 610072, China*
[3]*University of Macau, Macau 999078, China*

Correspondence should be addressed to Qing Zhang; zhangqcdutcm@163.com, Qiang Ren; 401627406@qq.com, and Yunhui Chen; chenyunhui@cdutcm.edu.cn

Received 7 April 2022; Revised 11 August 2022; Accepted 18 August 2022; Published 15 September 2022

Academic Editor: Helena Moreira

Cinnamomi Ramulus (CR) has been extensively used as a remedy for inflammatory diseases in China. This study adopted an integrative approach of experimental research, phytochemistry, and network pharmacology to investigate its alleviative effects on rheumatoid arthritis (RA) and the underlying potential mechanisms. CR extract (50, 100, and 200 mg/kg) and methotrexate (MTX) significantly ameliorated RA symptoms in the collagen-induced arthritis (CIA) rat model. They also reduced paw volume, arthritis index, proinflammatory cytokines (TNF-α, IL-17A, IL-6, and IL-1β), and oxidative damage. Sixty-three compounds were systematically identified as the basic components of CR. Fifty-five common genes obtained from compounds and GEO databases were employed to construct the protein-protein interaction (PPI) network. Among them, 20 hub genes were identified via the cytoHubba. Enrichment analysis of the common genes indicated that the TNF signaling pathway and IL-17 signaling pathway might be the potential key pathways. Moreover, molecular docking methods confirmed the high affinity between the top 10 bioactive components of CR and the top 10 targets. In addition, *in vitro* results showed that CR extract (0.2, 0.4, and 0.8 mg/mL) inhibited inflammation and oxidative damage in MH7A cells stimulated by lipopolysaccharide (LPS). In summary, this study adopted multiple approaches to elucidate the protective effect and potential mechanisms of CR on RA, indicating that CR might be a promising herbal candidate for further investigation of RA treatment.

1. Introduction

Rheumatoid arthritis (RA) is a progressive inflammatory autoimmune disease that causes severe joint damage, local inflammation, cartilage destruction, and bone erosion. It is associated with multiple genetic and environmental factors, impacts approximately 1% of the population, and is most prevalent among the middle-aged women, imposing a substantial emotional and financial burden on individuals and society [1]. Abnormal activation of fibroblast-like synovial cells (FLS) is the initial event of synovitis and joint injury, leading to bone and cartilage tissue damage, pannus formation, and finally joint destruction [2]. As the disease progresses, patients with RA experience an upsurge of inflammation and oxidative stress, leading to widespread pain from synovitis, progressive histological alterations, and disabling symptoms [3]. Currently, the commonly prescribed drugs for RA include glucocorticoids, nonsteroidal anti-inflammatory drugs (NSAIDs), disease-modifying antirheumatic drugs (DMARDs), and biological therapies [4]. Although these medications are widely prescribed to control the pain, immune responses, and inflammation of RA, their limited efficacy with noticeable side effects are inadequate to address this multifactorial disease. Thus, in order to investigate the pathogenesis of RA and explore valuable natural drugs, bioinformatics approaches should be utilized to

identify disease biomarkers and effective targets of natural medicines and clarify their therapeutic effects.

Cinnamomi Ramulus, the dried twigs of the aromatic plant *Cinnamomum cassia* (L.) Presl, is an important component of *Guizhi-Shaoyao-Zhimu* decoction (an effective antiarthritic prescription) [5]. According to phytochemistry and pharmacology researches, CR contains a variety of active substances represented by cinnamaldehyde, which have anti-inflammatory, antioxidant, antitumor, antipyretic, and analgesic effects [6]. Modern studies suggested that volatile oil is the main active component of CR, accounting for about 1% of the total medicinal materials [7]. In 2016, Sun et al. found that CR volatile oil alleviates pain and inflammation in mice by inhibiting inflammatory mediator release and iNOS and COX-2 activation [8]. Besides, 80% ethanolic extract of CR exhibited anti-inflammatory and antiarthritic activity by reducing the volume of edema in the CFA-induced chronic arthritic paw of rats [9]. Our previous studies explored its therapeutic value in RA by inhibiting the proliferation, invasion, and migration of fibroblast-like synoviocyte MH7A cells, inducing cell cycle arrest and apoptosis [10]. Certain active compounds in CR may contribute to these biological activities, while their detailed molecular mechanisms remain unclear. With the development of comprehensive bioinformatics analysis, microarray technology provides new insights into identifying key biomarkers for multiple diseases by analyzing data with sophisticated statistical algorithms and investigating overall patterns of gene expression [11]. Network pharmacology is a novel discipline based on system biology, which analyzes the network of biological systems and selects specific signal nodes for a multi-target drug molecule design. In recent years, it has become a pragmatic strategy to decipher the correlations between multicompounds, multitargets, and multipathways of TCM [12].

In this study, the alleviative effect of CR on RA was observed in the collagen-induced arthritis (CIA) rat model. Next, the phytochemical analysis of CR was conducted using ultraperformance liquid chromatography-Q Exactive Orbitrap-mass spectrometry (UPLC-Q Exactive-MS) combined with gas chromatography-mass spectrometry (GC-MS). Then, network pharmacology was employed to systematically decode the potential mechanisms of CR's alleviative actions on RA, and molecular docking was applied to verify the molecular targets. Finally, its potential effects on inhibiting inflammation and oxidative damage were screened *in vitro* based on lipopolysaccharide- (LPS-) induced MH7A cells. This study is aimed at elucidating the therapeutic effect and exploring the potential mechanisms and active ingredients of CR in improving RA, providing useful insight into future drug research and development for RA treatment.

2. Materials and Methods

2.1. Chemicals and Reagents. Cinnamomi Ramulus original material was purchased from the Sichuan New Green Pharmaceutical Technology Development Co., Ltd. (Chengdu, China). Herbal medicine was identified by Prof. Chunjie Wu (School of Pharmacy, Chengdu University of TCM). The bovine type II collagen (CII) was provided by Chondrex Inc. (Chondrex, Seattle, WA, USA). Dimethyl sulfoxide (DMSO), methotrexate (MTX), complete Freund's adjuvant (CFA), and lipopolysaccharide (LPS) were provided by Sigma-Aldrich Co. (St. Louis, MO, USA). The hematoxylin and eosin (H&E) and Safranin O-fast green (SFG) were purchased from Solarbio (Beijing, China). The ELISA assay kits for tumor necrosis factor- (TNF-) α, interleukin- (IL-) 1β, IL-6, and IL-17A were obtained from Beijing 4A Biotech Co. (Beijing, China). Oxidative stress parameters of superoxide dismutase (SOD), glutathione peroxidase (GSH-Px), catalase (CAT), and malonaldehyde (MDA) were purchased from Suzhou Michy Biomedical Technology Co., Ltd. (Suzhou, China). CCK-8 kits and dihydroethidium (DHE) fluorescent probe were obtained from US Everbright® Inc. (Suzhou, China). The 4′,6-diamidino-2-phenylindole (DAPI) was purchased from BOSTER biological technology company (Wuhan, China). Antibodies against NF-κB p65 and goat-anti-rabbit/rat horseradish-peroxidase-conjugated (HRP) secondary antibodies were purchased from Abcam (Cambridge, MA, USA). High-performance liquid chromatography-grade acetonitrile, methyl alcohol, and formic acid were obtained from Merck KGaA (Merck, Darmstadt, Germany); analytical grade anhydrous diethyl ether, anhydrous sodium sulphate, petroleum ether, ethyl acetate, and n-butyl alcohol were provided by Chengdu Kelong Chemical Co., Ltd. (Chengdu, China).

2.2. Preparation of CR Freeze-Dried Powder. The CR freeze-dried powder was prepared as follows. Briefly, the dried plants (200 g) were powdered and soaked with 75% ethanol (1 : 8, *w*/*v*) for 30 min. Reflux extraction was performed 3 times for 1.5 h per time. Each filtrate was combined, and the resulting filtrate mixture was rotationally evaporated at 60°C using a rotary evaporator (EYELA, N-1300V, Tokyo, Japan). The concentrated filtrate was cooled to room temperature, freeze-dried using a lyophilizer (Labconco Co., Kansas, MI, USA) to obtain the dry extract, and stored at 4°C until later use. The yield of the CR extract was 9.85%.

2.3. Animals. Specific pathogen-free (SPF) Wistar rats (6-7 weeks old, 200 ± 20 g) were obtained from Chengdu Dossy Experimental Animals Co., Ltd. (Chengdu, China). The animals were acclimated for one week at room temperature (22-24°C) with 50%-65% relative humidity and an alternating 12 h light-dark cycle. All animal experiments were conducted in conformity with the international guidelines for animal experiments and approved by the Animal Care and Use Committee of Chengdu University of Traditional Chinese Medicine.

2.4. Establishment of CIA Animal Model and Treatment. Collagen-induced arthritis (CIA) model was prepared according to the description of previous literature [5]. Firstly, bovine type II collagen (2 mg/mL) was emulsified in an equal volume of complete Freund's adjuvant (2 mg/mL). Rats were immunized by subcutaneous injection with

0.1 mL emulsion into the back (left and right sides) and tail base, respectively. The same doses of collagen mixture was performed on day 14 to boost immunization. The normal group was injected with equal volumes of normal saline at the same sites. Rats with CIA on day 21 were randomized into five groups ($n = 8$) based on the volume of hind paw swelling and arthritis score, namely, the CIA model group, CIA+CR (50 mg/kg) group, CIA+CR (100 mg/kg) group, CIA+CR (200 mg/kg) group, and positive control CIA +MTX group (0.2 mg/kg, 3 times/week). CR freeze-dried powder was dissolved in 0.5% CMC-Na solution. Rats in the CR group were given CR freeze-dried powder orally for 24 days, and rats in the normal group and CIA model group were given 0.5% CMC-Na solution in the same volume. Rats in the CR group were given oral administration of CR freeze-dried powder for 24 consecutive days, and the normal group and CIA model group received normal saline simultaneously. Paw volume and arthritis index were measured every three days to evaluate the severity of arthritis. The scoring criteria were as follows: 0 for no erythema or swelling, 1 for slight erythema or swelling of one toe or finger, 2 for erythema and swelling of more than one toe or finger, 3 for erythema and swelling of the ankle or wrist, and 4 for erythema and swelling of all toes or fingers and ankle or wrist [13]. Two hind legs were graded, and a total arthritis score was given for each animal.

2.5. Micro-CT Analyses and Histopathological Examination. The hind limb of each rat was harvested after sacrifice and scanned using a PerkinElmer Quantum GX micro-CT system (Norwalk, CT, USA) with the following parameters: X-ray, 90 kV, and 80 μA; field of view (FOV), 72 mm; voxel size, 45-90; scan mode, high resolution; and scan time, 4 min. The 3D reconstruction images were analyzed using the PerkinElmer Analyze software (version 12.0, Norwalk, CT, USA). For histopathological analysis, ankle joints were fixed in 10% formalin after removing the skin and excess tissue. After decalcified in 10% ethylenediaminetetraacetic acid (EDTA) for one month, the samples were embedded in paraffin, sliced into 5 μm sections, stained with H&E, and examined under Nikon TS2 light microscope and high-resolution digital camera system (Nikon TS2, Tokyo, Japan).

2.6. Volatile Oil Preparation. In order to explore the main active components in CR, volatile oil was obtained by steam distillation for GC-MS analysis. A total of 200 g of plant material in 0.5 L water were subjected to hydrodistillation for 3 h in a standard apparatus set. The white-yellow or brown oil samples were extracted with anhydrous diethyl ether twice, dried using anhydrous sodium sulphate to remove traces of moisture, and stored in the dark at 4°C until further investigation.

2.7. GC-MS Analysis and Compound Identification. The collected essential oil solution was analyzed using a gas chromatography-mass spectrometry (GC-MS) (Agilent 5975C gas chromatography instrument, Agilent Technologies, USA). An HP-5MS capillary column (30 m × 250 μm × 0.25 μm) was employed for the separation. High-purity helium was used as the carrier gas, with a flow rate of 1.0 mL/min. In addition to the injection temperature and interface temperature of 250°C, standard electron impact mass spectrometry source temperature of 230°C and quadrupole temperature of 150°C, the resolution ratio was set as 30 : 1. The full scan monitoring mode was adopted for the mass spectrometry, and the scanning range was m/z 12-550. The column temperature was set at 60°C and programmed to rise at 4°C/min to 200°C (2 min held) and 15°C/min to 290°C (3 min held) kept for 40 min. Upon comparison with the mass spectrometry recorded by the National Institute of Standards and Technology (NIST) mass spectral library, the components contained in CR essential oil were obtained, and the area normalization method was adopted to determine the relative percentage content of each component.

2.8. CR Solvent Extraction Preparation. After extracting the volatile oil, the filtrates were concentrated using a vacuum rotary evaporator (Yarong RE 52AA). The obtained concentrate was mixed with water to form a suspension, and the corresponding extraction sections were extracted with petroleum ether, ethyl acetate, and n-butanol successively. Each solvent was extracted 5 times per 200 mL, and the remaining section was the water part. After lyophilization, an appropriate amount of each extracted part was dissolved in methanol and filtered by 0.22 μm microporous membrane. The chemical constituents of each part were qualitatively analyzed by UPLC-Q Exactive-MS.

2.9. UPLC-Q Exactive-MS Conditions. Mass spectrum identification was performed using Thermo Scientific Q Exactive Orbitrap HRMS (Thermo Fisher Scientific, Massachusetts, USA) connected to Thermo Scientific Vanquish UPLC (Thermo Fisher Scientific, Massachusetts, USA). Chromatographic separation was achieved on a Thermo ScientificTM AccucoreTM C18 (3 × 100 mm, 2.6 μm) with a flow rate of 0.2 mL/min at 30°C. The mobile phase A was acetonitrile, and the mobile phase B was deionized water (0.1% formic acid). The gradient elution procedures of each part was described in detail: petroleum ether (0-15 min, 40-75% A; 15-30 min,75-85% A; 30-35 min, 85-95% A; 35-40 min, 95-95% A), ethyl acetate (0-15 min, 20-40% A; 15-20 min, 40-80% A; 20-35 min, 80-95% A; 35-40 min, 95-95% A), n-butanol (0-5 min, 10-20% A; 5-15 min, 20-50% A; 15-35 min, 50-95% A; 35-40 min, 95-95% A), and water (0-5 min, 10-30% A; 5-15 min, 30-50% A; 15-25 min, 50-70% A; 25-35 min, 70-95% A; 35-40 min, 95-95% A). After guiding into the electrospray ionization (ESI) source, MS conditions were performed as follows: heath gas flow rate, 35 L/min; spray voltage, 3000 V; capillary temperature, 320°C; aux gas flow rate, 10.00 L/min; and probe heater temperature, 350°C. Full scan spectra were recorded in the mass range of m/z 100-1500. Based on retention time, fragmentation patterns, literature, and the Thermo Scientific™ Compound Discoverer™ software (3.0), the chemical composition was identified in UPLC-Q Exactive-MS positive and negative ion mode.

2.10. Network Pharmacology Analysis of CR against RA

2.10.1. Acquisition of RA Targets. In this study, GSE55457 and GSE55235 datasets containing gene expression profiles were downloaded from the Gene Expression Omnibus (GEO) database. Dataset GSE55457, containing synovial tissue samples from 13 RA patients and 10 healthy individuals, was constructed by the Affymetrix Human Genome U133A Array (GPL96 platform). Dataset GSE55235 consisted of 20 samples (10 RA synovial tissue samples and 10 healthy samples) and was based on Affymetrix Human Genome U133A Array (GPL96 platform). To identify the differentially expressed genes (DEGs) between RA and normal samples, GSE55457 and GSE55235 were normalized and visualized by the Limma R package. Based on the threshold of p value < 0.05 and $|\log FC| > 1$ judgment, the volcano plot and heat map were obtained through the ggplot2 package and heat map package, respectively. After filtering according to the threshold, these DEGs were collected to form the RA targets library.

2.10.2. Acquisition of CR Targets. We collected the targets of extracted compounds from the Chinese Medicine Systems Pharmacology Database and Analysis Platform (TCMSP), SwissTargetPrediction, PharmMapper online database, and available literature reports [14–17]. After deleting duplicated targets, the Uniprot database was utilized to convert the target names into corresponding gene names to obtain the CR targets library, and then, Cytoscape (3.8.0) software was applied to construct the compound-target network diagram.

2.10.3. Construction of a Protein-Protein Interaction Network. The screened CR and RA targets were imported into the draw Venn diagram for analysis, and overlapping genes were identified as the potential therapeutic targets for CR acting on RA. After the overlapping genes were uploaded to the STRING database, a protein-protein interaction (PPI) network was performed to show interactions between individual targets. The PPI network identified using STRING was further integrated, analyzed, and visualized using the Cytoscape 3.8.0, and hub genes were selected from the PPI networks using the cytoHubba plug-in. Afterwards, a compound-common gene network was constructed by calculating the degrees of each node.

2.10.4. Gene Ontology and Kyoto Encyclopedia of Genes and Genomes Pathway. To comprehensively analyze the biological processes and signaling pathways involved in common genes, the clusterProfiler software package of R (4.0.2) was utilized to perform Gene Ontology (GO) enrichment analysis and Kyoto Encyclopedia of Genes and Genomes (KEGG) pathway analysis. GO biological processes and KEGG pathways with p value < 0.05 were considered to be significantly enriched. The top 10 results of GO enrichment and the top 20 results of KEGG pathway enrichment analyses were visualized with bubble plots and column charts by the R software package.

2.11. Docking Verification of Compound and Target Molecule. Discovery Studio 4.5 software was used to build the molecular docking model between the top 10 key active ingredients and the top 10 hub genes. We obtained 3D structures of these compounds from ChemDraw software and downloaded "PDB" format files of optimal protein crystal structures for corresponding targets from the RCSB PDB database. Subsequently, ligand and receptor were prepared using Discovery Studio 4.5 software to determine the location of the receptor's active site. Small molecule compounds matching the protein active site were screened by the ligand docking module. The compounds with higher docking scores than the prototype ligand were selected as active molecules.

2.12. Cell Culture and Treatment. Human synovial cells MH7A were purchased from the Beina Biological Company (Beijing, China) and cultured in DMEM containing 10% FBS at 37°C in a 5% CO_2 humidified atmosphere. CCK-8 assay was used to determine the optimal concentration of LPS-induced MH7A cells and the optimal intervention concentration of CR. In brief, MH7A cells (5×10^3) were seeded in 96-well plates and treated with various concentrations of LPS for 6 h [18]. The optimal concentration of LPS-stimulated MH7A cells was treated with CR extract at different doses for 24 h. Then, 10 μL CCK-8 was added to each well and incubated at 37°C for 2 h. The absorbance of each well at 450 nm was measured by an iMARK microplate reader (Bio-Rad, Hercules, CA, USA), and the cell survival rate was calculated.

2.13. ELISA Assays of the Proinflammatory Cytokines. Rats were sacrificed, and the serum was collected from the abdominal aorta by centrifugation at 3000 rpm for 15 min and stored at -80°C until assayed. Concentrations of TNF-α, IL-1β, IL-6, and IL-17A in the serum were measured using ELISA according to the manufacturer's instructions. MH7A cells were treated with LPS (1 μg/mL) for 6 h and then intervened with various doses of CR for 24 h. Then, the concentrations of TNF-α, IL-1β, IL-6, and IL-17A in MH7A cells were determined using commercial ELISA kits.

2.14. Assessment of Oxidative Stress Parameters. All experimental rats were sacrificed, and the serum was obtained by centrifugation at 3000 rpm for 15 min. The serum SOD, CAT, and GSH-Px activities and MDA level were determined by the corresponding assay kit following the manufacturer's protocols. Meanwhile, MH7A cells were treated with LPS (1 μg/mL) for 6 h and then treated with various doses of CR for 24 h. The levels of SOD, CAT, GSH-Px, and MDA in MH7A cells were determined following the manufacturer's protocols.

2.15. Determination of Reactive Oxygen Species (ROS). The DHE fluorescent probe was adopted to detect the level of intracellular reactive oxygen species. In brief, MH7A cells (1×10^5) were incubated in a 6-well plate and treated with LPS and different concentrations of CR. Subsequently, the cells were incubated with DHE (10 μM) for 30 min at 37°C in a dark environment, followed by washing three times with PBS. Cells were collected for intracellular ROS analysis using a FACSCanto II Flow cytometer (BD Company, New York, NY, USA).

2.16. Immunofluorescence Assay. MH7A cells were seeded into a confocal laser dish and treated with LPS and different concentrations of CR. At the end of the intervention, the cells were fixed with 4% paraformaldehyde for 20 min and then permeated with 0.1% Triton X-100 in PBS for 1 h at room temperature. The cells were incubated with NF-κB p65 antibody (diluted 1 : 200) overnight at 4°C. Anti-rabbit IgG (H+L) Alexa Fluor® was incubated at room temperature for 1 h in the dark, and the nuclei were visualized using DAPI staining. After washing with PBS for three times, the fluorescence intensity was observed using a confocal laser microscope (Leica, SP8 SR, Wetzlar, Germany).

2.17. Statistical Analysis. Data were expressed as mean ± standard deviation. Differences between multiple groups were assessed using one-way analysis of variance. p values < 0.05 were deemed statistically significant. Analysis and graphing were completed utilizing GraphPad Prism 8.0 software (San Diego, CA, USA).

3. Results

3.1. CR Alleviated the Severity of RA in CIA Rats. As shown in Figure 1(a), the CIA rat model was established to validate the efficacy of CR against RA. Photographs of paw edema showed that joint swelling in CIA rats was significantly reduced after 24 days of MTX and CR treatment (Figure 1(b)). The arthritis index in CIA rats peaked on day 9 after administration (day 30 after primary immunization) compared with the normal control group. After MTX and CR treatment, arthritic symptoms and arthritic scores of CIA rats were significantly improved (Figures 1(c) and 1(d)). As shown in Figure 1(e), the levels of inflammatory cytokines (TNF-α, IL-1β, IL-6, and IL-17A) were significantly higher in the model group than in the normal group. The results of the CR group and MTX group were consistent, and the effects of different CR concentrations on TNF-α, IL-1β, IL-6, and IL-17A levels were dose-dependent. As displayed in Figure 1(f), CIA rats developed oxidative stress with a decreased antioxidant enzyme activity (SOD, CAT, and GSH-Px) and an increased serum MDA level compared to the normal group. However, CR and MTX treatments were observed to significantly reduce oxidative damage. As expected, intervention of CR at different doses (50, 100, and 200 mg/kg) significantly reduced the serum level of MDA and elevated the activity of antioxidant enzyme.

3.2. CR Inhibited Ankle and Cartilage Damage in CIA Rats. The results of H&E and Safranin O staining demonstrated that the ankle joint and synovial tissue in the normal group were intact without damage. On the contrary, synovial cell proliferation and inflammatory cell infiltration were noted in the model group. CR (50, 100, and 200 mg/kg) and MTX treatment all reduced synovial hyperplasia, synovial inflammation, and cartilage erosion in CIA rats. Micro-CT imaging revealed that normal rats had smooth articular surface, clear and complete articular structure, normal bone and articular space, and absence of soft tissue swelling. CIA rats showed joint surface fusion, joint space narrowing, severe structural erosion, and destructive bone resorption and dissolution. CR and MTX intervention reduced soft tissue swelling and bone destruction, as well as deterioration of articular surface structure and space clarity (Figure 2(a)). The quantitative analysis for synovitis and cartilage damage is shown in Figures 2(b) and 2(c).

3.3. Analysis of the Constituents of Volatile Oil Obtained from CR. A total of 28 volatile compounds were identified utilizing the NIST mass spectral library and literature data [19–21] (Figure 3(a)). The retention time, formula, molecular weight, and area percentage of benzaldehyde (1), 4-hydroxybenzaldehyde (2), acetophenone (3), benzenepropanal (4), linderol (5), (-)-alpha-terpineol (6), *cis*-cinnamaldehyde (7), 3-phenylpropanol (8), 2-methoxybenzaldehyde (9), cinnamaldehyde (10), alpha-copaene (11), beta-caryophyllene (12), coumarin (13), cinnamyl acetate (14), gamma-muurolene (15), alpha-curcumene (16), alpha-muurolene (17), beta-bisabolene (18), trans-calamenene (19), 2-methoxycinnamaldehyde (20), alpha-calacorene (21), spathulenol (22), cedrol (23), tetradecanal (24), tau-cadinol (25), alpha-cadinol (26), cadalene (27), and alpha-bisabolol (28) are shown in Table 1. The structures of these compounds are presented in Figure 3(b).

3.4. Identification and Analysis of Active Constituents in CR Extract. Total ion chromatograms of each part in positive and negative ion modes are presented in Figures 4(a)–4(d). A total of 35 compounds were preliminarily isolated and identified from CR extract, including azelaic acid (29), syringaldehyde (30), coniferyl aldehyde (31), caryophyllene oxide (32), benzyl cinnamate (33), oleoyl ethanolamide (34), oleamide (35), stearoyl ethanolamide (36), stearamide (37), benzoic acid (38), catechin (39), 4-methoxybenzaldehyde (40), caffeic acid (41), 4-methoxycinnamaldehyde (42), p-coumaric acid (43), quercetin (44), taxifolin (45), ferulic acid (46), kaempferol (47), cinnamic acid (48), methyl eugenol (49), methyl cinnamate (50), ethyl 4-methoxycinnamate (51), 4-methoxycinnamic acid (52), 2-hydroxycinnamic acid (53), 3,4-dimethoxycinnamic acid (54), 2,3-dihydroxybenzoic acid (55), syringic acid (56), 2,4-dihydroxybenzoic acid (57), sebacic acid (58), 2-methoxybenzoic acid (59), 2-methoxycinnamic acid (60), isoquercetin (61), kaempferol-3-O-glucoside (62), and quercitrin (63) [22–42]. The retention time, formula, molecular weight, error value, fragment ion, and other details of 35 compounds are shown in Table 2, and the structures of these compounds are displayed in Figure 4(e).

3.5. Results of Network Pharmacology Analysis

3.5.1. Prediction of Related Targets of RA. After standardized processing of the two datasets downloaded from the GEO database, 419 DEGs were obtained from the RA synovial tissues and normal controls, including 183 upregulated genes (red dots) and 236 downregulated genes (green dots). Volcano map and heat map analysis of the DEGs were performed by R software (Figures 5(a) and 5(b)).

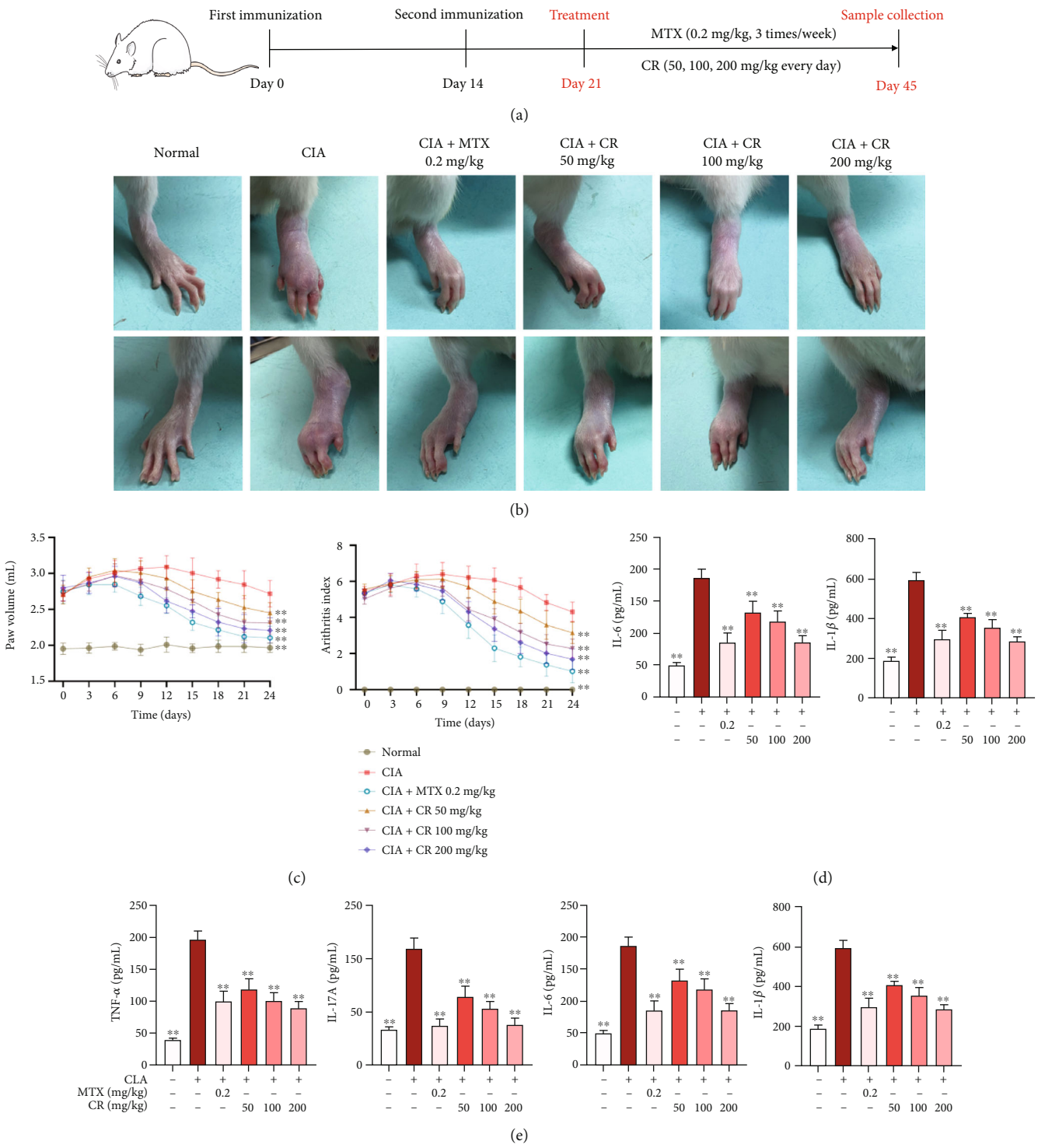

Figure 1: Continued.

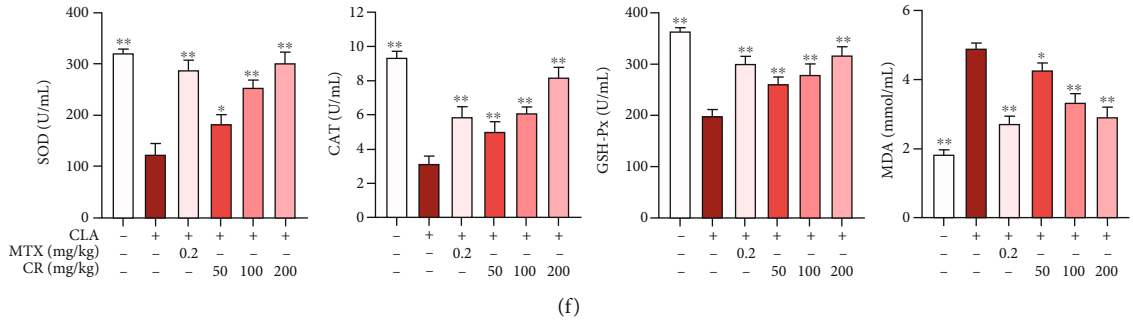

Figure 1: CR attenuated CIA-induced RA in rats. (a) The experimental procedure was illustrated. (b) Representative photographic images of rats in different treatment groups. (c) Effects of CR extract on paw volume of CIA rats. (d) Effects of CR extract on arthritis index of CIA rats. (e) Effects of CR extract on serum levels of pro-inflammatory cytokines (TNF-α, IL-17A, IL-6, and IL-1β). (f) Effects of CR extract on serum SOD, CAT, GSH-Px, and MDA levels. Data are expressed as mean ± SD; $^{*}p < 0.05$, $^{**}p < 0.01$ vs. the model group.

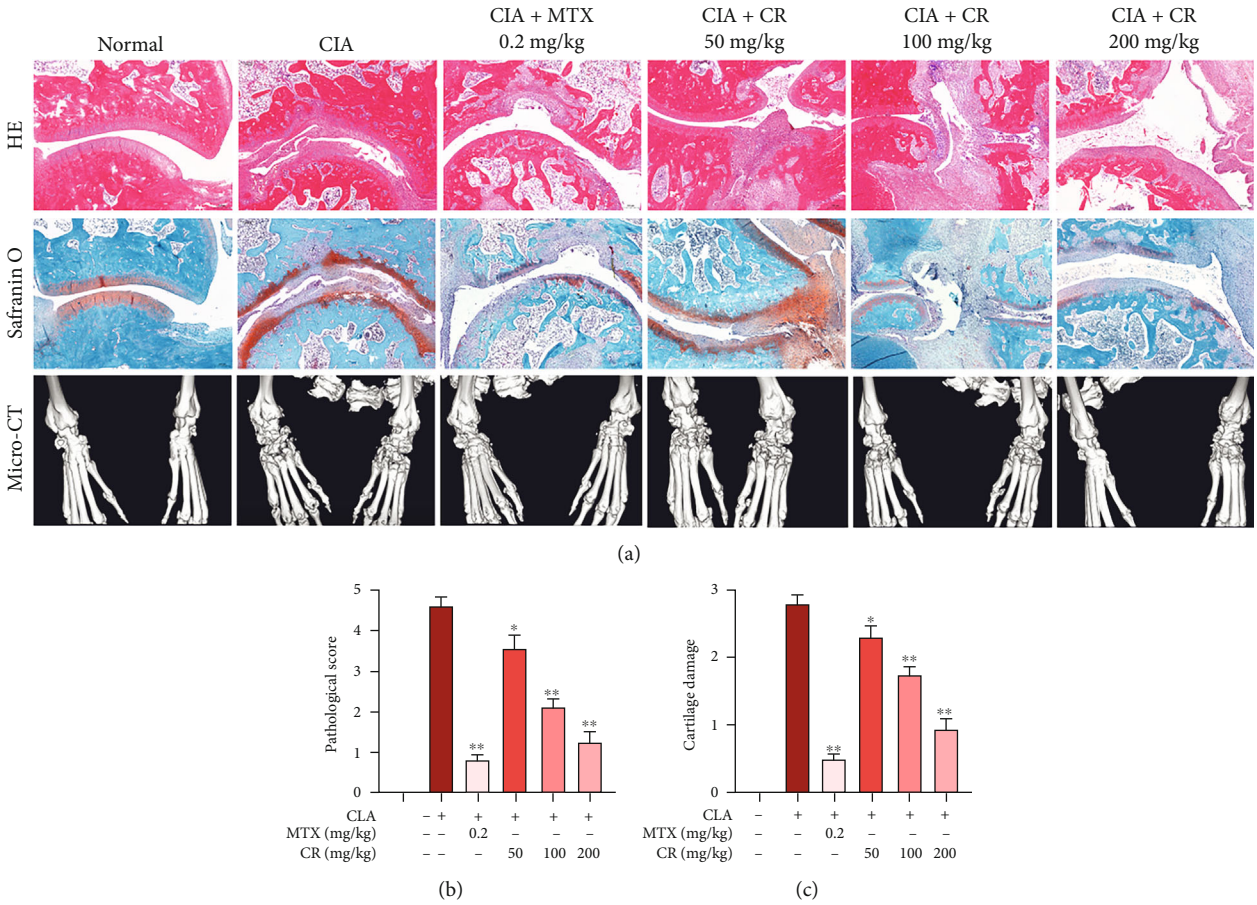

Figure 2: Effects of CR on histopathological changes and joint destruction of CIA rats. (a) Representative H&E staining and Safranin O staining of ankle joint sections, and representative images of the micro-CT determination. The quantitative results for (b) synovitis and (c) cartilage damage. Data are expressed as mean ± SD; $^{*}p < 0.05$, $^{**}p < 0.01$ vs. the model group.

3.5.2. Prediction of Anti-RA Targets of CR. We obtained targets for 63 compounds from TCMSP, PharmMapper, and SwissTargetPrediction databases, and a total of 559 unduplicated targets were collected. A compound-target network was constructed based on the interaction relationship between these 63 compounds and their corresponding targets (Figure 5(c)). The network consists of 622 nodes (63 compounds and 559 targets) and 2075 edges. Red circular nodes represent compounds, blue circular nodes symbolize targets, green circular nodes represent common targets, and edges symbolize interactions between compounds and targets. The 559 active compound targets and the 419 disease targets were used to draw a Venn diagram, and 55 common targets were obtained (Figure 5(d)).

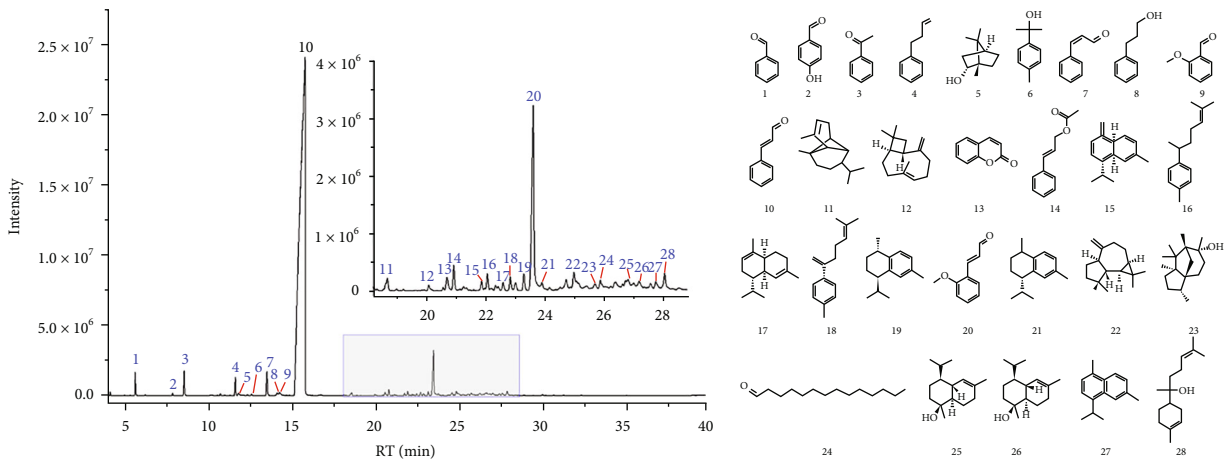

Figure 3: (a) The total ion chromatograms of volatile oil from *Cinnamomi Ramulus*. (b) Compounds in volatile oil from *Cinnamomi Ramulus*.

Table 1: Compounds identified in volatile oil from CR.

Peak no.	RT (min)	Compound	Formula	Molecular weight	Relative amount (%)
1.	5.705	Benzaldehyde	C_7H_6O	106.12	0.74
2.	7.947	4-Hydroxybenzaldehyde	$C_7H_6O_2$	122.12	0.1
3.	8.64	Acetophenone	C_8H_8O	120.15	0.97
4.	11.722	Benzenepropanal	$C_9H_{10}O$	134.17	0.74
5.	11.918	Linderol	$C_{10}H_{18}O$	154.25	0.19
6.	12.696	Alpha-terpineol	$C_{10}H_{18}O$	154.25	0.08
7.	13.621	*cis*-Cinnamaldehyde	C_9H_8O	132.16	1.20
8.	14.252	3-Phenylpropanol	$C_9H_{12}O$	136.19	0.22
9.	14.393	2-Methoxybenzaldehyde	$C_8H_8O_2$	136.15	0.32
10.	15.919	*trans*-Cinnamaldehyde	C_9H_8O	132.16	88.30
11.	18.719	Alpha-copaene	$C_{15}H_{24}$	204.35	0.22
12.	20.116	Beta-baryophyllene	$C_{15}H_{24}$	204.35	0.09
13.	20.729	Coumarin	$C_9H_6O_2$	146.14	0.21
14.	20.962	Cinnamyl acetate	$C_{11}H_{12}O_2$	176.21	0.28
15.	21.899	Gamma-muurolene	$C_{15}H_{24}$	204.35	0.11
16.	22.095	Alpha-curcumene	$C_{15}H_{22}$	202.33	0.2
17.	22.628	Alpha-muurolene	$C_{15}H_{24}$	204.35	0.1
18.	22.867	Beta-bisabolene	$C_{15}H_{24}$	204.35	0.16
19.	23.327	*trans*-Calamenene	$C_{15}H_{22}$	202.33	0.19
20.	23.639	2-Methoxycinnamaldehyde	$C_{10}H_{10}O_2$	162.18	2.88
21.	23.939	Alpha-calacorene	$C_{15}H_{20}$	200.32	0.14
22.	25.018	Spathulenol	$C_{15}H_{24}O$	220.35	0.45
23.	25.729	Cedrol	$C_{15}H_{26}O$	222.37	0.08
24.	25.912	Tetradecanal	$C_{14}H_{28}O$	212.37	0.12
25.	26.844	Tau-cadinol	$C_{15}H_{26}O$	222.37	0.23
26.	27.218	Alpha-cadinol	$C_{15}H_{26}O$	222.37	0.13
27.	27.781	Cadalene	$C_{15}H_{18}$	198.3	0.12
28.	28.075	Alpha-bisabolol	$C_{15}H_{26}O$	222.37	0.25

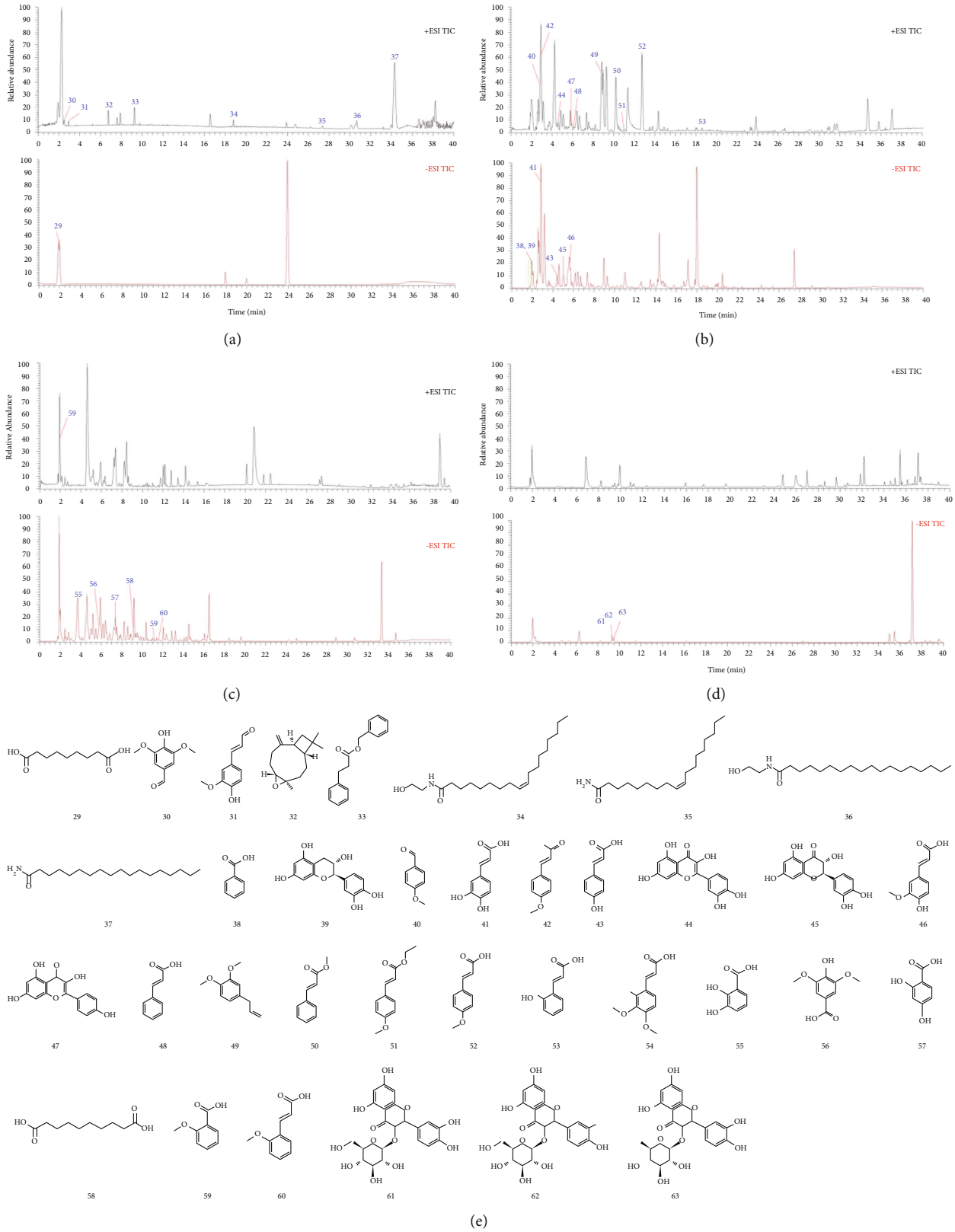

Figure 4: The total ion chromatograms of different fractions of *Cinnamomi Ramulus*: (a) petroleum ether fraction, (b) ethyl acetate fraction, (c) n-butanol fraction and (d) water fraction. (e) Compounds in different fractions of *Cinnamomi Ramulus*.

Table 2: Compounds identified in the CR by UPLC-QE-MS/MS.

Peak no.	RT (min)	Formula	Molecular weight	ESI-MS	Error (ppm)	Fragment ions (m/z)	Name	Ref
29	1.94	$C_9H_{16}O_4$	188.10469	187.09741[M-H]$^-$	-0.9	169, 125, 97	Azelaic acid	22
30	2.509	$C_9H_{10}O_4$	182.05843	183.06576[M+H]$^+$	2.85	168, 155, 140, 123, 95	Syringaldehyde	23
31	2.98	$C_{10}H_{10}O_3$	178.06265	179.06978[M+H]$^+$	-1.93	164, 161, 147, 133, 119, 105, 55	Coniferyl aldehyde	24
32	6.763	$C_{15}H_{24}O$	220.18333	221.19066[M+H]$^+$	2.81	207, 175, 161, 147, 133, 121, 109, 95, 81, 69, 55	Caryophyllene oxide	25
33	9.261	$C_{16}H_{14}O_2$	238.09984	239.10710[M+H]$^+$	1.93	192, 131, 91	Benzyl cinnamate	26
34	18.823	$C_{20}H_{39}NO_2$	325.29875	326.30603[M+H]$^+$	2.07	308, 62	Oleoyl ethanolamide	27
35	27.451	$C_{18}H_{35}NO$	281.27245	282.27982[M+H]$^+$	2.07	97, 83, 55	Oleamide	28
36	30.611	$C_{20}H_{41}NO_2$	327.31456	328.32178[M+H]$^+$	2.54	311, 62	Stearoyl ethanolamide	29
37	34.293	$C_{18}H_{37}NO$	283.2883	284.29556[M+H]$^+$	2.7	266, 88, 57	Stearamide	30
38	1.981	$C_7H_6O_2$	122.03708	121.04431[M-H]$^-$	2.44	93, 65	Benzoic acid	31
39	1.999	$C_{15}H_{14}O_6$	290.07902	289.08643[M-H]$^-$	-0.07	245, 203, 151, 125, 109, 97	Catechin	22
40	2.813	$C_8H_8O_2$	136.05254	137.05983[M+H]$^+$	0.84	122, 109, 94	4-Methoxybenzaldehyde	23
41	2.861	$C_9H_8O_4$	180.04176	179.03433[M-H]$^-$	-2.76	135, 107	Caffeic acid	22
42	2.947	$C_{10}H_{10}O_2$	162.06806	163.07544[M+H]$^+$	0.05	145, 135, 121, 105, 79, 55	4-Methoxycinnamaldehyde	26
43	4.396	$C_9H_8O_3$	164.04719	163.03949[M-H]-	-0.93	119, 93	p-Coumaric acid	22
44	4.584	$C_{15}H_{10}O_7$	302.0428	303.05014[M+H]$^+$	0.5	257, 229, 201, 165, 153, 137	Quercetin	32
45	5.018	$C_{15}H_{12}O_7$	304.05854	303.05130[M-H]$^-$	-3.62	285, 217, 151, 125, 109	Taxifolin	22
46	5.661	$C_{10}H_{10}O_4$	194.0578	193.05026[M-H]$^-$	-0.59	161, 151, 134	Ferulic acid	33
47	5.863	$C_{15}H_{10}O_6$	286.04805	287.05533[M+H]$^+$	1.1	165, 153	Kaempferol	32
48	6.15	$C_9H_8O_2$	148.05288	149.04446[M+H]$^+$	-4.55	131, 123, 103	Cinnamic acid	26
49	8.789	$C_{11}H_{14}O_2$	178.0629	179.07045[M+H]$^+$	-0.54	103, 91	Methyl eugenol	34
50	10.21	$C_{10}H_{10}O_2$	162.06814	163.07553[M+H]$^+$	0.4	131, 103, 95	Methyl cinnamate	35
51	11.111	$C_{12}H_{14}O_3$	206.09453	207.10184[M+H]$^+$	1.13	161, 134, 133	Ethyl 4-methoxycinnamate	36
52	12.743	$C_{10}H_{10}O_3$	178.06343	179.07039[M+H]$^+$	1.34	133, 117, 105	4-Methoxycinnamic acid	35
53	18.67	$C_9H_8O_3$	164.04758	165.05475[M+H]$^+$	1.43	147, 123, 103, 91	2-Hydroxycinnamic acid	26
54	2.013	$C_{11}H_{12}O_4$	208.0738	209.08141[M +H]+	0.92	191, 163, 91	3,4-Dimethoxycinnamic acid	37
55	3.699	$C_7H_6O_4$	154.0259	153.0186[M-H]-	-4.57	153, 109	2,3-Dihydroxybenzoic acid	38
56	5.75	$C_9H_{10}O_5$	198.0534	197.06065[M-H]-	2.8	182, 167, 153, 139, 123	Syringic acid	22
57	7.366	$C_7H_6O_4$	154.0259	153.01859[M-H]-	-4.85	153, 109	2,4-Dihydroxybenzoic acid	38
58	9.367	$C_{10}H_{18}O_4$	202.1203	201.12743[M-H]-	-1.04	183, 139	Sebacic acid	39
59	11.23	$C_8H_8O_3$	152.0477	153.05493[M +H]+	2.09	135, 92, 77	2-Methoxybenzoic acid	40
60	11.561	$C_{10}H_{10}O_3$	178.063	179.07036[M +H]+	-0.01	161, 131, 103, 77	2-Methoxycinnamic acid	41
61	8.225	$C_{21}H_{20}O_{12}$	464.0958	463.08865[M-H]-	0.66	317, 287, 259, 151, 125, 109	Isoquercetin	22
62	9.335	$C_21H_{20}O_{11}$	448.101	447.09409[M-H]-	0.97	285, 255, 227	Kaempferol-3-O-glucoside	31
63	9.496	$C_{21}H_{20}O_{11}$	448.101	447.09372[M-H]-	0.97	301, 300, 255, 179	Quercitrin	42

3.5.3. Compound-Common Gene Network. The PPI network was obtained by importing 55 common targets into STRING and removing five disconnected points. The downloaded TSV data were imported into Cytoscape 3.8.0 to visualize the protein interaction network, with darker node colors representing larger degree values (Figure 6(a)). The 20 hub targets were calculated by the cytoHubba plug-in, and the ranks were represented by color changes from red to yellow (Figure 6(b)). After removing 12 compounds without related targets, 51 active candidate compounds were obtained. Cytoscape 3.8.0 was utilized to construct a network diagram of 51 compounds and 55 common gene targets, as shown in Figure 6(c), consisting of 106 nodes and 244 edges. The results showed that cinnamaldehyde (10), caffeic acid (41), benzyl cinnamate (33), cinnamyl acetate (14), 4-methoxy-cinnamaldehyde (42), 2-methoxy-cinnamaldehyde (20), quercetin (44), kaempferol (47), 3, 4-dimethoxy-4-methoxy-cinnamic acid (52), cinnamic acid (54), ethyl 4-methoxycinnamate (51), 4-methoxy-benzaldehyde (40), 2-methoxybenzaldehyde (9), and coniferyl aldehyde (31) might be candidate bioactive substances for the treatment of RA.

3.5.4. GO and KEGG Pathway Enrichment Analyses. We performed GO and KEGG pathway enrichment analyses to further elucidate the biological functions of 55 common genes systematically. As shown in Figure 6(d), the top 10 terms in the BPs, CCs, and MFs were selected. The enrichment

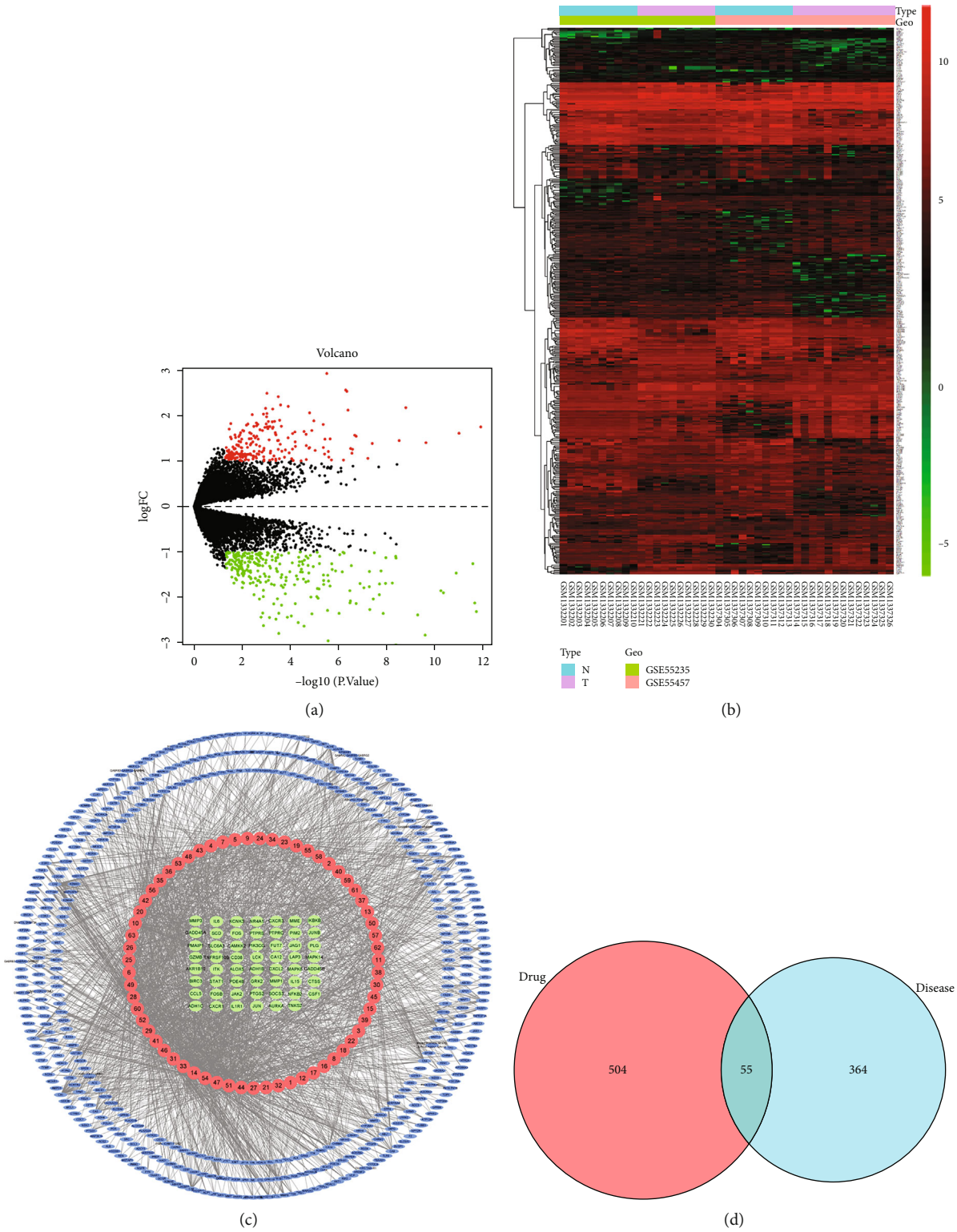

Figure 5: Prediction of anti-RA targets of CR. (a) Volcano map of DEGs in the GSE55235 and GSE55457 microarray datasets, with logFC on the vertical axis and log10 (p value) on the horizontal axis. (b) Heat map of DEGs in the GSE55235 and GSE55457 microarray datasets, with the vertical axis representing samples and the horizontal axis representing differentially expressed genes. (c) Compound-target network. The red circular node, blue ellipse nodes, and green ellipse nodes represented the compounds, targets, and overlapping genes, respectively. (d) Common genes between DEGs and compound targets.

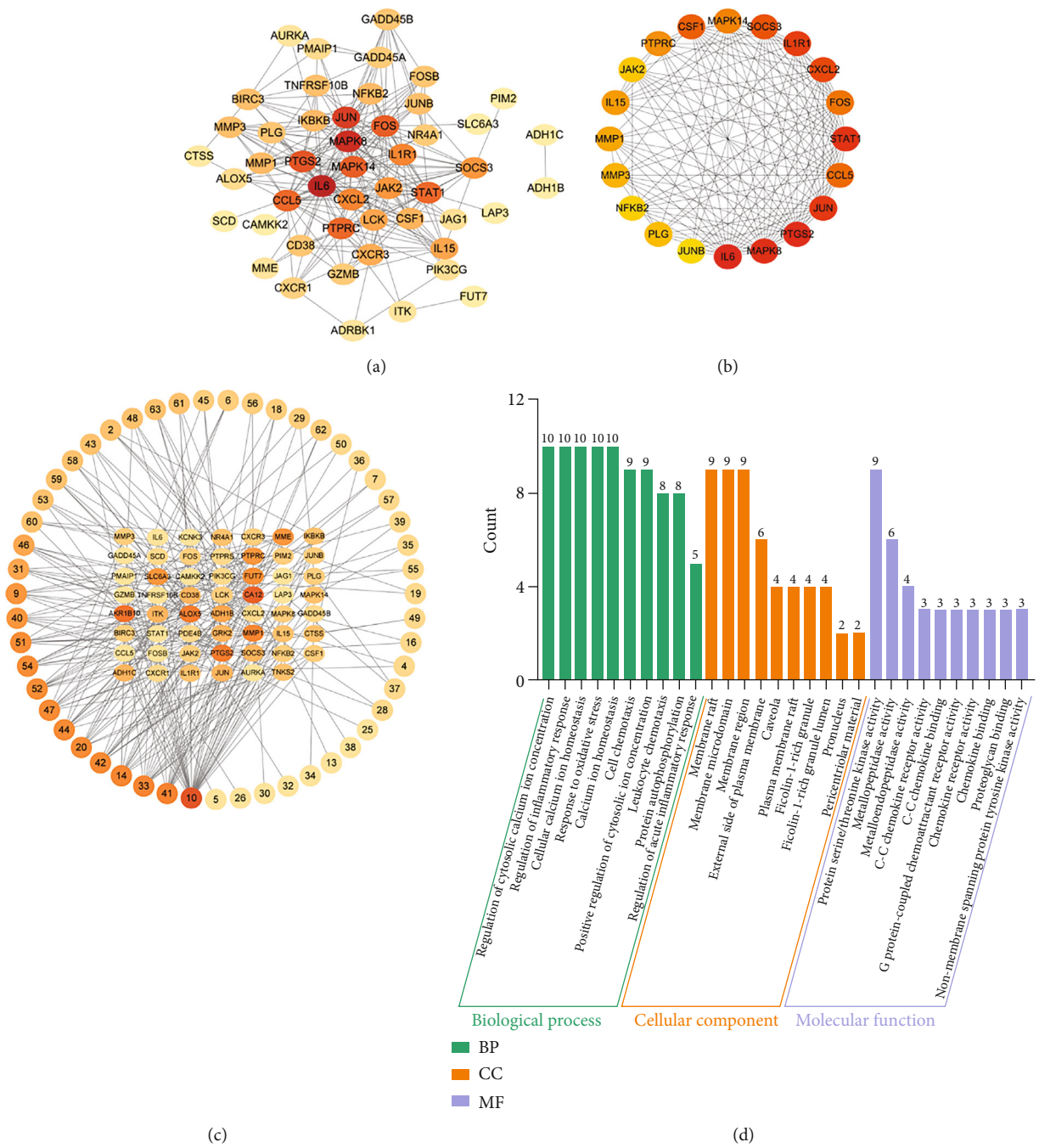

Figure 6: Continued.

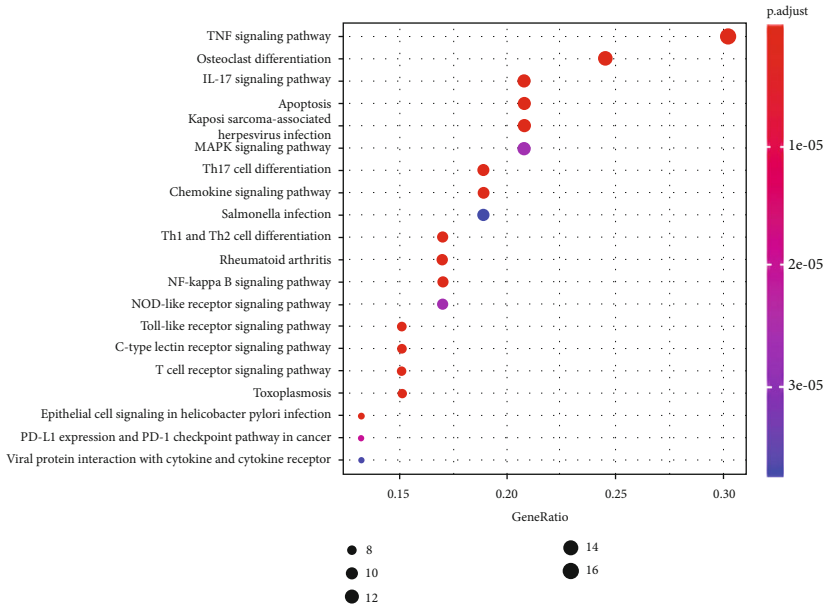

(e)

Figure 6: GO and KEGG enrichment analysis results. (a) PPI networks for common genes. (b) The top 20 hub genes of the common genes. (c) Active compound-common gene network. (d) The top 10 items with significant enrichment in BP, CC, and MF of GO analysis. The y-axis represents the enrichment count of target genes, and the x-axis represents the GO category of target genes. (e) The KEGG analysis diagram including the top 20 significant enrichment pathways. The y-axis represents the enrichment pathways, and the x-axis represents the enrichment score.

of BPs involved the regulation of cytosolic calcium ion concentration, cell chemotaxis, regulation of inflammatory response, and cellular calcium ion homeostasis. Enrichment to CCs mainly included membrane raft, membrane microdomain, and membrane region. The MFs most enriched in protein serine/threonine kinase activity, metallopeptidase activity, and metalloendopeptidase activity. Additionally, the KEGG pathways were most enriched in apoptosis and inflammatory-associated pathways, such as the TNF signaling pathway, osteoclast differentiation, IL-17 signaling pathway, apoptosis, Th17 cell differentiation, Th1 and Th2 cell differentiation, rheumatoid arthritis, and NF-kappa B signaling pathway. The top 20 pathways are shown in Figure 6(e).

3.6. Molecular Docking Verification. We searched the 3D structure of these 10 hub genes in the PDB database: IL6 (PDB: 4CNI), MAPK8 (PDB: 4HYS), PTGS2 (PDB: 5KIR), JUN (PDB: 2NO3), CCL5 (PDB: 5UIW), STAT1 (PDB: 6HHO), FOS (PDB: 6W3E), IL1R1 (PDB: 4GAF), SOCS3 (PDB: 6C7Y), and MAPK14 (PDB: 6SFO). The higher the molecular docking score, the better the receptor-ligand binding ability. According to Figure 7, the optimal docking results of the 10 hub genes and the top 10 bioactive compounds were presented in 3D topological structures of the drug-target binding model. Notably, these compounds were closely bound to the receptors through hydrogen bonds, hydrophobic interaction of amino acids, and π-conjugated effects. The above results indicated that the interaction between these core targets and core components was the biological basis for the multitarget action of CR against RA.

3.7. CR Ameliorated LPS-Induced Inflammatory Injury in MH7A Cells. MH7A cells were treated with different doses of LPS for 6 h to establish the LPS-induced inflammatory injury model. As shown in Figure 8(a), 1 μg/mL of LPS increased the viability of MH7A cells compared to the untreated control group, while LPS-induced survival decreased from 4 μg/mL. Given the effect of LPS on enhancing the viability of MH7A cells, 1 μg/mL LPS was selected as the stimulation condition for subsequent experiments. LPS-induced MH7A cells were treated with different doses of CR to detect cytotoxicity. Data in Figure 8(b) showed that 0.2 mg/mL CR began to decrease the viability of MH7A cells compared with the LPS group. Thus, 0.2, 0.4, and 0.8 mg/mL were selected as a CR-intervention condition for follow-up experiments. Since inflammation is a major contributor to LPS damage, the release of proinflammatory cytokines was also measured in this study. ELISA assay showed that CR significantly decreased the LPS-induced release of four proinflammatory cytokines (Figure 8(c)). NF-κB plays a crucial role in modulating synovial inflammation and joint destruction. Immunofluorescence results were shown in Figure 8(d), indicating that the activated NF-κB P65 in MH7A cells was significantly translocated into the nucleus after LPS treatment. However, this translocation effect was restrained by CR.

3.8. CR Ameliorated LPS-Induced Oxidative Stress in MH7A Cells. The effect of CR treatment on ROS overproduction in LPS-stimulated MH7A cells was determined by the DHE probe. The results showed that ROS accumulation in 1 μg/mL LPS-induced cells increased dramatically compared with

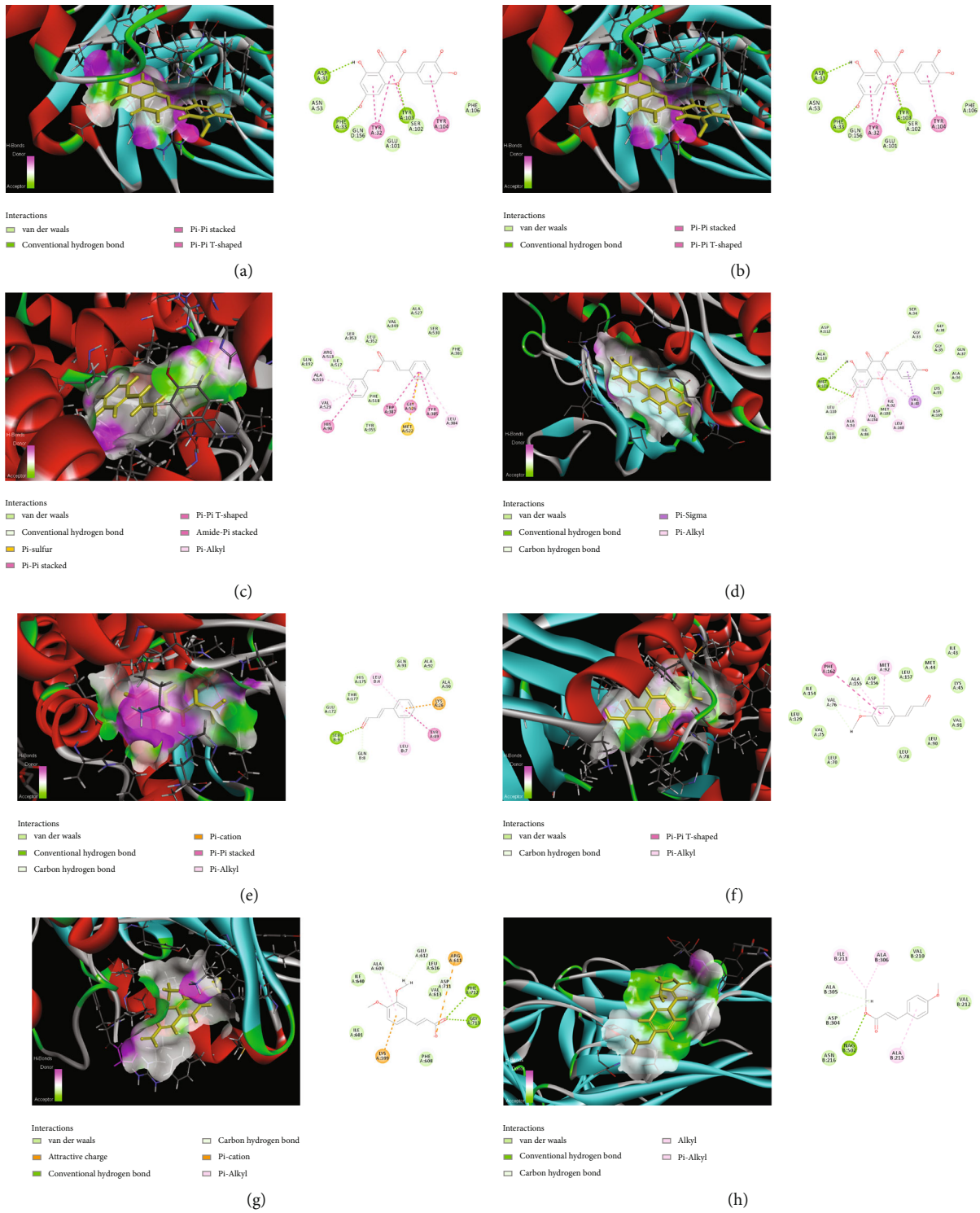

Figure 7: Continued.

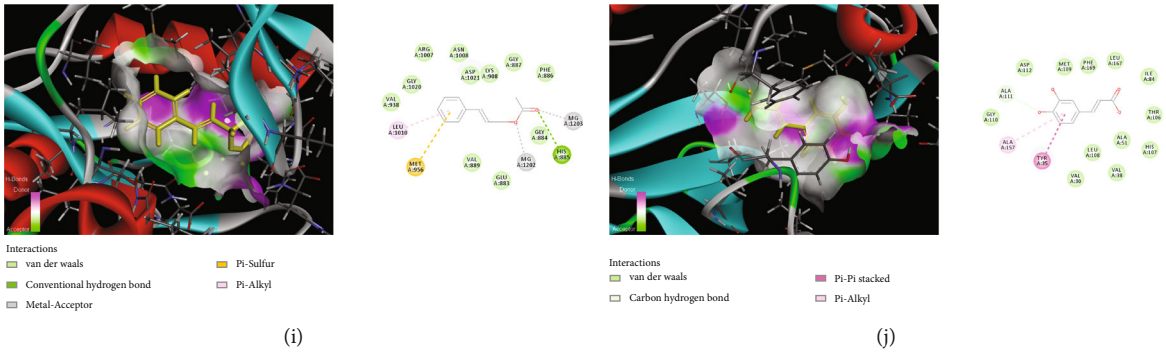

Figure 7: Molecular docking results of the 10 hub genes and the top 10 bioactive compounds: (a) IL6 and 44, (b) MAPK8 and 47, (c) PTGS2 and 33, (d) JUN and 47, (e) CCL5 and 10, (f) STAT1 and 42, (g) FOS and 54, (h) IL1R1 and 51, (i) SOCS3 and 14, and (j) MAPK14 and 41.

normal cells. However, CR treatment significantly reduced the intracellular ROS production in LPS-induced MH7A cells (Figure 9(a)). In addition, the antioxidant activity of CR was evaluated by determining the contents of antioxidant enzymes SOD, CAT, GSH-Px, and lipid peroxidation product MDA in LPS-induced MH7A cells. As shown in Figure 9(b), the MDA content of MH7A cells was significantly increased after LPS treatment, while activities of SOD, CAT, and GSH-Px were decreased. Nevertheless, the level of MDA was significantly downregulated and the activities of SOD, CAT, and GSH-Px were upregulated after CR treatment, indicating CR at different doses exerted therapeutic effects. These results suggested that CR could balance the LPS-induced oxidative stress in MH7A cells, which might be associated with the increased ROS scavenging enzyme activity.

4. Discussion

Cinnamomi Ramulus is a commonly prescribed Chinese medicine for arthritis treatment. There are many effective antiarthritis prescriptions containing CR in the Chinese Pharmacopoeia, and some studies on the anti-inflammatory and antiarthritic effects of CR in animal models of RA have been published. Notably, in addition to CR volatile oil and its extracts significantly alleviating inflammation and pain in CFA-induced chronic arthritis rats, active components such as cinnamaldehyde in CR volatile oil could also reduce RA symptoms by ameliorating oxidative stress and the release of inflammatory factors [14, 15]. However, due to the complex chemical composition of CR, its potential active components and the exact pharmacological mechanism for the treatment of RA remain difficult to elucidate. In our study, a comprehensive investigation approach integrating the CIA rat model, GC-MS, UPLC-Q Exactive-MS analysis, and bioinformatics were adopted to reveal the material basis and molecular mechanism of CR for RA treatment, and corresponding *in vitro* data were provided for verification.

A CIA rat model with similar clinical symptoms and pathological changes to RA was used for the *in vivo* exploration. Compared with the normal group, CIA rats showed obvious arthritis symptoms such as joint swelling, increased paw volume, and arthritic index. Since the initial phase of RA involves an imbalance of proinflammatory and anti-inflammatory cytokine activities, increasing proinflammatory cytokines such as TNF-α, IL-6, and IL-17 could stimulate inflammation and degradation of bone and cartilage [43]. Therefore, analysis of the expression of inflammatory cytokines has been deemed an important index to study the occurrence of RA. In this study, ELISA results showed that serum levels of inflammatory cytokines TNF-α, IL-17A, IL-1β, and IL-6 in CIA rats were higher than in the normal group, while MTX and CR extract significantly reversed these changes. In addition to inflammatory factors, the total ROS in peripheral blood and synovial tissue of RA patients were also significantly increased. After ROS inhibitor treatment, the expression of inflammatory cytokines in RA-FLS was distinctly inhibited [44]. As part of the endogenous antioxidant system, SOD, CAT, and GSH-Px protect tissues from oxidative damage by scavenging free radical superoxides. MDA is a decomposition product of lipid hydroperoxides and is correlated with the increased oxidative stress activity in inflammatory sites [45]. Our study demonstrated that CR attenuated the lipid peroxidation, enhanced the activity of antioxidant defense enzymes, and inhibited the oxidative stress state in RA rats. The H&E and safranin O-fast green staining results revealed that the cartilage tissue structure in the model group was significantly changed with hyperplastic and disordered synovial cells and infiltrating inflammatory cells, while CR extract could improve these pathological changes. Micro-CT scanning imaging results demonstrated that normal rats had obvious articular space, clear articular structure, and no bone erosion or hyperplasia changes, while CIA rats presented bone erosion-like changes, coarse articular surface, and notably narrowed joint space. After CR treatment, only slight erosive changes and joint space narrowing were observed in CIA rats.

Furthermore, 63 compounds were identified from the volatile oil and extract of CR, among which cinnamaldehyde, caffeic acid, benzyl cinnamate, cinnamyl acetate, 4-methoxy-cinnamaldehyde, and quercetin were closely correlated with anti-RA bioactivity. Cinnamaldehyde effectively ameliorated oxidative stress and inflammation in RA rats by activating enzymatic antioxidants and inhibiting the

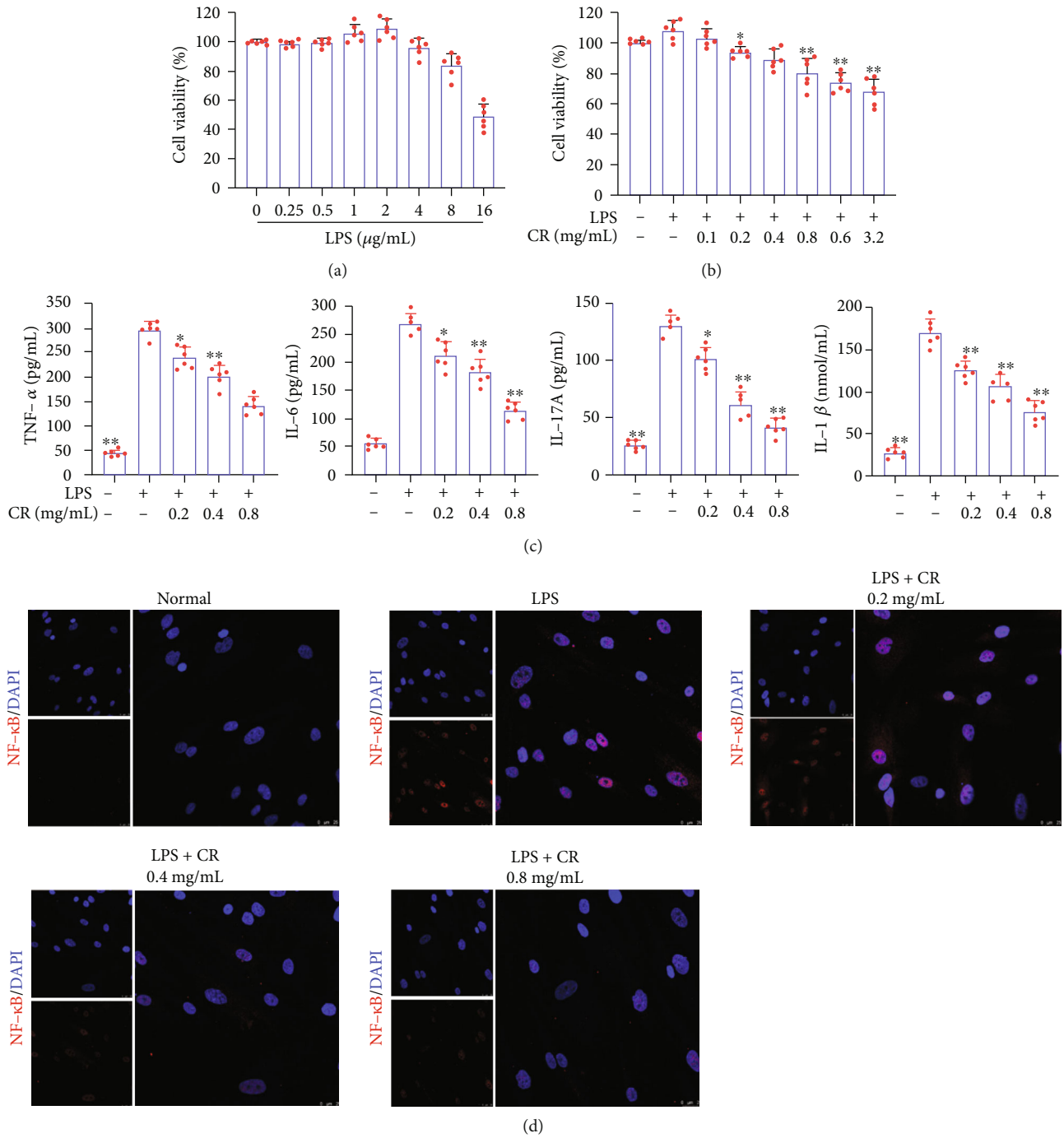

Figure 8: CR inhibited inflammation in LPS-induced MH7A cells. (a) The cell viability of MH7A cells treated with various doses of LPS for 6 h. (b) The cell viability of LPS-induced MH7A cells treated with different concentrations of CR for 24 h. (c) Effects of CR extract on the levels of proinflammatory cytokines (TNF-α, IL-17A, IL-6, and IL-1β) in LPS-induced MH7A cells. (d) Effect of CR on LPS-induced nuclear translocation of NF-κB p65. Data are expressed as mean ± SD; $^{*}p < 0.05$, $^{**}p < 0.01$ vs. the model group.

release of pro-inflammatory factors (TNF-α, IL-6, and IL-10) [14]. Caffeic acid not only mitigated adjuvant-induced paw edema and inflammatory cell infiltration in arthritic rats but also lowered the paw expression of NF-κB, chitinase-3-like protein-1, and angiogenesis [46]. Quercetin provided better protection against arthritis than MTX in terms of body weight, edema, joint damage, and cytokine production in mice [47]. Multiple compounds of CR acted on multiple targets at the same time, indicating that the anti-RA effect of CR was realized through the synergistic interaction of its compounds. IL6, MAPK8, PTGS2, JUN, and CCL5 were the core target proteins of CR for the treatment of RA. IL-6 is a highly expressed proinflammatory cytokine in the rheumatoid synovium, causing inflammation, pannus formation, and cartilage destruction. As an established target for the treatment of RA, its receptor

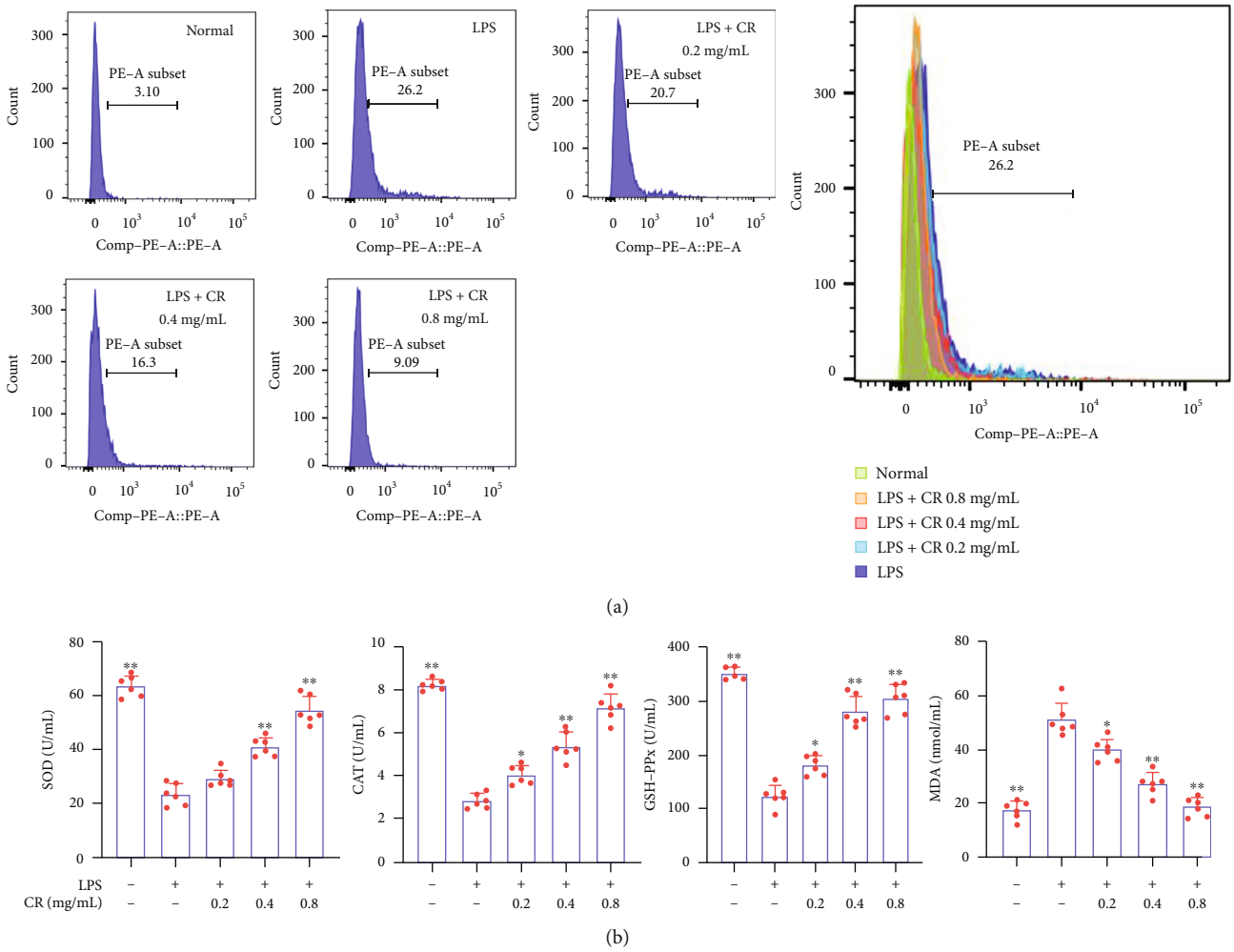

Figure 9: CR maintained redox balance in LPS-induced MH7A cells. (a) Effects of CR extract on ROS levels in LPS-stimulated MH7A cells. (b) Effects of CR extract on SOD, CAT, GSH-Px, and MDA levels in LPS-induced MH7A cells. Data are expressed as mean ± SD; $^{*}p < 0.05$, $^{**}p < 0.01$ vs. the model group.

antagonist tocilizumab has been widely accepted in the market [48]. The mitogen-activated protein kinase (MAPKs) signaling cascade is involved in the inflammation and tissue destruction of RA [49]. C-Jun N-terminal kinase (JNK) is highly activated in RA fibroblast-like synovial cells and synovium, which participated in cellular inflammation and cartilage degradation [50]. Selective cyclooxygenase-2 (COX-2) inhibitors (such as celecoxib) are commonly utilized to treat RA due to their significant anti-inflammatory, analgesic, and antipyretic activities [51]. Chemokine (C-C motif) ligand 5 (CCL5) regulates the immunopathological mechanism of RA joint inflammation and also increases MMP expression to induce collagen degradation [52]. The main compounds in CR binded well to these core proteins, which was further confirmed by molecular docking. These results provide supporting evidence that cinnamaldehyde, caffeic acid, benzyl cinnamate, cinnamyl acetate, 4-methoxy-cinnamaldehyde, and quercetin may be the main active compounds of CR in the treatment of RA, as they affect most of the targets associated with RA.

The actions of CR on RA are primarily based on effective pathophysiological mechanisms. According to the functional enrichment analysis results, CR interferes with the occurrence and development of RA mainly through the TNF signaling pathway, osteoclast differentiation, IL-17 signaling pathway, apoptosis, Th17 cell differentiation, and NF-kappa B signaling pathway. TNF is a pleiotropic cytokine widely involved in multiple aspects of RA modulation, and anti-TNF biological therapy has been deemed a second-line treatment for RA after methotrexate [53]. High levels of IL-17 produced by Th17 cells in RA promote osteoclast formation, bone resorption, marginal erosions, and release of other proinflammatory cytokines [54]. NF-κB is an important regulator of inflammatory response and immune stability, controlling normal development and the pathological destruction of cartilage. Meanwhile, NF-κB pathway is the major upstream signaling pathway controlling the production of TNF-α, IL-1β, IL-6, and IL-17A [55]. In the current study, MH7A cells were treated with LPS to establish the RA cell model. LPS stimulated MH7A cells to generate proinflammatory cytokines, such as TNF-α, IL-1β, IL-6, and IL-17A, and increased NF-κB P65 nuclear translocation. However, cells treated with CR significantly attenuated LPS-triggered inflammatory damage. RA symptoms are also

attributed to oxidative imbalance, with ROS resulting in altered chondrocyte metabolic function, which subsequently leads to impaired extracellular matrix synthesis and activation of inflammatory-related events [56]. Consequently, in addition to the inflammatory pathway, we further observed that CR treatment could upregulate the activities of SOD, CAT, and GSH-Px and downregulate the levels of ROS and MDA in a concentration-dependent manner, indicating that CR maintained ROS homeostasis in MH7A cells. Therefore, these results suggested that inhibition of ROS-NF-κB-related inflammation and oxidative damage is an effective pathway for CR to relieve RA.

5. Conclusion

In summary, the present study revealed the protective effect of CR on experimental RA cartilage destruction and inflammation. Specifically, its effects against RA were mediated via improving synovial hyperplasia and inflammation, reducing ROS-mediated lipid peroxidation, and enhancing antioxidant defense mechanisms. Hopefully, this study may also provide useful insight for screening and investigating the complex pharmacodynamic components and mechanisms of natural medicine.

Abbreviations

BP:	Biological process
CC:	Cellular component
CIA:	Type II collagen-induce arthritis
CR:	*Cinnamomi Ramulus*
CXCL8:	C-X-C motif chemokine ligand 8
DAVID:	Database for Annotation, Visualization and Integrated Discovery
DMARDs:	Disease-modifying antirheumatic drugs
EDTA:	Ethylenediaminetetraacetic acid
ELISA:	Enzyme-linked immunosorbent assays
ESI:	Electrospray ionization
GC-MS:	Gas chromatography-mass spectrometry
GEO:	Gene Expression Ominibus
GO:	Gene Ontology
H&E:	Hematoxylin and eosin
IL:	Interleukin
KEGG:	Kyoto Encyclopedia of Genes and Genomes
MAPK:	Mitogen-activated protein kinase
MF:	Molecular function
MMP:	Matrix metalloproteinases
MTX:	Methotrexate
NIST:	National Institute of Standards and Technology
NSAIDs:	Nonsteroidal anti-inflammatory drugs
PDB:	Protein Data Bank
PPI:	Protein-protein interaction
RA:	Rheumatoid arthritis
STRING:	Search Tool for the Retrieval of Interacting Genes/Proteins
TCM:	Traditional Chinese medicine
TCMSP:	Traditional Chinese medicine systems pharmacology database and analysis platform
TNF:	Tumor necrosis factor
UPLC-Q Exactive-MS:	Ultraperformance liquid chromatography-Q Exactive Orbitrap-mass spectrometry.

Data Availability

The datasets generated for this study are available.

Conflicts of Interest

There are no conflicts of interest associated with this paper.

Authors' Contributions

Jia Liu and Qing Zhang contributed equally to this paper, and both should be considered the first author. Qing Zhang, Qiang Ren, and Yunhui Chen conceived and designed this paper. Jia Liu, Qing Zhang, Yuanyuan Chen, Lingyu Wang, and Ting Tao completed the experiments. Jia Liu, Qing Zhang, and Yunhui Chen drafted the paper. Yunhui Chen and Xiuping Chen reviewed and edited the paper. All authors have read and approved the final submitted manuscript.

Acknowledgments

The research was supported by the International Cooperation and Exchange Project of Science & Technology Department of Sichuan Province (No. 2017HH0004), the National Natural Science Foundation of China (No. 81603537), and the Sichuan Provincial Administration of Traditional Chinese Medicine (No. 2021MS464). The authors thank Jiayi Sun (Innovative Institute of Chinese Medicine and Pharmacy, Chengdu University of Traditional Chinese Medicine, Chengdu, China) for his technological assistance in fluorescence microscope and flow cytometry analysis.

References

[1] D. van der Woude and A. H. M. van der Helm-van Mil, "Update on the epidemiology, risk factors, and disease outcomes of rheumatoid arthritis," *Best Practice & Research Clinical Rheumatology*, vol. 32, no. 2, pp. 174–187, 2018.

[2] Q. Zhang, J. Liu, M. Zhang et al., "Apoptosis induction of fibroblast-like synoviocytes is an important molecular-mechanism for herbal medicine along with its active components in treating rheumatoid arthritis," *Biomolecules*, vol. 9, no. 12, p. 795, 2019.

[3] D. Dragos, M. Gilca, L. Gaman et al., "Phytomedicine in joint disorders," *Nutrients*, vol. 9, no. 1, p. 70, 2017.

[4] M. Abbasi, M. J. Mousavi, S. Jamalzehi et al., "Strategies toward rheumatoid arthritis therapy; the old and the new,"

Journal of Cellular Physiology, vol. 234, no. 7, pp. 10018–10031, 2019.

[5] Q. Zhang, W. Peng, S. Wei et al., "*Guizhi-Shaoyao-Zhimu* decoction possesses anti-arthritic effects on type II collagen-induced arthritis in rats *via* suppression of inflammatory reactions, inhibition of invasion & migration and induction of apoptosis in synovial fibroblasts," *Biomedicine & Pharmacotherapy*, vol. 118, article 109367, 2019.

[6] J. Liu, Q. Zhang, R. L. Li et al., "The traditional uses, phytochemistry, pharmacology and toxicology of *Cinnamomi ramulus*: a review," *The Journal of Pharmacy and Pharmacology*, vol. 72, no. 3, pp. 319–342, 2020.

[7] F. Xu, D. Wang, and N. Zeng, "Review on chemical components of *Rimulus cinnamon* essential oil," *Natural Product Research and Development*, vol. 29, no. 3, pp. 532–541, 2017.

[8] L. Sun, S. B. Zong, J. C. Li et al., "The essential oil from the twigs of *Cinnamomum cassia* Presl alleviates pain and inflammation in mice," *Journal of Ethnopharmacology*, vol. 194, pp. 904–912, 2016.

[9] J. Lee and S. Lim, "Anti-inflammatory, and anti-arthritic effects by the twigs of *Cinnamomum cassia* on complete Freund's adjuvant-induced arthritis in rats," *Journal of Ethnopharmacology*, vol. 278, article 114209, 2021.

[10] J. Liu, Q. Zhang, R. L. Li et al., "Anti-proliferation and anti-migration effects of an aqueous extract of *Cinnamomi ramulus* on MH7A rheumatoid arthritis-derived fibroblast-like synoviocytes through induction of apoptosis, cell arrest and suppression of matrix metalloproteinase," *Pharmaceutical Biology*, vol. 58, no. 1, pp. 863–877, 2020.

[11] C. Xu, L. B. Meng, Y. C. Duan et al., "Screening and identification of biomarkers for systemic sclerosis via microarray technology," *International Journal of Molecular Medicine*, vol. 44, no. 5, pp. 1753–1770, 2019.

[12] F. Lu, D. Wang, R. L. Li, L. Y. He, L. Ai, and C. J. Wu, "Current strategies and technologies for finding drug targets of active components from traditional Chinese medicine," *Frontiers in Bioscience-Landmark*, vol. 26, no. 9, pp. 572–589, 2021.

[13] F. Gao, Q. Yuan, P. Cai et al., "Au clusters treat rheumatoid arthritis with uniquely reversing cartilage/bone destruction," *Advanced Science*, vol. 6, no. 7, article 1801671, 2019.

[14] S. Mateen, S. Shahzad, S. Ahmad et al., "Cinnamaldehyde and eugenol attenuates collagen induced arthritis via reduction of free radicals and pro-inflammatory cytokines," *Phytomedicine*, vol. 53, pp. 70–78, 2019.

[15] A. A. Azouz, E. Saleh, and A. A. Abo-Saif, "Aliskiren, tadalafil, and cinnamaldehyde alleviate joint destruction biomarkers; MMP-3 and RANKL; in complete Freund's adjuvant arthritis model: Downregulation of IL-6/JAK2/STAT3 signaling pathway," *Saudi Pharmaceutical Journal*, vol. 28, no. 9, pp. 1101–1111, 2020.

[16] P. Liu, J. Wang, W. Wen et al., "Cinnamaldehyde suppresses NLRP3 derived IL-1β via activating succinate/HIF-1 in rheumatoid arthritis rats," *International Immunopharmacology*, vol. 84, article 106570, 2020.

[17] X. Li and Y. Wang, "Cinnamaldehyde attenuates the progression of rheumatoid arthritis through down-regulation of PI3K/AKT signaling pathway," *Inflammation*, vol. 43, no. 5, pp. 1729–1741, 2020.

[18] D. Meng, J. Li, H. Li, and K. Wang, "Salvianolic acid B remits LPS-induced injury by up-regulating miR-142-3p in MH7A cells," *Biomedicine & Pharmacotherapy*, vol. 115, article 108876, 2019.

[19] X. Deng, Q. Liao, X. Xu et al., "Analysis of essential oils from Cassia bark and Cassia twig samples by GC-MS combined with multivariate data analysis," *Food Analytical Methods*, vol. 7, no. 9, pp. 1840–1847, 2014.

[20] P. N. Kaul, A. K. Bhattacharya, B. R. R. Rao, K. V. Syamasundar, and S. Ramesh, "Volatile constituents of essential oils isolated from different parts of cinnamon (Cinnamomum zeylanicum Blume)," *Journal of Science and Food Agriculture*, vol. 83, no. 1, pp. 53–55, 2003.

[21] C. J. Xu, Y. Z. Liang, Y. Q. Song, and J. S. Li, "Resolution of the essential constituents of *Ramulus cinnamomi* by an evolving chemometric approach," *Fresenius' Journal of Analytical Chemistry*, vol. 371, no. 3, pp. 331–336, 2001.

[22] Y. G. Zhang, H. Kan, S. X. Chen et al., "Comparison of phenolic compounds extracted from *Diaphragma juglandis* fructus, walnut pellicle, and flowers of *Juglans regia* using methanol, ultrasonic wave, and enzyme assisted-extraction," *Food Chemistry*, vol. 321, article 126672, 2020.

[23] R. Flamini, A. Dalla Vedova, D. Cancian, A. Panighel, and M. De Rosso, "GC/MS-positive ion chemical ionization and MS/MS study of volatile benzene compounds in five different woods used in barrel making," *Journal of Mass Spectrometry*, vol. 42, no. 5, pp. 641–646, 2007.

[24] N. Sahu, S. Meena, V. Shukla et al., "Extraction, fractionation and re-fractionation of *Artemisia nilagirica* for anticancer activity and HPLC-ESI-QTOF-MS/MS determination," *Journal of Ethnopharmacology*, vol. 213, pp. 72–80, 2018.

[25] A. Aliboni, A. D'Andrea, and P. Massanisso, "Propolis specimens from different locations of Central Italy: chemical profiling and gas chromatography-mass spectrometry (GC-MS) quantitative analysis of the allergenic esters benzyl cinnamate and benzyl salicylate," *Journal of Agricultural and Food Chemistry*, vol. 59, no. 1, pp. 282–288, 2011.

[26] P. Y. Chen, J. W. Yu, F. L. Lu, M. C. Lin, and H. F. Cheng, "Differentiating parts of Cinnamomum cassia using LC-qTOF-MS in conjunction with principal component analysis," *Biomedical Chromatography*, vol. 30, no. 9, pp. 1449–1457, 2016.

[27] J. Palandra, J. Prusakiewicz, J. S. Ozer, Y. Zhang, and T. G. Heath, "Endogenous ethanolamide analysis in human plasma using HPLC tandem MS with electrospray ionization," *Journal of Chromatography B, Analytical Technologies in the Biomedical and Life Sciences*, vol. 877, no. 22, pp. 2052–2060, 2009.

[28] A. M. Zaher, A. M. Moharram, R. Davis, P. Panizzi, M. A. Makboul, and A. I. Calderón, "Characterisation of the metabolites of an antibacterial endophyte *Botryodiplodia theobromae* Pat. of *Dracaena draco* L. by LC-MS/MS," *Natural Product Research*, vol. 29, no. 24, pp. 2275–2281, 2015.

[29] S. Gouveia-Figueira and M. L. Nording, "Development and validation of a sensitive UPLC-ESI-MS/MS method for the simultaneous quantification of 15 endocannabinoids and related compounds in milk and other biofluids," *Analytical Chemistry*, vol. 86, no. 2, pp. 1186–1195, 2014.

[30] L. S. Castillo-Peinado, M. A. López-Bascón, A. Mena-Bravo, M. D. Luque de Castro, and F. Priego-Capote, "Determination of primary fatty acid amides in different biological fluids by LC-MS/MS in MRM mode with synthetic deuterated standards: influence of biofluid matrix on sample preparation," *Talanta*, vol. 193, pp. 29–36, 2019.

[31] J. Chen, S. Mangelinckx, H. Lü, Z. T. Wang, W. L. Li, and N. De Kimpe, "Profiling and elucidation of the phenolic

compounds in the aerial parts of *Gynura bicolor* and G. *divaricata* collected from different Chinese origins," *Chemistry & Biodiversity*, vol. 12, no. 1, pp. 96–115, 2015.

[32] M. H. Liu, Q. Zhang, Y. H. Zhang, X. Y. Lu, W. M. Fu, and J. Y. He, "Chemical analysis of dietary constituents in Rosa roxburghii and Rosa sterilis fruits," *Molecules*, vol. 21, no. 9, p. 1204, 2016.

[33] G. Zengin, M. F. Mahomoodally, G. Rocchetti et al., "Chemical characterization and bioactive properties of different extracts from Fibigia clypeata, an unexplored plant food," *Food*, vol. 9, no. 6, p. 705, 2020.

[34] X. C. Liu, L. G. Zhou, Z. L. Liu, and S. S. Du, "Identification of insecticidal constituents of the essential oil of Acorus calamus rhizomes against Liposcelis bostrychophila Badonnel," *Molecules*, vol. 18, no. 5, pp. 5684–5696, 2013.

[35] G. Zengin, A. Uysal, A. Diuzheva et al., "Characterization of phytochemical components of *Ferula halophila* extracts using HPLC-MS/MS and their pharmacological potentials: a multifunctional insight," *Journal of Pharmaceutical and Biomedical Analysis*, vol. 160, pp. 374–382, 2018.

[36] Y. Nishidono, T. Fujita, A. Kawanami, M. Nishizawa, and K. Tanaka, "Identification of PGC-1α activating constituents in Zingiberaceous crude drugs," *Fitoterapia*, vol. 122, pp. 40–44, 2017.

[37] H. He, L. Qin, Y. Zhang et al., "3,4-Dimethoxycinnamic acid as a novel matrix for enhanced in situ detection and imaging of low-molecular-weight compounds in biological tissues by MALDI-MSI," *Analytical Chemistry*, vol. 91, no. 4, pp. 2634–2643, 2019.

[38] K. P. Cheiran, V. P. Raimundo, V. Manfroi et al., "Simultaneous identification of low-molecular weight phenolic and nitrogen compounds in craft beers by HPLC-ESI-MS/MS," *Food Chemistry*, vol. 286, pp. 113–122, 2019.

[39] D. Leyva, R. Jaffe, and F. Fernandez-Lima, "Structural characterization of dissolved organic matter at the chemical formula level using TIMS-FT-ICR MS/MS," *Analytical Chemistry*, vol. 92, no. 17, pp. 11960–11966, 2020.

[40] S. Oelschlaegel, M. Gruner, P. N. Wang, A. Boettcher, I. Koelling-Speer, and K. Speer, "Classification and characterization of manuka honeys based on phenolic compounds and methylglyoxal," *Journal of Agricultural and Food Chemistry*, vol. 60, no. 29, pp. 7229–7237, 2012.

[41] G. P. Lv, W. H. Huang, F. Q. Yang, J. Li, and S. P. Li, "Pressurized liquid extraction and GC-MS analysis for simultaneous determination of seven components in Cinnamomum cassia and the effect of sample preparation," *Journal of Separation Science*, vol. 33, no. 15, pp. 2341–2348, 2010.

[42] D. Singh, Y. Y. Siew, T. I. Chong et al., "Identification of phytoconstituents in *Leea indica* (Burm. F.) Merr. leaves by high performance liquid chromatography micro time-of-flight mass spectrometry," *Molecules*, vol. 24, no. 4, p. 714, 2019.

[43] S. Mateen, A. Zafar, S. Moin, A. Q. Khan, and S. Zubair, "Understanding the role of cytokines in the pathogenesis of rheumatoid arthritis," *Clinica Chimica Acta*, vol. 455, pp. 161–171, 2016.

[44] H. R. Lee, S. J. Yoo, J. Kim, C. K. Park, and S. W. Kang, "Reduction of oxidative stress in peripheral blood mononuclear cells attenuates the inflammatory response of fibroblast-like synoviocytes in rheumatoid arthritis," *International Journal of Molecular Sciences*, vol. 22, no. 22, article 12411, 2021.

[45] S. Luo, H. Li, J. Liu et al., "Andrographolide ameliorates oxidative stress, inflammation and histological outcome in complete Freund's adjuvant-induced arthritis," *Chemico-Biological Interactions*, vol. 319, article 108984, 2020.

[46] E. M. Fikry, A. M. Gad, A. H. Eid, and H. H. Arab, "Caffeic acid and ellagic acid ameliorate adjuvant-induced arthritis in rats via targeting inflammatory signals, chitinase-3-like protein-1 and angiogenesis," *Biomedicine & Pharmacotherapy*, vol. 110, pp. 878–886, 2019.

[47] N. Haleagrahara, S. Miranda-Hernandez, M. A. Alim, L. Hayes, G. Bird, and N. Ketheesan, "Therapeutic effect of quercetin in collagen-induced arthritis," *Biomedicine & Pharmacotherapy*, vol. 90, pp. 38–46, 2017.

[48] F. Pandolfi, L. Franza, V. Carusi, S. Altamura, G. Andriollo, and E. Nucera, "Interleukin-6 in rheumatoid arthritis," *International Journal of Molecular Sciences*, vol. 21, no. 15, p. 5238, 2020.

[49] R. Wang, J. Liu, Z. Wang et al., "Mangiferin exert protective effects on joints of adjuvant-induced arthritis rats by regulating the MAPKs/NF-κB pathway of fibroblast-like synoviocytes," *International Immunopharmacology*, vol. 101, Part B, article 108352, 2021.

[50] C. Xie, J. Jiang, J. Liu, G. Yuan, and Z. Zhao, "Ginkgolide B attenuates collagen-induced rheumatoid arthritis and regulates fibroblast-like synoviocytes-mediated apoptosis and inflammation," *Annals of Translational Medicine*, vol. 8, no. 22, p. 1497, 2020.

[51] E. Alaaeldin, H. A. Abou-Taleb, S. A. Mohamad, M. Elrehany, S. S. Gaber, and H. F. Mansour, "Topical nano-vesicular spanlastics of celecoxib: enhanced anti-inflammatory effect and down-regulation of TNF-α, NF-κB and COX-2 in complete Freund's adjuvant-induced arthritis model in rats," *International Journal of Nanomedicine*, vol. 16, pp. 133–145, 2021.

[52] S. A. Agere, N. Akhtar, J. M. Watson, and S. Ahmed, "RANTES/CCL5 induces collagen degradation by activating MMP-1 and MMP-13 expression in human rheumatoid arthritis synovial fibroblasts," *Frontiers in Immunology*, vol. 8, p. 1341, 2017.

[53] J. L. Davignon, B. Rauwel, Y. Degboé et al., "Modulation of T-cell responses by anti-tumor necrosis factor treatments in rheumatoid arthritis: a review," *Arthritis Research & Therapy*, vol. 20, no. 1, p. 229, 2018.

[54] R. Kugyelka, Z. Kohl, K. Olasz et al., "Enigma of IL-17 and Th17 cells in rheumatoid arthritis and in autoimmune animal models of arthritis," *Mediators of Inflammation*, vol. 2016, Article ID 6145810, 11 pages, 2016.

[55] E. Jimi, H. Fei, and C. Nakatomi, "NF-κB signaling regulates physiological and pathological chondrogenesis," *International Journal of Molecular Sciences*, vol. 20, no. 24, p. 6275, 2019.

[56] A. R. Phull, B. Nasir, I. U. Haq, and S. J. Kim, "Oxidative stress, consequences and ROS mediated cellular signaling in rheumatoid arthritis," *Chemico-Biological Interactions*, vol. 281, pp. 121–136, 2018.

Hindawi
Oxidative Medicine and Cellular Longevity
Volume 2022, Article ID 7657876, 25 pages
https://doi.org/10.1155/2022/7657876

Review Article

The Influence of Clusterin Glycosylation Variability on Selected Pathophysiological Processes in the Human Body

Ewa Janiszewska, Agnieszka Kmieciak, Monika Kacperczyk, Aleksandra Witkowska, and Ewa Maria Kratz

Department of Laboratory Diagnostics, Division of Laboratory Diagnostics, Faculty of Pharmacy, Wroclaw Medical University, Borowska Street 211A, 50-556 Wroclaw, Poland

Correspondence should be addressed to Ewa Maria Kratz; ewa.kratz@umw.edu.pl

Received 9 March 2022; Revised 12 August 2022; Accepted 16 August 2022; Published 28 August 2022

Academic Editor: Abdur Rauf

The present review gathers together the most important information about variability in clusterin molecular structure, its profile, and the degree of glycosylation occurring in human tissues and body fluids in the context of the utility of these characteristics as potential diagnostic biomarkers of selected pathophysiological conditions. The carbohydrate part of clusterin plays a crucial role in many biological processes such as endocytosis and apoptosis. Many pathologies associated with neurodegeneration, carcinogenesis, metabolic diseases, and civilizational diseases (e.g., cardiovascular incidents and male infertility) have been described as causes of homeostasis disturbance, in which the glycan part of clusterin plays a very important role. The results of the discussed studies suggest that glycoproteomic analysis of clusterin may help differentiate the severity of hippocampal atrophy, detect the causes of infertility with an immune background, and monitor the development of cancer. Understanding the mechanism of clusterin (CLU) action and its binding epitopes may enable to indicate new therapeutic goals. The carbohydrate part of clusterin is considered necessary to maintain its proper molecular conformation, structural stability, and proper systemic and/or local biological activity. Taking into account the wide spectrum of CLU action and its participation in many processes in the human body, further studies on clusterin glycosylation variability are needed to better understand the molecular mechanisms of many pathophysiological conditions. They can also provide the opportunity to find new biomarkers and enrich the panel of diagnostic parameters for diseases that still pose a challenge for modern medicine.

1. Introduction

Each year, medical research provides a large amount of significant information that contributes to improved disease diagnosis as well as treatment development. Although the achievements of medicine provide hope and the chance for a healthier, longer life for many patients, numerous cases still pose a challenge to clinicians and researchers. One of the most important and popular directions of scientific research in medicine is based on the recognition of human disease mechanisms, including those occurring on a molecular level, the understanding of which forms the basis for the development of new personalized therapies and, as a consequence, typing more sensitive and specific biomarkers to enrich medical laboratory diagnostics. The primary aim of many research projects is to propose effective diagnostic parameters that will enable the detection of a disease in its early stages as well as to find applications for monitoring its course, making the appropriate choice of therapy, controlling the body's response to the implemented treatment and the differentiation of diseases with a similar clinical view or non-specific symptoms.

The discovery of clusterin (CLU) presence in almost all body tissues and fluids and the multidirectional biological role which it plays in the human body have become the basis of many studies concerning the use of this glycoprotein as a potential new biomarker in the diagnosis of numerous human diseases. Clusterin, also known as apolipoprotein J (ApoJ), is a glycoprotein that exists in two forms: the highly glycosylated secretory form of clusterin (sCLU) and its

intracellular nuclear form (nCLU), which is still not well characterized [1, 2]. Secretory clusterin is considered a molecule with the properties of a chaperone protein, and its activity depends on the degree of glycosylation [3, 4]. Clusterin binds to specific cell surface receptors and thus mediates many biological processes such as endocytosis and apoptosis [5, 6]. Although the biological role of clusterin remains to be fully understood, it is undeniable that increased clusterin concentrations are associated with homeostasis disorders in many pathophysiological conditions, including atherosclerosis [7], obesity [8], diabetes [9], and Alzheimer's disease (AD) [10, 11]. The analysis of scientific reports on changes in the concentration of clusterin and the degree and/or profile of its glycosylation will allow us to check whether CLU can be an additional diagnostic marker helpful in the diagnosis of various diseases.

Our review is based on literature research performed in the PubMed and Google Scholar databases using search terms and their combinations, including clusterin, clusterin glycosylation, glycoprotein glycosylation, cardiovascular diseases, metabolic diseases, male infertility, cancer, and neoplasm. As a result, over 7000 entries, published from 1983 to the present, mostly in English, were found. Finally, the 165 items, mainly from original papers, which in our opinion seemed to be most useful for our investigation, were selected. Investigations on cell lines and animal models are also covered in the present review, as their goal is usually to understand mechanisms of reactions and their interrelationships that reflect those occurring in the human body. This article comprises a review of the recently available literature concerning variability in clusterin molecular structure, with a focus on particular changes in its profile and degree of glycosylation occurring in human tissues and body fluids, analyzed in the context of the utility of these characteristics as the potential diagnostic biomarkers of selected civilizational diseases.

2. Clusterin

The name of the discussed glycoprotein was coined in 1983 by Blaschuk and coworkers, who identified a high-molecular-weight protein in the fluid of a ram testicle and named CLU for its ability to cluster Sertoli cells [12]. The human clusterin (apolipoprotein J, ApoJ) is also sometimes called a complement-lysis inhibitor (CLI) or a complement-associated protein SP-40,40, but these names are not commonly used. Clusterin is involved in many biological processes such as cell adhesion, cell membrane restoration, complement system inhibition, sperm maturation, lipid transport, and apoptosis [13]. For example, human seminal plasma proteomic analysis has demonstrated the existence of at least 43 isoforms of sCLU, the presence of which is probably related to the maintenance of homeostasis in the body [14].

2.1. Clusterin Structure. Clusterin is a heterodimeric glycoprotein with a molecular weight of about 75-80 kDa, encoded by a single gene located on the short arm of chromosome 8, near the lipoprotein lipase gene locus. The primary clusterin polypeptide chain, composed of 449 amino acids, undergoes proteolytic cleavage, resulting in the formation of alpha and beta chains. The chains are linked by five disulfide bonds and form a two-chain, antiparallel glycoprotein structure. The core of the clusterin molecule is surrounded by three amphipathic α-helices and two α-helices with a coiled-coil structure. About 30% of the molecular weight of clusterin is constituted by N-linked glycans attached to the protein structure at six specific sites. Three of them are located within the α-chain (α64Asn, α81Asn, and α123Asn) and the rest on the β-chain (β64Asn, β127Asn, and β147Asn) [15, 16]. Clusterin is present in all human body fluids: urine, blood plasma, cerebrospinal fluid, semen, and even breast milk. It possesses the ability to form oligomers and may also interact with many ligands, forming complexes of various diameter and mass. The structure of this glycoprotein is flexible due to the presence of both hydrophilic and hydrophobic regions [17]. The schematic structure of secretory clusterin is presented in Figure 1.

2.2. Clusterin Properties. Clusterin shows extracellular chaperone properties, binding to proteins damaged by various factors, such as high temperature, oxidative stress (OS), or chemical reducing compounds. The combination of clusterin with misfolded proteins is ATP-independent and leads to the formation of high molecular weight soluble complexes, which are then removed by endocytosis and lysosomal degradation. This mechanism prevents the formation of pathological aggregates and may take place both inside or outside the cells [14, 20]. Clusterin, released into the cytosol after posttranslational ER modification, interacts with misfolded proteins, forming complexes, which are subsequently degraded in proteasomes and/or autophagosomes (Figure 2). CLU secreted into extracellular matrix (ECM) generates complexes not only with misfolded proteins, but also with plasmin-generated protein fragments (PGPF), which are formed due to the action of the circulating protease, plasmin. Such complexes bind to specific cell receptors, are internalized by receptor-mediated endocytosis, and then transported to autophagosomes for degradation, as shown in Figure 3 [21]. The effect of clusterin as a chaperone protein is enhanced under the environmental conditions below pH=7 that occur during local acidosis resulting from tissue damage or inflammation. This is due to the increased exposure of clusterin's hydrophobic regions under conditions of lowered pH [22]. Stewart et al. have hypothesized that the presence of numerous hydrophilic carbohydrate groups in the clusterin structure enables its chaperone activity [23]. To confirm this hypothesis, the authors compared the structure and function of the native and deglycosylated forms of human CLU. It was proven that although the deglycosylation of clusterin does not cause significant changes in the secondary protein structure, it raises the molecules' tendency to aggregation [23]. Disturbances in the function of clusterin as a chaperone protein contribute to the development of storage diseases such as amyloidosis, atherosclerosis, Alzheimer's or Creutzfeldt-Jakob disease [14, 20]. Blood plasma CLU combines with apolipoproteins A and E to form the HDL (high density lipoprotein)

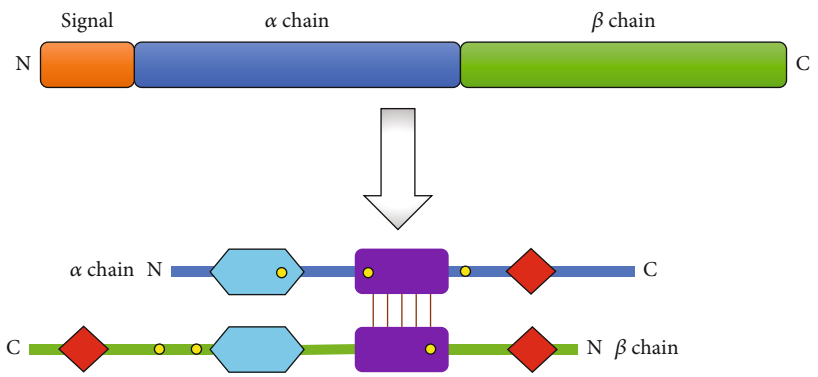

Figure 1: A scheme of the secretory isoform of clusterin. The purple color shows cysteine-rich centers connected to each other by five disulfide bounds. Two coiled-coil α-helices are indicated in blue, while three amphipathic α-helices are shown in red. N-glycosylation sites are indicated by yellow dots. Self-modification based on Wilson and Easterbrook-Smith [18] and Fini et al.[19].

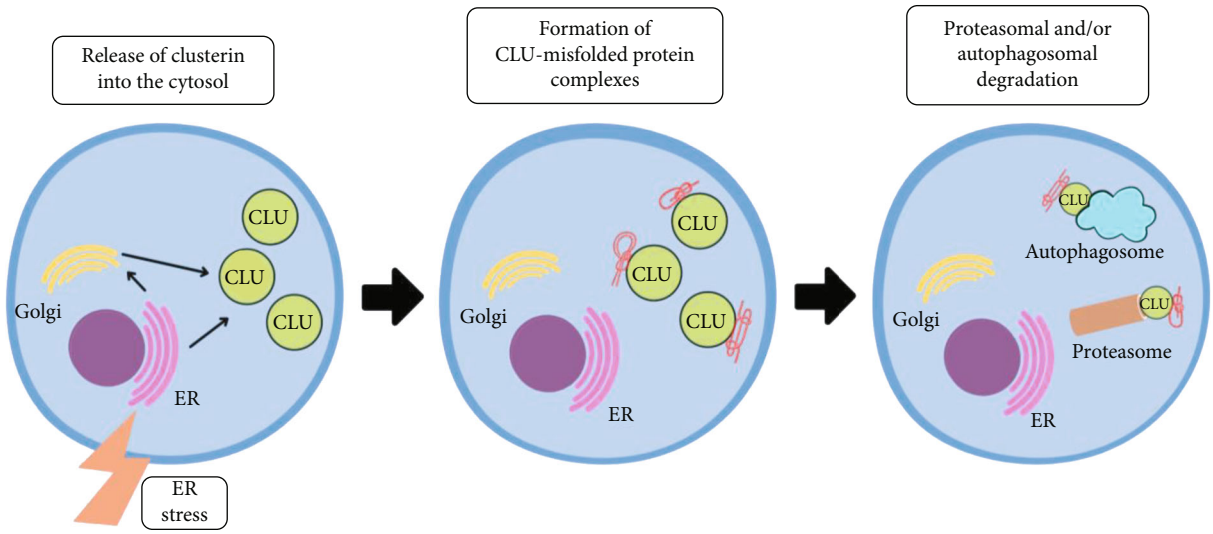

Figure 2: Schematic representation of intracellular role of CLU in misfolded protein degradation. CLU: clusterin; ER: endoplasmic reticulum. Self-modification based on Satapathy and Wilson [29] and Nizard et al. [30].

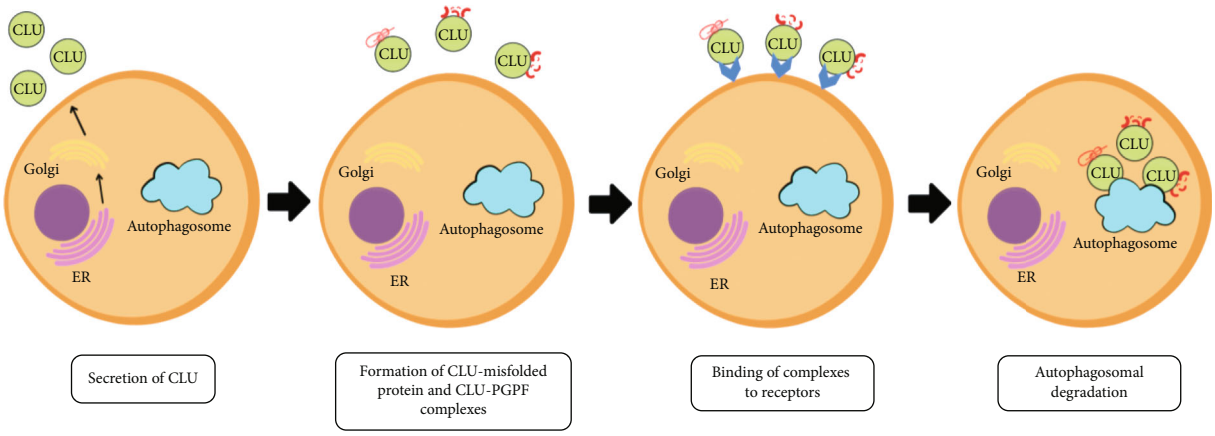

Figure 3: Schematic representation of extracellular role of CLU in misfolded protein degradation. CLU: clusterin; ER: endoplasmic reticulum; PGPF: plasmin-generated protein fragments. Self-modification based on Wyatt et al. [31].

molecule so that it can participate in the transport of cholesterol from peripheral tissues to the liver. Clusterin promotes the export of cholesterol and phospholipids from foam cells, which are characteristic of atherosclerotic lesions [24]. Clusterin is an integral component of the plasma-present C5b-9 complex which takes part in the initiation of the

complement cascade. Studies on the role of clusterin in the human body have shown its inhibitory effect on membrane attack complex (MAC) production, which prevents the lysis of cell membranes, thus protecting cells from the uncontrolled action of MAC, which leads to cell apoptosis. The presence of CLU may prevent uncontrolled attack on the cell membrane by proteins that are a part of the complement system, but also may protect the cell against other damaging factors originating from the extracellular environment [17]. It is worth paying attention to the bipolar action of clusterin. It has been documented that a decrease in CLU concentration in the heart muscle tissue is associated with reduction in the degree of its damage and the inhibition of the neuronal apoptosis process under conditions of hypoxia or ischemia. On the other hand, the decreased CLU concentration observed in immune myocarditis leads to an increase in myocardial tissue damage [16].

In the male reproductive tract, clusterin is produced by Sertoli cells and then attaches to the cell membranes of spermatids and mature sperm, taking part in the process of spermatogenesis. There are two main forms of clusterin: antiapoptotic secretory (sCLU) and nuclear (nCLU) with proapoptotic properties. Secretory clusterin protects cells against toxic factors that activate apoptosis due to the suppression of p53 and Bax protein (Bcl-2-associated X protein). Inhibition of the secretory clusterin gene expression leads to an increase in the apoptotic index [25]. The induction of clusterin gene expression was first associated with cell apoptosis in rat prostate regression. The effect of the degree of clusterin expression on cell survival and death was investigated [26]. It was reported that in human prostate cells, overexpression of clusterin provides protection against the action of TNF-α, which induces apoptosis [27]. The results of the above studies suggest that nuclear clusterin may play a cytoprotective role against epithelial cells. At this stage of the investigation, there is no clear evidence that clusterin is directly involved in the mechanism of programmed cell death or that the induction of CLU gene expression is a secondary process to apoptosis. To assess the significance of CLU in the apoptosis process, monoclonal antibodies that recognize the wild-type clusterin molecule and a unique isoform related to apoptosis were used [28]. Results of a study concerning the impact of apoptosis factors on clusterin present in Michigan Cancer Foundation 7 cells (MCF-7) confirmed that significant changes in the biogenesis of clusterin occur in the process of apoptosis and result in the appearance of a non-glycosylated CLU isoform in the cell nucleus, which initiates DNA fragmentation, proving that nCLU has proapoptotic properties [26].

The concentration of clusterin in human seminal plasma is considered a prognostic factor for regeneration of sperm production in azoospermic patients (nonobstructive azoospermia due to inhibition of sperm production). Therefore, the analysis of clusterin concentration changes in seminal plasma may be an important element in the diagnosis of male infertility linked with lack or lowered count of sperm [25]. It has been shown that antisense mutations in the CLU gene, resulting in the silencing of gene expression, may increase the chemosensitivity of prostate cancer cells, which is probably caused by blocking the antiapoptotic properties of clusterin [16].

2.3. Clusterin as DC-SIGN Ligand. The clusterin present in seminal plasma contains highly fucosylated Lewis^x (Le^x) and Lewis^y (Le^y) structures, which are responsible for its ability to bind to DC-SIGN (dendritic cell–specific intercellular adhesion molecule-3-grabbing non-integrin), a type C lectin receptor selectively expressed on dendritic cells (DCs) [32, 33]. In contrast, glycans of serum CLU contain mainly sialylated structures without Lewis-type sugar ligands [15, 33], and consequently blood plasma clusterin does not bind to the DC-SIGN receptor [32]. Seminal plasma CLU not only possesses chaperone activity similar to the blood plasma clusterin, but also addresses stress-altered proteins to the DCs via DC-SIGN. The complexes composed from clusterin and pathologically altered proteins are then processed inside the DCs and presented on their surface in antigen form (Figure 4). It is hypothesized that this mechanism may play an important role in the maintenance of immunological tolerance to paternal antigens in the fertilization process and proper pregnancy development. It should be underlined that the acquisition of female tolerance to the partner's antigens requires an active immune response that includes the participation of both DCs and regulatory T lymphocytes [34, 35]. Induction of tolerance to the semen antigens requires interaction with DCs. Steinman et al. [36] suggested that clusterin present in the seminal plasma may play a role in this interaction, promoting the endocytosis of antigens in semen by DCs via DC-SIGN. One of the most important functions of the seminal plasma clusterin is not to remove misfolded proteins from the extracellular space, but to direct these proteins to the DCs for antigen presentation, which results in immune tolerance induction [36]. The interaction of clusterin with DCs via DC-SIGN induces differentiation of dendritic cells with a tolerogenic profile (Figure 4). This process enables maternal tolerance towards male alloantigens [37].

2.3.1. The Importance of Clusterin Expression in Pathophysiological Conditions. The physiological concentration of blood plasma clusterin is about 100 μg/mL, and in semen, it is at least 20 times higher, assuming values in the range of 2-10 mg/mL [38]. However, the particular values obtained for human seminal plasma vary between different authors, which may be the result of using different methods for determination of CLU concentration, differing in sensitivity. In contrast, mean seminal plasma CLU levels obtained by Fukuda et al. [39] expressed in ng/mL (from 14.48±9.74 ng/mL in nonobstructive azoospermic patients, up to 48.31 ±38.59 ng/mL in the control group) were comparable with findings of Janiszewska et al., who reported the following mean seminal plasma CLU levels in infertile normozoospermic, teratozoospermic, asthenoteratozoospermic, and oligoasthenoteratozoospermic groups: 36.46 ng/mL, 33.08 ng/mL, 29.43 ng/mL, and 66.59 ng/mL [33]. On the other hand, the CLU levels in the blood sera of infertile patients were as follows: 21.53 μg/mL, 37.53 μg/mL, 38.25 μg/mL, and 36.73 μg/mL for normozoospermic, teratozoospermic,

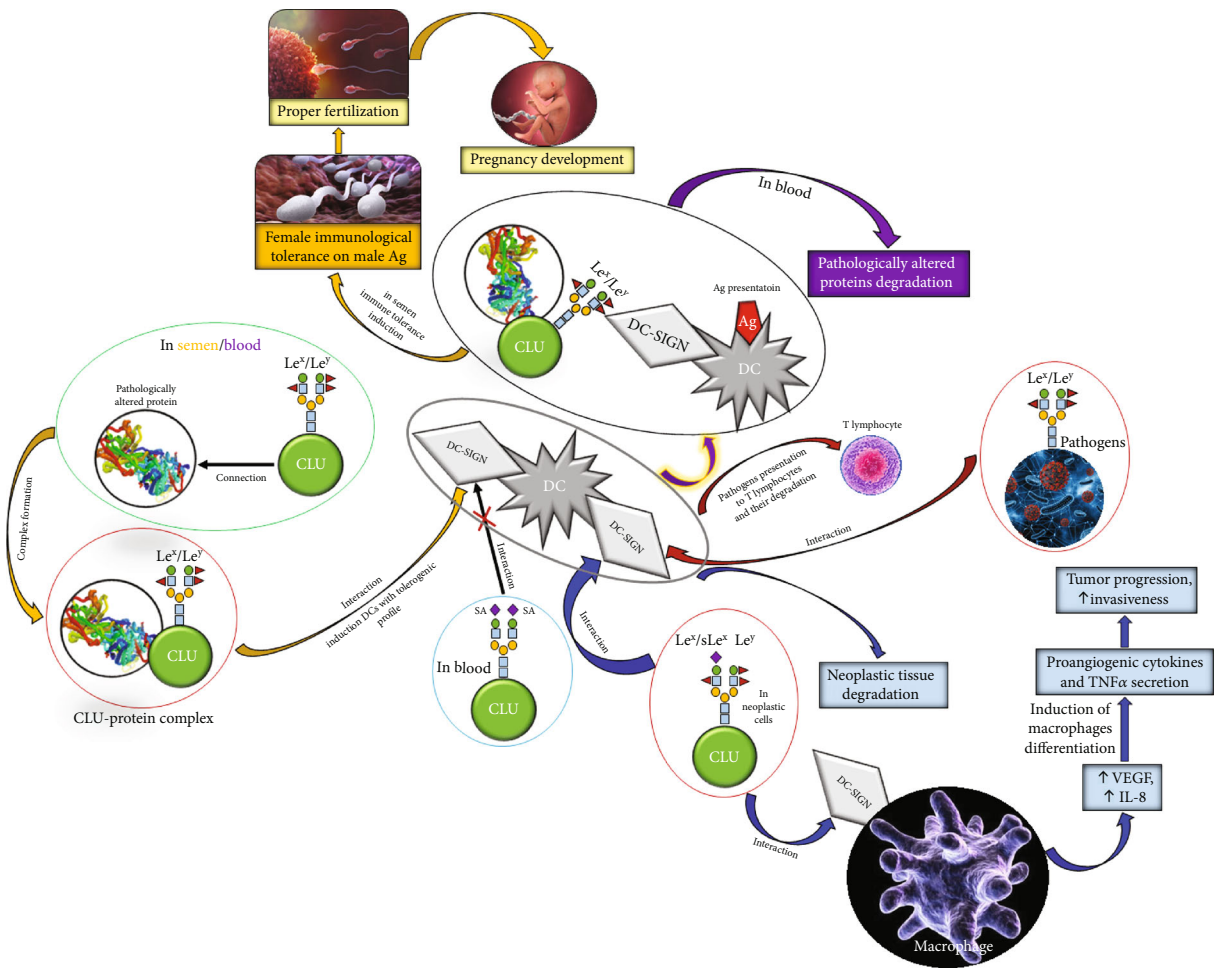

Figure 4: A scheme of the main processes occurring as a result of the interaction between CLU and DC-SIGN. Ag: antigen; CLU: clusterin; DC: dendritic cell; DC-SIGN: dendritic cell–specific intercellular adhesion molecule-3-grabbing non-integrin; IL-8: interleukin 8; VEGF: vascular endothelial growth factor; Le^X/Le^Y: $Lewis^X/Lewis^Y$ oligosaccharide structures; SA: sialic acid. Yellow arrows: CLU participation in reproduction process; purple arrows: CLU activity in the degradation of pathologically altered proteins in blood; blue arrows: CLU participation in neoplastic tissue degradation and/or tumor progression; red arrows: CLU activity in pathogens' degradation.

asthenoteratozoospermic, and oligoasthenoteratozoospermic men, respectively [33]. An increase in concentration of clusterin can be observed *inter alia* in the course of type 2 diabetes, ischemic heart disease, prostate cancer, and hepatocellular carcinoma (HCC) [40–42]. Determination of the particular role of CLU in various diseases based on changes in CLU gene expression is difficult. It is assumed that the expression of the CLU gene promotes cell survival, which may have two effects in the context of the whole organism, either beneficial, promoting neuronal survival by combating toxic agents, or detrimental, enabling tumor cells to survive. It was noticed that increased expression of the CLU gene occurs in treatment-resistant neoplasms [43]. CLU binds to low density lipoproteins such as very low density lipoproteins (VLDL) and low density lipoprotein-related protein 2 (LRP2) [44, 45]. The combination of clusterin with LRP2 induces the activation of serine-threonine kinase, also known as protein kinase B (PKB), promoting cell survival [45], and inhibits the transduction of proapoptotic signals through interaction with cell surface receptors [46].

To conclude, the issue of CLU gene expression under pathophysiological conditions, as well as its concentration in *inter alia* human blood serum and seminal plasma, is not completely defined. No simple relationship between CLU level and the expression of the CLU gene was found, and thus further studies concerning this subject are needed.

2.3.2. The Importance of Clusterin in the Formation of Neoplastic Metastases. Clusterin can play a variety of functions in carcinogenesis and tumor invasion processes [47]. First and foremost, it enables neoplastic cells to survive in places distant from the primary tumor, which makes it possible for them to form metastases [48]. Increased expression of CLU has been demonstrated in the metastatic or cancerous cells of colon, bladder, and hepatocellular carcinoma [49–51]. Miyake et al. introduced CLU complementary DNA into human renal cell carcinoma cells, which do not express a detectable level of clusterin expression, and their findings suggest that clusterin overexpression prolongs cell survival under unfavorable conditions in the metastatic

process, resulting in the enhanced metastatic potential of renal cell carcinoma, which confirms the positive effect of clusterin on neoplastic cell migration [52]. The results of the above studies, as well as the studies carried out by Chou et al. [53], proved that the increase in the expression of clusterin is associated with the degree of tumor invasiveness. Knowledge of the mechanism of metastasis formation induced by increased expression of clusterin has been used to create new anticancer therapies aimed at metastasis formation inhibition and tumor growth blockage [54]. Shiota et al. observed that overexpression of CLU is associated with low tumor histological differentiation and high advancement in clinical TNM classification (tumor node metastasis scale) [55]. The ability of clusterin to promote tumor invasion is based on epithelial-mesenchymal transition (EMT) induction [56], a process by which epithelial cells transform into mesenchymal tissue, losing the ability to adhere and gaining the possibility of moving to other parts of the body [56].

It has also been documented that clusterin increases the resistance of ovarian cancer to treatment, preventing drug interactions with neoplastic cells, thus preventing the induction of apoptosis and, consequently, the fight against cancer [57]. It has been proven that sCLU enhances the neoplastic process by facilitating Ku70 binding to the apoptotic protein Bax, as a result of which the Bax protein cannot reach the outer membrane of the mitochondria and transmit the signal to direct the cell to the apoptotic pathway [58].

Over 90% of fatal cancer cases are associated with the appearance of metastases, which are linked with lack of effective therapy—surgical treatment with adjuvant therapy is successful only in the case of primary, well-defined tumors [59, 60]. Still, many fundamental questions regarding the development of neoplastic metastases remain unanswered. It has been suggested that the determination of CLU concentration in neoplastic tissue or serum may be a potential diagnostic marker of early neoplastic metastases [61]. The results of the latest preclinical studies showed that inhibition of clusterin expression delays the development of metastases and increases sensitivity to cytotoxic chemotherapy, significantly improving the survival rate of cancer patients [62].

In summary, CLU enables neoplastic cell survival, as proven in particular in cases of colon, bladder, ovarian, and hepatocellular neoplasms. High CLU expression is also related to tumor invasiveness as well as metastasis formation, especially within the EMT mechanism. There is also some information about the potential role of CLU in treatment resistance in ovarian cancer. On the other hand, it has also been suggested that in some neoplasms, CLU concentration in serum and/or tissue may become an early metastasis biomarker.

3. The Biological Role of CLU Glycosylation

3.1. The Dependence of CLU Function as a Chaperone on Glycosylation. Clusterin is one of the few known extracellular chaperone proteins. Similarly to other chaperones, the mRNA of CLU undergoes positive regulation during heat shock [63, 64]. The organism's response to the conditions created during heat shock is reflected by increased production of proteolytic enzymes, detoxification proteins, and chaperones [65]. This is a form of defense against negative effects of UV and ionizing radiation or oxidative factors which lead to the formation of reactive oxygen species (ROS), resulting in cumulation of abnormally folded proteins [66]. Such interference disrupts protein homeostasis and may cause toxic stress. CLU, playing the chaperone role, prevents oxidative stress effects through binding with the proteins undergoing denaturation, and thus preventing their accumulation, as well as allowing them to be removed from the extracellular space [22].

Apart from extracellular secretory CLU, the cytoplasm of cells undergoing OS contains a small amount of another isoform of CLU, mainly non-glycosylated, which did not undergo proteolytic degradation, forming a dimeric structure consisting of alpha and beta subunits as in the case of sCLU formation [64]. Rohne et al. in their study [4] investigated whether intracellular CLU (iCLU) possesses chaperone properties. The authors reported that non-glycosylated iCLU cannot perform its chaperone activity. In contrast, the proper composition of antennary oligosaccharides in sCLU glycans was not obligatory to maintain the chaperone activity of this glycoprotein, whereas proper core oligosaccharide structure was crucial to maintaining its chaperone activity [4]. Debure et al. demonstrated the high sensitivity of iCLU to reducing factors, proving that intracellular forms of CLU only become active under oxidative stress conditions or in subcellular regions with altered reduction potential, e.g., in mitochondria [67]. It may be assumed that, in terms of homeostasis disturbance due to an inflammation process or other pathological conditions, iCLU may exhibit chaperone activity [67]. The results of the aforementioned research prove that CLU glycosylation is crucial to the maintenance of its function and proteolytic cleavage is the key to chaperone activity exhibition by CLU under reducing conditions, e.g., in atherosclerosis [4].

It has been proven that sCLU, as one of the few well-known extracellular chaperones, with a proper composition of core oligosaccharide structure can perform chaperone activity. Another intracellular, non-glycosylated isoform of CLU is formed in response to oxidative stress. Resistant to proteolytic cleavage, its chaperone activity is possible only under oxidative stress conditions or in subcellular regions with altered reduction potential.

3.2. The Impact of CLU Deglycosylation on the Cytotoxicity Development. Apart from sCLU, there are several variants of intracellular clusterin, which differ in their molecular weight. In cells stimulated by various factors, such as those that induce apoptosis, TGF-β (transforming growth factor β), TNF-α (tumor necrosis factor α), and ionizing radiation, the formation of reduced, nuclear forms of CLU with a molecular weight of 43-55 kDa were observed [26, 68]. Elevated nCLU expression constitutes a proapoptotic factor. Moreover, a fully non-glycosylated iCLU variant with molecular weight of 60 kDa was found in the mitochondria of human cancer cells, promoting neoplasm progression through disruption of the pro-apoptotic activity of the Bax protein [46, 69]. The differences in molecular weights

observed in iCLU forms were explained by changes in the process of posttranslational modifications caused by various factors [26].

CLU is sensitive to homeostasis disruption in the endoplasmic reticulum (ER) area, where the glycosylation process takes place [70]. Pathological factors present in the ER area disrupt the glycosylation process and lead to structural instability and/or impairment of intra- and extracellular clusterin function [71]. Kang et al. conducted studies to assess the effect of glycosylation on the accumulation of iCLU [72]. The results of these studies provide important information on the molecular basis of pathological conditions caused by impaired CLU biogenesis. To determine whether clusterin responds to stress factors within ER, researchers assessed CLU expression in cell cultures exposed to three different stress inducers of ER: dithiothreitol (DTT), thapsigargin (Tg), and tunicamycin (Tm). Western blot analysis, performed after previous electrophoresis under reducing conditions, showed the existence of two different forms of CLU: one with a mass of 60 kDa (probably a native CLU molecule) and the other with a mass of 40 kDa, which appeared to be an α subunit of the native CLU form. Moreover, DTT and Tg lowered the expression of both CLU forms, and Tm initiated the synthesis of the non-glycosylated forms with reduced solubility that were accumulated in ER [72]. The results of a study performed by Kang et al. [72] also suggested that disturbed CLU glycosylation leads to the accumulation of its abnormal molecules in ER, causing cytotoxicity with simultaneous activation of unfolded protein response (UPR)—a process of degradation of misfolded proteins which takes place in the proteasome. It has been documented that the oligosaccharides of CLU N-glycans are important determinants preventing CLU misfolding and aggregation in ER as well as N-glycans deficiency in CLU, which results in its accumulation in ER and induces cytotoxicity, which may be the cause of various diseases. The authors suggested that the discussed disorders are involved in the pathomechanism of cellular dysfunction in slowly progressive neurodegenerative diseases caused by excessive pathological protein accumulation [72].

In summary, it was documented that elevated levels of glycosylated nuclear CLU isoform have a proapoptotic effect. On the other hand, deglycosylation of CLU promotes its antiapoptotic properties. Moreover, the fully non-glycosylated CLU variant disturbs the proapoptotic activity of Bax, leading to neoplasm progression. Abnormal, disturbed, CLU glycosylation process leads to the accumulation of its abnormal form in the ER. It has been suggested that the aforementioned mechanisms lead to neurodegenerative diseases associated with excessive abnormal protein accumulation.

3.3. The Importance of Clusterin Glycosylation for Regulating the Immune System in Human Reproduction. Human seminal plasma proteome analysis expanded our current knowledge concerning the mechanisms of the fertilization process. Posttranslational modifications, including glycosylation, have a strong effect on cell-cell interactions and interactions between the inside of the cell and surface proteins, or proteins present in secretory fluids. It has been documented that the sialylated form of Le^x structures is the most important carbohydrate ligand present on the oocyte cell membrane, mediating sperm binding [73]. Another example documenting the importance of the glycosylation process is glycodelin, which in its glycosylated form is responsible for the acrosomal reaction [74]. Glycoproteins also play an important role in maternal immune response modulation, and glycans present on the sperm surface suppress the activity of maternal NK (natural killers) cells [75]. Le^x and Le^y oligosaccharide structures present in seminal plasma glycoproteins also exhibit an inhibitory effect on the female immune system [76]. Analysis of the seminal plasma glycome has made it possible to divide N-glycans into three main classes: high mannose; fucosylated bi-, tri-, and tetra-antennary Le^x and/or Le^y type oligosaccharide structures, and fucosylated and sialylated bi-, tri-, and tetra-antennary N-glycans [77].

A study by Saraswat et al. [78] enabled to establish the glycosylation profile and the glycan structure of glycoproteins present in seminal plasma, creating an opportunity to determine the role of glycoproteins in immune system modulation and gamete interaction. In subsequent studies, the same authors proved that all clusterin N-glycans were of the complex type, of which: 12 were sialylated and others, at the end of sugar antennas, contained an exposed galactose residue; 21 glycans contained Le^x/Le^a type oligosaccharide structures; another 3 had a sugar structure characteristic for the H antigen of the blood group; and one contained Le^y/Le^b oligosaccharide structures [78]. The role of seminal plasma proteins in the fertilization process has not been fully understood, and their biological function apparently includes participation in sperm protection from premature capacitation and sperm transport inside the cervix [79], as previously shown for glycosylated glycodelin, which, contrary to its non-glycosylated counterpart, inhibits the premature capacitation process [80].

A recent study by Janiszewska et al. [33] concerning blood serum and seminal plasma CLU concentration and fucosylation analysis indicates that serum CLU concentrations, as well as the expression of core fucose and antennary fucose α1,2-linked in CLU glycans, differ between an infertile normozoospermic group and groups of patients with sperm disorders and seem to be good markers for differentiation of normozoospermic men from those with sperm abnormalities. The authors [33] also suggest that disturbances in sperm count, motility, and morphology are not the only causes of male infertility. Moreover, the lack of similarities in levels of blood serum and seminal plasma CLU, as well as in fucose expression in CLU glycans, is probably due to the different mechanisms leading to CLU glycosylation in both body fluids analyzed by the authors [33].

Human clusterin is known as a ligand for DC-SIGN [78]. DC-SIGN has the ability to bind the Le^x/Le^y type oligosaccharide structures present on the surface of many pathogens and enables dendritic cells to recognize surface antigens of pathogens and present them to T lymphocytes (Figure 4) [81]. Glycosylation analysis of seminal CLU revealed that it contains Le^x/Le^a and/or Le^y/Le^b types of oligosaccharide

structures at the Asn374, Asn354, and Asn86 sites, which may indicate that clusterin is involved in immunomodulation in seminal plasma [78]. It has been proven that the major carbohydrate structure in N-glycans of zona pellucida (ZP), participating in sperm-oocyte interaction, is sialo-Le^x type, a well-known selectin ligand. Thus, any alterations in the zona pellucida glycoepitopes, as well as sperm surface glycans, may cause an unsuccessful fertilization process [73].

CLU is a very important glycoprotein in human semen that takes part in sperm maturation and thus in the fertilization process. Seminal plasma CLU, but not blood serum clusterin, expresses an extreme abundance of fucosylated glycans. These glyco-motifs enable seminal plasma clusterin to bind DC-SIGN with very high affinity. By inducing the endocytosis of stress-damaged proteins by DCs via DC-SIGN, clusterin present in seminal plasma may promote female tolerance to seminal antigens (Figure 4).

Sialo-Le^x oligosaccharide structures on the oocyte membrane are considered the main carbohydrate ligands mediating sperm binding. Moreover, it has been proven that not only Le-type oligosaccharide structures present in the glycan part of seminal plasma CLU are of crucial importance in the context of reproduction, but also the expression of core fucose differs between patients with abnormal semen parameters and those without sperm disorders. Further analyses concerning changes in glycosylation profile and degree of seminal plasma and serum CLU may shed new light on the complex mechanisms of proper fertilization processes.

3.4. The Importance of Fucosylated Clusterin in Breast Cancer. The disturbance of blood plasma clusterin expression has been documented in many types of cancer, including breast cancer [82]. Increased expression of blood plasma CLU usually correlates with negative prognosis, disease recurrence, or the development of resistance to treatment [83]. Chen et al. [84] have reported significantly higher serum CLU levels in invasive breast cancer patients in comparison to the healthy controls. Moreover, strong correlations between CLU concentration and clinical tumor stage, lymph node metastasis, shorter overall survival, and disease-free survival were observed. Patients after surgery treatment revealed lower CLU concentrations when compared to the presurgery stage. The diagnostic sensitivity and specificity of serum CLU level determinations in this study were 82.26% and 73.46%, respectively [84]. While the expression of CLU in the cytosol of neoplastic cells inhibits their apoptosis, promoting tumor growth and the development of resistance to chemotherapy, nCLU shows proapoptotic properties [1]. Secretory CLU is present in the extracellular space and body fluids, but its influence on the microenvironment of the developing tumor is poorly understood. It is worth underlining that CLU glycans in neoplastic tissues possess different glycan motives than those occurring in healthy tissues, which is often termed "abnormal glycosylation" [85].

Changes in the expression of Le structures are some of the most common alterations in protein glycosylation in neoplastic processes [86]. Neoexpression of sialo-Le^x structures makes the tumor cells capable of binding to the endothelial selectins, resulting in the formation of metastases [87]. Merlotti et al. analyzed the expression of fucosylated clusterin in breast cancer cells [88]. A tumor fragment and a piece of tumor-free tissue adjacent to the tumor were collected from each of 21 patients. Subsequent immunohistochemical analysis revealed the CLU expression, which enabled researchers to observe its presence both in the cytoplasm of tumor cells and in the apical parts of the cells of healthy tissues. The ELISA test (enzyme-linked immunosorbent assay) enabled CLU level quantification in tumor and healthy tissue samples, but there were no significant differences in clusterin concentrations between the compared groups [88]. The changes in the glycosylation profile of neoplastic tissues have been well documented, and the increased fucosylation degree of glycoproteins of neoplastic cells is probably associated with their increased invasiveness and ability to metastasis [86]. Merlotti et al. documented that breast tumor tissues are characterized by a higher expression of fucosylated CLU containing Le^x and Le^y structures in comparison to tissues without tumor transformation [88]. The authors reported that the fucosylated CLU of neoplastic cells, in contrast to the CLU present in healthy cells, has the ability to bind to DC-SIGN, proving that CLU of breast cancer cells contains fucosylated glycans of Le^x and/or Le^y type, enabling effective binding to DC-SIGN. Considering the fact that fucosylated clusterin effectively interacts with macrophages by interacting with DC-SIGN, the authors analyzed the effect of this interaction on macrophage phenotype and function. They conducted a study in which monocytes were cultured with M-CSF (macrophage colony-stimulating factor) for 5 days in the absence or presence of fucosylated CLU isolated from seminal plasma. It has been observed that the addition of fucosylated clusterin to the cell culture significantly increased the expression of angiogenic factors such as vascular endothelial growth factor (VEGF) and interleukin 8 (IL-8), suggesting that fucosylated CLU induces the differentiation of macrophages into cells that secrete proangiogenic cytokines and TNF-α. It has also been suggested that the fucosylated form of CLU produced by luminal breast cancer cells might play an important role in tumor advancement (Figure 4) [88].

It has been documented that CLU levels are associated with breast cancer development and correlate with tumor stage, lymph node metastasis, and disease-free survival as well as overall survival. After surgery, lowered CLU concentrations in comparison to the presurgery state were observed. Several studies have reported that neoplastic tissues express glycan motives distinct from those in healthy tissues. Increased CLU glycans fucosylation and sialo-Le^x expression is associated with elevated invasiveness and metastasis formation, via interactions with DC-SIGN, leading to pathological angiogenesis, as shown in Figure 4.

3.5. The Importance of Clusterin Glycoforms in Colorectal Cancer. Understanding the function of clusterin in carcinogenesis has been the subject of research for several decades. Chen et al. observed the presence of increased CLU concentrations in neoplastic cells among patients with human colorectal cancer (CRC) at an early stage of its development, i.e.,

with early intestinal lesions, benign polyps, or adenocarcinoma [89]. Pucci et al. [90] proved that increased sCLU expression in the cytoplasm of neoplastic cells also applies to patients with malignant colon tumors in the course of metastases to the lymph nodes. Many factors indicate that clusterin is involved in the mechanism of regulation of contrary processes such as cell survival and apoptosis [91], which has been observed both in colon cancer [90, 92] and other types of cancer, e.g., bladder cancer [93], kidney cancer [52], and prostate cancer [94]. It has been shown that increased expression of sCLU in neoplastic cells leads to the development of resistance to the cytotoxic pharmaceuticals used in anticancer therapy, which aim to induce apoptosis of cancer cells [95].

Chen et al. observed the presence of a correlation between the expression of an intracellular CLU isoform and tumor progression, which led to clusterin being considered a potential prognostic and predictive colon cancer marker [89]. In their study on tissue specimens, Artemaki et al. [50] showed that patients with significantly higher levels of CLU mRNA in tumors were at higher risk of recurrence or death and that the expression of CLU mRNA increased together with tumor growth and disease progression. Based on the results obtained, the authors suggested that the high levels of CLU mRNA may be usable as an adverse prognostic biomarker for disease-free survival and overall survival in colorectal cancer [50]. Rodríguez-Piñeiro et al. undertook studies related to the expression of blood plasma CLU isoforms in patients with CRC to determine whether the CLU molecule present in the blood plasma of CRC patients is altered, compared to the CLU present in the blood plasma of healthy subjects [92]. Increased concentration of sCLU and decreased expression of the deglycosylated form of nCLU were associated with increased viability of cancer cells and the possibility of metastasis [92]. Chromatographic analysis using ConA (*Concanavalin A* agglutinin, binds multimannose N-glycans, complex and hybrid type), combined with two-dimensional gel electrophoresis (2D-PAGE), enabled the isolation of two serum fractions: FI, rich in O-glycosylated proteins, but without N-glycans, and FII fraction, rich in N-glycoproteins. Anti-CLU antibodies were added to the obtained fractions and to the non-fractionated serum samples, which demonstrated the presence of heterodimeric, glycosylated 70-85 kDa clusterin molecule in the native serum samples and in the FII fraction [92]. In the FI fraction, obtained from the sera of patients with CRC, the presence of CLU with a molecular weight of about 40 kDa was additionally demonstrated. This was most likely a CLU molecule with reduced N-glycan expression (the molecular weight of the double-stranded CLU protein chain is no more than 30 kDa). As a result of deglycosylation of this 40-kDa molecule, a protein with a molecular mass of about 28 kDa was obtained, confirming previous assumptions. Structural analysis of specific CLU isoforms, isolated from the serum of patients with CRC, showed the presence of significant differences in comparison to CLU isoforms present in the control serum. In CRC patients, increased expression of five isoforms in the 40-kDa band in the FI fraction and one isoform in the FII fraction was observed, while the isoforms present in the 40-kDa band probably corresponded to the isoform detected by Pucci et al., who observed increased expression of cytoplasmic glycosylated CLU in the advanced stage of cancer with metastases to the lymph nodes [90]. This isoform has also been shown to be released into the extracellular space [90]. Rodríguez-Piñeiro et al. [92] also noted that the CLU isoforms in the 40-kDa band, present in the FI fraction isolated from the sera of CRC patients, were highly glycosylated. However, this glycosylation was probably abnormal, while their molecular mass corresponded to the molecular mass of CLU (approximately 40 kDa) described by Pucci et al. [90]. The results of studies performed by Rodríguez-Piñeiro et al. clearly show that the analysis of expression of individual CLU isoforms in the blood plasma of patients with CRC may become an effective diagnostic tool for this type of cancer [92]. Taking into account that there is still a great need for new, specific, and sensitive markers that would find application for CRC diagnosis and monitoring of its treatment, it seems justified to undertake further research on the use of CLU isoforms expression analysis for this purpose.

Several studies confirmed elevated CLU levels in neoplastic cells of colorectal cancer. The correlation between iCLU and tumor progression has also been demonstrated; thus, clusterin may become a prognostic and predictive CRC biomarker. As in the case of other tumors, the role of CLU is associated with inhibitory activity on the Bax protein. Some analysis concerning CLU structure and glycosylation revealed that patients with colorectal cancer are characterized by an increased CLU glycosylation, which was probably abnormal. Further glycomic studies will help to improve our knowledge about the molecular mechanisms concerning this issue.

3.6. The Importance of Secretory Clusterin Glycosylation in Hepatocellular Carcinoma. Hepatocellular carcinoma is one of the most common causes of death among cancer patients worldwide [96]. Factors involved in the development of HCC include chronic hepatitis B (HBV) or C (HCV), nonalcoholic steatohepatitis, and aflatoxin B1 poisoning. The prognosis of HCC patients depends on early diagnosis and the effectiveness of the selected treatment method. Despite the progress of therapy, the prognosis of patients is still poor, due to the frequent relapse of the disease after surgery and the risk of metastases. Therefore, selecting markers whose expression level would be closely related to the clinical advancement of HCC and enable the monitoring of metastasis formation is necessary to increase the chances of patients' survival [97].

Monitoring the course of liver disease, including the control of tumor cell growth, is currently based on the determination of α-fetoprotein (AFP) concentration or analysis of the degree of its glycan core fucosylation. However, AFP synthesis is associated not only with liver cancer but also with other non-oncological pathologies of this organ [98], and its secretion is not observed in all cases of HCC [99]. Therefore, more specific biomarkers useful in the diagnosis of HCC are still being sought.

In the liver, sCLU is often overexpressed in response to hypoxia, which contributes to increased risk of

carcinogenesis, metastasis formation, and multiple drug resistance (MDR) development [100]. Secretory CLU has a proven ability to inhibit cell apoptosis induced by activated Bax protein or protect liver cancer cells from death by interacting with apoptogenic glucose regulated protein 78 (GRP78) [101]. Studies in which the development of HCC in rats was induced by chemical carcinogens confirmed that differences in blood plasma and hepatic CLU expression may become specific early biomarkers of hepatocyte malignant transformation [102].

Comunale et al. analyzed the glycosylation profile of serum clusterin in the context of searching for a new specific diagnostic marker for HCC [103]. Comparison of serum CLU levels in patients with liver lesions with a control group of healthy people revealed no significant differences between the analyzed groups, and the obtained results lay within the reference values range, probably due to the deliberate selection of patients with similar clusterin concentrations for the study groups [103]. The analysis of blood serum CLU glycosylation profile using DSL lectin (DSL; *Datura stramonium* lectin), specific to β1,4-linked N-acetylglucosamine of triantennary N-glycans, in three groups of patients (HCC, cirrhosis and control) showed a significant decrease in the expression of triantennary N-glycans in serum samples of HCC patients in comparison to controls and cirrhosis patients. In contrast, no significant differences in the glycosylation profile of CLU between patients with different stages of HCC were observed. In addition, it was noted that a reduction of expression of clusterin β1,4-triantennary N-glycans in HCC patients was accompanied by an increase in the expression of biantennary N-glycans [103, 104], which may have been caused by decreased expression of N-acetylglucosamine transferase IV, an enzyme which initiates the formation of an additional third branch on the biantennary glycan, resulting in the formation of triantennary glycan [105]. In conclusion, the analysis of the degree of β1,4-linked triantennary glycan expression in clusterin, together with the determination of AFP concentration, can be used as a screening test for patients at high risk of developing HCC as well as for monitoring the treatment of HCC patients and possible recurrence of the disease [103].

In summary, current literature data concerning the role of sCLU in HCC indicates that an increase of sCLU levels in the blood serum and liver may become an early marker of malignant transformation of hepatocytes and increased sCLU levels may also suggest disease progression. Another promising aspect of CLU examination in the context of liver cancer development is the analysis of its glycosylation profile. Up to date, decreased expression of triantennary N-glycans together with an increase of biantennary N-glycans in patients with HCC was revealed. Further studies in this field may not only shed new light on the molecular processes associated with hepatocellular carcinoma pathogenesis but may also contribute to the invention of some new HCC biomarkers. The role of sCLU in the development of liver cancer is schematically presented in Figure 5.

3.7. The Importance of the Clusterin Glycopeptide Variant in Clear Cell Renal Cell Carcinoma. Clear cell renal cell carcinoma (ccRCC) is the most common and at the same time the most aggressive renal cancer, representing 75% of cases of neoplasms of this organ. Patients with genetically determined Von Hippel-Lindau syndrome (retinal-cerebellar angioma) are particularly at risk of developing ccRCC. Clear cell renal cell carcinoma is characterized by rapid growth and metastasis formation; therefore, increasing emphasis is being placed on the identification of new markers for early detection and/or prediction of disease recurrence. Most often ccRCC is diagnosed accidentally during ultrasound or computed tomography. Detection of this cancer at an early stage enables surgical treatment to take place, while therapeutic options for advanced ccRCC are severely limited [106].

The low blood concentrations of potentially diagnostically relevant glycoproteins pose a difficult challenge for glycoproteomic studies. In addition, the observed variability of glycans attachment at many different glycosylation sites of N-glycoprotein (macroheterogeneity) and variability in the profile and degree of N-glycan expression at one or more glycosylation sites (microheterogeneity) further complicate this analysis. The most common method of N-glycosylation analysis is the determination of oligosaccharide or glycopeptide profile. Oligosaccharide profile analysis is based on the release of a single N-glycan from a purified glycoprotein, using PNGase F (peptide N-glycosidase F), which is then analyzed by chromatography or mass spectrometry. In contrast, the assessment of the glycopeptide profile is based on the analysis of a single glycoprotein or multiple glycoproteins, which are analyzed by liquid chromatography with a mass spectrometer (LC-MS) [107, 108]. The analysis of glycopeptides by LC-MS provides information on the heterogeneity of glycoprotein oligosaccharides as well as on their attachment sites, whereas the analysis of oligosaccharides provides information only on glycan structure [110].

Observation of changes associated with the glycosylation site may help to understand the mechanism of glycoprotein action and improve the specificity of glycan detection, which may have potential therapeutic applications [110–112]. Studies by Kurahashi et al. have shown that high expression of CLU in surgically removed ccRCC tumor tissue may correlate with shorter survival, even if the patient does not experience recurrence [113]. A study with the use of highly invasive Caki-1 human RCC cells with expression shRNA of clusterin, targeting clusterin (Caki-1/clusterin shRNA), documented that clusterin significantly intensifies the activity of S100A4, one of the members of the S100 proteins family occurring in human RCC, which positively affects tumor growth and invasion. CLU was also observed to enhance metastasis formation, and its expression was noticeably higher during the invasion process [62]. However, not so much is known so far about the importance of blood plasma clusterin expression in detecting or monitoring ccRCC progression. Tousi et al. analyzed blood plasma clusterin glycosylation in patients with ccRCC [114]. The authors compared the N-glycans profile of clusterin present in the

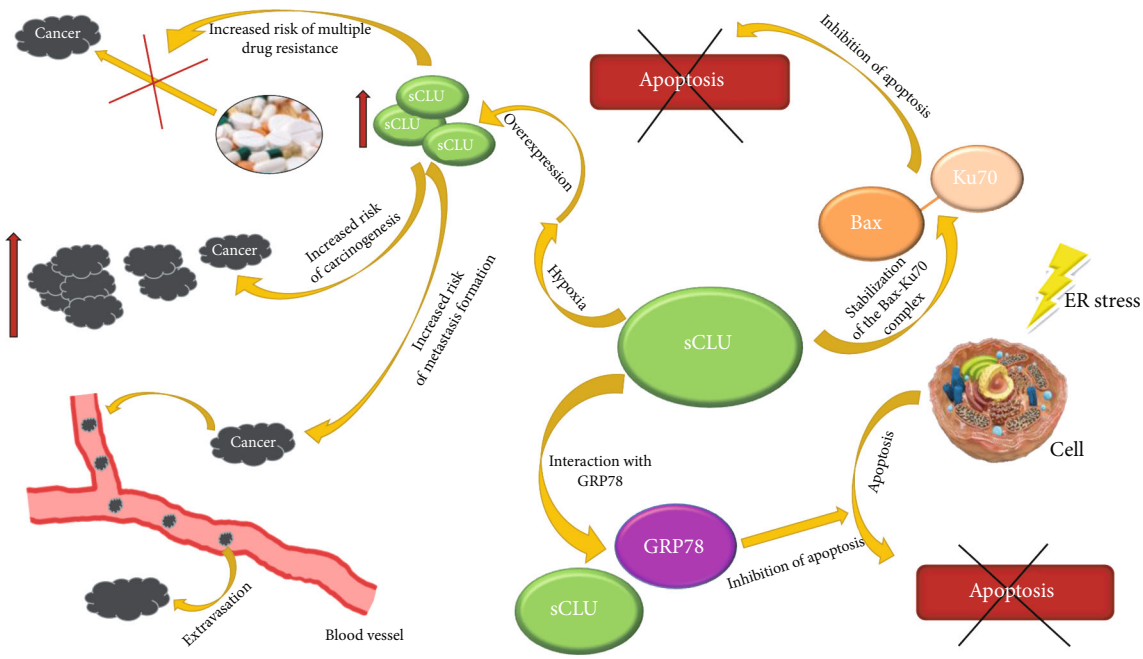

Figure 5: Schematic representation of the role of sCLU in the development of liver cancer. sCLU: secretory clusterin; Bax: Bcl-2-associated X protein; Ku70: Lupus Ku autoantigen p70; GRP78: glucose-regulated protein 78; ER: endoplasmic reticulum.

blood plasma of patients before and after nephrectomy (RCC(+) and RCC(-), respectively) of subjects with diagnosed ccRCC [114]. The expressions of A2G2S(3)2 (biantennary digalactosylated disialylated glycan) and FA2G2S(3)2 (core fucosylated biantennary digalactosylated disialylated glycan) were significantly lower in patients before curative nephrectomy in comparison to the results obtained from the same patients after surgical intervention. Moreover, an increase of A3G3S(6)2 (triantennary, trigalactosylated disialylated glycan) expression was observed in the blood plasma samples of patients after surgery [114]. In subsequent studies, Gbormittah et al. [115] confirmed that the expression of FA2G2S2 (core fucosylated biantennary disialylated digalactosylated glycans) and A2G2S2 (biantennary disialylated digalactosylated glycans) best differentiate blood plasma samples of patients with ccRCC before and after nephrectomy. A significant increase in the expression of FA2G2S2 and A2G2S2 glycans was observed in RCC(-) samples, i.e., after nephrectomy of a localized tumor, whereas blood plasma samples of RCC(+) patients before nephrectomy were characterized by a significant decrease in FA2G2S2 and A2G2S(3)2 expression in clusterin glycans [115]. The results of the above studies have shown that changes in clusterin glycosylation may be used to differentiate blood plasma samples from patients with ccRCC from those without renal neoplastic changes. So far, only the total blood plasma CLU concentration of patients with ccRCC before and after nephrectomy has been determined, with mean values in the range of 285-295 μg/mL, but no significant difference between these two groups of studied patients was observed. Hence, the value of total CLU concentration cannot be used as a diagnostic parameter of ccRCC development. However, glycoproteomic analysis of specific CLU glycoforms may become a useful marker for monitoring the development of ccRCC [115]. As the study performed by Gbormittah et al. [115] also documented decreased expression of core-fucosylated CLU glycans in the blood plasma of patients with ccRCC, the question arises whether ccRCC cells directly produce altered clusterin with reduced fucosylation or whether the observed changes in CLU fucosylation are a secondary effect of the influence of the tumor microenvironment [115].

Scientific studies reported that elevated clusterin expression in the ccRCC tumor tissue may correlate with shorter patient survival times. Current literature data suggests that the examination of CLU glycosylation profile in ccRCC patients is more interesting from a diagnostic point of view than the analysis of blood plasma clusterin levels. It has been demonstrated that CLU glycosylation profiles before and after nephrectomy are distinct. The expression of core fucosylated biantennary disialylated digalactosylated glycans and biantennary disialylated digalactosylated glycans in the CLU molecule significantly decreased in patients before nephrectomy in comparison to patients after nephrectomy. However, it is still an open question whether the observed changes in CLU glycosylation are the cause or the result of ccRCC development.

3.8. The Importance of Clusterin Glycosylation in the Pathophysiology of Neurodegenerative Diseases. Among all the human tissues examined, the highest expression of CLU is observed in brain tissue. Clusterin has been proven to play an important role in the pathogenesis of Alzheimer's disease. Elevated CLU concentrations were found in both the affected brain areas: the hippocampus and frontal cortex, as well as in blood plasma [116–118]. Based on the above findings, Desikan et al. have suggested that elevated levels of blood plasma CLU are associated with the occurrence

and severity of AD as well as with increased β-amyloid deposition and brain atrophy; however, these changes were not observed in all AD patients [118]. The authors suggested that CLU contributes to both increased β-amyloid aggregation and β-amyloid elimination, raising the question of whether an increase in CLU concentration in AD pathogenesis is beneficial or perhaps detrimental to the patient [116–118].

Tau protein is one of the most important proteins involved in AD pathogenesis. It has been demonstrated that the concentration of this protein increases after CLU injection into the rat hippocampus [119]. Yuste-Checa et al. have proposed a cellular model describing the relationships between CLU and tau protein, pointing to the chaperone role of CLU promoting the Tau protein aggregation in the whole process [120]. Lidström et al. [121] expected that increased CLU levels in the brain tissue of AD patients would positively correlate with increased CLU levels also in the cerebrospinal fluid (CSF); however, this assumption turned out to be incorrect [121, 122]. To prove that the potential involvement of clusterin in synaptic degradation, the correlations between CLU concentrations, and the concentrations of neurogranin (NG), a potential marker reflecting synaptic degradation, were examined in CSF. A significant positive correlation was found between the concentrations of both substances in CSF, occurring independently of other factors [123]. Since clusterin is a highly glycosylated protein, Nilselid et al. [124] decided to check whether the results obtained by Lidström et al. [121] were associated with differences in the glycosylation profile of CLU derived from brain tissue and the one present in the CSF, which could disturb the binding of specific CLU-detecting antibodies, consequently leading to falsely underestimated results. Glycosylation analysis of the clusterin present in CSF showed that it contains partially sialylated N-glycans, while the presence of O-glycans was not identified. The lower molecular weight of CSF clusterin compared to blood plasma CLU was probably associated with different glycosylation degrees of the CLU present in both body fluids [124]. Pilot studies concerning determinations of native CLU concentrations in the CSF of AD patients and in control samples of healthy subjects did not show significant differences between the studied groups. The CLU deglycosylation process is also accompanied by an increased concentration of deglycosylated CLU in the CSF samples of AD patients in comparison to controls [125]. Based on the results of the above pilot study, the authors suggested the determinations of native and deglycosylated CSF CLU concentrations in larger groups of participants. Interestingly, despite the fact that deglycosylation of CLU resulted in higher deglycosylated CLU concentrations in CSF, elevated CLU concentrations of about 25% in AD patients were noted in CSF samples for both native and deglycosylated CLU. This provides evidence that the deglycosylation of CLU was not necessary to demonstrate the elevated concentrations of this glycoprotein in the CSF of AD patients, but contributed to a more efficient detection of CLU by specific antibodies when its levels were determined [125].

Sihlbom et al. [126] demonstrated the presence of clusterin glycosylation changes in the CSF of AD patients, but because these changes also affected other proteins, the researchers suspected that this was a generalized variation in glycoproteins' glycosylation in the course of AD. The elevated concentrations observed after CLU deglycosylation suggested that clusterin microheterogeneity analysis may become a severity assessment marker in AD patients and determining the profile and degree of CLU glycosylation in CSF or the total glycosylation profile of CSF glycoproteins of AD patients would enable CSF differentiation between AD patients and healthy individuals [124].

Molecular studies on the CLU gene revealed that the presence of AD risk alleles rs9331888 and rs11136000 is associated with decreased blood plasma CLU levels [127]. Moreover, the presence of the single nucleotide polymorphism (SNP) rs11136000 in the CLU gene is associated with reduced risk of late-onset Alzheimer's disease (LOAD), which is more frequent in female than in male subjects [128]. The neuroprotective role of clusterin in the pathogenesis of AD is based on its activity as β-amyloid transporter, thus preventing the accumulation of β-amyloid deposits removing them from brain tissue, simultaneously inhibiting the complement system and neuronal apoptosis process, and promoting neurite growth [129].

An ideal prognostic and diagnostic biomarker should be characterized by variability while monitoring disease progression and treatment effects, thus contributing to a more accurate and earlier diagnosis of AD. It was suggested that the altered glycosylation profile of CLU may provide important information about disease progression. As mentioned above, blood plasma and CSF clusterin contains sialylated N-glycans [15], and changes in the degree of CLU glycan sialylation are associated with AD development [130, 131]. Liang et al. reported the results of blood plasma CLU glycosylation analysis of patients with mild and severe hippocampal atrophy [132]. Three glycosylation sites, α64Asn, β64Asn, and β147Asn, showed significant differences in glycosylation pattern between the study groups. The greatest changes were observed in the composition of glycans attached to β64Asn; 8 glycoforms were identified, and their expression was significantly reduced in patients with advanced hippocampal atrophy compared to subjects in the early stages of the disease, indicating the diagnostic utility of CLU glycoform examination as a prognostic marker of AD [132].

Following the discovery of single nucleotide polymorphisms in the CLU gene that contribute to the development of Alzheimer's disease, a possible role for clusterin in the pathogenesis of other neurodegenerative diseases was suggested. Researchers have paid particular attention to Parkinson's disease (PD), which is characterized by the formation of abnormal α-synuclein aggregates. The expression of CLU rs9331896 allele was shown to be associated with a significantly higher risk of Parkinson's disease development in the Chinese Han population, especially in males [133]. Another study reported increased cognitive changes in PD patients homozygous for the C allele of CLU rs11136000 [134]. In a study performed on a cell line with α-synuclein

overexpression, it was shown that reduced CLU expression enhances the formation of α-synuclein aggregates [135]. Clusterin levels also appear to be a potential candidate biomarker for Parkinson's disease, and blood plasma CLU levels in PD patients have been documented to be significantly higher than in healthy subjects [133]. A similar relationship was observed for CLU levels in CSF [136], but recent studies do not support these observations, reporting only increased CLU levels in CSF in healthy subjects with high-risk of PD [134].

In conclusion, several studies have confirmed the association between CLU and β-amyloid formation, indicating its role in Alzheimer's disease. Increased blood CLU levels are related to the occurrence and the severity of AD. However, the particular role of CLU in this disease, especially its role in the β-amyloid metabolism, is not fully understood and requires further analysis. Another aspect of this issue is the analysis of CLU glycosylation profile and degree in CSF and blood plasma. The observed changes in the profile and degree of CLU glycans sialylation in blood plasma and CSF, associated with AD development, suggest the need for further experiments concerning the analysis of CLU glycosylation heterogeneity in context of the development and progression of neurodegenerative disorders. CLU has also been documented to play an important role in Parkinson's disease, being significantly related to a higher risk of PD development, especially in males; a potential role of clusterin in preventing α-synuclein aggregation has also been suggested. Moreover, blood plasma clusterin levels appear to be a potential candidate biomarker for Parkinson's disease development, as they are significantly increased in PD patients in comparison to healthy subjects. The main CLU functions in development of neurodegenerative diseases as well as its neuroprotective properties are presented in Figure 6.

3.9. The Harmful Effects of Ethanol on Glycosylation of Clusterin Present in Brain Tissue. The destructive effect of ethanol on living organisms has been the subject of numerous studies. Most scientific reports detail the results of studies on the effects of chronic ethanol exposure on liver function [137, 138]. Long-term exposure of the body to ethanol not only results in hepatic steatosis, but can also lead to changes in liver protein synthesis and/or secretion [139].

Studies in rats have shown that ethanol selectively impairs glycoprotein metabolism, resulting in their alteration [137]. Ethanol has been documented to reduce the sialylation of brain tissue proteins [140]. The determination of the functions of glycoprotein carbohydrate structures has been the subject of studies for many years. Hale et al. analyzed how glycosylation of brain tissue proteins is affected by chronic ethanol exposure, using CLU as a model of N-glycosylated protein [71]. CLU, as one of the proteins present in brain tissue, is involved in cell aggregation, lipid transportation, remodeling of synapses, and cell membrane protection [141, 142]. The biosynthesis of CLU is regulated *inter alia* by the consistent action of two enzymes: sialotransferases and sialidases, present in brain microsomes, Golgi apparatus, cytosol, and plasma membranes [143]. Studies performed by Hale et al. [71] showed that sialylation is a key step in clusterin biosynthesis and that long-term ethanol exposure significantly impairs this stage of CLU biosynthesis. In previous studies in rats, Ghosh et al. showed that chronic ethanol exposure can lead to the modification of Golgi apparatus membranes, which form a key cell compartment for clusterin sialylation [138]. Loss of sialic acid by the clusterin molecule may result in a change in its molecular conformation, which may in turn affect its stability, antigenic expression, or receptor recognition (Figure 6). Javors and Johnson [144] proved that this process is reversible: Sialylation of CLU increased after alcohol overdose reduction. The amphipathic nature of the clusterin molecule potentially provides its ability to transport lipids, which can be incorporated into axonal membranes, maturing neurons, and neurons undergoing dendritic reorganization. In cases of nerve cell degeneration as well as mechanical, metabolic, or chemical damage of brain cells, clusterin expression can be increased due to the promotion of tissue repair and remodeling. This process probably requires the structural stability of the clusterin molecule and its correct structure [71]. Changes in degree of clusterin sialylation due to long-term ethanol exposure alter its structure, leading to impairment of its function related to the transport of lipids and neuropeptides used in ischemic brain tissue repair and remodeling [145, 146].

In conclusion, it has been documented that sialylation is a crucial step in CLU biosynthesis. Chronic ethanol exposure results in CLU sialylation disturbance, *inter alia* via Golgi apparatus impairment—the main compartment where the CLU glycosylation process takes place. The altered CLU structure disables its proper activity bound with lipid and neuropeptide transportation, which is crucial to ischemic brain tissue repair. The most important impacts of chronic ethanol exposure on the structure and functions of CLU are presented in Figure 7.

3.10. Structural Analysis of Clusterin Present in the Serum of ATTRwt Patients. Wild-type (wt) transthyretin amyloidosis (ATTR) is a disease that involves the accumulation of protein deposits in cardiac muscle fibers, causing heart failure in elderly people. These deposits result from the disassociation of the tetrameric protein transthyretin (TTR). Unlike inherited TTR amyloidosis, in which a change in amino acid sequence destabilizes the native transthyretin molecule, the amyloid protein in ATTRwt does not show an altered amino acid sequence. Therefore, scientists have searched for other factors that may be responsible for protein destabilization and the uncontrolled accumulation of wild-type TTR in myocardial fibers. The results of some research suggest that clusterin may play a role in the pathomechanism of this disease [147, 148].

Torres-Arancivia et al. [149] performed a comparative glycoproteomic analysis of CLU present in the blood sera of healthy and ATTRwt patients, which showed that the α81Asn clusterin glycosylation site, present in patients with this disease (CLUp), was characterized by lower diversity and glycosylation degree than in healthy patients; however, the oligosaccharide profile of glycans attached at the

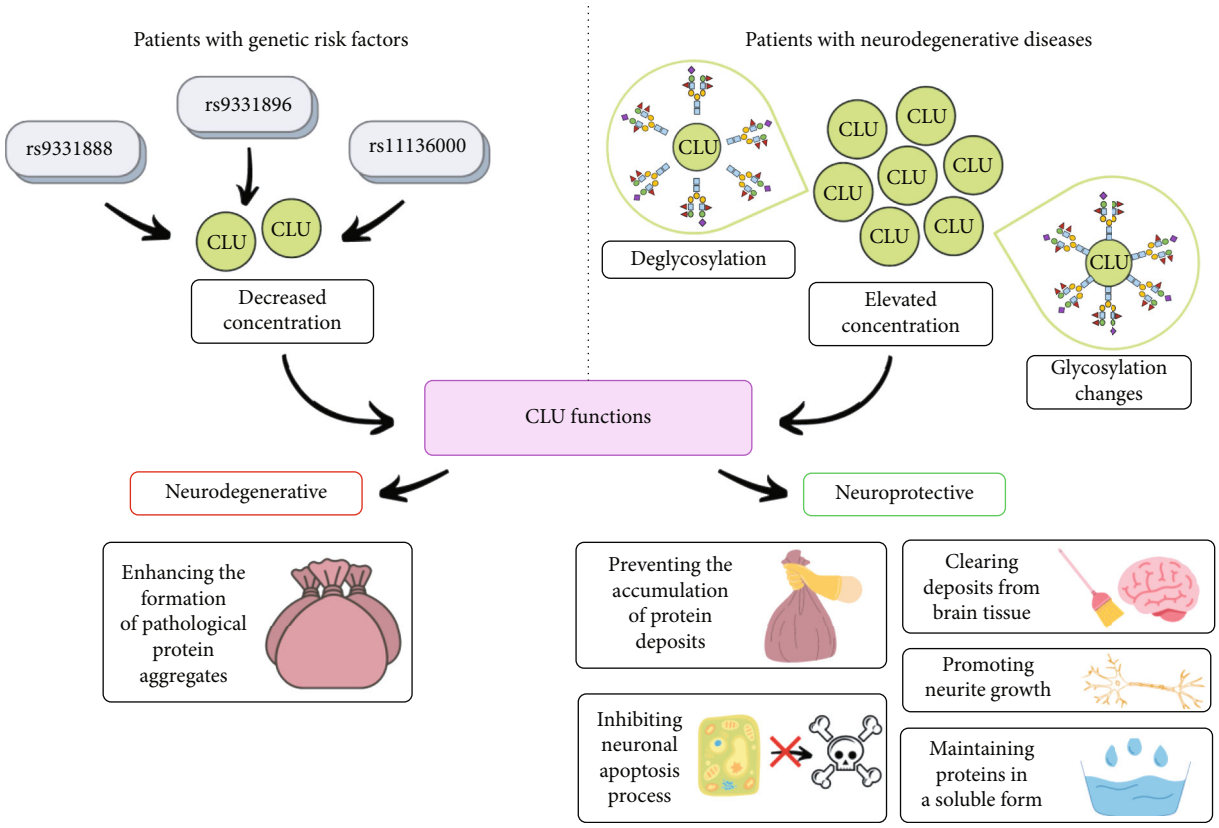

Figure 6: Schematic representation of the main CLU functions in neurodegenerative diseases and its possible neurodegenerative and neuroprotective activity. CLU: clusterin; rs9331888, rs9331896, and rs11136000: single nucleotide polymorphisms of clusterin gene.

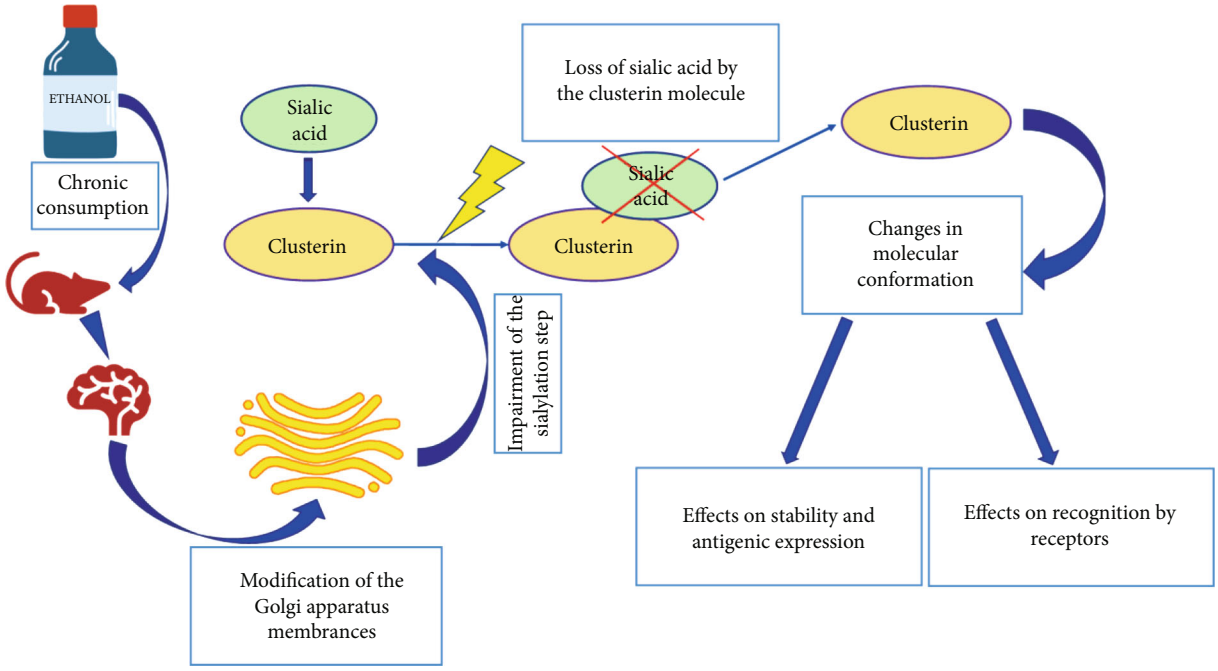

Figure 7: Schematic representation of chronic ethanol exposure on CLU structure and functions. Self-modification based on Ghosh et al. [138] and Hale et al. [71].

Table 1: The main changes in expression of sCLU glycans in selected disorders.

Disorder	Examined material	CLU glycan expression	Reference
Human reproduction	Blood serum	(i) Increased expressionof core and α1,2-linked fucosein infertile normozoospermic patientsin comparison to male patientswith sperm disorders (ii) Possibility of different CLU glycosylationmechanismsin seminal plasma and serum CLU	[33]
	Semen, human oocytes	(i) Expression of Le^x and Le^y oligosaccharide structures in seminal CLU make possible the reaction with DC-SIGN expressed in DCs of zona pellucidaand induction of maternal immunotolerance to male antigens	[32, 33, 78]
Breast cancer	Tumor tissue	(i) Ability to metastases formation through neoexpression of sialo-Le^x structures	[86, 87]
		(ii) Increased expression of fucose of Le^x and Le^y structures in tumor tissues in comparison to healthy nontumor tissue from the same patient (iii) Ability of fucosylated CLU, present in neoplastic cells, to bind to DC-SIGN (iv) Fucosylated form of CLU produced by tumor cells as a possible breast cancer advancement marker	[88]
Colorectal cancer	Blood serum	(i) Increased expression of five CLU isoforms in group of patients with CRC in the fraction containing O-glycosylated glycoproteins, but without N-glycans (ii) Increased expression of one CLU isoform in group of patients with CRC in fraction of N-glycosylated glycoproteins	[92]
	Tumor sections	(i) Expression of highly glycosylated cytoplasmic CLU in the advanced stage of cancer with metastases to the lymph nodes (ii) Extracellular expression of highly glycosylated CLU in the advanced CRC	[90]
Hepatocellular carcinoma	Blood serum	(i) Significant decrease in the expression of triantennary N-glycans in serum samples of HCC patients in comparison to controls and cirrhosis patients (ii) Reduction of expression of β1,4-triantennary N-glycans of clusterin in HCC patients, accompanied by an increase in the expression of biantennary N-glycans	[103]
Clear cell renal cell carcinoma	Blood plasma of patients before and after nephrectomy	(i) Significant decrease in the levels of a biantennary digalactosylated, disialylated glycans (A2G2S2) (ii) Increased levels of a core fucosylated biantennary digalactosylated, disialylated glycans (FA2G2S2) (iii) Increase of triantennary trigalactosylated, disialylated glycans (A3G3S(6)2) in blood plasma post-surgery	[114]
		(i) Increased expression of FA2G2S2 (core fucosylated biantennary digalactosylated, disialylated glycans) and A2G2S2 (biantennary digalactosylated, disialylated glycans) in blood plasma of patients following nephrectomy (ii) Expression of FA2G2S2 (core fucosylated biantennary digalactosylated, disialylated glycans) and A2G2S2 (biantennary digalactosylated, disialylated glycans) as a differentiating biomarker of patients with ccRCC before and after nephrectomy	[115]

Table 1: Continued.

Disorder	Examined material	CLU glycan expression	Reference
Alzheimer's disease	Cerebrospinal fluid	(i) CLU glycans partially sialylated	[124]
		(ii) Lack of O-glycans in the CSF CLU molecule	
		(iii) Elevated deglycosylated CLU concentrations in the CSF samples of AD patients compared to controls	[125]
		(iv) Decreased CLU sialylation degree	[130, 131]
	Blood plasma	(i) Decreased expression of the eight glycoforms attached to the β64Asn site in patients with advanced hippocampal atrophy compared to those in the early stages of the disease	[132]
Chronic ethanol overdose	Rat brain tissue	(i) Sialylation as a key step of the CLU biosynthesis	[71]
		(ii) Desialylated form of CLU as a result of chronic ethanol overdose	
	Blood serum	(i) Decreased blood serum CLU sialylation in alcohol-overdosing patients	[144]
		(ii) Reversibility of CLU desialylation process during abstinence	
Wild-type (wt) transthyretin amyloidosis	Blood serum	(i) Lower diversity and glycosylation degree of CLU glycans attached to α81Asn glycosylation site in comparison to the control group	[149]
		(ii) Similar oligosaccharide profile of glycans attached at the β352Asn position	
		(iii) CLU glycan sequence characteristic for patients with ATTRwt: HexNAc:4, Hex:5, Fuc:0, and Neu5Ac:2 frequently present at the β332Asn position	
		(i) No variation in the amino acid sequence of blood serum CLU between the group of patients with ATTRwt and the control group	[150]
		(ii) Differences in the degree of oligosaccharide expression in CLU between the ATTRwt patients and control group	
		(iii) The highest amount of CLU glycoforms in ATTRwt, present at position α—confirmation of the hypothesis that the alterations in glycan expression in the N-terminal part of the α subunit of circulating CLU may negatively affect the chaperoning capacity of clusterin in ATTRwt patients, influencing its ability to prevent the deposition of amyloid fibrils	
Acute myocardial infarction	Blood serum	(i) Reduced CLU glycosylation degree in group of AMI patients in comparison to the healthy control group	[160]
Bovine spongiform encephalopathy	Cattle urine	(i) Differential expression of certain isoforms of clusterin in urine of infected cattle compared to controls	[164]
	Cow urine	(i) Identification of high mannose complex CLU N-glycans	[74]
		(ii) Different CLU isoform expression in infected and uninfected cow urine	

AD: Alzheimer's disease; AMI: acute myocardial infarction; Asn: asparagine; ATTRwt: wild-type (wt) transthyretin amyloidosis; CRC: colorectal cancer; CSF: cerebrospinal fluid; DC-SIGN: dendritic cell–specific intercellular adhesion molecule-3-grabbing non-integrin; Fuc: fucose; HCC: hepatocellular carcinoma; Hex: hexose; Le^x: $Lewis^x$ oligosaccharide structure; Le^y: $Lewis^y$ oligosaccharide structure; Neu5Ac: N-acetylneuraminic acid.

β352Asn position was similar for both CLUp and controls (CLUc). Furthermore, the glycans HexNAc:4, Hex:5, Fuc:0, and Neu5Ac:2 were frequently present at the β332Asn position and were identified only for CLUc. The presented structural differences between CLUc and CLUp, concerning the oligosaccharide profile, may be the reason for the reduced

ability of clusterin to bind nonnative TTR, thus reducing the activity of clusterin as a chaperone and causing accumulation of wild-type TTR amyloid deposits in myocardial tissue, leading to myocardial failure [149].

In 2020, Torres-Arancivia et al. [150] published the results of a continued study on the role of CLU in the pathobiology of ATTRwt amyloidosis. They examined the amino acid content and oligosaccharide occupancy of CLU and compared the results with data obtained for control blood sera of healthy subjects. The authors concluded that there was no variation in the amino acid sequence of CLU between the sera of patients with ATTRwt and the control group, while differences between both groups were found in the degree of oligosaccharide expression in CLU. The highest amount of glycoforms in ATTRwt CLU was present at position α, which confirmed the hypothesis that the occurrence of alterations in glycan expression in the N-terminal region of the α subunit of circulating CLU may negatively affect the chaperoning capacity of clusterin in ATTRwt patients, influencing its ability to prevent the deposition of amyloid fibrils [150].

Current literature data concerning ATTRwt suggest that the differences in one of the glycosylation sites (α81Asn) between blood plasma CLU of ATTRwt patients and the control group of healthy subjects may lead to the reduction of clusterin ability to bind nonnative TTR and thus diminish the activity of clusterin as a chaperone, causing accumulation of wild-type TTR amyloid deposits in myocardial tissue and leading to myocardial failure.

3.11. The Importance of Clusterin Glycosylation in the Early Phase of Myocardial Infarction. Ischemic atherothrombotic syndromes cause pathological changes in the body, which are reflected in fluctuations of serum protein concentrations. Increased concentrations of C-reactive protein (CRP), amyloid A, or interleukin 6 (IL-6) were observed in a significant percentage in patients with acute coronary syndromes. Ischemia-modified albumin (IMA) is one of the best-known markers of myocardial ischemia [151], while the determination of troponin concentration is now a common test performed both for diagnostic purposes and for monitoring the degree of myocardial damage [152]. However, the fact that markers used to diagnose heart disease are characterized by low tissue specificity and rapid normalization of concentrations remains problematic. Moreover, in the case of the assessment of myoglobin concentration, the obtained value may be burdened with a large error among patients with renal insufficiency. From the clinicians' point of view, the time elapsed between the onset of myocardial infarction and its correct diagnosis is of crucial prognostic importance for the patient, because the immediate application of revascularization treatment of the coronary artery has the most effective results and gives the patient a chance to recover [153].

The identification of a biomarker that would indicate cardiac damage already in the first hours after an incident of myocardial infarction is still the subject of many studies. The known biomarkers used in the diagnosis of vascular atherosclerotic lesions include LDL, HDL, and apolipoproteins ApoA1 and ApoB [154, 155]. The analysis of HDL composition showed that the HDL structure includes proteins involved in the activation of the complement system, the regulation of proteolysis, and acute phase proteins [156]. In some reports, scientists suggest that the participation of HDL in the development of cardiovascular diseases is not based on its concentration in the blood but on its qualitative composition, structure, and biological function. Moreover, the results of clinical trials suggest that the HDL molecule may exert anti-inflammatory and cytoprotective effects during the ongoing inflammatory process [157, 158]. Clusterin bound to ApoA1 is a part of the HDL molecule [159], and the level of its expression in the blood serum depends on the maintenance or disturbance of the organism's homeostatic conditions [92]. The presence of high CLU concentrations in the sera of patients with diagnosed atherosclerotic lesions was observed. Cubedo et al. performed a proteomic analysis of proteins present in blood sera of patients in the early phase of acute myocardial infarction (AMI) [160]. Significant changes in the expression of individual clusterin isoforms, with a predominance of those with lower molecular weight, have been demonstrated in the sera of patients with AMI in comparison to the control group due to a reduced degree of CLU glycosylation in the sera of AMI patients. In addition, immunohistochemical analysis revealed the presence of CLU in ischemic myocardial tissue, which was not observed in myocardial muscle fibers without lesions [160]. The analysis of changes in CLU glycosylation degree may help to understand the role played by this glycoprotein in the pathomechanism of the development of AMI and may also become a more reliable biomarker to detect the early phase of AMI than parameters measured so far [160]. In addition to changes in the degree of clusterin glycosylation, a significant decrease in CLU blood serum levels was also demonstrated in patients within the first 6 hours of myocardial injury, and within 24 hours, CLU levels began to return to physiological values, reaching a value in the reference range within 72-96 hours. The observed decrease in the concentration of clusterin is probably the result of its action as an anti-inflammatory protein [160].

In summary, the presence of CLU in ischemic myocardial tissue was proven, suggesting the important role of this glycoprotein in the AMI. Moreover, serum CLU concentrations were significantly higher in the group of patients with AMI in comparison to the control group. It is worth noting that blood serum CLU levels are characterized by dynamic changes during the time after ischemia. Their levels decrease within 6 hours of ischemia and are normalized within 24 hours. The aforementioned information suggests that blood serum CLU may become an additional, sensitive myocardial infarction biomarker.

3.12. Analysis of Clusterin Glycoforms in the Urine of Cows with Spongiform Encephalopathy. Bovine spongiform encephalopathy (BSE) is a fatal neurodegenerative disease associated with prion infection that causes damage of the central nervous system, manifesting as vacuolization and gliosis of the grey matter of brain tissue [161]. Considering the fact that people can become infected with this disease

by eating meat from sick animals, it is very important to detect it early in cattle. Formerly, the diagnosis of BSE was based on a combination of symptoms of aggressive behavior in animals and lack of motor coordination. Among deceased animals, in order to confirm the diagnostic hypothesis and unequivocally identify the cause of death, an analysis of the abnormally folded PrPd protein present in brain tissue was performed and collected post-mortem [162]. It has been shown that in transmissible spongiform encephalopathy (TSE), which includes BSE, the concentration of clusterin mRNA increases [163]. Using two-dimensional differential gel electrophoresis (2D-DIGE), Simon et al. found that only certain isoforms of clusterin showed differential expression in urine from infected cattle compared to controls [164]. The difficulty in using specific clusterin isoforms as a biomarker in BSE diagnostics is the observed background interference in the form of other proteins with identical amino acid sequences, whose presence is not characteristic for BSE [164]. Lamoureux et al. performed a study to determine the diagnostic potential of clusterin isoforms present in the urine of BSE-infected cattle [165]. The use of CAB1 and CAB2 (CAB; custom polyclonal antibodies) specific for α and β subunits of clusterin, respectively, confirmed that the detected proteins, present in the urine of BSE cattle, were isoforms of the CLU β chain. The 3 β subunits of CLU characteristic for BSE as well as 2 β chains with lower molecular weight and a lower isoelectric point (pI) were identified [165]. In the next step, the glycosylation profiles of three potentially diagnostically relevant clusterin isoforms, typical for BSE, were analyzed and showed reactivity with lectins specific to: hybrid N-glycan structures (WGA; *Wheat germ* agglutinin) and high mannose oligosaccharide (ConA) structures, meaning that all three clusterin isoforms have complex glycans in their structure. However, Western blot analysis showed that all urine samples from uninfected cattle were characterized by the presence of a single band, reactive with anti-CLU antibodies, at a site corresponding to a molecular weight of about 37 kDa, while urine samples from infected cattle additionally showed a second band, with a molecular weight higher than 37 kDa. Deglycosylation of CLU from the urine of affected cattle, followed by Western blot analysis, revealed the presence of a single band with a molecular weight of approximately 37 kDa, which seems to support the hypothesis that the clusterin molecule undergoes stronger glycosylation during BSE development. The authors concluded that the analysis of the degree of glycosylation of clusterin isoforms, present in a readily available biological material such as urine, could serve as a basis for the creation of a quick and specific diagnostic test that could be applied to the diagnosis of BSE in breeding cattle [165].

To summarize, studies concerning the usefulness of CLU as a potential biomarker of bovine spongiform encephalopathy showed differential expression of CLU in the urine of infected cattle in comparison to the healthy controls. Glycosylation profile analysis revealed that CLU in BSE had a stronger degree of glycosylation as an effect of disease occurrence and progression. Further analysis of urine CLU glycosylation may result in the development of a quick and specific diagnostic test. Such a test could be applied to the diagnosis of BSE in breeding cattle in an easy and convenient way, especially in the context of preventing the transmission of the disease from infected cattle to humans.

Table 1 summarizes the main changes in expression of sCLU glycans in selected disorders.

4. Conclusions

Clusterin is a very interesting glycoprotein with a multifunctional role in the human body. Several pieces of research have proven that its concentration as well as its structure differs in many pathological conditions. The glycosylation process is essential for proper CLU biosynthesis, enabling chaperone activity as well as the formation of soluble complexes with misfolded proteins. In such a manner, damaged proteins are then removed by endocytosis and lysosomal degradation in an ATP-independent way, thus playing a great role in homeostasis maintenance. With its proapoptotic properties, the nuclear form of clusterin present in neoplastic cells inhibits tumor progression, whereas secretory clusterin performs chaperone activity and may contribute to metastasis formation. It is worth pointing out that CLU lacking in N-glycans is cumulated in the ER, which results in cytotoxicity induction. The presence of oligosaccharide structures type Le^x/Le^a and Le^y/Le^b enable CLU and DC-SIGN interactions, which influence the immunological properties of seminal plasma as well as neoplastic cell modulation and induce macrophage differentiation, leading to proangiogenic cell formation. Since CLU plays a variety of important roles in the human body, further studies concerning the use of CLU as a potential biomarker in many civilizational diseases may shed more light on the molecular mechanisms involved in the pathogenesis of these disorders and, in addition, may also contribute to the development of new therapeutic strategies.

Abbreviations

2D-DIGE:	Two-dimensional differential gel electrophoresis
2D-PAGE:	Two-dimensional gel electrophoresis
A2G2S(3)2:	Biantennary disialylated digalactosylated glycan
AD:	Alzheimer's disease
AFP:	α-fetoprotein
AMI:	Acute myocardial infarction
ApoA1:	Apolipoprotein A1
ApoB:	Apolipoprotein B
ApoJ:	Apolipoprotein J
AT:	Asthenoteratozoospermia
ATP:	Adenosine triphosphate
ATTRwt:	Wild-type transthyretin amyloidosis
Bax:	Bcl-2-associated X protein
BSE:	Bovine spongiform encephalopathy
CAB:	Custom polyclonal antibodies
ccRCC:	Clear cell renal cell carcinoma
CLI:	Complement-lysis inhibitor
CLU:	Clusterin
CLUc:	Clusterin concentration in control group

CLUp: Clusterin concentration in patients
ConA: *Concanavalin A* agglutinin
CRC: Human colorectal cancer
CRP: C-reactive protein
CSF: Cerebrospinal fluid
DCs: Dendritic cells
DC-SIGN: Dendritic cell–specific Intercellular adhesion molecule-3-grabbing non-integrin
DNA: Deoxyribonucleic acid
DSL: *Datura stramonium* lectin
DTT: Dithiothreitol
ECM: Extracellular matrix
ELISA: Enzyme-linked immunosorbent assay
EMT: Epithelial-mesenchymal transition
ER: Endoplasmic reticulum
FA2G2S(3)2: Core fucosylated biantennary disialylated digalactosylated glycan
GRP78: Glucose-related protein 78
HBV: *Hepatitis B* virus
HCC: Hepatocellular carcinoma
HCV: *Hepatitis C* virus
HDL: High density lipoprotein
iCLU: Intracellular clusterin
IL-6: Interleukin 6
IL-8: Interleukin 8
IMA: Ischemia-modified albumin
Le^x: Lewis^x oligosaccharide structure
Le^y: Lewis^y oligosaccharide structure
LC-MS: Liquid chromatography with mass spectrometry
LDL: Low density lipoprotein
LRP2: Low density lipoprotein-related protein 2
MAC: Membrane attack complex
MCF-7: Michigan Cancer Foundation 7 cells
M-CSF: Macrophage colony-stimulating factor
MDR: Multiple drug resistance
mRNA: Messenger ribonucleic acid
nCLU: Nuclear clusterin
N: Normozoospermia
Neu5Ac: N-acetylneuraminic acid
NG: Neurogranin
NK: Natural killers
OAT: Oligoasthenoteratozoospermia
OS: Oxidative stress
PD: Parkinson's disease
PGPF: Plasmin-generated protein fragments
PKB: Protein kinase B
PNGase F: Peptide N-glycosidase F
RCC(-): Patients after nephrectomy
RCC(+): Patients before nephrectomy
ROS: Reactive oxygen species
SA: Sialic acid
sCLU: Secretory clusterin
SNP: Single nucleotide polymorphism
SP-40,40: Secretory protein-40
T: Teratozoospermia
Tg: Thapsigargin
TGF-β: Transforming growth factor β
Tm: Tunicamycin
TNF-α: Tumor necrosis factor α
TNM: Tumor node metastasis scale
TSE: Transmissible spongiform encephalopathy
TTR: Transthyretin
UPR: Unfolded protein response
VEGF: Vascular endothelial growth factor
VLDL: Very low density lipoprotein
WGA: *Wheat germ* agglutinin
ZP: Zona pellucida.

Conflicts of Interest

The authors declare no conflict of interest.

Authors' Contributions

Conceptualization was carried out by E.M.K.; methodology was carried out by E.J., A.W., and E.M.K.; writing-original draft preparation was carried out by E.J., A.K., M.K., A.W., and E.M.K.; writing-review and editing was carried out by E.J., and E.M.K.; visualization was carried out by E.J., A.K., M.K., and E.M.K.; supervision was carried out by E.M.K.; E.M.K. was responsible for funding acquisition. All authors have read and agreed to the published version of the manuscript.

References

[1] F. Rizzi, M. Coletta, and S. Bettuzzi, "Chapter 2 Clusterin (CLU): From One Gene and Two Transcripts to Many Proteins," *Advances in Cancer Research*, vol. 104, pp. 9–23, 2009.

[2] E. M. Foster, A. Dangla-Valls, S. Lovestone, E. M. Ribe, and N. J. Buckley, "Clusterin in Alzheimer's disease: mechanisms, genetics, and lessons from other pathologies," *Frontiers in Neuroscience*, vol. 13, 2019.

[3] J. N. Lakins, S. Poon, S. B. Easterbrook-Smith, J. A. Carver, M. P. R. Tenniswood, and M. R. Wilson, "Evidence that clusterin has discrete chaperone and ligand binding sites," *Biochemistry*, vol. 41, no. 1, pp. 282–291, 2002.

[4] P. Rohne, H. Prochnow, S. Wolf, B. Renner, and C. Koch-Brandt, "The chaperone activity of clusterin is dependent on glycosylation and redox environment," *Cellular Physiology and Biochemistry*, vol. 34, no. 5, pp. 1626–1639, 2014.

[5] J. Herz and H. H. Bock, "Lipoprotein receptors in the nervous system," *Annual Review of Biochemistry*, vol. 71, no. 1, pp. 405–434, 2002.

[6] T. Chen, J. Turner, S. McCarthy, M. Scaltriti, S. Bettuzzi, and T. J. Yeatman, "Clusterin-mediated apoptosis is regulated by adenomatous polyposis coli and is p21 dependent but p53 independent," *Cancer Research*, vol. 64, no. 20, pp. 7412–7419, 2004.

[7] Y. Miwa, S. Takiuchi, K. Kamide et al., "Insertion/deletion polymorphism in clusterin gene influences serum lipid levels and carotid intima-media thickness in hypertensive Japanese females," *Biochemical and Biophysical Research Communications*, vol. 331, no. 4, pp. 1587–1593, 2005.

[8] S. Y. Gil, B. S. Youn, K. Byun et al., "Clusterin and LRP2 are critical components of the hypothalamic feeding regulatory pathway," *Nature Communications*, vol. 4, no. 1, p. 1862, 2013.

[9] T. Kujiraoka, H. Hattori, Y. Miwa et al., "Serum apolipoprotein J in health, coronary heart disease and type 2 diabetes mellitus," *Journal of Atherosclerosis and Thrombosis*, vol. 13, no. 6, pp. 314–322, 2006.

[10] M. Thambisetty, A. Simmons, L. Velayudhan et al., "Association of plasma clusterin concentration with severity, pathology, and progression in Alzheimer disease," *JAMA Psychiatry*, vol. 67, pp. 739–748, 2010.

[11] R. B. DeMattos, M. A. O'dell, M. Parsadanian et al., "Clusterin promotes amyloid plaque formation and is critical for neuritic toxicity in a mouse model of Alzheimer's disease," *Proceedings of the National Academy of Sciences*, vol. 99, no. 16, pp. 10843–10848, 2002.

[12] I. B. Fritz, K. Burdzy, B. Setchell, and O. Blaschuk, "Ram rete testis fluid contains a protein (clusterin) which influences cell-cell interactions in vitro," *Biology of Reproduction*, vol. 28, pp. 1173–1188, 1983.

[13] Z. Han, Z. Wang, G. Cheng et al., "Presence, localization, and origin of clusterin in normal human spermatozoa," *Journal of Assisted Reproduction and Genetics*, vol. 29, no. 8, pp. 751–757, 2012.

[14] A. R. Wyatt, J. J. Yerbury, H. Ecroyd, and M. R. Wilson, "Extracellular chaperones and proteostasis," *Annual Review of Biochemistry*, vol. 82, no. 1, pp. 295–322, 2013.

[15] J. T. Kapron, G. M. Hilliard, J. N. Lakins et al., "Identification and characterization of glycosylation sites in human serum clusterin," *Protein Science*, vol. 6, no. 10, pp. 2120–2133, 1997.

[16] S. E. Jones and C. Jomary, "Clusterin," *The International Journal of Biochemistry & Cell Biology*, vol. 34, no. 5, pp. 427–431, 2002.

[17] V. Naponelli and S. Bettuzzi, "Clusterin," in *Complement Factsb*, pp. 341–349, Elsevier, 2018.

[18] M. R. Wilson and S. B. Easterbrook-Smith, "Clusterin is a secreted mammalian chaperone," *Trends in Biochemical Sciences*, vol. 25, no. 3, pp. 95–98, 2000.

[19] M. E. Fini, S. Jeong, and M. R. Wilson, "Therapeutic Potential of the Molecular Chaperone and Matrix Metalloproteinase Inhibitor Clusterin for Dry Eye," *International Journal of Molecular Sciences*, vol. 22, no. 1, p. 116, 2021.

[20] A. R. Wyatt and M. R. Wilson, "Acute phase proteins are major clients for the chaperone action of α2-macroglobulin in human plasma," *Cell Stress & Chaperones*, vol. 18, no. 2, pp. 161–170, 2013.

[21] P. Constantinescu, R. A. Brown, A. R. Wyatt, M. Ranson, and M. R. Wilson, "Amorphous protein aggregates stimulate plasminogen activation, leading to release of cytotoxic fragments that are clients for extracellular chaperones," *Journal of Biological Chemistry*, vol. 292, no. 35, pp. 14425–14437, 2017.

[22] S. Poon, M. S. Rybchyn, S. B. Easterbrook-Smith, J. A. Carver, G. J. Pankhurst, and M. R. Wilson, "Mildly Acidic pH Activates the Extracellular Molecular Chaperone Clusterin∗," *Journal of Biological Chemistry*, vol. 277, no. 42, pp. 39532–39540, 2002.

[23] E. M. Stewart, J. A. Aquilina, S. B. Easterbrook-Smith et al., "Effects of glycosylation on the structure and function of the extracellular chaperone clusterin," *Biochemistry*, vol. 46, no. 5, pp. 1412–1422, 2007.

[24] I. C. Gelissen, T. Hochgrebe, M. R. Wilson et al., "Apolipoprotein J (clusterin) induces cholesterol export from macrophage-foam cells: a potential anti-atherogenic function?," *Biochemical Journal*, vol. 331, no. 1, pp. 231–237, 1998.

[25] H. Saleh, A. Afify, W. Ahmed, and M. Daruish, "Seminal plasma clusterin as a biomarker for spermatogenesis in patients with varicocele before and after varicocelectomy," *Human Andrology*, vol. 8, no. 4, pp. 111–114, 2019.

[26] J. O'Sullivan, L. Whyte, J. Drake, and M. Tenniswood, "Alterations in the post-translational modification and intracellular trafficking of clusterin in MCF-7 cells during apoptosis," *Cell Death and Differentiation*, vol. 10, no. 8, pp. 914–927, 2003.

[27] J. A. Sensibar, D. M. Sutkowski, A. Raffo et al., "Prevention of cell death induced by tumor necrosis factor α in LNCaP cells by overexpression of sulfated glycoprotein-2 (clusterin)," *Cancer Research*, vol. 55, pp. 2341–2347, 1995.

[28] J. Lakins, S. A. L. Bennett, J. H. Chen et al., "Clusterin Biogenesis Is Altered during Apoptosis in the Regressing Rat Ventral Prostate∗," *Journal of Biological Chemistry*, vol. 273, no. 43, pp. 27887–27895, 1998.

[29] S. Satapathy and M. R. Wilson, "The dual roles of clusterin in extracellular and intracellular proteostasis," *Trends in Biochemical Sciences*, vol. 46, no. 8, pp. 652–660, 2021.

[30] P. Nizard, S. Tetley, Y. Le Dréan et al., "Stress-induced retrotranslocation of Clusterin/ApoJ into the cytosol," *Traffic*, vol. 8, no. 5, pp. 554–565, 2007.

[31] A. R. Wyatt, J. J. Yerbury, P. Berghofer et al., "Clusterin facilitates in vivo clearance of extracellular misfolded proteins," *Cellular and Molecular Life Sciences*, vol. 68, no. 23, pp. 3919–3931, 2011.

[32] J. Sabatte, W. Faigle, A. Ceballos et al., "Semen clusterin is a novel DC-SIGN ligand," *Journal of Immunology*, vol. 187, pp. 5299–5309, 2011.

[33] E. Janiszewska, I. Kokot, I. Gilowska, R. Faundez, and E. M. Kratz, "The possible association of clusterin fucosylation changes with male fertility disorders," *Scientific Reports*, vol. 11, pp. 1–16, 2021.

[34] L. M. Moldenhauer, K. R. Diener, D. M. Thring, M. P. Brown, J. D. Hayball, and S. A. Robertson, "Cross-presentation of male seminal fluid antigens elicits T cell activation to initiate the female immune response to pregnancy," *Journal of Immunology*, vol. 182, pp. 8080–8093, 2009.

[35] S. A. Robertson, J. R. Prins, D. J. Sharkey, and L. M. Moldenhauer, "Seminal fluid and the generation of regulatory T cells for embryo implantation," *American Journal of Reproductive Immunology*, vol. 69, no. 4, pp. 315–330, 2013.

[36] R. M. Steinman, D. Hawiger, and M. C. Nussenzweig, "Tolerogenic dendritic cells," *Annual Review of Immunology*, vol. 21, no. 1, pp. 685–711, 2003.

[37] A. Merlotti, E. Dantas, F. Remes Lenicov et al., "Fucosylated clusterin in semen promotes the uptake of stress-damaged proteins by dendritic cells via DC-SIGN," *Human Reproduction*, vol. 30, pp. 1545–1556, 2015.

[38] N. H. Choi, T. Tobe, K. Hara, H. Yoshida, and M. Tomita, "Sandwich ELISA assay for quantitative measurement of SP-40, 40 in seminal plasma and serum," *The Journal of Immunological Methods*, vol. 131, no. 2, pp. 159–163, 1990.

[39] T. Fukuda, H. Miyake, N. Enatsu, K. Matsushita, and M. Fujisawa, "Seminal level of clusterin in infertile men as a significant biomarker reflecting spermatogenesis," *Andrologia*, vol. 48, no. 10, pp. 1188–1194, 2016.

[40] I. P. Trougakos, M. Poulakou, M. Stathatos, A. Chalikia, A. Melidonis, and E. S. Gonos, "Serum levels of the senescence biomarker clusterin/apolipoprotein J increase significantly in diabetes type II and during development of coronary heart disease or at myocardial infarction," *Experimental Gerontology*, vol. 37, no. 10-11, pp. 1175–1187, 2002.

[41] H. Miyake, M. Muramaki, J. Furukawa, T. Kurahashi, and M. Fujisawa, "Serum level of clusterin and its density in men with prostate cancer as novel biomarkers reflecting disease extension," *Urology*, vol. 75, no. 2, pp. 454–459, 2010.

[42] A. M. Nafee, H. F. Pasha, S. M. A. El Aal, and N. A. Mostafa, "Clinical significance of serum clusterin as a biomarker for evaluating diagnosis and metastasis potential of viral-related hepatocellular carcinoma," *Clinical Biochemistry*, vol. 45, no. 13-14, pp. 1070–1074, 2012.

[43] M. R. Wilson and A. Zoubeidi, "Clusterin as a therapeutic target," *Expert Opinion on Therapeutic Targets*, vol. 21, no. 2, pp. 201–213, 2017.

[44] M. Z. Kounnas, E. B. Loukinova, S. Stefansson et al., "Identification of Glycoprotein 330 as an Endocytic Receptor for Apolipoprotein J/Clusterin ∗," *Journal of Biological Chemistry*, vol. 270, no. 22, pp. 13070–13075, 1995.

[45] C. Leeb, C. Eresheim, and J. Nimpf, "Clusterin Is a Ligand for Apolipoprotein E Receptor 2 (ApoER2) and Very Low Density Lipoprotein Receptor (VLDLR) and Signals via the Reelin-signaling Pathway∗," *Journal of Biological Chemistry*, vol. 289, no. 7, pp. 4161–4172, 2014.

[46] H. Zhang, J. K. Kim, C. A. Edwards, Z. Xu, R. Taichman, and C. Y. Wang, "Clusterin inhibits apoptosis by interacting with activated Bax," *Nature Cell Biology*, vol. 7, no. 9, pp. 909–915, 2005.

[47] F. Fang, R. Chang, and L. Yang, "Heat shock factor 1 promotes invasion and metastasis of hepatocellular carcinoma in vitro and in vivo," *Cancer*, vol. 118, no. 7, pp. 1782–1794, 2012.

[48] K. Guitart, G. Loers, F. Buck, U. Bork, M. Schachner, and R. Kleene, "Improvement of neuronal cell survival by astrocyte-derived exosomes under hypoxic and ischemic conditions depends on prion protein," *Glia*, vol. 64, no. 6, pp. 896–910, 2016.

[49] B. Shapiro, P. Tocci, G. Haase, N. Gavert, and A. Ben-Ze'ev, "Clusterin, a gene enriched in intestinal stem cells, is required for L1-mediated colon cancer metastasis," *Oncotarget*, vol. 6, no. 33, pp. 34389–34401, 2015.

[50] P. I. Artemaki, A. D. Sklirou, C. K. Kontos et al., "High *clusterin* (CLU) mRNA expression levels in tumors of colorectal cancer patients predict a poor prognostic outcome," *Clinical Biochemistry*, vol. 75, pp. 62–69, 2020.

[51] M. Makridakis, M. G. Roubelakis, V. Bitsika et al., "Analysis of secreted proteins for the study of bladder cancer cell aggressiveness," *Journal of Proteome Research*, vol. 9, no. 6, pp. 3243–3259, 2010.

[52] H. Miyake, M. E. Gleave, S. Arakawa, S. Kamidono, and I. Hara, "Introducing the clusterin gene into human renal cell carcinoma cells enhances their metastatic potential," *The Journal of Urology*, vol. 167, no. 5, pp. 2203–2208, 2002.

[53] T. Y. Chou, W. C. Chen, A. C. Lee, S. M. Hung, N. Y. Shih, and M. Y. Chen, "Clusterin silencing in human lung adenocarcinoma cells induces a mesenchymal- to-epithelial transition through modulating the ERK/Slug pathway," *Cell Signaling*, vol. 21, no. 5, pp. 704–711, 2009.

[54] M. Xu, X. Chen, Y. Han, C. Ma, L. Ma, and S. Li, "Clusterin silencing sensitizes pancreatic cancer MIA-PaCa-2 cells to gmcitabine via regulation of NF-KB/BCL-2 signaling," *International Journal of Clinical and Experimental Medicine*, vol. 8, no. 8, pp. 12476–12486, 2015.

[55] M. Shiota, A. Zardan, A. Takeuchi et al., "Clusterin mediates TGF-β-induced epithelial-mesenchymal transition and metastasis via Twist1 in prostate cancer cells," *Cancer Research*, vol. 72, no. 20, pp. 5261–5272, 2012.

[56] X. Chen, A. M. Bode, Z. Dong, and Y. Cao, "The epithelial-mesenchymal transition (EMT) is regulated by oncoviruses in cancer," *The FASEB Journal*, vol. 30, no. 9, pp. 3001–3010, 2016.

[57] D. C. Park, S. G. Yeo, M. R. Wilson et al., "Clusterin interacts with paclitaxel and confer paclitaxel resistance in ovarian cancer," *Neoplasia*, vol. 10, pp. 964–972, 2008.

[58] S. M. Sintich, J. Steinberg, J. M. Kozlowski et al., "Cytotoxic sensitivity to tumor necrosis factor-in PC3 and LNCaP prostatic cancer cells is regulated by extracellular levels of SGP-2 (clusterin)," *Prostate*, vol. 39, pp. 87–93, 1999.

[59] P. S. Steeg, "Tumor metastasis: mechanistic insights and clinical challenges," *Nature Medicine*, vol. 12, pp. 895–904, 2006.

[60] G. P. Gupta and J. Massagué, "Cancer metastasis: building a framework," *Cell*, vol. 127, pp. 679–695, 2006.

[61] G. S. Zamay, O. S. Kolovskaya, T. N. Zamay et al., "Aptamers selected to postoperative lung adenocarcinoma detect circulating tumor cells in human blood," *Molecular Therapy*, vol. 23, pp. 1486–1496, 2015.

[62] W. Zheng, M. Yao, M. Wu, J. Yang, D. Yao, and L. Wang, "Secretory clusterin promotes hepatocellular carcinoma progression by facilitating cancer stem cell properties via AKT/GSK-3β/β-catenin axis," *Journal of Translational Medicine*, vol. 18, pp. 1–16, 2020.

[63] F. Loison, L. Debure, P. Nizard, P. Le Goff, D. Michel, and Y. Le Dréan, "Up-regulation of the clusterin gene after proteotoxic stress: implication of HSF1-HSF2 heterocomplexes," *The Biochemical Journal*, vol. 395, pp. 223–231, 2006.

[64] H. Prochnow, R. Gollan, P. Rohne, M. Hassemer, C. Koch-Brandt, and M. Baiersdörfer, "Non-secreted clusterin isoforms are translated in rare amounts from distinct human mRNA variants and do not affect Bax-mediated apoptosis or the NF-κB signaling pathway," *PLoS One*, vol. 8, pp. 1–15, 2013.

[65] A. Mogk, C. Schlieker, K. L. Friedrich, H. J. Schönfeld, E. Vierling, and B. Bukau, "Refolding of substrates bound to small Hsps relies on a disaggregation reaction mediated most efficiently by ClpB/DnaK," *The Journal of Biological Chemistry*, vol. 278, pp. 31033–31042, 2003.

[66] F. Seyffer, E. Kummer, Y. Oguchi et al., "Hsp70 proteins bind Hsp100 regulatory M domains to activate AAA+ disaggregase at aggregate surfaces," *Nature Structural & Molecular Biology*, vol. 19, pp. 1347–1355, 2012.

[67] L. Debure, J. L. Vayssière, V. Rincheval, F. Loison, Y. Le Drŕean, and D. Michel, "Intracellular clusterin causes juxtanuclear aggregate formation and mitochondrial alteration," *Journal of Cell Science*, vol. 116, pp. 3109–3121, 2003.

[68] K. S. Leskov, D. Y. Klokov, J. Li, T. J. Kinsella, and D. A. Boothman, "Synthesis and functional analyses of nuclear clusterin, a cell death protein," *The Journal of Biological Chemistry*, vol. 278, pp. 11590–11600, 2003.

[69] K. S. Leskov, S. Araki, J. P. Lavik et al., "CRM1 protein-mediated regulation of nuclear clusterin (nCLU), an ionizing radiation-stimulated, bax-dependent pro-death factor," *The Journal of Biological Chemistry*, vol. 286, pp. 40083–40090, 2011.

[70] B. F. Burkey, H. V. DeSilva, and J. A. K. Harmony, "Intracellular processing of apolipoprotein J precursor to the mature heterodimer," *Journal of Lipid Research*, vol. 32, pp. 1039–1048, 1991.

[71] E. A. Hale, S. K. Raza, R. G. Ciecierski, and P. Ghosh, "Deleterious actions of chronic ethanol treatment on the glycosylation of rat brain clusterin," *Brain Research*, vol. 785, pp. 158–166, 1998.

[72] S. W. Kang, S. Y. Yoon, J. Y. Park, and D. H. Kim, "Unglycosylated clusterin variant accumulates in the endoplasmic reticulum and induces cytotoxicity," *The International Journal of Biochemistry & Cell Biology*, vol. 45, pp. 221–231, 2013.

[73] P. C. Pang, P. C. N. Chiu, C. L. Lee et al., "Human sperm binding is mediated by the sialyl-Lewisx oligosaccharide on the zona pellucida," *Science*, vol. 333, pp. 1761–1764, 2011.

[74] M. Seppälä, H. Koistinen, R. Koistinen, P. C. N. Chiu, and W. S. B. Yeung, "Glycosylation related actions of glycodelin: gamete, cumulus cell, immune cell and clinical associations," *Human Reproduction Update*, vol. 13, pp. 275–287, 2007.

[75] M. Yoshimura, Y. Ihara, A. Ohnishi et al., "Bisecting N-acetylglucosamine on K562 cells suppresses natural killer cytotoxicity and promotes spleen colonization," *Cancer Research*, vol. 56, no. 2, pp. 412–418, 1996.

[76] P. C. Pang, B. Tissot, E. Z. Drobnis, H. R. Morris, A. Dell, and G. F. Clark, "Analysis of the human seminal plasma glycome reveals the presence of immunomodulatory carbohydrate functional groups," *Journal of Proteome Research*, vol. 8, pp. 4906–4915, 2009.

[77] M. Ferens-Sieczkowska, B. Kowalska, and E. M. Kratz, "Seminal plasma glycoproteins in male infertility and prostate diseases: is there a chance for glyco-biomarkers?," *Biomarkers*, vol. 18, pp. 10–22, 2013.

[78] M. Saraswat, S. Joenväärä, A. K. Tomar, S. Singh, S. Yadav, and R. Renkonen, "N-Glycoproteomics of human seminal plasma glycoproteins," *Journal of Proteome Research*, vol. 15, pp. 991–1001, 2016.

[79] J. P. Rickard, T. Pini, C. Soleilhavoup et al., "Seminal plasma aids the survival and cervical transit of epididymal ram spermatozoa," *Reproduction*, vol. 148, pp. 469–478, 2014.

[80] B. Dutta, R. Ain, P. B. Seshagiri, and A. A. Karande, "Differential influence of recombinant non-glycosylated and glycosylated glycodelin on human sperm function: comparative studies with hamster spermatozoa," *Reproduction, Fertility, and Development*, vol. 13, pp. 111–118, 2001.

[81] J. Sabatté, A. Ceballos, S. Raiden et al., "Human seminal plasma abrogates the capture and transmission of human immunodeficiency virus type 1 to CD4+ T cells mediated by DC-SIGN," *Journal of Virology*, vol. 81, pp. 13723–13734, 2007.

[82] T. Tellez, M. Garcia-Aranda, and M. Redondo, "The role of clusterin in carcinogenesis and its potential utility as therapeutic target," *Current Medicinal Chemistry*, vol. 23, pp. 4297–4308, 2016.

[83] M. García-Aranda, T. Téllez, M. Muñoz, and M. Redondo, "Clusterin inhibition mediates sensitivity to chemotherapy and radiotherapy in human cancer, anticancer," *Drugs*, vol. 28, pp. 702–716, 2017.

[84] Q. F. Chen, L. Chang, Q. Su, Y. Zhao, and B. Kong, "Clinical importance of serum secreted clusterin in predicting invasive breast cancer and treatment responses," *Bioengineered*, vol. 12, pp. 278–285, 2021.

[85] S. Miyamoto, L. R. Ruhaak, C. Stroble et al., "Glycoproteomic analysis of malignant ovarian cancer ascites fluid identifies unusual glycopeptides," *Journal of Proteome Research*, vol. 15, pp. 3358–3376, 2016.

[86] A. Blanas, N. M. Sahasrabudhe, E. Rodríguez, Y. van Kooyk, and S. J. van Vliet, "Fucosylated antigens in cancer: an alliance toward tumor progression, metastasis, and resistance to chemotherapy," *Frontiers in oncology*, vol. 8, pp. 2–14, 2018.

[87] E. Miyoshi, K. Moriwaki, and T. Nakagawa, "Biological function of fucosylation in cancer biology," *Journal of Biochemistry*, vol. 143, pp. 725–729, 2008.

[88] A. Merlotti, A. L. Malizia, P. Michea et al., "Aberrant fucosylation enables breast cancer clusterin to interact with dendritic cell-specific ICAM-grabbing non-integrin (DC-SIGN)," *Oncoimmunology*, vol. 8, pp. 1–10, 2019.

[89] X. Chen, R. B. Halberg, W. M. Ehrhardt, J. Torrealba, and W. F. Dove, "Clusterin as a biomarker in murine and human intestinal neoplasia," *Proceedings of the National Academy of Sciences of the United States of America*, vol. 100, pp. 9530–9535, 2003.

[90] S. Pucci, E. Bonanno, F. Pichiorri, C. Angeloni, and L. G. Spagnoli, "Modulation of different clusterin isoforms in human colon tumorigenesis," *Oncogene*, vol. 23, pp. 2298–2304, 2004.

[91] I. P. Trougakos, M. Lourda, G. Agiostratidou, D. Kletsas, and E. S. Gonos, "Differential effects of clusterin/apolipoprotein J on cellular growth and survival," *Free Radical Biology & Medicine*, vol. 38, pp. 436–449, 2005.

[92] A. M. Rodríguez-Piñeiro, M. Páez de la Cadena, Á. López-Saco, and F. J. Rodríguez-Berrocal, "Differential expression of serum clusterin isoforms in colorectal cancer," *Molecular & Cellular Proteomics*, vol. 5, pp. 1647–1657, 2006.

[93] H. Miyake, M. E. Gleave, H. Miyake, I. Hara, and S. Kamidono, "Synergistic chemsensitization and inhibition of tumor growth and metastasis by the antisense oligodeoxynucleotide targeting clusterin gene in a human bladder cancer model," *Clinical Cancer Research*, vol. 7, pp. 4245–4252, 2001.

[94] M. E. Gleave, H. Miyake, T. Zellweger et al., "Use of antisense oligonucleotides targeting the antiapoptotic gene, clusterin/testosterone-repressed prostate message 2, to enhance androgen sensitivity and chemosensitivity in prostate cancer," *Urology*, vol. 58, pp. 39–48, 2001.

[95] H. Miyake, C. Nelson, P. S. Rennie, and M. E. Gleave, "Acquisition of chemoresistant phenotype by overexpression of the antiapoptotic gene testosterone-repressed prostate message-2 in prostate cancer xenograft models," *Cancer Research*, vol. 60, no. 9, pp. 2547–2554, 2000.

[96] J.-G. Chen, J. Zhu, Y.-H. Zhang et al., "Cancer survival in Qidong between 1972 and 2011: a population-based analysis," *Molecular and Clinical Oncology*, vol. 6, pp. 944–954, 2017.

[97] M. Yao, M. Fang, W. Zheng, Z. Dong, and D. Yao, "Role of secretory clusterin in hepatocarcinogenesis," *Translational Gastroenterology and Hepatology*, vol. 3, p. 48, 2018.

[98] J. Choi, G. A. Kim, S. Han, W. Lee, S. Chun, and Y. S. Lim, "Longitudinal assessment of three serum biomarkers to

detect very early-stage hepatocellular carcinoma," *Hepatology*, vol. 69, pp. 1983–1994, 2019.

[99] J. A. Marrero, P. R. Romano, O. Nikolaeva et al., "GP73, a resident Golgi glycoprotein, is a novel serum marker for hepatocellular carcinoma," *Journal of Hepatology*, vol. 43, pp. 1007–1012, 2005.

[100] P. Xiu, X. Dong, X. Dong et al., "Secretory clusterin contributes to oxaliplatin resistance by activating Akt pathway in hepatocellular carcinoma," *Cancer Science*, vol. 104, pp. 375–382, 2013.

[101] C. Wang, K. Jiang, D. Gao et al., "Clusterin protects hepatocellular carcinoma cells from endoplasmic reticulum stress induced apoptosis through GRP78," *PLoS One*, vol. 8, pp. 1–9, 2013.

[102] X. Sheng, T. Huang, J. Qin, L. Yang, Z. Sa, and Q. Li, "Identification of the differential expression profiles of serum and tissue proteins during rat hepatocarcinogenesis," *Technology in Cancer Research & Treatment*, vol. 17, pp. 1–13, 2018.

[103] M. A. Comunale, M. Wang, L. Rodemich-Betesh et al., "Novel changes in glycosylation of serum Apo-J in patients with hepatocellular carcinoma," *Cancer Epidemiology, Biomarkers & Prevention*, vol. 20, pp. 1222–1229, 2011.

[104] K. L. Abbott and J. M. Pierce, "Lectin-based glycoproteomic techniques for the enrichment and identification of potential biomarkers," *Methods in enzymology*, vol. 480, pp. 461–476, 2010.

[105] Y. Hu, J. Feng, and F. Wu, "The multiplicity of polypeptide GalNAc-transferase: assays, inhibitors, and structures," *ChemBioChem*, vol. 19, pp. 2503–2521, 2018.

[106] R. H. Weiss and P. Y. Lin, "Kidney cancer: identification of novel targets for therapy," *Kidney International*, vol. 69, pp. 224–232, 2006.

[107] J. Bones, N. McLoughlin, M. Hilliard, K. Wynne, B. L. Karger, and P. M. Rudd, "2D-LC analysis of BRP 3 erythropoietin N-glycosylation using anion exchange fractionation and hydrophilic interaction UPLC reveals long poly-N-acetyl lactosamine extensions," *Analytical Chemistry*, vol. 83, pp. 4154–4162, 2011.

[108] A. Lee, J. M. Chick, D. Kolarich et al., "Liver membrane proteome glycosylation changes in mice bearing an extra-hepatic tumor," *Molecular & Cellular Proteomics*, vol. 10, no. 9, pp. M900538–MMCP200, 2011.

[109] P. Pompach, K. B. Chandler, R. Lan, N. Edwards, and R. Goldman, "Semi-automated identification of N-glycopeptides by hydrophilic interaction chromatography, nano-reverse-phase LC-MS/MS, and glycan database search," *Journal of Proteome Research*, vol. 11, pp. 1728–1740, 2012.

[110] R. K. Sterling, L. Jeffers, F. Gordon et al., "Clinical utility of AFP-L3% measurement in North American patients with HCV-related cirrhosis," *The American Journal of Gastroenterology*, vol. 102, pp. 2196–2205, 2007.

[111] S. Hua, C. Lebrilla, and H. J. An, "Application of nano-LC-based glycomics towards biomarker discovery," *Bioanalysis*, vol. 3, pp. 2573–2585, 2011.

[112] S. Hua, C. C. Nwosu, J. S. Strum et al., "Site-specific protein glycosylation analysis with glycan isomer differentiation," *Analytical and Bioanalytical Chemistry*, vol. 403, pp. 1291–1302, 2012.

[113] T. Kurahashi, M. Muramaki, K. Yamanaka, I. Hara, and H. Miyake, "Expression of the secreted form of clusterin protein in renal cell carcinoma as a predictor of disease extension," *BJU International*, vol. 96, pp. 895–899, 2005.

[114] F. Tousi, J. Bones, O. Iliopoulos, W. S. Hancock, and M. Hincapie, "Multidimensional liquid chromatography platform for profiling alterations of clusterin N-glycosylation in the plasma of patients with renal cell carcinoma," *Journal of Chromatography A*, vol. 1256, pp. 121–128, 2012.

[115] F. O. Gbormittah, J. Bones, M. Hincapie, F. Tousi, W. S. Hancock, and O. Iliopoulos, "Clusterin glycopeptide variant characterization reveals significant site-specific glycan changes in the plasma of clear cell renal cell carcinoma," *Journal of Proteome Research*, vol. 14, pp. 2425–2436, 2015.

[116] S. Baig, L. E. Palmer, M. J. Owen, J. Williams, P. G. Kehoe, and S. Love, "Clusterin mRNA and protein in Alzheimer's disease," *Journal of Alzheimer's Disease*, vol. 28, pp. 337–344, 2012.

[117] J. T. Yu and L. Tan, "The role of clusterin in Alzheimer's disease: pathways, pathogenesis, and therapy," *Molecular Neurobiology*, vol. 45, pp. 314–326, 2012.

[118] R. S. Desikan, W. K. Thompson, D. Holland et al., "The role of clusterin in amyloid-β-associated neurodegeneration," *JAMA Neurology*, vol. 71, pp. 180–187, 2014.

[119] M. D. Martin-Rehrmann, H. S. Hoe, E. M. Capuani, and G. W. Rebeck, "Association of apolipoprotein J-positive β-amyloid plaques with dystrophic neurites in Alzheimer's disease brain," *Neurotoxicity Research*, vol. 7, pp. 231–241, 2005.

[120] P. Yuste-Checa, V. A. Trinkaus, I. Riera-Tur et al., "The extracellular chaperone clusterin enhances Tau aggregate seeding in a cellular model," *Nature Communications*, vol. 12, pp. 1–15, 2021.

[121] A. M. Lidström, N. Bogdanovic, C. Hesse, I. Volkman, P. Davidsson, and K. Blennow, "Clusterin (apolipoprotein J) protein levels are increased in hippocampus and in frontal cortex in Alzheimer's disease," *Experimental Neurology*, vol. 154, pp. 511–521, 1998.

[122] P. Bertrand, J. Poirier, T. Oda, C. E. Finch, and G. M. Pasinetti, "Association of apolipoprotein E genotype with brain levels of apolipoprotein E and apolipoprotein J (clusterin) in Alzheimer disease," *Molecular Brain Research*, vol. 33, pp. 174–178, 1995.

[123] J. Wang, X. Zhang, B. Zhu, and P. Fu, "Association of clusterin levels in cerebrospinal fluid with synaptic degeneration across the Alzheimer's disease continuum," *Neuropsychiatric Disease and Treatment*, vol. 16, pp. 183–190, 2020.

[124] A. M. Nilselid, P. Davidsson, K. Nägga, N. Andreasen, P. Fredman, and K. Blennow, "Clusterin in cerebrospinal fluid: analysis of carbohydrates and quantification of native and glycosylated forms," *Neurochemistry International*, vol. 48, pp. 718–728, 2006.

[125] A. M. Lidström, C. Hesse, L. Rosengren, P. Fredman, and P. Davidsson, "Normal levels of clusterin in cerebrospinal fluid in Alzheimer's disease, and no change after acute ischemic stroke," *Journal of Alzheimer's Disease*, vol. 3, pp. 435–442, 2001.

[126] C. Sihlbom, P. Davidsson, M. Sjögren, L. O. Wahlund, and C. L. Nilsson, "Structural and quantitative comparison of cerebrospinal fluid glycoproteins in Alzheimer's disease patients and healthy individuals," *Neurochemical Research*, vol. 33, pp. 1332–1340, 2008.

[127] Y. Y. Xing, J. T. Yu, W. Z. Cui et al., "Blood clusterin levels, rs 9331888 polymorphism, and the risk of Alzheimer's disease," *Journal of Alzheimer's Disease*, vol. 29, pp. 515–519, 2012.

[128] V. J. Balcar, T. Zeman, V. Janout, J. Janoutová, J. Lochman, and O. Šerý, "Single nucleotide polymorphism rs11136000 of CLU gene (Clusterin, ApoJ) and the risk of late-onset Alzheimer's disease in a Central European Population," *Neurochemical Research*, vol. 46, pp. 411–422, 2021.

[129] J. J. Yerbury, S. Poon, S. Meehan et al., "The extracellular chaperone clusterin influences amyloid formation and toxicity by interacting with prefibrillar structures," *The FASEB Journal*, vol. 21, pp. 2312–2322, 2007.

[130] T. M. Maguire, A. M. Gillian, D. O'Mahony, C. M. Coughlan, and K. C. Breen, "A decrease in serum sialyltransferase levels in Alzheimer's disease," *Neurobiology of Aging*, vol. 15, no. 1, pp. 99–102, 1994.

[131] L. R. Fodero, J. Sáez-Valero, M. S. Barquero, A. Marcos, C. A. McLean, and D. H. Small, "Wheat germ agglutinin-binding glycoproteins are decreased in Alzheimer's disease cerebrospinal fluid," *Journal of Neurochemistry*, vol. 79, pp. 1022–1026, 2001.

[132] H. C. Liang, C. Russell, V. Mitra et al., "Glycosylation of human plasma clusterin yields a novel candidate biomarker of Alzheimer's disease," *Journal of Proteome Research*, vol. 14, pp. 5063–5076, 2015.

[133] Y. Lin, L. Lu, M. Zhou et al., "Association of CLU gene polymorphism with Parkinson's disease in the Chinese Han population," *The Journal of Gene Medicine*, vol. 23, pp. 1–6, 2021.

[134] F. Sampedro, J. Marín-Lahoz, S. Martínez-Horta, R. Pérez-González, J. Pagonabarraga, and J. Kulisevsky, "CLU rs11136000 promotes early cognitive decline in Parkinson's disease," *Movement Disorders*, vol. 35, pp. 508–513, 2020.

[135] D. R. Whiten, D. Cox, M. H. Horrocks et al., "Single-molecule characterization of the interactions between extracellular chaperones and toxic α-synuclein oligomers," *Cell Reports*, vol. 23, pp. 3492–3500, 2018.

[136] H. P. Vranová, J. Mareš, M. Nevrlý et al., "CSF markers of neurodegeneration in Parkinson's disease," *Journal of Neural Transmission*, vol. 117, pp. 1177–1181, 2010.

[137] P. Ghosh, S. J. Chirtel, and M. R. Lakshman, "Effect of chronic ethanol on apolipoprotein (Apo) E synthesis and glycosylation in rats," *Alcoholism, Clinical and Experimental Research*, vol. 15, pp. 725–729, 1991.

[138] P. Ghosh, Q. H. Liu, and M. R. Lakshman, "Long-term ethanol exposure impairs glycosylation of both N- and O-glycosylated proteins in rat liver," *Metabolism*, vol. 44, pp. 890–898, 1995.

[139] T. M. Donohue, N. A. Osna, K. K. Kharbanda, and P. G. Thomes, "Lysosome and proteasome dysfunction in alcohol-induced liver injury," *Liver Research*, vol. 3, pp. 191–205, 2019.

[140] T. Jayaraman, S. Kannappan, M. K. Ravichandran, and C. V. Anuradha, "Impact of essentiale L on ethanol-induced changes in rat brain and erythrocytes," *Singapore Medical Journal*, vol. 49, no. 4, pp. 320–327, 2008.

[141] H. V. De Silva, W. D. Stuart, C. R. Duvic et al., "A 70-kDa apolipoprotein designated ApoJ is a marker for subclasses of human plasma high density lipoproteins," *The Journal of Biological Chemistry*, vol. 265, pp. 13240–13247, 1990.

[142] P. C. May and C. E. Finch, "Sulfated glycoprotein 2: new relationships of this multifunctional protein to neurodegeneration," *Trends in Neurosciences*, vol. 15, pp. 391–396, 1992.

[143] G. P. Bhide and K. J. Colley, "Sialylation of N-glycans: mechanism, cellular compartmentalization and function," *Histochemistry and Cell Biology*, vol. 147, pp. 149–174, 2017.

[144] M. A. Javors and B. A. Johnson, "Current status of carbohydrate deficient transferrin, total serum sialic acid, sialic acid index of apolipoprotein J and serum β-hexosaminidase as markers for alcohol consumption," *Addiction*, vol. 98, pp. 45–50, 2003.

[145] D. E. Jenne and J. Tschopp, "Clusterin: the intriguing guises of a widely expressed glycoprotein," *Trends in Biochemical Sciences*, vol. 17, pp. 154–159, 1992.

[146] E. Kida, R. Pluta, A. S. Lossinsky et al., "Complete cerebral ischemia with short-term survival in rat induced by cardiac arrest. II. Extracellular and intracellular accumulation of apolipoproteins E and J in the brain," *Brain Research*, vol. 674, pp. 341–346, 1995.

[147] K. Bettens, S. Vermeulen, C. Van Cauwenberghe et al., "Reduced secreted clusterin as a mechanism for Alzheimer-associated CLU mutations," *Molecular Neurodegeneration*, vol. 10, p. 30, 2015.

[148] H. M. Dingerdissen, J. Torcivia-Rodriguez, Y. Hu, T. C. Chang, R. Mazumder, and R. Kahsay, "BioMuta and BioXpress: mutation and expression knowledge bases for cancer biomarker discovery," *Nucleic Acids Research*, vol. 46, pp. D1128–D1136, 2018.

[149] C. Torres-Arancivia, D. Chang, J. Zaia, and L. H. Connors, "Structural studies of serum clusterin in ATTRwt amyloidosis," *Amyloid*, vol. 26, pp. 51-52, 2019.

[150] C. M. Torres-Arancivia, D. Chang, W. E. Hackett, J. Zaia, and L. H. Connors, "Glycosylation of serum clusterin in wild-type transthyretin-associated (ATTRwt) amyloidosis: a study of disease-associated compositional features using mass spectrometry analyses," *Biochemistry*, vol. 59, pp. 4367–4378, 2020.

[151] D. A. Morrow, C. P. Cannon, R. L. Jesse et al., "National Academy of Clinical Biochemistry Laboratory Medicine Practice Guidelines: clinical characteristics and utilization of biochemical markers in acute coronary syndromes," *Circulation*, vol. 115, pp. e356–e375, 2007.

[152] H. A. Katus, "Diagnostic efficiency of troponin T measurements in acute myocardial infarction," *Circulation*, vol. 83, pp. 902–912, 1991.

[153] L. Babuin and A. S. Jaffe, "Troponin: the biomarker of choice for the detection of cardiac injury," *CMAJ*, vol. 173, pp. 1191–1202, 2005.

[154] C. Kabaroglu, I. Mutaf, B. Boydak et al., "Association between serum paraoxonase activity and oxidative stress in acute coronary syndromes," *Acta Cardiologica*, vol. 59, pp. 606–611, 2004.

[155] G. G. Schwartz, "High-density lipoprotein cholesterol as a risk factor and target of therapy after acute coronary syndrome," *The American Journal of Cardiology*, vol. 104, pp. 46E–51E, 2009.

[156] T. Vaisar, S. Pennathur, P. S. Green et al., "Shotgun proteomics implicates protease inhibition and complement activation in the antiinflammatory properties of HDL," *The Journal of Clinical Investigation*, vol. 117, pp. 746–756, 2007.

[157] B. J. Van Lenten, A. C. Wagner, D. P. Nayak, S. Hama, M. Navab, and A. M. Fogelman, "High-density lipoprotein loses its anti-inflammatory properties during acute influenza A infection," *Circulation*, vol. 103, pp. 2283–2288, 2001.

[158] P. Keul, A. Polzin, K. Kaiser et al., "Potent anti-inflammatory properties of HDL in vascular smooth muscle cells mediated by HDL-S1P and their impairment in coronary artery disease

due to lower HDL-S1P: a new aspect of HDL dysfunction and its therapy," *The FASEB Journal*, vol. 33, pp. 1482–1495, 2019.

[159] W. D. Stuart, B. Krol, J. A. K. Harmony, and S. H. Jenkins, "Structure and stability of apolipoprotein J-containing high-density lipoproteins," *Biochemistry*, vol. 31, pp. 8552–8559, 1992.

[160] J. Cubedo, T. Padró, X. García-Moll, X. Pintó, J. Cinca, and L. Badimon, "Proteomic signature of apolipoprotein J in the early phase of new-onset myocardial infarction," *Journal of Proteome Research*, vol. 10, pp. 211–220, 2011.

[161] S. B. Prusiner, "Molecular biology of prion diseases," *Science*, vol. 252, pp. 1515–1522, 1991.

[162] U. Braun, E. Schicker, and B. Hörnlimann, "Diagnostic reliability of clinical signs in cows with suspected bovine spongiform encephalopathy," *The Veterinary Record*, vol. 143, pp. 101–105, 1998.

[163] F. Xu, E. Karnaukhova, and J. G. Vostal, "Human cellular prion protein interacts directly with clusterin protein," *Biochimica et Biophysica Acta, Molecular Basis of Disease*, vol. 1782, pp. 615–620, 2008.

[164] S. L. R. Simon, L. Lamoureux, M. Plews et al., "The identification of disease-induced biomarkers in the urine of BSE infected cattle," *Proteome Science*, vol. 6, no. 1, 2008.

[165] L. Lamoureux, S. L. R. Simon, M. Plews et al., "Analysis of clusterin glycoforms in the urine of BSE-infected Fleckvieh-Simmental cows," *Journal of Toxicology and Environmental Health, Part A*, vol. 74, pp. 138–145, 2011.

Hindawi
Oxidative Medicine and Cellular Longevity
Volume 2022, Article ID 8122532, 24 pages
https://doi.org/10.1155/2022/8122532

Research Article

Identification and Experimental Validation of Marker Genes between Diabetes and Alzheimer's Disease

Cheng Huang,[1,2] Xueyi Wen,[1,2] Hesong Xie,[1,2] Di Hu,[1,2] and Keshen Li[1,2]

[1]*Department of Neurology and Stroke Center, The First Affiliated Hospital of Jinan University, Guangzhou, China*
[2]*Clinical Neuroscience Institute of Jinan University, Guangzhou, China*

Correspondence should be addressed to Keshen Li; likeshen1971@126.com

Received 17 May 2022; Revised 15 June 2022; Accepted 1 August 2022; Published 12 August 2022

Academic Editor: Amjad Islam Aqib

Currently, Alzheimer's disease (AD) and type 2 diabetes mellitus (T2DM) are widely prevalent in the elderly population, and accumulating evidence implies a strong link between them. For example, patients with T2DM have a higher risk of developing neurocognitive disorders, including AD, but the exact mechanisms are still unclear. This time, by combining bioinformatics analysis and in vivo experimental validation, we attempted to find a common biological link between AD and T2DM. We firstly downloaded the gene expression profiling (AD: GSE122063; T2DM: GSE161355) derived from the temporal cortex. To find the associations, differentially expressed genes (DEGs) of the two datasets were filtered and intersected. Based on them, enrichment analysis was carried out, and the least absolute shrinkage and selection operator (LASSO) logistic regression and support vector machine-recursive feature elimination (SVM-RFE) algorithms were used to identify the specific genes. After verifying in the external dataset and in the samples from the AD and type 2 diabetes animals, the shared targets of the two diseases were finally determined. Based on them, the ceRNA networks were constructed. Besides, the logistic regression and single-sample gene set enrichment analysis (ssGSEA) were performed. As a result, 62 DEGs were totally identified between AD and T2DM, and the enrichment analysis indicated that they were much related to the function of synaptic vesicle and MAPK signaling pathway. Based on the evidence from external dataset and RT-qPCR, CARTPT, EPHA5, and SERPINA3 were identified as the marker genes in both diseases, and their clinical significance and biological functions were further analyzed. In conclusion, discovering and exploring the marker genes that are dysregulated in both 2 diseases could help us better comprehend the intrinsic relationship between T2DM and AD, which may inspire us to develop new strategies for facing the dilemmas of clinical or basic research in cognitive dysfunction.

1. Introduction

Alzheimer's disease (AD), the leading cause of dementia, is emerging as a major global health challenge. Clinically, patients show a cognitive decline, accompanied by significant psychobehavioral abnormalities and impaired social life [1]. However, the molecular mechanism that can effectively explain this abnormal alteration is not yet clear. Usually, several nonspecific factors, such as age, vascular disease, infection, and environmental changes, are thought to play a role [2]. Currently available drugs developed to target these factors only slow the progression of the disease, not cure or prevent it. The realistic quandary forces us to expand theoretical hypotheses. Now, dysglycaemia involving the central nervous system (CNS) appears to be the next frontier in AD research [3].

Approximately 6% of the global population is affected by type 2 diabetes mellitus, and the prevalence of this chronic endocrine disease is rising [4, 5]. In-depth research on glucose metabolism brings new insights into our understanding of AD-related mechanisms. At present, a close association between AD and T2DM has been found. Epidemiological evidence shows much greater impairments in executive function, processing speed, and verbal memory plague adults with T2DM [6], and they have a higher incidence of cognitive dysfunction compared with the general population [7, 8]. Insulin is a major polypeptide hormone that plays crucial roles in the brain, including the release or reuptake of neurotransmitters,

the improvement of learning and memory abilities, and the activation of signal transduction cascades leading to long-term memory consolidation [9]. Besides, research shows the involvement of insulin in the activation of glycogen synthase kinase 3β, which leads to the phosphorylation of tau and the formation of neurofibrillary tangles [10]. It can be seen that the disorder of blood glucose metabolism in the brain may be closely involved in the pathological changes of Alzheimer's disease. So some people refer to Alzheimer's disease as "brain diabetes" [11]. On this basis, studies on specific brain regions are still preliminary.

Studies have demonstrated that impairment of executive ability and memory is associated with the reduced gray matter density and glucose metabolism in the temporal cortex (middle gyrus, parahippocampus, and uncinate lobe) [12]. Diabetics are at risk for brain structural changes [13], and the medial temporal structures are vulnerable to being involved, causing abnormal atrophy of the hippocampus and amygdala [14]. This has some similarities with Alzheimer's disease and maybe one of the neural mechanisms of type 2 diabetes patients' easy transformation to dementia. These suggest that temporal lobe abnormalities play an important role in type 2 diabetes-related cognitive impairment [15].

To figure out the association between Alzheimer's disease and type 2 diabetes as precisely as possible and determine the mechanisms and targets that potentially regulate their interrelationships in the temporal lobe, an exploratory method that combines high-throughput gene expression detection technology with bioinformatics was mainly employed to discover the molecular markers and quest their subtle physiological functions in this research. Based on the Gene Expression Omnibus (GEO) database (https://www.ncbi.nlm.nih.gov/geo/), we firstly identified the codysregulated genes in the temporal cortex, respectively, obtained from the patients of type 2 diabetes and AD to try to find a genetic bridge. The protein-protein interaction (PPI) and enrichment analysis were then performed. Besides, the machine learning algorithms were introduced to further screen the potential markers. With the validation in the external dataset and animal samples, targets were finally confirmed. Their disease-related risks and regulatory factors, such as miRNAs and interacting drugs, were predicted. These findings may provide a deeper insight into the molecular interactions between type 2 diabetes and Alzheimer's disease, assisting us in discovering new regimens for the disease transformation.

2. Materials and Methods

The whole analysis flow of this study is shown in Figure 1.

2.1. Microarray Data. Gene expression profiling in this work was downloaded from the NCBI-GEO database [16]. Specifically, the GSE161355 [17] dataset for the human temporal cortex (T2DM: 6 cases; normal controls: 5 cases) was executed on the GPL570 platform; the GSE122063 [18] (AD: 28 cases; normal controls: 22 cases) and GSE5281 (AD: 16 cases; normal controls: 12 cases) datasets for the human temporal cortex were, respectively, based on the GPL16699 and the GPL570 platforms.

2.2. Data Processing. R software (version 4.0.2) and Bioconductor packages (http://www.bioconductor.org/) [19] were subsequently applied in the data processing.

For the .CEL format files (GSE161355), the "affy" [20] (version 1.66.0), and "affyPLM" [21] (version 1.64.0) packages are used to process the raw data by the RMA (robust multiarray average) function firstly [22]. Then, the probe identification numbers were converted into the official gene symbols according to the GPL570 platform. If multiple probes correspond to one gene, the average value was selected. After processing the missing value of the gene expression profile file by the KNN (k-nearest neighbor) algorithm [23], the "LIMMA" package [24] (version 3.44.3) built-in R was used to identify the differentially expressed genes (DEGs; adjusted $P < 0.05$ and $|\text{logFC}| > 1$ were set as the cutoff criteria).

For the .txt format files (GSE122063 and GSE5281), the probe identification numbers were converted into the official gene symbols according to the GPL16699 and GPL570 platforms. The average expression was taken when multiple probes corresponded to the one. After log2 transformation and normalization, the "LIMMA" package (version 3.44.3) was used to identify the DEGs (adjusted $P < 0.05$ and $|log\ FC| > 1$ were set as the cutoff criteria). The GSE5281 dataset served as the validation set in this research.

2.3. Gene Ontology and Pathway Enrichment Analysis. Gene Ontology (GO) and Kyoto Encyclopedia of Genes and Genomes (KEGG) pathway enrichment analyses [25] were executed by using clusterProfiler package [26] (version 3.16.0) in R software (version 4.0.2) for function annotating and pathway predicting. When the results met the cutoff criterion ($P < 0.05$), it was considered statistically significant.

2.4. Construction of Protein-Protein Interaction (PPI) Network and Module Analysis. STRING (Search Tool for the Retrieval of Interacting Genes/Proteins; https://www.string-db.org/) [27] integrating multiple databases that provide information on candidate genes was employed for predicting the potential PPI network and detecting the possible associations (confidence score 0.4). Furthermore, the MCODE (version 1.6.1) and cytoHubba (version 0.1) plugin [28] built in the Cytoscape software (http://cytoscape.org/; version 3.7.2) were, respectively, used to identify the significant module and hub genes in the constructed network.

2.5. Screening and Validation of the Specific Genes in the Disease. The least absolute shrinkage and selection operator (LASSO) logistic regression [29] with the "glmnet" package (version 4.1-1) and the support vector machine-recursive feature elimination (SVM-RFE) [30] with the "e1071" package (version 1.7-6) were applied to screen the specific genes. The obtained results of the two algorithms were intersected and displayed in a Venn diagram, and all of them were further screened through the combination of Comparative Toxicogenomics Database (CTD; http://ctdbase.org/) [31] and the GSE5281 dataset. Besides, we used the pROC package (version 1.18.0) [32] of R to analyze the receiver operating characteristic (ROC) curve to evaluate their performance.

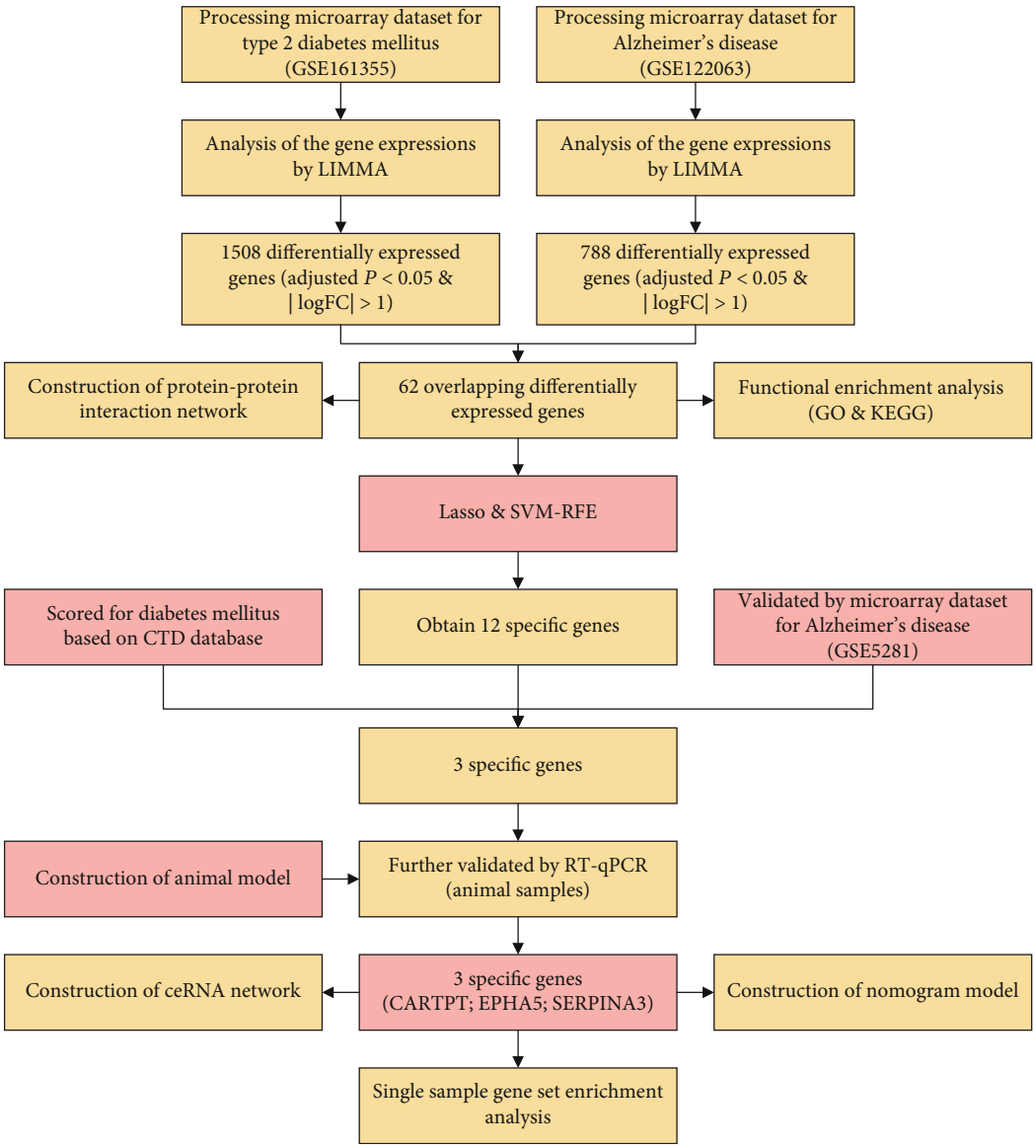

Figure 1: The whole analysis flow for this study.

2.6. Experimental Animals. Adult C57BL/6 mice (male; 4-week-old; $n = 10$) were purchased for type 2 diabetes model construction, and they were randomly divided into the control ($n = 5$) and the diabetic group ($n = 5$). The newly purchased animals were fed with regular chow diet for one week. In the following 4 weeks, the control mice were continued to be regular fed, while the model mice were given high-fat diet [33]. Eight-month-old APP/PS1 mice (male; $n = 5$) were used as AD model in vivo, and age-matched C57BL/6 mice were the controls (male; $n = 5$). All animals were housed in standard polypropylene cages. During the period, they were allowed to free diet under a stable condition (lights on: 08 : 00 am; lights off: 20 : 00 pm; optimum temperature: $23 \pm 2^{\circ}$C; suitable humidity: $55 \pm 5\%$). All the animal experiments were approved by the Institutional Animal Care and Use Committee of Jinan University.

2.7. Type 2 Diabetes Model. Before the start of the experiment, another week of environmental adaptation was carried out. For the diabetic group, 45 mg/kg streptozocin (STZ; Solarbio Beijing) was intraperitoneally injected for one week, while the same volume of saline was injected into the controls. During the week of drug injection, we trained the mice on the Y maze for the first six days and performed the final behavioral test on the seventh day. The blood glucose in caudal venous was detected every two days. When random blood glucose > 16.7 mmol/L [34], they were considered diabetic.

2.8. Behavioral Test. The Y maze was applied to detect the memory ability of mice. The maze consists of three arms divided into 1 start arm and 2 nonstart arms. Each arm was 30 cm long, 15 cm high, and 10 cm wide with an angle of 120 degrees. Markers were set around the maze. The first

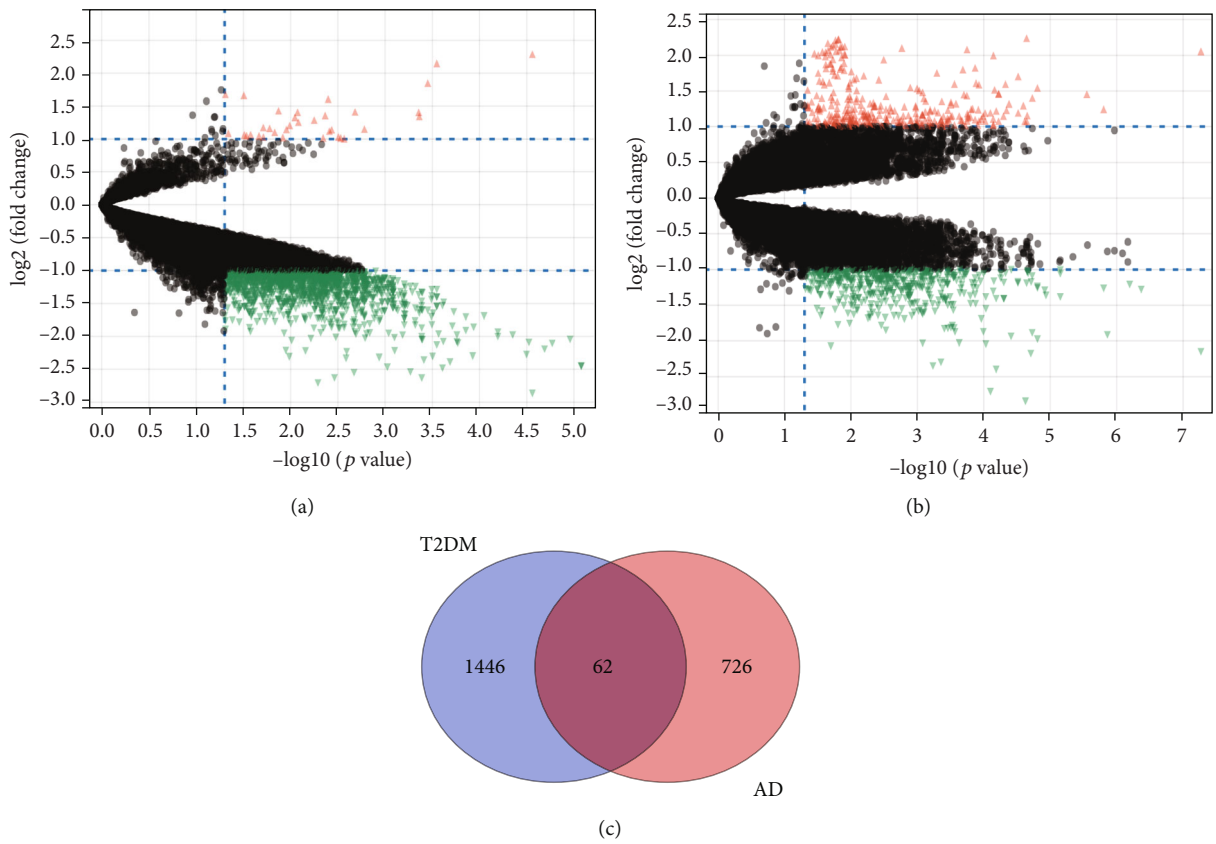

Figure 2: Volcano plot of differently expressed genes. (a) GSE161355 (T2DM), (b) GSE122063 (AD), and (c) the intersection of the two sets of DEGs: 62 genes.

six days are the training period. Each mouse was placed at the end of one start arm and allowed to freely move through the maze for adaptation over the course of 5 minutes. One (target arm) was randomly selected in the two nonstart arms, with food placed on the end and well marked, and the another (nontarget arm) was left untreated. After the adaptation, put the animal back into the end of the start arm, timing was initiated, and the latency and times for the animal to correctly enter the food arm were recorded. Each animal repeated 6 times daily. On the seventh day, the mark of the target arm was changed, and no food was put in. After the animal was put into the start arm, the duration and times of the animal entering the target arm were recorded. The test period of each mice was 5 minutes. The maximum number of arm alternations was defined as the number of occurrences in all arms minus 2, and the percentage of arm alternations was (number of occurrences in the target arm/maximum number of alternations) × 100 [35].

2.9. Sample Collection. After completing all tests, the experimental mice were decapitated. The mice were anesthetized with 15% pentobarbital sodium solution (intraperitoneal injection; 0.4 ml/100 g). Then, cardiac perfusion was performed by irrigation with 0.9% sodium chloride solution [36]. The temporal cortex was collected and stored at −80°C until molecule experiments.

2.10. Reverse Transcription Quantitative Real-Time Polymerase Chain Reaction (RT-qPCR). RNAs were extracted from the temporal cortex of mice using TRIzol reagent (Invitrogen, CA, USA), and the concentration and purity were detected by Nanodrop. According to the manufacturer's instructions, we reverse-transcribed the RNAs into cDNAs with the PrimerScript RT Reagent Kit (Takara). With the SYBR Premix Ex Taq (Takara), RT-qPCR proceeded in the Bio-Rad CFX96 TouchTM system. The primer of different genes needed in our research is shown in the Supplementary Table 1. Target genes were normalized to GAPDH using the comparative CT method.

2.11. ceRNA Network Construction. The miRNAs interacting with the DEGs were predicted by the StarBase (http://starbase.sysu.edu.cn) database [37] or miRSystem (http://mirsystem.cgm.ntu.edu.tw/) database [38]. StarBase integrates seven well known miRNA target gene prediction programs: PITA, RNA22, miRmap, microT, miRanda, PicTar, and TargetScan, while miRSystem integrates DIANA, miRanda, miRBridge, PicTar, PITA, RNA22, and TargetScan. After comprehensive evaluation, the miRNAs hitting the most programs will be included in our research. The interaction between miRNA and lncRNAs/circRNAs was also predicted by using the StarBase. During the operation, we refer to the ClipExpNum to remove the weak interactions with miRNAs for net simplifying.

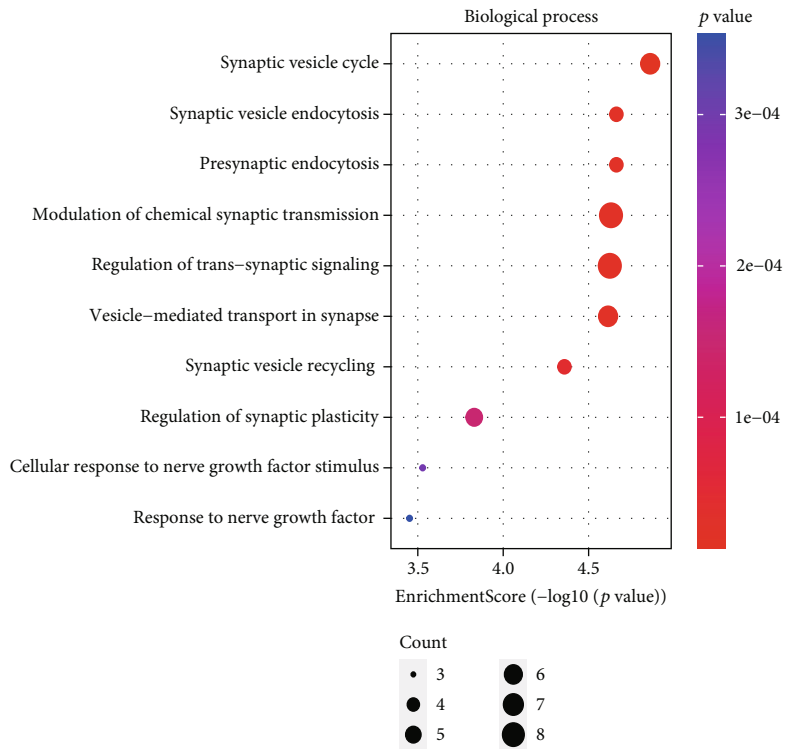

(a)

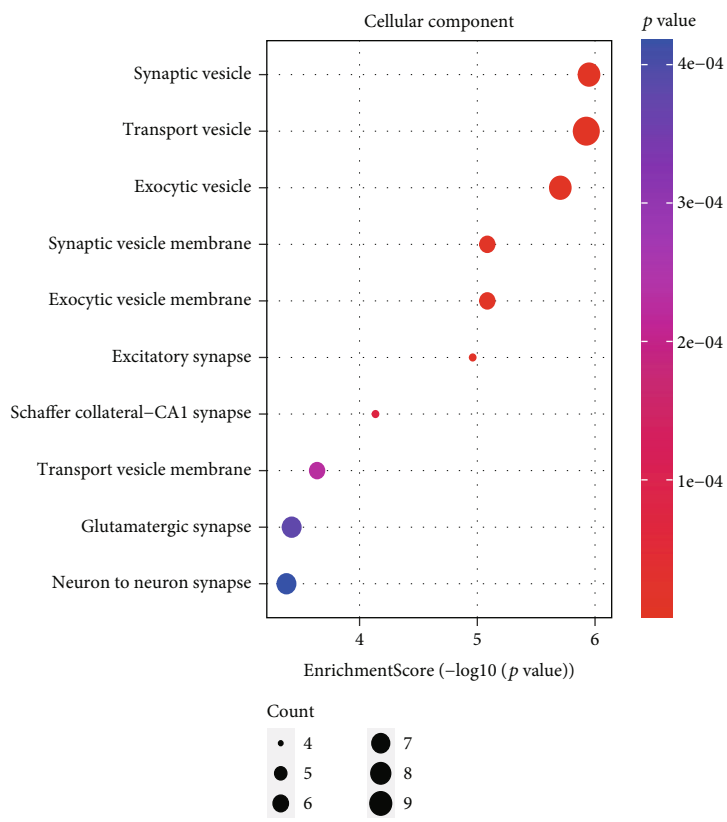

(b)

Figure 3: Continued.

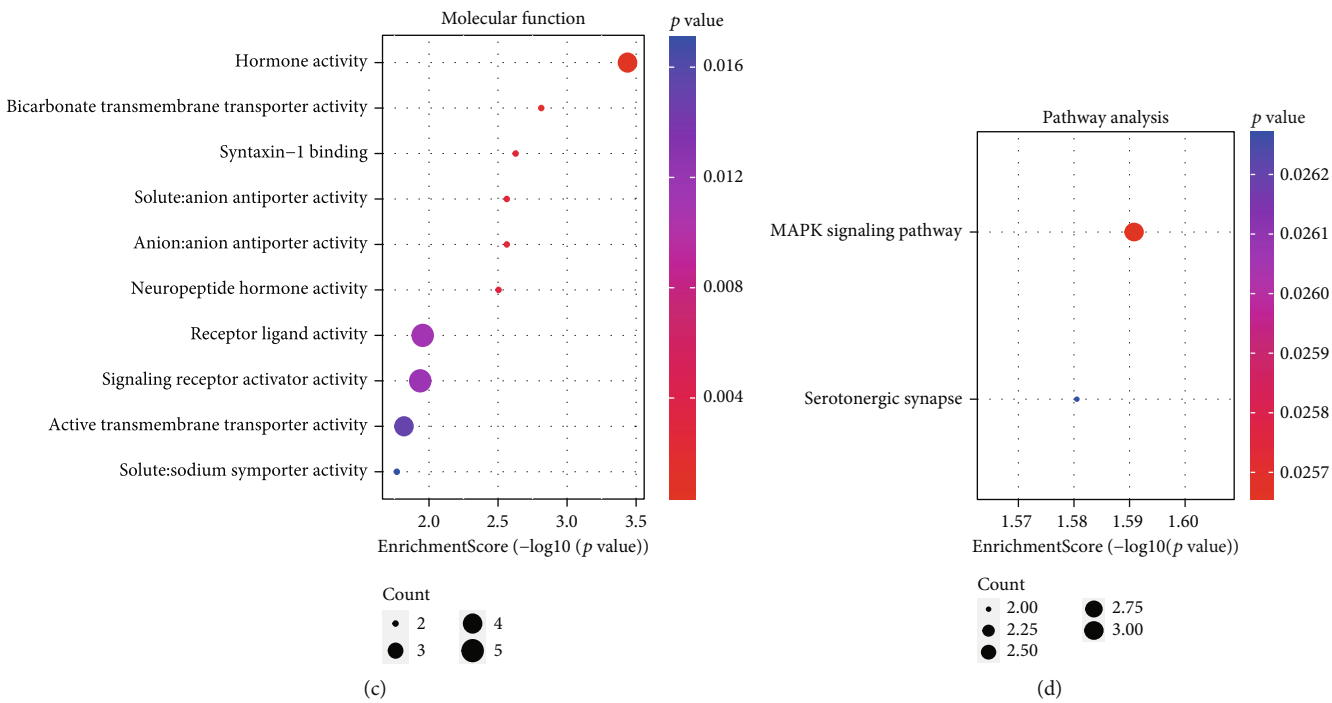

Figure 3: Bubble diagram displays the significant enrichment terms for the 62 DEGs. (a) BP terms, (b) CC terms, (c) MF terms, and (d) KEGG terms.

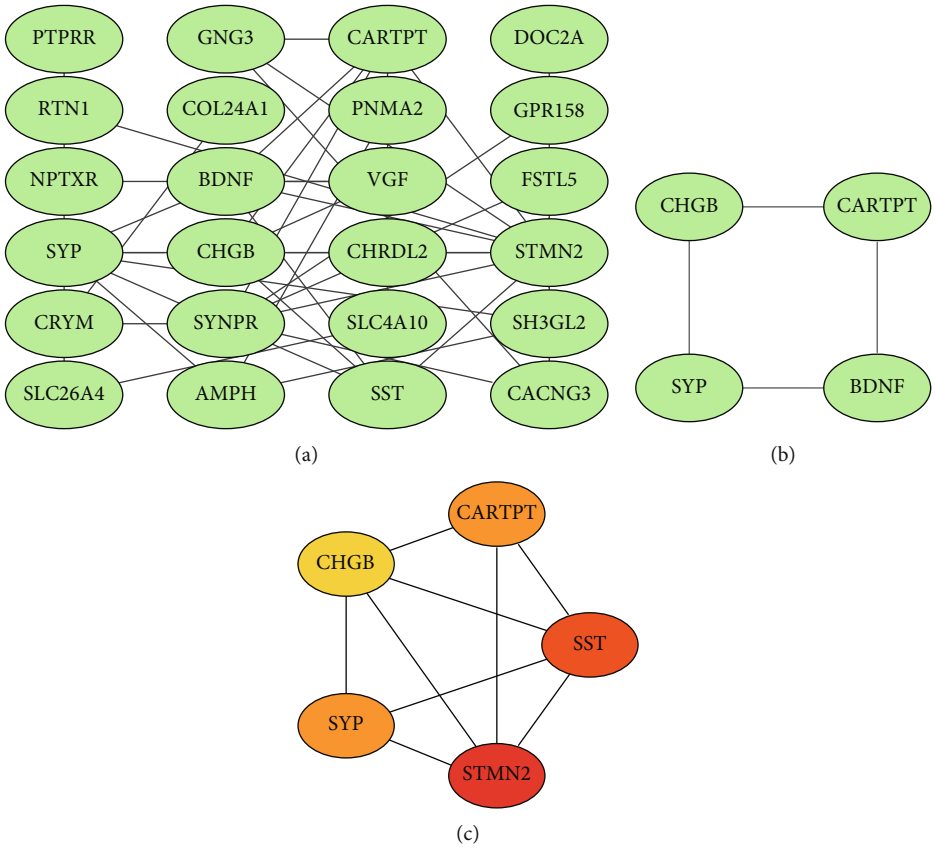

Figure 4: (a) PPI network constructed by the 62 DEGs (the disconnected nodes were hidden), (b) the most significant module in the network (score: 2.7), and (c) top 5 genes computed by the MCC algorithm (the darker the color, the higher the score).

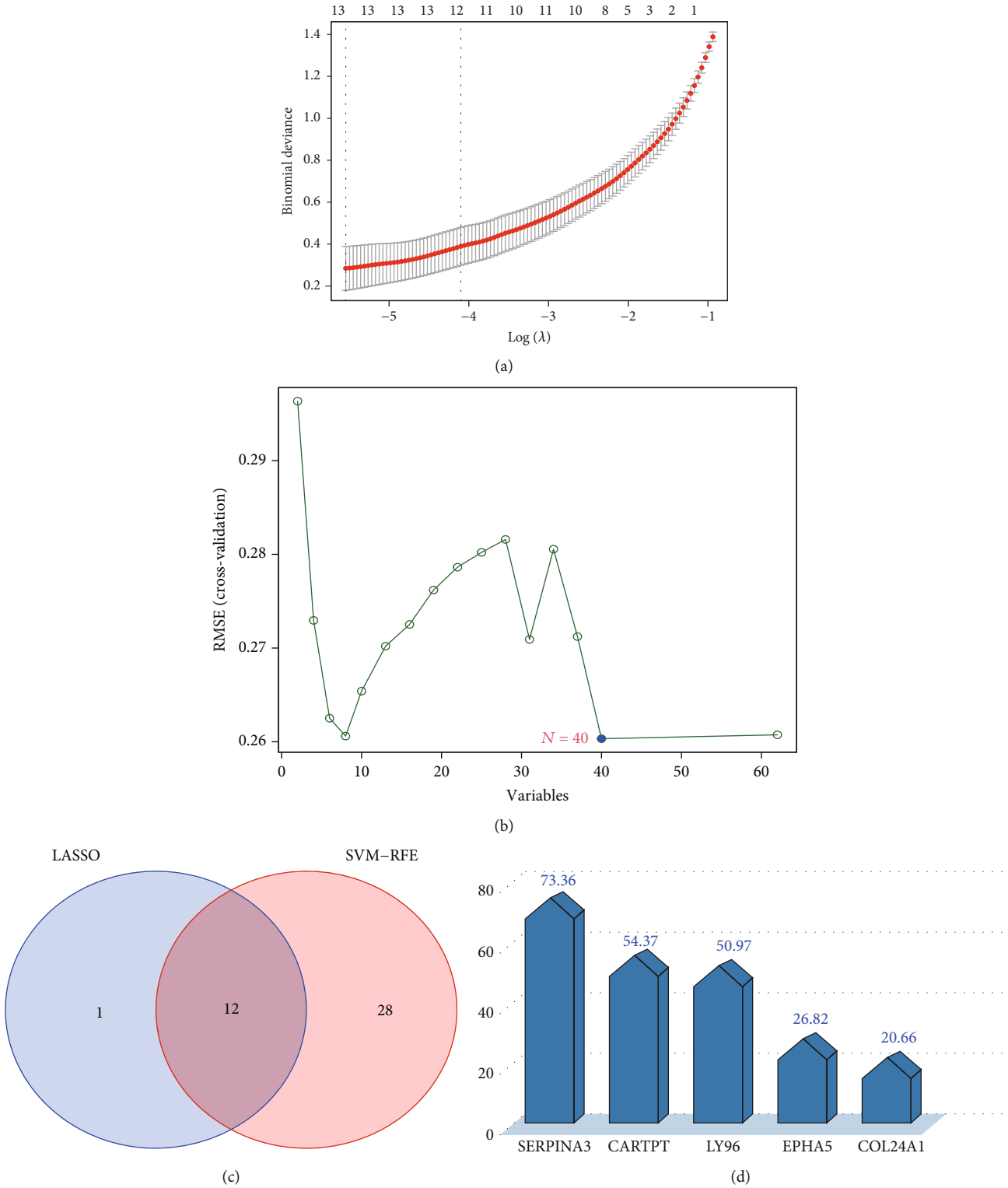

Figure 5: Machine learning algorithms for finding characteristic genes. (a) The LASSO logistic regression algorithm (13 genes). (b) The SVM-RFE algorithm (40 genes). (c) The intersection of the two algorithms (12 genes). (d) The inference score of T2DM based on the CTD database (of these overlapping 12 genes, the top 5 ranked were visualized).

2.12. Nomogram Model. A nomogram model ("rms" package; version 6.2-0) [39] was built to predict the risk of AD. Using the calibration curve, the predictive ability of nomogram model was evaluated. In addition, decision curve analysis and clinical impact curve were used to assess the clinical value of the model.

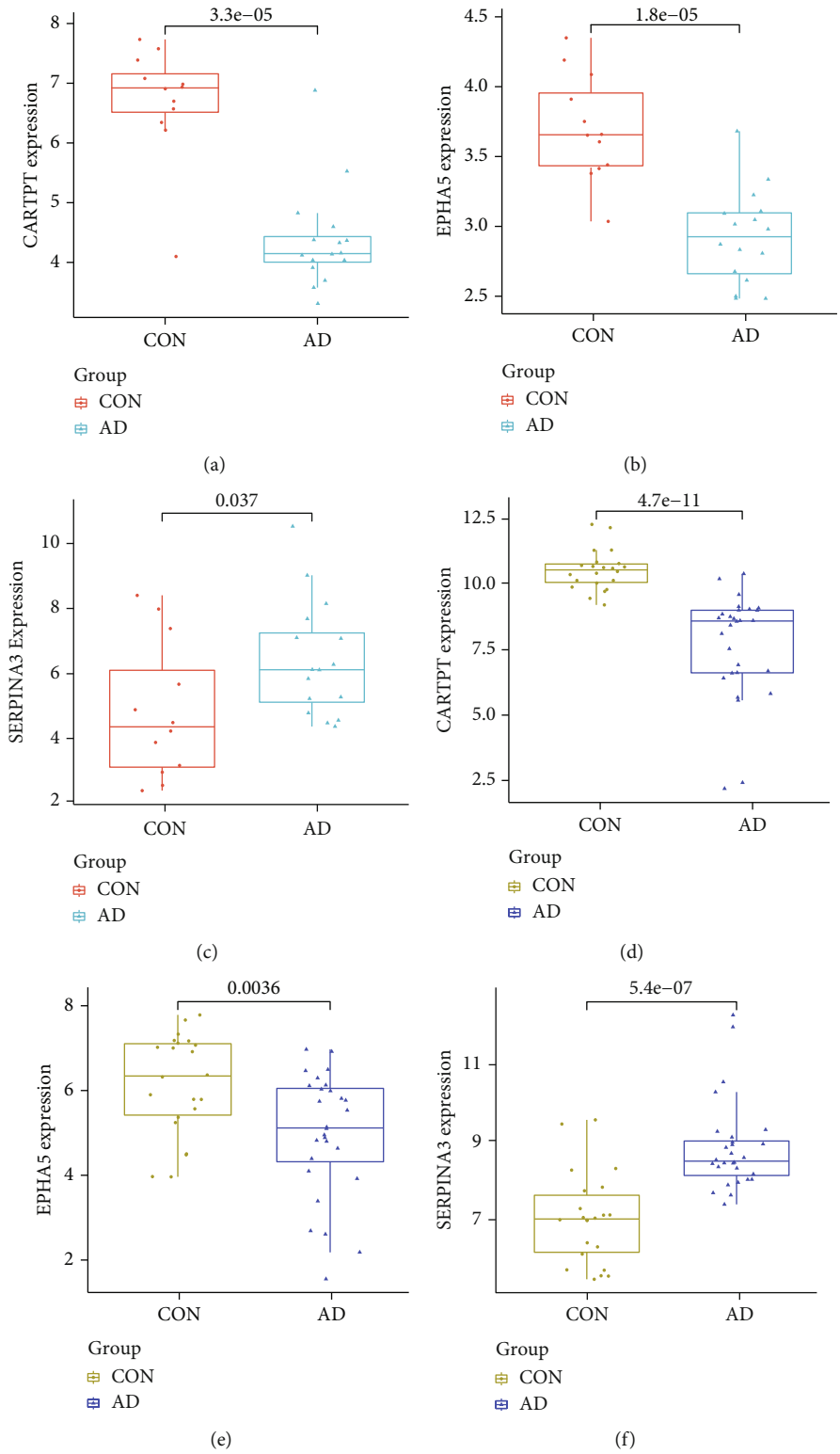

Figure 6: Continued.

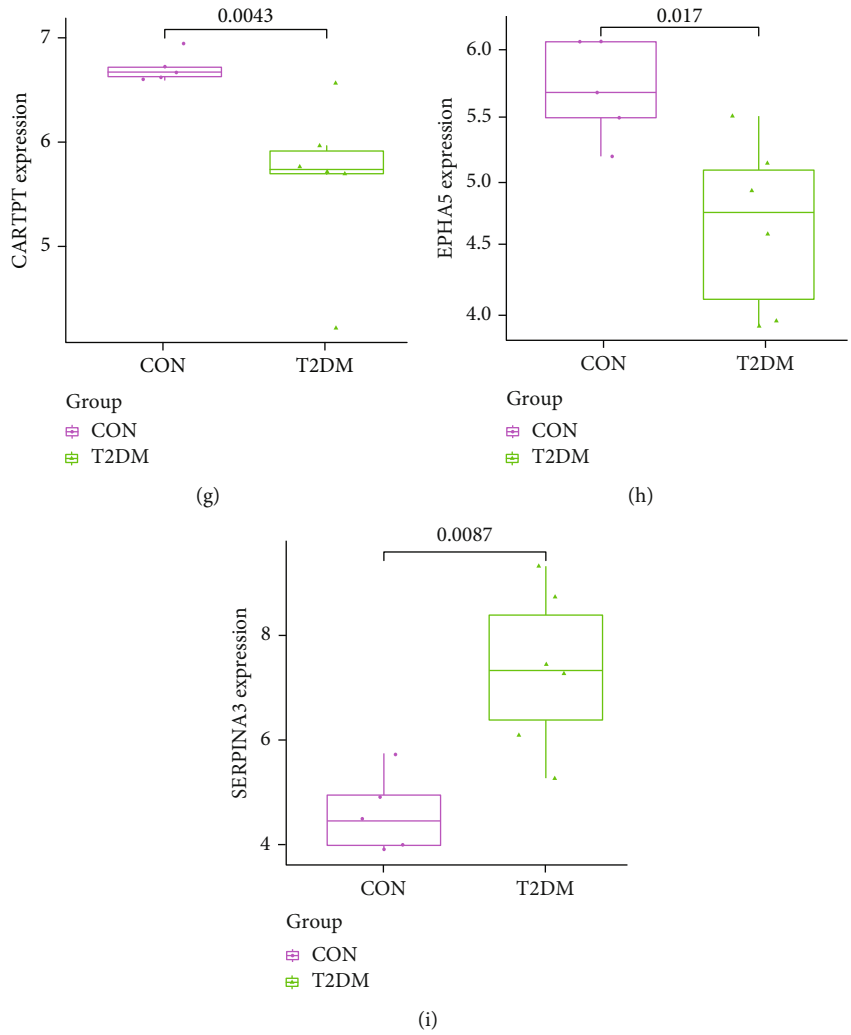

Figure 6: The expression value of CARTPT, EPHA5, and SERPINA3. (a) Validated in the GSE5281 (AD, $P < 0.05$), (b) expression value calculated based on the GSE122063 (AD, $P < 0.05$), and (c) expression value calculated based on the GSE161355 (T2DM, $P < 0.05$).

2.13. The Gene-Drug Interaction Analysis. The Drug Gene Interaction Database (DGIdb) [40] (https://www.dgidb.org) provides information about the association of genes with their known or potential drugs. We searched the specific genes in it to explore their possible drugs and their directions.

2.14. Assessment of Hallmark Gene Sets and Immune Cell Infiltration. The relative levels of the 50 hallmark gene sets and the 28 immune cells in the GSE122063 dataset (AD) were quantified using ssGSEA algorithm [41]. Plots were generated to present the differential expression levels between the controls and AD. In addition, Spearman's correlations for the 50 hallmark gene sets and the 28 immune cells with the specific genes were calculated, which were visualized by using the "ggplot2" package [42] (version 3.3.2).

2.15. Statistical Analysis. Statistical analyses were executed using SPSS 23.0 (Chicago, USA). The results for the behavior test and molecular experiments are presented as mean ± SEM. For data examination, the parametric Student's t-test was employed. All tests were two-tailed. When $P < 0.05$, it was considered statistically significant.

3. Results

3.1. DEG Identification. The analysis of differentially expressed genes (GSE161355 or GSE122063) was executed by the "LIMMA" package (version 3.44.3) with the criteria of the $|\log 2\,\mathrm{FC}| > 1$ and adjusted P value < 0.05. In general, a total of 1508 DEGs (Supplementary file 1) were screened in human diabetes-associated temporal cortex, including 1473 downregulated genes and 35 upregulated genes, which were intuitively presented in a volcano map (Figure 2(a)). On the other side, 788 DEGs (Supplementary file 2) were identified in AD temporal cortex when compared to controls, including 475 downregulated genes and 313 upregulated genes, which were also exhibited in a volcano map (Figure 2(b)). Among the two sets of DEGs, there were 62 overlapping items (Figure 2(c)). Here, we used the overlapping for subsequent studies to explore the mechanisms linking diabetes to

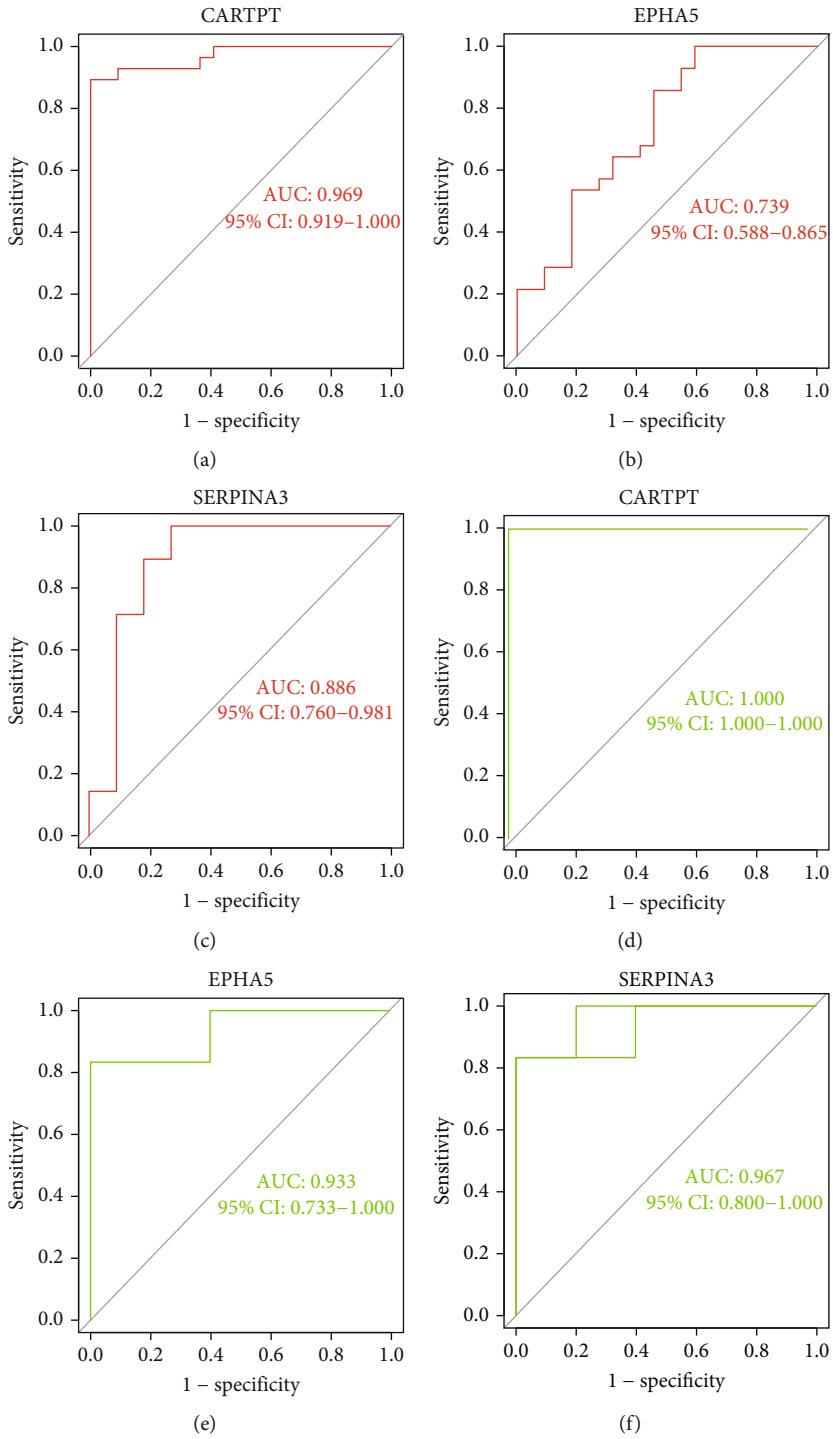

Figure 7: Diagnostic performance of CARTPT, EPHA5, and SERPINA3. (a–c) The ROC curves based on the GSE122063 (AD) and (d–f) the ROC curves based on GSE161355 (T2DM).

AD. Supplementary Figure 1 visualizes the expression level of these 62 genes in GSE122063 (AD) in the form of a heatmap.

3.2. Enrichment Analysis for the 62 Overlapping DEGs. The terms of GO mainly consist of biological process (BP), cellular component (CC), and molecular function (MF). As shown in Figure 3(a), synaptic vesicle cycle (GO:0099504), synaptic vesicle endocytosis (GO:0048488), and presynaptic endocytosis (GO:0140238) were the most remarkable annotations in BP. For the CC (Figure 3(b)), most of the overlapping genes were enriched in synaptic vesicle (GO:0008021), transport vesicle (GO:0030133), and exocytic vesicle (GO:0070382). Among the significant MF enrichments (Figure 3(c)), hormone activity (GO:0005179), bicarbonate transmembrane transporter activity (GO:0015106), and

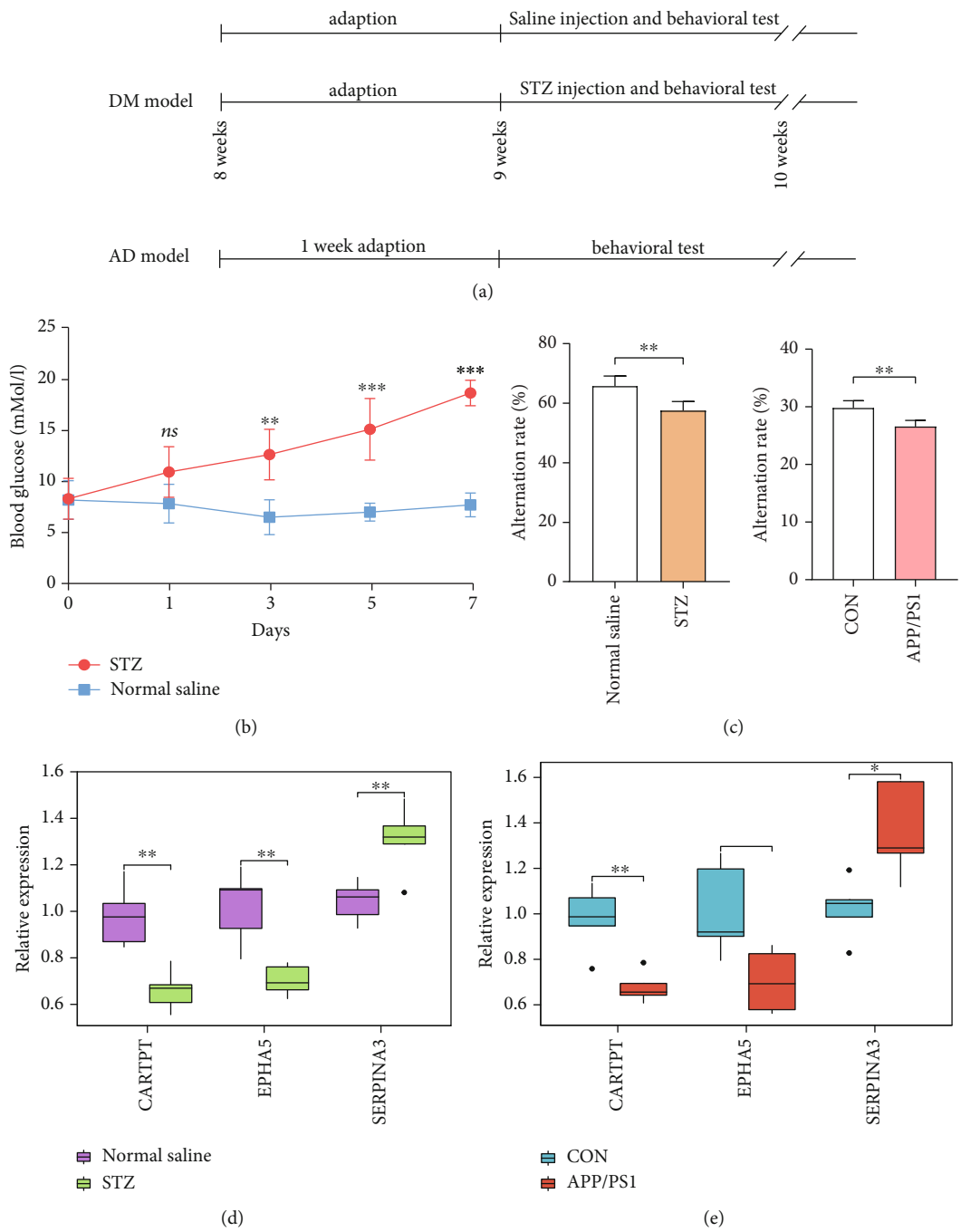

Figure 8: Temporal cortex tissue for external validation: (a) time-flow diagram; (b) changes in blood glucose; (c) results of behavioral test (Y maze); (d) RT-qPCR for CARTPT, EPHA5, and SERPINA3 ($n = 5$ in the control mice; $n = 5$ in the T2DM mice); and (e) RT-qPCR for CARTPT, EPHA5, and SERPINA3 ($n = 5$ in the control mice; $n = 5$ in the APP/PS1 mice). The significance of differences indicated in figures: $^{*}P < 0.05$, $^{**}P < 0.01$, and $^{***}P < .001$.

syntaxin-1 binding (GO:0017075) were dominant. On the other hand, the MAPK signaling pathway (hsa04010) is highlighted in the KEGG pathway enrichments (Figure 3(d)).

3.3. PPI Network. All the 62 overlapping DEGs were then imported into the STRING for the PPI network construction, which were finally visualized by the Cytoscape (http://cytoscape.org/;version 3.7.2). This resulting network contained 24 nodes and 39 edges (Figure 4(a)) with a most significant module (Figure 4(b); score: 2.7) obtained by using the MCODE plugin (version 1.6.1) of the Cytoscape. Relying on the same software, we further captured the top 5 hub genes in the network through the MCC algorithm with the cytoHubba plugin (version 0.1) (Figure 4(c)).

3.4. Identification of the Specific Genes in Disease. We believe that these 62 overlapping genes are differentially altered in

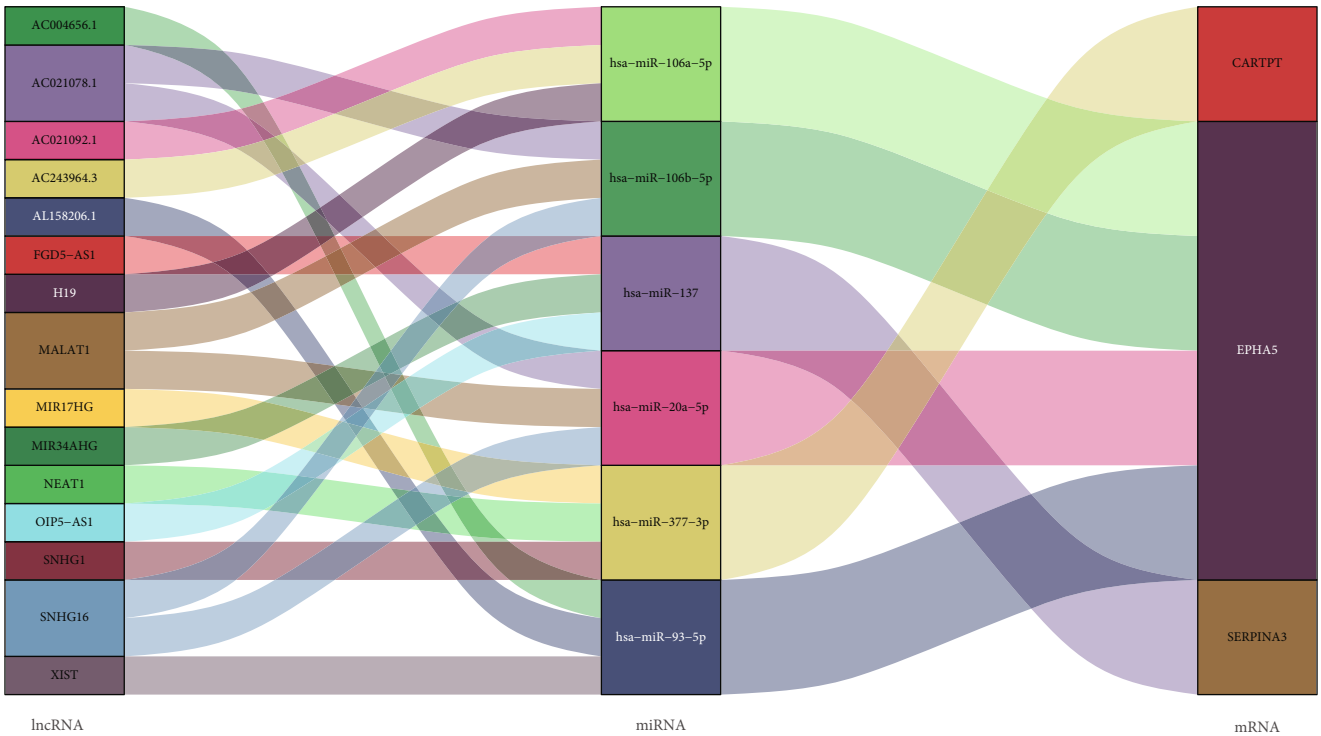

(a)

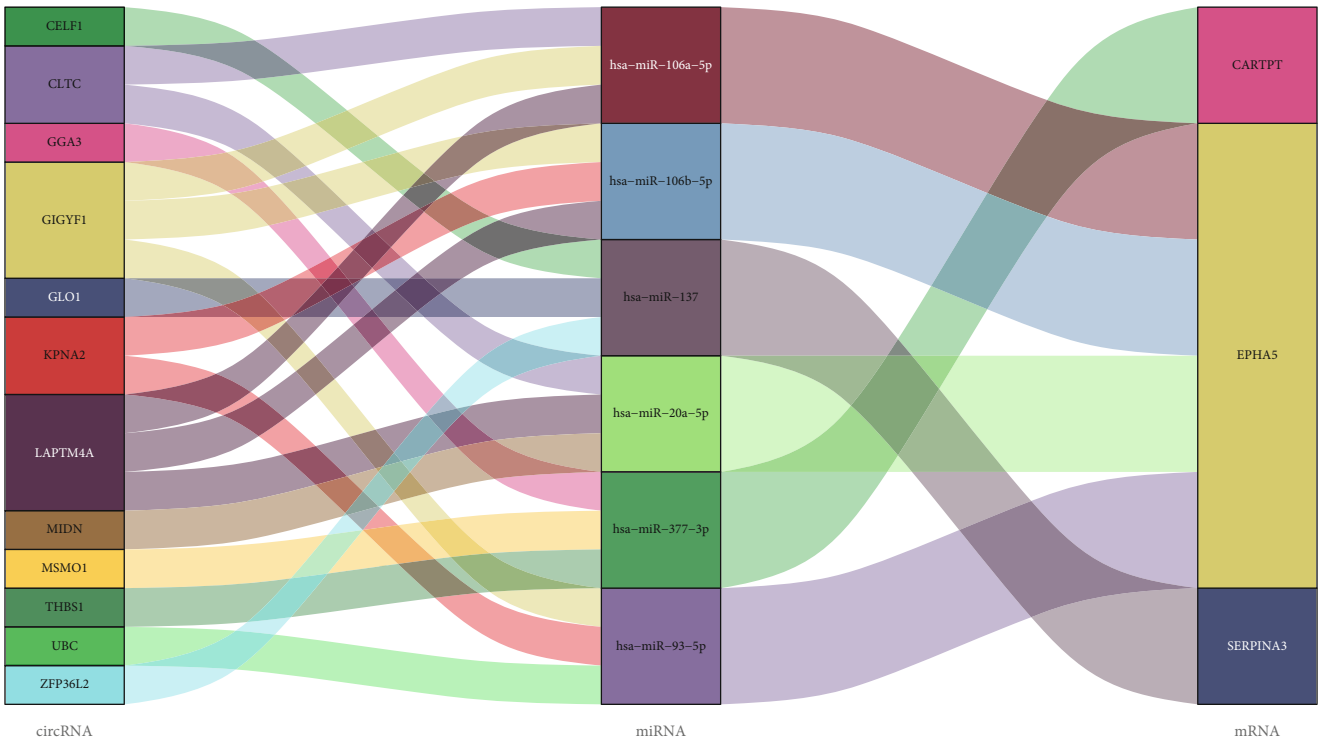

(b)

Figure 9: Sankey diagram for the ceRNA network of CARTPT, EPHA5, and SERPINA3. (a) lncRNA-miRNA-mRNA network and (b) circRNA-miRNA-mRNA network.

AD patients and susceptible to glycemic disturbances. Therefore, we extracted their expression values in the AD dataset for further study. Base on the gene expression matrix from the GSE122063 dataset, we identified 13 specific genes (IGLL5, COL24A1, C20orf195, LOC283737, SERPINA3, LPP-AS2, ZCCHC12, OSR1, CHRDL2, LY96, LOC100507165, EPHA5, and CARTPT) from the 62 overlapping DEGs with the LASSO logistic regression algorithm

Table 1: The potential drugs targeting the specific genes based on the DGIdb.

Gene	Drug	Sources	PMIDs	Query score	Interaction score
CARTPT	AMPHETAMINE	TdgClinicalTrial	15597110, 15661821, 15680473, 16713658, 15644956, and 15680478	2.04	7.43
	INSULIN	NCI	12883265	0.17	0.62
	DEXAMETHASONE	NCI	12591118	0.12	0.44
	PROGESTERONE	NCI	18598674	0.1	0.38
EPHA5	VANDETANIB	ChemblInteractions	/	0.23	1.09
	HESPERADIN	DTC	19035792	0.11	0.53
	PACLITAXEL	PharmGKB	26133776, 22843789, 26763541, and 26133777	0.08	0.39
SERPINA3	/	/	/	/	/

(Figure 5(a)). Furthermore, 40 specific genes (CARTPT, LOC283737, SERPINA3, RNF165, LOC100507165, COL24A1, TSPAN7, CHRDL2, C5orf55, DGKI, VGF, IGLL5, LY96, LOC100129973, KDM4D, SLC26A4, OSR1, C20orf195, SLC5A11, NPTXR, WDR54, MYOT, SST, LPP-AS2, ABCC12, BDNF, LY86-AS1, SYNPR, FSTL5, AMPH, ZWILCH, NRSN1, CHGB, CACNG3, PTPRR, COPG2IT1, CASQ1, NLGN4Y, C2orf80 and EPHA5) were also filtered using the SVM-RFE algorithm (Figure 5(b)). Subsequently, 12 genes (SERPINA3, CARTPT, LY96, EPHA5, COL24A1, OSR1, CHRDL2, IGLL5, LPP-AS2, C20orf195, LOC283737, and LOC100507165) were determined by the combination of the two algorithms (Figure 5(c)). We ranked these 12 genes according to their reference score involving diabetes in the CTD and chose the top five ranked genes (Figure 5(d)) for expression validation.

3.5. Verification of the Specific Genes in Datasets. We validated the expression value of the five specific genes in the GSE5281 dataset (AD; the validation set; $P < 0.05$ was considered significant), and the results presented that CARTPT, EPHA5, and SERPINA3 met the criteria (Figures 6(a)–6(c)). Because the P value of COL24A1 (Supplementary Figure 2) and LY96 (Supplementary Figure 3) was 0.37 and 0.7, respectively, they were not available for the subsequent analysis. In addition, the expression value of CARTPT, EPHA5, and SERPINA3 in the GSE122063 (AD; the training set; Figures 6(d)–6(f)) and GSE161355 (T2DM; Figures 6(g)–6(i)) datasets was also calculated. The trend of the dysregulated expression for the three genes was consistent in the three different datasets.

Consequently, we drew receiver operating characteristic (ROC) curve to further test their efficacy in the GSE122063 dataset (AD; the training set). For CARTPT, the area under the curve (AUC) was 0.969 and 95% CI: 0.919–1.000 (Figure 7(a)). For EPHA5, the area under the curve (AUC) was 0.739 and 95% CI: 0.588–0.865 (Figure 7(b)). For SERPINA3, the area under the curve (AUC) was 0.886 and 95% CI: 0.760–0.981 (Figure 7(c)). We also evaluated them in the GSE161355 dataset (T2DM). For CARTPT, the area under the curve (AUC) was 1.000 and 95% CI: 1.000–1.000 (Figure 7(d)); for EPHA5, the area under the curve (AUC) was 0.933 and 95% CI: 0.733–1.000 (Figure 7(e)); for SERPINA3, the area under the curve (AUC) was 0.967 and 95% CI: 0.800–1.000 (Figure 7(f)). All results indicated that CARTPT, EPHA5, and SERPINA3 had high diagnostic values in both AD and T2DM.

3.6. Animal Model Evaluation. The flow of the animal experiment is shown in Figure 8(a). After STZ injection within 1 week, the level of random blood glucose in C57BL/6 mice was significantly increased (Figure 8(b); >16.7 mmol/L; $P < 0.05$) when compared with the controls (normal saline injection), indicating that STZ treatment successively induced diabetic model. Besides, the percentage of correct alternation arm was significantly decreased in the diabetic and APP/PS1 mice when compared with the controls ($P < 0.05$, Figure 8(c)), signifying that diabetic and 8-month-old APP/PS1 mice had already developed memory impairment.

3.7. RT-qPCR. Following our successfully constructed animal models, RT-qPCR was conducted to finally verify the specific genes in the mice temporal cortex of T2DM and AD. In Figure 8(d), CARTPT and EPHA5 showed a significant decrease ($P < 0.05$), while the expression of SERPINA3 statistically increased ($P < 0.05$) in STZ group when compared with the control. In the aspect of AD model (Figure 8(e)), CARTPT and EPHA5 decreased significantly ($P < 0.05$), while the expression of SERPINA3 was significantly enhanced ($P < 0.05$). Based on these data, we judge that the previous speculations are reliable.

3.8. ceRNA Network. In miRSystem database, hsa-miR-377-3p was predicted to interact with CARTPT by 3 programs. In StarBase database, hsa-miR-20a-5p, hsa-miR-93-5p, hsa-miR-106a-5p, and hsa-miR-106b-5p were, respectively, predicted to interact with EPHA5 by 6 programs; hsa-miR-137 was predicted to interact with SERPINA3 by 4 programs. To better comprehend the regulation, we further constructed 2 ceRNA networks based on the StarBase database. The simplified lncRNA-miRNA-mRNA network and circRNA-miRNA-mRNA network are, respectively, exhibited in Figures 9(a) and 9(b).

3.9. Prediction of the Potential Drugs. DGIdb was utilized to quest the possible pharmaceutical compounds. Briefly, 4 compounds (amphetamine, insulin, dexamethasone, and

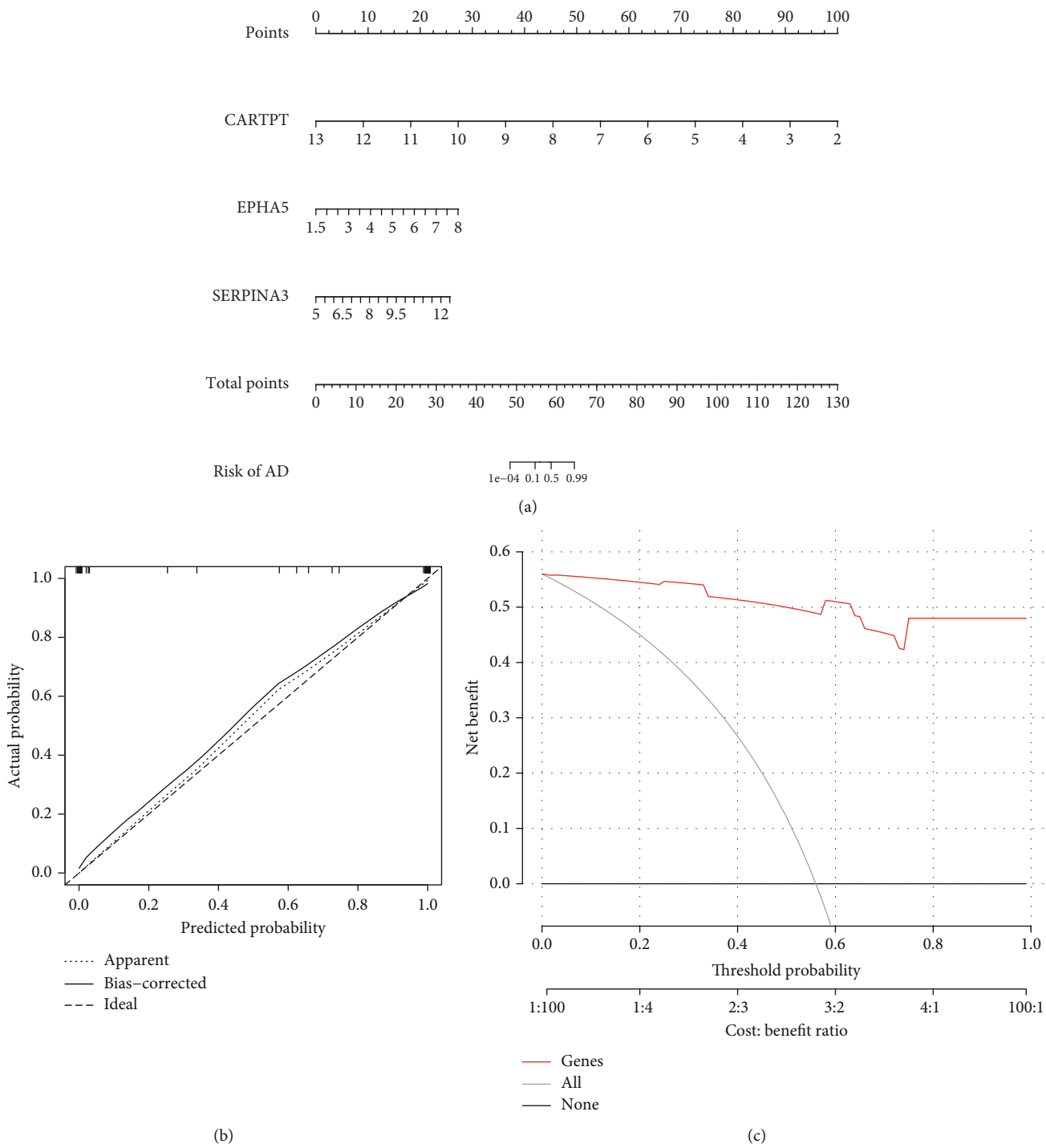

Figure 10: Continued.

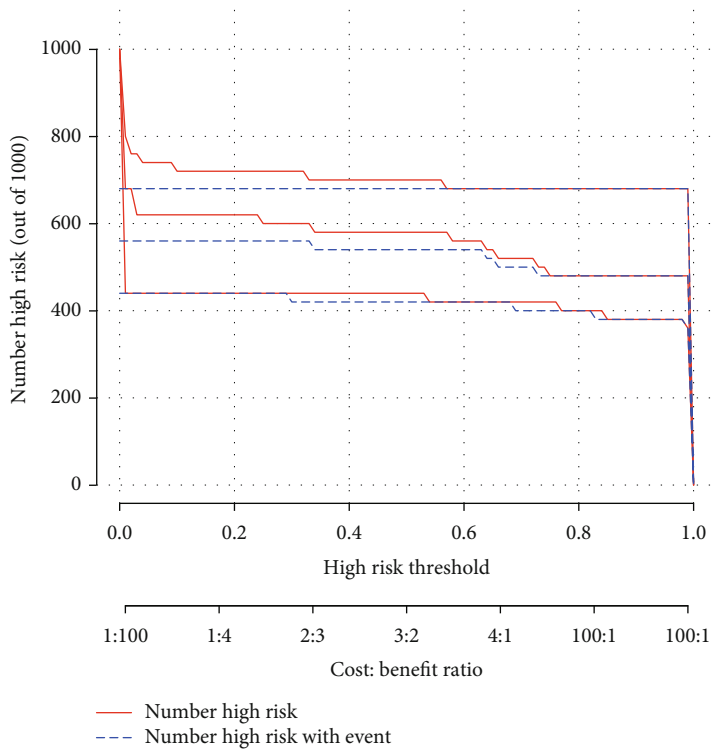

(d)

Figure 10: The nomogram model based on the gene expression in GSE122063 (AD). (a) The nomogram, (b) the calibration curve, (c) the DCA curve, and (d) the clinical impact curve.

progesterone) were recognized to interplay with CARTPT; the potential agents of EPHA5 may include vandetanib, hesperadin, and paclitaxel. Unfortunately, no drugs for SERPINA3 have been predicted. More details are shown in Table 1.

3.10. Construction of the Nomogram Model. Using the "rms" package (version 6.2-0) in R (version 4.0.2), a nomogram model based on the 3 specific genes (CARTPT, EPHA5, and SERPINA3) was constructed to predict the risk of Alzheimer's disease (Figure 10(a); GSE122063). As shown in Figure 10(b), the calibration curve suggested a high predictive accuracy of the nomogram model. From 0 to 1 on the abscissa (Figure 10(c)), the red line in the DCA curve is far from and consistently above the gray and black lines, manifesting that decision-making based on the nomogram model may benefit AD patients. At last, we evaluated the clinical impact of the nomogram model through a clinical impact curve (Figure 10(d)).

3.11. Hallmark Gene Sets and Immune Cell Infiltration. To further assess the differences in the hallmark gene sets and the immune cell infiltration between controls and AD, the ssGSEA algorithm was employed. The detailed distribution of the 50 hallmark gene sets between AD and control (GSE122063) was illuminated in Figure 11(a) (the significance in the figure as follows: $^{ns}P < 1$, $^{\#}P < 0.2$, $^{*}P < 0.05$, $^{**}P < 0.01$, and $^{***}P < .001$). In addition, the infiltration of 28 immune cells between the two groups is shown in Figures 12(a) and 12(b). Briefly, we can find that there are 14 differentially infiltrating immune cells between AD and control groups; they are activated dendritic cell, immature B cell, immature dendritic cell, MDSC, macrophage, natural killer T cell, natural killer cell, neutrophil, plasmacytoid dendritic cell, regulatory T cell, type 1 T helper cell, type 17 T helper cell, central memory CD8 T cell, and effector memory CD8 T cell. Figure 11(b) shows the correlation of the hallmark gene sets with the specific genes (CARTPT, EPHA5, and SERPINA3), and Figure 12(c) shows the details of their related immune cells. $P < 0.05$ was considered statistically significant. We can find that CARTPT and EPHA5 are generally consistent, while SERPINA3 has the opposite. For instance, both CARTPT and EPHA5 are negatively correlated with the HALLMARK_APICAL_JUNCTION, but SERPINA3 is positively correlated with that; both CARTPT and EPHA5 are negatively correlated with the natural killer T cell, but SERPINA3 is positively correlated with that. These data will help us further appreciate the critical role of the specific genes.

4. Discussion

Alzheimer's disease is a neurodegenerative disease with insidious progression [43]. Despite nearly 100 years of research on it, the etiology, pathogenesis, and risk factors are far from being elucidated, which has also led to repeated setbacks in AD drug development. Therefore, finding the risk factors affecting AD, identifying AD high-risk

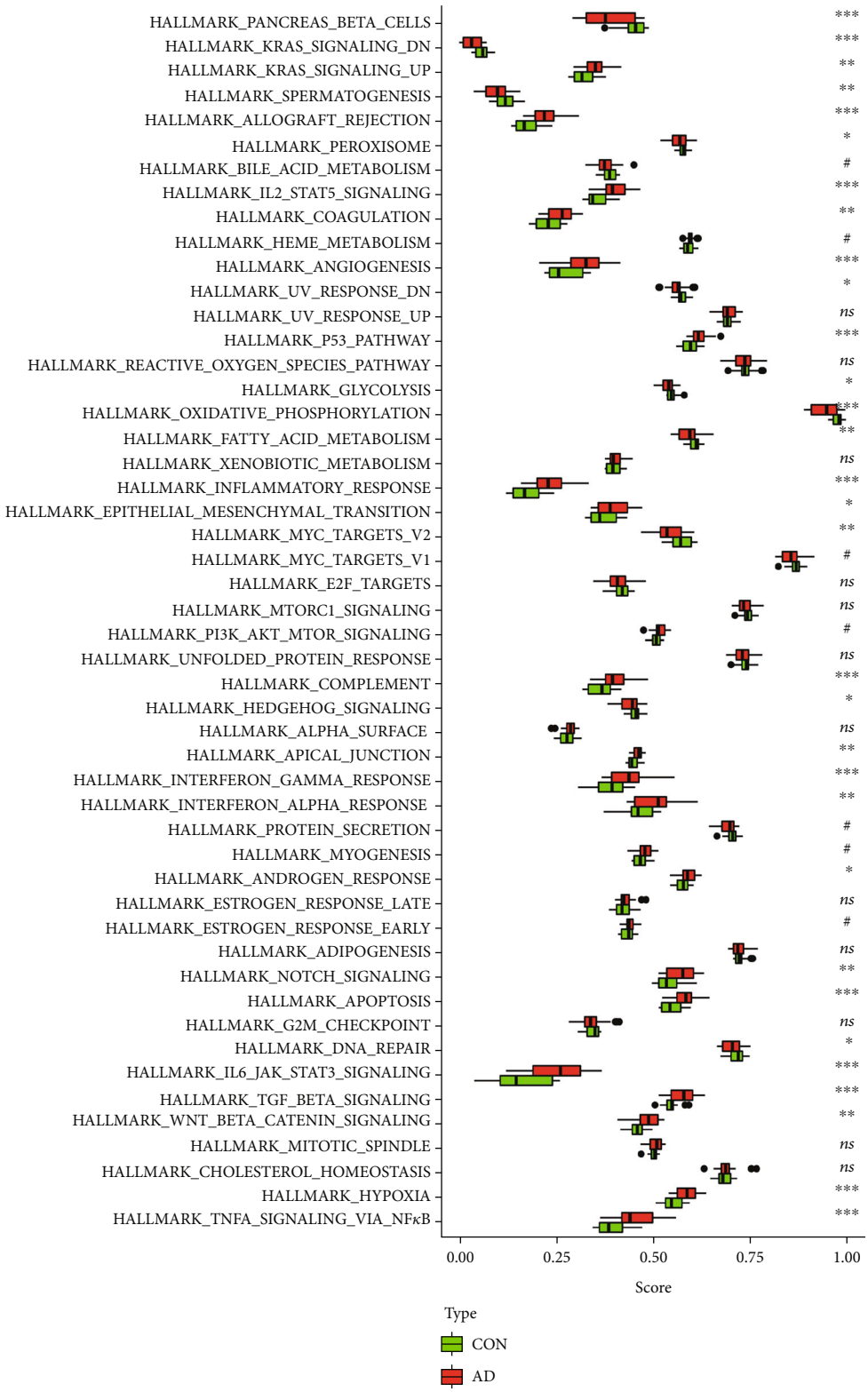

(a)

Figure 11: Continued.

(b)

Figure 11: Analysis of hallmark gene sets associated with AD (GSE122063): (a) the specific distribution of the 50 hallmark gene sets in AD and (b) the correlation analysis of the 50 hallmark gene sets with CARTPT, EPHA5, and SERPINA3.

populations, and intervening in novel therapeutic targets have become hot spots in AD research. Recent studies have shown that diabetes can accelerate the decline of executive function in patients [44, 45]. This impairment is significantly related to the time of suffering from diabetes and the level of aging glycosylated hemoglobin in the blood [46]. Due to the

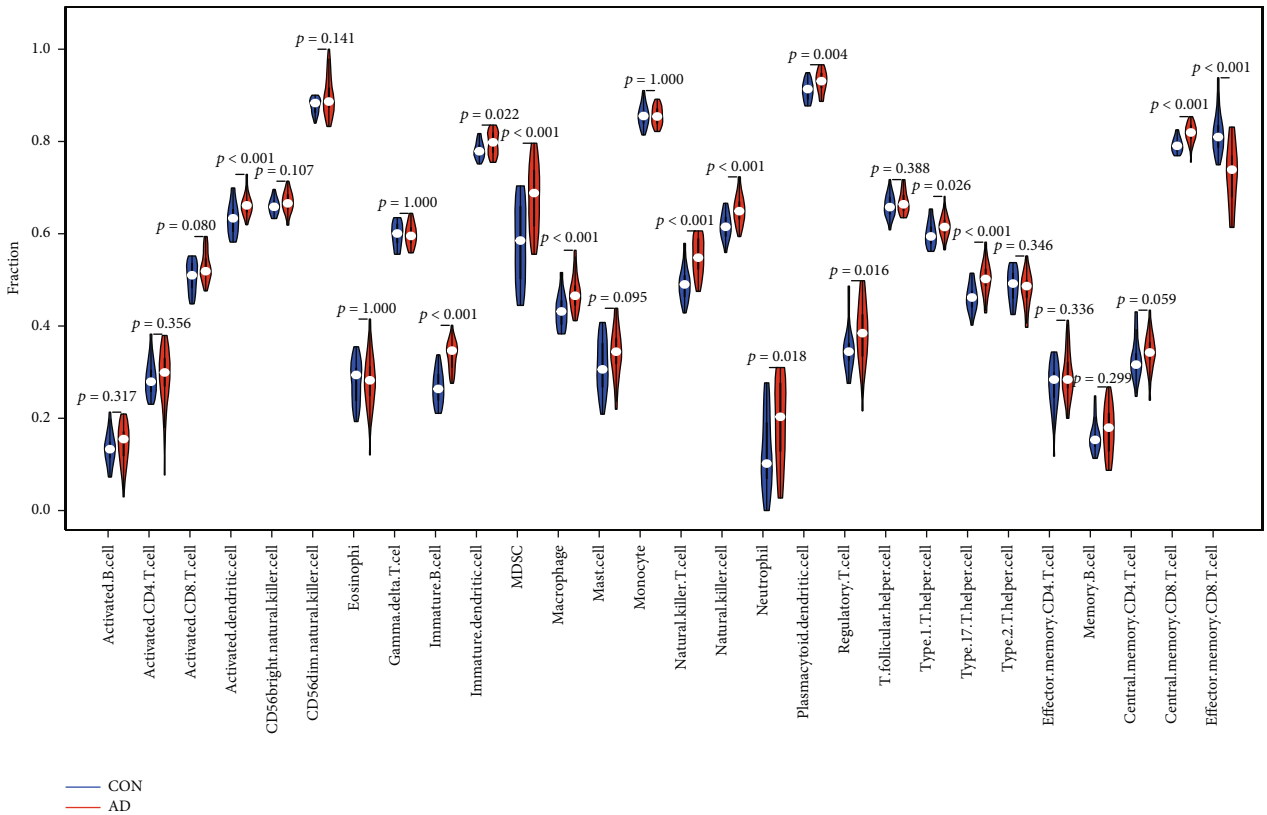

(a)

Figure 12: Continued.

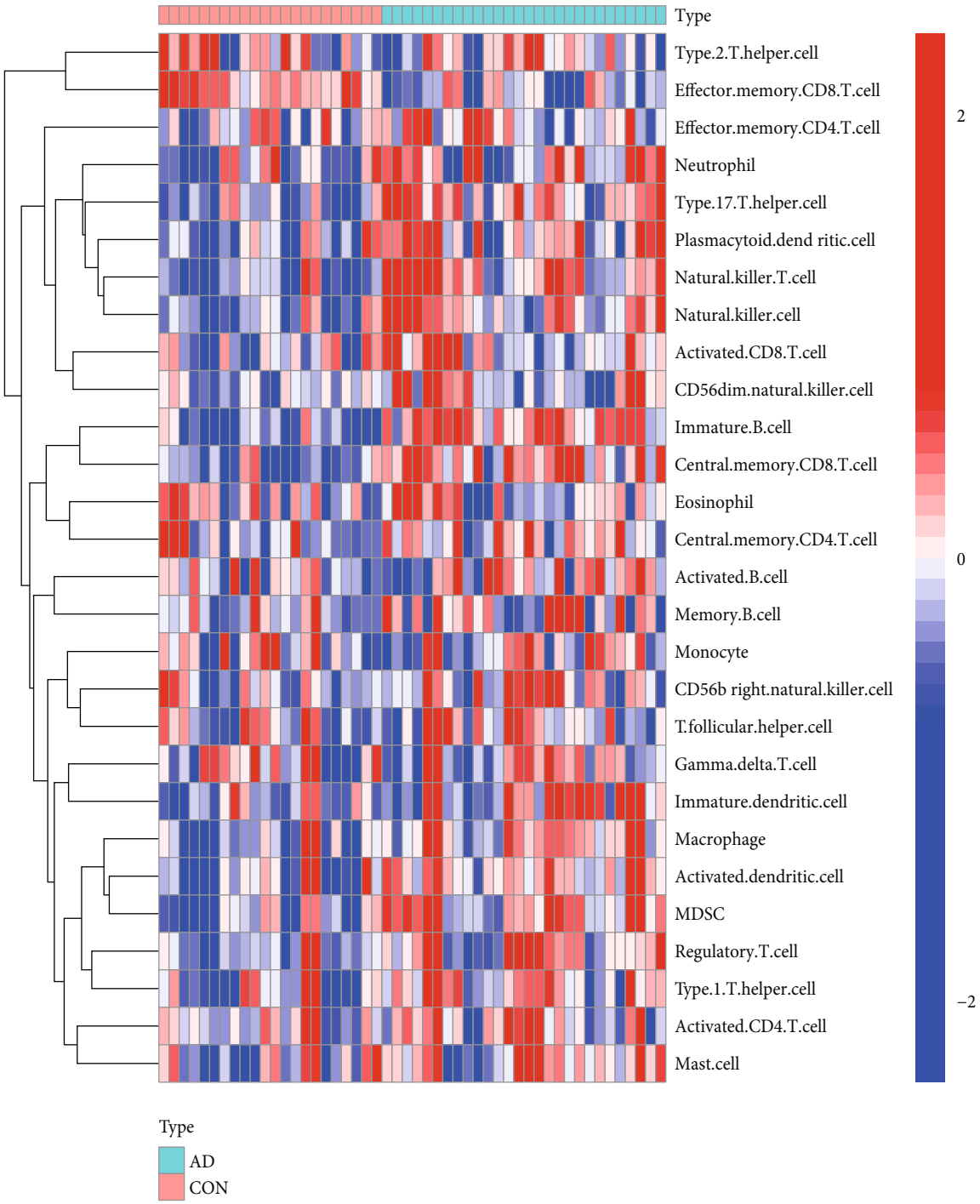

(b)

Figure 12: Continued.

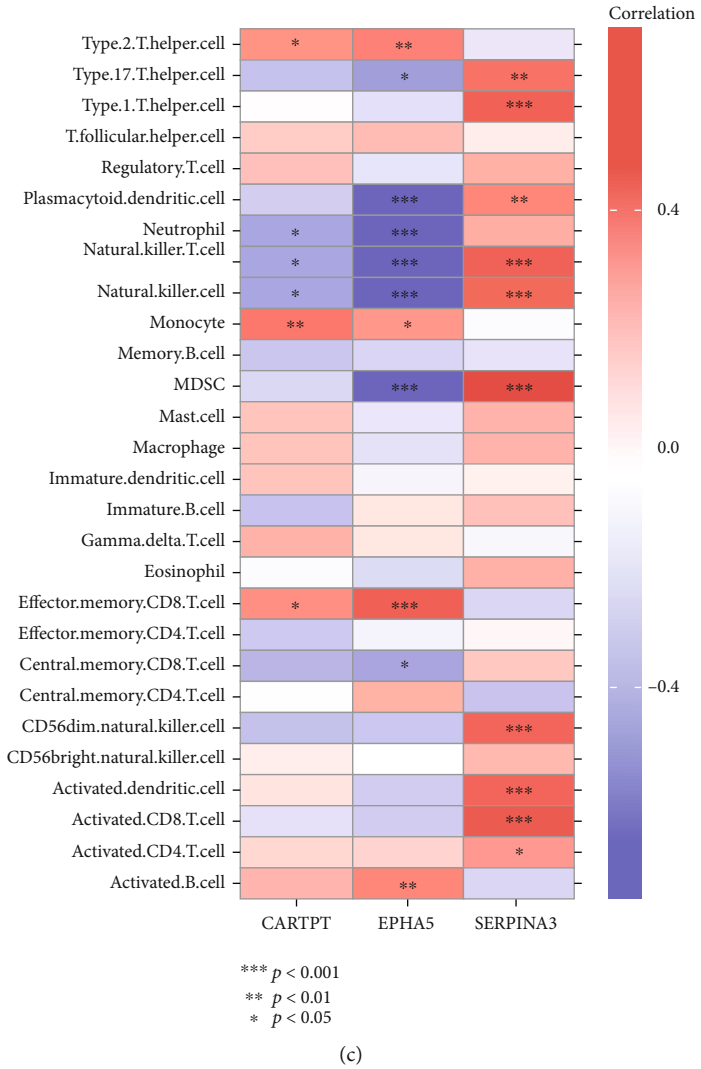

(c)

Figure 12: Analysis of immune landscape associated with AD (GSE122063) (a) violin plot: 14 types of immune cells were differently distributed between healthy control and AD (b) heatmap; (c) the relationship between 3 genes (CARTPT, EPHA5, and SERPINA3) and immune cell infiltration.

lack of a complete cure, it is urgent to reduce the risk of dementia. Understanding how diabetes affects cognition through which targets, and taking early interventions to delay its progression, is of great help to current research.

This time, our GEO-based research discovered 62 DEGs overlapping in the dataset of GSE122063 (AD) and GSE161355 (T2DM) by integrated bioinformatics. The resulting GO enrichments indicated that these genes were closely related to the synaptic function. Synapses are important mediators for maintaining connections between neurons, and their function and structure can change with the activity of neurons, that is, synaptic plasticity [47]. The loss of neurons and the destruction of synaptic plasticity in the brain are the key to cognitive defects. Studies have reported that the volume of the hippocampal CA1 region was significantly reduced in the streptozotocin-induced diabetic rats [48], accompanied by a decrease in the number of spinophilin-/neurabin II-positive cells; in addition, ultrastructural observations revealed widening of the synaptic cleft and reduction of vesicles, along with atrophy, cristae rupture, and ruffling of mitochondrial chromatin and nuclei [49]. Therefore, targeted regulation of synaptic plasticity may be an important mechanism of diabetes-related cognitive impairment [50].

As we all know, insulin can enter the CNS through the blood-cerebrospinal fluid barrier, regulating brain glucose metabolism and the brain structural plasticity to improve memory [51]. To exert this function, insulin mainly activates the mitogen-activated protein kinase (MAPK) [52] and phosphatidylinositol 3-kinase (PI3-K)/Akt [53] signaling pathways. In our pathway enrichment analysis, MAPK signaling (hsa04010) ranked at the top. MAPKs are a group of serine-threonine protein kinases that can be activated by diverse extracellular stimuli. Insulin resistance (IR) can cause strong MAPK immunoreactivity, leading to tau hyperphosphorylation, and a positive correlation between the number of MAPKs and tau protein accumulations was found in transgenic mice accompanied by hyperphosphorylated tau [54].

All this evidence points to the unique role of MAPK signaling in diabetes-related cognitive impairment, and the involved genes are equally worthy of our attention.

Among the overlapping 62 dysregulated genes, we finally identified 3 targets by the machine learning algorithm; they are CARTPT, EPHA5, and SERPINA3. To be specific, we found that CARTPT (logFC: -2.84) and EPHA5 (logFC: -1.18) were significantly downregulated in AD (GSE122063), and they had a good performance as a marker of the disease (GSE122063; the AUC of CARTPT was 0.969; the AUC of EPHA5 was 0.739). On the other side, the expression of SERPINA3 (logFC: 1.82) in samples from AD individuals was higher than that of controls (GSE122063). Likewise, its ROC curve performed well (the AUC of SERPINA3 was 0.886). After further calculation of the AD validation set (GSE5281), we spotted the same trend in the expression of these genes. Similarly, CARTPT (logFC: -1.09) and EPHA5 (logFC: -1.02) were downregulated in T2DM (GSE161355); the AUC of them was 1.00 and 0.933, respectively. As for SERPINA3, the expression of it (logFC: 2.76; GSE161355) in T2DM samples was also higher than the controls (the AUC of its ROC curve was 0.967). We further successfully constructed diabetic and AD animal models, after which brain tissue samples were collected and RT-qPCR was performed to verify our bioinformatics-based predictions. The experimental results (the mRNA level of CARTPT and EPHA5 was significantly decreased, while SERPINA3 increased; $P < 0.05$) were consistent with the previous analyses. Therefore, we concluded that CARTPT, EPHA5, and SERPINA3 might constitute a molecular bridge between T2DM and AD.

According to the ROC curve of the three genes (Figure 7), it is not difficult to recognize that CARTPT has the highest diagnostic efficacy, whether in diabetes or AD (the AUC of CARTPT was 0.969 and 1.00, respectively, in GSE122063 and GSE161355). More than this, CARTPT is also the core gene of the constructed PPI network (Figures 4(b) and 4(c)). We speculate that the role of the CARTPT in the transformation of diseases may be relatively more significant. Also as a metabolic disorder, middle-aged obesity may increase the risk of AD, and CARTPT was now identified as a target for antiobesity drugs, having a high value in connecting obesity and AD [55]. This provides a reference for us to study the relationship between diabetes and AD. CARTPT is capable of encoding the CART protein [56]. CART, fully known as the cocaine- and amphetamine-regulated transcript, is an endogenous neuropeptide, broadly expressed in the CNS [57]. It has also been documented that the expression of CART is decreased in the CSF of AD patients, and the treatment of exogenous CART can partially ameliorate the deficits of learning and memory in mice [58] by improving the synaptic ultrastructure [59]. This evidence fits well with our enrichment analysis and experimental results. Therefore, we believe that CARTPT has the potential to be a target for metabolic-related neurodegenerative changes.

Eph family proteins include Eph receptors with ephrin ligands and are mainly expressed in the CNS [60]. They bidirectionally regulate synaptic signal transmission with neuronal morphogenesis and participate in neural functions such as learning and memory [61]. EphA5 is mainly involved in the formation of dendritic spines, and EphA5 knockout mice exhibit abnormal dendritic spine morphology and neuronal aggregation in the cerebral cortex [62]. The experiments found that the use of EphA5 receptor agonists was able to improve spatial memory in mice [63]. As an acute phase response protein, SERPINA is thought to be a major component of neuritic plaques in the brain, which promotes the assembly of amyloid and its deposition, affecting individual cognition [64]. Their phenotype in the cognitive impairment is consistent with our findings. Nevertheless, the specific relationship between the 2 specific genes and glucose metabolism is also not clear so far. Therefore, EPHA5 and SERPINA3 were equally valuable in subsequent studies.

The relatively small sample size used for bioinformatics analysis and experimental validation in this study may limit our final conclusions to a certain extent. Consequently, the potential mechanisms for glucose metabolism in AD etiology deserve future investigation.

5. Conclusion

Gene expression data involving AD and type 2 diabetes were downloaded from the public GEO database platform and subjected to a comprehensive bioinformatics analysis with machine learning algorithms in our study, presenting us with the DEGs linking AD and T2DM. The subsequent enrichment and network analysis about these genes conveyed us their biological functions. Through external dataset validation, as well as construction of animal models, collection of brain tissues, and further verification by RT-qPCR, we located and captured the crucial targets among the DEGs. They are, respectively, CARTPT, EPHA5, and SERPINA3, which are perhaps of great value in studying the molecular regulatory mechanisms shared by type 2 diabetes and Alzheimer's disease. The key factors regulating them, such as miRNA and drugs, as well as the clinical prediction and diagnostic value in type 2 diabetes and Alzheimer's disease, were further analyzed. Our finding may shed new light on the treatment of Alzheimer's disease or diabetic cognitive impairment, but follow-up studies still need to be unfolded.

Abbreviations

AD: Alzheimer's disease
T2DM: Type 2 diabetes mellitus
CNS: Central nervous system
GEO: Gene Expression Omnibus
DEGs: Differentially expressed genes
GO: Gene Ontology
MF: Molecular function
BP: Biological process
CC: Cellular component
KEGG: Kyoto Encyclopedia of Genes and Genomes
PPI: Protein-protein interaction
STRING: Search Tool for the Retrieval of Interacting Genes
LASSO: Least absolute shrinkage and selection operator
SVM-RFE: Support vector machine-recursive feature elimination

CTD: Comparative Toxicogenomics database
ROC: Receiver operating characteristic
STZ: Streptozocin.

Data Availability

The public gene data (GSE161355, GSE122063, and GSE5281) analyzed in this article were downloaded from the NCBI-GEO database (https://www.ncbi.nlm.nih.gov/geo/).

Ethical Approval

All experimental procedures and animal care were approved by the Jinan University Laboratory Animal Ethics Committee.

Conflicts of Interest

The authors declared no potential conflicts of interest with respect to the research, authorship, and/or publication of this article.

Authors' Contributions

Cheng Huang and Keshen Li designed the study. Cheng Huang and Xueyi Wen collected and analyzed the data. Xueyi Wen conducted the experiments. Cheng Huang wrote the initial draft of the manuscript. Hesong Xie and Di Hu contributed to find references. Keshen Li reviewed and edited the manuscript. All authors read and approved the manuscript. Cheng Huang and Xueyi Wen contributed equally to this work.

Acknowledgments

This work was supported by the National Natural Science Foundation of China (Grant No. 81971079).

Supplementary Materials

Supplementary 1. Supplementary Table 1: primer pairs for RT-qPCR in mice temporal cortex.

Supplementary 2. Supplementary file 1: the DEGs identified in patients with T2DM compared with controls (GSE161355; a total of 1508 DEGs; including 1473 downregulated genes and 35 upregulated genes).

Supplementary 3. Supplementary file 2: the DEGs identified in patients with AD compared with controls (GSE122063; a total of 788 DEGs; including 475 downregulated genes and 313 upregulated genes).

Supplementary 4. Supplementary Figure 1: the heatmap for the expression level of 62 overlapping genes in GSE122063.

Supplementary 5. Supplementary Figure 2: the expression value of COL24A1 validated in the GSE5281 (no significance).

Supplementary 6. Supplementary Figure 3: the expression value of LY96 validated in the GSE5281 (no significance).

References

[1] H. Feldman and M. Woodward, "The staging and assessment of moderate to severe Alzheimer disease," *Neurology*, vol. 65, no. 6, Supplement 3, pp. S10–S17, 2005.

[2] Z. Breijyeh and R. Karaman, "Comprehensive review on Alzheimer's disease: causes and treatment," *Molecules (Basel, Switzerland)*, vol. 25, no. 24, 2020.

[3] W. Xu, C. Qiu, B. Winblad, and L. Fratiglioni, "The effect of borderline diabetes on the risk of dementia and Alzheimer's disease," *Diabetes*, vol. 56, no. 1, pp. 211–216, 2007.

[4] E. Adeghate, P. Schattner, and E. Dunn, "An update on the etiology and epidemiology of diabetes mellitus," *Annals of the New York Academy of Sciences*, vol. 1084, no. 1, pp. 1–29, 2006.

[5] C. Eberle and S. Stichling, "Clinical improvements by telemedicine interventions managing type 1 and type 2 diabetes: systematic meta-review," *Journal of Medical Internet Research*, vol. 23, no. 2, article e23244, 2021.

[6] L. Zilliox, K. Chadrasekaran, J. Kwan, and J. Russell, "Diabetes and cognitive impairment," *Current Diabetes Reports*, vol. 16, no. 9, p. 87, 2016.

[7] C. Brady, J. Vannest, L. Dolan et al., "Obese adolescents with type 2 diabetes perform worse than controls on cognitive and behavioral assessments," *Pediatric Diabetes*, vol. 18, no. 4, pp. 297–303, 2017.

[8] M. Xue, W. Xu, Y. Ou et al., "Diabetes mellitus and risks of cognitive impairment and dementia: a systematic review and meta-analysis of 144 prospective studies," *Ageing Research Reviews*, vol. 55, article 100944, 2019.

[9] L. Li and C. Hölscher, "Common pathological processes in Alzheimer disease and type 2 diabetes: a review," *Brain Research Reviews*, vol. 56, no. 2, pp. 384–402, 2007.

[10] R. Kandimalla, V. Thirumala, and P. Reddy, "Is Alzheimer's disease a type 3 diabetes? A critical appraisal," *Molecular Basis Of Disease*, vol. 1863, no. 5, pp. 1078–1089, 2017.

[11] G. Stanciu, V. Bild, D. Ababei et al., "Link between diabetes and Alzheimer's disease due to the shared amyloid aggregation and deposition involving both neurodegenerative changes and neurovascular damages," *Journal Of Clinical Medicine*, vol. 9, no. 6, p. 1713, 2020.

[12] N. Garcia-Casares, R. E. Jorge, J. A. Garcia-Arnes et al., "Cognitive dysfunctions in middle-aged type 2 diabetic patients and neuroimaging correlations: a cross-sectional study," *Journal of Alzheimer's Disease*, vol. 42, no. 4, pp. 1337–1346, 2014.

[13] A. Moheet, S. Mangia, and E. Seaquist, "Impact of diabetes on cognitive function and brain structure," *Annals of the New York Academy of Sciences*, vol. 1353, no. 1, pp. 60–71, 2015.

[14] C. Moran, T. G. Phan, J. Chen et al., "Brain atrophy in type 2 diabetes: regional distribution and influence on cognition," *Diabetes Care*, vol. 36, no. 12, pp. 4036–4042, 2013.

[15] Y. Cui, T.-Y. Tang, C.-Q. Lu, and S. Ju, "Insulin resistance and cognitive impairment: evidence from neuroimaging," *Journal of Magnetic Resonance Imaging: JMRI*, 2022.

[16] T. Barrett, T. O. Suzek, D. B. Troup et al., "NCBI GEO: mining millions of expression profiles—database and tools," *Nucleic Acids Research*, vol. 33, supplement 1, pp. D562–D566, 2004.

[17] J. J. Bury, A. Chambers, P. R. Heath et al., "Type 2 diabetes mellitus-associated transcriptome alterations in cortical neurones and associated neurovascular unit cells in the ageing brain," *Acta Neuropathologica Communications*, vol. 9, no. 1, pp. 1–16, 2021.

[18] E. C. McKay, J. S. Beck, S. K. Khoo et al., "Peri-infarct upregulation of the oxytocin receptor in vascular dementia," *Journal of Neuropathology & Experimental Neurology*, vol. 78, no. 5, pp. 436–452, 2019.

[19] J. L. Sepulveda, "Using R and bioconductor in clinical genomics and transcriptomics," *The Journal of Molecular Diagnostics*, vol. 22, no. 1, pp. 3–20, 2020.

[20] Z. Zhan, Y. Chen, Y. Duan et al., "Identification of key genes, pathways and potential therapeutic agents for liver fibrosis using an integrated bioinformatics analysis," *PeerJ*, vol. 7, article e6645, 2019.

[21] W. H. Ge, Y. Lin, S. Li, X. Zong, and Z. C. Ge, "Identification of biomarkers for early diagnosis of acute myocardial infarction," *Journal of Cellular Biochemistry*, vol. 119, no. 1, pp. 650–658, 2018.

[22] C. Huang, J. Luo, X. Wen, and K. Li, "Linking Diabetes Mellitus with Alzheimer's Disease: Bioinformatics Analysis for the Potential Pathways and Characteristic Genes," *Biochemical Genetics*, vol. 60, pp. 1–27, 2021.

[23] J. Y. Lee and M. P. Styczynski, "NS-kNN: a modified k-nearest neighbors approach for imputing metabolomics data," *Metabolomics*, vol. 14, no. 12, pp. 1–12, 2018.

[24] M. E. Ritchie, B. Phipson, D. Wu et al., "limma powers differential expression analyses for RNA-sequencing and microarray studies," *Nucleic Acids Research*, vol. 43, no. 7, pp. e47–e47, 2015.

[25] W. Liang, F. Sun, Y. Zhao, L. Shan, and H. Lou, "Identification of susceptibility modules and genes for cardiovascular disease in diabetic patients using WGCNA analysis," *Journal of Diabetes Research*, vol. 2020, 11 pages, 2020.

[26] M. Zhang, K. Zhu, H. Pu et al., "An immune-related signature predicts survival in patients with lung adenocarcinoma," *Frontiers in Oncology*, vol. 9, p. 1314, 2019.

[27] Z. Lan, X. Yao, K. Sun, A. Li, S. Liu, and X. Wang, "The interaction between lncRNA SNHG6 and hnRNPA1 contributes to the growth of colorectal cancer by enhancing aerobic glycolysis through the regulation of alternative splicing of PKM," *Frontiers in Oncology*, vol. 10, p. 363, 2020.

[28] A. S. Nangraj, G. Selvaraj, S. Kaliamurthi, A. C. Kaushik, W. C. Cho, and D. Q. Wei, "Integrated PPI-and WGCNA-retrieval of hub gene signatures shared between Barrett's esophagus and esophageal adenocarcinoma," *Frontiers in Pharmacology*, vol. 11, p. 881, 2020.

[29] Y. Xv, F. Lv, H. Guo et al., "Machine learning-based CT radiomics approach for predicting WHO/ISUP nuclear grade of clear cell renal cell carcinoma: an exploratory and comparative study," *Insights Into Imaging*, vol. 12, no. 1, pp. 1–14, 2021.

[30] Y. Liu, S. Cui, J. Sun, X. Yan, and D. Han, "Identification of potential biomarkers for psoriasis by DNA methylation and gene expression datasets," *Frontiers In Genetics*, vol. 12, 2021.

[31] A. P. Davis, C. J. Grondin, R. J. Johnson et al., "The comparative toxicogenomics database: update 2019," *Nucleic Acids Research*, vol. 47, no. D1, pp. D948–D954, 2019.

[32] X. Robin, N. Turck, A. Hainard et al., "pROC: an open-source package for R and S+ to analyze and compare ROC curves," *BMC Bioinformatics*, vol. 12, no. 1, pp. 1–8, 2011.

[33] Z.-F. Guan, X.-L. Zhou, X.-M. Zhang et al., "Beclin-1-mediated autophagy may be involved in the elderly cognitive and affective disorders in streptozotocin-induced diabetic mice," *Translational Neurodegeneration*, vol. 5, no. 1, pp. 1–10, 2016.

[34] Y. Qin, Y.-H. He, N. Hou et al., "Sonic hedgehog improves ischemia-induced neovascularization by enhancing endothelial progenitor cell function in type 1 diabetes," *Molecular and Cellular Endocrinology*, vol. 423, pp. 30–39, 2016.

[35] F. Dellu, A. Contarino, H. Simon, G. Koob, and L. Gold, "Genetic differences in response to novelty and spatial memory using a two- trial recognition task in mice," *Neurobiology of Learning and Memory*, vol. 73, no. 1, pp. 31–48, 2000.

[36] C.-n. Zhou, F.-l. Chao, Y. Zhang et al., "Sex differences in the white matter and myelinated fibers of APP/PS1 mice and the effects of running exercise on the sex differences of AD mice," *Frontiers in Aging Neuroscience*, vol. 10, p. 243, 2018.

[37] J. Xu, X. Shen, X. Wei et al., "Identification of blood-based key biomarker and immune infiltration in immunoglobulin A nephropathy by comprehensive bioinformatics analysis and a cohort validation," *Journal of Translational Medicine*, vol. 20, no. 1, pp. 1–16, 2022.

[38] C.-S. Rau, S.-C. Wu, T.-H. Lu et al., "Effect of low-fat diet in obese mice lacking toll-like receptors," *Nutrients*, vol. 10, no. 10, p. 1464, 2018.

[39] X. Pan, X. Jin, J. Wang, Q. Hu, and B. Dai, "Placenta inflammation is closely associated with gestational diabetes mellitus," *American Journal of Translational Research*, vol. 13, no. 5, pp. 4068–4079, 2021.

[40] K. C. Cotto, A. H. Wagner, Y.-Y. Feng et al., "DGIdb 3.0: a redesign and expansion of the drug–gene interaction database," *Nucleic Acids Research*, vol. 46, no. D1, pp. D1068–D1073, 2018.

[41] W. Chong, L. Shang, J. Liu et al., "m6A regulator-based methylation modification patterns characterized by distinct tumor microenvironment immune profiles in colon cancer," *Theranostics*, vol. 11, no. 5, pp. 2201–2217, 2021.

[42] R. A. M. Villanueva and Z. J. Chen, *ggplot2: Elegant Graphics for Data Analysis*, vol. 17, Taylor & Francis, 2019.

[43] L. Lin, L. J. Zheng, and L. J. Zhang, "Neuroinflammation, gut microbiome, and Alzheimer's disease," *Molecular Neurobiology*, vol. 55, no. 11, pp. 8243–8250, 2018.

[44] F.-P. Lu, K.-P. Lin, and H.-K. Kuo, "Diabetes and the risk of multi-system aging phenotypes: a systematic review and meta-analysis," *PLoS One*, vol. 4, no. 1, article e4144, 2009.

[45] P. Palta, M. Carlson, R. Crum et al., "Diabetes and cognitive decline in older adults: the Ginkgo evaluation of memory study," *The Journals of Gerontology Series A, Biological Sciences and Medical Sciences*, vol. 73, no. 1, pp. 123–130, 2018.

[46] E. L. Goldwaser, N. K. Acharya, A. Sarkar, G. Godsey, and R. G. Nagele, "Breakdown of the cerebrovasculature and blood-brain barrier: a mechanistic link between diabetes mellitus and Alzheimer's disease," *Journal of Alzheimer's Disease*, vol. 54, no. 2, pp. 445–456, 2016.

[47] Y. Wu, L. Dissing-Olesen, B. A. MacVicar, and B. Stevens, "Microglia: dynamic mediators of synapse development and plasticity," *Trends in Immunology*, vol. 36, no. 10, pp. 605–613, 2015.

[48] K. Chandrasekaran, J. Choi, M. Arvas et al., "Nicotinamide mononucleotide administration prevents experimental diabetes-induced cognitive impairment and loss of hippocampal neurons," *International Journal of Molecular Sciences*, vol. 21, no. 11, 2020.

[49] F. Zhao, J. Li, L. Mo et al., "Changes in neurons and synapses in hippocampus of streptozotocin-induced type 1 diabetes rats: a stereological investigation," *The Anatomical Record*, vol. 299, no. 9, pp. 1174–1183, 2016.

[50] K. Pu, M. Wu, T. Jiang et al., "Involvement of paired immunoglobulin-like receptor B in diabetes-associated cognitive dysfunction through modulation of axon outgrowth and dendritic remodeling," *Molecular Neurobiology*, vol. 59, no. 4, pp. 2563–2579, 2022.

[51] J. Freiherr, M. Hallschmid, I. I. William, and Y. Brünner, "Intranasal insulin as a treatment for Alzheimer's disease: a review of basic research and clinical evidence," *Drugs*, vol. 27, no. 7, pp. 505–514, 2013.

[52] A. Sdzikowska and L. Szablewski, "Insulin and insulin resistance in Alzheimer's disease," *International Journal of Molecular Sciences*, vol. 22, no. 18, p. 9987, 2021.

[53] Y. Yang and W. Song, "Molecular links between Alzheimer's disease and diabetes mellitus," *Neuroscience*, vol. 250, pp. 140–150, 2013.

[54] S. C. Correia, R. X. Santos, C. Carvalho et al., "Insulin signaling, glucose metabolism and mitochondria: major players in Alzheimer's disease and diabetes interrelation," *Brain Research*, vol. 1441, pp. 64–78, 2012.

[55] Q.-S. Zhuang, L. Meng, Z. Wang, L. Shen, and H.-F. Ji, "Associations between obesity and Alzheimer's disease: multiple bioinformatic analyses," *Journal of Alzheimer's Disease*, vol. 80, no. 1, pp. 271–281, 2021.

[56] P. Kristensen, M. E. Judge, L. Thim, U. Ribel, and S. Hastrup, "Hypothalamic CART is a new anorectic peptide regulated by leptin," *Nature*, vol. 393, no. 6680, pp. 72–76, 1998.

[57] P. R. Couceyro, E. O. Koylu, and M. J. Kuhar, "Further studies on the anatomical distribution of CART by in situ hybridization," *Journal of Chemical Neuroanatomy*, vol. 12, no. 4, pp. 229–241, 1997.

[58] K. Schultz, S. Wiehager, K. Nilsson, J. E. Nielsen, and A. Petersén, "Reduced CSF CART in dementia with Lewy bodies," *Neuroence Letters*, vol. 453, no. 2, pp. 104–106, 2009.

[59] J. L. Jin, A. K. F. Liou, Y. Shi et al., "CART treatment improves memory and synaptic structure in APP/PS1 mice," *Scientific Reports*, vol. 5, p. 10224, 2015.

[60] Y. Yamaguchi and E. B. Pasquale, "Eph receptors in the adult brain," *Current Opinion in Neurobiology*, vol. 14, no. 3, pp. 288–296, 2004.

[61] D. B. Nikolov, K. Xu, and J. P. Himanen, "Eph/ephrin recognition and the role of Eph/ephrin clusters in signaling initiation," *Biochimica et Biophysica Acta (BBA)-Proteins and Proteomics*, vol. 1834, no. 10, pp. 2160–2165, 2013.

[62] G. Das, Q. Yu, R. Hui, K. Reuhl, N. W. Gale, and R. Zhou, "EphA5 and EphA6: regulation of neuronal and spine morphology," *Cell & Bioscience*, vol. 6, no. 1, pp. 1–12, 2016.

[63] R. Gerlai, N. Shinsky, A. Shih et al., "Regulation of learning by EphA receptors: a protein targeting study," *Journal of Neuroscience*, vol. 19, no. 21, pp. 9538–9549, 1999.

[64] M. I. Kamboh, R. L. Minster, M. Kenney et al., "Alpha-1-antichymotrypsin (ACT or SERPINA3) polymorphism may affect age-at- onset and disease duration of Alzheimer's disease," *Neurobiology of Aging*, vol. 27, no. 10, pp. 1435–1439, 2006.

Hindawi
Oxidative Medicine and Cellular Longevity
Volume 2022, Article ID 8059622, 10 pages
https://doi.org/10.1155/2022/8059622

Research Article

Leukocyte-Rich Platelet-Rich Plasma as an Effective Source of Molecules That Modulate Local Immune and Inflammatory Cell Responses

Maciej Dejnek,[1] Helena Moreira,[2] Sylwia Płaczkowska,[3] Ewa Barg,[2] Paweł Reichert,[1] and Aleksandra Królikowska[4]

[1]*Clinical Department of Trauma and Hand Surgery, Department of Trauma Surgery, Faculty of Medicine, Wroclaw Medical University, 50-556 Wroclaw, Poland*
[2]*Department of Medical Science Foundation, Faculty of Pharmacy, Wroclaw Medical University, 50-556, Wroclaw, Poland*
[3]*Teaching and Research Diagnostic Laboratory, Department of Laboratory Diagnostics, Faculty of Pharmacy, Wroclaw Medical University, 50-556 Wroclaw, Poland*
[4]*Ergonomics and Biomedical Monitoring Laboratory, Department of Physiotherapy, Faculty of Health Sciences, Wroclaw Medical University, 50-355 Wroclaw, Poland*

Correspondence should be addressed to Maciej Dejnek; maciej.dejnek@student.umw.edu.pl

Received 4 May 2022; Accepted 18 July 2022; Published 2 August 2022

Academic Editor: Ana Lloret

Autologous platelet-rich plasma (PRP) injection is a safe biological method used to treat various musculoskeletal diseases. By downregulation of inflammatory cytokines and stimulation of synovial fibroblasts, PRP injection is a promising adjunctive treatment for patients with chronic autoimmune inflammatory diseases such as rheumatoid arthritis. A major problem in comparing the results of clinical trials in this area is the considerable variability in the cytokine content of PRP. We presented the profile of selected growth factors and inflammatory cytokines in the obtained PRP samples and compared them with baseline serum levels to assess the efficacy of PRP as a source of those paracrine molecules. Additionally, we wanted to determine whether the difference is only quantitative, which would suggest the use of a cheaper alternative by injecting a large amount of autologous serum. For this purpose, we analyzed whole blood and PRP samples prepared using the Mini GPS III Platelet Concentration System (Biomet Inc., USA) in 31 subjects aged 35-60 years. Cellular content, seven selected growth factors, and 13 human inflammatory cytokines were evaluated. Multiplex bead immunoassays that use fluorescence-encoded beads LEGENDplex™ (BioLegend, USA) and flow cytometer measurements were used. As a result, we found a statistically significant increase in four of the growth factors tested and eight of the inflammatory cytokines tested in PRP compared to blood serum. The difference is not only quantitative but also in the composition of paracrine molecules. In conclusion, the study confirmed that PRP is an efficient source of several growth factors and some inflammatory cytokines. These data provide additional insight into the potential mechanisms of PRP's effects on cellular metabolism and inflammatory response and may contribute to a better understanding of its clinical efficacy.

1. Introduction

Autologous platelet-rich plasma (PRP) injection is a treatment method used in various soft tissue degenerative conditions. It is widely used in orthopedic, sports medicine, stomatology, and aesthetic medicine [1–3]. A growing number of reports indicate a potential role for PRP in the treatment of involved joints in patients with chronic autoimmune inflammatory diseases such as rheumatoid arthritis [4, 5].

Rheumatoid arthritis (RA) is a chronic autoimmune inflammatory disease that affects approximately 1% of the world's population and is characterized by synovial hyperplasia, articular inflammation, and invasion of the synovium

into the adjacent bone and cartilage [6]. The underlying cause of the disease is an abnormal immune response that activates fibroblast-like synoviocytes (FLS), provoking an inflammatory response that leads to disease progression [4]. In the initial stage, the disease usually affects small joints, but when advanced, it can lead to massive destruction of large joints such as the knee, shoulder, or hip, causing significant disability. The exact cause of the disease is not sufficiently understood, although many different therapies targeting the molecular pathways of the ongoing inflammatory process have been proposed [4]. One of the new methods supporting the treatment of patients is the intra-articular injection of PRP. Studies have shown high safety of the therapy resulting in suppression of the inflammatory process [4, 5, 7].

PRP is obtained by the separation of plasma with an excessive amount of platelets from the blood sample. The most common preparation method is manually extracting platelet-rich plasma from the blood sample after centrifugation in a specially designed tube [8]. Many different commercially available kits existing on the market are helping to prepare PRP as easily as possible in ambulatory conditions.

This treatment is aimed at providing a high amount of platelet-derived growth factors to enhance healing issues and stimulate degenerative tissue to regenerate or modulate the local inflammatory response [9]. In the human body, high amounts of growth factors and cytokines are released from platelets alpha-granules at the site of injury. Their role is to stimulate cell migration, proliferation, differentiation, angiogenesis, extracellular matrix production, and scar formation [10]. An enormous amount of various cytokines affect the local environment and interact with each other through the processes of stimulation and inhibition [9]. The function of many of them remains unclear and is difficult to assess in the living organism.

There are many doubts about the effectiveness of PRP treatment in different conditions. The results presented by various researchers are often mutually exclusive, and most meta-analyses do not provide clear answers in this field [1]. There may be several reasons for this situation. Significant differences in the content of biologically active components in PRPs prepared by different commercially available kits and their repeatability in the platelet and leukocyte concentrations are among the problems to be solved [11]. Furthermore, significant differences due to the patients' characteristics, such as age, sex, smoking status, diseases, drugs usage, or physical activity, can affect the quality of the final PRP product [12–14]. Incorrect interpretation of the results may also be due to the incompletely understood function of all cytokines in the PRP samples and their interaction with each other and the surrounding tissues. Many more studies are still needed both on the content of biologically active components in PRP samples and their influence on the effectiveness of treatment of various diseases.

The aim of the study was to assess if PRP samples would have a significantly higher amount of selected growth factors and inflammatory cytokines than baseline level in patients' serum and if the difference would be only quantitative or qualitative as well. We hypothesized that PRP would contain a proportionally higher concentration of paracrine molecules than patients' serum. Confirmation of the above hypothesis could lead to the development of a new, cheaper orthobiological treatment method by intra-articular injection of a higher volume of autologous serum, which could be beneficial for large joints affected by rheumatoid arthritis.

2. Materials and Methods

2.1. Ethical Standards. The study was carried out according to the Declaration of Helsinki and was approved by the Institutional Ethics Committee of Wroclaw Medical University (KB–26/2019, 21.01.2019). All patients agreed to participate in the study and signed an informed consent.

2.2. Study Design. The study was designed as a single-center prospective descriptive laboratory study and is an additional part of the investigation of the correlation between the concentration of cytokines in PRP and the effectiveness of epicondylopathy treatment registered in clinicaltrials.gov under identifier NCT04521387.

2.3. Population. The study was conducted on 31 patients who were enrolled in the years 2021-2022. The population contained 15 men and 16 women aged 35-60 years old ($x = 49.10$; SD = 6.03). Patients' height and weight were measured to calculate Body Mass Index (BMI). Three patients regularly smoked cigarettes, 15 regularly practiced sports activity (≥3 sessions per week), 22 drank alcohol occasionally (≤1 dose per week), and nine did not drink alcohol at all. Patients with hematologic diseases, diabetes, and suspicion of the infectious process; those who are pregnant; and those taking medications that may affect platelet function or the coagulation system were excluded.

2.4. PRP Preparation. From each patient, 27 ml of blood was collected into a 30 ml syringe filled with 3 ml of anticoagulant citrate dextrose solution A (ACD-A). Additional 6 ml of blood was taken and divided to a 2 ml probe with ethylenediaminetetraacetic acid (EDTA) for complete blood count analysis and a 4 ml probe with clotting activator for serum preparation. A 30 ml syringe blood sample mixed with ACD-A was transferred to a specially designed tube with a membrane for PRP separation—Mini GPS III Platelet Concentration System (Biomet Inc., USA). The tube was placed in a dedicated centrifuge for the separation process, which took 15 minutes with 3200 revolutions per minute (RPM). After centrifugation, platelet-poor plasma placed above the separation membrane was removed, and 3 ml liquid-form leukocyte-rich platelet-rich plasma was collected in the sterile 3 ml syringe according to the manufacturer manual. The step-by-step process for preparing PRP is shown in Figure 1. Two ml of PRP was used for patient treatment, and 1 ml of PRP was reinjected into an Eppendorf polypropylene tube and then gently shaken for 30 seconds just before laboratory analysis. The time between blood draw, PRP separation, and further analysis did not exceed 1 hour, and the whole process was conducted in daylight at room temperature.

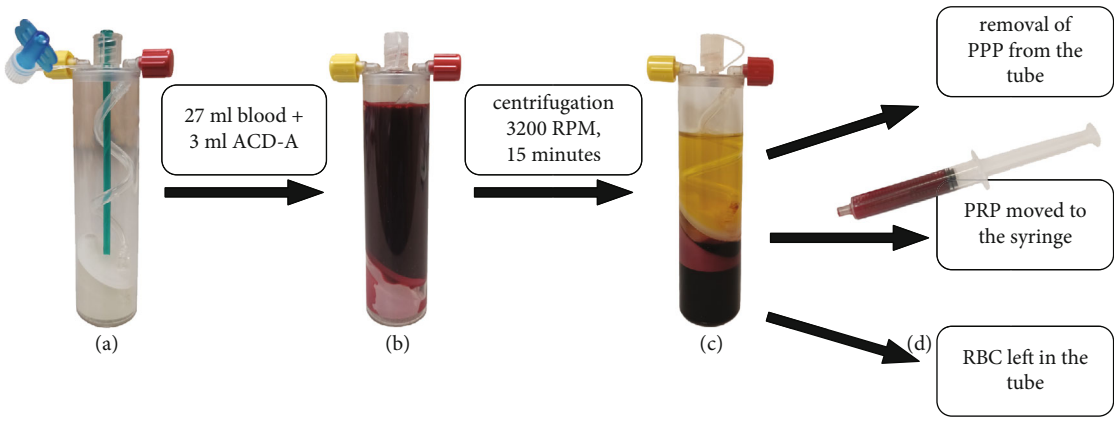

Figure 1: PRP preparation process by Mini GPS III. (a) The empty Mini GPS III tube. (b) The tube filled with 3 ml of anticoagulant citrate dextrose solution A (ACD-A) and 27 ml of patients' own blood. (c) The tube after centrifugation containing three separate layers: platelet-poor plasma (PPP), platelet-rich plasma (PRP), and red blood cells (RBC). (d) The syringe filled with PRP taken from the tube after the removal of PPP.

2.5. Evaluation of Cellular Components. The complete blood count was analyzed from a 2 ml probe with EDTA using the Mindray BC-5150 automatic laboratory analyzer (Shenzhen Mindray Bio-Medical Electronics Co., PRC). Then, the PRP sample was analyzed in the same fashion from the Eppendorf tube.

2.6. Serum Sample Preparation and Storage. Blood was collected into BD Vacutainer® Plus Plastic Serum Tubes (BD, Biosciences, Warsaw, Poland). The blood samples were allowed to clot at room temperature for approximately 20–30 min and centrifuged at 500 × g for 15 minutes. The serum was transferred to a polypropylene tube and stored at -80°C until the time of analysis.

2.7. PRP Activation and Storage. PRP samples were activated through a double freeze-thaw process for 30 minutes in each step as proposed by Zimmermann et al. [15]. The activated samples were frozen to -80°C and stored for further analysis.

2.8. Growth Factor and Inflammatory Cytokine Evaluation. LEGENDplex™ Custom Human 7-plex Panel and LEGENDplex™ Human Inflammation Panel 1 (BioLegend, USA) were used to estimate the concentration of selected growth factors and inflammatory cytokines in PRP and serum samples. The first one is a customized panel dedicated to our study, containing the most frequently studied and the most important platelet-derived growth factors. The second one is a commercially available standard set for inflammatory cytokine testing (see Table 1). LEGENDplex is a multiplex immunoassays based on fluorescence-encoded beads and flow cytometric measurements. Just before the assay, all samples were thawed to room temperature, centrifuged for 5 minutes at 2500 RPM in a Micro Star 17 microcentrifuge (VWR International Company, Thermo Electron LED, Germany), and 2x diluted. A LEGENDplex assay was performed according to the manufacturer's procedure. The samples were acquired on a CyFlow Cube 8 flow cytometer (Sysmex-Partec, Görlitz, Germany) applying a 488 nm laser with 536/40 (BP) filter for the PE fluorochrome and a 638 nm laser with 675/20 (BP) for the APC fluorochrome. The results were analyzed using LEGENDplex™ Data Analysis Software V.8.0 (Vigene Tech Inc., USA). The concentration of each growth factor/cytokine was determined by means of a standard curve generated during the performance of the assay.

2.9. Statistical Analysis. For statistical assessment, Statistica 13.3 software (TIBCO Software Inc, USA) was used. For compliance of the result distribution, the Shapiro-Wilk test was used. Arithmetic means and standard deviations (SD) were calculated. For data with nonnormal distribution, the median and quartile distribution (Q1-Q3) were additionally given. The outliers (more than 3 standard deviations) were removed for the calculations. For comparison of two variables with normal distribution, dependent t-test for paired samples was performed. For variables without normal distribution, the Wilcoxon signed rank test was performed. Pearson's correlation coefficient (r) was used to establish a relationship between blood cell components and growth factors or inflammatory cytokines. The level equal to or greater than 0.8 was assumed to be the satisfactory power of the tests ($1 - \beta > 0.8$). Based on an earlier pilot study, we calculated that 30 patients would be sufficient to achieve the power target for the growth factor comparison [11]. The results were assessed as significant at $p \leq 0.05$.

3. Results

3.1. Cellular Components. Differences between whole blood and PRP samples in cellular content are highlighted in Table 2. All differences except the content of eosinophils ($p = 0.52$) were significant ($p \leq 0.001$). WBC and PLT but not RBC content in whole blood correlate ($r > 0.30$) to their concentrations in PRP. There was significant difference between men and women in RBC content in whole blood (5.15 *vs.* 4.56, $p \leq 0.001$), which is a physiological difference within the normal range for both sexes. WBC content in PRP also differed between males and females (34.64 *vs.* 25.83, $p < 0.05$). Current smoking status was connected with

Table 1: All paracrine molecules tested by flow cytometry with the use of LEGENDplex™ panels.

LEGENDplex™ Custom Human 7-plex Panel	LEGENDplex™ Human Inflammation Panel 1
Transforming growth factor-β1 (TGF-β1, free active)	Interleukin-1β (IL-1β)
Epidermal growth factor (EGF)	Interferon-α2 (IFN-α2)
Fibroblast growth factor-basic (FGF-basic)	Interferon-γ (IFN-γ)
Vascular endothelial growth factor (VEGF)	Tumor necrosis factor α (TNF-α)
Hepatocyte growth factor (HGF)	Monocyte chemoattractant Protein-1 (MCP-1)
Platelet-derived growth factor-AA (PDGF-AA)	Interleukin-6 (IL-6)
Platelet-derived growth factor-BB (PDGF-BB)	Interleukin-8 (IL-8)
	Interleukin-10 (IL-10)
	Interleukin-12p70 (IL-12p70)
	Interleukin-17A (IL-17A)
	Interleukin-18 (IL-18)
	Interleukin-23 (IL-23)
	Interleukin-33 (IL-33)

Table 2: Differences in cellular content between whole blood (WB) and platelet-rich plasma (PRP). Values are presented as arithmetic mean (standard deviation). The ability to concentrate the cell components in PRP vs. WB is presented as the "ratio." The Pearson correlation coefficient between the cell components of WB and PRP is presented as a value r ($^*p < 0.050$). The significance of the comparison is shown as p value.

	WB	PRP	Ratio	p	r
WBC ($10^3/\mu$l)	6.60 (1.34)	30.09 (9.58)	×4.59	≤0.001	0.66*
Neutrophils	4.03 (1.22)	12.72 (6.66)	×3.19	≤0.001	0.47*
Lymphocytes	1.96 (0.51)	14.18 (5.04)	×7.31	≤0.001	0.64*
Monocytes	0.4 (0.1)	2.81 (1.07)	×7.25	≤0.001	0.73*
Eosinophils	0.15 (0.11)	0.17 (0.17)	×1.06	0.52	0.78*
Basophiles	0.03 (0.02)	0.19 (0.12)	×6.44	≤0.001	0.85*
RBC ($10^6/\mu$l)	4.85 (0.44)	0.92 (0.49)	×0.19	≤0.001	0.14
PLT ($10^3/\mu$l)	253.27 (59.37)	1083.87 (493.55)	×4.41	≤0.001	0.47*

a significantly higher concentration of PLT in whole blood and PRP ($p < 0.05$). Alcohol consumption and sports activity did not influence the cellular content of the whole blood and PRP.

3.2. Growth Factors. The differences between the serum and PRP growth factor content are presented in Table 3. All growth factors increased in PRP, but the difference was not significant for VEGF. Sex did not influence any of the growth factors. Smokers had significantly higher concentration of PDGF-BB (70486.93 *vs.* 46856.9, $p < 0.05$) which could be explained by a higher PLT content in their whole blood and PRP samples. Alcohol consumption and sports activity did not influence growth factor content in the whole blood and PRP.

3.3. Inflammatory Cytokines. Differences between serum and PRP inflammatory cytokine content are highlighted in Table 4. All inflammatory cytokine concentrations in the PRP were lower in women, and these differences were significant ($p < 0.05$) in all except MCP-1 ($p = 0.63$), IFN-γ ($p = 0.10$), TNF-α ($p = 0.12$), and IL-6 ($p = 0.27$). Comparison between both sexes is shown in Supplementary Table 1. Smoking status, alcohol consumption, and sports activity did not influence the content of cytokines in the PRP samples. More than 80% of the IL-23 results were below the lower cut-off point for measurement; therefore, it was excluded.

3.4. Correlations between Cell Content and Growth Factors or Inflammatory Cytokines. Significant high positive correlation was found between PLT content in PRP and three growth factors: EGF ($r = 0.74$; $p \leq 0.001$), PDGF-AA ($r = 0.77$; $p \leq 0.001$), and PDGF-BB ($r = 0.79$; $p \leq 0.001$). Significant but low positive correlation was found between PLT and VEGF ($r = 0.46$; $p < 0.05$) (see Figure 2). No significant correlations between PLT content and inflammatory cytokines were observed.

Significant moderate positive correlation was found between WBC and VEGF ($r = 0.69$; $p \leq 0.001$), and significant low correlation between WBC and HGF ($r = 0.42$; $p < 0.05$). For inflammatory cytokines, a significant positive low correlation was found between WBC and IL-8 ($r = 0.45$; $p < 0.05$) (see Figure 3). Subpopulation of neutrophils correlated moderately with IL-8 ($r = 0.62$; $p \leq 0.001$) and on a low level with IL-1β ($r = 0.41$; $p < 0.05$) and IL-18

Table 3: Differences in growth factor content between serum and platelet-rich plasma (PRP). Values (pg/ml) are presented as arithmetic mean (standard deviation) and median (Q1-Q3). The ability to concentrate growth factors in PRP vs. serum is presented as the "ratio." The significance of the comparison is shown as p value.

	Serum		PRP		Ratio	p
	Mean (SD)	Median (Q1-Q3)	Mean (SD)	Median (Q1-Q3)		
TGF-β1, free active	151.67 (72.41)	158.02 (94.86-204.24)	383.33 (251.75)	343.26 (257.65-443.32)	×3.79	≤0.001
EGF	110.04 (44.88)	103.575 (76.33-140.36)	243.96 (155.21)	219.13 (116.43-319.81)	×2.5	≤0.001
FGF-basic	1094.06 (487.25)	1048.33 (667.71-1436.06)	746.30 (2043.42)	315.30 (254.70-428.24)	×0.68	≤0.001
VEGF	152.88 (52.91)	152.925 (128.87-171.73)	324.53 (394.54)	180.67 (40.95-313.17)	×2.34	0.43
HGF	534.72 (210.44)	497.91 (375.67-679.67)	231.23 (114.08)	204.03 (156.05-258.75)	×0.51	≤0.001
PDGF-AA	25462.54 (13742.23)	23429.45 (16404.90-32176.13)	132725.23 (53608.77)	137269.89 (90062.55-183956.91)	×6.19	≤0.001
PDGF-BB	9070.09 (6484.37)	6807.38 (5424.22-13513.71)	49143.68 (18068.74)	51779.04 (29826.86-62573.63)	×6.43	≤0.001

Table 4: Differences in inflammatory cytokine content between serum and platelet-rich plasma (PRP). Values (pg/ml) are presented as arithmetic mean (standard deviation) and median (Q1-Q3). The ability to concentrate the cytokines in PRP vs. serum is shown as the "ratio." The significance of the comparison is presented as p value.

	Serum		PRP		Ratio	p
	Mean (SD)	Median (Q1-Q3)	Mean (SD)	Median (Q1-Q3)		
IL-1β	34.09 (48.04)	18.12 (18.12-19.78)	67.09 (58.67)	43.24 (30.36-82.03)	×2.99	0.002
IFN-α2	16.90 (2.54)	16.16 (16.16-16.16)	39.0 (28.68)	26.38 (16.16-50.14)	×2.40	≤0.001
IFN-γ	4.98 (0.56)	4.87 (4.87-4.87)	6.66 (3.09)	4.87 (4.87-7.13)	×1.39	0.03
TNF-α	18.50 (7.45)	13.17 (13.02-20.98)	33.1 (27.09)	23.56 (13.02-42.72)	×2.12	0.02
MCP-1	140.22 (162.49)	80.3 (30.82-194.90)	107.90 (66.07)	88.71 (63.97-148.27)	×2.13	0.99
IL-6	13.14 (2.61)	12.16 (12.16-12.50)	18.70 (9.77)	14.64 (12.16-22.04)	×1.52	0.009
IL-8	47.45 (96.35)	16.39 (12.14-33.46)	125.99 (131.44)	64.38 (46.77-157.73)	×5.89	≤0.001
IL-10	13.62 (4.09)	11.76 (11.76-12.59)	18.84 (8.12)	15.81 (11.76-23.69)	×1.46	0.007
IL-12p70	13.89 (4.22)	12.01 (10.66-17.21)	20.75 (11.30)	16.12 (10.66-27.8)	×1.62	0.01
IL-17A	2.50 (0.87)	1.94 (1.94-2.85)	3.18 (1.69)	2.56 (1.94-4.28)	×1.41	0.15
IL-18	251.82 (167.62)	189.23 (151.49-308.10)	403.01 (292.19)	323.65 (183.26-507.57)	×2.45	0.14
IL-33	117.58 (46.18)	101.795 (83.24-143.64)	176.58 (99.23)	159.09 (95.95-229.86)	×1.75	0.11

($r = 0.48$; $p < 0.05$). Subpopulation of lymphocytes correlated moderately with FGF-basic ($r = 0.53$; $p < 0.05$) and on a low level with EGF ($r = 0.43$; $p < 0.05$) and VEGF ($r = 0.48$; $p < 0.05$).

Age and BMI did not influence the content of PLT, WBC, RBC, and all growth factors in PRP. Among inflammatory cytokines, age significantly negatively correlates with IL-1β ($r = -0.50$; $p < 0.05$), IFN-α2 ($r = -0.38$; $p < 0.05$), and TNF-α ($r = -0.39$; $p < 0.05$). BMI was positively correlated only with IL-1β ($r = 0.40$; $p < 0.05$). However, these correlations were on a low level.

4. Discussion

We hypothesized that PRP prepared with Mini GPS III Platelet Concentration System would contain a proportionally higher concentration of paracrine molecules than patients' serum. The results show that PRP delivers higher doses of TGF-β1 free active, EGF, VEGF, PDGF-AA, and PDGF-BB but not HGF and FGF-basic. However, the profile of inflammatory cytokines differed significantly only for eight from thirteen measured: IL-1β, IFN-α2, IFN-γ, TNF-α, IL-6, IL-8, IL-10, and IL-12p70. These differences cannot be simply explained by a higher concentration of platelets or white blood cells. Increases in platelet-derived growth factor concentration (PDGF-AA, PDGF-BB) and TGF-β1 were closest to the achieved increase in platelet concentration (×6.19, ×6.43, and 3.79, respectively, vs. ×4.41). The two other growth factors increased more than two times (VEGF × 2.34, EGF × 2.5) and the other two decreased. Those inflammatory cytokines, the concentration of which increased significantly, increased from 1.39 to 5.89. This leads to the assumption that in PRP, we obtain a different cytokine profile, not just a quantitative increase in concentration. There is a risk of bias due to the serum preparation protocol, which requires cloth formation. Attention should be paid to this critical detail, as it can directly impact the clinical effectiveness of the proposed treatment.

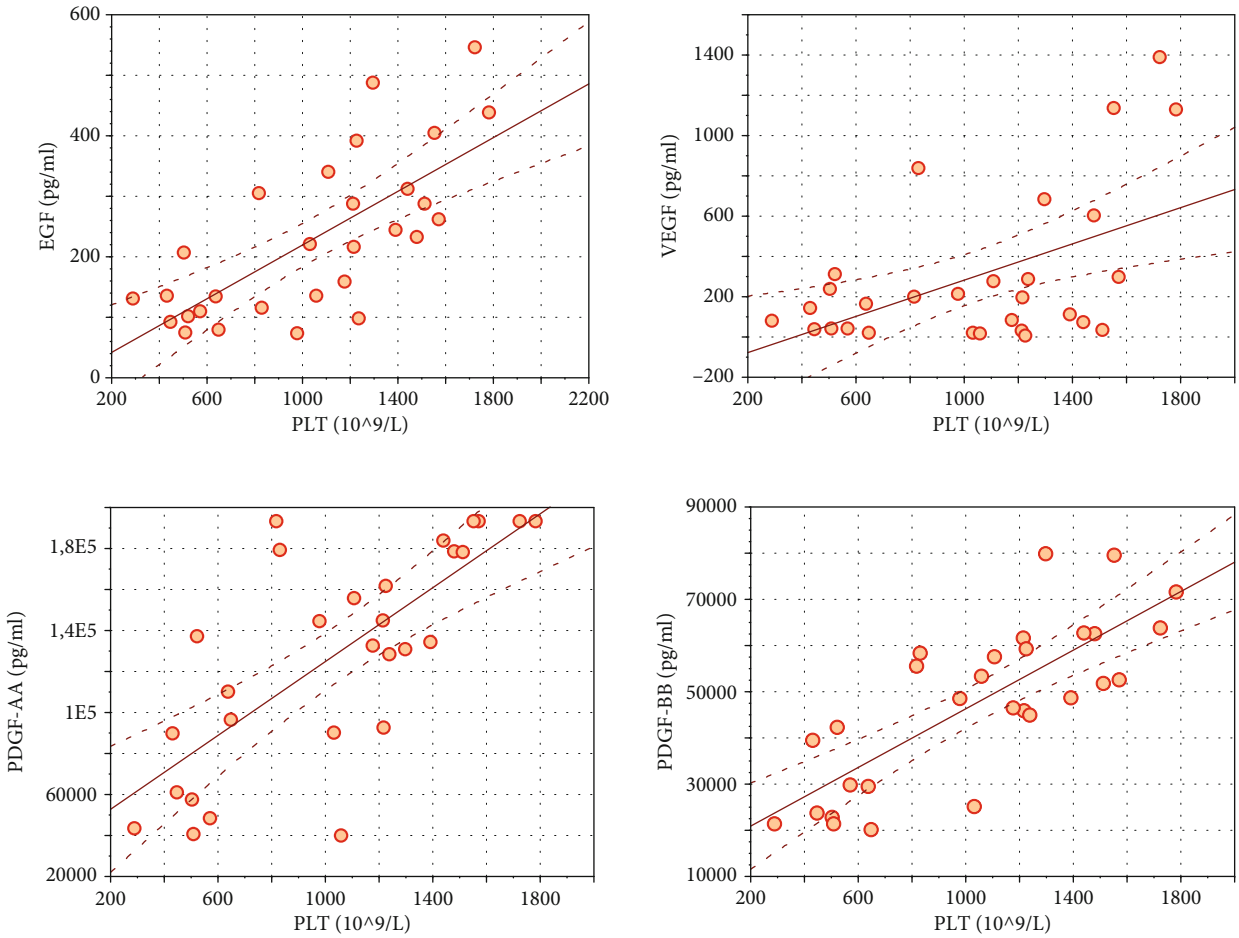

Figure 2: Significant ($p < 0.05$) Pearson correlation coefficient (r) between platelets (PLT) and growth factors: EGF ($r = 0.74$), VEGF ($r = 0.46$), PDGF-AA ($r = 0.77$), and PDGF-BB ($r = 0.79$).

Multiple protocols have been developed for PRP preparation. Many commercially available techniques differ in the shape of the separator used; the amount of blood collected and PRP obtained; the amount, time, and force of centrifugation; and the separation technique. As a result, they differ in the concentration of platelets, leukocytes, and red cell contamination obtained. These differences significantly affect the content of biologically active molecules that may have a therapeutic effect [8, 11]. Different divisions have been proposed to facilitate the comparison of PRP treatment results. The most commonly used takes into account fibrin and leukocyte content, dividing PRP into four categories: leukocyte-rich or pure platelet-rich plasma (L-PRP, P-PRP) and leukocyte-rich (L-PRF) or pure platelet-rich fibrin (P-PRF) [16]. Additionally, it is worth distinguishing systems enabling high (5-9×) and low (2.5-3×) concentrations of platelets [17]. Currently, the most complex classification system was proposed by Lana et al. [18]. The system called MARSPILL includes interalia, specifying the number of platelets, white blood cells, red blood cells, spins, activation process, and image guidance during PRP administration. The above classification perfectly illustrates the complexity of assessing the effectiveness of different PRP treatments.

Most researchers define PRP as plasma with platelet concentrations above 1 million per microliter [19, 20]. Commercially available systems do not always meet this criterion. The US Food and Drug Administration (FDA) allows the term PRP to be applied to products that have platelet concentrations above 250,000 per microliter. In addition, Mazzucco et al.'s work concluded that platelet concentrations above 200,000 per microliter are sufficient for a therapeutic effect [21]. This can lead to confusion as this platelet count is within the normal range for whole blood, and it is hard to expect a higher density of active cytokines in it. In our work, we used the Mini GPS III Platelet Concentration System, one of the most widely used PRP preparation systems globally. It allows obtaining reproducible results with 4-5 times platelet density and higher than baseline concentration of white blood cells [11].

The WBC content of the obtained PRP can influence the concentration of various cytokines and modulate local immune and inflammatory responses. Both negative and positive effects of leukocyte-rich PRP on tissue healing have been reported in the literature. Threats arise from the potential catabolic effects of leukocytes on surrounding tissues through the release of proinflammatory cytokines

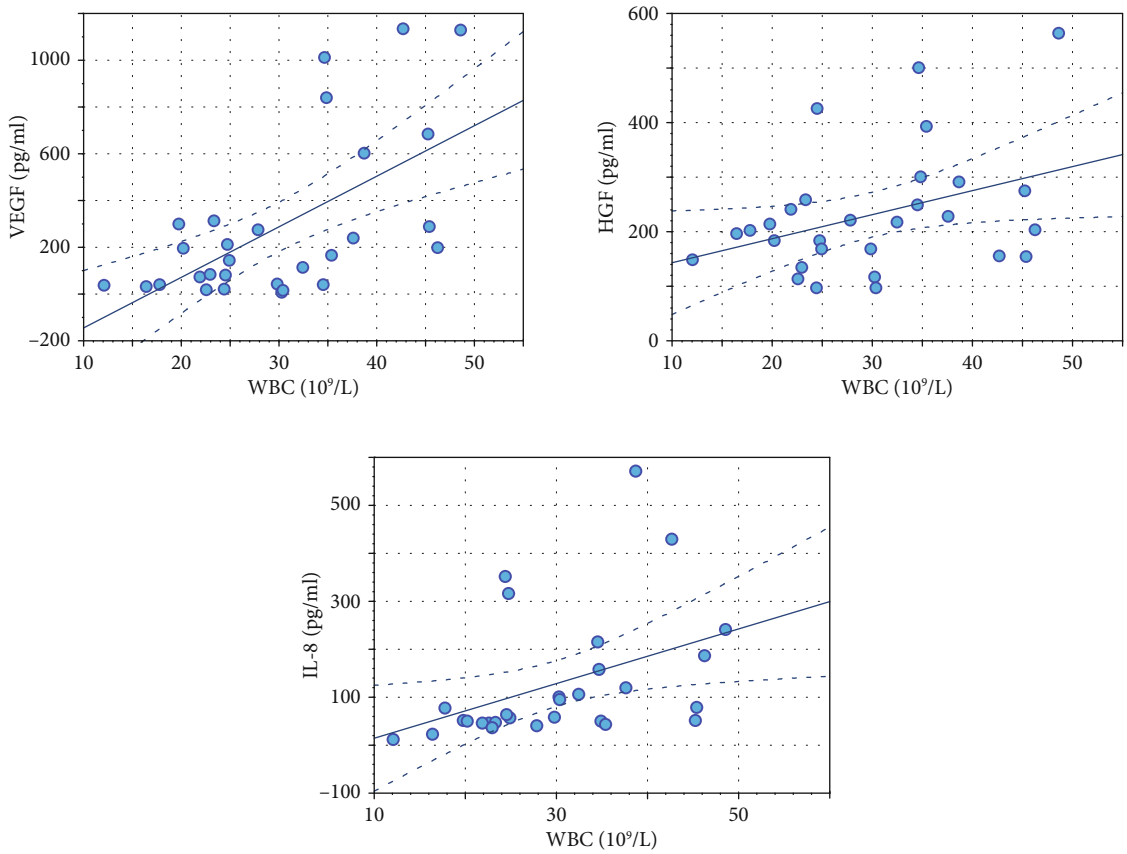

Figure 3: Significant ($p < 0.05$) Pearson correlation coefficient (r) between white blood cells (WBC) and growth factors/cytokines: VEGF ($r = 0.69$), HGF ($r = 0.42$), and IL-8 ($r = 0.45$).

and proteinases. The benefits of a high WBC content are associated with positive correlations with certain growth factors, the ability of leukocytes to modulate immune responses, antimicrobial properties, and reported favourable clinical outcomes [22–25].

Previous studies have shown correlations between some cytokines and cell contents in PRP, but only a few have compared their contents and those in whole blood [25, 26]. A significant positive correlation was found between PLT content in PRP and EGF, VEGF, PDGF-AA, and PDGF-BB in these studies. Magalon et al. evaluated the content of EGF, VEGF, TGF-β1, and PDGF-AB in PRP obtained with Mini GPS III. The PLT and WBC concentrations were similar to our findings, but the growth factor content was much higher for VEGF and EGF (×3.2 and ×9.3, respectively) than in our study. The concentration of the representative of PDGF family in their research (PDGF-AB) was much lower than that of PDGF-AA or PDGF-BB in our study [27]. The possible reason for these differences is the addition of calcium chloride for platelet activation. The double freeze-thaw process activates platelets in a more physiological way, which is why it was used in our study [15]. Similar to our finding, they presented a significant positive correlation between EGF, VEGF, PDGF, and PLT concentration in PRP. Contrary to our results, they also found a correlation between PLT and TGF-β1 [27]. The concentration of WBC in PRP correlates with the content of VEGF and EGF in their study. Our findings support only the correlation between WBC and VEGF. Another study reporting growth factor content in PRP obtained by GPS III was carried out by Castillo et al. [28]. The concentration of WBC in the final sample was similar to that presented in our study, but PLT mean concentration was almost two times lower. That could be due to the fact that they used a different version of the GPS III system, which requires approximately 55 ml of blood donation and other centrifugation parameters. They assessed the final concentrations of PDGF-AB, PDGF-BB, TGF-β1, and VEGF. In their results, PDGF-BB was two times lower, but VEGF 6 times higher than those found in our study. Just as a decreased PDGF level can be explained by a lower platelet content, the differences in other factors are difficult to explain. In the literature review, Oudelaar et al. collected seven studies presenting the content of PLT, WBC, PDGF-AB, VEGF, and TGF- β1 in PRP obtained with the GPS III system [8]. The contents of PLT and WBC were similar between the studies and comparable to our results. However, the content of growth factors varied considerably, especially TGF-β1. In most of the mentioned studies, the concentration of VEGF was higher than in our samples. Concentrations of TGF-β1 were much higher because we evaluated the concentration of TGF- β1 free active, whose levels are about 65 times lower than total TGF-β1 in serum [29].

Among the best described is the platelet-derived growth factor family (PDGF) role in the healing process both in vitro, in animal models, and in patients with wound healing disorders. It stimulates neutrophils, monocytes, and fibroblasts to migrate to the wound site and activates the latter mentioned to proliferate and produce an extracellular matrix [9]. The fibroblast growth factor (FGF) family has mitogenic activity and a positive effect on cell migration and differentiation and participates in cytoprotection during stress conditions [10]. Angiogenesis at the wound site is induced and stimulated by vascular endothelial growth factor (VEGF) [9]. Other growth factors such as hepatocyte growth factor (HGF), epidermal growth factor (EGF), and transforming growth factor-β1 (TGF-β1) have an impact on proper cell proliferation and differentiation during the healing process [9, 10, 30].

Among a wide spectrum of tested inflammatory cytokines, a significant positive correlation was found only between WBC and IL-8. This cytokine has some potential positive effects on healing and immunomodulation by its ability to stimulate reepithelialization and to attract neutrophils to the site of injury. In the literature, only a few authors have performed an analysis of inflammatory cytokines in PRP. The concentrations of IL-1β and matrix metalloproteinase-9 (MMP-9) in PRP were presented in two studies [25, 26]. The authors found that MMP-9 and IL-1β levels were much higher in leukocyte-rich PRP and were significantly correlated with neutrophil concentration [25]. Those two are catabolic cytokines known for their role in inflammation and matrix degradation. MMP-9 has been implicated as a predictor of improper healing [26]. We also found significant but low correlation between neutrophil concentration and IL-1β. The healing process is also modulated by a number of different cytokines that can stimulate migration of macrophages like monocyte chemoattractant protein (MCP), stimulate reepithelialization such as interleukin-8 (IL-8), inhibit inflammation and scar formation such as interleukin-10 (IL-10) [10]. A complex process of interaction between numerous anti- and proinflammatory cytokines regulates the course of tissue healing, leading in the most desirable case to recovery.

In our study, age and BMI did not influence the content of PLT, WBC, RBC, and all growth factors in PRP. Dragoo et al., in their study, found a significant negative correlation between age and PDGF-BB. The concentration of PDGF-BB in the PRP was higher in 18-30-year-old subpopulation; however, among the older subpopulations, the values were stable and oscillated about 31 ng/ml [31]. Among inflammatory cytokines in our research, age was significantly negatively correlated with IL-1β, IFN-α2, and TNF-α. The statistically significant differences in the cytokine content in PRP between the sexes are difficult to explain, especially since they were not shown when comparing the serum samples. A possible explanation would be the uneven distribution of cytokines during centrifugation, forced by other components. Solving this problem would require further, more detailed research.

Rheumatoid arthritis is a chronic autoimmune inflammatory disease characterized by progressive destruction of cartilage and bone with periods of acute exacerbation [32]. The correlation of cytokines such as TNF-α, IL-6, and IL-1β with the intensity of the disease has been demonstrated [32]. This is also the reason why TNF-α inhibitors were developed to treat RA. The increased level of VEGF is probably related to the stimulation of neovascularization during the ongoing inflammatory process. In an animal model of arthritis, Lippross et al. found that PRP injection leads to the reduction of IL-6, IL-1, IGF-1, and VEGF in cartilage and synovium. TNF-α did not change after injection of PRP [32]. Tong et al. presented results on a type II collagen-induced arthritis mouse model treated with PRP. The study reported a downregulation of the expression of IL-6, IL-8, IL-17A, IL-1β, TNF-α, receptor activator for nuclear factor-κB, and IFN-γ in inflammatory tissue [7]. They also found that PRP can be beneficial due to decreased joint inflammation, cartilage destruction, bone damage, and increased joint tissue repair [7]. On the other hand, in their papers, both Yan et al. and Wang et al. highlighted the risk of rheumatoid arthritis fibroblast-like synoviocytes cell migration, invasion, and adhesion stimulated by MMP-1, whose expression was increased after PRP administration [6, 33].

Only two studies evaluating PRP efficacy on rheumatoid arthritis have been published. Badsha et al. presented results of PRP injection to the knee joint of four subjects. They reported a significant improvement in the disease activity score, reduced pain, and a decrease of joint inflammation during ultrasound examination [5]. Saif et al. evaluated the therapeutic effect of intra-articular PRP versus steroid in RA patients and their impact on inflammatory cytokines, local joint inflammation, disease activity, and quality of life. In this randomized controlled trial, 60 patients with RA were divided into two equal groups. Both groups showed improvements at 3 months after injection, but only in the PRP group this improvement lasted up to 6 months. Downregulating effects on inflammatory cytokines (IL-1β, TNF-α) with subsequent improvement of local joint inflammation, disease activity, and quality of life were presented in the PRP group. The authors concluded that PRP injections were a safe and valuable treatment option for RA patients [34].

These findings lead us to the hypothesis that intra-articular PRP injections could help patients with RA through two main mechanisms. The first is the positive role of growth factors such as PDGF, EGF, FGF, or TGF-β1 in stimulating healing, regeneration, and protecting articular cartilage. The second is the ability of PRP to downregulate the expression of major inflammatory cytokines such as IL-1β, IL-6, and TNF-α leading to a reduction in local inflammation. The exact molecular pathway of the PRP interaction will be challenging to determine due to the multitude of biologically active ingredients it contains.

There are some limitations of the presented study. The major limitation is that we evaluated only one particular PRP preparation protocol, which, due to its distinctiveness, may in itself influence the final cytokine profile. Some of the existing numerous cytokines that may affect the local cellular response have been omitted for technical reasons. The direction of further research should be to compare the

biological effect in vitro or in vivo depending on the profile of biologically active components in PRP.

5. Conclusions

The study showed that autologous leukocyte-rich platelet-rich plasma obtained with the Mini GPS III Platelet Concentration System is an efficient source of paracrine molecules such as TGF-β1, EGF, PDGF-AA, PDGF-BB, IL-1β, IFN-α2, TNF-α, and IL-8 with the ability to concentrate those molecules above twice as baseline. The profile of growth factors and cytokines is different in PRP than in patients' own blood serum. For the above reason, PRP cannot simply be replaced by an increased serum volume, which may, however, be considered for selected cases as an alternative treatment option.

Data Availability

The data used to support the findings of this study are available from the corresponding author upon reasonable request.

Conflicts of Interest

The authors declare that they have no conflict of interest with respect to the publication of this article.

Acknowledgments

This work was financially supported by the grant from the project entitled "Wroclaw Medical University as a Regional Center of Excellence in the field of medical sciences and health sciences" implemented under the funds of the Ministry of Science and Higher Education (Republic of Poland) in the program "Regional Initiative of Excellence" in the years 2019-2022, project number 016/RID/2018/19 (grant number RID.Z501.20.008).

Supplementary Materials

Supplementary Table 1: differences between males and females according to age, BMI, and biologically active compounds in whole blood, serum, and PRP. Values are presented as arithmetic mean (standard deviation) and median (Q1-Q3). The significance of the comparison is shown as p value. *(Supplementary Materials)*

References

[1] N. Hussain, H. Johal, and M. Bhandari, "An evidence-based evaluation on the use of platelet rich plasma in orthopedics - a review of the literature," *Sicot-J*, vol. 3, 2017.

[2] D. Man, H. Plosker, and J. E. Winland-Brown, "The use of autologous platelet-rich plasma (platelet gel) and autologous platelet-poor plasma (fibrin glue) in cosmetic surgery," *Plastic and Reconstructive Surgery*, vol. 107, no. 1, pp. 229–237, 2001.

[3] D. C. Tietze, K. Geissler, and J. Borchers, "The effects of platelet-rich plasma in the treatment of large-joint osteoarthritis: a systematic review," *The Physician and Sportsmedicine*, vol. 42, no. 2, pp. 27–37, 2014.

[4] G. Chellamuthu, S. Muthu, M. Khanna, and V. Khanna, "'Platelet-rich plasma holds promise in management of rheumatoid arthritis'—systematic review," *Rheumatology International*, vol. 41, no. 11, pp. 1895–1903, 2021.

[5] H. Badsha, G. Harifi, and W. D. Murrell, "Platelet rich plasma for treatment of rheumatoid arthritis: case series and review of literature," *Case Reports in Rheumatology*, vol. 2020, Article ID 8761485, 7 pages, 2020.

[6] S. Yan, B. Yang, C. Shang et al., "Platelet-rich plasma promotes the migration and invasion of synovial fibroblasts in patients with rheumatoid arthritis," *Molecular Medicine Reports*, vol. 14, no. 3, pp. 2269–2275, 2016.

[7] S. Tong, C. Zhang, and J. Liu, "Platelet-rich plasma exhibits beneficial effects for rheumatoid arthritis mice by suppressing inflammatory factors," *Molecular Medicine Reports*, vol. 16, no. 4, pp. 4082–4088, 2017.

[8] B. W. Oudelaar, J. C. Peerbooms, R. Huis In 't Veld, and A. J. Vochteloo, "Concentrations of blood components in commercial platelet-rich plasma separation systems: a review of the literature," *The American Journal of Sports Medicine*, vol. 47, no. 2, pp. 479–487, 2019.

[9] D. J. Sánchez-González, E. Méndez-Bolaina, and N. I. Trejo-Bahena, "Platelet-rich plasma peptides: key for regeneration," *International Journal of Peptide*, vol. 2012, pp. 1–10, 2012.

[10] S. Werner and R. Grose, "Regulation of wound healing by growth factors and cytokines," *Physiological Reviews*, vol. 83, no. 3, pp. 835–870, 2003.

[11] M. Dejnek, H. Moreira, S. Płaczkowska et al., "Analysis and comparison of autologous platelet-rich plasma preparation systems used in the treatment of enthesopathies: a preliminary study," *Advances in Clinical and Experimental Medicine*, vol. 30, no. 7, pp. 757–764, 2021.

[12] R. Evanson, M. K. Guyton, D. L. Oliver et al., "Gender and age differences in growth factor concentrations from platelet-rich plasma in adults," *Military Medicine*, vol. 179, no. 7, pp. 799–805, 2014.

[13] P. Jayaram, P. Yeh, S. J. Patel et al., "Effects of aspirin on growth factor release from freshly isolated leukocyte-rich platelet-rich plasma in healthy men: a prospective fixed-sequence controlled laboratory study," *The American Journal of Sports Medicine*, vol. 47, no. 5, pp. 1223–1229, 2019.

[14] G. Weibrich, W. K. G. Kleis, G. Hafner, and W. E. Hitzler, "Growth factor levels in platelet-rich plasma and correlations with donor age, sex, and platelet count," *Journal of Craniomaxillofacial Surgery*, vol. 30, no. 2, pp. 97–102, 2002.

[15] R. Zimmermann, D. Arnold, E. Strasser et al., "Sample preparation technique and white cell content influence the detectable levels of growth factors in platelet concentrates," *Vox Sanguinis*, vol. 85, no. 4, pp. 283–289, 2003.

[16] D. M. Dohan Ehrenfest, L. Rasmusson, and T. Albrektsson, "Classification of platelet concentrates: from pure platelet-rich plasma (P-PRP) to leucocyte- and platelet-rich fibrin (L-PRF)," *Trends in Biotechnology*, vol. 27, no. 3, pp. 158–167, 2009.

[17] R. Dhurat and M. Sukesh, "Principles and methods of preparation of platelet-rich plasma: a review and author's perspective," *Journal of Cutaneous and Aesthetic Surgery*, vol. 7, no. 4, pp. 189–197, 2014.

[18] J. F. S. D. Lana, J. Purita, C. Paulus et al., "Contributions for classification of platelet rich plasma - proposal of a new classification: MARSPILL," *Regenerative Medicine*, vol. 12, no. 5, pp. 565–574, 2017.

[19] R. E. Marx, "Platelet-rich plasma (PRP): what is PRP and what is not PRP?," *Implant Dentistry*, vol. 10, no. 4, pp. 225–228, 2001.

[20] A. Mishra and T. Pavelko, "Treatment of chronic elbow tendinosis with buffered platelet-rich plasma," *The American Journal of Sports Medicine*, vol. 34, no. 11, pp. 1774–1778, 2006.

[21] L. Mazzucco, V. Balbo, E. Cattana, R. Guaschino, and P. Borzini, "Not every PRP-gel is born equal Evaluation of growth factor availability for tissues through four PRP-gel preparations: Fibrinet®, RegenPRP-Kit®, Plateltex® and one manual procedure," *Vox Sanguinis*, vol. 97, no. 2, pp. 110–118, 2009.

[22] Y. Kobayashi, Y. Saita, H. Nishio et al., "Leukocyte concentration and composition in platelet-rich plasma (PRP) influences the growth factor and protease concentrations," *Journal of Orthopaedic Science*, vol. 21, no. 5, pp. 683–689, 2016.

[23] A. Cieślik-Bielecka, T. Bold, G. Ziółkowski, M. Pierchała, A. Królikowska, and P. Reichert, "Antibacterial activity of leukocyte- and platelet-rich plasma: an in vitro study," *BioMed Research International*, vol. 2018, Article ID 9471723, 8 pages, 2018.

[24] L. Zhang, S. Chen, P. Chang et al., "Harmful effects of leukocyte-rich platelet-rich plasma on rabbit tendon stem cells in vitro," *The American Journal of Sports Medicine*, vol. 44, no. 8, pp. 1941–1951, 2016.

[25] E. A. Sundman, B. J. Cole, and L. A. Fortier, "Growth factor and catabolic cytokine concentrations are influenced by the cellular composition of platelet-rich plasma," *The American Journal of Sports Medicine*, vol. 39, no. 10, pp. 2135–2140, 2011.

[26] J. H. Oh, W. O. O. Kim, K. U. Park, and Y. H. Roh, "Comparison of the cellular composition and cytokine-release kinetics of various platelet-rich plasma preparations," *The American Journal of Sports Medicine*, vol. 43, no. 12, pp. 3062–3070, 2015.

[27] J. Magalon, O. Bausset, N. Serratrice et al., "Characterization and comparison of 5 platelet-rich plasma preparations in a single-donor model," *Arthroscopy: The Journal of Arthroscopic & Related Surgery*, vol. 30, no. 5, pp. 629–638, 2014.

[28] T. N. Castillo, M. A. Pouliot, H. J. Kim, and J. L. Dragoo, "Comparison of growth factor and platelet concentration from commercial platelet-rich plasma separation systems," *The American Journal of Sports Medicine*, vol. 39, no. 2, pp. 266–271, 2011.

[29] S. A. Khan, J. Joyce, and T. Tsuda, "Quantification of active and total transforming growth factor-β levels in serum and solid organ tissues by bioassay," *BMC Research Notes*, vol. 5, no. 1, p. 1, 2012.

[30] T. Molloy, Y. Wang, and G. A. C. Murrell, "The roles of growth factors in tendon and ligament healing," *Sports Medicine*, vol. 33, no. 5, pp. 381–394, 2003.

[31] J. L. Dragoo, T. Korotkova, A. S. Wasterlain, M. A. Pouliot, H. J. Kim, and S. R. Golish, "Age-related changes of chondrogenic growth factors in platelet-rich plasma," *Operative Techniques in Orthopaedics*, vol. 22, no. 2, pp. 49–55, 2012.

[32] S. Lippross, B. Moeller, H. Haas et al., "Intraarticular injection of platelet-rich plasma reduces inflammation in a pig model of rheumatoid arthritis of the knee joint," *Arthritis and Rheumatism*, vol. 63, no. 11, pp. 3344–3353, 2011.

[33] W. Wang, J. Liu, B. Yang et al., "Modulation of platelet-derived microparticles to adhesion and motility of human rheumatoid arthritis fibroblast-like synoviocytes," *PLoS One*, vol. 12, no. 7, pp. 1–12, 2017.

[34] D. S. Saif, N. N. Hegazy, and E. S. Zahran, "Evaluating the efficacy of intra-articular injections of platelet rich plasma (PRP) in rheumatoid arthritis patients and its impact on inflammatory cytokines, disease activity and quality of life," *Current Rheumatology Reviews*, vol. 16, 2020.

Hindawi
Oxidative Medicine and Cellular Longevity
Volume 2022, Article ID 1735204, 17 pages
https://doi.org/10.1155/2022/1735204

Research Article

The Examination of the Influence of Caffeinated Coffee Consumption on the Concentrations of Serum Prolactin and Selected Parameters of the Oxidative-Antioxidant Balance in Young Adults: A Preliminary Report

Kamil Rodak, Izabela Kokot, Aleksandra Kryla, and Ewa Maria Kratz

Department of Laboratory Diagnostics, Division of Laboratory Diagnostics, Faculty of Pharmacy, Wroclaw Medical University, Borowska Street 211A, 50-556 Wroclaw, Poland

Correspondence should be addressed to Ewa Maria Kratz; ewa.kratz@umw.edu.pl

Received 26 March 2022; Revised 15 April 2022; Accepted 6 July 2022; Published 25 July 2022

Academic Editor: Alin Ciobica

We verified whether caffeinated coffee consumption influenced the concentrations of prolactin (PRL) and oxidative stress parameters: total antioxidant status (TAS), ferric reducing antioxidant power (FRAP), total oxidant status (TOS), oxidative stress index (OSI), advanced oxidation protein products (AOPP), uric acid (UA), total bilirubin (T-Bil), albumin (ALB), iron (Fe), calcium (Ca), magnesium (Mg), and inflammatory marker C-reactive protein (CRP)—in blood sera obtained at 15, 60, and 120 minutes after caffeinated coffee intake, in relation to the fasting point. The study participants were 33 young, healthy, nonsmoking volunteers (15 men, 18 women) aged 19-29 years. PRL concentrations significantly decreased ($p < 0.05$) after consumption, except at time point 15' in men ($p > 0.05$). In women, FRAP levels significantly increased over time, and significant changes were also observed for UA at 120' and ALB at 15'. In men, significant changes were found for levels of AOPP at 15', T-Bil and ALB at 15', iron at 60' and 120', and calcium at 120'. There were no significant differences in the levels of other examined parameters between the defined time points. In conclusion, the substances contained in caffeinated coffee decrease the level of prolactin and may also have an impact on selected parameters of oxidative stress, which could be the basis of future research focused on the identification of new therapeutic targets.

1. Introduction

Coffee is the most popular stimulant among people all around the world. Its main active compound is caffeine (1,3,7-trimethylxanthine) [1], which has both positive (e.g., better concentration, higher agitation, reduced risk of Alzheimer's Disease and Parkinson's Disease development, and anti-inflammatory properties) and negative (e.g., increased risk of lung cancer, anxiety, and urinary incontinence) effects on body functioning [2]. Also, caffeine is considered to have antioxidant properties, as evidenced by the affinity for scavenging hydroxyl radicals [3]. Ninety-nine percent of caffeine is absorbed from the gastrointestinal tract within 45 minutes of consumption of caffeinated beverages, and the maximum blood plasma concentration of this compound is observed 15–120 minutes after oral intake [4]. However, it is worth remembering that coffee contains not only caffeine but is composed of many bioactive compounds with an anti-free-radical or antioxidant effect, including phenolic compounds (e.g., tocopherols), trigonelline, diterpenes, soluble fiber, chlorogenic acids (CGAs), cafestol, and kahweol in various quantities, depending on the source [5–8]. The total content of polyphenols ranges from 200 to 550 mg per cup [9]. Another important contribution may be the action of some compounds generated during the thermal reactions of the roasting process, such as melanoidins, which show strong antioxidant properties [10]. The main antioxidant substances present in coffee are shown in Figure 1. The effects of coffee on the human organism depend mainly on its type, quantity, the blend of coffee (i.e., Arabica

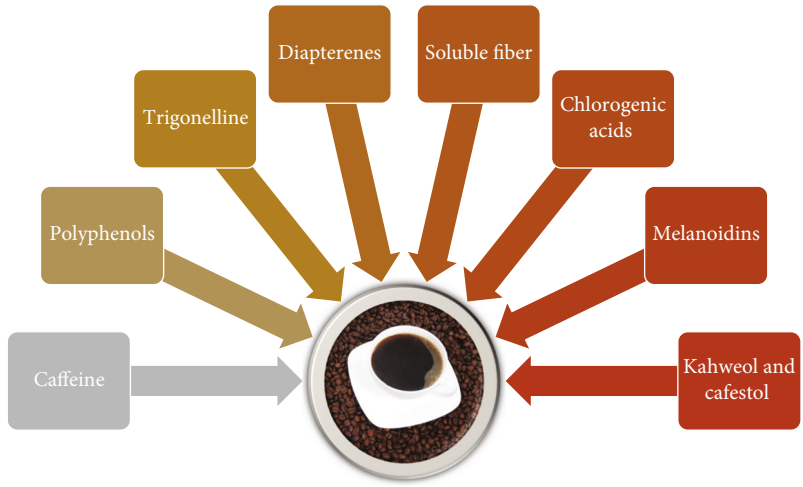

Figure 1: The main ingredients of coffee with an antioxidant effect.

or Robusta), the growing area, the extent of roasting, the method of brewing [11], and the age and sex of the person who drinks it. The observed changes are mainly caused by the interaction of its ingredients with receptors such as adenosine receptors [2]. For example, Gorjanović et al. [12] compared 24 different types of coffee and showed that instant coffees contain the highest amount of antioxidants because they are the richest in polyphenols out of all coffee types. Moreover, Czachor et al. [13] compared Robusta and Arabica and showed that Robusta had a greater amount of caffeine, polyphenols, and antioxidant activity.

For decades, scientists have debated the effects of coffee on human health. The controversy surrounding this topic even led to the fact that in 1991 the International Agency for Research on Cancer (IARC) classified coffee as "possibly carcinogenic to humans" because of a weak positive relationship between coffee consumption and the risk of bladder, pancreatic, and ovarian cancer [14]. Recently, caffeinated coffee became a subject of interest for scientists because of its antioxidant properties [6, 9, 15, 16]. Long-term consumption of coffee and caffeine has been shown to play an important role in preventing age-related cognitive decline by protecting the antioxidant system and regulating oxidative stress [17]. A study conducted by Qureshi et al. [18] documented that coffee ranked in the top places among drinks contributing the most to the total antioxidant intake through dietary habits in women. More and more substances of natural origin were tested for their antioxidant and anti-inflammatory properties. One of the most recent reports in this field is the work of Taysi et al. [19], which noted that thymoquinone derived from the herb *Nigella sativa*, commonly used in alternative medicine, exhibits the above-mentioned healing properties. Studies carried out in recent decades confirmed that excessive accumulation in body fluids of reactive oxygen species (ROS), such as the superoxide anion, hydroxyl radical, and hydroperoxyl radical, is a major cause of oxidative stress (OS) and consequently leads to pathological changes in the human body, resulting in premature aging and many diseases. Excessive formation of reactive nitrogen species (RNS) is also among the factors that can trigger oxidative stress and cause nitrosative stress [20]. Oxidative/nitrosative stress occurs when the cellular production of ROS/RNS exceeds the availability of human antioxidants able to defeat these insults. Prolonged oxidative stress may lead to macromolecular oxidative damage, induce tissue protein denaturation, DNA damage, and lipid peroxidation, and interfere with the body's normal metabolic activity, leading to dangerous diseases such as cancer, cardiovascular diseases, or diabetes. In addition, ROS can induce platelet adhesion and aggregation, leading to intravascular coagulopathy, which causes placental infarction and impairs the uteroplacental blood flow, which may consequently lead to deficiencies in oxygen and nutrients necessary for normal fetal development, and thus, oxidative stress can also negatively influence the course of pregnancy [21]. ROS can be produced as a response to various negative factors, such as gamma or UV radiation [22], smoking [23], alcoholism [24], environmental factors [25], polluted and poor-quality food [26], stress [27], some medications or treatments [28], and elements deficiencies (e.g., zinc) [29]. Since higher prolactin levels have also been documented to induce oxidative stress and damage [30], PRL was in our area of interest in the current research.

Prolactin (PRL) is a protein hormone produced by the pituitary gland and has over 300 described functions, including regulation of reproductive function, the immune system, osmotic balance, and angiogenesis. Although the concentration of PRL in body fluids has seemed important only for women, the latest research suggests that PRL is involved in reproduction processes in both women and men, which is of great importance, especially in the case of people of reproductive age. In women, its concentration is related to the onset of ovulation, while the mechanisms of its effects on male fertility remain unclear [31]. Some animal studies reported its role in spermatogenesis [32]. Low PRL levels have also been associated with reduced volume of ejaculate and dysfunction of seminal vesicles in infertile individuals. Moreover, in men, lower PRL levels were associated with erectile dysfunction and premature ejaculation, as confirmed in the general European population and in infertile men

[33]. Studies conducted on human sperm have suggested that PRL contributes to the survival of male germ cells, because after incubation with PRL, their mobility was maintained for a longer time, and the spontaneous fragmentation of DNA strands was reduced [34]. Sex hormones, including prolactin, have also been implicated in the etiology of breast and ovarian cancer [31]. Prolactin excess (hyperprolactinemia) may lead to hypogonadism, galactorrhea, etc. In addition to physiological causes such as ovulation and pregnancy, hyperprolactinemia may also be caused by prolactin-secreting pituitary adenoma, liver cirrhosis, polycystic ovarian syndrome, and stress, which may be related to oxidative stress [35]. Due to the widespread consumption of caffeinated coffee by people of reproductive age and the key role of prolactin in processes related to female and male fertility, it seems important to determine the influence of the commonly known stimulant, coffee, on the concentration of this hormone. Some studies emphasized the effects of coffee on levels of sex hormones in the human circulatory system [36–38]. Data from these studies suggest that caffeine and caffeinated coffee may alter levels of circulating luteal estrogens and prolactin, which are possible mechanisms by which caffeinated coffee or caffeine may be associated with malignancies in the reproductive system as well as with fertility disorders.

Currently, measurements of oxidative-antioxidant balance in the human body are based, among others, on the determination of oxidative stress markers such as total antioxidant capacity (TAC), which can be measured by various methods such as total antioxidant status (TAS) and ferric reducing antioxidant power (FRAP), total oxidant status (TOS), and advanced oxidation protein products (AOPP). TOS is usually used to estimate the body's overall oxidation status [39], while the antioxidant capacity of TAS and FRAP is measured using single electron transfer (SET) analytical methods, in which the reducing capacity toward any molecule by electron donation is measured [40].

Apart from the parameters determining the overall oxidative or antioxidant status, single parameters assessing the influence of oxidative stress, such as AOPP, can be analyzed. Due to the high amount of total proteins in human serum and their potential to scavenge ROS, especially by albumin, AOPP appears to be a good marker of oxidative damage induced in the body. As they are factors long circulating in the blood, arising in response to oxidative stress, they can be determined for many hours or even days after the activation of human neutrophil and monocyte oxidative metabolism [41].

The aims of our study focused on the effects of caffeinated coffee consumption on levels of serum prolactin and selected parameters of the oxidative-antioxidant balance of the human body. The objective of the present preliminary study was to assess the short-term effects of caffeinated coffee intake on levels of prolactin and selected parameters of oxidative stress—TAS, FRAP, TOS, AOPP, uric acid (UA), total bilirubin (T-Bil), albumin (ALB), and iron (Fe)—in human serum. We also were interested in the impact of caffeinated coffee on levels of some other elements such as calcium (Ca), magnesium (Mg), and inflammatory markers: C-reactive protein (CRP), which, together with white blood cell (WBC) count, may also be used to verify the health status of the volunteers who participated in our study.

2. Materials and Methods

2.1. Participants. We enrolled 33 healthy, young adults from Wroclaw Medical University (aged 19-29 years; 15 men and 18 women) in this study. All participants gave written informed consent after being fully informed of the study's aims and procedures. The participants were qualified for the study based on the initial screening questions. The exclusion criteria were a history of hyperprolactinemia, chronic disease, past cancer, inflammation, or cigarette smoking, as reported by the participants. Afterward, an extensive interview included information such as age, gender, medical history, drugs, sports condition, diet, coffee and caffeine consumption, and general health status. All participants were free from any known immune, cardiovascular, metabolic diseases, or illnesses and were not taking any medication. They were all habitual caffeine consumers (from brewed coffee, espresso coffee, instant coffee, or tea). Volunteers included in the project assessed their health as good on the day of the examination and in the preceding two weeks. Due to procedures related to the COVID-19 pandemic at Wroclaw Medical University, each person's body temperature was verified (the acceptable measurement was <37.4°C). Moreover, in fasting samples (time point 0'), we verified the basic parameters of inflammation (WBC < 10 G/L and CRP < 10 mg/L), based on which we made the final decision to include the participants in the study group. The characteristics of the analyzed groups are presented in Table 1.

2.2. Study Design. Venous blood was collected from the participants at four time points, as presented in Figure 2. All the participants were asked to drink one dose of such prepared coffee. For each participant, the dose of coffee was the same, regardless of body weight. In the collected biological material CBC analysis was performed using auto 5-Diff Hematology Analyzer Mindray BC-5150 (Mindray Bio-Medical Electronics Co., Ltd., Shenzhen, China). The serum concentrations of PRL, selected parameters of oxidative stress (TAS, FRAP, TOS, AOPP, T-Bil, UA, ALB and Fe), calcium, magnesium, and levels of the inflammatory marker CRP were determined using methods/tests as described below. This study was conducted according to the guidelines of the Helsinki II declaration, and the protocol was approved by the Bioethics Human Research Committee of Wroclaw Medical University (No. 862/2020 and No. 865/2021).

2.3. Blood Collection and Handling. Whole blood samples were collected by venipuncture from an antecubital vein into four vacutainer tubes with a clotting activator and one K_2EDTA tube. The first sampling, between 7.00 a.m. and 9.00 a.m., concerned fasting conditions (minimum 8-hour fast) before oral coffee administration. Two tubes were used—the first with a clotting activator to obtain blood

Table 1: General characteristics of the study groups.

Parameters	Gender	
	Women $N = 18$ Mean ± SD	Men $N = 15$ Mean ± SD
Age (years)	22.17 ± 1.86	23.80 ± 2.60
Height (m)	1.68 ± 0.07	1.82 ± 0.05
Body mass (kg)	64.87 ± 15.38	75.02 ± 11.11
BMI (kg/m^2)	22.85 ± 4.54	22.52 ± 2.62
WHR	0.77 ± 0.06	0.84 ± 0.11
WBC (G/L)	6.75 ± 1.86	5.63 ± 1.08
Caffeine consumption (% of people who consume caffeine)	100%	100%
The mean frequency of consumption of caffeinated beverages (times/day)	2.06 ± 1.47	2.27 ± 1.03
The frequency of consumption of caffeinated coffee (cups/day)	1.50 ± 0.86	1.93 ± 0.96
The type of consumed coffee (number of volunteers)		
Instant	3	3
Brewed coffee	7	6
Espresso coffee	7	6
Other	1	0

BMI: body mass index (body mass (kg)/height (m^2)); WHR: waist-hip ratio (waist circumference/hip circumference); WBC: white blood cell count; SD: standard deviation; N: number of participants.

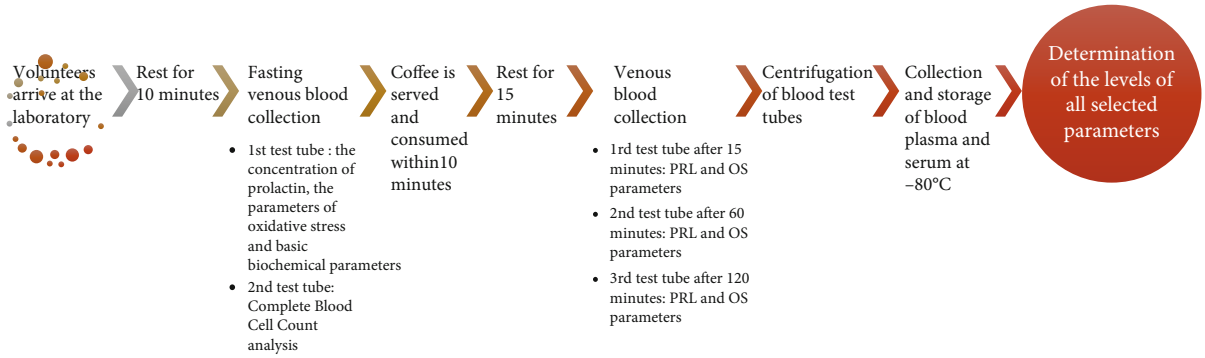

Figure 2: Schematic representation of experimental procedures. PRL: prolactin; OS: oxidative stress.

serum and the second with K_2EDTA to Complete Blood Cell Count (CBC) analysis. The second, third and fourth collections took place 15, 60, and 120 minutes after drinking coffee (a total of 3 clotting tubes to obtain serum). According to the coffee manufacturer's (Tchibo, product reference number: tcs81037, United Kingdom) information, one dose of coffee (100% Arabica instant coffee, freeze-dried, harmoniously mild, subtle acidity) contained 72 mg of caffeine/2.4 kcal/< 0.12 g of fat/<0.12 carbohydrates/<0.012 g of salt/0.36 g of proteins in 1.8 g instant coffee, and a dose of coffee drink was prepared by dissolving 1.8 g instant coffee in 200 mL hot water. Subsequently, samples were centrifuged at 1500 g for 10 min. After centrifugation, blood plasma was collected from the K_2EDTA tube and blood serum was collected from vacutainer clotting activator tubes and stored at −80°C for future analysis.

2.4. Statistical Analysis. The Statistica 13.3 PL software (StatSoft Poland Sp. z o.o., Krakow, Poland) was used to analyze the results statistically. All data were tested with the Shapiro–Wilk test for normality distribution. Due to the lack of a normal distribution for examined parameters at some time points and the small size of the study groups, nonparametric tests for dependent variables were used for data analysis. In the first step, Friedman's ANOVA rank test was used to determine whether there were differences between concentrations of each parameter, depending on the time the blood sample was taken. This test is analogous to Repeated Measures ANOVA, but with the advantage of being nonparametric, and not requiring the assumptions of normality or homogeneity of variances. Friedman's ANOVA was used to determine if the consumption of caffeinated coffee significantly influences the measurements obtained in any of the

four time points. In the second step, in both groups, the Wilcoxon Signed-Rank test was used to compare the differences between values at 15', 60', and 120' time points in reference to values obtained at time point 0'. The results were presented as the mean ± SD (standard deviation) and median (Me) with interquartile range (Q1–Q3) and as Me and minimum-maximum range in Figure S1 (Supplementary materials (available here)). Spearman's rank correlation was used to check the relationships between the measured parameters, separately for each time point. The strength of Spearman's rank correlations was rated based on the following classification: $0.0 \leq |R| \leq 0.2$—lack of correlation; $0.2 < |R| \leq 0.4$—weak correlation; $0.4 < |R| \leq 0.7$—moderate correlation; $0.7 < |R| \leq 0.9$—strong correlation; and $0.9 < |R| \leq 1.0$—very strong correlation. A two-tailed p value of less than 0.05 was considered significant.

2.5. Assay Measurements

2.5.1. Prolactin. Prolactin concentrations were determined with the commercially available ELISA test–DRG Prolactin ELISA (EIA-1291) (DRG Instruments GmbH, Marburg, Germany), according to the recommendations of the manufacturer. The linearity range was up to 200 ng/mL. A Mindray-96A reader (Mindray, Shenzhen, China) was used to measure the absorbance in this assay.

2.5.2. TAS. TAS was measured using the 2,2′-azino-di-3-ethylbenzthiazoline sulfonate $(ABTS)^+$ colorimetric method (Randox TAS Kit, Crumlin, United Kingdom). This method depends on the ability of antioxidants contained in the serum to inhibit the formation of $ABTS^+$ from the oxidation of ABTS by metmyoglobin (a peroxidase). The concentration of TAS was analyzed using the biochemical analyzer Konelab 20i® (ThermoScientific, Vantaa, Finland) and given in mmol/L of Trolox equivalents, with the linearity of up to 2.50 mmol/L.

2.5.3. FRAP. FRAP reagent was prepared *ex tempore* by mixing 300 mmol/L acetate buffer, 10 mmol/L 2,4,6-tripyridyl-s-triazine (TPTZ) in 40 mM hydrochloric acid (HCl), and 20 mmol/L aqueous solution of $FeCl_3 \times 6H_2O$ with proportion 10 : 1 : 1. A calibration curve was performed for the known amounts of Fe^{2+} in the solution, from 0.05 to 0.25 mmol/L Fe^{2+}. 500 μL of FRAP reagent was mixed with 100 μL of a diluted sample (1 : 9), incubated for 5 min at 37°C, and then centrifuged at 2000 g for 10 min at room temperature. The supernatants were analyzed spectrophotometrically at 593 nm against a reagent blank using a UV/Vis spectrophotometer (UV-6300PC, VWR, Shanghai, China). The FRAP concentrations were read from the calibration curve and expressed in mmol/L.

2.5.4. TOS. TOS concentrations were measured according to a method previously published by Erel [39]. In the first step, two reagents were prepared—reagent 1 was made by mixing 22.8 mg of xylenol orange and 1.636 g NaCl with 180 mL 25 mmol/L H_2SO_4 and 20 mL glycerol, and reagent 2 was made by mixing 19.6 mg of ferrum ammonium sulfate and 31.7 mg of o-dianisidine dihydrochloride with 10 mL 25 mmol/L H_2SO_4. Then, 450 μL of reagent 1 and 70 μL of serum were mixed, and absorbance was measured at 560 nm with a side wave of 800 nm against a reagent blank. After measurement, reagent 2 was added, and after 3 minutes of incubation at room temperature, absorbance was measured again at 560 nm with a side wave of 800 nm. The difference between absorbance measurements at the two time points was used for further calculations. A calibration curve was performed for the absorbance of an aqueous solution of perhydrol, made by perhydrol dilution with distilled water from 0 μmol/L to 25 μmol/L. The concentration of TOS was analyzed using a UV/Vis spectrophotometer (UV-6300PC, VWR, Shanghai, China), read from the calibration curve, and expressed in μmol/L.

2.5.5. OSI. Oxidative stress index was calculated as the ratio of TOS concentration to TAS concentration [42]:

$$\mathrm{OSI(arbitrary\ units)} = \frac{\mathrm{TOS}\ (\mu\mathrm{mol/L})}{\mathrm{TAS}\ (\mathrm{mmol/L})}. \quad (1)$$

2.5.6. AOPP. AOPP concentrations were measured by using 1.16 mol/L potassium iodide solution (4.825 g KI in 25 mL H_2O). Determinations were conducted in ELISA Nunc™ MaxiSorp plates. In the first step, sera were diluted by PBS in proportion 1 : 9 (200 μL) and shacked for 2 minutes at 500 rotations per minute. Then, 10 μL of KI was added, followed by 20 μL of 100% glacial acetic acid added after 2 minutes of incubation at room temperature. A control sample was prepared simultaneously by mixing 200 μL of PBS with 10 μL of KI, to which, after 2 minutes of incubation at room temperature, 20 μL of 100% glacial acetic acid was added. Both samples were measured at 340 nm and 600 nm using a UV/Vis spectrophotometer (Multiskan GO, Thermo Scientific). The results were expressed in μmol/L of chloramine T equivalent because a calibration curve was constructed for chloramine T concentrations ranging from 0 to 80 μmol/L.

2.5.7. Low-Molecular-Weight Antioxidants and Iron Measurements. Concentrations of albumin, total bilirubin, uric acid, and iron were measured by colorimetric method using the biochemical analyzer Konelab 20i® (ThermoScientific, Vantaa, Finland). All procedures were performed following the manufacturers' instructions. Lower test limits were 2.00 g/dL, 0.06 mg/dL, 0.20 mg/dL, and 6.00 μg/dL, respectively.

2.5.8. Calcium and Magnesium Concentrations. The concentrations of calcium and magnesium were measured by using a diagnostic reagent for quantitative *in vitro* determination produced by DiaSys Diagnostic Systems (Calcium AS FS and Magnesium XL FS, DiaSys Diagnostic Systems GmbH, Holzheim, Germany). Calcium levels were measured using the Arsenazo III test according to the manufacturer's recommendations. The test measuring range was within 0.04–20.00 mg/dL. Magnesium concentrations were measured by photometric test using xylidyl blue according to the manufacturer's procedures. The test measurements range was from

0.05 to 5.00 mg/dL, and the analyzer Konelab 20i® (ThermoScientific, Vantaa, Finland) was used for determinations.

2.5.9. Inflammatory Markers. To determine C-reactive protein (CRP) concentrations, commercial reagents for the immunoturbidimetric test were used (highly sensitive for CRP, U-hs, DiaSys Diagnostic Systems GmbH, Germany), and measurements were made using an automatic analyzer Konelab 20i® (ThermoScientific, Vantaa, Finland). All procedures were performed according to the recommendations of the manufacturer. The measuring range was from 0.3 mg/L up to the concentration of the highest calibrator, at least up to 350 mg/L. White blood cell count (WBC) was obtained from a Complete Blood Cell Count analysis (5-Diff Hematology Analyzer Mindray BC-5150, Mindray Bio-Medical Electronics Co., Ltd., Shenzhen, China).

3. Results

3.1. Prolactin. The results of the determinations of PRL concentrations are shown in Figure 3.

Fasting PRL levels (0') were higher in women than in men (median values: 16.56 ng/mL in women, 8.85 ng/mL in men). Prolactin concentrations in women after caffeinated coffee consumption were significantly lower, at 15', 60', and 120' in comparison to time point 0' (13.43 ng/mL, 8.80 ng/mL, and 6.91 ng/mL, respectively) with a significance of $p < 0.001$ for each time point, and in men at 60' and 120' (5.74 ng/mL, $p = 0.001$, and 4.80 ng/mL, $p = 0.017$, respectively). No significant differences were found in men at time point 15' (9.59 ng/mL) when compared to time point 0'.

3.2. Oxidative Stress Markers. The results of the determinations of TAS, FRAP, TOS, OSI, AOPP, low-molecular-weight antioxidants (UA, T-Bil, and ALB), Fe, Ca, Mg, and inflammatory marker (CRP) concentrations are shown in Table 2, with marked significant differences in levels of investigated parameters in relation to time point 0'.

3.2.1. TAC. Friedman's rank test showed that in time, after drinking coffee, there were significant differences between TAS concentrations in women ($p = 0.044$) and no differences in men. The median values at 0', 15', 60', and 120' time points for women were 1.57 mmol/L, 1.55 mmol/L, 1.56 mmol/L, and 1.57 mmol/L, respectively, and for men, they were at levels of 1.65 mmol/L, 1.70 mmol/L, 1.66 mmol/L, and 1.64 mmol/L, respectively. The Wilcoxon test indicated a lack of significant differences between TAS concentrations in 15', 60', and 120' in comparison to time point 0' in both groups. FRAP concentrations significantly differed in time for women ($p = 0.002$) and were similar for men at all time points. The median of FRAP levels at 15', 60', and 120' time points for women was 1.13 mmol/L, 1.15 mmol/L, and 1.13 mmol/L, respectively, and was significantly higher when compared to time point 0' (1.11 mmol/L), with the significance of $p < 0.001$, $p < 0.001$, and $p = 0.028$, respectively. Such differences were not observed for men (median values: 1.34 mmol/L, 1.39 mmol/L, 1.37 mmol/L, and 1.38 mmol/L at time points 0', 15', 60', and 120', respectively).

3.2.2. TOS and OSI. No significant differences were found in TOS levels and OSI, neither for women nor men. In women, the median values of TOS concentrations at time points 0', 15', 60', and 120' were 1.50 μmol/L, 1.57 μmol/L, 1.44 μmol/L, and 1.38 μmol/L, respectively. In the male group, the median values for TOS levels at time points 0', 15', 60', and 120' were 1.38 μmol/L, 1.71 μmol/L, 1.40 μmol/L, and 1.45 μmol/L, respectively. The OSI values calculated for women at time points 0', 15', 60', and 120' were 0.95, 1.00, 0.93, and 0.92, respectively, and for men, they were 0.91, 1.08, 0.85, and 0.88, respectively.

3.2.3. AOPP. There were no significant differences in AOPP concentrations between time points 15', 60', and 120' in reference to time point 0', neither in women (median values for 0', 15', 60', and 120': 85.65 μmol/L, 84.99 μmol/L, 86.31 μmol/L, and 82.02 μmol/L, respectively) nor in men at time points 60' and 120' (median values: 87.96 μmol/L and 84.66 μmol/L, respectively). Significant differences in reference to time point 0' (median value: 87.96 μmol/L) were observed in men at 15' (median value: 90.61 μmol/L) with significance of $p = 0.047$.

3.2.4. Low-Molecular-Weight Antioxidants. The differences in uric acid concentrations were not significant at the examined time points, neither for women nor men. Median values of UA concentrations for women were 4.68 mg/dL at 0', 4.50 mg/dL at 15', 4.66 mg/dL at 60', and 4.54 mg/dL at 120', and only the concentrations at time point 120' were significantly lower when compared to these at time point 0' ($p = 0.048$). No significant differences were found in men, where the median values of UA concentrations at time points 0', 15', 60', and 120' were 5.71 mg/dL, 5.77 mg/dL, 5.63 mg/dL, and 5.70 mg/dL, respectively.

Total bilirubin concentrations were similar in women (median values at 0', 15', 60', and 120' were 0.55 mg/dL, 0.55 mg/dL, 0.57 mg/dL, and 0.54 mg/dL, respectively) while in men T-Bil concentrations significantly increased over time ($p < 0.001$) and the differences between time point 15' (median value: 0.62 mg/dL, $p = 0.005$), 60' (median value: 0.67 mg/dL, $p < 0.001$), and 120' (median value: 0.69 mg/dL, $p < 0.001$) were significant in reference to time point 0' (median value: 0.61 mg/dL).

Albumin concentrations changed over time in both women and men, with a significance of $p = 0.006$ and $p = 0.002$, respectively. Among women, the median values of ALB concentrations were 4.45 g/dL, 4.30 g/dL, 4.42 g/dL, and 4.52 g/dL, while among men the median values of ALB levels were 4.59 g/dL, 4.54 g/dL, 4.55 g/dL, and 4.59 g/dL for 0', 15', 60', and 120', respectively. Only at time point 15' in women ($p < 0.001$) and at time point 15' in men ($p < 0.001$) ALB concentrations were significantly lower in comparison to time point 0'.

3.3. Elements. Based on the results of Friedman's ANOVA test, we observed that the consumption of caffeinated coffee influences the concentration of serum elements, as the analyzed groups differed significantly at four time points in both women and men for Fe ($p = 0.038$ and $p = 0.018$,

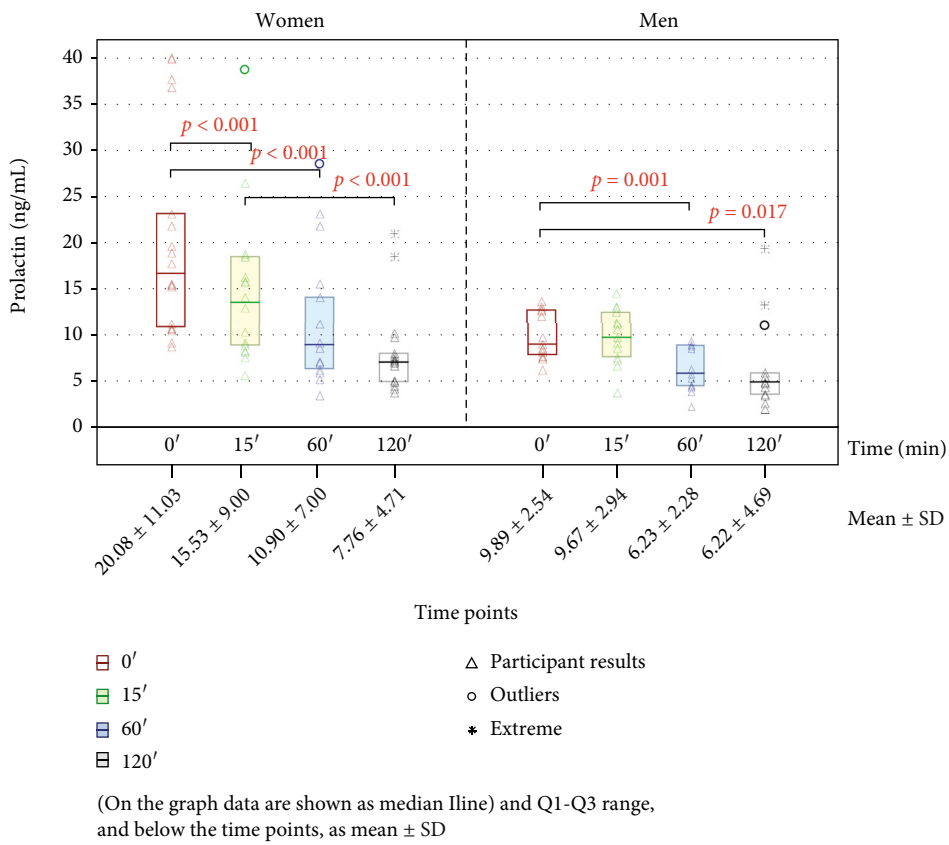

Figure 3: The concentration values of prolactin for women and men. SD: standard deviation; p value was calculated versus time point 0', and a two-tailed p value of less than 0.05 was considered significant. 0', 15', 60', and 120': time points of measurements.

respectively), in women for Mg ($p = 0.032$) and in men for Ca ($p = 0.019$). The median values of concentrations of Fe at time points 0', 15', 60', and 120' in women were 101.50 μg/dL, 98.50 μg/dL, 108.00 μg/dL, and 108.50 μg/dL, respectively, and in men, they were 109.00 μg/dL, 106.00 μg/dL, 105.00 μg/dL, and 108.00 μg/dL, respectively. In men only at time points 60' and 120' were Fe levels significantly higher in reference to time point 0' with $p = 0.023$ and $p = 0.011$, respectively. For Ca concentrations in women, the median values at 15', 60', and 120' time points were 9.55 mg/dL, 9.60 mg/dL, and 9.70 mg/dL, respectively, and there were no significant differences in relation to time point 0' (9.45 mg/dL). For Mg concentrations in women, no significant differences between time point 0' and the other time points were observed (2.30 mg/dL, 2.20 mg/dL, 2.30 mg/dL, and 2.35 mg/dL, respectively). On the other hand, in men, the median values of Ca levels measured at all defined time points were 9.50 mg/dL, 9.50 mg/dL, 9.50 mg/dL, and 9.70 mg/dL, respectively, with significantly higher values observed for time point 120' ($p = 0.018$) in reference to time point 0'. Meanwhile, the following Mg levels were observed: 2.30 mg/dL, 2.30 mg/dL, 2.20 mg/dL, and 2.40 mg/dL, respectively, and did not differ significantly.

3.4. Inflammatory Marker. The CRP concentrations were similar for women and men and did not differ significantly between the analyzed time points, neither in women (median values: 1.33 mg/L, 1.17 mg/L, 1.25 mg/L, and 1.23 mg/L, respectively) nor in men (0.47 mg/L, 0.46 mg/L, 0.45 mg/L, and 0.42 mg/L, respectively).

3.5. Correlations. In Table 3, we presented the results of Spearman's rank correlations only for pairs of analyzed parameters that correlated significantly at least at three time points of measurements. The results were analyzed separately for women and men, as blood serum prolactin physiological levels significantly differ between genders. Additionally, it was documented that uric acid levels are physiologically lower in women than in men, and simultaneously UA, as a component of TAS and FRAP, influence these levels, although to a different extent.

We observed a positive moderate correlation between calcium and albumin levels at all time points in both genders, except time point 0' in men. Calcium concentrations also showed positive, moderate, and strong correlations with magnesium levels in men. In turn, for women, we found a negative moderate correlation between CRP and calcium concentrations and a negative strong correlation between CRP and albumin levels. Strong or very strong positive correlations were observed between uric acid and FRAP levels, regardless of gender. In men, we also showed a strong positive correlation between UA and TAS concentrations and between TAS and FRAP levels.

Table 2: The concentrations of oxidative-antioxidant balance parameters, elements, and inflammatory marker.

	Women $N = 18$				Men $N = 15$			
	0' Mean ± SD Median (Q1-Q3)	15' Mean ± SD Median (Q1-Q3)	60' Mean ± SD Median (Q1-Q3)	120' Mean ± SD Median (Q1-Q3)	0' Mean ± SD Median (Q1-Q3)	15' Mean ± SD Median (Q1-Q3)	60' Mean ± SD Median (Q1-Q3)	120' Mean ± SD Median (Q1-Q3)
				TAC				
TAS (mmol/L)	1.58 ± 0.08 1.57 (1.52–1.65)	1.55 ± 0.07 1.55 (1.51–1.60)	1.59 ± 0.08 1.56 (1.54–1.65)	1.58 ± 0.08 1.57 (1.50–1.62)	1.65 ± 0.08 1.65 (1.58–1.74)	1.68 ± 0.13 1.70 (1.61–1.74)	1.66 ± 0.08 1.67 (1.59–1.72)	1.66 ± 0.08 1.64 (1.61–1.75)
FRAP (mmol/L)	1.11 ± 0.11 1.11 (1.04–1.20)	1.14 ± 0.11 1.13 (1.10–1.22) $p < 0.001$	1.14 ± 0.10 1.15 (1.09–1.20) $p < 0.001$	1.13 ± 0.10 1.13 (1.08–1.19) $p = 0.028$	1.31 ± 0.19 1.34 (1.17–1.44)	1.33 ± 0.16 1.39 (1.18–1.43)	1.31 ± 0.17 1.37 (1.18–1.43)	1.33 ± 0.16 1.38 (1.20–1.45)
				TOS and OSI				
TOS (μmol/L)	1.72 ± 0.99 1.50 (1.07–2.16)	1.74 ± 0.96 1.57 (1.10–2.14)	2.04 ± 1.76 1.44 (0.89–3.04)	1.99 ± 2.27 1.38 (0.68–2.53)	1.94 ± 1.17 1.38 (1.20–2.38)	1.86 ± 1.01 1.71 (0.75–2.66)	1.55 ± 0.60 1.40 (1.07–1.77)	1.45 ± 0.68 1.45 (0.94–2.12)
OSI (arbitrary units)	1.10 ± 0.66 0.95 (0.68–1.42)	1.12 ± 0.62 1.00 (0.72–1.43)	1.27 ± 1.03 0.93 (0.58–2.00)	1.24 ± 1.32 0.92 (0.43–1.65)	1.17 ± 0.70 0.91 (0.68–1.44)	1.13 ± 0.64 1.08 (0.44–1.80)	0.93 ± 0.35 0.85 (0.64–1.07)	0.88 ± 0.43 0.88 (0.59–1.25)
				AOPP				
AOPP (μmol/L)	95.46 ± 30.15 85.65 (77.39–110.45)	87.49 ± 14.16 85.00 (78.71–97.22)	87.08 ± 16.76 86.31 (75.40–99.89)	87.56 ± 23.74 82.02 (70.77–91.93)	106.83 ± 39.79 87.97 (80.69–140.20)	97.00 ± 32.38 90.61 (74.08–113.09) $p = 0.047$	101.98 ± 35.05 87.97 (76.73–122.35)	98.72 ± 36.40 84.67 (75.40–108.46)
				Low-molecular-weight antioxidants				
UA (mg/dL)	4.58 ± 0.71 4.68 (3.97–4.96)	4.54 ± 0.70 4.50 (3.94–4.93)	4.50 ± 0.67 4.66 (3.90–4.94)	4.48 ± 0.59 4.54 (3.97–4.85) $p = 0.048$	5.70 ± 1.16 5.71 (5.03–6.53)	5.74 ± 0.96 5.77 (5.00–6.45)	5.74 ± 1.01 5.63 (4.98–6.60)	5.76 ± 0.93 5.70 (5.00–6.61)
T-Bil (mg/dL)	0.52 ± 0.21 0.55 (0.42–0.60)	0.53 ± 0.22 0.55 (0.41–0.60)	0.56 ± 0.27 0.57 (0.40–0.64)	0.55 ± 0.27 0.54 (0.46–0.64)	0.78 ± 0.51 0.61 (0.42–1.17)	0.82 ± 0.53 0.62 (0.45–1.21) $p = 0.005$	0.87 ± 0.53 0.67 (0.46–1.24) $p < 0.001$	0.89 ± 0.56 0.69 (0.47–1.24) $p < 0.001$
ALB (g/dL)	4.59 ± 0.46 4.45 (4.24–4.67)	4.42 ± 0.30 4.30 (4.24–4.57) $p < 0.001$	4.65 ± 0.50 4.42 (4.35–5.19)	4.67 ± 0.53 4.52 (4.32–4.70)	4.72 ± 0.38 4.59 (4.50–5.13)	4.50 ± 0.18 4.54 (4.41–4.65) $p < 0.001$	4.55 ± 0.28 4.55 (4.35–4.70)	4.78 ± 0.44 4.59 (4.39–5.27)

Table 2: Continued.

	Women $N = 18$				Men $N = 15$			
	0' Mean ± SD Median (Q1-Q3)	15' Mean ± SD Median (Q1-Q3)	60' Mean ± SD Median (Q1-Q3)	120' Mean ± SD Median (Q1-Q3)	0' Mean ± SD Median (Q1-Q3)	15' Mean ± SD Median (Q1-Q3)	60' Mean ± SD Median (Q1-Q3)	120' Mean ± SD Median (Q1-Q3)
Elements								
Fe (μg/dL)	96.39 ± 41.15 101.50 (68.00–125.00)	95.06 ± 41.33 98.50 (67.00–124.00)	100.78 ± 45.73 108.00 (63.00–132.00)	101.44 ± 47.71 108.50 (63.00–132.00)	114.47 ± 43.59 109.00 (87.00–127.00)	114.80 ± 43.59 106.00 (86.00–126.00)	118.27 ± 46.04 105.00 (88.00–135.00) $p = 0.023$	121.40 ± 45.13 108.00 (90.00–140.00) $p = 0.011$
Ca (mg/dL)	9.48 ± 0.47 9.45 (9.10–9.60)	9.51 ± 0.39 9.55 (9.20–9.70)	9.63 ± 0.40 9.60 (9.40–9.90)	9.63 ± 0.41 9.70 (9.40–9.90)	9.49 ± 0.36 9.50 (9.20–9.80)	9.49 ± 0.40 9.50 (9.20–9.70)	9.59 ± 0.44 9.50 (9.20–9.90)	9.66 ± 0.37 9.70 (9.30–9.90) $p = 0.018$
Mg (mg/dL)	2.29 ± 0.14 2.30 (2.20–2.40)	2.25 ± 0.15 2.20 (2.20–2.30)	2.30 ± 0.11 2.30 (2.20–2.40)	2.34 ± 0.15 2.35 (2.20–2.40)	2.33 ± 0.15 2.30 (2.20–2.40)	2.31 ± 0.16 2.30 (2.20–2.40)	2.27 ± 0.18 2.20 (2.20–2.40)	2.33 ± 0.20 2.40 (2.20–2.50)
Inflammatory marker								
CRP (mg/L)	2.06 ± 2.34 1.33 (0.44–2.35)	2.01 ± 2.28 1.17 (0.45–2.41)	2.07 ± 2.42 1.25 (0.29–2.40)	2.09 ± 2.45 1.23 (0.36–2.43)	0.58 ± 0.62 0.47 (0.15–0.62)	0.58 ± 0.60 0.46 (0.18–0.61)	0.58 ± 0.62 0.45 (0.19–0.55)	0.59 ± 0.62 0.42 (0.22–0.68)

The Wilcoxon test was used to check the differences between time point 0' and other analyzed time points. A two-tailed p value of less than 0.05 was considered significant. p: significant differences versus time point 0'. ALB: albumin; AOPP: advanced protein oxidation products; Ca: calcium; CRP: C-reactive protein; SD: standard deviation; Fe: iron; FRAP: ferric reducing antioxidant power; Mg: magnesium; OSI: oxidative stress index (TOS/TAS); TAC: total antioxidant capacity; TAS: total antioxidant status; TOS: total oxidant status; T-Bil: bilirubin; UA: uric acid.

Table 3: The significant correlations between concentrations of determined parameters.

Parameters compared	0'		15'		60'		120'	
	R	*p*	*R*	*p*	*R*	*p*	*R*	*p*
Women								
Ca vs. ALB	0.586	0.010	0.667	0.002	0.612	0.007	0.646	0.004
Ca vs. CRP	-0.559	0.016	-0.541	0.020	-0.552	0.017	-0.516	0.028
CRP vs. ALB	-0.717	<0.001	-0.735	<0.001	-0.717	0.001	-0.664	0.003
FRAP vs. UA	0.830	<0.001	0.904	<0.001	0.884	<0.001	0.687	0.002
Men								
Ca vs. ALB	0.503	0.056	0.560	0.030	0.704	0.003	0.558	0.031
Ca vs. Mg	0.636	0.011	0.548	0.034	0.710	0.003	0.757	0.001
FRAP vs. UA	0.961	<0.001	0.946	<0.001	0.968	<0.001	0.957	<0.001
TAS vs. UA	0.893	<0.001	0.821	<0.001	0.862	<0.001	0.811	<0.001
FRAP vs. TAS	0.859	<0.001	0.728	0.002	0.803	<0.001	0.706	0.003

A two-tailed *p* value of less than 0.05 was considered significant. ALB: albumin; Ca: calcium; CRP: C-reactive protein; FRAP: ferric reducing antioxidant power; Mg: magnesium; R: correlation coefficient; TAS: total antioxidant status; UA: uric acid.

4. Discussion

Hyperprolactinemia can threaten many processes in the human body through hormonal disorders, but also through the induction of oxidative stress [30], which is often overlooked in assessing the effects of excess prolactin in the organism. In our study, prolactin levels in healthy participants were independent of BMI (data not shown) and were generally higher in women than in men (median values: 16.56 ng/mL and 8.85 ng/mL, respectively), which is consistent with the physiological difference between the sexes. After administration of a single dose of caffeinated coffee, a decrease in prolactin levels was observed over time, both in men and in women. Our results also showed a significant reduction in prolactin levels at different time points of PRL measurements (15', 60', and 120') in reference to time point 0', except time point 15' in men. On the other hand, the study by Kotsopoulos et al. [36], who investigated the effect of caffeine and caffeinated coffee on the concentration of prolactin among pre- and postmenopausal women (aged 25–70 years), depending on the number of cups of coffee and caffeine consumed daily, have shown that there were no significant differences in the levels of this hormone. The differences between our observations and results obtained by Kotsopoulos et al. [36] may be caused by differing time periods in which PRL levels were examined after the consumption of caffeinated beverages. While Kotsopoulos et al. [36] analyzed the long-term impact of caffeine beverages on prolactin levels, our study showed a short-term decrease in serum prolactin concentrations. Differences in the age of participants included in the study groups are another possible cause of the observed dissimilarity in PRL concentration analyzed in relation to coffee consumption between the study of Kotsopoulos et al. [36] and our investigations. Our participants were 19-29 years old, while the subjects analyzed by Kotsopoulos et al. [36] were aged 25–70. However, due to the real short-term effect of coffee ingredients on the level of prolactin, further, more extensive research is needed to draw more significant conclusions. We were the first to investigate the influence of caffeinated coffee on the level of blood serum PRL not only in women but also in men. Although all the concentrations of prolactin observed were within the reference ranges, the evident effect of caffeinated coffee and its ingredients on the reduction of PRL levels may suggest that caffeine possibly has a similar effect in the case of hyperprolactinemia, which, after confirmation in further studies, may contribute to the development of new therapeutic strategies in its treatment.

Oxidative stress plays an important role in many pathological processes that take place in the human body and is responsible for the development of a variety of diseases. Parameters of oxidative-antioxidant balance may be examined by measurements of TAS, FRAP, and TOS concentrations to estimate the overall oxidation status of the body, as well as AOPP levels and the concentrations of low-molecular-weight antioxidants such as UA, T-Bil, and ALB, which may vary during the response to oxidative stress. It is already documented that TAS levels also provide information on the relative antioxidant capacity of different coffees [6]. FRAP test is a nonspecific, redox-related colorimetric test which is related to the concentration of antioxidants present in the tested sample, and the increase in absorbance is proportional to the total ferric reducing power of the sample [43]; however, it only reflects the reducing capacity and does not identify potential antioxidants [6, 9, 12].

The presence of antioxidant compounds in coffee leads to the disappearance of free radical chromogens [6]. Most of the evidence supporting the positive role of coffee in the reduction of oxidative stress comes from *in vitro* and epidemiological studies [44–46]. In women, the determined concentrations of serum TAS slightly decreased with time after drinking caffeinated coffee, but no differences between time points 15', 60', and 120' in comparison to time point 0' were observed. In men, TAS levels slightly increased at 15' and decreased at other time points, but the differences were not significant. The results obtained for men are in accordance with the findings of Teekachunhatean et al. [47], who used the same method for TAS determination as in our study.

The authors also did not find the significant differences in serum TAS levels (mean value: 1.51 mmol/L) among 11 healthy Thai male volunteers after a single dose of caffeinated coffee intake (180 mL) or measurements at time points: 10', 20', 30', 40', 60', 75', and 120' in reference to time point 0'. Significant reduction, versus baseline, in TAS levels was achieved only on the 6th and 12th day of the experiment (1.37 mmol/L and 1.39 mmol/L, respectively). Leelarungrayub et al. [48], using the same method for TAS measurements as us, examined 26 healthy men divided into three groups: subjects who consumed caffeinated coffee, subjects who consumed decaffeinated coffee, and a control group. The authors showed that there were no significant differences between the investigated groups ($p > 0.05$, mean values: 0.84 mmol/L [control], 0.98 mmol/L [decaffeinated coffee], and 1.00 mmol/L [caffeinated coffee]) in blood plasma TAS levels one hour after coffee consumption [48]. Our results for TAS concentration, analyzed in the context of caffeinated coffee intake, differ from those obtained by Leelarungrayub et al. [48], but this may be because the participants investigated by Leelarungrayub and coworkers were examined after a physical exercise test.

Another parameter that can be used to express TAC is FRAP. Our study showed that among women FRAP levels were higher over time, and differences between each time point with reference to time point 0' were significant ($p < 0.001$, $p < 0.001$, and $p = 0.028$, respectively), while among men the differences were not insignificant. Agudelo-Ochoa et al. [49] examined the impact of caffeinated coffee intake on blood plasma FRAP levels in 38 men and 37 women divided into 3 groups: control—no coffee consumption, and 2 groups that drank 1 of 2 types of coffee (400 mL/day) with different caffeine contents (188 mg/400 mL and 197 mg/400 mL) and content of other substances for 8 weeks. The authors [49] noticed that, one hour after drinking the first dose of coffee, the level of FRAP significantly increased in both groups in comparison to the baseline values, while in the control group FRAP concentrations were significantly lower. In our study, we observed similar changes in FRAP levels one hour after drinking caffeinated coffee, despite the different coffee concentrations given to our volunteers and those used in the studies of Agudelo-Ochoa et al. [49]. Moura-Nunes et al. [50] observed that blood plasma TAC levels determined using FRAP assay, measured 90 minutes after caffeinated coffee drinking (8 g of instant coffee/240 mg of caffeine/200 mL water), increased by 2.6% in a group of 10 healthy subjects (3 men and 7 women). Moreover, Metro et al. [51] reported an increase of blood plasma TAC levels for much longer than a few hours after drinking caffeine solution—it could be observed even after a week. Although the investigations of Metro et al. [51] were limited to men and different commercial tests were used to measure TAC levels, the results obtained by the authors are in accordance with our assumptions that caffeine increases TAC concentrations, which may suggest the potential influence of caffeinated coffee (polyphenols action) on total antioxidant capacity. Although in different human clinical trials coffee samples differ in their chemical composition (the variety of beans, roasting temperatures, and brewing methods), dosages, and lengths of coffee consumption examined, in general, it can be concluded that a short-term influence on oxidative-antioxidant balance parameters is observed as a result of the consumption of coffee.

The next parameters we examined were TOS levels and the OSI index. To the best of our knowledge, the effects of caffeinated coffee on TOS levels have not yet been measured. Although the OSI index is told to be a new tool for the measurement of consequences of oxidative stress [52], we are the first, to our knowledge, to use it to explore the short-term effect of caffeinated coffee on oxidative-antioxidant balance in the human body. Even though we did not observe significant differences in levels of TOS and values of OSI index between examined time points after coffee intake, both TOS levels and values of OSI index were different at each time point of measurement. The highest median value of the OSI index was observed 15 minutes after drinking caffeinated coffee; then, it stabilized at subsequent time points and the median values were comparable to the baseline value. The OSI index is the TOS/TAS ratio, which would explain these changes over time—in the initial stage after drinking caffeinated coffee, the activity of oxidative factors increases while antioxidant mechanisms are activated. Stabilization of oxidative and antioxidant mechanisms was observed 120 minutes after drinking caffeinated coffee in both sexes. We think that further extended study, using other types and/or doses of coffee, may give different results. It should also be noticed that long-term consumption of caffeinated beverages could have a potential influence on these parameters.

AOPP are products of blood plasma protein oxidation, mainly albumin. Due to the rapid response to any changes in oxidative-antioxidant balance by AOPP production, this parameter is considered suitable for measuring short-term changes in oxidative stress [53]. In our study, the changes in AOPP levels between examined time points after coffee consumption were insignificant in both groups of participants, except for time point 15' in men ($p = 0.047$). A slight decrease in AOPP levels was observed at each time point in women and at 60' and 120' in men. Nemzer et al. [54] reported that single-dose treatment with phenol-rich foods lowered blood AOPP levels by 39% in the first 60 minutes and this decrease was significant ($p < 0.05$) compared to the baseline level. AOPP concentrations returned close to baseline levels in the hour following treatment. It is very likely that our results would be in line with those obtained by Nemzer et al. [54] if we had used larger doses of coffee or a type of coffee that contained more polyphenols.

Human blood is equipped with a great number of antioxidants that can bind metal ions (for example iron and copper) and scavenge free radicals. The ability of blood plasma components to counteract oxidative stress is a useful indicator of oxidative-antioxidant status [55]. Known low-molecular-weight antioxidants include uric acid, bilirubin, and albumin—compounds that deactivate free radicals or oxidants by interacting with them [56].

UA is a powerful scavenger of blood serum oxidants, including the hydroxyl radical, singlet oxygen, ozone, and several organic and nitrogen oxidants such as peroxide

radicals [56], and can therefore be considered an indirect indicator of oxidative stress [39, 57]. Moura-Nunes et al. [50] reported no significant changes in UA concentration (mean value: 3.8 mg/dL) 90 minutes from caffeinated coffee consumption (baseline: 4.0 mg/dL). On the other hand, a study conducted by Choi and Curhan [58] documented that caffeinated coffee drinking was inversely associated with UA concentration in human blood serum. Our study showed no significant changes in blood serum UA concentrations between examined time points after coffee intake, apart from time point 120' in women ($p = 0.048$), in which the median value (4.54 mg/dL) was slightly below baseline (4.68 mg/dL). Moreover, the aforementioned study conducted by Natella et al. [59] documented an increase in UA levels after the 1st and 2nd hour from drinking coffee in relation to time point 0'. The increase was attributable to the interference of phenols in UA secretion and reabsorption, as phenol-rich compounds increase UA levels [60–62]. The effect of caffeinated coffee on the concentration of UA in the blood serum is still unclear and requires further exploration, but our study, like that of Moura-Nunes et al. [50], suggests that instant coffee has no influence on this parameter. However, further research is needed to confirm or exclude this hypothesis.

In the present study, we observed strong positive correlations, importantly, at each time point, between levels of UA vs. FRAP and TAS in men and between UA vs. FRAP concentrations in women, confirming the well-known and documented positive relationships between blood plasma antioxidant activity as measured by FRAP levels and blood serum uric acid concentrations. The estimated contribution of uric acid, measured by the FRAP method, in the total antioxidant capacity is about 60%, while albumin contributes only 10%. The small participation of albumin in the results of FRAP concentration determinations is most likely related to the influence of low pH on the thiol groups of proteins required for this method [43, 63]. In turn, in the method used for the determinations of TAS concentrations, the main component is albumin (28%), while the estimated amount of uric acid is approx. 19% [63]. Physiologically, men have a higher concentration of uric acid than women, and in our investigations, we also found significantly higher concentrations of UA in the group of men ($p = 0.002$; data not shown). This is also reflected by lower serum FRAP concentration in women compared to men ($p = 0.002$; data not shown), as also documented by Brock et al. [64]. The above finding may indicate a higher contribution of uric acid in the total antioxidant capacity of blood serum in men than in women. The mechanisms of homeostatic control are very complex and require many components. Maintaining oxidative-antioxidant balance is particularly important, as oxidative stress is believed to induce many diseases. Our study indicates that these mechanisms may differ by gender, which most likely explains the presence of correlations between TAS and FRAP levels in men and not in women. On the other hand, when we took the whole group of participants, without gender differentiation, we also observed the significant correlations between TAS and FRAP levels at each time point (data not shown). A study by Erel [65] reported the presence of significant correlations between FRAP and TAS levels ($R = 0.847$, $p < 0.0001$), although Cao et al. [63] did not observe such a relationship. However, their study group consisted of 31 women and only 14 men.

Another examined parameter was T-Bil. *In vitro*, bilirubin is a scavenger of peroxyl radicals and singlet oxygen. However, whether it also fulfills this function *in vivo* remains unclear. It should also be mentioned that bilirubin is capable of forming singlet oxygen in the presence of light [56]. Moura-Nunes et al. [50] observed no significant changes in T-Bil concentrations after 90 minutes from caffeinated coffee consumption (mean value: 0.60 mg/dL) in comparison to baseline (mean value: 0.60 mg/dL). Regular consumption of caffeinated coffee contributes to the reduction of total bilirubin in human blood serum [66, 67]. Although our results were similar in the group of women at all examined time points, median values of total bilirubin concentrations among men increased slightly over the time (from 0.61 mg/dL to 0.69 mg/dL).

Albumin is one of the main components of the antioxidant defense system, the primary target of blood plasma proteins under oxidative stress, and works through its multiple binding sites and free radical scavenging properties [68]. In the present study, albumin concentrations were significantly lower both in the group of women and men at time point 15' (median value: 4.30 g/dL and 4.54 g/dL, respectively) in reference to time point 0' (4.45 g/dL and 4.59 g/dL, respectively). No other significant changes were observed, which corresponds to the results obtained by Moura-Nunes et al. [50], who observed no significant changes in albumin concentrations (mean value: 4.50 g/dL) 90 minutes from caffeinated coffee consumption (baseline mean value: 4.20 g/dL). The decrease in albumin concentration shortly after drinking caffeinated coffee may be explained by damage to blood plasma proteins by the drink's ingredients, as described by some authors [69, 70].

Oxidative stress has been speculated to relate to the disturbance of ion homeostasis in the human body due to the modification of proteins and opening of ion channels [71, 72]. Iron is a microelement responsible for oxygen transport, energy metabolism, and electron transfer. It is a cofactor of many enzymes and therefore very important in the fight against free radicals when present in physiological amounts in the body. The reported increase of iron levels in the body may be due to iron's presence in coffee [73]. On the other hand, coffee can inhibit iron absorption by phenolic compounds, which can hinder the absorption of this element. However, we did not observe the presence of significant differences in iron levels between the analyzed time points in women and saw a slight, but significant, increase of iron concentrations in men at time points 60' and 120' in comparison to baseline time point 0' ($p = 0.023$ and $p = 0.011$, respectively).

In vitro studies suggest a relationship between the occurrence of oxidative stress and the increased concentration of calcium in cell cytoplasm due to disturbed thiol homeostasis increasing the flow of calcium from the endoplasmic reticulum through cell membranes to the cytosol of the cell [71, 72]. In an extensive review by Olechno et al. [74], instant coffee was reported to contain high amounts of calcium,

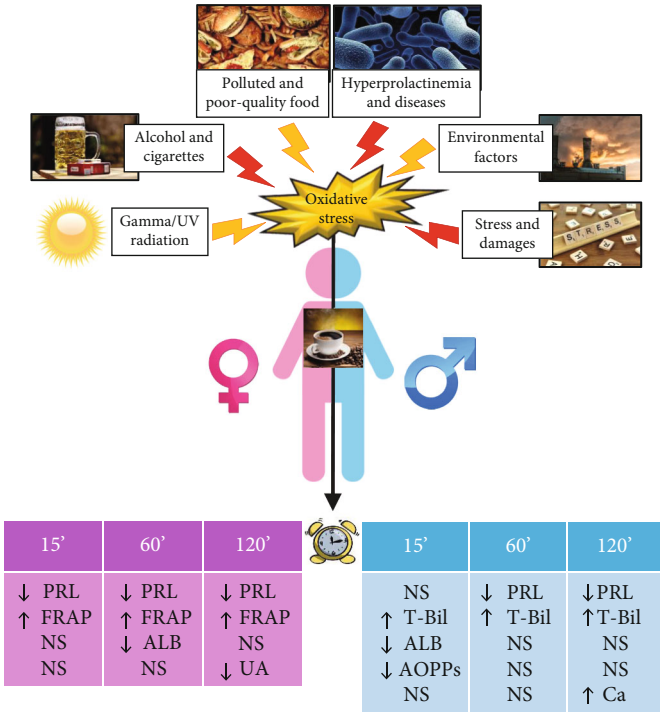

Figure 4: Scheme of interactions between oxidative stress development and levels of serum oxidative stress parameters in relation to time points of measurement after caffeinated coffee consumption. ALB: albumin; Ca: calcium; FRAP: ferric reducing antioxidant power; PRL: prolactin; T-Bil: total bilirubin; UA: uric acid. Versus time point 0': NS: not significant; ↑: significantly increased; ↓: significantly decreased.

but our results do not support this statement—a significant increase in calcium concentration was observed only in men at time point 120'. Analyses of NHANES 2011–2016 data by Rehm et al. [75] have also reported that there was no association between coffee consumption and calcium supply. In our studies, we observed the presence of strong positive correlations between Ca vs. ALB concentrations in both women and men, except at point 0' in men. A positive correlation between these parameters was shown earlier by Rajaraman et al. [76]. The observed correlations result from the fact that albumin binds calcium, and this ability of ALB is necessary for the maintenance of serum calcium levels. We also observed a positive correlation between Ca vs. Mg levels in men at each time point, which may be explained by the participation of magnesium in the conversion of the inactive form of vitamin D to the active form, which increases the body's ability to absorb calcium [77]. A possible cause of such correlations, which appeared in men only, is higher blood serum vitamin D levels in men than in women [78], due to which the effect of magnesium levels on calcium levels is more noticeable in males.

The results of some studies have confirmed the positive influence of magnesium in combating the effects of oxidative stress [79] and state that magnesium deficiency is accompanied by increased levels of oxidative stress markers, such as products of lipids, proteins, and DNA oxidative modification [80]. Olechno et al. [74] showed that instant coffee has a lower magnesium content than other types of coffee. Analyses of NHANES 2011–2016 Data made by Rehm et al. [75] showed that the supply of magnesium increases with the amount of caffeinated coffee consumed ($p < 0.001$), but in the present study, no significant changes in magnesium levels between analyzed time points were observed, neither in women nor men.

Inflammation is accompanied by increased oxidative stress, and the reduction of expression of inflammation-related biomarkers as a result of coffee consumption had an antioxidant effect that accompanied the reduction of inflammation [6]. Coffee contains a variety of aforementioned bioactive compounds with anti-inflammatory and antioxidative properties (Figure 1), which may reduce blood serum CRP levels. In a long-term study on the influence of coffee intake on the concentration of serum CRP, Hang et al. [81] reported that CRP levels were significantly lower (about 16.6%) among people consuming more than 4 cups of caffeinated coffee/day in reference to those who were not. Moreover, this relationship was stronger in women than in men. Similar results were obtained in many studies [82–85]; however, the results of our study did not support the hypothesis that short-term consumption of caffeinated coffee decreases blood serum CRP levels, as no significant changes between examined time points after caffeinated coffee consumption were observed. On the other hand, we observed the presence of negative correlations between CRP and ALB concentrations in women. This is most likely related to the role of these proteins in inflammation and the balance between their expression: albumin is a negative (decrease in concentration) and CRP is a positive (increase in concentration) acute phase protein [86]. The above correlations did not occur in men, probably due to the effect of

the amount and distribution of body fat on CRP level, which is greater in women than in men [87], and a faster decrease in the levels of albumin in women than in men [88]. We also showed a negative correlation between Ca and CRP levels in women only, which seems to be associated with negative correlations observed between CRP vs. ALB concentrations and positive correlations between Ca vs. ALB levels. This, in turn, may be associated with the abovementioned greater influence of body fat on CRP level in female participants.

5. Conclusions

We examined the short-term effect of caffeinated coffee consumption on the concentration of prolactin, selected parameters of oxidative stress, and some elements in blood sera of young healthy adults. Currently, there is very little data available on the effects of the consumption of caffeinated beverages on the body's hormone balance, especially on sex hormones. To the best of our knowledge, to date, there have been no studies analyzing the short-term effects of caffeine on values of the sex hormone PRL in both women and men. Due to the potential pharmaceutical use of caffeinated coffee ingredients, we hypothesized that caffeine may have therapeutic potential in hyperprolactinemia treatment, due to an observed reduction in the concentration of this parameter within 2 hours after consuming a caffeinated coffee. Although our results seem to be promising, further studies are needed to determine if this effect is of biological importance, especially in people struggling with hyperprolactinemia. The results of this study could help not only to understand the role of diet in maintaining the body's hormonal balance but also provide opportunities to verify the potential utility of coffee ingredients to create new therapeutic strategies and guide future research on this subject. The results obtained for the parameters of the oxidative-antioxidant balance suggest the presence of a relationship between the expression of caffeinated coffee components and a decrease in oxidative stress in the human body. The parameters of oxidative-antioxidant balance we investigated were TAS, FRAP, TOS, OSI index, AOPP, iron, calcium, magnesium, and low molecular weight antioxidants such as uric acid, total bilirubin, and albumin. We observed that caffeinated coffee increased the concentrations of some of the characteristic oxidative stress markers shortly after consumption. Although the antioxidant response after caffeinated coffee intake was not as high as expected, we may notice the potential positive role of coffee in the reduction and/or elimination of oxidative stress. An interesting direction for further, more detailed research, also based on the analysis of a wider spectrum of oxidative stress parameters, would be to check whether the ingredients of caffeinated coffee may have an important use in the prevention and treatment of the effects of oxidative stress. We hope that our findings will be helpful in developing new strategies for treating hyperprolactinemia and will contribute to increasing the significance of research on preventing the negative effects of oxidative stress. A scheme showing the interrelationships between oxidative stress development and the analyzed parameters, summarizing the results of our research, is presented in Figure 4.

Data Availability

The data presented in this study are available upon reasonable request from the corresponding author.

Conflicts of Interest

The authors declare that there is no conflict of interest regarding the publication of this paper.

Authors' Contributions

KR, IK, and EMK are responsible for the conceptualization. KR, IK, AK, and EMK are responsible for the methodology. KR, IK, AK, and EMK curated the data. KR, IK, and EMK did the formal analysis. KR, IK, AK, and EMK did the investigation. KR, AK, and EMK are assigned to the project administration. KR, IK, and EMK are assigned to the writing—original draft preparation. KR, IK, and EMK are assigned to the writing—review and editing. KR, IK, and EMK worked on visualization. IK and EMK did the supervision. KR and EMK acquired funding. All authors have read and agreed to the published version of the manuscript.

Acknowledgments

This research was partially financed from the funds of the Wroclaw Medical University allocated to the statutory activities of the Student Research Club, "Biomarkers in Medical Diagnostics", and partially financially supported by the Ministry of Health subvention according to number SUB.D270.21.096 from the IT Simple System of Wroclaw Medical University. Absorbance measurements for AOPP determinations were performed using a microplate reader located in the Screening Laboratory of Biological Activity Test and Collection of Biological Material, Faculty of Pharmacy, Wroclaw Medical University, supported by the ERDF Project within the Innovation Economy Operational Programme POIG.02.01.00-14-122/09.

Supplementary Materials

Figure S1: The concentration values of selected parameters in women and men. *(Supplementary Materials)*

References

[1] F. Burdan, "Pharmacology of caffeine: the main active compound of coffee," in *Coffee in Health and Disease Prevention*, pp. 823–829, Academic Press, 2015.

[2] K. Rodak, I. Kokot, and E. M. Kratz, "Caffeine as a factor influencing the functioning of the human body—friend or foe," *Nutrients*, vol. 13, no. 9, p. 3088, 2021.

[3] J. R. León-Carmona and A. Galano, "Is caffeine a good scavenger of oxygenated free radicals," *The Journal of Physical Chemistry B*, vol. 115, no. 15, pp. 4538–4546, 2011.

[4] Institute of Medicine (US) Committee on Military Nutrition Research, *2 Pharmacology of Caffeine, vol. 37, no. 1*, National Academies Press (US), 2001.

[5] Y. F. Chu, *Coffee: Emerging Health Effects and Disease Prevention, Vol. 59*, John Wiley & Sons, 2012.

[6] N. Liang and D. D. Kitts, "Antioxidant property of coffee components: assessment of methods that define mechanism of action," *Molecules*, vol. 19, no. 11, pp. 19180–19208, 2014.

[7] O. J. Lara-Guzmán, S. Medina, R. Álvarez et al., "Oxylipin regulation by phenolic compounds from coffee beverage: positive outcomes from a randomized controlled trial in healthy adults and macrophage derived foam cells," *Free Radical Biology & Medicine*, vol. 160, pp. 604–617, 2020.

[8] L. Bravo, "Polyphenols: chemistry, dietary sources, metabolism, and nutritional significance," *Nutrition Reviews*, vol. 56, no. 11, pp. 317–333, 1998.

[9] A. Yashin, Y. Yashin, J. Y. Wang, and B. Nemzer, "Antioxidant and antiradical activity of coffee," *Antioxidants*, vol. 2, no. 4, pp. 230–245, 2013.

[10] G. V. de Melo Pereira, D. P. de Carvalho Neto, A. I. M. Júnior et al., "Chemical composition and health properties of coffee and coffee by-products," *Advances in Food and Nutrition Research*, vol. 91, pp. 65–96, 2020.

[11] I. A. Ludwig, P. Mena, L. Calani et al., "Variations in caffeine and chlorogenic acid contents of coffees: what are we drinking?," *Food & Function*, vol. 5, no. 8, pp. 1718–1726, 2014.

[12] S. Gorjanović, D. Komes, J. Laličić-Petronijević et al., "Antioxidant efficiency of polyphenols from coffee and coffee substitutes-electrochemical versus spectrophotometric approach," *Journal of Food Science and Technology*, vol. 54, no. 8, pp. 2324–2331, 2017.

[13] J. Czachor, M. Miłek, S. Galiniak, K. Stępień, M. Dżugan, and M. Mołoń, "Coffee extends yeast chronological lifespan through antioxidant properties," *International Journal of Molecular Sciences*, vol. 21, no. 24, pp. 1–18, 2020.

[14] International Agency for Research on Cancer, International Agency for Research on Cancer, and Weltgesundheitsorganisation, "Coffee, tea, mate, methylxanthines and methylglyoxal," *IARC Monographs on the Evaluation of Carcinogenic Risks to Humans*, vol. 51, pp. 217–233, 1991.

[15] V. Brezová, A. Šlebodová, and A. Staško, "Coffee as a source of antioxidants: an EPR study," *Food Chemistry*, vol. 114, no. 3, pp. 859–868, 2009.

[16] H. Kolb, K. Kempf, and S. Martin, "Health effects of coffee: mechanism unraveled," *Nutrients*, vol. 12, no. 6, pp. 1–14, 2020.

[17] R. V. Abreu, E. M. Silva-Oliveira, M. F. D. Moraes, G. S. Pereira, and T. Moraes-Santos, "Chronic coffee and caffeine ingestion effects on the cognitive function and antioxidant system of rat brains," *Pharmacology, Biochemistry, and Behavior*, vol. 99, no. 4, pp. 659–664, 2011.

[18] S. A. Qureshi, A. C. Lund, M. B. Veierød et al., "Food items contributing most to variation in antioxidant intake; a cross-sectional study among Norwegian women," *BMC Public Health*, vol. 14, no. 1, pp. 1–9, 2014.

[19] S. Taysi, F. S. Algburi, Z. Mohammed, O. A. Ali, and M. E. Taysi, "Thymoquinone: a review of pharmacological importance, oxidative stress, COVID-19, and radiotherapy," *Mini Reviews in Medicinal Chemistry*, vol. 22, 2022.

[20] A. Hausladen and J. S. Stamler, "Nitrosative stress," *Methods in Enzymology*, vol. 300, pp. 389–395, 1999.

[21] S. Taysi, A. S. Tascan, M. G. Ugur, and M. Demir, "Radicals, oxidative/nitrosative stress and preeclampsia," *Mini Reviews in Medicinal Chemistry*, vol. 19, no. 3, pp. 178–193, 2019.

[22] J. Renzing, S. Hansen, and D. P. Lane, "Oxidative stress is involved in the UV activation of p53," *Journal of Cell Science*, vol. 109, no. 5, pp. 1105–1112, 1996.

[23] H. Van Der Vaart, D. S. Postma, W. Timens, and N. H. T. Ten Hacken, "Acute effects of cigarette smoke on inflammation and oxidative stress: a review," *Thorax*, vol. 59, no. 8, pp. 713–721, 2004.

[24] D. Wu and A. I. Cederbaum, "Alcohol, oxidative stress, and free radical damage," *Alcohol Research and Health*, vol. 27, no. 4, pp. 277–284, 2003.

[25] M. Puttabyatappa, M. Banker, L. Zeng et al., "Maternal exposure to environmental disruptors and sexually dimorphic changes in maternal and neonatal oxidative stress," *The Journal of Clinical Endocrinology and Metabolism*, vol. 105, no. 2, pp. 492–505, 2020.

[26] B. L. Tan, M. E. Norhaizan, and W. P. P. Liew, "Nutrients and oxidative stress: friend or foe," *Oxidative Medicine and Cellular Longevity*, vol. 2018, Article ID 9719584, 24 pages, 2018.

[27] J. Egea, I. Fabregat, Y. M. Frapart et al., "European contribution to the study of ROS: a summary of the findings and prospects for the future from the COST action BM1203 (EU-ROS)," *Redox Biology*, vol. 13, pp. 94–162, 2017.

[28] D. J. Hassett and J. A. Imlay, "Bactericidal antibiotics and oxidative stress: a radical proposal," *ACS Chemical Biology*, vol. 2, no. 11, pp. 708–710, 2007.

[29] S. Taysi, O. Cikman, A. Kaya et al., "Increased oxidant stress and decreased antioxidant status in erythrocytes of rats fed with zinc-deficient diet," *Biological Trace Element Research*, vol. 123, no. 1–3, pp. 161–167, 2008.

[30] B. S. Veena, S. Upadhya, S. K. Adiga, and K. N. Pratap, "Evaluation of oxidative stress, antioxidants and prolactin in infertile women," *Indian Journal of Clinical Biochemistry*, vol. 23, no. 2, pp. 186–190, 2008.

[31] M. E. Freeman, B. Kanyicska, A. Lerant, and G. Nagy, "Prolactin: structure, function, and regulation of secretion," *Physiological Reviews*, vol. 80, no. 4, pp. 1523–1631, 2000.

[32] G. Rastrelli, G. Corona, and M. Maggi, "The role of prolactin in andrology: what is new," *Reviews in Endocrine and Metabolic Disorders*, vol. 16, no. 3, pp. 233–248, 2015.

[33] G. Corona, F. C. Wu, G. Rastrelli et al., "Low prolactin is associated with sexual dysfunction and psychological or metabolic disturbances in middle-aged and elderly men: the European Male Aging Study (EMAS)," *The Journal of Sexual Medicine*, vol. 11, no. 1, pp. 240–253, 2014.

[34] D. A. Pujianto, B. J. Curry, R. J. Aitken, and A. Di Santo, "Prolactin exerts a prosurvival effect on human spermatozoa via mechanisms that involve the stimulation of Akt phosphorylation and suppression of caspase activation and capacitation," *Endocrinology*, vol. 151, no. 3, pp. 1269–1279, 2010.

[35] P. O. Fiebai and N. C. Orazulike, "Hyperprolactinaemia," *Amenorrhea*, vol. 8, no. 12, pp. 121–131, 2016.

[36] J. Kotsopoulos, A. H. Eliassen, S. A. Missmer, S. E. Hankinson, and S. S. Tworoger, "Relationship between caffeine intake and plasma sex hormone concentrations in premenopausal and postmenopausal women," *Cancer*, vol. 115, no. 12, pp. 2765–2774, 2009.

[37] C. Nagata, M. Kabuto, and H. Shimizu, "Association of coffee, green tea, and caffeine intakes with serum concentrations of

estradiol and sex hormone-binding globulin in premenopausal Japanese women," *Nutrition and Cancer*, vol. 30, no. 1, pp. 21–24, 1998.

[38] J. Lucero, B. L. Harlow, R. L. Barbieri, P. Sluss, and D. W. Cramer, "Early follicular phase hormone levels in relation to patterns of alcohol, tobacco, and coffee use," *Fertility and Sterility*, vol. 76, no. 4, pp. 723–729, 2001.

[39] O. Erel, "A new automated colorimetric method for measuring total oxidant status," *Clinical Biochemistry*, vol. 38, no. 12, pp. 1103–1111, 2005.

[40] I. Kokot, A. Piwowar, M. Jędryka, and E. M. Kratz, "Is there a balance in oxidative-antioxidant status in blood serum of patients with advanced endometriosis," *Antioxidants*, vol. 10, no. 7, p. 1097, 2021.

[41] V. Witko-Sarsat, V. Gausson, A. T. Nguyen et al., "AOPP-induced activation of human neutrophil and monocyte oxidative metabolism: a potential target for N -acetylcysteine treatment in dialysis patients," *Kidney International*, vol. 64, no. 1, pp. 82–91, 2003.

[42] K. Zabłocka-Słowińska, S. Płaczkowska, K. Skórska et al., "Oxidative stress in lung cancer patients is associated with altered serum markers of lipid metabolism," *PLoS One*, vol. 14, no. 4, p. e0215246, 2019.

[43] I. F. F. Benzie and J. J. Strain, "The Ferric Reducing Ability of Plasma (FRAP) as a measure of "Antioxidant Power": the FRAP assay," *Analytical Biochemistry*, vol. 239, no. 1, pp. 70–76, 1996.

[44] R. Poole, O. J. Kennedy, P. Roderick, J. A. Fallowfield, P. C. Hayes, and J. Parkes, "Coffee consumption and health: umbrella review of meta-analyses of multiple health outcomes," *BMJ*, vol. 359, article j5024, 2017.

[45] S. Buscemi, S. Marventano, M. Antoci et al., "Coffee and metabolic impairment: Aan updated review of epidemiological studies," *NFS Journal*, vol. 3, pp. 1–7, 2016.

[46] G. Grosso, J. Godos, F. Galvano, and E. L. Giovannucci, "Coffee, caffeine, and health outcomes: an umbrella review," *Annual Review of Nutrition*, vol. 37, pp. 131–156, 2017.

[47] S. Teekachunhatean, N. Tosri, C. Sangdee et al., "Antioxidant effects after coffee enema or oral coffee consumption in healthy Thai male volunteers," *Human & Experimental Toxicology*, vol. 31, no. 7, pp. 643–651, 2012.

[48] D. Leelarungrayub, M. Sallepan, and S. Charoenwattana, "Effects of acute caffeinated coffee consumption on energy utilization related to glucose and lipid oxidation from short submaximal treadmill exercise in sedentary men," *Nutrition and Metabolic Insights*, vol. 4, p. NMI-S8299, 2011.

[49] G. M. Agudelo-Ochoa, I. C. Pulgarín-Zapata, C. M. Velásquez-Rodriguez et al., "Coffee consumption increases the antioxidant capacity of plasma and has no effect on the lipid profile or vascular function in healthy adults in a randomized controlled trial," *The Journal of Nutrition*, vol. 146, no. 3, pp. 524–531, 2016.

[50] N. Moura-Nunes, D. Perrone, A. Farah, and C. M. Donangelo, "The increase in human plasma antioxidant capacity after acute coffee intake is not associated with endogenous non-enzymatic antioxidant components," *International Journal of Food Sciences and Nutrition*, vol. 60, no. sup6, pp. 173–181, 2009.

[51] D. Metro, V. Cernaro, D. Santoro et al., "Beneficial effects of oral pure caffeine on oxidative stress," *Journal of Clinical & Translational Endocrinology*, vol. 10, pp. 22–27, 2017.

[52] A. Abuelo, J. Hernández, J. L. Benedito, and C. Castillo, "Oxidative stress index (OSi) as a new tool to assess redox status in dairy cattle during the transition period," *Animal*, vol. 7, no. 8, pp. 1374–1378, 2013.

[53] L. Selmeci, L. Seres, M. Antal, J. Lukács, A. Regöly-Mérei, and G. Acsády, "Advanced oxidation protein products (AOPP) for monitoring oxidative stress in critically ill patients: a simple, fast and inexpensive automated technique," *Clinical Chemistry and Laboratory Medicine*, vol. 43, no. 3, pp. 294–297, 2005.

[54] B. V. Nemzer, L. C. Rodriguez, L. Hammond, R. Disilvestro, J. M. Hunter, and Z. Pietrzkowski, "Acute reduction of serum 8-iso-PGF2-alpha and advanced oxidation protein products in vivo by a polyphenol-rich beverage; a pilot clinical study with phytochemical and in vitro antioxidant characterization," *Nutrition Journal*, vol. 10, no. 1, p. 67, 2011.

[55] M. Kiely, P. A. Morrissey, P. F. Cogan, and P. J. Kearney, "Low molecular weight plasma antioxidants and lipid peroxidation in maternal and cord blood," *European Journal of Clinical Nutrition*, vol. 53, no. 11, pp. 861–864, 1999.

[56] T. Grune, P. Schröder, and H. Biesalski, "Low molecular weight antioxidants," *Reactions, Processes*, vol. 2, pp. 77–90, 2005.

[57] A. Gupta, R. P. S. Mohan, S. Gupta, S. S. Malik, S. Goel, and N. Kamarthi, "Roles of serum uric acid, prolactin levels, and psychosocial factors in oral lichen planus," *Journal of Oral Science*, vol. 59, no. 1, pp. 139–146, 2017.

[58] H. K. Choi and G. Curhan, "Coffee, tea, and caffeine consumption and serum uric acid level: the third National Health and Nutrition Examination Survey," *Arthritis Care and Research*, vol. 57, no. 5, pp. 816–821, 2007.

[59] F. Natella, M. Nardini, I. Giannetti, C. Dattilo, and C. Scaccini, "Coffee drinking influences plasma antioxidant capacity in humans," *Journal of Agricultural and Food Chemistry*, vol. 50, no. 21, pp. 6211–6216, 2002.

[60] I. A. Bobulescu and O. W. Moe, "Renal transport of uric acid: evolving concepts and uncertainties," *Advances in Chronic Kidney Disease*, vol. 19, no. 6, pp. 358–371, 2012.

[61] A. Ghiselli, F. Natella, A. Guidi, L. Montanari, P. Fantozzi, and C. Scaccini, "Beer increases plasma antioxidant capacity in humans," *The Journal of Nutritional Biochemistry*, vol. 11, no. 2, pp. 76–80, 2000.

[62] R. A. A. Caccetta, K. D. Croft, L. J. Beilin, and I. B. Puddey, "Ingestion of red wine significantly increases plasma phenolic acid concentrations but does not acutely affect ex vivo lipoprotein oxidizability," *The American Journal of Clinical Nutrition*, vol. 71, no. 1, pp. 67–74, 2000.

[63] G. Cao and R. L. Prior, "Comparison of different analytical methods for assessing total antioxidant capacity of human serum," *Clinical Chemistry*, vol. 44, no. 6, pp. 1309–1315, 1998.

[64] G. R. Brock, C. J. Butterworth, J. B. Matthews, and I. L. C. Chapple, "Local and systemic total antioxidant capacity in periodontitis and health," *Journal of Clinical Periodontology*, vol. 31, no. 7, pp. 515–521, 2004.

[65] O. Erel, "A novel automated direct measurement method for total antioxidant capacity using a new generation, more stable ABTS radical cation," *Clinical Biochemistry*, vol. 37, no. 4, pp. 277–285, 2004.

[66] M. A. Elhadad, N. Karavasiloglou, W. Wulaningsih et al., "Metabolites, nutrients, and lifestyle factors in relation to

coffee consumption: an environment-wide association study," *Nutrients*, vol. 12, no. 5, p. 1470, 2020.

[67] E. Casiglia, P. Spolaore, G. Inocchio, and B. Ambrosio, "Unexpected effects of coffee consumption on liver enzymes," *European Journal of Epidemiology*, vol. 9, no. 3, pp. 293–297, 1993.

[68] M. Roche, P. Rondeau, N. R. Singh, E. Tarnus, and E. Bourdon, "The antioxidant properties of serum albumin," *FEBS Letters*, vol. 582, no. 13, pp. 1783–1787, 2008.

[69] C. Hoelzl, S. Knasmüller, K. H. Wagner et al., "Instant coffee with high chlorogenic acid levels protects humans against oxidative damage of macromolecules," *Molecular Nutrition & Food Research*, vol. 54, no. 12, pp. 1722–1733, 2010.

[70] K. Kempf, C. Herder, I. Erlund et al., "Effects of coffee consumption on subclinical inflammation and other risk factors for type 2 diabetes: a clinical trial," *The American Journal of Clinical Nutrition*, vol. 91, no. 4, pp. 950–957, 2010.

[71] S. Orrenius, M. J. Burkitt, G. E. N. Kass, J. M. Dypbukt, and P. Nicotera, "Calcium ions and oxidative cell injury," *Annals of Neurology: Official Journal of the American Neurological Association and the Child Neurology Society*, vol. 32, no. S1, pp. S33–S42, 1992.

[72] G. J. Burton and E. Jauniaux, "Oxidative stress," *Best Practice and Research: Clinical Obstetrics and Gynaecology*, vol. 25, no. 3, pp. 287–299, 2011.

[73] E. Olechno, A. Puścion-jakubik, K. Socha, and M. E. Zujko, "Coffee infusions: can they be a source of microelements with antioxidant properties?," *Antioxidants*, vol. 10, no. 11, p. Nov, 2021.

[74] E. Olechno, A. Puścion-Jakubik, K. Socha, and M. E. Zujko, "Coffee brews: are they a source of macroelements in human nutrition," *Foods*, vol. 10, no. 6, p. 1328, 2021.

[75] C. D. Rehm, J. C. Ratliff, C. S. Riedt, and A. Drewnowski, "Coffee consumption among adults in the United States by demographic variables and purchase location: analyses of NHANES 2011–2016 data," *Nutrients*, vol. 12, no. 8, pp. 1–13, 2020.

[76] S. Rajaraman, S. Selvanayagam, R. Chidambaram, A. S. Hospitals, and T. Nadu, "Correlation study between total calcium , ionized calcium, serum albumin and their significance with vitamin D," *Journal of Experimental Sciences*, vol. 2, no. 12, pp. 17–21, 2011.

[77] A. M. Uwitonze and M. S. Razzaque, "Role of magnesium in vitamin d activation and function," *Journal of the American Osteopathic Association*, vol. 118, no. 3, pp. 181–189, 2018.

[78] M. Verdoia, A. Schaffer, L. Barbieri et al., "Impact of gender difference on vitamin D status and its relationship with the extent of coronary artery disease," *Nutrition, Metabolism, and Cardiovascular Diseases*, vol. 25, no. 5, pp. 464–470, 2015.

[79] R. Morabitoa, A. Remigante, and A. Marino, "Protective Role of Magnesium against Oxidative Stress on SO," *Cellular Physiology and Biochemistry*, vol. 52, no. 6, pp. 1292–1308, 2019.

[80] A. A. Zheltova, M. V. Kharitonova, I. N. Iezhitsa, and A. A. Spasov, "Magnesium deficiency and oxidative stress: an update," *BioMedicine (Taiwan)*, vol. 6, no. 4, pp. 8–14, 2016.

[81] D. Hang, A. S. Kværner, W. Ma et al., "Coffee consumption and plasma biomarkers of metabolic and inflammatory pathways in US health professionals," *The American Journal of Clinical Nutrition*, vol. 109, no. 3, pp. 635–647, 2019.

[82] E. Loftfield, M. S. Shiels, B. I. Graubard et al., "Associations of coffee drinking with systemic immune and inflammatory markers," *Cancer Epidemiology, Biomarkers & Prevention*, vol. 24, no. 7, pp. 1052–1060, 2015.

[83] S. Jacobs, J. Kröger, A. Floegel et al., "Evaluation of various biomarkers as potential mediators of the association between coffee consumption and incident type 2 diabetes in the EPIC-Potsdam study," *The American Journal of Clinical Nutrition*, vol. 100, no. 3, pp. 891–900, 2014.

[84] E. Lopez-Garcia, R. M. Van Dam, L. Qi, and F. B. Hu, "Coffee consumption and markers of inflammation and endothelial dysfunction in healthy and diabetic women," *The American Journal of Clinical Nutrition*, vol. 84, no. 4, pp. 888–893, 2006.

[85] K. Yamashita, H. Yatsuya, T. Muramatsu, H. Toyoshima, T. Murohara, and K. Tamakoshi, "Association of coffee consumption with serum adiponectin, leptin, inflammation and metabolic markers in Japanese workers: a cross-sectional study," *Nutrition & Diabetes*, vol. 2, no. APRIL, p. e33, 2012.

[86] S. Jain, V. Gautam, and S. Naseem, "Acute-phase proteins: as diagnostic tool," *Journal of Pharmacy and Bioallied Sciences*, vol. 3, no. 1, pp. 118–127, 2011.

[87] A. Khera, G. L. Vega, S. R. Das et al., "Sex differences in the relationship between c-reactive protein and body fat," *The Journal of Clinical Endocrinology and Metabolism*, vol. 94, no. 9, pp. 3251–3258, 2009.

[88] G. Weaving, G. F. Batstone, and R. G. Jones, "Age and sex variation in serum albumin concentration: an observational study," *Annals of Clinical Biochemistry*, vol. 53, no. 1, pp. 106–111, 2016.

Hindawi
Oxidative Medicine and Cellular Longevity
Volume 2022, Article ID 7009863, 15 pages
https://doi.org/10.1155/2022/7009863

Review Article

Selenium Status and Its Antioxidant Role in Metabolic Diseases

Jing Huang, Ling Xie, Anni Song, and Chun Zhang

Department of Nephrology, Union Hospital, Tongji Medical College, Huazhong University of Science and Technology, Wuhan 430022, China

Correspondence should be addressed to Chun Zhang; drzhangchun@hust.edu.cn

Received 14 May 2022; Revised 11 June 2022; Accepted 23 June 2022; Published 6 July 2022

Academic Editor: Helena Moreira

Selenium (Se), in the form of selenoproteins, is an essential micronutrient that plays an important role in human health and disease. To date, there are at least 25 selenoproteins in humans involved in a wide variety of biological functions, including mammalian development, metabolic progress, inflammation response, chemoprotective properties, and most notably, oxidoreductase functions. In recent years, numerous studies have reported that low Se levels are associated with increased risk, poor outcome, and mortality of metabolic disorders, mainly related to the limited antioxidant defense resulting from Se deficiency. Moreover, the correlation between Se deficiency and Keshan disease has received considerable attention. Therefore, Se supplementation as a therapeutic strategy for preventing the occurrence, delaying the progression, and alleviating the outcomes of some diseases has been widely studied. However, supranutritional levels of serum Se may have adverse effects, including Se poisoning. This review evaluates the correlation between Se status and human health, with particular emphasis on the antioxidant benefits of Se in metabolic disorders, shedding light on clinical treatment.

1. Introduction

The trace element selenium (Se), originally regarded as a toxin, is now recognized as an essential micronutrient [1]. Researchers have found that the Se-containing amino acid selenocysteine (Sec) is the major form of Se in cells. The Sec-containing protein, selenoprotein, is largely responsible for the biological effects of Se [2]. Although selenoproteins are widely expressed in many species, the distribution of selenoproteins varies greatly among species. It has been established that there are 25 genes coding for selenoproteins in the human genome [3]. Most selenoproteins, including glutathione peroxidases (GPx), thioredoxin reductases (TrxR), and iodothyronine deiodinases (DIO) have well-defined oxidoreductase functions, exerting an important role in preventing oxidative injury as an intracellular antioxidant [4]. In addition, several selenoproteins, such as selenoprotein F (SEP15), selenoprotein S (SELS), selenoprotein M (SELM), selenoprotein T (SELT), selenoprotein N (SELN), and selenoprotein K (SELK), are regarded as endoplasmic reticulum-(ER-) resident selenoproteins and are involved in redox sensing and regulation, the unfolded protein response (UPR), and calcium homeostasis [5]. Selenoprotein P (SEPP1), selenoprotein H (SELH), selenoprotein M (SELM), SELT, SEP15, and selenoprotein W (SELW) possess thioredoxin-like domains, suggesting a potential redox-related functions [2]. Selenoproteins represent diverse molecular pathways and biological functions, most notably oxidoreductase functions [2, 3].

In recent years, many studies have shown that the antioxidant effects of Se and selenoproteins have led to great advances in human health and treatment of disease [1, 6–8]. Moreover, the importance of Se supplementation in the prevention and treatment of some diseases has been highlighted. Recently, numerous studies have illustrated the crucial role of Se in chronic metabolic diseases, including cardiovascular disease (CVD), type 2 diabetes mellitus (T2DM), and nonalcoholic fatty liver disease (NAFLD) [9–12]. Previous studies have highlighted the role of excess reactive oxygen species (ROS) in the complex pathogenesis of metabolic diseases [13]. Se, as an antioxidant, shows great potential for redox regulation and the maintenance of cellular homeostasis and metabolism [14]. Many studies have reported that serum Se status is related to the risk of metabolic diseases, and Se supplementation may be a

promising approach in patients with low Se levels. In addition, Se levels have been positively associated with blood glucose levels, insulin resistance (IR), and total cholesterol (TC), triglyceride (TG), high-density lipoprotein (HDL), and low-density lipoprotein (LDL) levels, indicating a significant role of Se in glucose and lipid metabolism [15, 16]. Therefore, the protective action of Se, mainly focused on boosting internal antioxidant defense in metabolic diseases, has attracted much attention. However, the molecular mechanism underlying the action of Se in metabolic diseases has yet to be elucidated.

This review summarizes the current knowledge regarding Se status in human health, including Se hierarchy, Se evaluation, Se deficiency, and Se poisoning. Furthermore, we elaborate on the antioxidant properties of Se in the risk of metabolic diseases and from the perspective of Se supplementation trials in the treatment of metabolic diseases.

2. Selenium Status in Human Health

Diet is the main source of Se, and approximately 80% of dietary Se is absorbed, depending on the type of food consumed [17]. The Se content in food varies geographically, both within and between countries, and the amount of Se in the diet largely depends on where crops are grown and cultivated, the soil to which animals are exposed, and the foods consumed [1]. Dietary Se is obtained from a wide variety of food sources, including bread and cereals, meat, fish, eggs, vegetables, nuts, milk, and dairy [1, 7, 8]. Knowing the distribution of Se in each food group can provide a basis for dietary recommendations to maintain a Se balance. At nutritional levels, Se is mainly incorporated into selenoproteins, such as SEPP1 and GPx, to exert its biological functions. Studies have shown that dietary Se is mainly absorbed from the duodenum and cecum through a sodium pump via active transport [18]. SEPP1, which accounts for approximately 60% of serum Se, is the major form of Se circulating in the bloodstream. SEPP1 is synthesized and secreted by the liver and transported to other tissues through systemic circulation, and the plasma SEPP1 is absorbed by apolipoprotein E receptor-2 (apoER2) in the brain, testis, and other tissues and by megalin in the kidney (Figure 1) [1, 19–21].

3. Se Hierarchy

Although all tissues can synthesize selenoproteins, the amount of Se supplied and the consequences of Se deficiency differ across tissue types. In general, Se is stored in organs and tissues at varying densities: 30% in the liver, 30% in the muscle, 15% in the kidney, 10% in plasma, and 15% in other organs [18]. However, selenoprotein synthesis is regulated by Se availability in the diet. Under conditions of Se deficiency, not all organs or tissues obtain Se equally. In fact, Se retention and redistribution occur in the brain, thyroid gland, testis, and skeletal muscle (SKM), while the levels of Se in the liver, muscle, skin, and other tissues decrease, resulting in the formation a tissue Se hierarchy (Figure 1) [19, 22–24].

As previously reported, the brain expresses all types of selenoproteins [25, 26]. The results obtained from the study of rats fed on a Se-deficient diet showed that while most organs lose up to 90% of Se, the brain retains >75% of Se [27]. Moreover, the thyroid gland is rich in Se and expresses a variety of selenoproteins [28]. Similarly, it was reported that the level of serum Se was decreased in SEPP1-knockout mice, while the thyroid gland morphology, thyroid GPx activity, thyroid Se concentration, and serum levels of thyroid-stimulating hormone (TSH), triiodothyronine (T3), or thyroxine (T4) were all within the normal range, suggesting that low levels of serum Se or SEPP1 do not necessarily interfere with the regular functioning of the thyroid hormone (TH) axis [24]. As for the testes, some studies have indicated that testicular mRNA abundances of GPx4, selenoprotein V (SELV), and TrxR3 are not affected by levels of dietary Se supplementation and were much higher at 6-21 weeks old than at 2 and 104 weeks of age [29]. The total testicular GPx4 level was found to be unaffected in response to diets containing <0.01–5 mg Se/kg, suggesting that selenoproteins in the testis are resistant to the impact of dietary Se levels in order to maintain male reproductive activity [30]. Similarly, neither late nor early developmental disruption of DIO2 in mouse SKM was found to impair muscle function. It is conceivable that, as in the brain and thyroid gland, residual DIO2 in other SKM cells relies on paracrine function and is supplied with sufficient T3 to develop skeletal myocytes in order to maintain SKM function [31–33]. In summary, when Se was deficient, the brain, thyroid gland, testes, and SKM were resistant to Se deficiency (Figure 1). More importantly, selenoproteins in the thyroid were preferentially supplied and even less dependent on serum Se or SEPP1 levels than those in the brain, thyroid gland, and SKM, which indicates the priority of the Se and selenoenzyme supply in the thyroid gland under Se deficiency. On the other hand, previous studies have shown that selenoprotein expression is differentially regulated by Se availability. For example, some selenoproteins (GPx1, SELW, and SELH) are highly regulated by Se availability and belong to the group of stress-related selenoproteins. Other selenoproteins (GPx4, TrxR1, and TrxR3) are less regulated by dietary Se intake and belong to a subclass of housekeeping selenoproteins, indicative of the greatest changes in selenoprotein levels under Se availability conditions [2]. Further studies are required to validate the specific mechanisms that dictate the hierarchy of selenoprotein expression.

4. Se Evaluation

At the individual level, Se status can be assessed from hair, toenails, and urinary analyses or blood analysis (including whole blood, plasma, serum, or erythrocyte/platelet fractions) [1]. In general, the level of plasma or serum Se is one of the most used methods for evaluating Se status and intake [34]. For long-term Se status, the toenail and hair Se levels are often employed as markers. Se urinary excretion is closely correlated with plasma and serum levels and can be used to monitor recent dietary intake of Se [34, 35]. Moreover, bioassays of selenoproteins in different blood

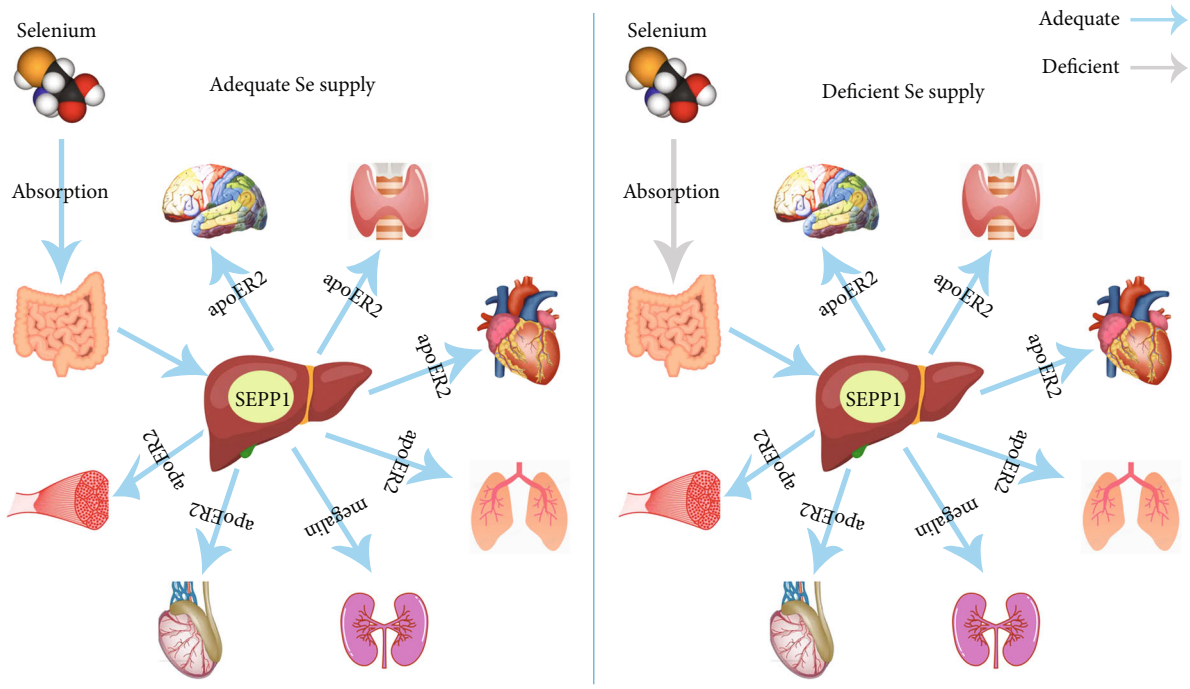

Figure 1: Outline of selenium absorption and transportation under the conditions of adequate and deficient Se supply. In general, Se is mainly obtained through the diet and absorbed via the duodenum and caecum. SEPP1, the major transport form of Se, is synthesized and secreted by the liver and transported to other tissues through systemic circulation. When Se supply is adequate, plasma SEPP1 is absorbed by apoER2 in the brain, thyroid gland, testis, and other tissues and by megalin in the kidney. When Se supply is deficient, the brain, thyroid gland, testis, and SKM retain or redistribute Se to maintain physiological function, while the levels of Se in the liver, lung, and other tissues rapidly decrease, resulting in a tissue Se hierarchy.

fractions may provide more accurate estimates of physiological Se status [36]. For example, the concentration of serum SEPP1 is sensitive to dietary Se content; therefore, the level of serum SEPP1 was considered an index of Se nutritional status [37, 38]. However, a high correlation between serum SEPP1 concentration and total Se content in elderly men, young men, and elderly women has been reported, but not in young women, suggesting sexual dimorphism of SEPP1 as a biomarker of Se status in young subjects [39]. Platelet GPx1 and GPx4 activities are recommended as accurate indicators of Se status [40–42]. Burk et al. conducted a randomized controlled trial (RCT) to evaluate the effect of chemical form of Se (sodium selenite, high-Se yeast, and selenomethionine) on plasma biomarkers (Se level, SEPP1 concentration, and GPx activity) and urinary Se excretion in a high-dose human supplementation trial. This study found that supplementation with selenomethionine (SeMet) and Se yeast increased the plasma Se concentration in a dose-dependent manner, but selenite did not [43]. The increased Se levels were related to the amount of SeMet administered. Neither GPx activity nor SEPP1 concentration responded to Se supplementation. Urinary Se excretion was greater after SeMet than after selenite, with excretion after yeast being intermediate and not significantly different from either of the other two [43]. This indicates that plasma Se levels are useful in monitoring the compliance and safety of Se supplementation as SeMet, but not as selenite. Plasma Se levels seem to reflect the SeMet content of yeast but not the other yeast Se forms. As judged by urinary Se excretion, Se in the form of SeMet is better absorbed than selenite [43]. In conclusion, there is a need to select a more appropriate index to reflect the Se status according to specific situations, such as Se deficiency, Se supplementation, individuals, and environmental factors. Further studies are needed to evaluate the strengths and limitations of all potentially available biomarkers of Se measurement in different population groups, including the effects of intake, baseline Se status, duration of intervention, and the possible confounding effects of genotype.

5. Se Intake and Diseases

In contrast to many other micronutrients, the intake of Se varies hugely worldwide, ranging from deficiency (associated with Se-deficiency diseases) to toxic concentrations (associated with Se poisoning) [7, 44]. Dietary Se intake ranges from 7 to 4990 μg per day, with mean values of 40 μg per day in Europe and 93 (in women) to 134 μg (in men) per day in the USA [1, 45, 46]. Data from various Asian, European, and Middle Eastern countries show that dietary Se intake and Se status are suboptimal or even low in these populations [47]. The World Health Organization (WHO) indicated that over 40 countries and regions globally suffer from Se deficiency [48]. The recommended dietary allowance of Se ranges from 55 to 70 μg per day, which is typically based on the Se intake needed to saturate GPx activity [49]. However, there is no consensus on a specific cut-off to define Se deficiency, and what is considered a normal range is

usually defined based on Se levels in a healthy population in a specific geographical area [50]. Therefore, the minimum requirement for Se intake is to prevent the occurrence of Se-deficient diseases, such as Keshan disease (KD), an endemic cardiomyopathy. The recommended intake of Se has been calculated from the requirement for optimum plasma GPx activity that must, because of the hierarchy of selenoproteins, also consider the amounts needed for normal levels of other biologically necessary Se compounds [50].

6. Se Deficiency and Keshan Disease (KD)

KD is a primary endemic cardiomyopathy that only occurs in severely low-Se areas from the northeast to the southwest of mainland China [51]. In other words, the main cause of KD is Se deficiency. Although KD has been effectively controlled in most endemic areas with Se supplementation therapy, chronic and latent KD still exist in some endemic areas with poor economic conditions [52]. Extensive evidence has shown that Se deficiency is strongly associated with KD from an etiological perspective; thus, Se levels are useful for assessing the effectiveness of KD prevention, control, and elimination [1, 7, 51].

Recently, a large and wide scope study, including a total of 6,382 individuals recruited from 1,688 counties in 29 provinces in mainland China, was conducted to explore the role of serum Se and SEEP1 levels in KD. The results showed that Se deficiency may still exist among residents living in some KD-endemic areas, who are still at risk of KD, suggesting the need for a diet rich in Se for the residents in KD-endemic areas [53]. However, the mean serum SEPP1 levels of the residents living in the KD-endemic counties were not significantly lower than those of the residents living in the KD nonendemic counties, which indicated that SEPP1 may not properly reflect the Se status [53]. However, the serum SEPP1 levels in 2,351 subjects living in rural areas, general cities, and developed cities in 15 KD-endemic provinces and 13 KD nonendemic provinces in China were measured [54]. The mean serum SEPP1 levels of residents in KD-endemic areas were significantly lower than those in nonendemic areas, and serum SEPP1 levels were low among individuals in the KD-endemic provinces of Shandong, Inner Mongolia, and Heilongjiang, which indicated that the spatial distribution of SEPP1 was positively correlated with per capita consumption expenditure and soil Se [54]. A local study provided further evidence of SEPP1 as a biomarker for KD [55]. In addition, a spatial ecological study on hair Se levels in KD in Heilongjiang Province, China, showed that the median hair Se levels of the residents in the KD-endemic areas were significantly lower than those in nonendemic areas. Measuring the Se levels in the hair of residents of KD-endemic areas can be a molecular marker of Se nutritional status and provide visualized evidence for the evaluation of KD elimination from the aspect of Se nutrition [56, 57]. Taken together, these data support the idea that Se deficiency is widely accepted as a fundamental cause of KD, and serum Se levels, serum SEPP1 levels, and hair Se levels can be used as biomarkers for monitoring Se status in residents in KD-endemic areas to some degree.

As Se deficiency contributes to the risk of KD, Se supplementation has been proposed to play an important role in the prevention and elimination of KD. In a retrospective long-term follow-up analysis performed on a group of 302 chronic KD patients, 173 (56.3%) of the KD patients were administered Se supplementation until the endpoint of follow-up. Using multivariate analyses, this study clarified that Se supplementation was associated with a decreased risk of cardiac death [58]. Moreover, a randomized double-blind design of children with KD was conducted to assess the relative bioavailability of selenite versus organic Se yeast in a Se-deficient area in China and showed that both forms of Se supplementation (selenite and organic Se-yeast) were equally effective in increasing GPx activity, and Se-yeast provided a longer-lasting body pool of Se [59]. Furthermore, a systematic review and meta-analysis were conducted to evaluate the effectiveness of Se supplementation in the prevention of KD. The administration of Se supplements among the residents of KD-endemic areas significantly reduced the incidence of KD. The protection rates of Se supplements were >80% in 35 studies, and the overall effect (risk ratio) was 0.14 [60]. Therefore, Se supplementation may be a potential strategy for KD prevention and treatment.

7. Se Poisoning

Although Se is an essential micronutrient for humans, high levels of Se are harmful, and acute or chronic toxicity resulting from high Se exposure has attracted much attention. Acute symptoms of Se intoxication include abdominal symptoms, such as vomiting, pain, and nausea, as well as garlic breath and cardiac symptoms [61]. Mortality is a serious consequence of acute selenium poisoning. In general, the normal intake levels of Se are between 11 and 280 μg/day [62], the plasma levels of Se are approximately 100 μg/L, and the urinary levels of Se range from 10 to 85 μg/L in the general population [63–65]. Death from Se poisoning has been characterized by plasma Se levels of 300, or as high as 3,000 μg/L, compared to normal levels of 100 μg/L. Nevertheless, individuals with plasma Se levels up to 3,000 μg/L without mortality have also been documented [61]. Similarly, urinary levels of Se related to mortality ranging from 170 to 30,000 μg/L have been reported, and no deaths have been observed in humans with urinary Se levels as high as 1,000 μg/L compared to normal levels of 20–90 μg/L [61]. In recent years, many Se poisoning events have been reported, including large food poisoning incidents and individual dietary poisoning cases.

In 1983–1984, a misformulated Se supplement containing 27,300 μg Se per tablet was taken by 13 individuals, resulting in selenosis symptoms, including abdominal pain, diarrhea, nausea, peripheral neuropathy, fatigue, irritability, hair, and nail changes [66]. Moreover, a March 2008 voluntary market recalls supplement products responsible for the most serious Se toxicity outbreak that occurred in the US, warning consumers that these products caused serious adverse reactions, including significant hair loss, muscle

cramps, diarrhea, joint pain, and fatigue, within 10 days of ingestion [66]. The peak levels of Se in these subjects were up to 18.3 μg/g in toenails and 44.1 μg/g in fingernails. Nail samples accurately reflect exposure during this Se toxicity outbreak, which results in long-term or permanent adverse health effects [66]. As for the individual case, a 75-year-old man ingested 10 g of sodium selenite and gradually developed abdominal pain, diarrhea, hypotension, hypokalemia, poor perfusion, and cardiac arrest and ultimately died six hours after exposure [67]. Similarly, a 24-year-old man exhibited typical signs and symptoms of acute Se poisoning, presenting with nausea and vomiting, followed by pulmonary edema and rapid cardiovascular collapse approximately 3 to 4 h after ingestion of a gun bluing agent (likely containing selenous acid). One hour after the suspected ingestion, his serum Se levels reached up to 30,000 μg/L [68]. Moreover, deaths from different types of Se poisoning, such as Se dioxide, selenic acid, and sodium tetraoxoselenate poisoning, are not uncommon [69–71]. In addition, a 51-year-old man and a 44-year-old woman experimented with the daily ingestion of supplement containing Se powder, magnesium powder, zinc drops, and a teaspoon of laxative salts. A few days later, they experienced severe nausea, diarrhea, headache, weight loss, and worsening general condition, as well as considerable diffuse hair loss and white-brownish discoloration of the nails. The serum Se levels in the woman and man were 347 and 387 μg/L, respectively, suggesting a chronic Se poisoning status [72]. Moreover, a previously healthy woman suddenly presented with nausea, vomiting, headache, and dizziness a few days after the ingestion of paradise nuts, as well as massive hair loss after approximately two weeks and discoloration of the fingernails [73]. Detailed diagnostic procedures did not reveal any pathological results, and therapeutic measures did not show any effect. While the thallium and arsenic levels were within the normal range in plasma, the plasma Se levels reached toxic values approximately 8-9 weeks later [73]. This case suggests that we cannot overlook the possibility of Se poisoning in the clinical diagnosis.

In summary, although acute or chronic Se poisoning is rarely observed, its consequences can be serious and even fatal. Thus, attention must be paid to foods with a high Se content to avoid eating too much by mistake. Studies on the Se content in humans have revealed that toxic effects occur following a daily intake of at least 300 μg [72]. In addition, noncritical Se intake without a physician's recommendation should be urgently dissuaded. As a part of the therapeutic strategy, there is a need to consider its limited therapeutic range to avoid overdose and related toxicity.

8. Se Levels and Metabolic Diseases

Prospective studies have found that a high Se status is associated with decreased mortality, wherein low plasma Se was related to increased overall and cancer mortality [74–76]. Moreover, Se levels were also associated with the incidence of new-onset heart failure, anemia, iron deficiency, high C-reactive protein (CRP) levels, and current smoking [74]. Recently, it was reported that serum Se is related to multiple indicators of metabolic syndrome, including high levels of blood glucose, cholesterol, and body mass index (BMI) in the general adult population [74]. For instance, a cross-sectional analysis of 4,339 participants found that Se levels were positively associated with IR and blood glucose; that is, a 10 μg/L increase in Se was associated with a 1.5% increase in insulin [15]. On the other hand, a large cross-sectional study of 8,198 rural Chinese reported that serum Se levels were positively correlated with total cholesterol (TC), TG, HDL, and LDL, and elevated serum Se levels were related to an increased risk of dyslipidemia, which indicated the crucial role of Se status in lipid metabolism [16]. These studies indicate that high levels of Se are associated with IR and dyslipidemia. Therefore, it has been proposed that the relationship between Se status and various health outcomes, especially in metabolic diseases, requires close attention. In summary, these results indicate the relevance of Se status in public health. Understanding the association between Se status and human health is essential for developing effective public health policies, guiding applicable clinical practice, and counteracting health issues associated with Se deficiency.

Due to the antioxidant activity of Se, its protective role in metabolic diseases, including coronary heart disease (CHD), HT, T2DM, and nonalcoholic fatty liver disease (NAFLD), has been previously demonstrated [1, 6, 8, 77]. In addition, considering the crucial role of Se in the cellular antioxidant defense system, therapeutic strategies involving Se supplementation for the treatment of certain diseases have been underway for many years [77, 78]. Recently, this practice has achieved promising results in the prevention and treatment of metabolic diseases, including CHD, HT, NAFLD, and T2DM [6, 79–82].

9. Coronary Heart Disease (CHD)

Coronary atherosclerotic heart disease is caused by the narrowing or occlusion of the vascular lumen due to coronary atherosclerosis (AS), which eventually leads to myocardial ischemia, hypoxia, or necrosis, also known as CHD [83]. Oxidative stress, endothelial dysfunction, hyperlipidemia, and inflammation are involved in the pathogenesis of AS. As an antioxidant agent, several prospective investigations have declared the association between Se level and cardiovascular risk and outcomes [1, 2, 7].

Recently, a meta-analysis compared the Se levels between CHD patients and healthy individuals and found that the level of Se was lower in CHD patients than in healthy individuals, indicating that Se status may have some effect on the risk of CVD [84]. A nested case-control study of 1,621 CHD cases in the prospective Dongfeng-Tongji cohort also found that CHD risk was inversely associated with plasma Se levels [85]. Another meta-analysis, including 25 observational studies, further clarified that a 50% increase in Se level was associated with a 24% reduction in CHD risk in observational studies, suggesting an inverse correlation between Se levels and CHD risk [86]. Moreover, a meta-analysis including 16 prospective observational studies showed a nonlinear relationship between CHD risk and blood Se levels across a

range of 30-165 μg/L and a significant benefit of CHD within a narrow Se range of 55-145 μg/L [87]. In a small Chinese cohort study of 1,103 cohort participants, the inverse association between CHD mortality and serum Se level was 73 μg/L [88]. In addition, a study using data collected from 17,867 individuals showed a U-shaped association between dietary Se intake and all-cause mortality, wherein the serum Se levels were negatively but nonlinearly associated with the incidence of CHD [89]. These analyses highlight the significant benefit of higher levels of Se in the prevention of CHD. Furthermore, several selenoproteins play vital roles in the heart; for example, low Se levels disrupt the synthesis of a subgroup of stress-induced selenoproteins, including GPx1, leading to a shortage of one or more of these crucial proteins in the heart [90]. A case-control study on 85 CHD patients indicated a reduction in GPx1 activity related to increased CHD severity, which suggested that GPx1 activity may be a useful marker for predicting and monitoring CHD [91]. In summary, Se status and GPx1 are tightly related to the incidence and mortality of CHD. Additional research is needed to confirm whether Se may attenuate the adverse effects of CHD and to investigate the potential underlying mechanisms.

Based on the inverse relationship between Se levels and CHD risk, moderate Se supplementation may be beneficial in preventing CHD risk. Among six RCTs, including a total of 17,766 participants, four trials used Se supplementation combined with other vitamins or minerals, while two trials used Se supplementation alone. Se supplementation was found to result in a nonsignificant 11% reduction in coronary events, as the trials were small and Se was administered in combination with other vitamins or minerals in all but two trials [86]. Another RCT illustrated that probiotic and Se cosupplementation had a favorable effect on glucose and lipid metabolism and anti-inflammatory and antioxidant capacity, compared with placebo in CHD [92]. Moreover, a five-year prospective RCT among 443 Swedish citizens aged 70–88 years showed that the combined supplementation of Se and coenzyme Q10 significantly reduced CVD mortality, accompanied by a decreased level of N-terminal pro-BNP and a better cardiac function score, compared with the placebo group [93]. Even after 12 years, CVD mortality was significantly reduced in the actively supplemented group, as well as in subgroups of patients with diabetes, HT, ischemic heart disease, or impaired functional capacity, compared with the placebo group [94]. These results suggest that the protective action of Se supplementation was not confined to the intervention period but persisted during the follow-up period [94]. Alehagen et al. further indicated that supplementation with Se and coenzyme Q10 resulted in lower concentrations of both copeptin and MR-proADM (as oxidative stress biomarkers) in a four-year prospective RCT among 437 elderly Swedish citizens [95]. A secondary analysis of this RCT showed a decreased level of CRP and sP-selectin (as inflammation biomarkers) in the active supplementation group compared with the placebo group, indicating a significant effect of Se on inflammation and AS [96]. Recently, Alehagen et al. used structural equation modelling to explain the underlying mechanisms of the protective action of Se in CVD and found that Se supplementation reduced inflammation and oxidative stress, which reduced myocardial fibrosis and improved myocardial function [97]. However, a meta-analysis including 16 RCTs with 43,998 participants reported that Se supplementation significantly lowered serum CRP levels and increased GPx activity but had no effect on CHD mortality and lipid profile [98]. Another study showed that oral Se supplements (200 μg/day) for two weeks to 144 months significantly increased blood Se levels by 56.4 μg/L, whereas oral Se supplements (100 μg/day) for 6–114 months had no effect on CHD, suggesting that Se supplementation had no effect on CHD [87]. Although the results of these clinical trials are not entirely consistent and need to be further studied, evidence from animal studies suggests that Se may protect against experimental AS. In the apolipoprotein E-deficient mouse model of AS, dietary SeMet supplementation increased Se levels and GPx activities, reduced lesion burden and inflammatory response, and improved vessel function compared with the nonsupplemented group [99]. Xiao et al. also showed consistent results that oral administration of both Se nanoparticles (SeNPs) and Na_2SeO_3 for 10 weeks significantly reduced AS lesions in mouse aortae by alleviating vascular endothelial dysfunction [83]. In summary, few RCTs have addressed the efficacy of Se supplementation on CHD risk, and their findings remain inconclusive. The preliminary results of studies conducted on animal models may not truly reflect the effectiveness of Se supplementation in preventing or treating CHD; evidence from large RCT is needed to confirm the feasibility of Se supplementation as the treatment therapy for CHD.

10. Hypertension (HT)

HT is a cardiovascular syndrome that is characterized by elevated systemic arterial pressure. Oxidative stress, inflammation, and endothelial dysfunction are considered the major pathological factors associated with HT [100]. Some studies have shown that individuals with HT can produce more ROS and have an impaired antioxidant defense system, both of which increase oxidative stress and lead to an ongoing vicious cycle [101]. ROS, in turn, activate chemoreflex and suppress baroreflex, thereby stimulating the sympathetic nervous system and causing HT [102]. Se, an essential micronutrient with antioxidant properties, has been hypothesized to play a protective role against HT.

Xie et al. conducted a 20-year cohort study and found that the cumulative intake of Se was inversely associated with the risk of HT only in northern residents (low-Se zone), but not in southern residents, suggesting that the association between Se intake and the risk of HT varied according to regions in China [80]. A 10-year prospective study conducted in South Africa found that baseline Se levels were negatively associated with blood pressure (BP), indicating a vascular protective effect of Se [103]. Furthermore, in low soil Se zones, high Se intake may be beneficial for the prevention of HT, as low Se levels are associated with left ventricular hypertrophy, which is the main pathological change leading to HT [104]. Recently, Wang et al. conducted a secondary analysis and inferred a significant inverse association between plasma Se levels and HT risk [105]. These

studies suggested that low Se levels were a risk factor for HT; however, opposing findings have since been reported. For instance, a cross-sectional study of 9,076 urban and rural residents in Shandong Province of China indicated that higher Se levels were associated with an increased risk of HT in women, but not in men, by logistic regression analysis, suggesting that high Se levels in women were more likely to increase the risk of HT compared to similar levels in men [106]. Another cross-sectional study concluded that chronic overexposure to environmental Se elevated BP, particularly in women [107]. Moreover, a longitudinal study on 2,000 elderly individuals indicated that higher Se levels were associated with higher BP and HT risk [108]. Surprisingly, these studies showed that high Se levels may play a harmful role in the prevalence of HT, which is in contrast to the results of previous studies. In contrast, in a cross-sectional study in China, high environmental Se exposure increased the prevalence of HT, but there was no significant association between Se level and the risk of HT [109]. Tan et al. reported a U-shaped association between serum Se levels and all-cause or cardiovascular mortality in patients with HT [110]. The nadir mortality of all-cause and cardiovascular events occurred at serum Se levels of 136 and 130 μg/L, respectively [110]. In conclusion, the correlation between Se levels and HT risk remains unclear. Whether positive, negative, or U-shaped, further studies, especially large RCTs, will be needed to address these contrasting results.

Considering the controversial role of Se in HT, the potential benefit of Se supplementation on the risk of HT remains to be elucidated. Currently, no RCTs have been published wherein Se supplementation is the sole intervention for HT. However, cosupplementation in Se-depleted areas has been shown to reduce the risk of gastric cancer, stroke, and overall mortality, but not in HT and CVD [111]. In addition, a larger RCT that cosupplemented Se with β-carotene or α-tocopherol also showed no difference in BP compared to control groups [112]. Moreover, various studies have shown that increasing Se levels above the recommended daily intake are not beneficial and lead to HT, diabetes, and hyperlipidemia [113]. In summary, additional experimental evidence and RCT data are needed to gain further insights into the role of Se in the risk of HT, particularly to clarify the underlying mechanisms. The application of Se supplementation for the prevention of HT requires further discussion.

11. Nonalcoholic Fatty Liver Disease (NAFLD)

NAFLD, including simple steatosis (NAFL) and nonalcoholic steatohepatitis (NASH), is the most common cause of liver disease worldwide, and its incidence is increasing in parallel with obesity and diabetes [114]. NAFLD is a complex disease that is modulated by numerous mechanisms, including metabolic, genetic, and gut microbial factors [115]. Some injurious processes, such as oxidative stress, UPR response, and lipotoxicity, contribute to liver damage, progressive fibrosis, and cirrhosis [114]. Owing to the role of Se in lipid metabolism and antioxidant defense, extensive evidence has suggested that Se may contribute to the development of NAFLD.

Recently, a cross-sectional analysis of 3,827 adults without viral hepatitis, hemochromatosis, or alcoholic liver disease indicated a nonlinear association between serum Se levels and alanine aminotransferase (ALT) activity and NAFLD risk [81]. These positive associations were only found above a serum Se level of 130 μg/L, whereas no association was observed below this value [81]. Another large cross-sectional study of 8,550 adults in China demonstrated that increased plasma Se levels were associated with an increased risk of NAFLD, which may be mediated by IR and oxidative stress [116]. In addition, this study found that elevated plasma Se levels were related to higher TG, LDL, ALT, aspartate aminotransferase (AST), gamma-glutamyltransferase (γ-GT), fasting plasma glucose, post-loading plasma glucose, and IR [116]. However, previous studies have shown that Se levels are low in patients with NAFLD and cirrhosis. Reja et al. reported an inverse relationship between serum Se levels and the risk of advanced liver fibrosis, indicating that Se may be beneficial for the prevention of liver fibrosis in the development of NAFLD [117]. In contrast, several animal studies have indicated that Se exposure could induce increased serum liver enzyme levels, the activation of Kupffer cells, and higher hepatic IR and TG levels in animals, suggesting that Se exposure may be associated with the development of NAFLD [116]. Regarding the role of selenoproteins in NAFLD, Day et al. performed a transcriptomic exploration of the expression of selenoproteins in NAFLD and healthy individuals. Bioinformatics analysis revealed lower levels of TrxR3 and SELO expression in NAFLD, while SELM, DIO1, GPx2, and GPx3 were highly expressed in NAFLD compared with the healthy group [118]. A case-control study showed that SEPP1 levels were positively correlated with NAFLD risk factors including BMI, ALT, AST, and γ-GT. In addition, the overexpression of SEPP1 aggravated lipid accumulation and inhibited AMPK/ACC phosphorylation, providing insights into SEPP1 in the diagnosis and treatment of NAFLD [119]. Caviglia et al. also clarified a close association between SEPP1 levels and altered metabolic profiles and degree of hepatic fibrosis [120]. However, whether Se levels are positively or negatively associated with NAFLD risk in humans remains unclear. Thus, the importance of selenoproteins in NAFLD cannot be ignored, and further research is needed to demonstrate the precise role of Se in NAFLD.

Although the specific role of Se in NAFLD remains unclear, few studies have investigated the effects of Se supplementation in NAFLD patients. In animal experiments, feeding NAFLD mice with Se for four months decreased AST and ALT activity, hepatic damage-associated diagnostic markers, and serum lipid levels, suggesting a protective role of Se supplementation in NAFLD [121]. Another animal experiment found that Se supplementation had a beneficial effect on hepatic injury in mice [122]. Recently, Wang et al. found that Se supplementation was beneficial for alleviating hepatic injury and IR during NAFLD, which was mediated by activating the KEAP1/NRF2 pathway [123]. In conclusion, animal studies have indicated that Se supplementation may

be a potential therapy for the prevention and treatment of NAFLD. However, these preliminary experiments conducted on animal models may not truly reflect the specific value of Se supplementation in clinical trials. Therefore, further clinical trials will be needed to elucidate the role of Se supplementation in patients with NAFLD.

12. Type 2 Diabetes (T2DM)

T2DM is characterized by hyperglycemia, IR, and a relative decrease in insulin secretion, which often occurs in younger individuals [82]. The pathogenesis of T2DM is complex, and IR and β cell failure are two core pathophysiological defects in T2DM. Redox imbalance can provide a reasonable explanation for the occurrence and progression of T2DM [124]. Recently, several studies have reported that elevated ROS levels in pancreatic β cells are associated with elevated fasting plasma insulin levels and the absence of IR, resulting in pancreatic B cell dysfunction and subsequent progression to T2DM [102]. Moreover, intracellular ROS accumulation causes defective angiogenesis in response to ischemia, activates a number of proinflammatory pathways and genes, and inactivates antiatherosclerosis enzymes, resulting in the development of diabetes complications, such as AS and cardiomyopathy, which is caused in part by pathway-selective IR [125]. Thus, increased superoxide production is the central and major mediator of diabetic tissue damage. Based on the role of Se in glucose metabolism and antioxidant defense, Se may be involved in the pathogenesis of T2DM [126].

Several studies have demonstrated the importance of Se in T2DM patients. A case-control study showed that T2DM patients had higher levels of Se than healthy individuals [126]. A case cohort study also found that higher serum Se levels were associated with an increased risk of T2DM [127]. In a meta-analysis, eight observational studies demonstrated a statistically significant positive association between Se levels and the risk of T2DM [82]. Similarly, a linear association between plasma Se level and T2DM risk was observed in a Spanish study [128]. Moreover, a prospective cohort study in Italy showed that higher dietary Se intake increased the risk of the first hospitalization for T2DM [129]. Although many studies have reached a consensus that high Se exposure is a risk factor for T2DM, the relationship between dose and effect remains unclear. Thus, Vinceti et al. conducted a meta-analysis of 34 nonexperimental studies and found a direct relationship between Se exposure and T2DM risk. As a result, a clear and roughly linear trend was observed in subjects with a higher serum Se level of 140 μg/L. At Se levels up to 160 μg/L, the risk ratio was as high as 1.96, indicating a dose-response association between Se exposure and T2DM [130]. In contrast, serum Se levels have been reported to be positively correlated with insulin levels and IR markers [15]. Regarding the role of selenoproteins in T2DM, SEPP1 was highly expressed in T2DM patients, leading to IR by eliminating physiological ROS required for insulin signal transduction [131]. Mita et al. isolated SEPP1-neutralizing antibodies that improved glucose tolerance, IR, and insulin secretion in a T2DM mouse model, suggesting that elevated SEPP1 levels are an effective target for T2DM treatment [132]. A prospective study in the Japanese population even indicated that SEPP1 may be a marker for predicting hyperglycemia [133]. These studies clarified that the association between serum Se and T2DM may depend on the upregulation of hepatic SEPP1 biosynthesis under IR and hyperglycemia conditions [134]. Similarly, SELS is involved in the pathogenesis of T2DM through inflammatory responses, oxidative stress, and ER stress [135]. Taken together, these results highlight the significant role of Se and selenoprotein in T2DM. However, the relationship between Se and T2DM varies in RCTs and observational studies, and its specific role and mechanism have yet to be fully elucidated.

With respect to the contributing factor of Se in T2DM, it is worth exploring whether Se supplementation can increase the risk of T2DM. A meta-analysis showed that Se supplementation increased the risk of T2DM by 11% compared with placebo, with a higher risk ratio in women than in men [130]. In addition, an RCT on 54 patients with T2DM and CHD found that probiotics and Se cosupplementation improved mental health parameters and metabolic profiles in T2DM patients [92]. In contrast, some studies have reached inconsistent conclusions. To examine the effect of long-term Se supplementation on the prevalence of T2DM, a secondary analysis of 1,202 subjects without T2DM at baseline was performed [136]. During an average follow-up of 7.7 years, Se supplementation had no effect on the risk of T2DM in analyses stratified by age, sex, BMI, and smoking status [136]. Similarly, Stranges et al. reported that there was no significant change in HbA1c in an elderly European population with a low Se status after 2 years of Se supplementation [137]. Moreover, a meta-analysis of RCTs indicated that a higher risk of T2DM was not observed in the Se supplementation group compared to the placebo group [82]. A systematic review of RCTs also found no evidence to support the increased risk of Se supplementation in T2DM [138]. These studies suggest that Se supplementation does not increase the risk for T2DM. These inconsistent results may be explained by a possible U-shaped response of Se supplementation to glucose metabolism [137]. Overall, further longitudinal, cross-sectional studies and RCTs are needed to demonstrate whether Se supplementation can increase the prevalence of T2DM to further verify whether high Se levels are a risk factor for T2DM.

13. Conclusions

As an important microelement, Se is mainly obtained through the diet, including via supplements, absorbed from the duodenum and cecum, and transported to various tissues in the form of SEPP1 (Figure 1). It mainly exerts its nutritional and antioxidant activities on human health and diseases in the form of selenoproteins. Given the antioxidant defense of these selenoproteins, Se has been used to mitigate oxidative stress in multiple diseases, including CVD, T2DM, thyroid disease, neurodegeneration, infection, infertility, and cancer (Figure 2). Recently, extensive evidence has been reported that supports the significant role of Se in the

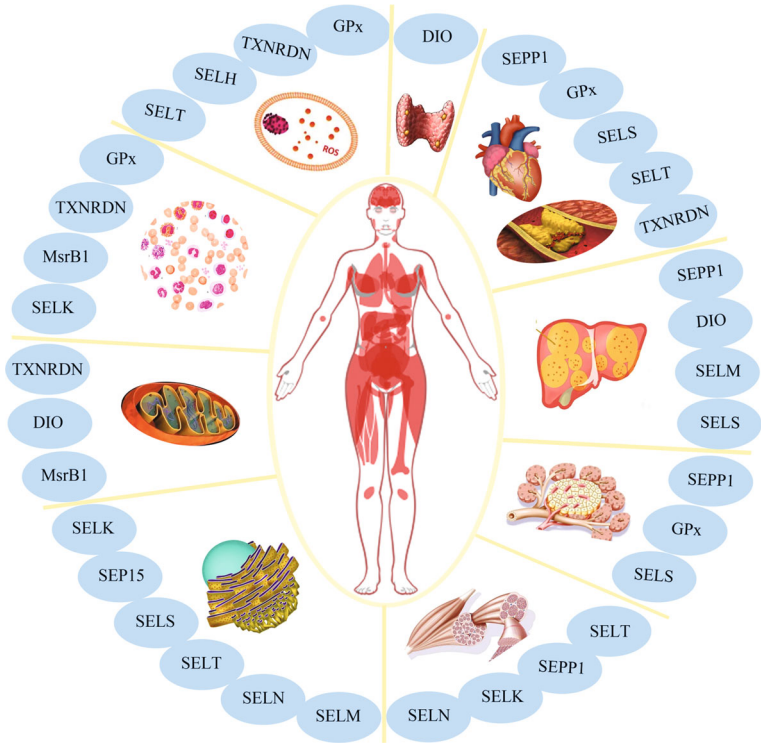

Figure 2: Graphical summary of the potential effects of the various selenoproteins in tissues and organelles. In general, Se is widely expressed in many organs, such as the thyroid gland, heart, liver, pancreas, and skeletal muscle. As an antioxidant agent, Se is incorporated into selenoproteins, which play an important role in the glucose and lipid metabolism and may be involved in metabolic disorders, including cardiovascular disease, atherosclerosis, type 2 diabetes, autoimmune thyroid disorders, and nonalcoholic fatty liver disease. In addition, selenoproteins are highly expressed in the mitochondria and endoplasmic reticulum, which indicates a close correlation between energy metabolism and selenoproteins. Furthermore, the importance of selenoproteins in antioxidant defense and anti-inflammatory capacity has been widely reported. These roles may partly contribute to the role of Se within the occurrence and development of diseases.

prevention, onset, and clinical outcomes of metabolic diseases, such as CVD, HT, NAFLD, and T2DM. Herein, we review these studies, focusing mainly on the last 20 years of research. According to the reported data, a close correlation between Se status and favorable prognosis of the above-mentioned pathologies has been generally observed. Se supplementation has been widely studied as a therapeutic approach for the prevention of metabolic diseases, delaying the progression, and alleviating the outcomes of metabolic diseases.

As an antioxidant agent, Se is incorporated into selenoproteins, which play important roles in glucose and lipid metabolism. Moreover, Se shows great potential for redox regulation to maintain cellular homeostasis and metabolism [14]. Previous studies have reported that excess ROS play a role in the complex pathogenesis of metabolic diseases [13]. Therefore, this review focused on the potential role of Se in the development of metabolic diseases. As mentioned above, we systematically reviewed current data on the correlation between Se status and the risk of metabolic diseases, including CHD, HT, NAFLD, and T2DM. Surprisingly, the specific role of Se levels in metabolic diseases remains controversial. Some studies indicate that higher levels of Se have significantly beneficial effects in the prevention of CHD. By contrast, other studies have indicated a positive correlation between Se levels and T2DM. With regard to the protective action of Se in HT and NAFLD, research opinions remain inconsistent. The results of different studies highlight the complex physiological role of Se. Although the role of Se in metabolic diseases remains unclear, the antioxidant activity of Se in the pathogenesis of diseases cannot be ignored, and the molecular mechanisms underlying these paradoxical effects need to be further explored. Some studies have shown that high levels of Se reduce NO bioavailability and impair angiogenesis, and high Se concentrations induce ER stress and increase ROS accumulation, which may lead to cell apoptosis [139]. ROS can activate chemoreflex and suppress baroreflex, thereby stimulating the sympathetic nervous system and causing HT [102]. In addition, the elevated level of ROS in pancreatic β cells is accompanied by elevated fasting plasma insulin levels and the absence of IR, resulting in pancreatic β cell dysfunction and subsequent progression to T2DM [102]. These results suggest that Se may affect the redox balance in humans by regulating ROS levels, which contributes to the development of metabolic diseases. On the other hand, Cardoso et al. found that xanthine dehydrogenase (XDH) was the interacting protein that connected the pathogenesis with the molecular action of Se by searching the STITCH 4.0 and STRING databases [15]. A previous study showed an inverse correlation between GPx enzyme

levels and XDH levels in diabetic rats, suggesting that Se may be related to xanthine metabolism [140]. Taken together, the mechanism underlying the role of Se in metabolic diseases, which may be dependent on or independent of the internal antioxidant defense system, should be studied in future experimental investigations.

Se is vital for many physiological processes, and adequate Se intake and status are very important for human health. Based on the importance of Se in the cellular antioxidant defense system, Se intake higher than the dietary recommendations may be protective against cancer or result in other additional health benefits which have been proposed. The therapeutic strategy of Se supplementation for metabolic diseases has been studied for many years. When studying Se supplementation in clinical trials, several aspects need to be considered, including the different types of Se used for supplementation, the level of Se at baseline in the subjects, the level of nutritional or supernutritional Se supplementation, and the duration of Se supplementation in the trial. Burk et al. noted that supplementation with SeMet and Se yeast increased plasma Se levels in a dose-dependent manner, but selenite did not [43]. Plasma Se levels were useful in monitoring the compliance and safety of Se supplementation as SeMet, but not selenite, and plasma Se levels seemed to reflect the SeMet content of yeast, but not the other yeast Se forms [43]. In addition, next-generation Se supplements, such as zerovalent Se nanoparticles (SeNPs) and selenized polysaccharides, slowly release active Se through an equilibrium reaction, which has a lower risk of Se excess supplementation due to their lower toxicity, higher bioavailability, and controlled release [141]. Since Se deficiency contributes to the risk of KD, administering Se supplements to the residents of KD-endemic areas significantly reduced the incidence of KD. Therefore, Se supplementation may be a potential strategy for KD prevention and treatment. Regarding the role of Se supplementation in metabolic diseases, although many studies have shown the protective action of Se supplementation in trials, some studies have shown that Se supplementation has no effect, even contributing to the development of CVD and T2DM. Evidence from large RCTs is needed to confirm the feasibility of Se supplementation as a potential therapy for metabolic diseases and to investigate the potential underlying mechanisms and the possibility of public health interventions.

However, supernutritional Se supplementation may result in acute or chronic Se poisoning, and the difference between potential beneficial and toxic Se level doses should be considered when recommending dosages. According to the dietary 5recommendation from the RDA, Se intake ranges from 55 to 70 μg per day, which is typically based on the Se intake needed to saturate GPx activity. In general, plasma Se levels are approximately 100 μg/L, and urinary Se levels range from 10 to 85 μg/L in the general population [48, 49]. Mortality has been associated with blood/plasma Se levels ranging from 300 μg/L to 30,000 μg/L compared to normal levels of 100 μg/L. As mentioned above, Se deficiency is closely related to the occurrence, development, prognosis, and outcome of many diseases, as well as the all-cause mortality rate. Therefore, the minimum requirement for Se is to prevent the prevalence of Se-deficient diseases, such as KD. In addition, owing to the toxicity of high Se levels, including acute or chronic Se poisoning, noncritical Se intake without a physician's recommendation should be urgently dissuaded. As part of a therapeutic approach, there is a need to consider its limited therapeutic range to avoid overdose and related toxicity.

To summarize, this review presents an up-to-date overview of the current understanding of Se intake and human health, including Se deficiency and Se poisoning, with an emphasis on the correlation between Se status and metabolic diseases. In addition, the prospects of Se supplementation as a therapeutic strategy for prevention of related diseases are briefly summarized and discussed. Within this context, understanding the association between Se status and human health is essential for developing effective public health policies, guiding applicable clinical practice, and counteracting health issues associated with Se deficiency. In light of the current state of this field of research, future studies on the protective action of Se in metabolic diseases and the corresponding molecular mechanisms are needed to clarify the paradoxical effects of this micronutrient.

Conflicts of Interest

The authors declare that there is no conflict of interest regarding the publication of this paper.

Authors' Contributions

Jing Huang and Ling Xie conceptualized and wrote the manuscript. Anni Song and Chun Zhang revised the manuscript. All authors have read and agreed to the published version of the manuscript. Jing Huang and Ling Xie contributed equally to this work.

Acknowledgments

This research was funded by the National Natural Science Foundation of China (Nos. 81961138007, 81974096, 81770711, and 81873602), the National Key R&D Program of China (2018YFC1314000), and the Program for HUST Academic Frontier Youth Team (2017QYTD20).

References

[1] S. J. Fairweather-Tait, Y. Bao, M. R. Broadley et al., "Selenium in human health and disease," *Antioxidants & Redox Signaling*, vol. 14, no. 7, pp. 1337–1383, 2011.

[2] V. M. Labunskyy, D. L. Hatfield, and V. N. Gladyshev, "Selenoproteins: molecular pathways and physiological roles," *Physiological Reviews*, vol. 94, no. 3, pp. 739–777, 2014.

[3] V. N. Gladyshev, E. S. Arnér, M. J. Berry et al., "Selenoprotein gene nomenclature," *The Journal of Biological Chemistry*, vol. 291, no. 46, pp. 24036–24040, 2016.

[4] U. Tinggi, "Selenium: its role as antioxidant in human health," *Environmental Health and Preventive Medicine*, vol. 13, no. 2, pp. 102–108, 2008.

[5] M. W. Pitts and P. R. Hoffmann, "Endoplasmic reticulum-resident selenoproteins as regulators of calcium signaling and homeostasis," *Cell Calcium*, vol. 70, pp. 76–86, 2018.

[6] G. Barchielli, A. Capperucci, and D. Tanini, "The role of selenium in pathologies: an updated review," *Antioxidants*, vol. 11, no. 2, p. 251, 2022.

[7] M. P. Rayman, "Selenium and human health," *Lancet*, vol. 379, no. 9822, pp. 1256–1268, 2021.

[8] M. P. Rayman, "The importance of selenium to human health," *Lancet*, vol. 356, no. 9225, pp. 233–241, 2000.

[9] Z. Y. Li, G. B. Xu, and T. A. Xia, "Prevalence rate of metabolic syndrome and dyslipidemia in a large professional population in Beijing," *Atherosclerosis*, vol. 184, no. 1, pp. 188–192, 2006.

[10] T. Lin, X. Zhu, D. Xu et al., "The association between dietary antioxidant micronutrients and cardiovascular disease in adults in the United States: a cross-sectional study," *Frontiers in Nutrition*, vol. 8, article 799095, 2022.

[11] L. N. Kohler, A. Florea, C. P. Kelley et al., "Higher plasma selenium concentrations are associated with increased odds of prevalent type 2 diabetes," *The Journal of Nutrition*, vol. 148, no. 8, pp. 1333–1340, 2018.

[12] L. Xu, Y. Lu, N. Wang, and Y. Feng, "The role and mechanisms of selenium supplementation on fatty liver-associated disorder," *Antioxidants*, vol. 11, no. 5, p. 922, 2022.

[13] A. Carrier, "Metabolic syndrome and oxidative stress: a complex relationship," *Antioxidants & Redox Signaling*, vol. 26, no. 9, pp. 429–431, 2017.

[14] N. Wang, H. Y. Tan, S. Li, Y. Xu, W. Guo, and Y. Feng, "Supplementation of micronutrient selenium in metabolic diseases: its role as an antioxidant," *Oxidative Medicine and Cellular Longevity*, vol. 2017, Article ID 7478523, 13 pages, 2017.

[15] B. R. Cardoso, S. Braat, and R. M. Graham, "Selenium status is associated with insulin resistance markers in adults: findings from the 2013 to 2018 National Health and Nutrition Examination Survey (NHANES)," *Frontiers in Nutrition*, vol. 8, article 696024, 2021.

[16] W. Ju, M. Ji, X. Li et al., "Relationship between higher serum selenium level and adverse blood lipid profile," *Clinical Nutrition*, vol. 37, no. 5, pp. 1512–1517, 2018.

[17] M. Wang, B. Li, S. Li, Z. Song, F. Kong, and X. Zhang, "Selenium in wheat from farming to food," *Journal of Agricultural and Food Chemistry*, vol. 69, no. 51, pp. 15458–15467, 2021.

[18] Y. Mehdi, J. L. Hornick, L. Istasse, and I. Dufrasne, "Selenium in the environment, metabolism and involvement in body functions," *Molecules*, vol. 18, no. 3, pp. 3292–3311, 2013.

[19] R. F. Burk and K. E. Hill, "Regulation of selenium metabolism and transport," *Annual Review of Nutrition*, vol. 35, pp. 109–134, 2015.

[20] G. E. Olson, V. P. Winfrey, K. E. Hill, and R. F. Burk, "Megalin mediates selenoprotein P uptake by kidney proximal tubule epithelial cells," *The Journal of Biological Chemistry*, vol. 283, no. 11, pp. 6854–6860, 2008.

[21] R. F. Burk, K. E. Hill, A. K. Motley et al., "Selenoprotein P and apolipoprotein E receptor-2 interact at the blood-brain barrier and also within the brain to maintain an essential selenium pool that protects against neurodegeneration," *The FASEB Journal*, vol. 28, no. 8, pp. 3579–3588, 2014.

[22] R. Brigelius-Flohe, C. Müller, J. Menard, S. Florian, K. Schmehl, and K. Wingler, "Functions of GI-GPx: lessons from selenium-dependent expression and intracellular localization," *BioFactors*, vol. 14, no. 1-4, pp. 101–106, 2001.

[23] K. E. Hill, J. Zhou, W. J. McMahan et al., "Deletion of selenoprotein P alters distribution of selenium in the mouse," *The Journal of Biological Chemistry*, vol. 278, no. 16, pp. 13640–13646, 2003.

[24] L. Schomburg, C. Riese, M. Michaelis et al., "Synthesis and metabolism of thyroid hormones is preferentially maintained in selenium-deficient transgenic mice," *Endocrinology*, vol. 147, no. 3, pp. 1306–1313, 2006.

[25] R. F. Burk, K. E. Hill, G. E. Olson et al., "Deletion of apolipoprotein E receptor-2 in mice lowers brain selenium and causes severe neurological dysfunction and death when a low-selenium diet is fed," *The Journal of Neuroscience*, vol. 27, no. 23, pp. 6207–6211, 2007.

[26] K. E. Hill, J. Zhou, L. M. Austin et al., "The selenium-rich C-terminal domain of mouse selenoprotein P is necessary for the supply of selenium to brain and testis but not for the maintenance of whole body selenium," *The Journal of Biological Chemistry*, vol. 282, no. 15, pp. 10972–10980, 2007.

[27] A. Nakayama, K. E. Hill, L. M. Austin, A. K. Motley, and R. F. Burk, "All regions of mouse brain are dependent on selenoprotein P for maintenance of selenium," *The Journal of Nutrition*, vol. 137, no. 3, pp. 690–693, 2007.

[28] J. Kohrle, F. Jakob, B. Contempre, and J. E. Dumont, "Selenium, the thyroid, and the endocrine system," *Endocrine Reviews*, vol. 26, no. 7, pp. 944–984, 2005.

[29] A. Liu, F. Li, P. Xu et al., "Correction to: Gpx4, Selenov, and Txnrd3 are three most testis-abundant selenogenes resistant to dietary selenium concentrations and actively expressed during reproductive ages in rats," *Biological Trace Element Research*, 2022.

[30] J. C. Zhou, S. Zheng, J. Mo et al., "Dietary selenium deficiency or excess reduces sperm quality and testicular mRNA abundance of nuclear glutathione peroxidase 4 in rats," *The Journal of Nutrition*, vol. 147, no. 10, pp. 1947–1953, 2017.

[31] J. P. Werneck-de-Castro, T. L. Fonseca, D. L. Ignacio et al., "Thyroid hormone signaling in male mouse skeletal muscle is largely independent of D2 in myocytes," *Endocrinology*, vol. 156, no. 10, pp. 3842–3852, 2015.

[32] M. Dentice, A. Marsili, R. Ambrosio et al., "The fox O3/type 2 deiodinase pathway is required for normal mouse myogenesis and muscle regeneration," *The Journal of Clinical Investigation*, vol. 120, no. 11, pp. 4021–4030, 2010.

[33] D. L. Ignacio, D. H. Silvestre, E. Anne-Palmer et al., "Early developmental disruption of type 2 deiodinase pathway in mouse skeletal muscle does not impair muscle function," *Thyroid*, vol. 27, no. 4, pp. 577–586, 2017.

[34] K. Ashton, L. Hooper, L. J. Harvey, R. Hurst, A. Casgrain, and S. J. Fairweather-Tait, "Methods of assessment of selenium status in humans: a systematic review," *The American Journal of Clinical Nutrition*, vol. 89, no. 6, pp. 2025–2039, 2009.

[35] T. Urbano, T. Filippini, D. Lasagni et al., "Associations between urinary and dietary selenium and blood metabolic parameters in a healthy Northern Italy population," *Antioxidants*, vol. 10, no. 8, 2021.

[36] R. Hurst, C. N. Armah, J. R. Dainty et al., "Establishing optimal selenium status: results of a randomized, double-blind, placebo-controlled trial," *The American Journal of Clinical Nutrition*, vol. 91, no. 4, pp. 923–931, 2010.

[37] O. Brodin, J. Hackler, S. Misra et al., "Selenoprotein P as biomarker of selenium status in clinical trials with therapeutic dosages of selenite," *Nutrients*, vol. 12, no. 4, article 1067, 2020.

[38] R. F. Burk and K. E. Hill, "Selenoprotein P: an extracellular protein with unique physical characteristics and a role in selenium homeostasis," *Annual Review of Nutrition*, vol. 25, no. 1, pp. 215–235, 2005.

[39] S. Hybsier, T. Schulz, Z. Wu et al., "Sex-specific and inter-individual differences in biomarkers of selenium status identified by a calibrated ELISA for selenoprotein P," *Redox Biology*, vol. 11, pp. 403–414, 2017.

[40] X. Wu, K. Huang, C. Wei, F. Chen, and C. Pan, "Regulation of cellular glutathione peroxidase by different forms and concentrations of selenium in primary cultured bovine hepatocytes," *The Journal of Nutritional Biochemistry*, vol. 21, no. 2, pp. 153–161, 2010.

[41] K. M. Brown, K. Pickard, F. Nicol, G. J. Beckett, G. G. Duthie, and J. R. Arthur, "Effects of organic and inorganic selenium supplementation on selenoenzyme activity in blood lymphocytes, granulocytes, platelets and erythrocytes," *Clinical Science (London, England)*, vol. 98, no. 5, pp. 593–599, 2000.

[42] W. C. Hawkes, B. D. Richter, Z. Alkan et al., "Response of selenium status indicators to supplementation of healthy North American men with high-selenium yeast," *Biological Trace Element Research*, vol. 122, no. 2, pp. 107–121, 2008.

[43] R. F. Burk, B. K. Norsworthy, K. E. Hill, A. K. Motley, and D. W. Byrne, "Effects of chemical form of selenium on plasma biomarkers in a high-dose human supplementation trial," *Cancer Epidemiology, Biomarkers & Prevention*, vol. 15, no. 4, pp. 804–810, 2006.

[44] C. C. Johnson, F. M. Fordyce, and M. P. Rayman, "Symposium on 'geographical and geological influences on nutrition': factors controlling the distribution of selenium in the environment and their impact on health and nutrition," *The Proceedings of the Nutrition Society*, vol. 69, no. 1, pp. 119–132, 2010.

[45] M. P. Rayman, "Food-chain selenium and human health: emphasis on intake," *The British Journal of Nutrition*, vol. 100, no. 2, pp. 254–268, 2008.

[46] M. P. Rayman, "Selenium in cancer prevention: a review of the evidence and mechanism of action," *The Proceedings of the Nutrition Society*, vol. 64, no. 4, pp. 527–542, 2005.

[47] R. Stoffaneller and N. L. Morse, "A review of dietary selenium intake and selenium status in Europe and the Middle East," *Nutrients*, vol. 7, no. 3, pp. 1494–1537, 2015.

[48] Q. T. Dinh, Z. Cui, J. Huang et al., "Selenium distribution in the Chinese environment and its relationship with human health: a review," *Environment International*, vol. 112, pp. 294–309, 2018.

[49] National Academies Press, *In dietary reference intakes for vitamin C, vitamin E, selenium, and carotenoids*, National Academy of Sciences, Washington (DC), 2000.

[50] C. D. Thomson, "Assessment of requirements for selenium and adequacy of selenium status: a review," *European Journal of Clinical Nutrition*, vol. 58, no. 3, pp. 391–402, 2004.

[51] J. Loscalzo, "Keshan disease, selenium deficiency, and the selenoproteome," *The New England Journal of Medicine*, vol. 370, no. 18, pp. 1756–1760, 2014.

[52] Q. Li, M. Liu, J. Hou, C. Jiang, S. Li, and T. Wang, "The prevalence of Keshan disease in China," *International Journal of Cardiology*, vol. 168, no. 2, pp. 1121–1126, 2013.

[53] Y. Jia, R. Wang, S. Su et al., "A county-level spatial study of serum selenoprotein P and Keshan disease," *Frontiers in Nutrition*, vol. 9, article 827093, 2022.

[54] X. Zhang, T. Wang, and S. Li, "A spatial ecological study of selenoprotein P and Keshan disease," *Journal of Trace Elements in Medicine and Biology*, vol. 51, pp. 150–158, 2019.

[55] Y. Wang, Y. Zou, T. Wang et al., "A spatial study on serum selenoprotein P and Keshan disease in Heilongjiang Province, China," *Journal of Trace Elements in Medicine and Biology*, vol. 65, article 126728, 2021.

[56] Y. Zou, X. Liu, T. Wang et al., "A spatial ecological study on hair selenium level of residents in Keshan disease endemic and non-endemic areas in Heilongjiang Province, China," *Biological Trace Element Research*, vol. 199, no. 12, pp. 4546–4554, 2021.

[57] X. Zhang, T. Wang, S. Li et al., "A spatial ecology study of Keshan disease and hair selenium," *Biological Trace Element Research*, vol. 189, no. 2, pp. 370–378, 2019.

[58] Y. H. Zhu, X. F. Wang, G. Yang et al., "Efficacy of long-term selenium supplementation in the treatment of chronic Keshan disease with congestive heart failure," *Current Medical Science*, vol. 39, no. 2, pp. 237–242, 2019.

[59] G. Alfthan, G. L. Xu, W. H. Tan et al., "Selenium supplementation of children in a selenium-deficient area in China: blood selenium levels and glutathione peroxidase activities," *Biological Trace Element Research*, vol. 73, no. 2, pp. 113–125, 2000.

[60] H. Zhou, T. Wang, Q. Li, and D. Li, "Prevention of Keshan disease by selenium supplementation: a systematic review and meta-analysis," *Biological Trace Element Research*, vol. 186, no. 1, pp. 98–105, 2018.

[61] N. Hadrup and G. Ravn-Haren, "Acute human toxicity and mortality after selenium ingestion: a review," *Journal of Trace Elements in Medicine and Biology*, vol. 58, article 126435, 2020.

[62] O. A. Levander, P. B. Moser, and V. C. Morris, "Dietary selenium intake and selenium concentrations of plasma, erythrocytes, and breast milk in pregnant and postpartum lactating and nonlactating women," *The American Journal of Clinical Nutrition*, vol. 46, no. 4, pp. 694–698, 1987.

[63] G. Alfthan, A. Aro, H. Arvilommi, and J. K. Huttunen, "Selenium metabolism and platelet glutathione peroxidase activity in healthy Finnish men: effects of selenium yeast, selenite, and selenate," *The American Journal of Clinical Nutrition*, vol. 53, no. 1, pp. 120–125, 1991.

[64] M. Sanz Alaejos and C. Díaz Romero, "Urinary selenium concentrations," *Clinical Chemistry*, vol. 39, no. 10, pp. 2040–2052, 1993.

[65] B. Kłapcińska, S. Poprzęcki, A. Danch, A. Sobczak, and K. Kempa, "Selenium levels in blood of upper Silesian population: evidence of suboptimal selenium status in a significant percentage of the population," *Biological Trace Element Research*, vol. 108, no. 1-3, pp. 001–016, 2005.

[66] J. S. Morris and S. B. Crane, "Selenium toxicity from a misformulated dietary supplement, adverse health effects, and the temporal response in the nail biologic monitor," *Nutrients*, vol. 5, no. 4, pp. 1024–1057, 2013.

[67] K. A. See, P. S. Lavercombe, J. Dillon, and R. Ginsberg, "Accidental death from acute selenium poisoning," *The Medical Journal of Australia*, vol. 185, no. 7, pp. 388-389, 2006.

[68] D. M. Hunsaker, H. A. Spiller, and D. Williams, "Acute selenium poisoning: suicide by ingestion," *Journal of Forensic Sciences*, vol. 50, no. 4, pp. 926–942, 2005.

[69] R. Wietecha-Posłuszny, T. Lech, and P. Kościelniak, "Application of three spectrometric methods to total selenium determination in postmortem material in a case of acute selenium compound poisoning," *Journal of Forensic Sciences*, vol. 6, no. 2, pp. 518–521, 2011.

[70] Y. Kise, S. Yoshimura, K. Akieda et al., "Acute oral selenium intoxication with ten times the lethal dose resulting in deep gastric ulcer," *The Journal of Emergency Medicine*, vol. 26, no. 2, pp. 183–187, 2004.

[71] A. Gasmi, R. Garnier, M. Galliot-Guilley et al., "Acute selenium poisoning," *Veterinary and Human Toxicology*, vol. 39, no. 5, pp. 304–308, 1997.

[72] B. Schuh and U. Jappe, "Selenium intoxication: undesirable effect of a fasting cure," *The British Journal of Dermatology*, vol. 156, no. 1, pp. 177-178, 2007.

[73] D. Müller and H. Desel, "Acute selenium poisoning by paradise nuts (Lecythis ollaria)," *Human & Experimental Toxicology*, vol. 29, no. 5, pp. 431–434, 2010.

[74] A. A. Al-Mubarak, N. Grote Beverborg, N. Suthahar et al., "High selenium levels associate with reduced risk of mortality and new-onset heart failure: data from PREVEND," *European Journal of Heart Failure*, vol. 24, no. 2, pp. 299–307, 2022.

[75] S. Giovannini, G. Onder, F. Lattanzio et al., "Selenium concentrations and mortality among community-dwelling older adults: results from IlSIRENTE study," *The Journal of Nutrition, Health & Aging*, vol. 22, no. 5, pp. 608–612, 2018.

[76] E. Garcia-Esquinas, M. Carrasco-Rios, R. Ortolá et al., "Selenium and impaired physical function in US and Spanish older adults," *Redox Biology*, vol. 38, article 101819, 2021.

[77] F. P. Bellinger, A. V. Raman, M. A. Reeves, and M. J. Berry, "Regulation and function of selenoproteins in human disease," *The Biochemical Journal*, vol. 422, no. 1, pp. 11–22, 2009.

[78] E. Zoidis, I. Seremelis, and N. Kontopoulos, "Selenium-dependent antioxidant enzymes: actions and properties of selenoproteins," *Antioxidants*, vol. 7, no. 5, article 66, 2018.

[79] T. Yin, X. Zhu, D. Xu et al., "The association between dietary antioxidant micronutrients and cardiovascular disease in adults in the United States: a cross-sectional study," *Frontiers in Nutrition*, vol. 8, article 799095, 2021.

[80] C. Xie, J. Xian, M. Zeng et al., "Regional difference in the association between the trajectory of selenium intake and hypertension: a 20-year cohort study," *Nutrients*, vol. 13, no. 5, article 1501, 2021.

[81] X. Wang, Y. A. Seo, and S. K. Park, "Serum selenium and non-alcoholic fatty liver disease (NAFLD) in U.S. adults: National Health and Nutrition Examination Survey (NHANES) 2011-2016," *Environmental Research*, vol. 197, article 111190, 2021.

[82] E. D'Adamo and S. Caprio, "Type 2 diabetes in youth: epidemiology and pathophysiology," *Diabetes Care*, vol. 34, pp. 161–165, 2011.

[83] J. Xiao, N. Li, S. Xiao, Y. Wu, and H. Liu, "Comparison of selenium nanoparticles and sodium selenite on the alleviation of early atherosclerosis by inhibiting endothelial dysfunction and inflammation in apolipoprotein E-deficient mice," *International Journal of Molecular Sciences*, vol. 22, no. 21, article 11612, 2021.

[84] L. Yang, M. Qi, X. Du et al., "Selenium concentration is associated with occurrence and diagnosis of three cardiovascular diseases: a systematic review and meta-analysis," *Journal of Trace Elements in Medicine and Biology*, vol. 70, article 126908, 2022.

[85] Y. Yuan, Y. Xiao, W. Feng et al., "Plasma metal concentrations and incident coronary heart disease in Chinese adults: the Dongfeng-Tongji cohort," *Environmental Health Perspectives*, vol. 125, article 107007, no. 10, 2017.

[86] G. Flores-Mateo, A. Navas-Acien, R. Pastor-Barriuso, and E. Guallar, "Selenium and coronary heart disease: a meta-analysis," *The American Journal of Clinical Nutrition*, vol. 84, no. 4, pp. 762–773, 2006.

[87] X. Zhang, C. Liu, J. Guo, and Y. Song, "Selenium status and cardiovascular diseases: meta-analysis of prospective observational studies and randomized controlled trials," *European Journal of Clinical Nutrition*, vol. 70, no. 2, pp. 162–169, 2016.

[88] W. Q. Wei, C. C. Abnet, Y. L. Qiao et al., "Prospective study of serum selenium concentrations and esophageal and gastric cardia cancer, heart disease, stroke, and total death," *The American Journal of Clinical Nutrition*, vol. 79, no. 1, pp. 80–85, 2004.

[89] B. Xie, J. Wang, J. Zhang, and M. Chen, "Dietary and serum selenium in coronary heart disease and all-cause mortality: an international perspective," *Asia Pacific Journal of Clinical Nutrition*, vol. 29, no. 4, pp. 827–838, 2020.

[90] A. A. Al-Mubarak, P. van der Meer, and N. Bomer, "Selenium, selenoproteins, and heart failure: current knowledge and future perspective," *Current Heart Failure Reports*, vol. 18, no. 3, pp. 122–131, 2021.

[91] D. Wickremasinghe, H. Peiris, L. G. Chandrasena, V. Senaratne, and R. Perera, "Case control feasibility study assessing the association between severity of coronary artery disease with glutathione peroxidase-1 (GPX-1) and GPX-1 polymorphism (Pro198Leu)," *BMC Cardiovascular Disorders*, vol. 16, no. 1, p. 111, 2016.

[92] F. Raygan, V. Ostadmohammadi, and Z. Asemi, "The effects of probiotic and selenium co-supplementation on mental health parameters and metabolic profiles in type 2 diabetic patients with coronary heart disease: a randomized, double-blind, placebo-controlled trial," *Clinical Nutrition*, vol. 38, no. 4, pp. 1594–1598, 2019.

[93] U. Alehagen, P. Johansson, M. Björnstedt, A. Rosén, and U. Dahlström, "Cardiovascular mortality and N-terminal-pro BNP reduced after combined selenium and coenzyme Q10 supplementation: a 5-year prospective randomized double-blind placebo-controlled trial among elderly Swedish citizens," *International Journal of Cardiology*, vol. 67, no. 5, pp. 1860–1866, 2013.

[94] U. Alehagen, J. Aaseth, J. Alexander, and P. Johansson, "Still reduced cardiovascular mortality 12 years after supplementation with selenium and coenzyme Q10 for four years: a validation of previous 10-year follow-up results of a prospective randomized double-blind placebo-controlled trial in elderly," *PLos One*, vol. 13, no. 4, article e0193120, 2018.

[95] U. Alehagen, J. Aaseth, and P. Johansson, "Less increase of copeptin and MR-proADM due to intervention with selenium and coenzyme Q10 combined: results from a 4-year

prospective randomized double-blind placebo-controlled trial among elderly Swedish citizens," *BioFactors*, vol. 41, no. 6, pp. 443–452, 2015.

[96] U. Alehagen, T. L. Lindahl, J. Aaseth, E. Svensson, and P. Johansson, "Levels of sP-selectin and hs-CRP decrease with dietary intervention with selenium and coenzyme Q10 combined: a secondary analysis of a randomized clinical trial," *PLos One*, vol. 10, no. 9, article e0137680, 2015.

[97] U. Alehagen, P. Johansson, E. Svensson, J. Aaseth, and J. Alexander, "Improved cardiovascular health by supplementation with selenium and coenzyme Q10: applying structural equation modelling (SEM) to clinical outcomes and biomarkers to explore underlying mechanisms in a prospective randomized double-blind placebo-controlled intervention project in Sweden," *European Journal of Nutrition*, 2022.

[98] W. Ju, X. Li, Z. Li et al., "The effect of selenium supplementation on coronary heart disease: a systematic review and meta-analysis of randomized controlled trials," *Journal of Trace Elements in Medicine and Biology*, vol. 44, pp. 8–16, 2017.

[99] Y. Zhang, S. P. Cartland, R. Henriquez et al., "Selenomethionine supplementation reduces lesion burden, improves vessel function and modulates the inflammatory response within the setting of atherosclerosis," *Redox Biology*, vol. 29, article 101409, 2020.

[100] H. F. Chiu, K. Venkatakrishnan, O. Golovinskaia, and C. K. Wang, "Impact of micronutrients on hypertension: evidence from clinical trials with a special focus on meta-analysis," *Nutrients*, vol. 13, no. 2, article 588, 2021.

[101] C. Russo, O. Olivieri, D. Girelli et al., "Anti-oxidant status and lipid peroxidation in patients with essential hypertension," *Journal of Hypertension*, vol. 16, no. 9, pp. 1267–1271, 1998.

[102] N. R. Prabhakar, Y. Peng, and J. Nanduri, "Hypoxia-inducible factors and obstructive sleep apnea," *The Journal of Clinical Investigation*, vol. 130, no. 10, pp. 5042–5051, 2020.

[103] R. Swart, A. E. Schutte, J. M. van Rooyen, and C. M. C. Mels, "Selenium and large artery structure and function: a 10-year prospective study," *European Journal of Nutrition*, vol. 58, no. 8, pp. 3313–3323, 2019.

[104] P. Gać, K. Czerwińska, M. Poręba et al., "Serum zinc and selenium concentrations in patients with hypertrophy and remodelling of the left ventricle secondary to arterial hypertension," *Antioxidants*, vol. 10, no. 11, article 1803, 2021.

[105] Z. Wang, H. Ma, Y. Song et al., "Plasma selenium and the risk of first stroke in adults with hypertension: a secondary analysis of the China Stroke Primary Prevention Trial," *The American Journal of Clinical Nutrition*, vol. 115, no. 1, pp. 222–231, 2022.

[106] G. Wu, Z. Li, W. Ju, X. Yang, X. Fu, and X. Gao, "Cross-sectional study: relationship between serum selenium and hypertension in the Shandong Province of China," *Biological Trace Element Research*, vol. 185, no. 2, pp. 295–301, 2018.

[107] M. Vinceti, R. Chawla, T. Filippini et al., "Blood pressure levels and hypertension prevalence in a high selenium environment: results from a cross-sectional study," *Nutrition, Metabolism, and Cardiovascular Diseases*, vol. 29, no. 4, pp. 398–408, 2019.

[108] L. Su, Y. Y. Jin, F. W. Unverzagt et al., "Longitudinal association between selenium levels and hypertension in a rural elderly Chinese cohort," *The Journal of Nutrition, Health & Aging*, vol. 20, no. 10, pp. 983–988, 2016.

[109] W. Wu, S. Jiang, Q. Zhao et al., "Environmental exposure to metals and the risk of hypertension: a cross-sectional study in China," *Environmental Pollution*, vol. 233, pp. 670–678, 2018.

[110] Q. H. Tan, Y. Q. Huang, X. C. Liu et al., "A U-shaped relationship between selenium concentrations and all-cause or cardiovascular mortality in patients with hypertension," *Frontiers in Cardiovascular Medicine*, vol. 8, article 671618, 2021.

[111] H. Y. Huang, B. Caballero, S. Chang et al., "The efficacy and safety of multivitamin and mineral supplement use to prevent cancer and chronic disease in adults: a systematic review for a National Institutes of Health state-of-the-science conference," *Annals of Internal Medicine*, vol. 145, no. 5, pp. 372–385, 2006.

[112] D. Kuruppu, H. C. Hendrie, L. Yang, and S. Gao, "Selenium levels and hypertension: a systematic review of the literature," *Public Health Nutrition*, vol. 17, no. 6, pp. 1342–1352, 2014.

[113] S. Stranges, A. Navas-Acien, M. P. Rayman, and E. Guallar, "Selenium status and cardiometabolic health: state of the evidence," *Nutrition, Metabolism, and Cardiovascular Diseases*, vol. 20, no. 10, pp. 754–760, 2010.

[114] M. E. Rinella, "Nonalcoholic fatty liver disease: a systematic review," *JAMA*, vol. 313, no. 22, pp. 2263–2273, 2015.

[115] A. G. Singal, H. Manjunath, A. C. Yopp et al., "The effect of PNPLA3 on fibrosis progression and development of hepatocellular carcinoma: a meta-analysis," *The American Journal of Gastroenterology*, vol. 109, no. 3, pp. 325–334, 2014.

[116] Z. Yang, C. Yan, G. Liu et al., "Plasma selenium levels and nonalcoholic fatty liver disease in Chinese adults: a cross-sectional analysis," *Science Reports*, vol. 6, article 37288, 2016.

[117] M. Reja, M. Makar, A. Visaria, D. Marino, and V. Rustgi, "Increased serum selenium levels are associated with reduced risk of advanced liver fibrosis and all-cause mortality in NAFLD patients: National Health and Nutrition Examination Survey (NHANES) III," *Annals of Hepatology*, vol. 19, no. 6, pp. 635–640, 2020.

[118] K. Day, L. A. Seale, R. M. Graham, and B. R. Cardoso, "Selenotranscriptome network in non-alcoholic fatty liver disease," *Frontiers in Nutrition*, vol. 8, article 744825, 2021.

[119] Y. Chen, X. He, X. Chen, Y. Li, and Y. Ke, "SeP is elevated in NAFLD and participates in NAFLD pathogenesis through AMPK/ACC pathway," *Journal of Cellular Physiology*, vol. 236, no. 5, pp. 3800–3807, 2021.

[120] G. P. Caviglia, C. Rosso, A. Armandi et al., "Interplay between oxidative stress and metabolic derangements in non-alcoholic fatty liver disease: the role of selenoprotein P," *International Journal of Molecular Sciences*, vol. 21, no. 22, article 8838, 2020.

[121] M. Miyata, K. Matsushita, R. Shindo, Y. Shimokawa, Y. Sugiura, and M. Yamashita, "Selenoneine ameliorates hepatocellular injury and hepatic steatosis in a mouse model of NAFLD," *Nutrients*, vol. 12, no. 6, article 1898, 2020.

[122] Y. I. Hong-Wei, Z. H. U. Xiao-Xiao, X. L. Huang, L. A. I. Yu-Zhu, and T. A. N. G. Yue, "Selenium-enriched Bifidobacterium longum protected alcohol and high fat diet induced hepatic injury in mice," *Chinese Journal of Natural Medicines*, vol. 18, no. 3, pp. 169–177, 2020.

[123] Y. Wang, B. Liu, P. Wu et al., "Dietary selenium alleviated mouse liver oxidative stress and NAFLD induced by obesity

by regulating the KEAP1/NRF2 pathway," *Antioxidants*, vol. 11, no. 2, article 349, 2022.

[124] R. A. DeFronzo, "From the triumvirate to the ominous octet: a new paradigm for the treatment of type 2 diabetes mellitus," *Diabetes*, vol. 58, no. 4, pp. 773–795, 2009.

[125] F. Giacco and M. Brownlee, "Oxidative stress and diabetic complications," *Circulation Research*, vol. 107, no. 9, pp. 1058–1070, 2010.

[126] X. L. Liao, Z. H. Wang, X. N. Liang et al., "The association of circulating selenium concentrations with diabetes mellitus," *Diabetes Metab Syndr Obes*, vol. Volume 13, pp. 4755–4761, 2020.

[127] M. Cabral, O. Kuxhaus, F. Eichelmann et al., "Trace element profile and incidence of type 2 diabetes, cardiovascular disease and colorectal cancer: results from the EPIC-Potsdam cohort study," *European Journal of Nutrition*, vol. 60, no. 6, pp. 3267–3278, 2021.

[128] I. Galan-Chilet, M. Grau-Perez, G. De Marco et al., "A gene-environment interaction analysis of plasma selenium with prevalent and incident diabetes: the Hortega study," *Redox Biology*, vol. 12, pp. 798–805, 2017.

[129] M. Vinceti, M. Bonaccio, T. Filippini et al., "Dietary selenium intake and risk of hospitalization for type 2 diabetes in the Moli-sani study cohort," *Nutrition, Metabolism, and Cardiovascular Diseases*, vol. 31, no. 6, pp. 1738–1746, 2021.

[130] M. Vinceti, T. Filippini, and K. J. Rothman, "Selenium exposure and the risk of type 2 diabetes: a systematic review and meta-analysis," *European Journal of Epidemiology*, vol. 33, no. 9, pp. 789–810, 2018.

[131] T. Takamura, "Hepatokine selenoprotein P-mediated reductive stress causes resistance to intracellular signal transduction," *Antioxidants & Redox Signaling*, vol. 33, no. 7, pp. 517–524, 2020.

[132] Y. Mita, K. Nakayama, S. Inari et al., "Selenoprotein P-neutralizing antibodies improve insulin secretion and glucose sensitivity in type 2 diabetes mouse models," *Nature Communications*, vol. 8, no. 1, 2017.

[133] S. M. Oo, H. Misu, Y. Saito et al., "Serum selenoprotein P, but not selenium, predicts future hyperglycemia in a general Japanese population," *Scientific Reports*, vol. 8, no. 1, 2018.

[134] H. Steinbrenner, L. H. Duntas, and M. P. Rayman, "The role of selenium in type-2 diabetes mellitus and its metabolic comorbidities," *Redox Biology*, vol. 50, article 102236, 2022.

[135] S. S. Yu and J. L. Du, "Selenoprotein S: a therapeutic target for diabetes and macroangiopathy," *Cardiovascular Diabetology*, vol. 16, no. 1, p. 101, 2017.

[136] S. Stranges, J. R. Marshall, R. Natarajan et al., "Effects of long-term selenium supplementation on the incidence of type 2 diabetes: a randomized trial," *Annals of Internal Medicine*, vol. 147, no. 4, pp. 217–223, 2007.

[137] S. Stranges, M. P. Rayman, K. H. Winther, E. Guallar, S. Cold, and R. Pastor-Barriuso, "Effect of selenium supplementation on changes in HbA1c: results from a multiple-dose, randomized controlled trial," *Diabetes, Obesity & Metabolism*, vol. 21, no. 3, pp. 541–549, 2019.

[138] A. Stróżyk, Z. Osica, J. D. Przybylak et al., "Effectiveness and safety of selenium supplementation for type 2 diabetes mellitus in adults: a systematic review of randomised controlled trials," *Journal of Human Nutrition and Dietetics*, vol. 32, no. 5, pp. 635–645, 2019.

[139] M. Zachariah, H. Maamoun, L. Milano, M. P. Rayman, L. B. Meira, and A. Agouni, "Endoplasmic reticulum stress and oxidative stress drive endothelial dysfunction induced by high selenium," *Journal of Cellular Physiology*, vol. 236, no. 6, pp. 4348–4359, 2021.

[140] Y. Aliciguzel, I. Ozen, M. Aslan, and U. Karayalcin, "Activities of xanthine oxidoreductase and antioxidant enzymes in different tissues of diabetic rats," *The Journal of Laboratory and Clinical Medicine*, vol. 142, no. 3, pp. 172–177, 2003.

[141] D. Constantinescu-Aruxandei, R. M. Frîncu, L. Capră, and F. Oancea, "Selenium analysis and speciation in dietary supplements based on next-generation selenium ingredients," *Nutrients*, vol. 10, no. 10, article 1466, 2018.

Hindawi
Oxidative Medicine and Cellular Longevity
Volume 2022, Article ID 4777434, 13 pages
https://doi.org/10.1155/2022/4777434

Research Article

ATR-IR Spectroscopy Application to Diagnostic Screening of Advanced Endometriosis

Izabela Kokot,[1] **Sylwester Mazurek**,[2] **Agnieszka Piwowar**,[3] **Roman Szostak**,[2] **Marcin Jędryka**,[4,5] **and Ewa Maria Kratz**[1]

[1]*Department of Laboratory Diagnostics, Division of Laboratory Diagnostics, Faculty of Pharmacy, Wroclaw Medical University, Borowska Street 211A, 50-556 Wroclaw, Poland*
[2]*Faculty of Chemistry, University of Wrocław, F. Joliot-Curie 14, 50-383 Wrocław, Poland*
[3]*Department of Toxicology, Faculty of Pharmacy, Wroclaw Medical University, Borowska Street 211, 50-556 Wroclaw, Poland*
[4]*Department of Oncology, Gynecological Oncology Clinic, Faculty of Medicine, Wroclaw Medical University, Hirszfeld Square 12, 53-413 Wroclaw, Poland*
[5]*Department of Oncological Gynecology, Wroclaw Comprehensive Cancer Center, Hirszfeld Square 12, 53-413 Wroclaw, Poland*

Correspondence should be addressed to Izabela Kokot; izabela.kokot@umed.wroc.pl
and Sylwester Mazurek; sylwester.mazurek@chem.uni.wroc.pl

Received 31 March 2022; Revised 13 May 2022; Accepted 19 May 2022; Published 6 June 2022

Academic Editor: Alin Ciobica

Endometriosis is one of the most common gynecological diseases among young women of reproductive age. Thus far, it has not been possible to define a parameter that is sensitive and specific enough to be a recognized biomarker for diagnosing this disease. Nonspecific symptoms of endometriosis and delayed diagnosis are impulses for researching noninvasive methods of differentiating endometriosis from other gynecological disorders. We compared three groups of individuals in our research: women with endometriosis (E), patients suffering from other gynecological disorders (nonendometriosis, NE), and healthy women from the control group (C). Partial least squares discriminant analysis (PLS-DA) models were developed based on selected serum biochemical parameters, specific regions of the serum's infrared attenuated total reflectance (FTIR ATR) spectra, and combined data. Incorporating the spectral data into the models significantly improved differentiation among the three groups, with an overall accuracy of 87.5%, 97.3%, and 98.5%, respectively. This study shows that infrared spectroscopy and discriminant analysis can be used to differentiate serum samples among women with advanced endometriosis, women without this disease, i.e., healthy women, and, most importantly, also women with other benign gynecological disorders.

1. Introduction

Endometriosis (E) is a benign gynecological disease in which endometrial tissue grows outside the uterus and acts as a eutopic endometrium, causing local inflammation and fibrosis. The consequences of this process include chronic pain and changes leading to infertility [1]. Despite numerous studies, no clear cause for the development of endometriosis has yet been identified, suggesting multifactorial pathogenesis [2, 3]. This is the fundamental problem that makes proper disease diagnosis and treatment difficult since no highly specific diagnostic marker exists. So far, laparoscopy has been recognized as the golden standard of endometriosis diagnostics. However, the current ESHRE guideline (2022) does not support this recommendation anymore, and now, laparoscopy is recommended only for patients with negative imaging results and/or where empirical treatment was unsuccessful or inappropriate. However, members of the Endometriosis Guideline Core Group emphasize that there is still an urgent need for more research to gain more clarity on the most appropriate diagnostics, including laboratory diagnostics [4]. Therefore, there is a great need for a broadly understood, noninvasive diagnosis of endometriosis.

Infrared (IR) and Raman spectroscopy can provide information enabling correct and detailed characteristics of different diseases [5]. Changes in tissues, cells, and body

fluids due to lesions and infection are reflected in the spectroscopic data of biological material. Thus, disease-specific spectral biomarkers of blood or serum could support effective medical diagnostics and have a significant impact on rapid screening for potential patients in large-population tests [6–8].

Attenuated total reflection (ATR) allows IR data of samples to be collected in their native state. The major advantage of this method is that samples can be examined directly in the solid or liquid state without further preparation. For blood serum samples, spectra can be recorded directly for hydrated samples, as they are, or for thin films obtained by drying the fluid on an ATR crystal. In the former case, strong water bands obscure the shape of signals from the remaining components present in the sample. Formally, water contributions can be subtracted from serum spectra, but some specific features in a difference spectrum can be skewed due to hydrogen bonding stabilizing the molecules' structures. The most common procedure applied in blood spectroscopy is collecting IR data from dried, thin films. However, drying serum samples on the ATR crystal is a time-consuming procedure. As an alternative, the ATR spectra of the freeze-dried or lyophilized sera can be utilized. The quality of classification based on IR data depends on the sample storage, drying processes, and other preanalytical factors [9].

Spectroscopic methods usually generate large datasets consisting of thousands of variables, absorbances in the case of ATR spectroscopy. Very often, a strong correlation is observed between absorbances registered at different wavenumbers. Additionally, spectra can be distorted by spectral noise, depending on the instrumental factors and sample characteristics. Therefore, analysis is often supported by multivariate methods to extract relevant information from spectral data, reduce their dimensionality, and avoid overfitting. By applying principal component analysis (PCA) or discriminant analysis (DA), it is possible to distinguish among samples belonging to particular groups [10]. A conjunction of ATR spectroscopy and multivariate modeling techniques has found applications in molecular fingerprinting of disease development, including of breast, brain, and ovarian cancers [11–16]. Classification has been reported of sera samples from patients with Salmonella [17] or viral infections [18–20]. Serum spectra were also used to determine levels of total protein [21], glycated albumin [22], lipidic parameters [23, 24], and glucose [25].

In this study, we present multivariate models that can discriminate among advanced endometriosis, nonendometriosis, and healthy controls by applying previously determined biochemical parameters of serum samples [2, 26] and their ATR spectra. In a commonly used approaches, two groups, i.e., patients and healthy controls, are usually taken into account [27, 28]. However, in our research, two groups of women suffering from benign pathologic conditions, one with advanced endometriosis and one for which endometriosis was excluded, were compared with a group of healthy women without any symptoms of inflammation or medical history of endometriosis, to select biomarkers allowing for discrimination among these three groups of women.

2. Materials and Methods

2.1. Serum Samples. Serum samples from patients with advanced endometriosis (E, $n = 29$, interquartile range of age 31.0–43.0) and without endometriosis (reference group; nonendometriosis, NE, $n = 24$, interquartile range of age 33.0–43.5) were collected at the Department of Oncological Gynecology, Wroclaw Comprehensive Cancer Center. The control group comprised healthy female volunteers (control group, C, $n = 18$, interquartile range of age 35.0–41.0). The E and NE groups had undergone surgical interventions, mainly laparoscopy; following histological verification, they were assigned to the proper group. Patients belonging to E group had advanced endometriosis, corresponding to the revised American Fertility Society classifications of stages III ($n = 12$) and IV ($n = 17$). Women in the NE group were histologically confirmed to have leiomyomas, benign ovarian cysts or severe cervical dysplasia, and cervical intraepithelial neoplasia grade 3 (CIN 3). The control group consisted of healthy, nonpregnant women of reproductive age who were premenopausal, lacked gynecological problems, had no history or symptoms related to endometriosis, and had no symptoms of inflammation, therefore, they were not qualified for laparoscopy. The main exclusion criterion for all groups was cancer, present, treated, or past. Another exclusion criteria were menopause and previous hysterectomy. Due to the homogeneity of the study group (E), the exclusion criterion was endometriosis in the cyst of the abdominal integuments and the postoperative scar and adenomyosis. Only patients with confirmed stage III or IV of endometriosis according to the rAFS classification were included in the study. The reference group (NE) included only patients with histopathologically excluded endometriosis, but with mild gynecological disorders. Women from the control group were recruited from among employees of the Wroclaw Medical University and from our friends. All of the participants were of a similar age and had comparable body mass indexes.

All information regarding blood collection and handling was described in our previous work [2, 26]. The present study was conducted in agreement with the Helsinki II Declaration, and the protocol was approved by the Bioethics Human Research Committee of Wroclaw Medical University (No. 231/2019, No. 634/2019, and No. 685/2019). All of the subjects gave written and informed consent prior to their participation in the study. All of the biochemical analyses were carried out in accordance with the manufacturers' instructions.

2.2. Biochemical Analysis. High sensitive interleukin 1β (hsIL-1β), interleukin 6 (IL-6), chitinase-3-like protein 1 (YKL-40), sirtuins (SIRTs: SIRT3, SIRT5, and SIRT6), and telomerase (TE) levels were determined with commercially available ELISA tests. Human IL-1β ELISAPRO kits (MABTECH AB, Nacka Strand, Stockholm, Sweden) were used to measure hsIL-1β concentrations. High Sensitivity ELISA kit (The Covalab, Villeurbanne, France) and Human Chitinase-3-like Protein 1 ELISA Kit (Bioassay Technology Laboratory, Shanghai, China) were used for determining IL-6 and

YKL-40 concentrations, respectively. Sirtuin concentrations were measured with Human Sirtuin 3 ELISA Kit, Human Sirtuin 5 ELISA Kit, and Human Sirtuin 6 ELISA Kit (Bioassay Technology Laboratory, Shanghai, China), and TE levels were determined using Human Telomerase ELISA Kit (CUSABIO Technology LLC, Wuhan, China). A Mindray-96A ELISA plate reader (Mindray, Shenzhen, China) was used to measure the concentrations of these inflammatory parameters. C-reactive protein (CRP) and immunoglobulin G (IgG) concentrations were measured using the immunoturbidimetric method, highly sensitive for CRP (U-hs DiaSys Diagnostic Systems GmbH, Holzheim, Germany) and immunoglobulin G (FS DiaSys Diagnostic Systems GmbH, Holzheim, Germany), respectively, using the biochemical analyzer Konelab 20i® (ThermoScientific, Vantaa, Finland). This analyzer was also used to determine the levels of total antioxidant status (Randox TAS Kit, Crumlin, United Kingdom), glucose (GLU), total protein (T-P), albumin (ALB), total bilirubin (T-BIL), uric acid (UA), iron (Fe) (Thermo Scientific, Vantaa, Finland), calcium (Ca), magnesium (Mg), total cholesterol (T-CHOL), triglycerides (TG), and high-density lipoprotein (HDL) cholesterol (DiaSys Diagnostic Systems GmbH, Holzheim, Germany). LDL (low-density lipoprotein) cholesterol was calculated using Friedewald's formula. Carcinoma antigen 125 (CA 125), prolactin (PRL), and estradiol (E2) concentrations were measured by Cobas® 6000 analyzer (Roche, Mannheim, Germany). The concentrations of advanced protein oxidation products (AOPP) were measured according to the method of Witko-Sarsat et al. [29], and the ferric-reducing antioxidant power (FRAP) was measured using Benzie and Strain's method [30]. Levels of these parameters were measured using the UV/Vis spectrophotometer (UV-6300PC, VWR, Shanghai, China).

2.3. Spectroscopic Conditions. Attenuated total reflection (ATR) FTIR spectra of serum samples were recorded with an iS50 FTIR spectrometer (Thermo Nicolet, Madison, WI, USA) using a single-reflection Golden Gate (Specac, Slough, UK) diamond accessory. Measurements were performed using a KBr beamsplitter and a DTGS detector. Interferograms were averaged over 128 scans. Next, they underwent Happ-Genzel apodization and Fourier transformation using a zero-filling factor of 2 to give spectra in the 400-4000 cm^{-1} range with a resolution of 4 cm^{-1}. A single FTIR spectrum of serum consisted of 7,469 absorbance points.

Before measurement, the frozen serum samples were thawed at room temperature for 30 min. An aliquot of 10 μL of serum was deposited on ATR crystal and nitrogen-dried over 60 min to obtain a thin film of biological material to analyze. After each measurement, the crystal was cleaned with methanol. Serum samples belonging to various groups of women were measured alternately.

2.4. Computational Analysis. The studied datasets, i.e., matrices of the biochemical diagnostic parameters (71×29) and the absorbance intensities of the ATR spectra (71×7469), were analyzed by applying PCA and discriminant analysis using partial least squares regression through PLS-Toolbox in MATLAB (ver. R2010a, MathWorks, Natwick, MA, USA). The second derivatives of spectral data were computed utilizing the Savitzky–Golay algorithm, applying third-degree polynomial and 15-point windows. Biochemical data were autoscaled before chemometric modeling, while the ATR spectra were mean-centered. The constructed models were cross-validated by applying the leave-one-out procedure. General least squares weighting (GLSW) was applied to PCA performed on the serum parameters [31]. Variables were selected by applying the interval PLS (iPLS) algorithm, as implemented using PLS-Toolbox, working in a forward mode. The mean spectra, together with the standard deviation (SD) of absorbance at each wavenumber, were computed to determine and compare the average IR spectra for all three sample groups.

2.5. Principal Component Analysis (PCA). Data originating from modern spectrometers are characterized by highly redundant information. In typical analyses, the number of obtained variables, e.g., absorbance at a given wavenumber, is much greater than the number of analyzed objects. PCA transforms correlated explanatory variables into new ones that do not show any correlation. These new variables, i.e., principal components (PCs), are linear combinations of explanatory variables, and each PC is orthogonal to the others. The successive PCs explain decreasing variance present in the data not accounted for by previous PCs. When a specific variability resulting from the nature of the investigated objects is greater than undesirable random variability, only the k-first PCs are considered [32]. Therefore, using PCs can reduce data dimensionality significantly without information loss.

PCA decomposes the X data matrix, containing n rows (objects) and m columns (variables), into two smaller matrices:

$$X_{n,m} = T_{n,k} \times P^{T}{}_{k,m} + E_{n,m}, \quad (1)$$

where T (the scores matrix) describes the relations among the samples, P (loadings) provides the mutual dependencies between variables, and E shows differences between the data matrix values and those obtained from the product of matrices T and P.

2.6. Partial Least Squares Discriminant Analysis. Partial least squares discriminant analysis (PLS-DA) is a chemometric technique for separating groups of samples by combining a dataset matrix (X) with class membership (Y). This approach is aimed at maximizing the covariance between the independent variables X and the corresponding dependent variable Y of highly multidimensional data by finding a linear subspace of the explanatory variables. This new subspace allows Y to be predicted based on a reduced number of PLS factors or latent variables (LV). These factors describe the behavior of dependent variables and include a subspace onto which independent variables are projected [33, 34]. The main advantage of PLS-DA is its ability to handle highly collinear and noisy data, which are very common outputs from spectroscopic measurements or metabolomics experiments. This technique provides a visual interpretation of

Table 1: Serum biochemical parameters for the studied groups.

	Endometriosis $n = 29$ Mean ± SD	Nonendometriosis $n = 24$ Mean ± SD	Control $n = 18$ Mean ± SD
PRL (ng/mL)	29.01 ± 18.71	27.02 ± 18.62	12.84 ± 4.86
CA 125 (U/mL)	113.41 ± 129.42	23.64 ± 17.39	14.28 ± 7.40
IgG (mg/dL)	1065.46 ± 286.73	1078.22 ± 298.25	1237.28 ± 215.91
hsCRP (mg/L)	14.29 ± 19.45	13.88 ± 19.96	0.96 ± 1.19
Albumin (g/dL)	4.36 ± 0.64	4.13 ± 0.32	4.26 ± 0.19
Calcium (mg/dL)	9.62 ± 1.15	9.35 ± 0.49	9.29 ± 0.25
Magnesium (mg/dL)	2.44 ± 0.37	2.47 ± 0.18	2.22 ± 0.14
hsIL-1β (pg/ml)	0.57 ± 0.39	0.56 ± 0.46	0.27 ± 0.26
IL-6 (pg/ml)	19.33 ± 43.69	18.05 ± 34.09	1.47 ± 1.48
FRAP (mmol/L)	1.11 ± 0.26	1.18 ± 0.30	0.95 ± 0.22
AOPP (μmol/L)	235.16 ± 150.41	181.78 ± 156.00	105.16 ± 49.24
YKL-40 (ng/mL)	685.22 ± 1246.58	403.29 ± 934.76	104.12 ± 154.07

AOPP: advanced protein oxidation products; CA 125: carcinoma antigen 125; FRAP: ferric-reducing antioxidant power; hsCRP: high sensitive C-reactive protein; hsIL-1β: high sensitive interleukin 1β; IgG: immunoglobulin G; IL-6: interleukin 6; PRL: prolactin; YKL-40: chitinase-3-like protein 1. Data presented in the table are a part of previously published study results [2, 26].

complex datasets through low-dimensional, easily interpretable score plots that illustrate the separation between different groups [33].

2.7. Classifier Evaluation Criteria. Different criteria can be used to evaluate the quality of classifiers. In our analysis, classification accuracy, sensitivity, specificity, and receiver operating characteristic curves (ROC) were used to characterize the performance of the obtained PLS-DA models. In medical applications, the model characterized by higher area under the ROC is better suited for distinguishing patients from healthy subjects. "Positive" and "negative" results are classification predictions obtained from the model. "True" and "false" are the actual data. The sensitivity, specificity, and accuracy were calculated using the following equations:

$$\text{Sensitivity} = \frac{\text{TP}}{\text{TP} + \text{FN}}, \tag{2}$$

$$\text{Specificity} = \frac{\text{TN}}{\text{TN} + \text{FP}}, \tag{3}$$

$$\text{Accuracy} = \frac{\text{TP} + \text{TN}}{\text{TP} + \text{TN} + \text{FP} + \text{FN}}, \tag{4}$$

where TP and TN denote the true-positive and true-negative values and FP and FN represent false-positive and false-negative values, respectively.

3. Results and Discussion

Diagnosing endometriosis based on parameters of peripheral blood serum is not straightforward. The disease's development appears directly related to inflammatory processes, and since there is no specific biomarker [35], only a combination of commonly determined blood biochemical markers may allow endometriosis to be distinguished from other inflammatory conditions and, in the future, increase the chances of detecting endometriosis in large-scale tests of serum samples from women. Table 1 provides values of selected biochemical parameters for the three groups of subjects, and Table S1 in the Supplementary Materials contains a complete list of the examined serum parameters.

3.1. Multivariate Analysis of Serum Parameters. Our recent studies discussed the importance of selected blood serum parameters for advanced endometriosis diagnostics [2, 26]. The most promising serum parameters as markers of inflammation and oxidative-antioxidant balance were interleukin 6, prolactin, CA 125, FRAP, telomerase, and advanced protein oxidation products. Although these parameters are not specific to advanced endometriosis, they can serve as useful noninvasive diagnostic tools for identifying patients with high risk of developing advanced endometriosis. This itself is a challenge.

Principal component analysis (PCA) was performed on an autoscaled matrix of parameters without any additional pretreatment. The distribution of the objects in the PC1/PC2 coordination system, as presented in Fig. S1 in the Supplementary Materials, showed no specific grouping of samples, and combination of higher PCs did not improve the separation. Separation of the three samples groups became clearer when applying general least squares weighting (GLSW) which resulted in the expected sample arrangement in the PCA score plot. This plot together with the loadings on PCs is presented in Fig. S2 in the Supplementary Materials. Given these plots, the parameters displaying the most pronounced impact on differentiation among serum samples were CA 125, immunoglobulin G, albumin, magnesium, hsIL-1β, and FRAP. Our findings seem to be particularly important considering that during the development of

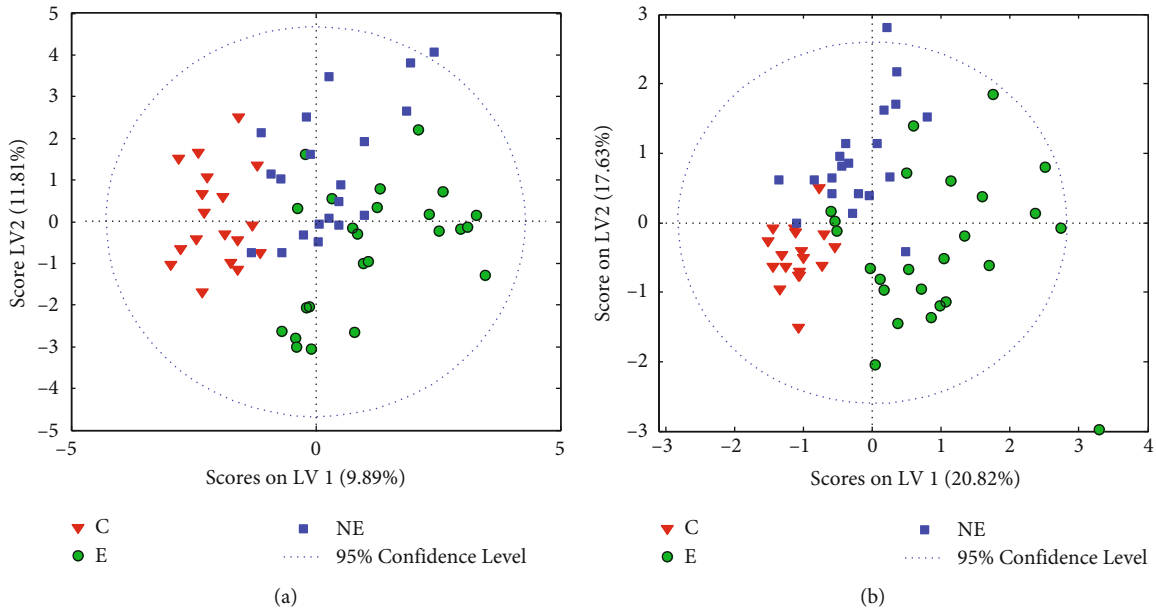

Figure 1: Score plots for PLS-DA modeling of biochemical data from serum samples: (a) all parameters included ($n = 29$) and (b) iPLS variable selection ($n = 6$). E: endometriosis; NE: nonendometriosis; C: control group of healthy women.

inflammation, an increase in the serum concentration of inflammatory markers CA 125 and IgG and the proinflammatory cytokine hsIL-1β is observed, with a simultaneous decrease in the level of albumin, i.e., acute phase protein. Increased FRAP, as one of the antioxidant markers reflecting blood plasma's antioxidant capacity, is associated with elevated free radical production; their concentration increases significantly in inflammatory conditions. On the other hand, magnesium deficiency may also be associated with inflammation and increased concentration of free radicals. Inflammatory mediators and free radicals could induce oxidative DNA damage [36, 37]. Previous studies have suggested that persons with endometriosis experience vascular inflammation [38, 39]. Magnesium relaxes smooth muscle [40, 41] and thus may be related to endometriosis through its influence on retrograde menstruation [41]. The obtained PCA score plots are even more important because PCA belongs to a group of an unsupervised methods and the algorithm does not take class affiliation into account during matrix decomposition.

In the next step, the PLS-DA model was constructed by applying the same dataset of serum parameters. The model including all available parameters separated the samples belonging to E, NE, and controls relatively well. The PLS-DA scores are shown in Figure 1, and Fig. S3 in the Supplementary Materials presents the variable importance in projection (VIP) scores. The latter plot indicates that CA 125, together with albumin and magnesium content, had the strongest impact on differentiation among the three studied groups. Our findings are in line with those of the previous studies, in which advanced endometriosis was associated with high serum CA 125 levels [36]. Due to the lack of a specific marker for endometriosis, CA 125 concentration in serum is considered an important prognostic factor in patients with endometriosis in clinical practice and should be considered when surgical treatment is suspected, particularly when assessing the disease's severity, the size of the lesion, and adhesions [42]. Interestingly, in comparison to PCA modeling, no pronounced differences were observed in sample classification when the GLSW pretreatment was used.

The interval PLS (iPLS) algorithm was applied to select variables, in order to reduce the dimensionality of the parameters' matrix and find the most significant determinants of serum. On this basis, six of the 29 diagnostic parameters were chosen. The obtained set, namely, CA 125, IgG, CRP, albumin, magnesium, and chitinase-3-like protein 1 (YKL-40), is quite similar to that one found using VIP scores. All of the selected parameters reflect the ongoing inflammation. It is believed that YKL-40 is a marker which excludes endometriosis, rather than confirms its presence or progression [2, 43]. The classifier constructed for four LVs (latent variables) applying selected inputs was characterized by accuracy of 91-92% (86-89%), sensitivity of 81-94% (75-94%), and specificity of 89-100% (87-95%), with the models' cross-validation results shown in parentheses. In our opinion, the results presented above clearly indicate the high clinical usefulness of the selected parameters for identifying advanced endometriosis diagnoses. Detailed characteristics of the obtained PLS-DA model are presented in Table 2 and Table S2 in the Supplementary Materials. The PLS-DA model's scores are shown in Figure 1, while plots of the receiver operating characteristic (ROC) curves, expressing the classification performance, are shown in Fig. S4 in the Supplementary Materials.

3.2. ATR Spectra of Serum. In parallel with biochemical analysis, FTIR ATR spectra of 71 human sera were collected. Figure 2 and Fig. S5 in the Supplementary Materials show the IR spectra of the samples from the three groups of women.

Table 2: Parameters of PLS-DA models.

Parameter	Biochemistry			FTIR ATR			Fused data		
	E	NE	C	E	NE	C	E	NE	C
Accuracy	92.2 (87.5)	92.2 (85.9)	90.6 (89.1)	98.6 (92.9)	97.1 (92.9)	98.6 (94.3)	98.5 (94.1)	98.5 (95.6)	100 (98.5)
Sensitivity (TPR)	80.8 (76.9)	90.0 (75.0)	94.4 (94.4)	96.6 (89.7)	95.8 (91.7)	100 (88.2)	96.3 (92.6)	100 (91.3)	100 (100)
Specificity (TNR)	100 (94.7)	93.2 (90.9)	89.1 (87.0)	100 (95.1)	97.8 (93.5)	98.1 (96.2)	100 (95.1)	97.8 (97.8)	100 (98.0)
Precision (PPV)	100 (90.9)	85.7 (78.9)	77.3 (73.9)	100 (92.9)	95.8 (88.0)	94.4 (88.2)	100 (92.6)	95.8 (95.5)	100 (94.7)
F1-score	89.4 (83.3)	87.8 (76.9)	85.0 (82.9)	98.2 (91.2)	95.8 (89.8)	97.1 (88.2)	98.1 (92.6)	97.9 (93.3)	100 (97.3)
Overall accuracy		87.5 (81.3)			97.3 (89.9)			98.5 (94.3)	

E: endometriosis; NE: nonendometriosis; C: control group of healthy women; TPR: true positive rate; TNR: true negative rate; PPV: positive predictive value. In parenthesis, the results of cross-validation are shown.

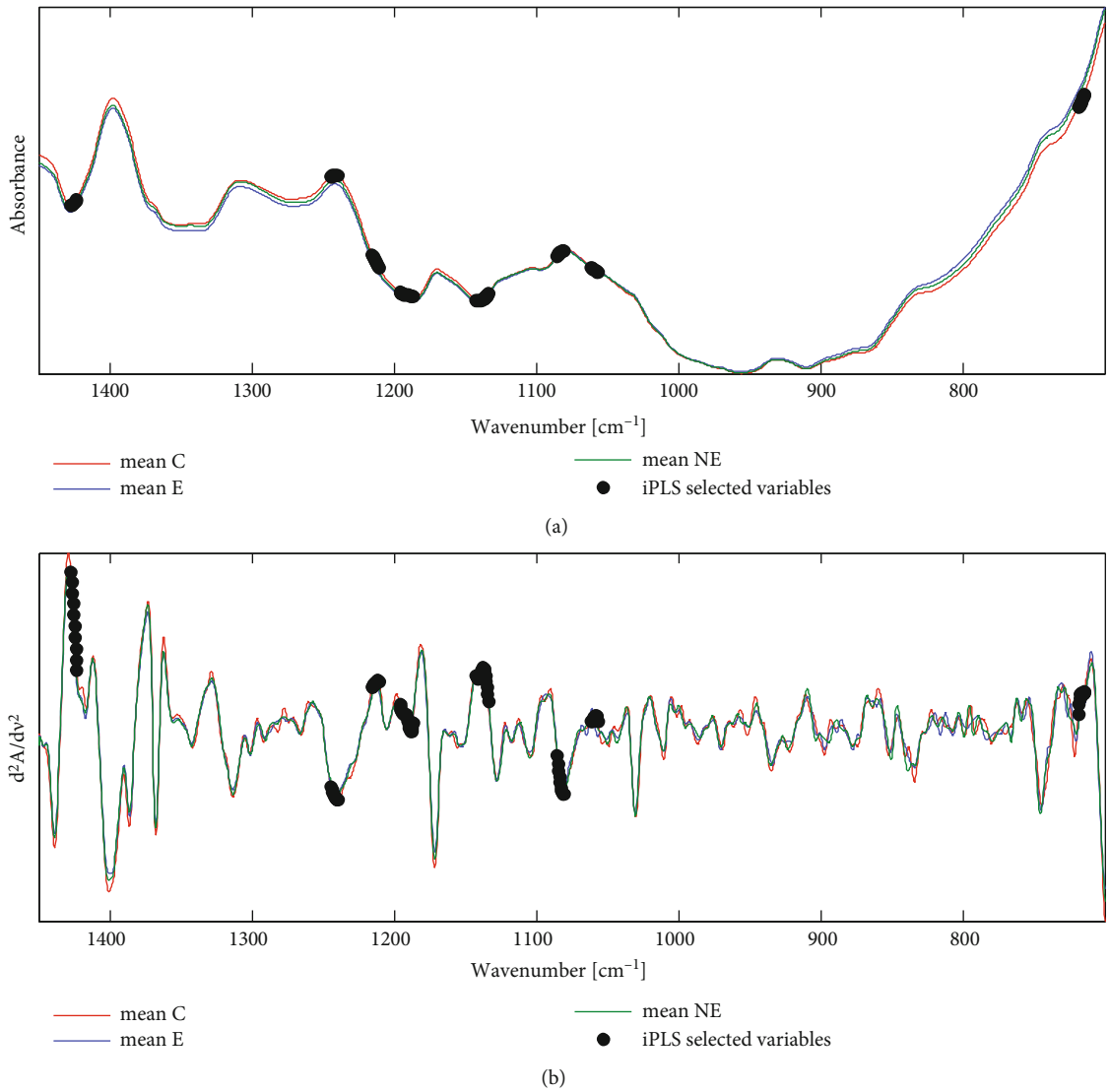

Figure 2: Average FTIR ATR spectra of sera in the 700-1450 cm^{-1} range for the three studied groups (a) and the second derivatives of the spectra (b); the black dots indicate variables selected by iPLS for the PLS-DA model. E: endometriosis; NE: nonendometriosis; C: control group of healthy women; cm^{-1}: unit of the wavenumbers presented as the reciprocal centimeters.

Tentative assignments of the vibrational bands present in ATR spectra can be found elsewhere [44, 45]. The spectra of the E, NE, and C groups are very similar, and subtraction plots (Fig. S6 in the Supplementary Materials) indicate that their differences exceeded the standard deviation of absorbance intensity for the mean spectra only at particular wavenumbers.

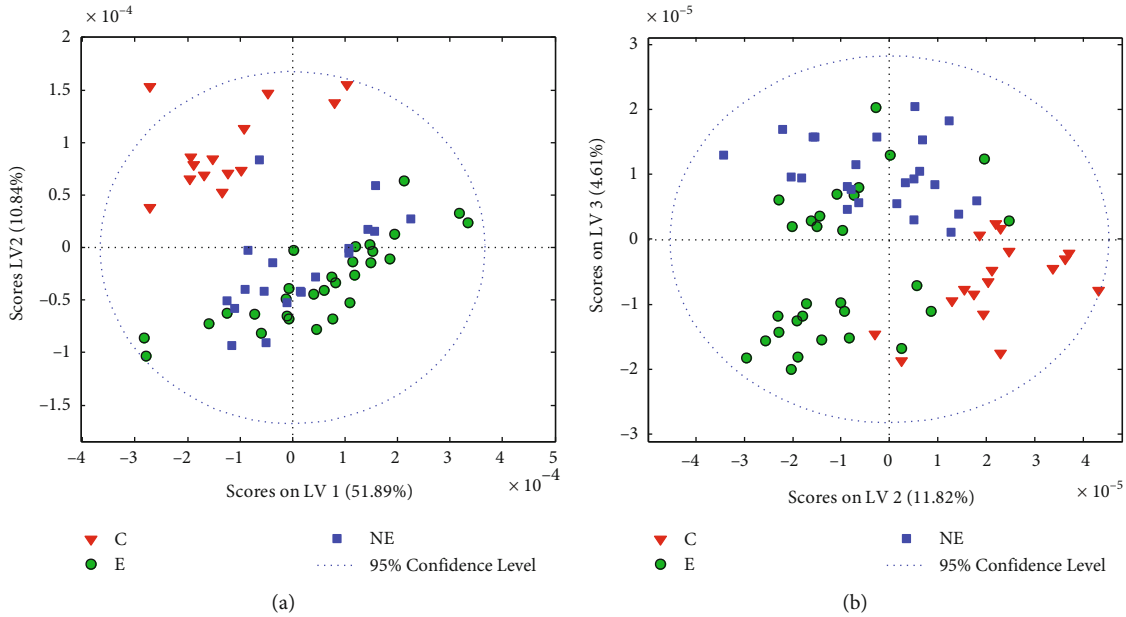

Figure 3: PLS-DA score plots obtained for the ATR spectra of the serum samples for the model applying the 700-1450 cm^{-1} range (a) and the model with variables selected via iPLS (b). E: endometriosis; NE: nonendometriosis; C: control group of healthy women.

Preparations of thin serum film onto an ATR crystal are not always reproducible and can result in nonequal sample deposition on the crystal, despite attempts to follow all established procedures. This can result in uneven drying of the samples, which generates undesirable spectral variation [46]. An effect of absorbance changes to IR spectra in a drying function is shown in Fig. S7 in the Supplementary Materials. The greatest variability of signal in the serum spectra was observed in the amide band regions. Drying resulted in strong changes to the intensity of the ν(OH) band in the 3000-3500 cm^{-1} range and the narrowing of the amide A band. Drying enhances spectral features originating from chemical components of serum, whereas strong water absorbance was observed in wet samples. These changes are observable for the amide I and II bands in the IR serum spectra, with maxima at about 1640 and 1540 cm^{-1}, respectively. As is visible in Fig. S7 in the Supplementary Materials, changes to the water content influence the band positions, which, in the case of unequal drying of serum samples, can be a source of additional variability influencing the classification results. This effect also may be important when analyzing signal intensity. Taking our observations into account, and based on the experiences of other researchers, we standardized the conditions of the analysis process to obtain reliable and repeatable results. In a series of preliminary experiments, the biological samples were dried for 60 min. After this time, changes in the IR spectra's absorbance were much smaller than those observed after shorter time intervals were. The scores and loadings of the PCA obtained for the dried samples are plotted in Fig. S8 in the Supplementary Materials.

3.3. Multivariate Modeling of Spectral Data. Special attention was paid to the 700-1450 cm^{-1} range of the ATR spectra. As other studies pointed out, spectral ranges outside of amide band regions are better suited to discriminating between ill and healthy subjects [28, 47]. The second derivatives of ATR spectra without additional pretreatment were used to construct chemometric models. The score plots of PCA for this spectral region did not allow the three groups of serum samples to be separated when considering the first two principal components. Only adding the third and fourth PCs allowed healthy controls to be distinguished from the E and NE groups but without clear distinction between advanced endometriosis and nonendometriosis patients. The score plots of PCA are shown in Fig. S9 in the Supplementary Materials. Discriminant analysis resulted in a quite similar distribution of samples. The score plots obtained from PLS-DA (Fig. S10 in the Supplementary Materials) show a clear separation between control and ill patients; however, similarly to PCA, E and NE objects were mixed. This suggests that the region of sera spectrum applied for modeling contains characteristic features that are correlated with overall inflammatory conditions but does not enable the recognition of different inflammation sources.

The VIP score plots were used to improve the quality of discrimination among the three studied groups based on the serum's ATR spectra (Fig. S11 in the Supplementary Materials). This method can indicate variables with differing spectra among the three examined groups. However, models constructed based on manually selected inputs did not enable satisfactory separation between the E and NE groups. Cleaner separation between samples was obtained with the PLS-DA model built with variables selected by the iPLS procedure. Taking into account the dimensionality of the absorbance data matrix, 10-variable intervals, corresponding to the spectral resolution of the ATR spectra, were established during the procedure. Eight intervals within the analyzed spectral range, i.e., 80 points of spectral data, were selected as inputs, as highlighted in Figure 2. The variables selected

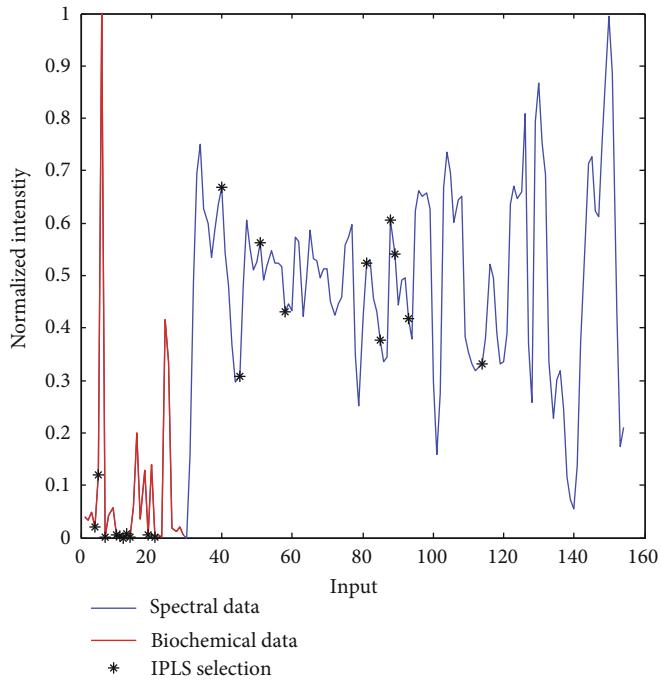

Figure 4: Representative input for fused data.

by the iPLS cover spectral regions containing some characteristic vibrations in the IR spectra of serum. These include the peaks at 1056 and 1080 cm^{-1}, characteristic of nucleic acids, the $\nu_{as}(PO_2^-)$ vibrations of phospholipids or ν(C-O) of ribose, and the band at 1186 cm^{-1}, which can be assigned to the C-O-C asymmetric vibrations of phospholipids, triglycerides, and cholesterol esters. The selected variables also included a peak at about 1137 cm^{-1}, which can be assigned to the ν_{as}(CO-O-C) vibration of glycan DNA and RNA and the ν(C-O) of ribose; the band at 1213 cm^{-1}, characteristic of A-DNA, $\nu_{as}(PO_2^-)$ and RNA vibrations; and a contribution at 1241 cm^{-1} from nucleic acids, the $\nu_{as}(PO_2^-)$ vibrations and immunoglobulins [44, 45].

In the resulting model, the two first latent variables described about 80% of the total variance present in spectral data, versus 63% by a model built without variable selection. The PLS-DA scores are presented in Figure 3; the ROC plots obtained for the developed model are shown in Fig. S12 in the Supplementary Materials. The modeling parameters are gathered in Table 2 and S2 in the Supplementary Materials. The model constructed using five PLS factors was characterized by accuracy of 97-99% (93-94%), sensitivity of 96-100% (88-92%), and specificity of 98-100% (93-96%) for the three studied groups; the cross-validation results are shown in parentheses. The quality parameters determined for the constructed classifier were significantly higher than those obtained from modeling biochemical data, and the overall accuracy reached 97% (Table 2).

The obtained results show compatibility between the biochemical and spectral data for the three studied patient groups, indicating that changes to the chemical composition of serum samples due to inflammatory conditions in advanced endometriosis and nonendometriosis patients have straightforward effects on their ATR spectra. Even when such differences are quite subtle, the variability present in spectral data can be separated effectively by PLS-DA, making vibrational spectroscopy a potential tool for detecting advanced endometriosis.

3.4. Models Based on Fused Data. It seems justified to check whether classification models built using both biochemical and spectral data from serum samples would allow for better separation of the analyzed patient groups. This is not a straightforward operation because biochemical and spectral data differ. First, the number of biochemical parameters is orders of magnitude smaller than the number of points in the analyzed spectra. Second, their values also differ by orders of magnitude. Third, a noticeable proportion of spectral data provides no useful information due to spectral noise. To select a set of IR intensities representing the 700-1450 cm^{-1} range of ATR spectra, PCA was performed on a transposed matrix of the spectra's second derivatives. The original data were reduced by a factor of 10 after selecting evenly distributed points from each quadrant of the PC1/PC2 scores plot (Fig. S13 in the Supplementary Materials). Next, range scaling was applied to obtain a fused dataset containing biochemical parameters values normalized between 0 and 1 as well as intensities at selected wavenumbers. A representative input is presented in Figure 4.

Prior to modeling, the iPLS algorithm was used again to select the most relevant variables in the matrix of fused data. Absorbances at 10 wavenumbers (731, 747, 796, 834 1060, 1078, 1094, 1100, 1125, and 1243 cm^{-1}) were selected by iPLS from the spectral portion of the combined dataset (Figure 4). Among them, the contributions can be distinguished from the C-C and C-O vibrations of carbohydrates (1094 and 1100 cm^{-1}), features originating from nucleic acids and phospholipids (intensities at 1060 and 1078 cm^{-1}) and

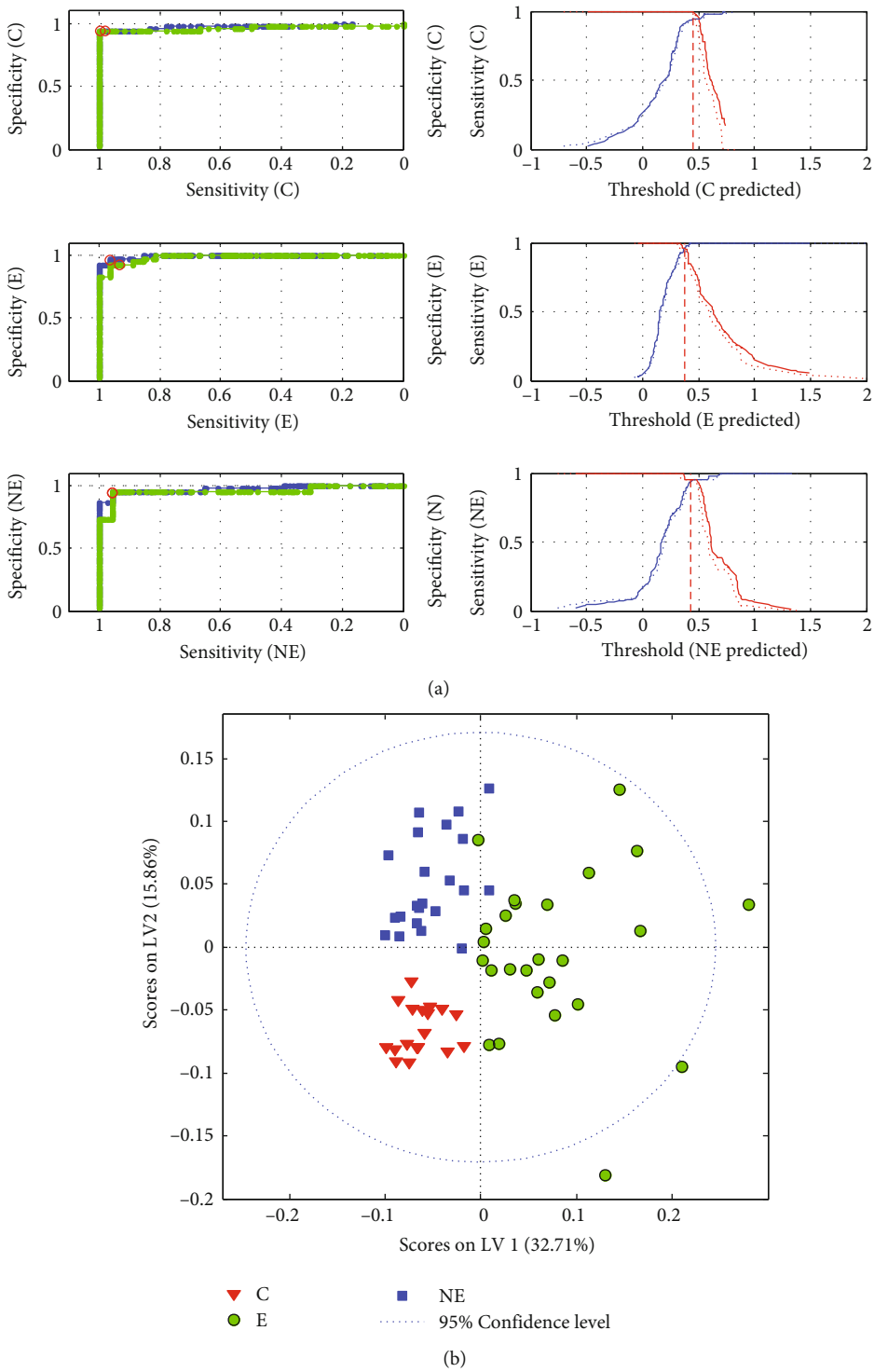

Figure 5: ROC curves (a) and scores plot (b) for the PLS-DA model based on the fused data. E: endometriosis; NE: nonendometriosis; C: control group of healthy women.

immunoglobulins (band at 1243 cm^{-1}) [44, 45]. Interestingly, among the 10 selected biochemical parameters of serum, three, CA 125, albumin, and magnesium, were the same as those selected for the classifier constructed for biochemical data, which seems to confirm their crucial role in separating the three patient groups. The remaining selected parameters include prolactin, total antioxidant status (TAS), total protein (T-P), total bilirubin (T-BIL), calcium (Ca), uric acid (UA), and hsIL-1β. These parameters are related to both the oxidative-antioxidant balance and inflammation state. Particular attention, except CA 125, should be paid to prolactin, which has a pleiotropic effect on the human body. Its most important functions are related to reproduction, calcium metabolism, osmoregulation, and behavior.

Prolactin has an immunostimulatory effect, including promoting autoimmunity, although it cannot initiate an immune reaction itself; rather, it is a factor that maintains homeostasis during immune reactions. Prolactin is involved in stimulating the immune response, providing specific interference in inducing B-lymphocyte tolerance, enhancing the proliferative response to antigens and mitogens and increasing immunoglobulin and cytokine production, including of IL-1β [48–50]. This positive acute-phase protein induces IL-6 production through, e.g., peritoneal mesothelial cells, which additionally contributes to the local inflammation in endometriosis patients [3]. Through the action of IL-1β in promoting endometrial cells' angiogenesis and proliferation, it may play a key role in the development of endometriosis [51, 52]. Uric acid also indirectly contributes to inducing IL-1β synthesis [53]. Additionally, attention should be paid to UA dualism. Under physiological conditions, UA reflects the body's metabolic state and has antioxidant properties. It is responsible for approximately 60% of total antioxidant capacity and, along with other low-molecular-weight antioxidants such as total bilirubin, is the first line of antioxidant defense. However, given reduced availability of other antioxidants, it begins to act as an oxidative factor in various pathological processes. UA's role and the mechanism of its action in reproductive system disorders have not yet been elucidated [53, 54], although our studies have also emphasized its importance in advanced endometriosis. Moreover, both prolactin and uric acid in the blood serum can serve as biomarkers for the activity of some autoimmune diseases [49].

The constructed classifier had accuracy of 99-100%, while its sensitivity and specificity were 96-100% and 98-100%, respectively (Table 2). Notably, this model required only two LVs to reach the best performance, versus 4-5 PLS factors needed by PLS-DA models built separately for biochemical parameters or spectra. The obtained PLS-DA score plots and ROC curves are shown in Figure 5, while classification errors are presented in Fig. S14 in the Supplementary Materials.

The parameters of the classifiers obtained based on different data blocks occurred to be quite similar, as were their separation of the three groups of women. However, incorporating spectral data significantly improved the robustness of the elaborated models, in comparison with the values obtained for the models based on biochemical parameters only (Table 2). Since no specific marker of endometriosis has been found that would allow unequivocal diagnosis of the disease, combining spectral data with routinely determined biochemical parameters used to assess the state of the body could provide a tool for detecting women with a high probability of advanced endometriosis.

4. Conclusions

PLS-DA models were developed based on selected biochemical parameters and regions of FTIR ATR spectra of serum that could identify women at risk of advanced endometriosis, women with a developing inflammatory process with another origin, and healthy women. The sensitivity, specificity, and accuracy of the obtained models were 81-100%, 89-100%, and 91-100%, respectively. This study shows that infrared spectroscopy and discrimination analysis can be used to differentiate serum samples originating from women with advanced endometriosis and without endometriosis. Standardization of this method, based on the results obtained for a larger group of participants, likely will allow for effective endometriosis screening and diagnostics of this disease with advanced stages. One remaining challenge is still the development of classifiers able to detect the early stages of endometriosis.

Abbreviations

ALB:	Albumin
AOPP:	Advanced protein oxidation products
BMI:	Body mass index
C:	Control group of healthy women
Ca:	Calcium
CA 125:	Carcinoma antigen 125
DA:	Discriminant analysis
E:	Endometriosis
E2:	Estradiol
Fe:	Iron
FRAP:	Ferric-reducing antioxidant power
FTIR ATR:	Fourier transform infrared spectroscopy-attenuated total reflectance
GLSW:	General least squares weighting
GLU:	Glucose
HDL:	High-density lipoprotein cholesterol
hsCRP:	High sensitive C-reactive protein
hsIL-1β:	High sensitive interleukin 1β
IgG:	Immunoglobulin G
IL-6:	Interleukin 6
iPLS:	Interval partial least squares
IR:	Infrared spectroscopy
LDL:	Low-density lipoprotein cholesterol
LV:	Latent variable
Mg:	Magnesium
NE:	Nonendometriosis
PC:	Principal component
PCA:	Principal component analysis
PLS-DA:	Partial least squares discriminant analysis
PPV:	Positive predictive value
PRL:	Prolactin
rAFS:	Revised American Fertility Society classification
ROC:	Receiver operating characteristic curve
SD:	Standard deviation
SIRT3:	Sirtuin 3
SIRT5:	Sirtuin 5
SIRT6:	Sirtuin 6
TAS:	Total antioxidant status
TE:	Telomerase
TG:	Triglycerides
TNR:	True negative rate
T-P:	Total protein
TPR:	True positive rate
T-BIL:	Total bilirubin
T-CHOL:	Total cholesterol

UA: Uric acid
VIP: Variable importance in projection
YKL-40: Chitinase-3-like protein 1.

Data Availability

The corresponding authors can provide the datasets for this study upon reasonable request.

Ethical Approval

The study was conducted according to the guidelines of the Declaration of Helsinki II and approved by the Bioethics Committee of Wroclaw Medical University (No. KB-231/2019, No. 634/2019, and No. KB-685/2019; Approval dates: 18 March 2019, 30 August 2019, and 7 October 2019, respectively).

Consent

Informed consent was obtained from all individual participants included in the study. All authors give their consent for the publication of this study.

Conflicts of Interest

The authors have no conflicts of interest to declare that are relevant to the content of this article.

Authors' Contributions

Conceptualization was carried out by I.K., S.M., and E.M.K.; M.J. was responsible for the resources; methodology was carried out by I.K. and S.M.; formal analysis was carried out by I.K. and S.M.; I.K., S.M., and E.M.K. wrote the original draft; I.K., S.M., A.P., R.S., M.J., and E.M.K. wrote, reviewed, and edited the manuscript; visualization was carried out by I.K., S.M., and E.M.K.; supervision over the analysis was carried out by S.M.; project supervision was carried out by A.P. and E.M.K.; I.K. and E.M.K were responsible for the funding acquisition. All authors have read and agreed to the published version of the manuscript.

Acknowledgments

This research was financially supported by the Ministry of Health Subvention according to number SUBZ.D270.22.047 from the IT Simple system of Wroclaw Medical University.

Supplementary Materials

Supplementary Materials Table S1: serum parameters. Table S2: confusion matrix for PLS-DA models after iPLS variable selection. Fig. S1: PCA scores based on biochemical parameters of serum samples. Fig. S2: PCA of biochemical serum parameters obtained with GLSW pretreatment. Fig. S3: VIP scores for PLS-DA modeling of biochemical data of serum samples. Fig. S4: PLS-DA of serum biochemical parameters. Fig. S5: Average FTIR ATR spectra of serum samples for three studied groups and second derivatives of spectra. Fig. S6: ATR difference spectra of average serum samples with ±SD of absorbance. Fig. S7: IR spectra of serum sample dried on an ATR crystal collected in 10 min intervals. Fig. S8: PCA for ATR spectra of serum sample during drying and thin film formation. Fig. S9: PCA scores for ATR spectra of serum samples obtained based on 700-1450 cm^{-1} spectral range. Fig. S10: PLS-DA scores for ATR spectra of serum samples obtained based on 700-1450 cm^{-1} spectral range. Fig. S11: VIP scores of PLS-DA and iPLS variable selection for ATR data in the 700-1450 cm^{-1} spectral range. Fig. S12: PLS-DA of ATR spectra of sera-ROC plots for all three groups of samples and calibration/cross-validation errors for the model constructed applying variables selected by iPLS. Fig. S13: ATR inputs selected by PCA for fused data modeling. Fig. S14: errors of classification for PLS-DA model constructed on the basis of fused data. *(Supplementary Materials)*

References

[1] L. C. Giudice and L. C. Kao, "Endometriosis," *Lancet*, vol. 364, no. 9447, pp. 1789–1799, 2004.

[2] I. Kokot, A. Piwowar, M. Jedryka, K. Solkiewicz, and E. M. Kratz, "Diagnostic significance of selected serum inflammatory markers in women with advanced endometriosis," *International Journal of Molecular Sciences*, vol. 22, no. 5, p. 20, 2021.

[3] S. H. Ahn, S. P. Monsanto, C. Miller, S. S. Singh, R. Thomas, and C. Tayade, "Pathophysiology and immune dysfunction in endometriosis," *BioMed Research International*, vol. 2015, 12 pages, 2015.

[4] C. M. Becker, A. Bokor, O. Heikinheimo et al., "ESHRE guideline: endometriosis," *Human Reproduction Open*, vol. 2022, no. 2, 2022.

[5] D. Perez-Guaita, S. Garrigues, and M. de la Guardia, "Infrared-based quantification of clinical parameters," *TrAC, Trends in Analytical Chemistry*, vol. 62, pp. 93–105, 2014.

[6] F. Bonnier, H. Blasco, C. Wasselet et al., "Ultra-filtration of human serum for improved quantitative analysis of low molecular weight biomarkers using ATR-IR spectroscopy," *Analyst*, vol. 142, no. 8, pp. 1285–1298, 2017.

[7] F. Bonnier, G. Brachet, R. Duong et al., "Screening the low molecular weight fraction of human serum using ATR-IR spectroscopy," *Journal of Biophotonics*, vol. 9, no. 10, pp. 1085–1097, 2016.

[8] H. J. Byrne, R. Bonnier, J. McIntyre, and D. J. Parachalil, "Quantitative analysis of human blood serum using vibrational spectroscopy," *Clinical Spectroscopy*, vol. 2, p. 100004, 2020.

[9] J. M. Cameron, H. J. Butler, D. J. Anderson et al., "Exploring pre-analytical factors for the optimisation of serum diagnostics: progressing the clinical utility of ATR-FTIR spectroscopy," *Vibrational Spectroscopy*, vol. 109, p. 103092, 2020.

[10] D. Perez-Guaita, J. Kuligowski, G. Quintas, S. Garrigues, and M. de la Guardia, "Modified locally weighted-partial least squares regression improving clinical predictions from infrared spectra of human serum samples," *Talanta*, vol. 107, pp. 368–375, 2013.

[11] V. E. Sitnikova, M. A. Kotkova, T. N. Nosenko, T. N. Kotkova, D. M. Martynova, and M. V. Uspenskaya, "Breast cancer detection by ATR-FTIR spectroscopy of blood serum and multivariate data-analysis," *Talanta*, vol. 214, p. 120857, 2020.

[12] J. M. Cameron, C. Rinaldi, H. J. Butler et al., "Stratifying brain tumour histological sub-types: the application of ATR-FTIR serum spectroscopy in secondary care," *Cancers*, vol. 12, no. 7, p. 16, 2020.

[13] J. R. Hands, K. M. Dorling, P. Abel et al., "Attenuated Total reflection Fourier transform infrared (ATR-FTIR) spectral discrimination of brain tumour severity from serum samples," *Journal of Biophotonics*, vol. 7, no. 3-4, pp. 189–199, 2014.

[14] K. M. G. Lima, K. B. Gajjar, P. L. Martin-Hirsch, and F. L. Martin, "Segregation of ovarian cancer stage exploiting spectral biomarkers derived from blood plasma or serum analysis: ATR-FTIR spectroscopy coupled with variable selection methods," *Biotechnology Progress*, vol. 31, no. 3, pp. 832–839, 2015.

[15] G. L. Owens, K. Gajjar, J. Trevisan et al., "Vibrational biospectroscopy coupled with multivariate analysis extracts potentially diagnostic features in blood plasma/serum of ovarian cancer patients," *Journal of Biophotonics*, vol. 7, no. 3-4, pp. 200–209, 2014.

[16] H. Ghimire, M. Venkataramani, Z. Bian, Y. Liu, and A. G. U. Perera, "ATR-FTIR spectral discrimination between normal and tumorous mouse models of lymphoma and melanoma from serum samples," *Scientific Reports*, vol. 7, no. 1, p. 16993, 2017.

[17] K. Naseer, S. Ali, S. Mubarik, S. Z. Hussain, and J. Qazi, "Use of ATR-FTIR for detection of Salmonella typhi infection in human blood sera," *Infrared Physics & Technology*, vol. 110, p. 103473, 2020.

[18] K. Naseer, S. Ali, and J. Qazi, "ATR-FTIR spectroscopy based differentiation of typhoid and dengue fever in infected human sera," *Infrared Physics & Technology*, vol. 114, p. 103664, 2021.

[19] M. C. D. Santos, Y. M. Nascimento, J. M. G. Araujo, and K. M. G. Lima, "ATR-FTIR spectroscopy coupled with multivariate analysis techniques for the identification of DENV-3 in different concentrations in blood and serum: a new approach," *RSC Advances*, vol. 7, no. 41, pp. 25640–25649, 2017.

[20] L. Sitole, F. Steffens, T. P. J. Kruger, and D. Meyer, "Mid-ATR-FTIR spectroscopic profiling of HIV/AIDS sera for novel systems diagnostics in global health," *Omics: a Journal of Integrative Biology*, vol. 18, no. 8, pp. 513–523, 2014.

[21] K. Spalding, F. Bonnier, C. Bruno et al., "Enabling quantification of protein concentration in human serum biopsies using attenuated total reflectance - Fourier transform infrared (ATR-FTIR) spectroscopy," *Vibrational Spectroscopy*, vol. 99, pp. 50–58, 2018.

[22] Y. P. Li, F. C. Li, X. H. Yang et al., "Quantitative analysis of glycated albumin in serum based on ATR-FTIR spectrum combined with SiPLS and SVM," *Spectrochimica Acta A*, vol. 201, pp. 249–257, 2018.

[23] A. Oleszko, J. Hartwich, A. Wojtowicz, M. Gasior-Glogowska, H. Huras, and M. Komorowska, "Comparison of FTIR-ATR and Raman spectroscopy in determination of VLDL triglycerides in blood serum with PLS regression," *Spectrochimica Acta A*, vol. 183, pp. 239–246, 2017.

[24] D. Perez-Guaita, A. Sanchez-Illana, J. Ventura-Gayete, S. Garrigues, and M. de la Guardia, "Chemometric determination of lipidic parameters in serum using ATR measurements of dry films of solvent extracts," *Analyst*, vol. 139, no. 1, pp. 170–178, 2014.

[25] D. R. Parachalil, C. Bruno, F. Bonnier et al., "Analysis of bodily fluids using vibrational spectroscopy: a direct comparison of Raman scattering and infrared absorption techniques for the case of glucose in blood serum," *Analyst*, vol. 144, no. 10, pp. 3334–3346, 2019.

[26] I. Kokot, A. Piwowar, M. Jedryka, and E. M. Kratz, "Is there a balance in oxidative-antioxidant status in blood serum of patients with advanced endometriosis," *Antioxidants*, vol. 10, no. 7, p. 1097, 2021.

[27] Z. Guleken, H. Bulut, J. Depciuch, and N. Tarhan, "Diagnosis of endometriosis using endometrioma volume and vibrational spectroscopy with multivariate methods as a noninvasive method," *Spectrochimica Acta A*, vol. 264, p. 120246, 2022.

[28] D. Mabwa, K. Gajjar, D. Furniss et al., "Mid-infrared spectral classification of endometrial cancer compared to benign controls in serum or plasma samples," *Analyst*, vol. 146, no. 18, pp. 5631–5642, 2021.

[29] V. Witko-Sarsat, M. Friedlander, C. Capeillere-Blandin et al., "Advanced oxidation protein products as a novel marker of oxidative stress in uremia," *Kidney International*, vol. 49, no. 5, pp. 1304–1313, 1996.

[30] I. F. F. Benzie and J. J. Strain, "The ferric reducing ability of plasma (FRAP) as a measure of "Antioxidant power": the FRAP assay," *Analytical Biochemistry*, vol. 239, no. 1, pp. 70–76, 1996.

[31] H. Martens, M. Hoy, B. M. Wise, R. Bro, and P. B. Brockhoff, "Pre-whitening of data by covariance-weighted pre-processing," *Journal of Chemometrics*, vol. 17, no. 3, pp. 153–165, 2003.

[32] S. Wold, K. Esbensen, and P. Geladi, "Principal component analysis," *Chemometrics and Intelligent Laboratory Systems*, vol. 2, no. 1-3, pp. 37–52, 1987.

[33] P. S. Gromski, H. Muhamadali, D. I. Ellis et al., "A tutorial review: metabolomics and partial least squares-discriminant analysis - a marriage of convenience or a shotgun wedding," *Analytica Chimica Acta*, vol. 879, pp. 10–23, 2015.

[34] R. G. Brereton and G. R. Lloyd, "Partial least squares discriminant analysis: taking the magic away," *Journal of Chemometrics*, vol. 28, no. 4, pp. 213–225, 2014.

[35] S. H. Ahn, V. Singh, and C. Tayade, "Biomarkers in endometriosis: challenges and opportunities," *Fertility and Sterility*, vol. 107, no. 3, pp. 523–532, 2017.

[36] M. Jamilian, N. Mirhosseini, M. Eslahi et al., "The effects of magnesium-zinc-calcium-vitamin D co-supplementation on biomarkers of inflammation, oxidative stress and pregnancy outcomes in gestational diabetes," *BMC Pregnancy and Childbirth*, vol. 19, no. 1, p. 107, 2019.

[37] E. Rabbani, F. Golgiri, L. Janani et al., "Randomized study of the effects of zinc, vitamin a, and magnesium co-supplementation on thyroid function, oxidative stress, and hs-CRP in patients with hypothyroidism," *Biological Trace Element Research*, vol. 199, no. 11, pp. 4074–4083, 2021.

[38] Y. J. Lin, M. D. Lai, H. Y. Lei, and L. Y. C. Wing, "Neutrophils and macrophages promote angiogenesis in the early stage of endometriosis in a mouse model," *Endocrinology*, vol. 147, no. 3, pp. 1278–1286, 2006.

[39] J. L. Mahnke, M. Y. Dawood, and J. C. Huang, "Vascular endothelial growth factor and interleukin-6 in peritoneal fluid of women with endometriosis," *Fertility and Sterility*, vol. 73, no. 1, pp. 166–170, 2000.

[40] A. E. Schindler, "Gonadotropin-releasing hormone agonists for prevention of postoperative adhesions: an overview," *Gynecological Endocrinology*, vol. 19, no. 1, pp. 51–55, 2004.

[41] H. R. Harris, J. E. Chavarro, S. Malspeis, W. C. Willett, and S. A. Missmer, "Dairy-food, calcium, magnesium, and vitamin

D intake and endometriosis: a prospective cohort study," *American Journal of Epidemiology*, vol. 177, no. 5, pp. 420–430, 2013.

[42] M. Karimi-Zarchi, N. Dehshiri-Zadeh, L. Sekhavat, and F. Nosouhi, "Correlation of CA-125 serum level and clinicopathological characteristic of patients with endometriosis," *International Journal of Reproductive Biomedicine*, vol. 14, no. 11, pp. 713–718, 2016.

[43] U. M. Ural, Y. B. Tekin, M. Cure, and F. K. Sahin, "Serum YKL-40 levels as a novel marker of inflammation in patients with endometriosis," *Clinical and Experimental Obstetrics & Gynecology*, vol. 42, no. 4, pp. 495–497, 2015.

[44] K. Kochan, D. E. Bedolla, D. Perez-Guaita et al., "Infrared spectroscopy of blood," *Applied Spectroscopy*, vol. 75, no. 6, pp. 611–646, 2021.

[45] S. Roy, D. Perez-Guaita, S. Bowden, P. Heraud, and B. R. Wood, "Spectroscopy goes viral: diagnosis of hepatitis B and C virus infection from human sera using ATR-FTIR spectroscopy," *Clinical Spectroscopy*, vol. 1, p. 100001, 2019.

[46] J. Huang, N. Ali, E. Quansah et al., "Vibrational spectroscopic investigation of blood plasma and serum by drop coating deposition for clinical application," *International Journal of Molecular Sciences*, vol. 22, no. 4, p. 18, 2021.

[47] J. Ingham, M. J. Pilling, D. S. Martin et al., "A novel FTIR analysis method for rapid high-confidence discrimination of esophageal cancer," *Infrared Physics & Technology*, vol. 102, p. 103007, 2019.

[48] L. J. Jara, G. Medina, M. A. Saavedra, O. Vera-Lastra, and C. Navarro, "Prolactin and autoimmunity," *Clinical Reviews in Allergy and Immunology*, vol. 40, no. 1, pp. 50–59, 2011.

[49] A. Gupta, R. P. S. Mohan, S. Gupta, S. S. Malik, S. Goel, and N. Kamarthi, "Roles of serum uric acid, prolactin levels, and psychosocial factors in oral lichen planus," *Journal of Oral Science*, vol. 59, no. 1, pp. 139–146, 2017.

[50] A. De Bellis, A. Bizzarro, R. Pivonello, G. Lombardi, and A. Bellastella, "Prolactin and autoimmunity," *Pituitary*, vol. 8, no. 1, pp. 25–30, 2005.

[51] M. Bilotas, G. Meresman, R. Buquet, C. Sueldo, and R. I. Baranao, "Effect of vascular endothelial growth factor and interleukin-1 beta on apoptosis in endometrial cell cultures from patients with endometriosis and controls," *Journal of Reproductive Immunology*, vol. 84, no. 2, pp. 193–198, 2010.

[52] S. Lambert, P. Santulli, S. Chouzenoux et al., "Endometriosis: increasing concentrations of serum interleukin-1 beta and interleukin-1sRII is associated with the deep form of this pathology," *Journal de Gynécologie Obstétrique et Biologie de la Reproduction*, vol. 43, no. 9, pp. 735–743, 2014.

[53] J. H. Hu, W. Y. Xu, H. Y. Yang, and L. S. Mu, "Uric acid participating in female reproductive disorders: a review," *Reproductive Biology and Endocrinology*, vol. 19, no. 1, p. 65, 2021.

[54] Y. Y. Sautin and R. J. Johnson, "Uric acid: the oxidant-antioxidant paradox," *Nucleosides, Nucleotides, and Nucleic Acids*, vol. 27, no. 6-7, pp. 608–619, 2008.

Hindawi
Oxidative Medicine and Cellular Longevity
Volume 2022, Article ID 3145938, 11 pages
https://doi.org/10.1155/2022/3145938

Research Article

Identification of Bioactive Compounds and Potential Mechanisms of Kuntai Capsule in the Treatment of Polycystic Ovary Syndrome by Integrating Network Pharmacology and Bioinformatics

Xiushen Li,[1,2,3] **Jingxin Ma**,[4] **Li Guo**,[5] **Chenle Dong**,[1] **Guli Zhu**,[1] **Wenli Hong**,[1] **Can Chen**,[1] **Hao Wang**,[1,2,3] **and Xueqing Wu**[1,2,6]

[1]*Department of Obstetrics and Gynecology, Shenzhen University General Hospital, Shenzhen, Guangdong, China*
[2]*Guangdong Key Laboratory for Biomedical Measurements and Ultrasound Imaging, School of Biomedical Engineering, Shenzhen University Health Science Center, Shenzhen, Guangdong, China*
[3]*Shenzhen Key Laboratory, Shenzhen University General Hospital, Shenzhen, Guangdong, China*
[4]*School of Biomedical Engineering, Health Science Center, Shenzhen University, Shenzhen, Guangdong, China*
[5]*School of Pharmaceutical Sciences, Health Science Center, Shenzhen University, Shenzhen, Guangdong, China*
[6]*Clinical Medical Academy, Shenzhen University, Shenzhen, Guangdong, China*

Correspondence should be addressed to Hao Wang; haowang0806@gmail.com and Xueqing Wu; wuxueqing0307@163.com

Received 24 February 2022; Accepted 30 March 2022; Published 28 April 2022

Academic Editor: Katarzyna G bczak

Context. Kuntai capsule (KTC), a proprietary Chinese medicine, have been used for the treatment of polycystic ovary syndrome (PCOS). *Objective*. This study elucidates the potential therapeutic targets and molecular mechanisms of KTC in the treatment of PCOS. *Materials and Methods*. Using the Traditional Chinese Medicine System Pharmacology Database and Analysis Platform (TCMSP), the active ingredients and potential targets of KTC were obtained. The Gene Expression Omnibus (GEO) database was used to find differentially expressed genes (DEGs) related to PCOS. Search the CTD, DisGeNet, genecards, NCBI, OMIM, and PharmGKB databases for therapeutic targets related to PCOS. The intersection of potential targets, DEGs, and therapeutic targets was submitted to perform bioinformatics analysis by R language. Finally, the analyses' core targets and their corresponding active ingredients were molecularly docked. *Results*. 88 potential therapeutic targets of KTC for PCOS were discovered by intersecting the potential targets, DEGs, and therapeutic targets. According to bioinformatics analysis, the mechanisms of KTC treatment for PCOS could be linked to IL-17 signaling route, p53 signaling pathway, HIF-1 signaling pathway, etc. The minimal binding energies of the 5 core targets and their corresponding ingredients were all less than -6.5. Further research found that quercetin may replace KTC in the treatment of PCOS. *Discussion and Conclusions*. We explored the active ingredients and molecular mechanisms of KTC in the treatment of PCOS and found that quercetin may be the core ingredient of KTC in the treatment of PCOS.

1. Introduction

Polycystic ovary syndrome (PCOS) is one of the most common endocrine and metabolic diseases in gynecology. The main symptom of PCOS is excessive androgen, which also affects ovarian function and causes infertility [1]. At present, the cause of PCOS is still unclear, but recent studies have shown that the predisposing factors of PCOS may be related to the patients' daily life style and psychological factors [2]. Oral contraceptives, antiandrogens, and other hormonal

interventional drugs are the clinically recognized therapy options [3, 4]. The efficacy and safety drugs for PCOS, on the other hand, have yet to be discovered.

In recent years, the curative effect of many classic prescriptions of traditional Chinese medicine (TCM) in the treatment of PCOS has been recognized by more and more people [5]. According to Chinese medicine theory, one of the core pathogenic processes of PCOS is kidney shortage and blood stasis [6]. Kuntai Capsule (KTC) nourishes the kidneys and also improves blood circulation, which helps to regulate estrogen levels and promote ovarian function (Zhang H et al. [7]). The mechanisms of KTC in the treatment of PCOS may be related to increasing the patient's sensitivity to insulin, inhibiting oocyte apoptosis, and improving impaired ovarian function, according to the literature (Zhang J et al. [8]; Zhang B et al. [9, 10]). However, the specific mechanisms of KTC in the therapy of PCOS remains unknown.

As one of the cutting-edge methods to explore the mechanisms of drug therapy, network pharmacology has achieved remarkable results in exploring the therapeutic mechanisms of TCM prescriptions and screening the active ingredients and therapeutic targets of TCM ([11]; Gao X et al. [12]). Therefore, we used network pharmacology, bioinformatics, molecular docking, and other methods to reveal the active ingredients, targets, and molecular mechanisms of KTC in the treatment of PCOS. The flow chart of the entire study is shown in Figure 1.

2. Materials and Methods

2.1. Screen the Active Ingredients and Targets of KTC. We searched the active ingredients of KTC through the TCMSP database (https://old.tcmsp-e.com/tcmsp.php) based on the conditions of drug-like properties ≥ 0.18 and bioavailability ≥ 30% [13]. Then, we searched for the targets of the active ingredients through the TCMSP database and converted the target names to the gene names through the uniprot database (https://www.uniprot.org/). Finally, the Cytoscape 3.7.2 software was used to construct the relationship network between the active ingredients and target genes of KTC.

2.2. Collect the Therapeutic Targets of PCOS. The therapeutic targets were attained by searching DisGeNet, genecards, NCBI, OMIM, and PharmGKB with "PCOS" and "polycystic ovary syndrome" as keywords. Then, we converted the target names to the gene names by the uniprot database.

2.3. Screen Targets Related to PCOS. We merged the three PCOS-related datasets (GSE5850, GSE98421, GSE34526) found in the Gene Expression Omnibus (GEO) database and further used the R language "sva" and "limma" packages for batch correction and differentially expressed genes (DEGs) screening $|\log 2\,(\text{foldchange})| > 1$ and p value < 0.05).

2.4. Potential Therapeutic Targets of KTC in the Treatment of PCOS. Therapeutic targets obtained from CTD, DisGeNet, genecards, NCBI, OMIM, and PharmGKB databases were combined with DEGs from the GEO database and screened for targets appearing in at least two databases. These targets were then intersected with KTC therapeutic targets to identify prospective KTC therapeutic targets for PCOS.

2.5. The Analysis of PPInetwork, GO, and KEGG. We obtained the interactions between potential therapeutic targets of KTC through the STRING database. The protein-protein interaction (PPI) network was constructed by the Cytoscape software, and the core therapeutic targets were further screened according to the degree value. To investigate the probable molecular mechanisms of KTC in the treatment of PCOS, R language was used to perform Gene Ontology (GO) and Kyoto Encyclopedia of Genes and Genomes (KEGG) enrichment analysis.

2.6. Molecular Docking. Firstly, identify the active ingredients that correlate to KTC's core targets in the treatment of PCOS. The active ingredient's two-dimensional structure was retrieved via the PubChem website and translated into the three-dimensional structure with the lowest free energy by using the ChemBio3D software. Then, the 3D structure of the core target was obtained through the PDB database, and the water molecules and small molecule ligands were deleted through the "PyMOL" software. Next, the "AutoDockTools" software was used to convert the protein and drug ingredient into PDBQT format files and identify active pockets. Finally, we used the "vina" software for molecular docking.

2.7. Identify the Core Ingredients of KTC. We intersected the therapeutic targets of all active ingredients in KTC with the therapeutic targets of KTC. The active ingredient with the most overlapping targets was considered to be the core ingredient of KTC. Further bioinformatics analysis of the potential therapeutic targets of the core ingredients was performed.

3. Results

3.1. The Active Ingredients and Targets of KTC. According to the screening conditions, 80 active ingredients and 204 therapeutic targets of KTC were obtained through the TCMSP database (Supplementary Table 1 and Supplementary Table 2). After converting target names to gene names, the KTC regulatory network was constructed though the "Cytoscape" software. As shown in Figure 2, the surrounding circles were the active ingredients of KTC, and different colors represented different drugs. The red triangles and blue rectangles represented the active ingredients shared by various TCM and therapeutic targets, respectively. The degree value represented the number of edges connected to the node in the graph. The top three pharmaceutical ingredients in terms of degree value were quercetin, kaempferol, and wogonin.

3.2. Therapeutic Targets for PCOS. We found 988, 2540, 477, 181, and 327 therapeutic targets in the DisGeNet, genecards (relevance score 1), NCBI, OMIM, and PharmGKB

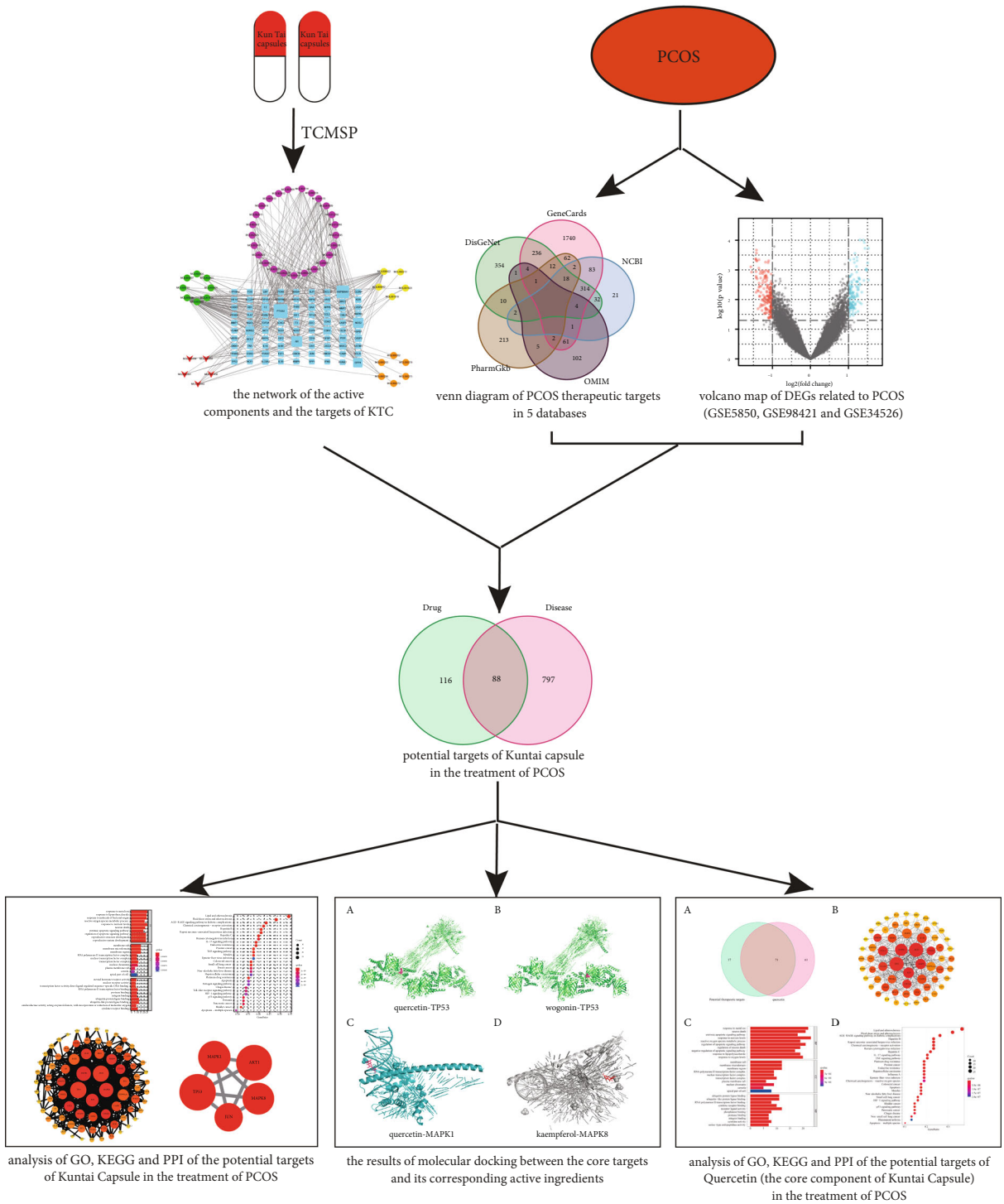

Figure 1: Flow chart.

databases, respectively, by using keywords “polycystic ovary syndrome” and “PCOS” (supplement table 3).

3.3. Targets Related to PCOS. We utilized the R language "limma" package to detect 315 DEGs after excluding batch effects in three data datasets linked to PCOS (supplement table 3). The red dots on the left represented genes with low expression in PCOS patients, whereas the blue dots on the right represented genes with high expression in PCOS patients (Figure 3(a)). Figure 3(b) shows the expression of the top 20 DEGs ranked high and low in PCOS patients versus healthy individuals.

3.4. Potential Therapeutic Targets of KTC. The obtained DEGs from the GEO database were combined with PCOS-related targets from the DisGeNet, genecards, NCBI, OMIM,

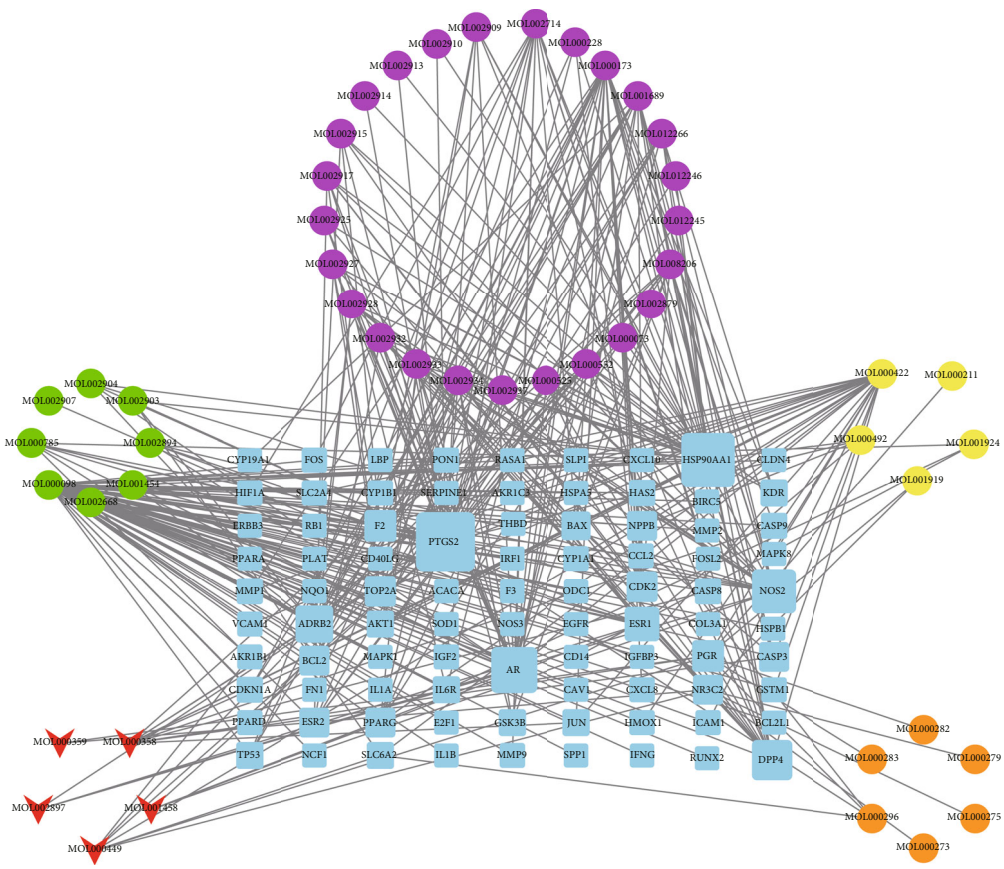

Figure 2: The network of the relationship between the active ingredients and the targets of KTC.

and PharmGKB databases. Targets that appeared at least twice were screened and intersected with therapeutic targets of KTC, resulting in 88 potential therapeutic targets for PCOS (Figures 4(a) and 4(b); Supplementary Table 4).

3.5. Analysis Results of GO, KEGG, and PPI Networks. In order to further explore the mechanisms of KTC in the treatment of PCOS, we performed R language to perform GO and KEGG enrichment analyses of potential therapeutic targets (supplement table 5). As shown in Figure 5(a), in terms of biological processes, targets were mostly enriched in reactions with metal ions, lipopolysaccharides, bacteria-derived molecules, nutritional levels, apoptosis, reactive oxygen metabolism, reproductive system, neuronal death, etc. In terms of cell components, targets were mostly enriched in membrane raft, membrane microdomain, membrane region, RNA polymerase II transcription factor complex, nuclear transcription factor complex, and so on. In terms of molecular function, the targets were mostly enriched in the activity of steroid hormone receptors, nuclear receptors, transcription factors, oxidoreductase factors, etc. KEGG enrichment analysis found that the targets were mostly enriched in IL-17 signaling pathway, TNF signaling pathway, p53 signaling pathway, Toll-like receptor signaling pathway, HIF-1 signaling pathway, etc. (Figure 5(b)). Figure 6(a) illustrates the PPI network of potential therapeutic targets. The darker the color, the larger the node area and the higher the degree and importance (Figure 6(a)). The selected core potential therapeutic targetswere shown in Figure 6(b). The R language scripts used in this study were shown in Supplementary Table 9.

3.6. The Results of Molecular Docking. By analyzing the PPI network, the five targets with the highest degree of MAPK1, MAPK8, TP53, AKT1, and JUN were identified and further searched for their corresponding active ingredients. Then, following the molecular docking steps described in the methods section, we executed the corresponding operations and acquired the molecular docking data for the targets and their corresponding active ingredients (Supplementary Table 6). We found that the binding energies of all molecular docking results were less than -6.5. The docking results for the four compounds with the lowest binding energies are shown in Figure 7.

3.7. The Core Ingredients of KTC. By intersecting the targets of each active ingredient with the potential therapeutic targets of KTC (supplement table 7), we finally determined that quercetin was the core ingredient of KTC. Quercetin had 71 targets that overlap with the potential therapeutic targets of KTC for PCOS (Figure 8(a)). We performed PPI network analysis on these 71 targets and found that the 5 core targets were almost the same as those of KTC (Figure 8(b)). As shown in Figure 8(c), the repetition rate of the GO and KEGG enrichment analysis results of

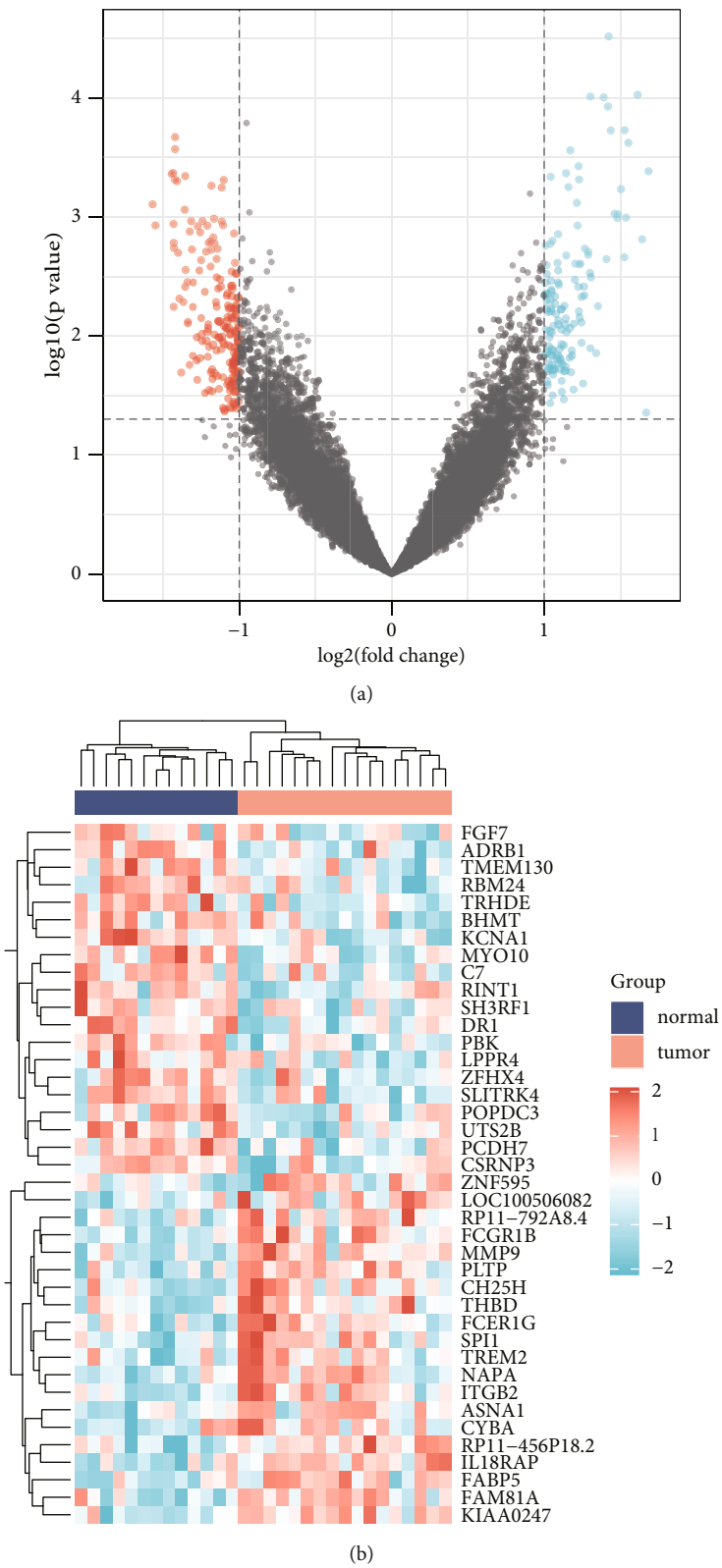

Figure 3: DEGs related to PCOS in the GEO dataset. (a) Volcano map of DEGs related to PCOS (GSE5850, GSE98421, and GSE34526). (b) Heat map of DEGs related to PCOS (GSE5850, GSE98421, and GSE34526).

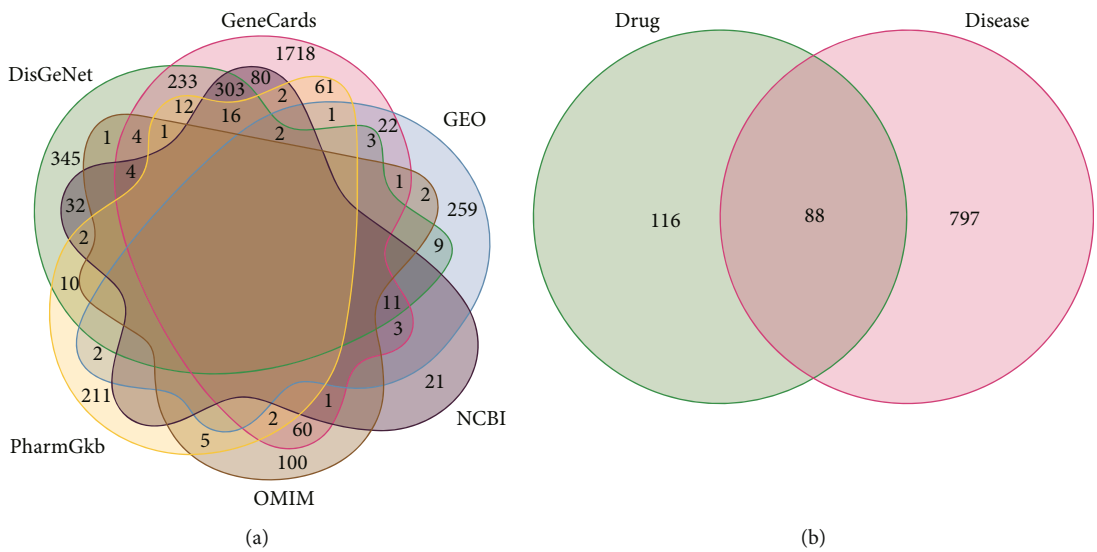

(a) (b)

Figure 4: Targets related to PCOS treatment. (a) The Venn diagram of PCOS therapeutic targets in 5 disease databases and GEO data sets. (b) The Venn diagram of the targets in at least two databases in (a) and the therapeutic targets of KTC.

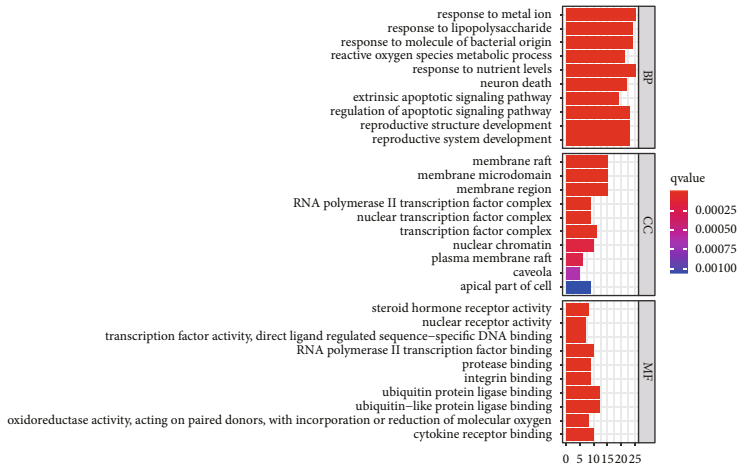

(a)

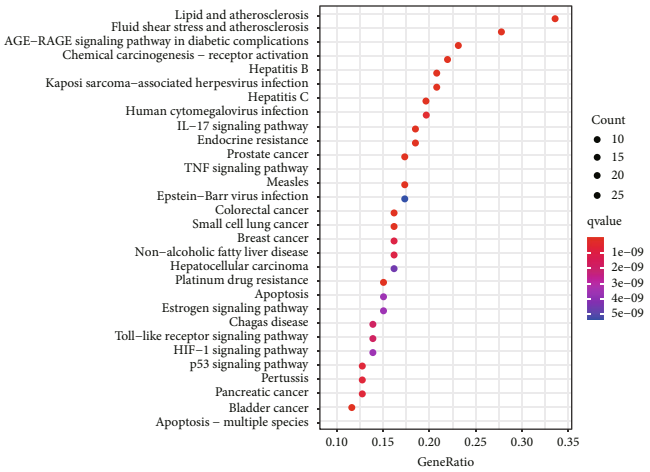

(b)

Figure 5: The GO and KEGG enrichment analyses of KTC's therapeutic target. (a) GO enrichment analysis (the top 10 results of BP, CC, MF enrichment analysis respectively). (b) KEGG enrichment analysis of therapeutic targets (the top 30 results).

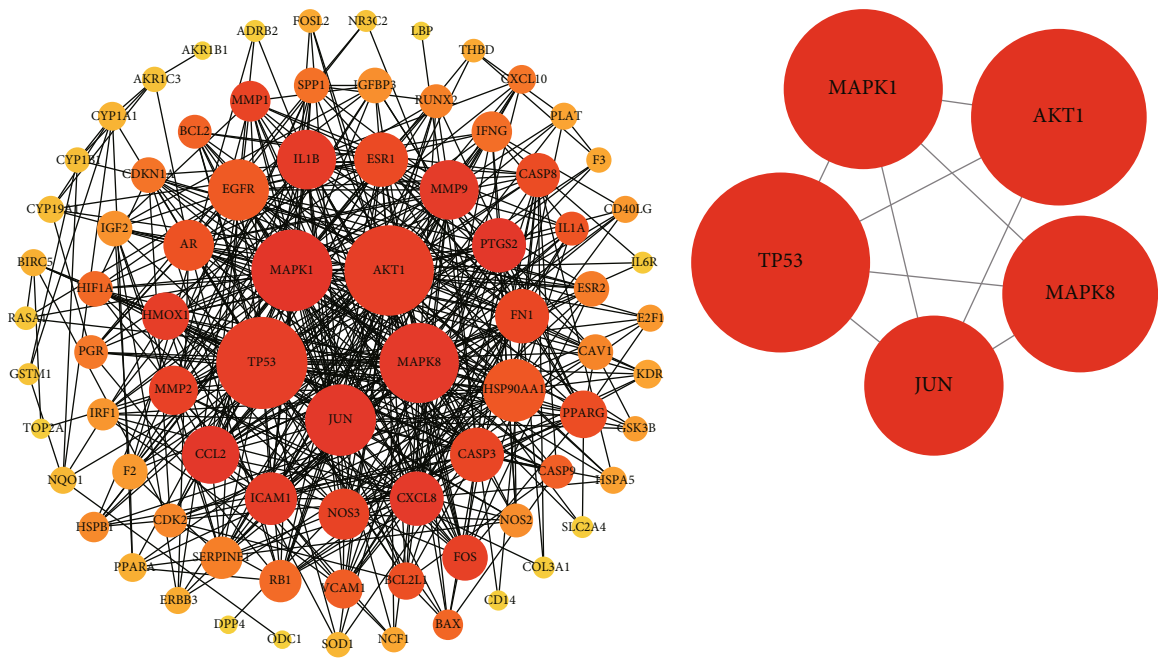

(a) (b)

Figure 6: The PPI network of KTC's targets for the treatment of PCOS. (a) Analysis results of PPI network. (b) The core targets of the PPI network.

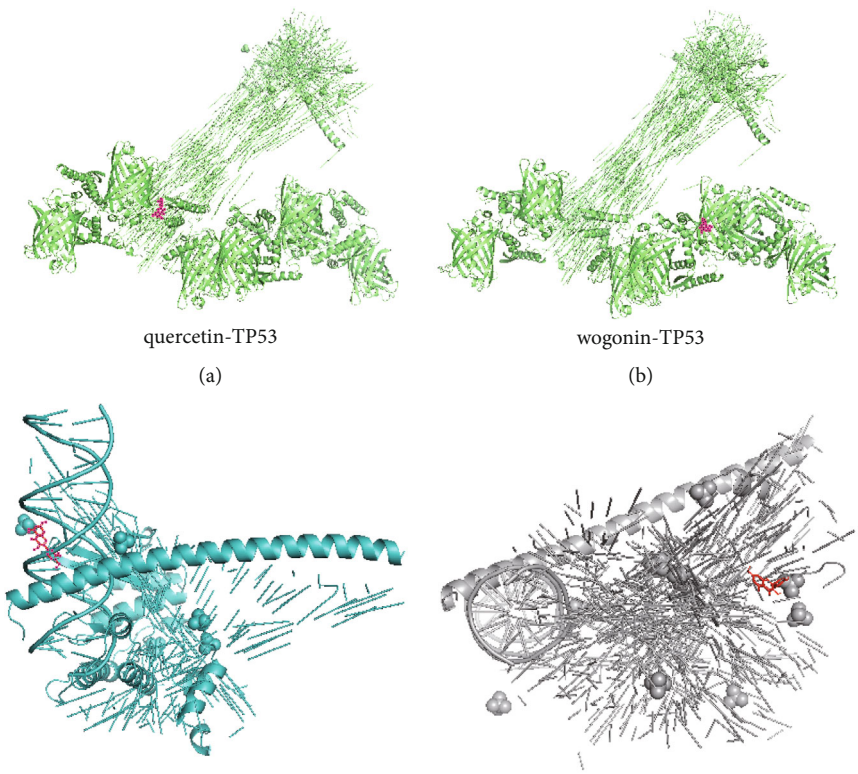

quercetin-TP53

(a)

wogonin-TP53

(b)

quercetin- MAPK1

(c)

kaempferol-MAPK8

(d)

Figure 7: The results of molecular docking between the core targets of the PPI network and their corresponding active ingredients (the four results with the lowest binding energy). (a) Molecular docking results of TP53 and quercetin (binding energy -8.9). (b) Molecular docking results of TP53 and wogonin (binding energy -8.8). (c) Molecular docking results of MAPK1 and quercetin (binding energy -8.7). (d) Molecular docking results of MAPK8 and kaempferol (binding energy -8.7).

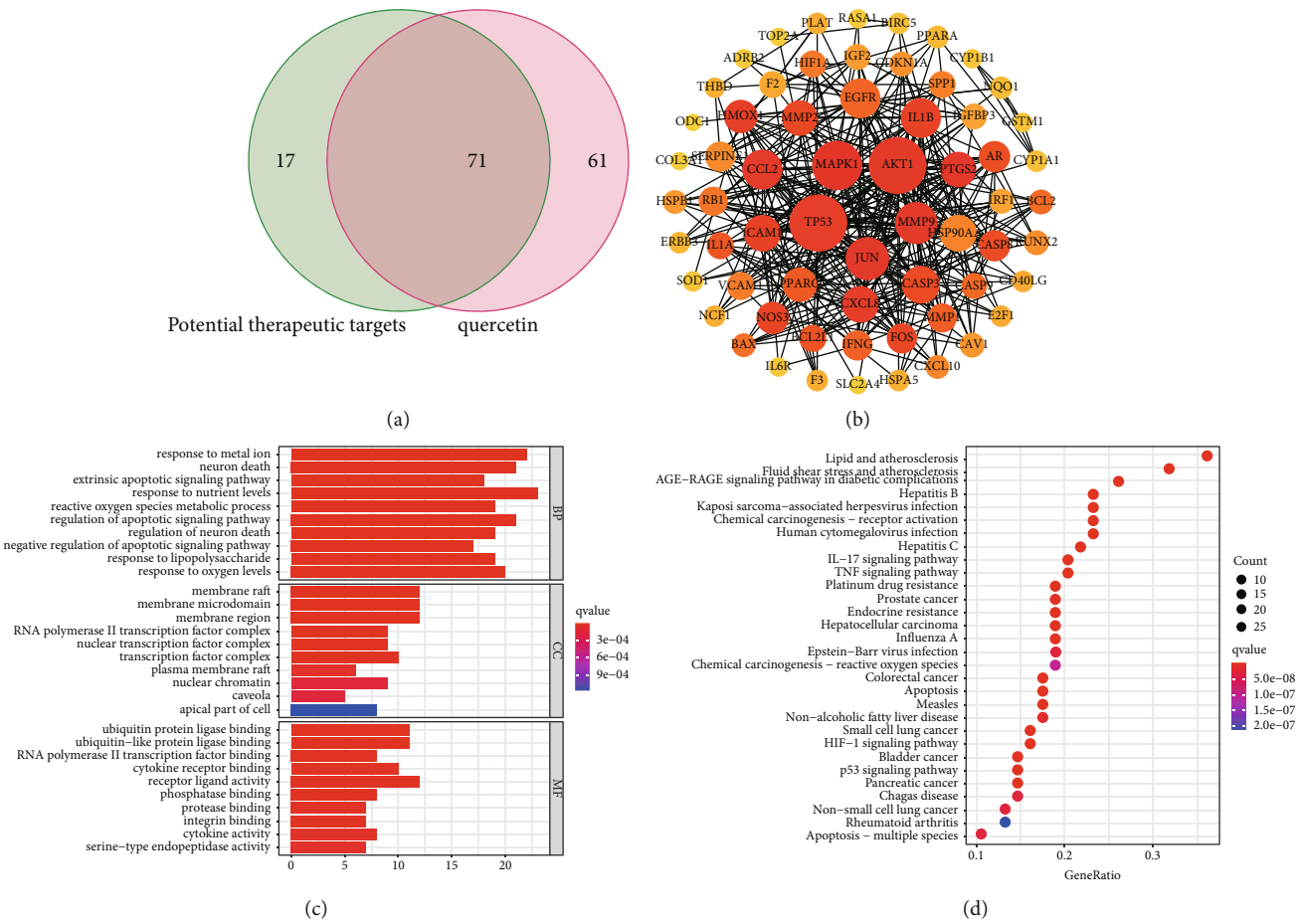

Figure 8: The bioinformatic analysis of quercetin's potential therapeutic target. (a) The Venn diagram of the potential therapeutic targets of quercetin and the therapeutic targets of KTC. (b) PPI network of therapeutic targets. (c) GO enrichment analysis of therapeutic targets (the top 10 results of BP, CC, MF enrichment analysis respectively). (d) KEGG enrichment analysis of therapeutic target (the top 30 results).

quercetin and KTC reached 75%, which were IL-17 signaling pathway, TNF signaling pathway, endocrine resistance, p53 signaling pathway, HIF-1 signaling pathway, apoptosis-multiple species, and so on (Figure 8(d); supplement table 8).

4. Discussion

Many TCM formulations have been used for the clinical treatment of PCOS. KTC targets the pathogenesis of PCOS by invigorating the kidney and promoting blood circulation, regulating the level of estrogen, and improving ovarian function. TCM formulations are difficult to examine at the molecular level due to their multi-ingredient and multitarget features. However, the emergence of network pharmacology has made it possible to systematically research TCM formulations. Therefore, this study relies on network pharmacology and bioinformatics to explore the molecular mechanisms of KTC in the treatment of PCOS.

By intersecting the therapeutic targets of KTC and PCOS in the bioinformatics database, 88 potential therapeutic targets of KTC for PCOS were finally obtained. We used potential therapeutic targets to construct a PPI network and further screened out 5 core targets (MAPK1, MAPK8, TP53, AKT1, and JUN). In mammals, the MAPK family participates in a variety of biological processes in the human body. Currently, the 14 MAPK family members that have been identified played important roles in transforming extracellular stimuli into cellular responses [14]. The cascades of MAPK are involved in many steps in the regulation of ovulation, including the recovery of meiosis and the rupture of follicles. MAPK1 plays a significant role in the mechanisms of insulin resistance and ovulation dysfunction in PCOS patients [15]. MAPK8 affects the progress of PCOS by regulating the autophagy of follicular cells [16]. TP53, a transcription factor, stabilizes and induces the transcription of genes related to cell cycle arrest, apoptosis, and metabolism [17]. TP53 participates in the occurrence and progression of PCOS by inducing the apoptosis of ovarian granulosa cells [18]. JUN belongs to the AP-1 transcription factor family, which causes fibrosis and regulates many core cell biological processes [19]. As an important regulator of ovarian function, AKT participates in multiple biological processes including the activation of primordial follicles

and the differentiation of granulosa cells [20]. AKT1 is involved in the proliferation of granular cells and follicle formation. The upregulated AKT1 in PCOS patients may be related to granule cell dysfunction [21].

We performed KEGG enrichment analysis on 88 potential therapeutic targets of KTC for PCOS, and found that molecular mechanisms of KTC's treatment of PCOS might be related to IL-17 signaling pathway, TNF signaling pathway, p53 signaling pathway, Toll-like receptor, and so on. IL17A, a proinflammatory cytokine, is mainly secreted by T-helper 17 cells. In PCOS patients, IL17A is abundantly expressed. The activation of the IL17A signaling pathway can result in the release of inflammatory mediators such as TNF, IL-6, and IL-1 ([22]; Gao Q et al. [23]). TNF is a cytokine with a wide range of biological activities, including TNF-α and TNF-β secreted by macrophages and T lymphocytes, respectively. As an adipokine of systemic inflammation, TNF-α is highly expressed in obese PCOS patients ([24]; Zhang Q et al. [25]). TNF-α signaling pathway is related to the uptake of glucose in tissues, which may lead to the decline of female fertility [26]. Increased androgen is a common clinical feature of PCOS patients, which can promote the expression of p53 [27]. P53 has previously been linked to cytokines including IL-1, IL-6, and TNF-α. The p53 signaling pathway may be involved in ovarian granulosa cell autophagy and death, which could be linked to PCOS pathophysiology [28]. The expression of Toll-like receptors in PCOS patients is significantly increased, which can lead to a decrease in the rate of available embryos in PCOS patients ([29]; Wang Y et al. [30]). Insulin resistance, the significant pathogenic feature of PCOS, is present in almost 85 percent of patients [31]. Recent studies have found that Toll-like receptors activate the NF-κB signaling pathway, leading to insulin resistance in PCOS patients ([32]; Wang D et al. [33]).

By molecular docking of the 5 core targets and their corresponding drug ingredients, we found that wogonin-TP53, kaempferol-MAPK8, quercetin-TP53, and quercetin-MAPK1 have excellent binding efficiency. Wogonin, a naturally occurring flavonoid compound, has anti-inflammatory, antioxidant, anticancer, and antiviral effects [34]. Wogonin regulates the redox process of chondrocytes and inhibits the biological activity of inflammatory mediators produced by macrophages and lymphocytes [35, 36]. In PCOS patients, endoplasmic reticulum stress induces granulosa cell apoptosis through death receptor 5 [37]. By controlling the process of endoplasmic reticulum stress, kaempferol, a natural flavonol active molecule, improves the survival rate of noncancer cells [38, 39]. The core ingredient of KTC was quercetin which had 71 targets that overlap with the potential therapeutic targets of KTC for PCOS. As one of the potential risk factors of PCOS, oxidative stress damages the insulin resistance, lipid metabolism, and follicular development of PCOS. Quercetin works as an antioxidant by lowering free radical generation, preventing lipid peroxidation, and altering antioxidants [40]. Studies have found that quercetin reduces the body weight, cysts, and ovarian diameter and restores healthy follicle function to alleviate the metabolic disorders of PCOS model rats [41]. Oral quercetin has been shown in clinical studies to successfully reduce adiponectin-mediated insulin resistance and hormone abnormalities in PCOS patients [42].

5. Conclusion

In this study, we uncovered the targets and molecular mechanisms of KTC in the treatment of PCOS and confirmed that quercetin may replace KTC for the treatment of PCOS patients through network pharmacology, bioinformatics, molecular docking, and other methods. These results may provide evidence for the clinical application of KTC in the treatment of PCOS.

Abbreviations

KTC: Kuntai capsule
PCOS: Polycystic ovary syndrome
TCMSP: Traditional Chinese Medicine System Pharmacology Database and Analysis Platform
GEO: Gene Expression Omnibus
TCM: Traditional Chinese medicine
GO: Gene Ontology
KEGG: Kyoto Encyclopedia of Genes and Genomes
PPI: Protein-protein interaction.

Data Availability

The data sets used and/or analyzed during the current study are available from the corresponding author on reasonable request.

Ethical Approval

No ethics approval was required in this study. All utilized public data sets were generated by others who had obtained ethical approval.

Conflicts of Interest

The authors declare that they have no conflicts of interest.

Authors' Contributions

Xiushen Li, Jingxin Ma, and Li Guo collected and analyzed the data. Xiushen Li, Guli Zhu, and Wenli Hong conducted experiments and wrote the manuscript. Jingxin Ma, Chenle Dong, Can Chen, and Li Guo contributed to find references. Xiushen Li, Jingxin Ma, and Li Guo contributed equally, so they are the cofirst authors. Hao Wang and Xueqing Wu are the guarantors of this work. Xiushen Li, Jingxin Ma, and Li Guo contributed equally to this work.

Acknowledgments

This study was supported by the Research fund of National Natural Science Foundation of China (81873822), the Shenzhen Science and Technology Innovation Committee (JCYJ20190808120807379 and JCYJ20210324100004013), the grant of 2019 Guangdong Recruitment Program of Foreign Experts (project name: Long-term effects of obesity on

hypothalamic-pituitary-ovarian axis in women and mechanisms study), the Shenzhen Pea-cock Program-Project Development Fund (No. 20210407618B), the Shenzhen University General Hospital (SUGH2018QD042), and the Shenzhen Key Laboratory Foundation (ZDSYS20200811143757022).

Supplementary Materials

Supplementary 1. Supplement Table 1: effective ingredients of KTC.

Supplementary 2. Supplement Table 2: therapeutic targets of effective ingredients.

Supplementary 3. Supplement Table 3: therapeutic targets of PCOS disease database and GEO database.

Supplementary 4. Supplement Table 4: the intersection of KTC's therapeutic targets and PCOS-related databases.

Supplementary 5. Supplement Table 5: analysis of PPI network, GO, and KEGG of KTC's potential therapeutic targets.

Supplementary 6. Supplement Table 6: molecular docking results of TP53, MAPK1, MAPK8, JUN, AKT1, and their corresponding effective ingredients.

Supplementary 7. Supplement Table 7: potential therapeutic targets of the active ingredients of KTC.

Supplementary 8. Supplement Table 8: analysis of PPI network, GO, and KEGG of quercetin's potential therapeutic targets.

Supplementary 9. Supplement Table 9: the R language scripts used in the study.

References

[1] C. J. Glueck and N. Goldenberg, "Characteristics of obesity in polycystic ovary syndrome: etiology, treatment, and genetics," *Metabolism*, vol. 92, pp. 108–120, 2019.

[2] H. F. Escobar-Morreale, "Polycystic ovary syndrome: definition, aetiology, diagnosis and treatment," *Nature Reviews. Endocrinology*, vol. 14, no. 5, pp. 270–284, 2018.

[3] A. H. Balen, L. C. Morley, M. Misso et al., "The management of anovulatory infertility in women with polycystic ovary syndrome: an analysis of the evidence to support the development of global WHO guidance," *Human Reproduction Update*, vol. 22, no. 6, pp. 687–708, 2016.

[4] P. Jin and Y. Xie, "Treatment strategies for women with polycystic ovary syndrome," *Gynecological Endocrinology*, vol. 34, no. 4, pp. 272–277, 2018.

[5] W. Shen, B. Jin, Y. Pan et al., "The effects of traditional Chinese medicine-associated complementary and alternative medicine on women with polycystic ovary syndrome," *Evidence-based Complementary and Alternative Medicine: eCAM*, vol. 2021, article 6619597, 2021.

[6] Z. Qiu, J. Dong, C. Xue et al., "Liuwei Dihuang Pills alleviate the polycystic ovary syndrome with improved insulin sensitivity through PI3K/Akt signaling pathway," *Journal of Ethnopharmacology*, vol. 250, article 111965, 2020.

[7] H. Zhang, F. Qin, A. Liu et al., "Retracted: Kuntai capsule attenuates premature ovarian failure through the PI3K/AKT/mTOR pathway," *Journal of Ethnopharmacology*, vol. 239, article 111885, 2019.

[8] J. Zhang, L. Fang, L. Shi et al., "Protective effects and mechanisms investigation of Kuntai capsule on the ovarian function of a novel model with accelerated aging ovaries," *Journal of Ethnopharmacology*, vol. 195, pp. 173–181, 2017, eng.

[9] R. Liang, Z. Liu, P. Li et al., "Kuntai capsules improve glucolipid metabolism in patients with polycystic ovary syndrome: a randomized, double-blind, placebo-controlled trial," *Medicine*, vol. 98, no. 39, article e16788, 2019eng.

[10] B. Zhang, N. Chu, X. M. Qiu et al., "Effects of Heyan Kuntai Capsule () on follicular development and oocyte cohesin levels in aged mice," *Chinese Journal of Integrative Medicine*, vol. 24, no. 10, pp. 768–776, 2018.

[11] Z. Wu, W. Li, G. Liu, and Y. Tang, "Network-based methods for prediction of drug-target interactions," *Frontiers in Pharmacology*, vol. 9, p. 1134, 2018.

[12] X. Gao, S. Li, C. Cong, Y. Wang, and L. Xu, "A network pharmacology approach to estimate potential targets of the active ingredients of epimedium for alleviating mild cognitive impairment and treating Alzheimer's disease," *Evidence-Based Complementary and Alternative Medicine: eCAM*, vol. 2021, article 2302680, 2021.

[13] J. Ru, P. Li, J. Wang et al., "TCMSP: A Database of Systems Pharmacology for Drug Discovery from Herbal Medicines," *Journal of Cheminformatics*, vol. 6, no. 1, p. 13, 2014.

[14] J. Yue and J. M. López, "Understanding MAPK signaling pathways in apoptosis," *International Journal of Molecular Sciences*, vol. 21, no. 7, p. 2346, 2020.

[15] M. Kupreeva, A. Diane, R. Lehner et al., "Effect of metformin and flutamide on insulin, lipogenic and androgen-estrogen signaling, and cardiometabolic risk in a PCOS-prone metabolic syndrome rodent model," *American Journal of Physiology. Endocrinology and Metabolism*, vol. 316, no. 1, pp. E16–E33, 2019.

[16] S. Kumariya, V. Ubba, R. K. Jha, and J. R. Gayen, "Autophagy in ovary and polycystic ovary syndrome: role, dispute and future perspective," *Autophagy*, vol. 17, no. 10, pp. 2706–2733, 2021.

[17] A. Ranjan and T. Iwakuma, "Non-canonical cell death induced by p 53," *International Journal of Molecular Sciences*, vol. 17, no. 12, 2016.

[18] R. Yang, J. Chen, L. Wang, and A. Deng, "LncRNA BANCR participates in polycystic ovary syndrome by promoting cell apoptosis," *Molecular Medicine Reports*, vol. 19, no. 3, pp. 1581–1586, 2019.

[19] G. Wernig, S. Y. Chen, L. Cui et al., "Unifying mechanism for different fibrotic diseases," *Proceedings of the National Academy of Sciences of the United States of America*, vol. 114, no. 18, pp. 4757–4762, 2017.

[20] A. Makker, M. M. Goel, and A. A. Mahdi, "PI3K/PTEN/Akt and TSC/mTOR signaling pathways, ovarian dysfunction, and infertility: an update," *Journal of Molecular Endocrinology*, vol. 53, no. 3, pp. R103–R118, 2014, eng.

[21] S. Nekoonam, M. Naji, M. S. Nashtaei et al., "Expression of AKT1 along with AKT2 in granulosa-lutein cells of hyperandrogenic PCOS patients," *Archives of Gynecology and Obstetrics*, vol. 295, no. 4, pp. 1041–1050, 2017, eng.

[22] O. Ozcaka, N. Buduneli, B. O. Ceyhan et al., "Is interleukin-17 involved in the interaction between polycystic ovary syndrome

and gingival inflammation?," *Journal of Periodontology*, vol. 84, no. 12, pp. 1827–1837, 2013.

[23] Q. Gao, H. Zhu, L. Dong et al., "Integrated proteogenomic characterization of HBV-related hepatocellular carcinoma," *Cell*, vol. 179, no. 2, pp. 561–577.e522, 2019.

[24] Q. Xie, X. Xiong, N. Xiao et al., "Mesenchymal stem cells alleviate DHEA-induced polycystic ovary syndrome (PCOS) by inhibiting inflammation in mice," *Stem Cells International*, vol. 2019, 9782312 pages, 2019.

[25] Q. Zhang, Y. Lou, J. Yang et al., "Integrated multiomic analysis reveals comprehensive tumour heterogeneity and novel immunophenotypic classification in hepatocellular carcinomas," *Gut*, vol. 68, no. 11, pp. 2019–2031, 2019.

[26] L. Oróstica, I. Astorga, F. Plaza-Parrochia et al., "Proinflammatory environment and role of TNF-α in endometrial function of obese women having polycystic ovarian syndrome," *International Journal of Obesity*, vol. 40, no. 11, pp. 1715–1722, 2016.

[27] F. Xu, R. Liu, and X. Cao, "Hyperandrogenism stimulates inflammation and promote apoptosis of cumulus cells," *Cellular and Molecular Biology (Noisy-le-Grand, France)*, vol. 63, no. 10, pp. 64–68, 2017.

[28] Y. Qin, T. Li, H. Zhao, Z. Mao, C. Ding, and Y. Kang, "Integrated transcriptomic and epigenetic study of PCOS: impact of Map3k1 and Map1lc3a promoter methylation on autophagy," *Frontiers in Genetics*, vol. 12, article 620241, 2021.

[29] B. X. Gu, X. Wang, B. L. Yin et al., "Abnormal expression of TLRs may play a role in lower embryo quality of women with polycystic ovary syndrome," *Systems Biology in Reproductive Medicine*, vol. 62, no. 5, pp. 353–358, 2016.

[30] Y. Wang, J. He, and J. Yang, "Eicosapentaenoic acid improves polycystic ovary syndrome in rats via sterol regulatory element-binding protein 1 (SREBP-1)/toll-like receptor 4 (TLR4) pathway," *Medical Science Monitor*, vol. 24, pp. 2091–2097, 2018.

[31] N. K. Stepto, S. Cassar, A. E. Joham et al., "Women with polycystic ovary syndrome have intrinsic insulin resistance on euglycaemic-hyperinsulaemic clamp," *Human Reproduction*, vol. 28, no. 3, pp. 777–784, 2013.

[32] B. Jiang, M. Xue, D. Xu, Y. Song, and S. Zhu, "Retracted article: Upregulation of microRNA-204 improves insulin resistance of polycystic ovarian syndrome via inhibition of HMGB1 and the inactivation of the TLR4/NF-κB pathway," *Cell Cycle*, vol. 19, no. 6, pp. 697–710, 2020.

[33] D. Wang, Y. Weng, Y. Zhang et al., "Exposure to hyperandrogen drives ovarian dysfunction and fibrosis by activating the NLRP3 inflammasome in mice," *Science of The Total Environment*, vol. 745, article 141049, 2020.

[34] J. Sharifi-Rad, J. Herrera-Bravo, L. A. Salazar et al., "The therapeutic potential of wogonin observed in preclinical studies," *Evidence-based Complementary and Alternative Medicine: eCAM*, vol. 2021, article 9935451, 2021.

[35] D. L. Huynh, T. H. Ngau, N. H. Nguyen, G. B. Tran, and C. T. Nguyen, "Potential therapeutic and pharmacological effects of Wogonin: an updated review," *Molecular Biology Reports*, vol. 47, no. 12, pp. 9779–9789, 2020.

[36] N. M. Khan, A. Haseeb, M. Y. Ansari, P. Devarapalli, S. Haynie, and T. M. Haqqi, "Wogonin, a plant derived small molecule, exerts potent anti-inflammatory and chondroprotective effects through the activation of ROS/ERK/Nrf2 signaling pathways in human osteoarthritis chondrocytes," *Free Radical Biology & Medicine*, vol. 106, pp. 288–301, 2017, eng.

[37] J. M. K. Azhary, M. Harada, N. Takahashi et al., "Endoplasmic reticulum stress activated by androgen enhances apoptosis of granulosa cells via induction of death receptor 5 in PCOS," *Endocrinology*, vol. 160, no. 1, pp. 119–132, 2019.

[38] M. Ashrafizadeh, S. Tavakol, Z. Ahmadi, S. Roomiani, R. Mohammadinejad, and S. Samarghandian, "Therapeutic effects of kaempferol affecting autophagy and endoplasmic reticulum stress," *Phytotherapy Research: PTR*, vol. 34, no. 5, pp. 911–923, 2020.

[39] J. Cao, Y. Wang, S. Hu et al., "Kaempferol ameliorates secretagogue-induced pseudo-allergic reactions via inhibiting intracellular calcium fluctuation," *The Journal of Pharmacy and Pharmacology*, vol. 72, no. 9, pp. 1221–1231, 2020, eng.

[40] F. Pourteymour Fard Tabrizi, F. Hajizadeh-Sharafabad, M. Vaezi, H. Jafari-Vayghan, M. Alizadeh, and V. Maleki, "Quercetin and polycystic ovary syndrome, current evidence and future directions: a systematic review," *Journal of Ovarian Research*, vol. 13, no. 1, p. 11, 2020, eng.

[41] S. Jahan, A. Abid, S. Khalid et al., "Therapeutic potentials of quercetin in management of polycystic ovarian syndrome using letrozole induced rat model: a histological and a biochemical study," *Journal Of Ovarian Research*, vol. 11, no. 1, p. 26, 2018.

[42] N. Rezvan, A. Moini, L. Janani et al., "Effects of quercetin on adiponectin-mediated insulin sensitivity in polycystic ovary syndrome: a randomized placebo-controlled double-blind clinical trial," *Hormone and Metabolic Research*, vol. 49, no. 2, pp. 115–121, 2017.

Hindawi
Oxidative Medicine and Cellular Longevity
Volume 2022, Article ID 5491038, 31 pages
https://doi.org/10.1155/2022/5491038

Research Article

Analysis of Immune and Inflammation Characteristics of Atherosclerosis from Different Sample Sources

HAN NIE,[1,2] Chen Yan,[1,2,3] Weimin Zhou,[4] and Tao-sheng Li[1]

[1]*Department of Stem Cell Biology, Atomic Bomb Diseases Institute, Nagasaki University, China*
[2]*Department of Stem Cell Biology, Nagasaki University Graduate School of Biomedical Sciences, 1-12-4 Sakamoto, Nagasaki 852-8523, Japan*
[3]*Department of Rheumatology, The Second Affiliated Hospital of Nanchang University, Nanchang City, Jiangxi Province 330006, China*
[4]*Department of Vascular Surgery, The Second Affiliated Hospital of Nanchang University, Nanchang City, Jiangxi Province 330006, China*

Correspondence should be addressed to Weimin Zhou; weiminzhouncu@163.com and Tao-sheng Li; litaoshe@nagasaki-u.ac.jp

Received 7 December 2021; Accepted 21 March 2022; Published 25 April 2022

Academic Editor: Helena Moreira

Background. Atherosclerosis is the predominant cause of cardiovascular diseases. Existing studies suggest that the development of atherosclerosis is closely related to inflammation and immunity, but whether there are differences and similarities between atherosclerosis occurring at different sites is still unknown. We elucidated the pathological characteristics of peripheral vascular diseases by using bioinformatic analyses on immune cells and inflammation-related gene expression in atherosclerotic arteries and plaques. *Methods*. Eight data sets regarding atherosclerosis were downloaded from the Gene Expression Omnibus database. Human immune genes were obtained from the IMMPORT website. The samples were scored and divided into high- and low-immune groups. Then the samples were analysed using weighted gene co-expression network analysis, while the modules were analysed using functional enrichment. The protein–protein interaction network was constructed using the STRING and Cytoscape databases. The hub immune genes were screened, and the correlation between hub immune genes and immune cells was analysed. *Results*. Immune cells and their functions were significantly different during atherosclerosis development. The infiltration proportion of immune cells was approximately similar in samples from different sources of patients with carotid atherosclerosis. However, the sensitivity of lower extremity atherosclerosis samples to immune cells is lower than that of carotid atherosclerosis samples.The samples from the plaque and artery were mainly infiltrated by macrophages, T cells and mast cells. After immune cells were assessed, resting NK cells, activated mast cells and M0 macrophages were found to be key immune cells in atherosclerosis and plaque formation. In addition, CCL4, TLR2, IL1B and PTPRC were considered to be immune marker genes in atherosclerosis development. Conclusion. Bioinformatic data analysis confirms the essential role of immune cells in cardiovascular diseases, and also indicates some differences of immune and inflammation characteristics of atherosclerosis between carotid and lower extremity arteries.

1. Introduction

Cardiovascular diseases remain a thorny public health problem in most low- and middle-income countries; however, the morbidity and mortality of cardiovascular diseases have decreased significantly in high-income countries with the improvements in living conditions, medical care and health management [1]. According to the World Health Organization, cardiovascular disease caused 13.2 million deaths in 2011, accounting for 24% of deaths worldwide. Moreover, the death rate due to cardiovascular diseases is expected to reach 23.3 million worldwide by 2030, which promotes

cardiovascular diseases as the leading cause of death [2]. Atherosclerosis is a chronic arterial disease that mainly causes most cardiovascular diseases, and its lesions are characterised by the gradual development of lipid deposits in the arterial wall into atheromatous plaques and characteristic plaques. Atherosclerotic plaque formation involves the partial or complete narrowing of the vascular lumen. Moreover, the acute rupture of plaques, a major cause of cerebrovascular disease, leads to local thrombosis and occlusion [3, 4], while plaque formation often leads to peripheral arterial disease. Atherosclerosis used to be considered a lipid metabolism disease [5, 6]; however, increasing experimental and clinical evidence points to atherosclerosis s a chronic immune-inflammatory disease [7–9]. Early-stage atherosclerosis formation involves flow-mediated inflammatory changes in the endothelial cells (ECs), and when ECs are damaged, inflammatory factors such as monocyte chemotactic protein-1, interleukin (IL)-8, vascular adhesion molecule-1, E-selectin and P-selectin are released, which attract lymphocytes and monocytes that infiltrate the arterial wall and lead to inflammation [10]. Following this, macrophages, mast cells, T cells, B cells, tumour necrosis factor (TNF) ILs and other immune cells and inflammatory mediators infiltrate the vessel wall in large numbers to promote atherosclerosis [11, 12]. Currently, the treatment for inflammation has been quite successful, and the strategy for controlling inflammation has been successfully used to treat many other diseases. Therefore, treating inflammation is the preferred target for atherosclerosis treatment. However, the lack of relevant clinical data hinders the effective development of anti-inflammatory drugs for atherosclerosis. Therefore, exploring the immune cells that play an important role in the occurrence and development of atherosclerotic plaque and identifying immune genes that play a key role in inflammation are of great significance for the anti-inflammatory immunotherapy of atherosclerosis.

2. Methods

2.1. Data Download and Processing. Eight data sets related to atherosclerotic plaque were obtained from the GEO database, namely, GSE21545, GSE24495, GSE28829, GSE163154, GSE43292, GSE24702, GSE100927 and GSE57691 [13–18], which included carotid plaque (N = 343), peripheral plaque (N = 290), carotid atherosclerotic artery (N = 29) and lower extremity atherosclerotic artery (N = 48). The 'SVA' package [19] in R software (4.0.2, http://www.r-project.org) was used to remove batch effects and for standardisation of data sets of different platforms.

2.2. Single-sample gene set enrichment analysis (ssGSEA) and sample clustering. ssGSEA were performed using GSVA (version 1.34.0) in R software, and the enrichment scores of 29 immune-related cells and their functions in each sample were calculated [20–23]. An unsupervised machine learning method was used to cluster the samples into two clusters. The clusters were further divided into high- and low-immune groups based on their immune scores. Additionally, principal component analysis (PCA) or t-distributed stochastic neighbor embedding (tSNE) was used to reduce the dimension of the grouping data.

2.3. Gene Set Enrichment Analysis (GSEA). The 'clusterprofiler' package [24] in R software and MSigDB (https://www.gsea-msigdb.org/gsea/msigdb/index.jsp) were used for GSEA analysis in the high- and low-immune groups.

2.4. Immune Cell Infiltration and Evaluation. R software was used to identify the cell type by estimating the relative subsets of RNA transcripts (CIBERSORT) [25] and calculate the scores of 22 types of human immune cells in the sample. A p-value <0.05 was considered the filtering standard. Differentially expressed immune cells in the high- and low-immune groups were analysed according to the score.

2.5. WGCNA. The 'WGCNA' package [26] in R software was used to analyse the samples based on the Pearson correlation matrix: amn = |cmn β (where amn is the proximity between genes m and n, cmn is the Pearson correlation and β is the soft power threshold). WGCNA is mainly used for gene co-expression network construction, key disease-related module identification and analysis, protein network construction and key module hub node identification and enrichment analysis.

Gene Ontology (GO) and Kyoto Encyclopedia of Genes and Genomes (KEGG) enrichment analyses.

The enrichment analyses of data obtained from GO and KEGG databases were analysed using the cluster profiler package [24].

2.6. Immune-Related Gene Expression Data. The expression profiles of 2498 genes related to immune infiltrating cells, including genes related to antigen-presenting cells, chemokines and their receptors, cytokines and their receptors, interferons and interleukin were downloaded from the ImmPort database (https://www.immport.org/home).

Screening of differentially expressed genes (DEGs) in the high- and low-immune groups.

The 'limma' package in R software was used to analyse differences in the high- and low-immune groups. The statistical significance of DEGs was set to more than the double change factor (≥1), and the corrected p-value error detection rate was <0.05.

2.7. Construction of PPI Networks and the Screening of Key Immune Genes. The most immune-related module genes in WGCNA were intersected with the DEGs and immune-related genes. Following this, the STRING database (https://www.string-db.org) was used to construct the PPI network using the intersected genes. The constructed PPI network was inputted into Cytoscape, using the MCC algorithm in cytohubba [27], and the top five genes obtained were identified as key immune genes.

2.8. Sensitivity Test and Immune Cell Correlation Test. The 'pROC' package in R software was used to analyse the subject working characteristic curve of key immune genes, which helped to detect gene sensitivity. The Spearman

method was used to detect the correlation between different immune cells and key immune genes.

3. Results

3.1. Data processing and classification. The procedure of this work shown in the analysis flow chart (Supplementary Figure 1).Based on the sample source and disease type, the samples were divided into plaque samples and artery samples. The plaque samples were further divided into carotid plaque group (343 carotid plaque and 32 control samples; fusion and batch effect of the carotid plaque samples; Supplementary Figure 2A) and peripheral plaque group (290 peripheral plaque samples). The artery samples were further divided into carotid atherosclerosis group (29 carotid atherosclerosis and 12 control samples) and lower limbs atherosclerotic artery group (48 lower limb atherosclerotic artery and 33 control samples; fusion and batch effect of the lower limbs atherosclerotic artery samples; Supplementary Figure 2B). Sample grouping and related information are shown in Table 1.

3.2. ssGSEA and Sample Clustering. Atherosclerotic plaque development was speculated to be closely related to immune cells and their function. Therefore, to substantiate this speculation, ssGSEA analysis was performed on GSE28829 (including 16 advanced and 13 early carotid plaque samples), GSE 43292 (including 32 carotid atherosclerotic plaques and 32 control samples) and GSE 100927 (including 29 carotid atherosclerotic artery and 12 control samples). The analysis revealed significant differences in immune cells and their functions between the early and advanced carotid plaque samples, carotid atherosclerotic plaque and control samples, and carotid atherosclerotic artery and control samples (Supplementary Figures 3A, B, C) Further, PCA analysis of the three data sets revealed that the samples in the data sets could be distinguished according to the immune score (Supplementary Figures 3D, E and F), which confirmed the close relation between atherosclerotic plaque development and immune cells and their functions.

Therefore, according to the previous grouping, the carotid plaque group was used as an example to obtain ssGSEA scores. The samples were divided into high immune and low immune groups according to the clustering and immune score (Figure 1(a), 1(b)). tSNE analysis was performed according to the immune score and high and low immune group classification, which showed that the samples could be distinguished according to immune score (Figure 1(c)). The other groups, namely, peripheral plaque (Figure 1(d), 1(e), (f)), carotid atherosclerotic artery (Figure 2(a), 2(b), (c)) and lower extremity atherosclerotic artery (Figure 2(d), 2(e), (f)) groups, underwent the same analyses. The tSNE analysis of all groups confirmed that the samples could be divided into high- and low-immune groups according to immune cells and their function.

3.3. Differential Gene Analysis and GSEA. Using the carotid plaque group as an example, 2396 genes were identified as DEGs (LogFC ≥ 1 or ≤ -1. $p < 0.05$, Supplementary Figure 4A). GSEA showed that the high- and low-immune groups were closely related to the chemokine signalling pathway and interleukin and inflammatory responses (Figure 3(a)). The same analysis performed on the other groups revealed 772 DEGs in the peripheral plaque group (Supplementary Figure 4B), 1042 DEGs in the carotid atherosclerotic artery group (supplementary Figure 4C) and 68 DEGs in the lower extremity atherosclerotic artery group (Supplementary Figure 4D). Additionally, GSEA showed that the high- and low-immune groups in these types were related to chemokine, interleukin, inflammation pathways and other processes (Figure 3(b); figure 3(c); Figure 3(d)), which further contributes to the credibility of the method to distinguish samples according to immune-related characteristics.

3.4. Immune Cell Infiltration and Evaluation. Using the carotid plaque group as an example, CIBERSORT was used to evaluate the infiltration of 22 immune cell types in the group. Figure 3(e), 3(f) shows that macrophages, mast cells, T cells and B cells mainly infiltrated the carotid plaque. Moreover, significant differences in the expression of nine immune cell types, such as M0 macrophages and activated mast cells, in the high- and low-immune groups, including four T cell types (Figure 3(e), 3(f), Table 2) The same analysis was performed to determine the difference in immune cell infiltration among the peripheral plaque (Figure 4(a), 4(b)), carotid atherosclerotic artery (Figure 4(c), 4(d)) and lower limbs atherosclerotic artery (Figure 4(e), 4(f)) groups. Differences in immune cell expression in the high- and low-immune groups of all samples are shown in Table 2. The results showed that the proportion of immune cells in the peripheral and carotid plaques was roughly the same, with macrophages, especially M2 macrophages, predominately seen in both plaque types (Figure 3(f), Figure 4(f)) Moreover, although the proportion of T cells, NK cells and mast cells was low, they accounted for the majority of immune cell types, such as activated mast cells activated, resting NK cells and CD4 T cells (Table 2).

Macrophages, especially M0 macrophages, were predominantly found in the lower extremity atherosclerotic artery group. Notably, a strong similarity was seen between the differentially expressed immune cells in the lower atherosclerotic artery and plaque groups. The expression of M0 macrophages, M1 macrophages, follicular helper T cells, gamma delta T cells and CD8 T cells was increased in the high-immune group, while the expression of naïve B cells and resting NK cells was increased in the low-immune group (Table 2). Therefore, despite the differences in sample source and sample site, macrophages, T cells and NK cells play a key role in atherosclerosis.

Interestingly, the differentially expressed immune cells of GSE28829 (including 16 advanced and 13 early carotid plaques) and the total carotid plaques group showed great similarity. The expression of M0 macrophages, activated mass cells and gamma delta T cells were increased in the advanced carotid plaque and high-immune groups, while the expression of regulatory T cells (Tregs) was increased in the early

Table 1: Dataset information.

Plaque(series)	Platform	Samples	Group
21545	570	Carotid plaque 126	
24495	10687	Carotid plaque 113	
28829	570	Carotid plaque 29 (advanced 16; early 13)	Carotid plaque
163154	6104	Carotid plaque 43 (non-IPH 16; IPH 27)	
43292	6244	Carotid plaque 32; control samples 32	
24702	10687	Peripheral plaque 290	Peripheral plaque
Artery	Platform	Samples	Group
100927	17077	Carotid atherosclerotic artery:29; carotid artery control:12	Carotid atherosclerotic artery
100927	17077	Femoral atherosclerotic artery:25; femoral artery control: 12	
100927	17077	Infra-popliteal atherosclerotic artery:14; infra-popliteal artery control: 11	Lower extremity atherosclerotic artery
57691	10558	Lower extremity aortic occlusive disease:9; control artery:10	

carotid plaque and low-immune groups (Supplementary Figure 5A, 5B).

Differentially expressed immune cells in the carotid plaque, peripheral plaque, carotid atherosclerotic artery and lower atherosclerotic artery groups are summarised in Table 2. Immune cells with different expressions in two or more groups, resting NK cells, mast cells, resting CD4 memory T cells, M0 macrophages, CD8 T cells, follicular helper T cells, naïve B cells and plasma cells were screened out. Among them, resting NK cells, M0 macrophages and activated mast cells showed differences in immune cell expression in three groups; therefore, they are considered to play an important role in atherosclerosis development.

3.5. WGCNA and Functional Enrichment Analysis. Using the carotid plaque group as an example, samples were analysed using WGCNA according to β value to cluster the samples, The β value was derived from 'sft$powerEstimate' choice. (Supplementary Figure 5C). The sample was divided into three modules with $\beta = 4$ (Figure 5(a), 5(b)), with the blue module showing the highest relation to immunity (Figure 5(c)). The blue module contained 308 genes (Supplementary Table 1), which further underwent GO and KEGG enrichment analyses. The results showed that these genes were related to metabolism, calcium signalling pathway, cell migration and cytokine activation (Figure 5(d)). The same analysis was performed for the other groups.

WGCNA analysis of the peripheral plaque group, with $\beta = 6$ (Supplementary Figure 5D), divided the group into 11 modules (Figure 5(e), 5(f)). The turquoise module showed the highest relation to immunity (Figure 5(g)) and contained 2120 genes (Supplementary Table 2), which are related to the MAPK pathway, NF-KB pathway, chemokines, cytokines, leukocyte proliferation and T cell activation (Figure 5(h)).

WGCNA analysis of the carotid atherosclerotic artery group, with $\beta = 12$ (Supplementary Figure 5E), divided the group into three modules (Figure 6(a), 6(b)). The turquoise module showed the highest relation to immunity (Figure 6(c)) and contained 1042 genes (Supplementary Table 3), which are related to THE NF-KB pathway, chemokines, mast cell granules, inflammatory response regulation and neutrophil activation (Figure 6(d)).

WGCNA analysis of the lower extremity atherosclerotic artery group, with $\beta = 5$ (Supplementary Figure 5F), divided the group into five modules (Figure 6(e), 6(f)). The blue module showed the highest relation to immunity (Figure 6(g)) and contained 361 genes (Supplementary Table 4), which are related to the toll-like receptor signalling pathway, Akt signalling pathway, chemokine signalling pathway, cytokine activity and T cell activation pathway (Figure 6(h)).

3.6. Construction of a PPI Network and Screening of Key Immune Genes. Using the carotid plaque group as an example, the blue module genes, which were closely related to immunity in WGCNA, were intersected with the high and low immune group genes and immune-related genes to obtain 21 intersecting genes (Figure 7(a)). These genes were introduced into the STRING website for PPI network construction (Figure 7(b)). Following this, the constructed PPI network was introduced into Cytoscape and analysed using the MCC algorithm in cytohubba to screen for the top five genes: CD40, NRP1, NRP2, NFATC2, IFNGR1 (Figure 7(c)). The same analysis was performed for the other groups. A total of 134 intersecting genes were obtained in the peripheral plaque group (Figure 7(d)), with PTPRC, CD4, CCL2, TLR2 and CD86 identified as key immune genes (Figure 7(e), 7(f)). A total of 108 intersecting genes were obtained in the carotid atherosclerotic artery group (Figure 8(a)), with TNF, PTPRC, CCl4, TLR2 and IL1B identified as key immune genes (Figure 8(b), 8(c)). A total of 12 intersecting genes were obtained in the lower extremity atherosclerotic artery group (Figure 8(d)), with HLA-DQA1, HLA-DQA2, CD3D, CD86 and MMP9 identified as key immune genes (Figure 8(e), 8(f)).

3.7. Correlation Analysis of Immune Cells. The correlation between the key immune genes screened in each group and differentially expressed immune cells of the corresponding groups were analysed: carotid plaque (Figure 9(a)), peripheral plaque (Figure 9(b)), carotid atherosclerotic artery (Figure 9(c)) and lower extremity atherosclerotic artery

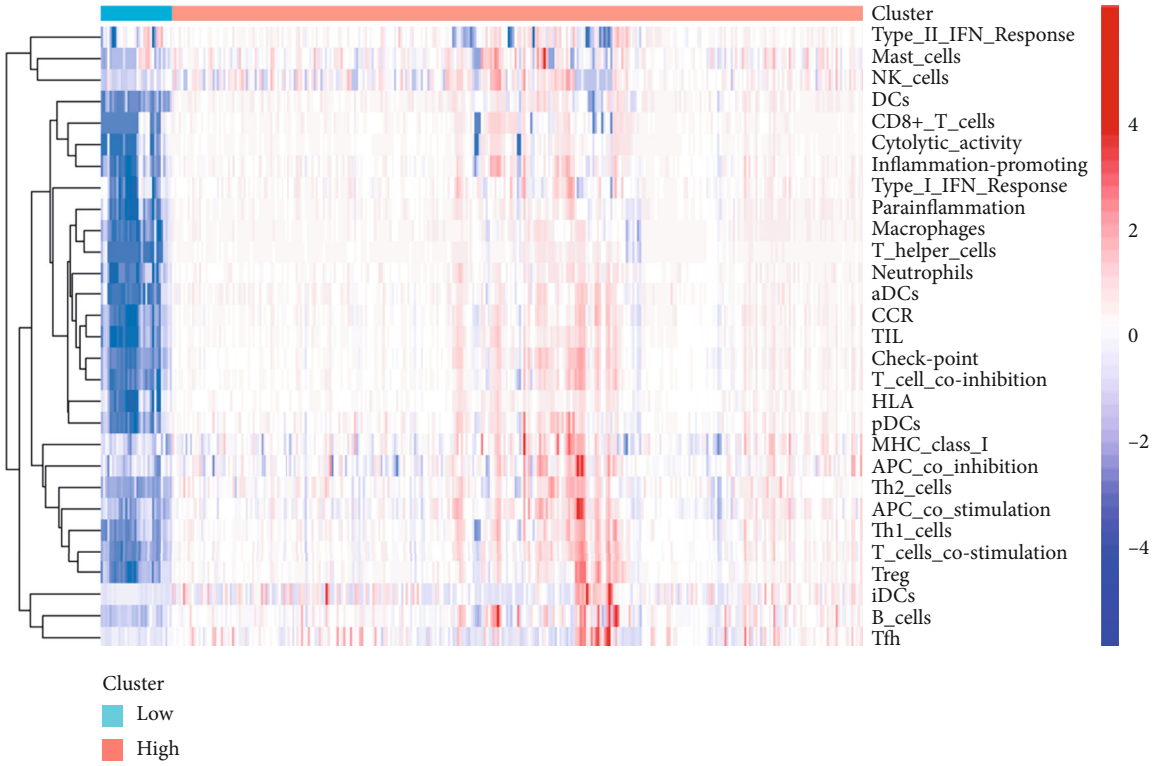

(a)

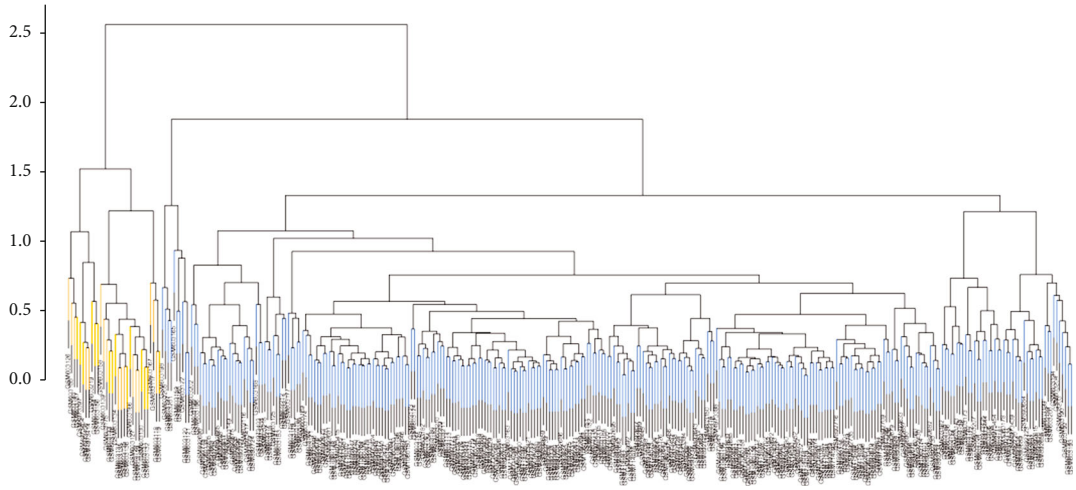

(b)

Figure 1: Continued.

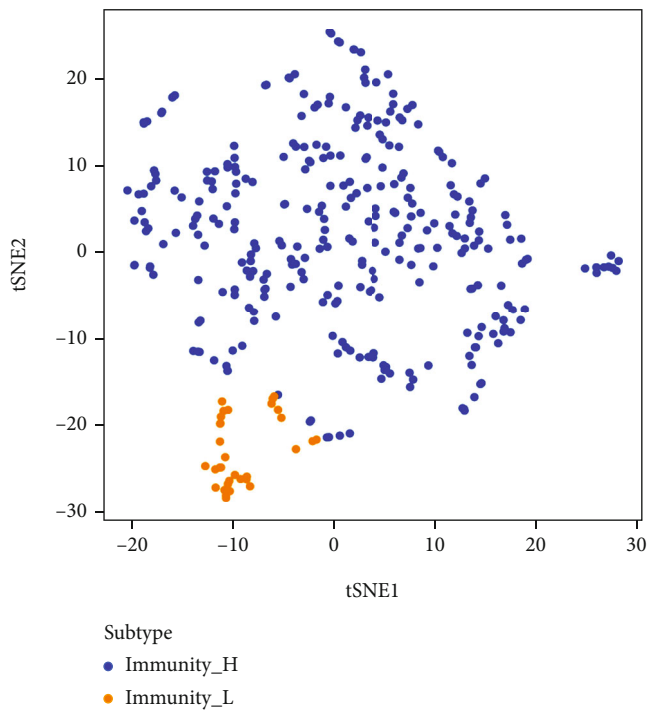

(c)

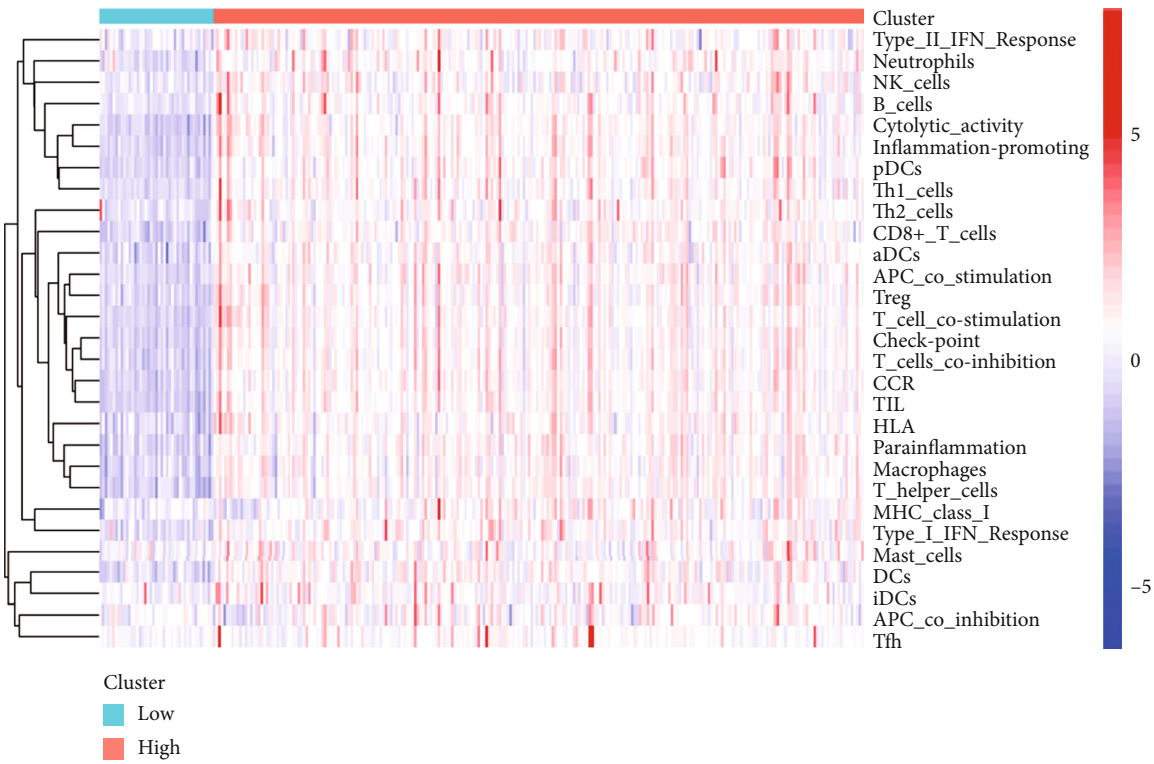

(d)

Figure 1: Continued.

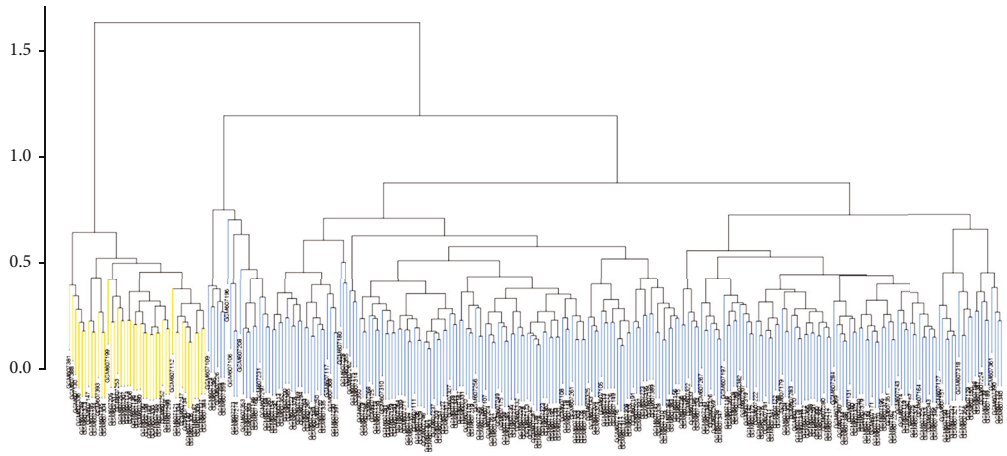

(e)

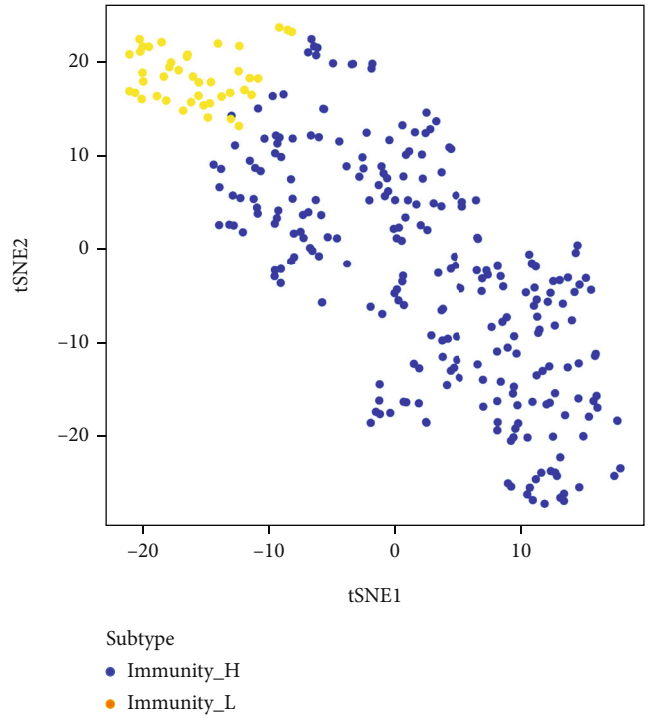

(f)

Figure 1: A: Heat map of the carotid artery plaque samples obtained using single-sample gene set enrichment analysis B: Cluster analysis divides the carotid artery plaque samples into the high- and low-immune groups C: t-distributed stochastic neighbor embedding analysis in carotid artery plaque samples. D: Heat map of the peripheral plaque samples obtained using single-sample gene set enrichment analysis E: Cluster analysis divides the carotid artery plaque samples into the high- and low-immune groups F: t-distributed stochastic neighbor embedding analysis in carotid artery plaque samples.

(Figure 9(d)) groups. The results are shown in Supplementary Table 5. Although most immune genes were correlated with immune cells ($p < 0.05$), the correlation was not very high ($r < 0.5$). Moreover, compared with the plaque and peripheral blood groups, the correlation between immune genes and immune cells in the artery group was very high ($r > 0.5$), especially the correlation between *CCL4* and activated mast cells was as high as 0.9 (Figure 9(c)). $r > 0.5$ was used as the standard to screen the key immune genes closely related to immune cells, which were then analysed according to the situation of each group. Since *PTPRC* and *TLR2* were common key immune genes in the PPI network of groups with strong correlations with most immune cells in both groups, they were identified as hub immune genes that were closely related to immune cells. Based on the correlation criteria and correlation criteria value, *CCL2*, *CCL4*, *TLR2*, *IL1B* and *PTPRC* were identified as hub immune genes in atherosclerosis.

3.8. Receiver Operating Characteristic Curve Analysis. To verify the reliability of the selected key immune genes, the receiver operating characteristic curve(ROC) analysis of

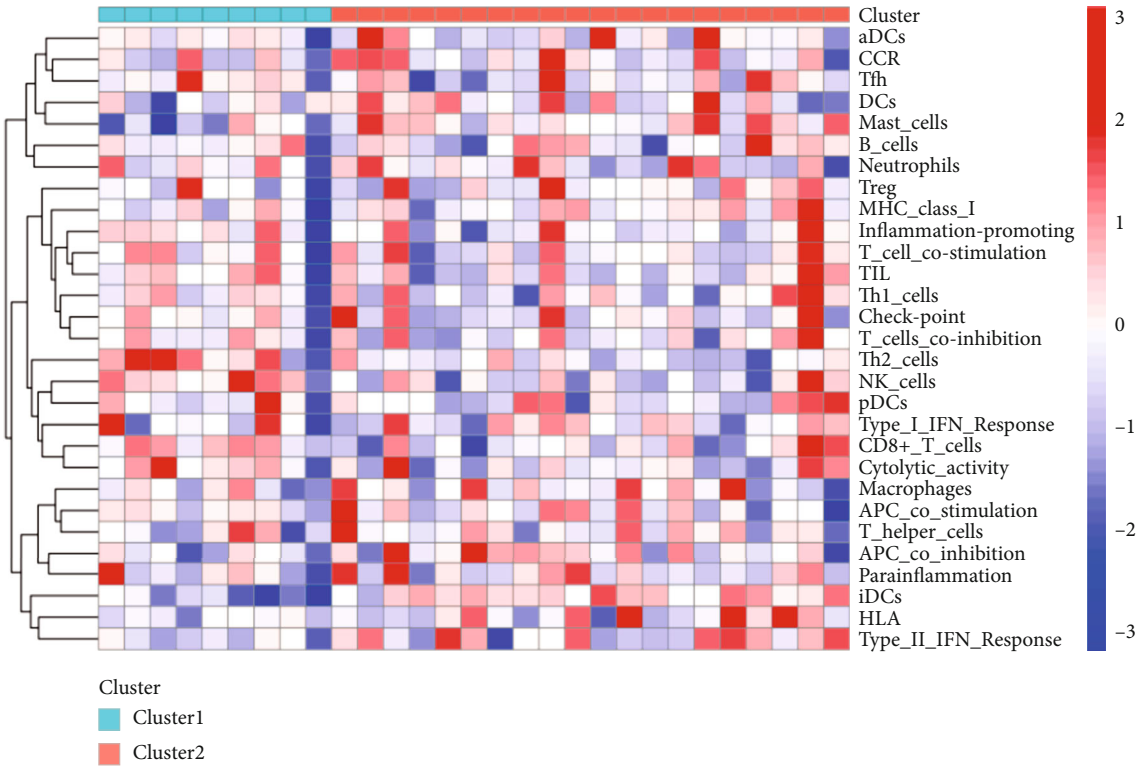

(a)

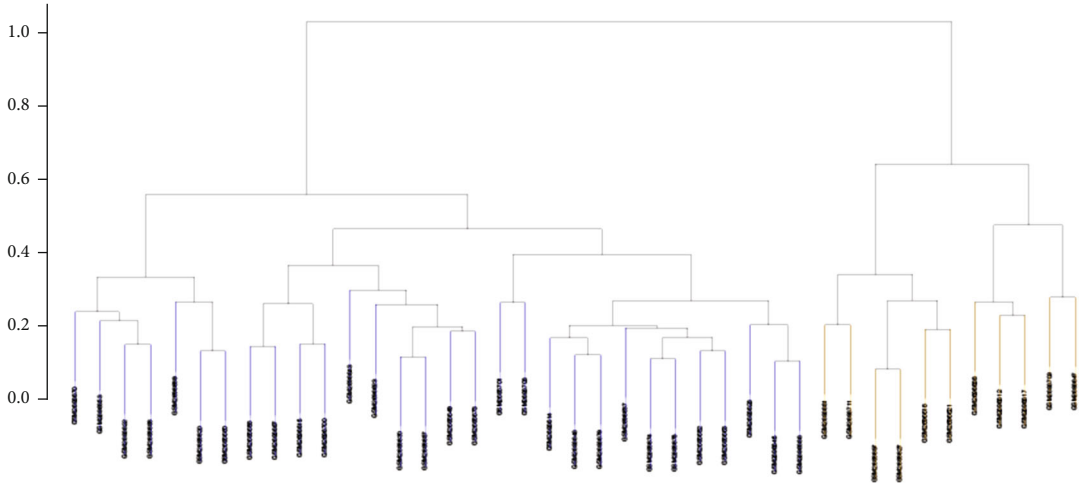

(b)

Figure 2: Continued.

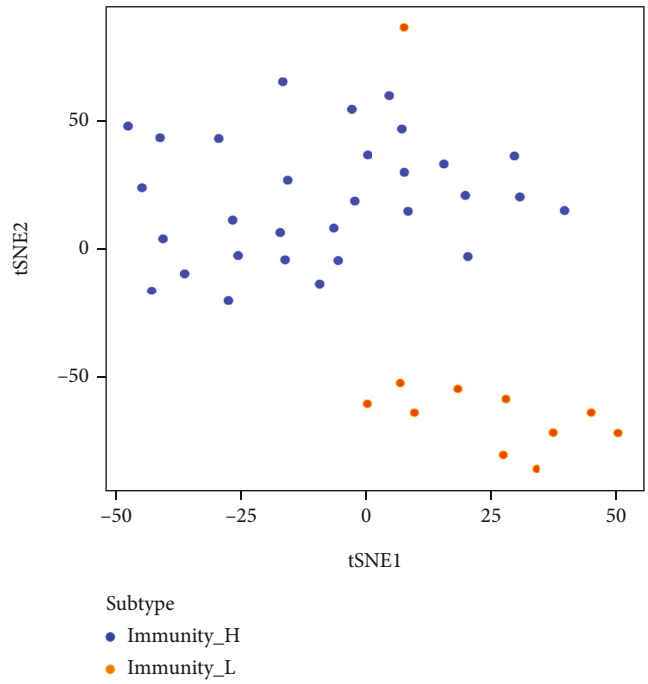

(c)

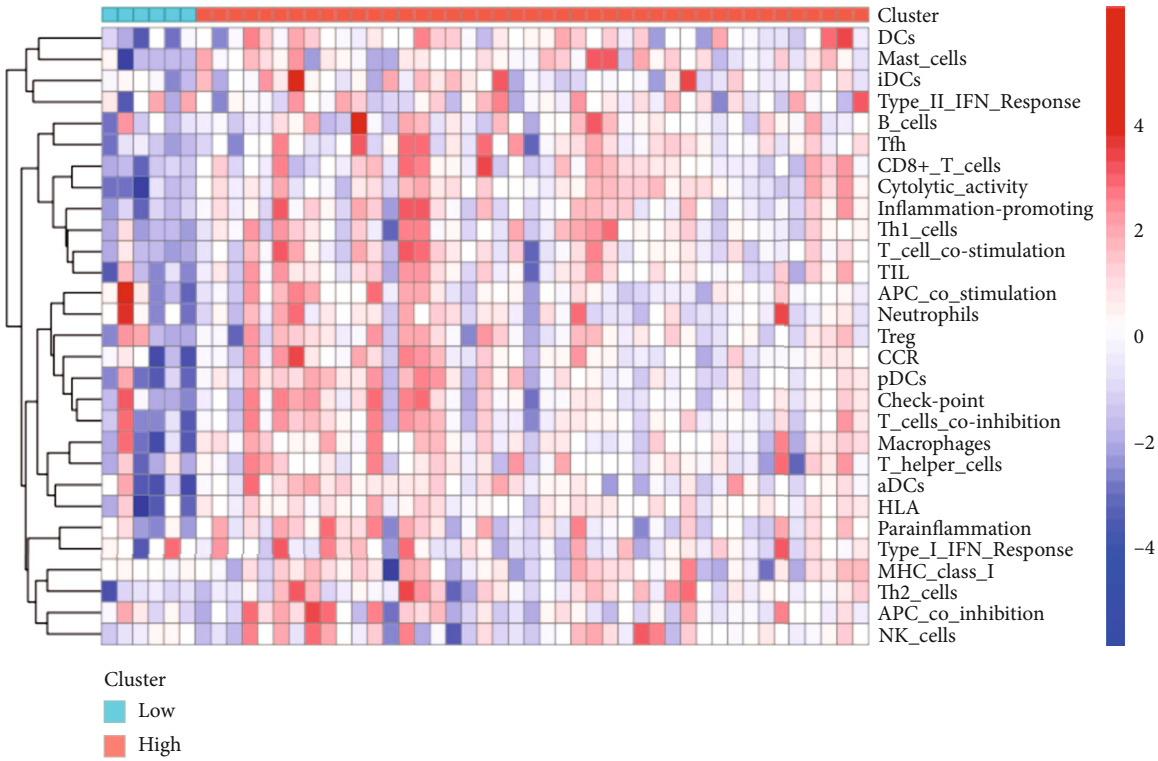

(d)

Figure 2: Continued.

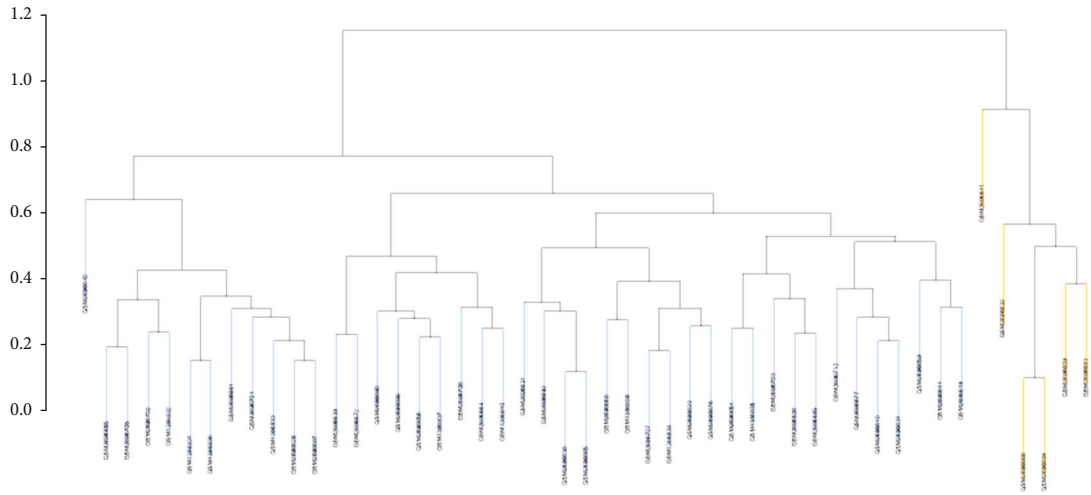

(e)

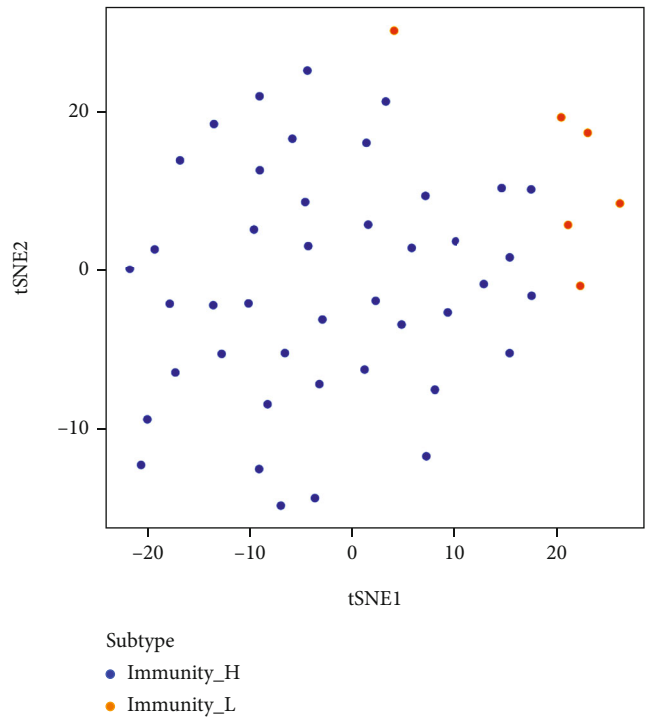

(f)

Figure 2: A: Heat map of the carotid atherosclerotic artery samples obtained using single-sample gene set enrichment analysis B: Cluster analysis divides the carotid atherosclerotic artery samples into the high- and low-immune groups C: t-distributed stochastic neighbor embedding analysis in carotid atherosclerotic artery samples D: Heat map of the lower extremity atherosclerotic artery samples obtained using single-sample gene set enrichment analysis E: Cluster analysis divides the lower extremity atherosclerotic artery samples into the high- and low-immunity groups F: t-distributed stochastic neighbour embedding analysis in lower extremity atherosclerotic artery samples.

CCL2, CCL4, TLR2, IL1B and PTPRC in the plaque and artery groups were analysed. The results showed that the five genes had high accuracy in all groups except the lower extremity atherosclerotic artery group (Figure 10(a), 10(b), (c), (d)). To further verify the accuracy of the genes, ROC analysis was performed on these five genes in the GSE28829 (including 16 advanced and 13 early carotid plaques), GSE163154 (including 27 intraplaque and 16 non intraplaque haemorrhage samples), GSE43292 (including 32 carotid plaques and 32 control samples), GSE100927 (including 29 carotid atherosclerotic artery samples and 12 control samples), GSE100927 (including 25 femoral atherosclerotic artery samples and 12 control samples) and GSE100927 (including 14 infrapopliteal atherosclerotic artery samples and 11 control samples) datasets. These five genes showed strong accuracy in identifying carotid plaque progression (Figure 10(e)), plaque

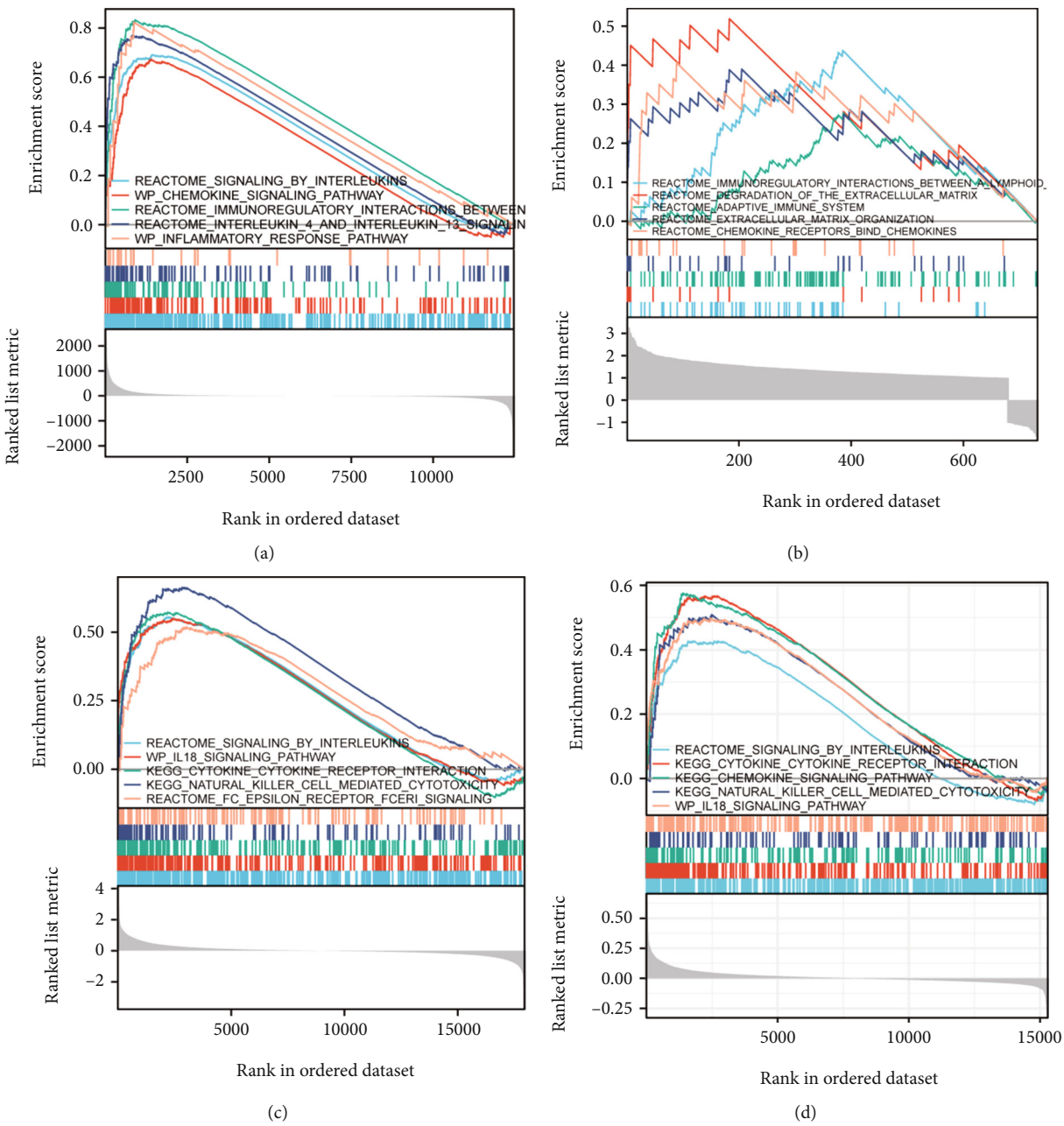

Figure 3: Continued.

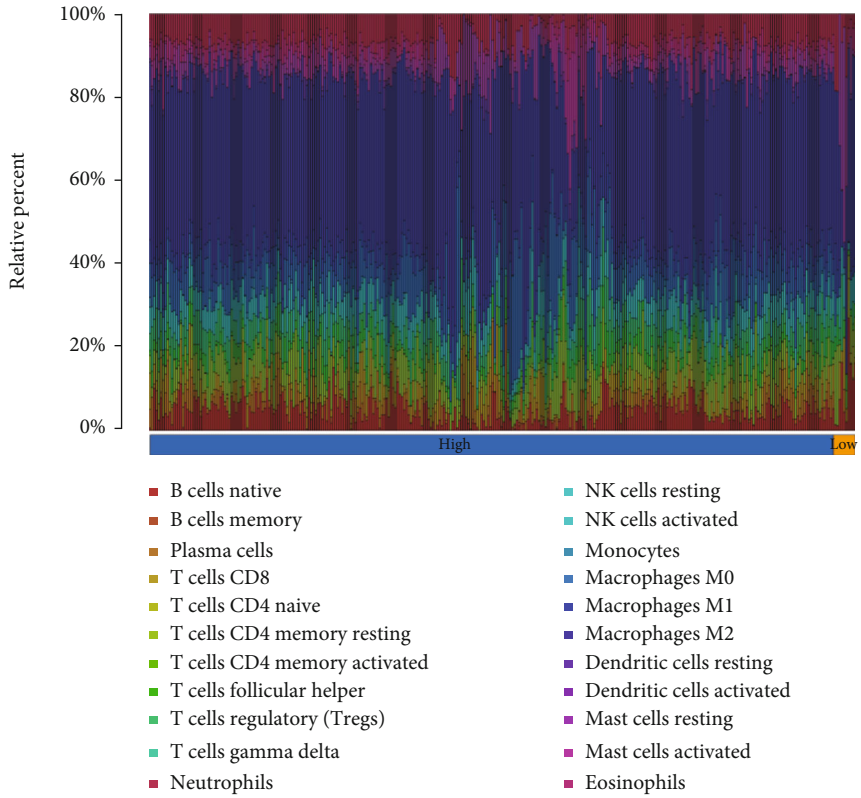

(e)

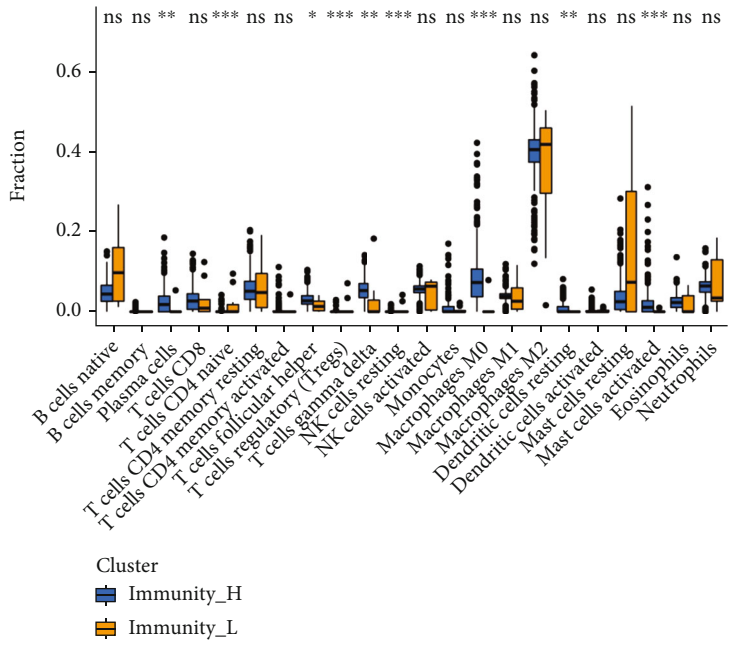

(f)

Figure 3: A: Gene set enrichment analysis of the high- and low-immunity groups in carotid artery plaque samples B: Gene set enrichment analysis of the high- and low-immunity groups in peripheral plaque samples C: Gene set enrichment analysis of the high- and low-immunity groups in carotid atherosclerotic artery samples D: Gene set enrichment analysis of the high- and low-immunity groups in lower extremity atherosclerotic artery samples E: The infiltration ratio of 22 immune cells in the carotid artery plaque samples F: The differential expression of 22 immune cells in the high- and low-immune groups in carotid artery plaque samples.

Table 2: Differentially expressed immune cells in each group (the immune cells with increased expression in each group are listed in the table).

Group	Immunity-High	Immunity-Low
Carotid plaque	Plasma cells	T cells regulatory (Tregs)
	T cells CD4 naive	NK cells resting
	T cells follicular helper	
	T cells gamma delta	
	Macrophages M0	
	Dendritic cells resting	
	Mast cells activated	
Peripheral plaque	T cells CD8	B cells naive
	T cells CD4 memory activated	T cells follicular helper
	Macrophages M1	NK cells resting
	Mast cells activated	Mast cells resting
	Eosinophils	
Carotid atherosclerotic artery	Macrophages M0	Plasma cells
	Mast cells activated	T cells CD4 memory resting
		Macrophages M1
		Macrophages M2
		Mast cells resting
Lower limbs atherosclerotic arteries	T cells CD8	B cells naive
	T cells follicular helper	Plasma cells
	T cells gamma delta	NK cells resting
	Macrophages M0	Dendritic cells activated
	Macrophages M1	Neutrophils

stability (Figure 10(f)) and carotid atherosclerosis and plaque occurrence (Figure 10(g), (h)), which indicates the close relationship of these five immune genes with atherosclerosis and plaque occurrence and plaque progression and stability. However, the accuracy of these five genes in the lower extremity atherosclerotic artery group was lower than that of the other three groups. Therefore, the lower extremity atherosclerotic artery group was further subdivided into the following groups: femoral artery and inferior popliteal artery. The verification of these subgroups showed the strong accuracy of the other four genes except CCL2 (Figure 10(i), (j)). However, differences were observed in immune responses between the lower extremity atherosclerosis, carotid atherosclerosis and atherosclerotic plaque groups. Moreover, the distinguishing accuracy between the high- and low-immune groups is lower than that of the other sample groups. In addition to CCL2, the four genes (CCL4, TLR2, IL1B and PTPRC) can distinguish between lower extremities atherosclerotic artery and lower extremities normal artery. Although CCL2 does not perform well in the lower extremity atherosclerotic artery, it performs well in the carotid atherosclerotic artery and plaque groups, which indicates that CCL2 is a specific immune gene for carotid atherosclerosis and plaque formation.

4. Discussion

To the best of our knowledge, this study is the first to comprehensively analyse and compare the immune characteristics of four different atherosclerosis sample types: carotid plaque, peripheral plaque, carotid atherosclerotic artery and lower extremity atherosclerotic artery.

Comprehensive analyses showed that despite differences in sample source, the immune cell infiltration in atherosclerotic plaque and artery samples were dominated by macrophages, especially in the carotid plaque and carotid atherosclerotic artery groups. M0 macrophages accounted for a large proportion of the infiltered cells and their expression in the high immune group was significantly higher than that in the low immune group. Macrophages play a central role in atherosclerosis as inflammation regulators. The main cells involved in atherosclerotic plaque formation are activated macrophages and foam cells, with macrophages promoting two key changes in plaque morphology: plaque necrosis and protective collagen scar (fibrous cap) thinning [28]. A study by Ginhoux et al. [29] showed that macrophages in the plaque can induce high inflammation tissue destruction. M0 macrophages are usually considered to be inactivated macrophages and are induced by IFN-γ, TLR4, IL-4, IL-13 and other factors, thus differentiating into pro-inflammatory M1 macrophage or anti-inflammatory M2 macrophage [30, 31]. Therefore, inducing macrophage differentiation may control atheroma, which is a key factor in the development of hardening.

Despite being present in smaller proportion as compared to macrophages, T cells, NK cells and mast cells showed strong heterogeneity in the high- and low-immunity group,

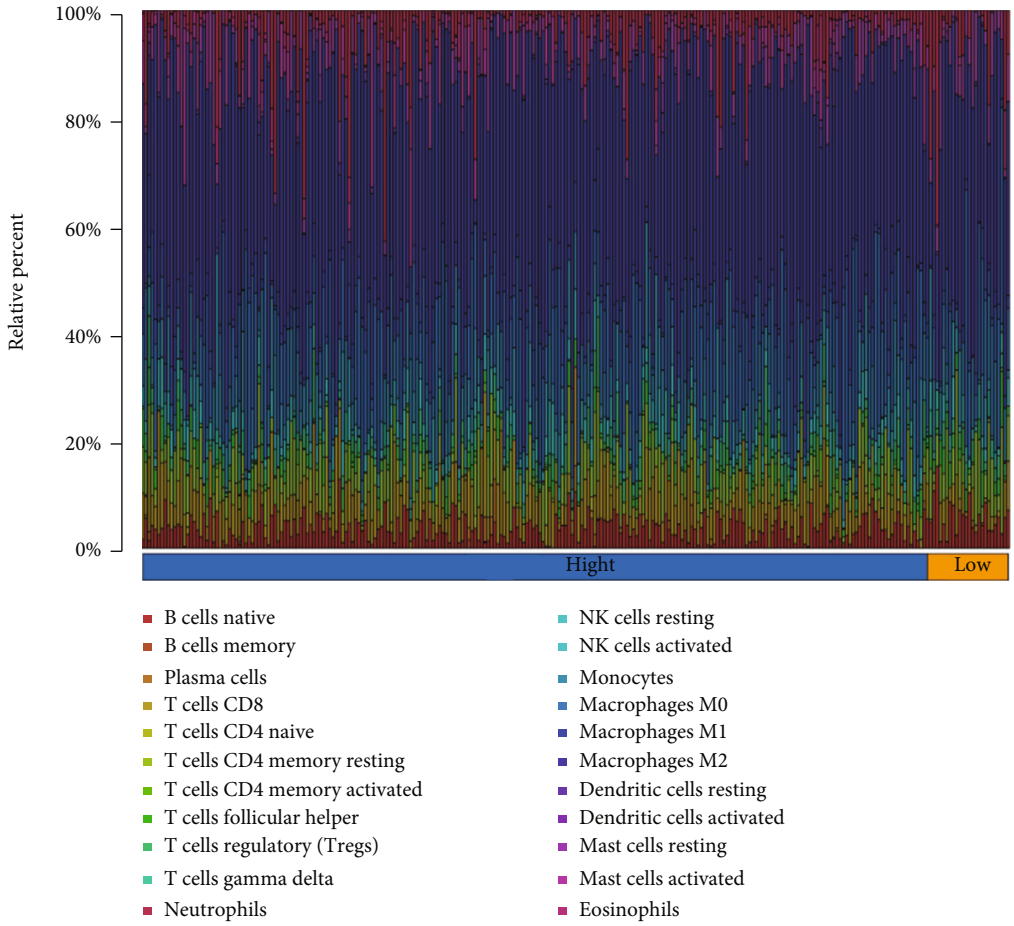

(a)

Figure 4: Continued.

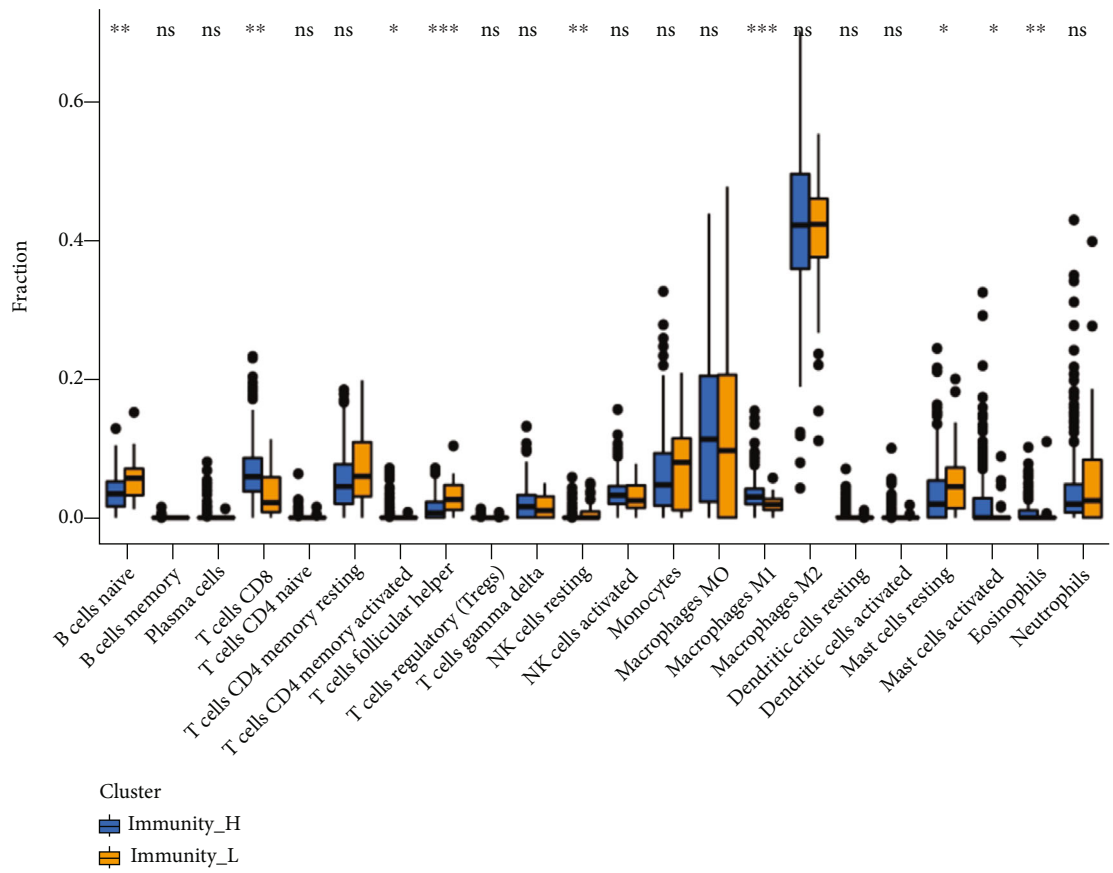

(b)

Figure 4: Continued.

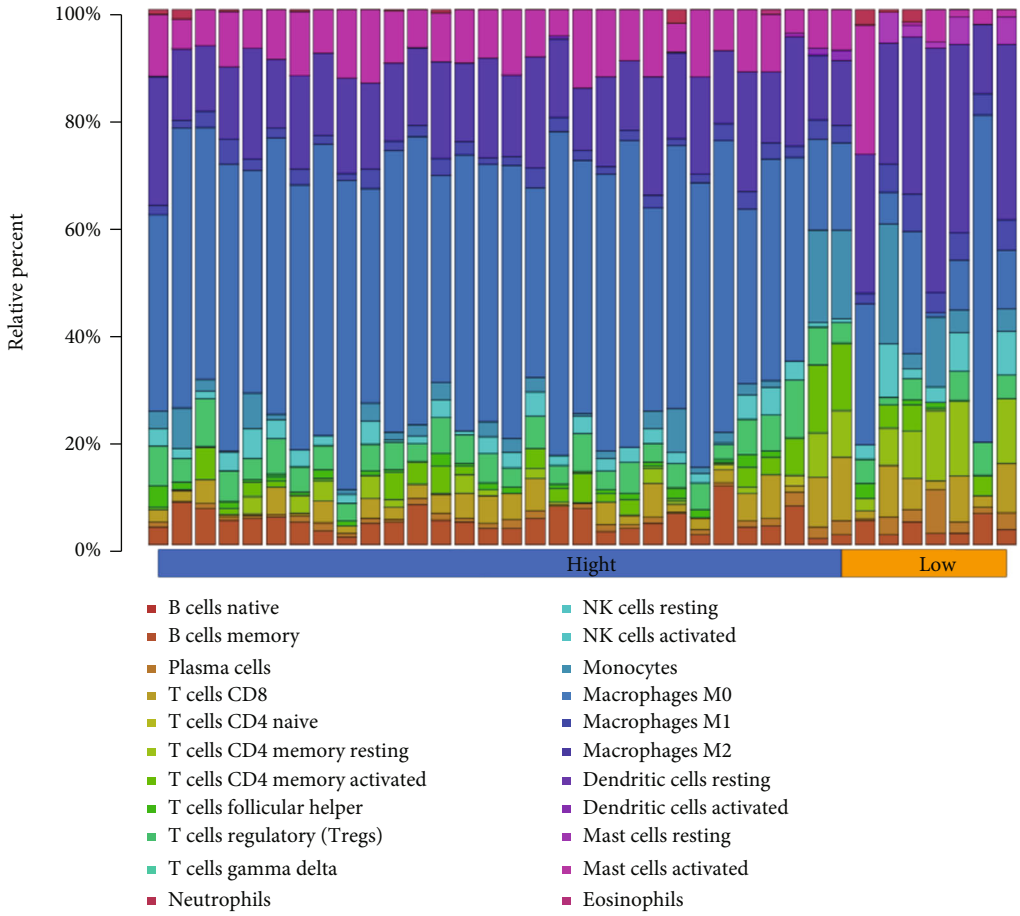

(c)

Figure 4: Continued.

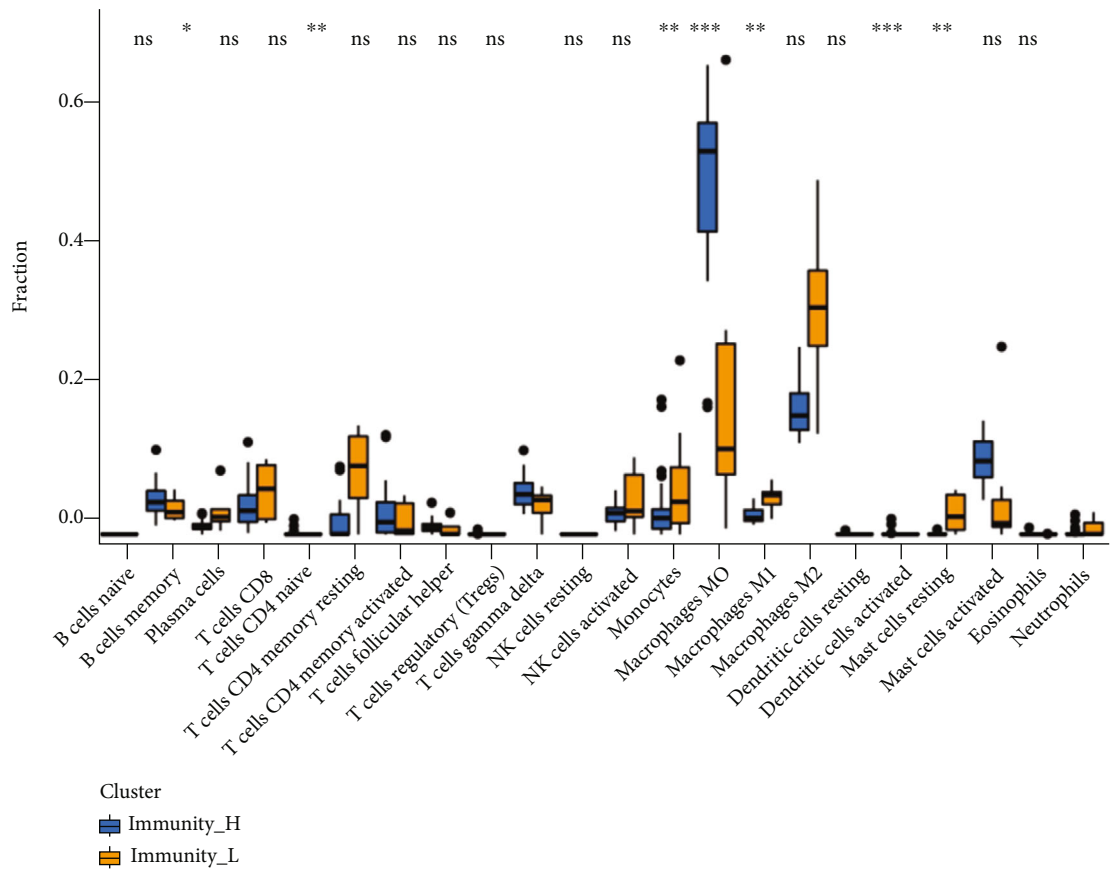

(d)

Figure 4: Continued.

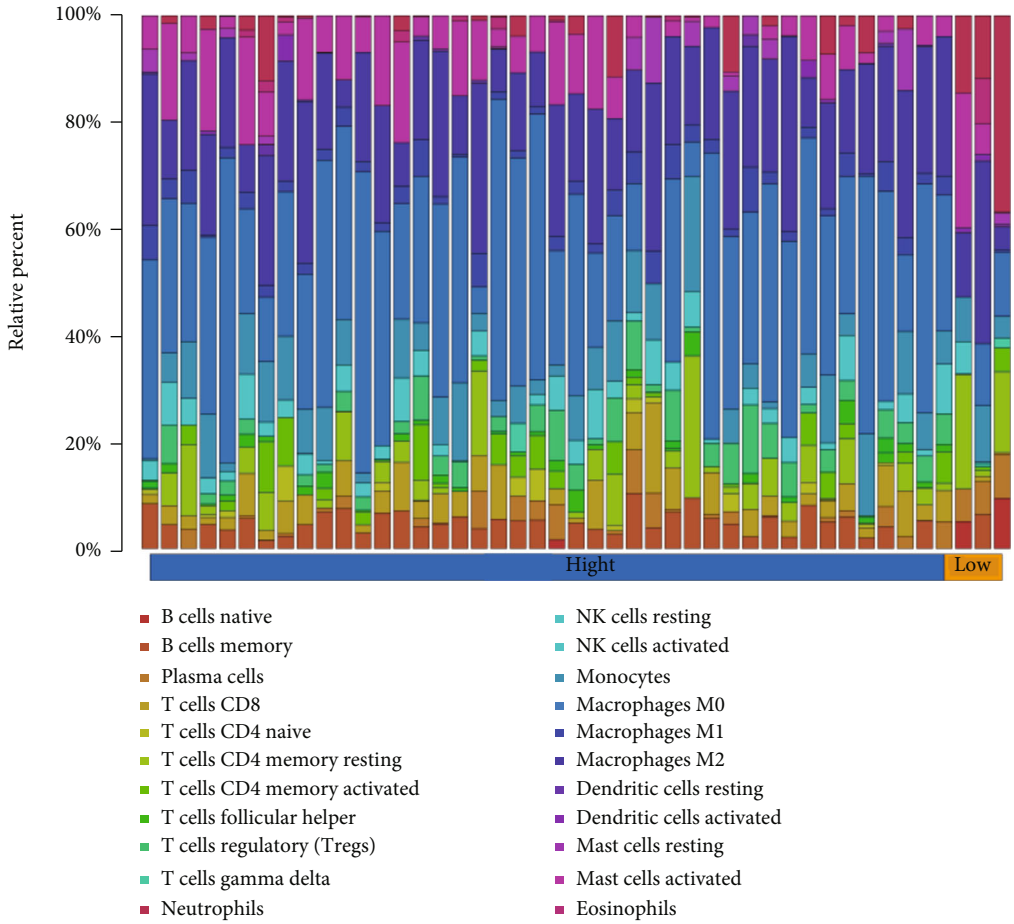

(e)

Figure 4: Continued.

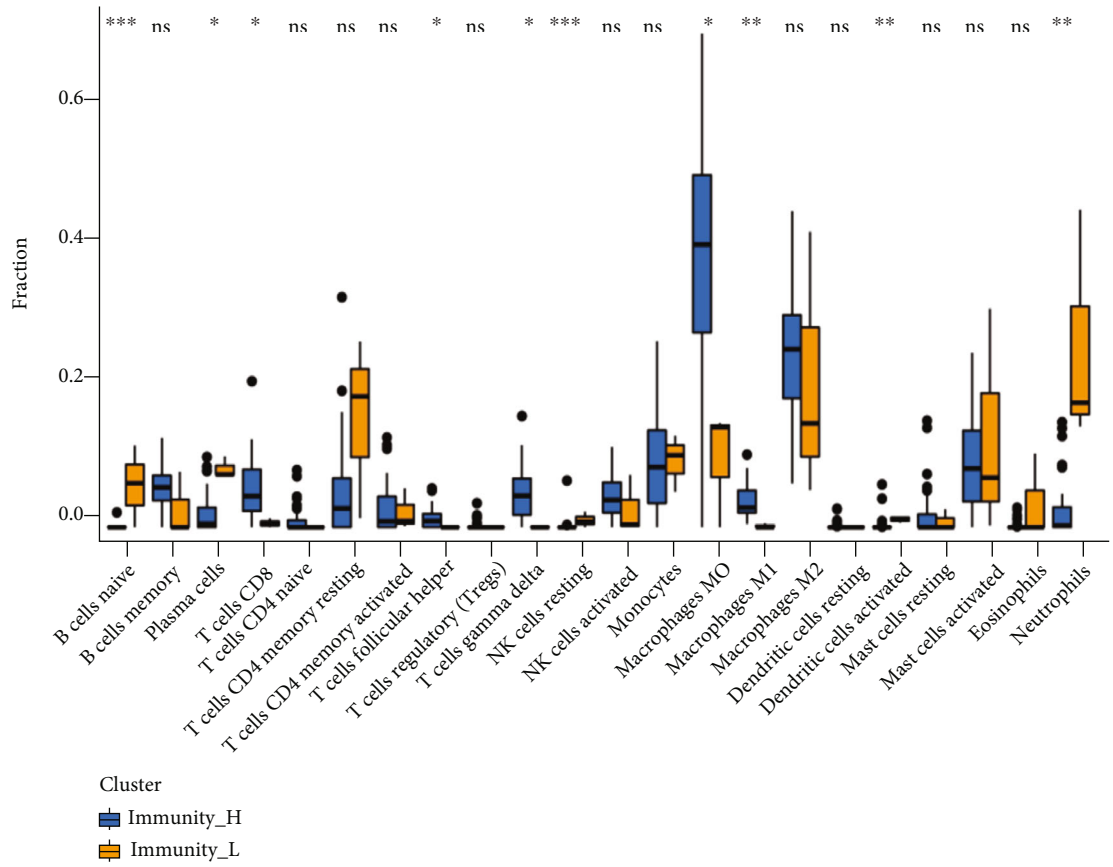

(f)

Figure 4: A: The infiltration ratio of 22 immune cells in the peripheral plaque samples B: The differential xpression of 22 immune cells in the high- and low-immune groups in the peripheral plaque sample C: The infiltration ratio of 22 immune cells in the carotid atherosclerotic artery samples D: The differential expression of 22 immune cells in the high- and low-immune groups in the carotid atherosclerotic artery samples E: The infiltration ratio of 22 immune cells in the lower extremity atherosclerotic artery samples F: The differential expression of 22 immune cells in the high- and low-immune groups in the lower extremity atherosclerotic artery samples.

especially T cells. T cell expression varied between the high- and low-immunity groups in plaque, artery and lower extremity atherosclerotic artery source samples. Among the differentially expressed T cells, CD4 memory T cells and CD8 T cells were dominant. Previous studies have shown that most T cells found in atherosclerotic plaques show memory phenotype and have large CD4 T cell numbers. After stimulation by antigens, stimulants and some cytokines, CD4 T cells differentiate into different T cell subsets and participate in the immune and inflammatory processes [32, 33]. Although CD8 T cells are rare compared to CD4 T cells in atherosclerotic plaques, CD8 T cells showed a significant increase in severe atherosclerotic plaque lesions, indicating that CD8 T cells are inextricably linked with plaque progression and inflammation. Additionally, some studies have reported that CD8 T cells contribute to plaque inflammation and necrotic core formation, suggesting their role in promoting plaque instability and causing cardiovascular events after plaque rupture [34–37]. Moreover, these studies have indicated that T cells, especially CD4 memory T cells and CD8 T cells, can be the key immune cells that promote atherosclerosis formation and plaque progression, which is consistent with this study. Notably, Tregs only showed high expression in the low-immune group in carotid plaque samples in comparison with other differential immune cells. Tregs also showed a higher correlation with key genes than the other immune cells, and Tregs expression increased in the early carotid plaque group compared with the advanced carotid plaque group. Liu et al. reported that the number of Tregs in the unstable plaques of human origin was reduced. Correspondingly, studies in animal models have also demonstrated that Tregs can secrete anti-inflammatory cytokine IL-10 and TGF in stable plaque- β and inhibit pro-inflammatory T cell proliferation, delaying atherosclerosis occurrence and development [38–40]. Further evidence suggests that Tregs promote the transformation from pro-inflammatory M1 macrophages to anti-inflammatory M2 macrophages by releasing IL-10 to prevent atherosclerosis occurrence. Therefore, Tregs play an anti-inflammatory role in carotid plaque and delay plaque progression.

The role of mast cells should not be underestimated despite their lower content in atherosclerosis and plaque compared to macrophages. Mast cells are mainly present in

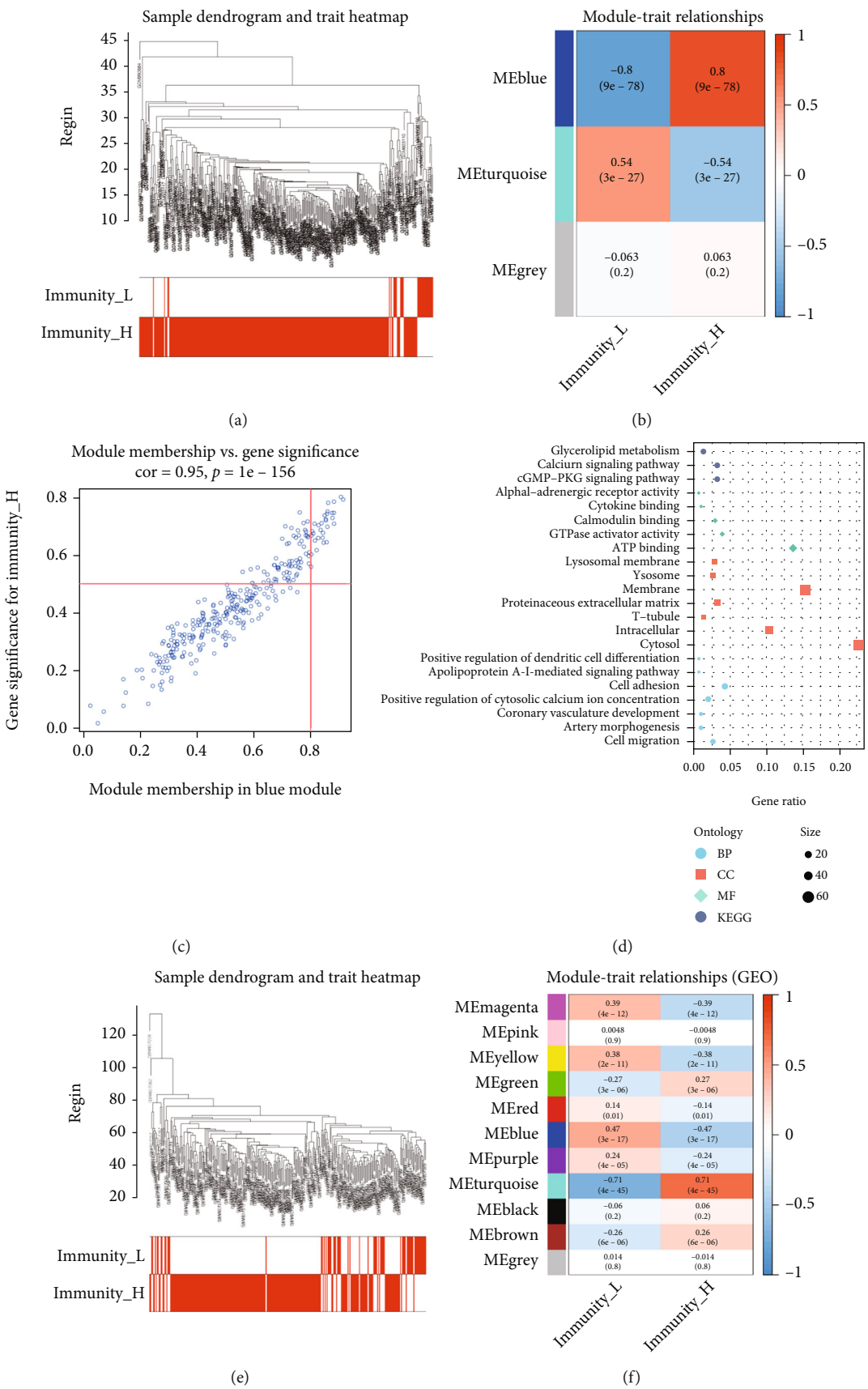

Figure 5: Continued.

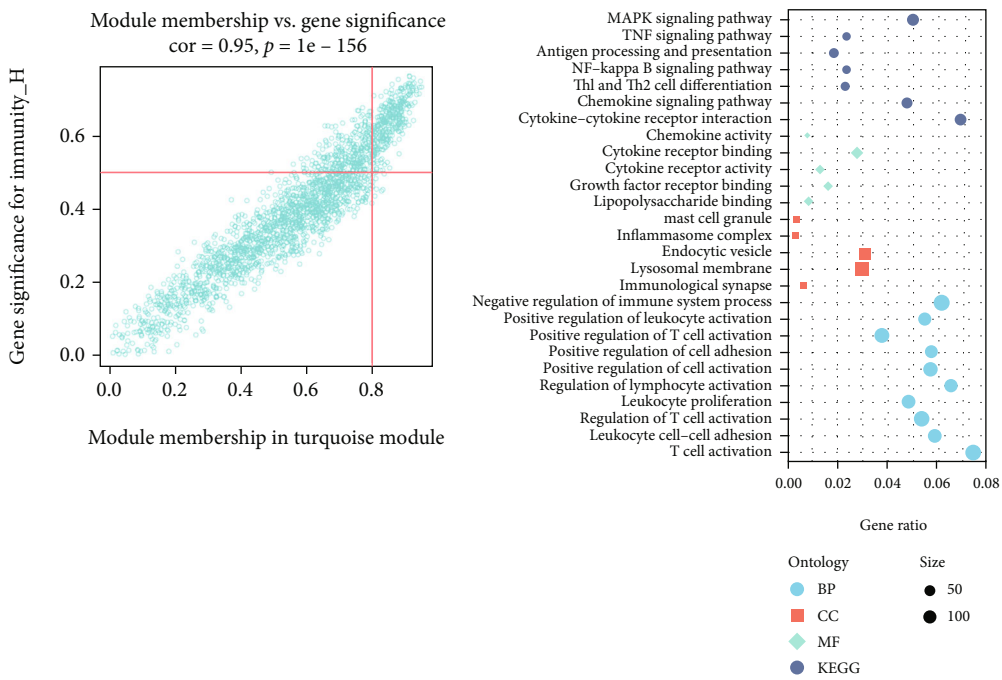

(g) (h)

Figure 5: A: Sample clustering dendrogram for detecting outliers in carotid artery plaque samples. B: Correlation diagram between modules and immune groups: each module contains a correlation value (first row) and p value (second row) in carotid artery plaque samples. C: The correlation between the genes in the blue module and the high-immunity group in carotid artery plaque samples D: Gene Ontology and Kyoto Encyclopedia of Genes and Genomes enrichment analyses of the genes in the blue module E: Sample clustering dendrogram for detecting outliers in peripheral plaque samples F: Correlation diagram between the modules and immune groups: each module contains a correlation value (first row) and p value (second row) in peripheral plaque samples G: The correlation between the genes in the turquoise module and the high-immunity group in peripheral plaque samples H: Gene Ontology and Kyoto Encyclopedia of Genes and Genomes enrichment analyses of the genes in the turquoise module.

the mucosal and connective tissues and distributed around the blood vessels, activating the release of proinflammatory cytokines, vasoactive substances and proteolytic enzymes. These characteristics of mast cells have extremely strong effects on the blood vessels [41, 42]. This study showed that activated mast cell numbers increased in the high-immune groups of the plaque and artery samples, showing a strong correlation between the screened key genes and activated mast cells. Wang et al. confirmed that mast cell density and degranulated cell proportion in the shoulder area of the carotid plaque were significantly higher than those in other areas, and mast cells were also found around plaque thrombosis, calcification and neovascularization, indicating their role in carotid atherosclerotic plaque formation and affecting plaque stability by activating degranulation [43]. Various studies have shown that mast cells located near plaque microvessels contain basic fibroblast growth factor (bFGF). Mast cells release angiogenesis-related compounds via bFGF, which enhances the ability of the matrix around cells to degrade protease, induces the leakage and rupture of neovascularization and leads to bleeding in plaque [44]. Den et al. reported that activated mast cells release chymotrypsin via the TLR4 pathway and promote vascular smooth muscle cell apoptosis in the body, which leads to plaque instability [45]. Therefore, previous reports and the current study mutually confirm that inhibiting mast cell activation is a potential therapeutic target and an important research direction for controlling atherosclerosis development and plaque stabilisation. However, the role of NK cells in atherosclerosis remains unclear. Selathurai et al. [46] speculated that perforin and granzyme B produced by NK cells can promote atherosclerosis and necrotic core development, whereas Nour-Eldine et al. [47] speculated that NK cells have no direct effect on hypercholesterolaemia induced atherosclerosis. However, NK cell may promote atherosclerosis formation when pathological NK cells are over-activated. This study shows that in the low-immunity group of the carotid and peripheral plaques, resting NK cell expression increased significantly and resting NK cells number in the early carotid plaque increased compared with the late carotid plaque. Therefore, NK cells contribute to atherosclerosis formation. Interestingly, we found that B-naïve cells were highly expressed in the low immune group of the peripheral plaques and lower limbs atherosclerotic arteries, but not in the carotid plaque and carotid atherosclerotic artery. In contrast to T cells and macrophages, the role of B cells in atherosclerosis has only recently begun to receive attention. Recent studies have shown that B cell production

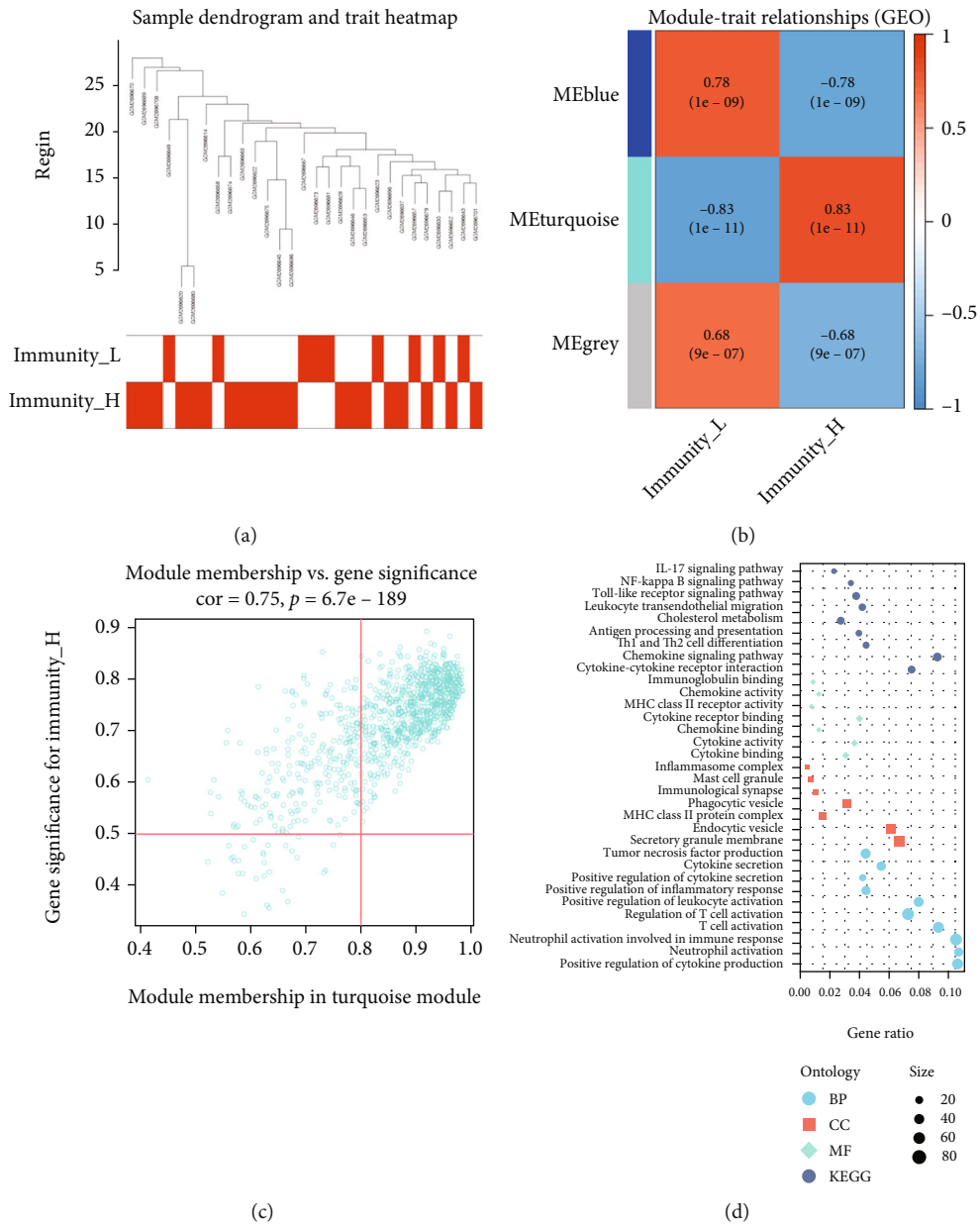

Figure 6: Continued.

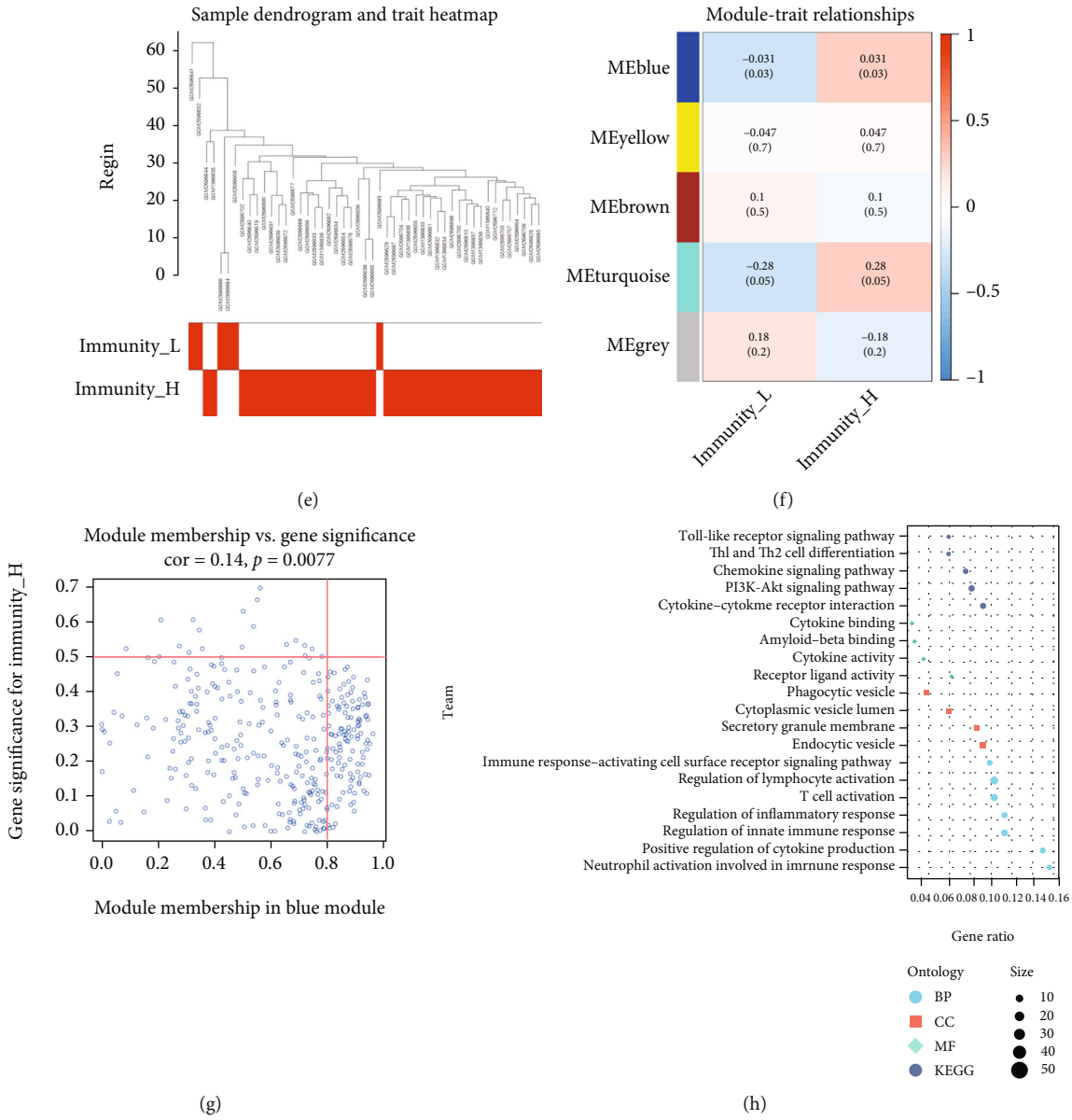

Figure 6: A: Sample clustering dendrogram for detecting outliers in carotid atherosclerotic artery samples B: Correlation diagram between modules and immune groups: each module contains a correlation value (first row) and p value (second row) in carotid atherosclerotic artery samples C: The correlation between the genes in the turquoise module and the high-immunity group in carotid atherosclerotic artery samples D: Gene Ontology and Kyoto Encyclopedia of Genes and Genomes enrichment analyses of the genes in the turquoise module E: Sample clustering dendrogram for detecting outliers in lower extremity atherosclerotic artery samples F: Correlation diagram between the modules and immune groups: each module contains a correlation value (first row) and p value (second row) in lower extremity atherosclerotic artery samples G: The correlation between the genes in the blue module and the high-immunity group in lower extremity atherosclerotic artery samples. H: Gene Ontology and Kyoto Encyclopedia of Genes and Genomes enrichment analyses of the genes in the blue module.

is significantly reduced in the bone marrow of aged mice and humans [48], Frasca et al. found that aging downregulates B cell type switching in humans and mice [49]; in addition, hypercholesterolemia Apoe-/- mice and low-density lipoprotein-deficient mice have also shown that protective immunity of B cells can delay the progression of atherosclerosis, while the lack of B cells increases the occurrence of atherosclerosis [50, 51]. Further studies have found that the lack of B cell in mice can lead to vascular endothelium dysfunction by inducing the increase of neutrophils, thereby leading to vascular diseases [52]. These studies demonstrate the importance of B cells in the development of atherosclerosis and may have a more significant impact on large vessel atherosclerosis than in carotid atherosclerosis, but more work is needed to confirm this speculation.

Bioinformatic and correlation analyses of differentially expressed immune cells helped to identify CCL4, TLR2, IL1B, and PTPRC as hub genes in atherosclerosis formation

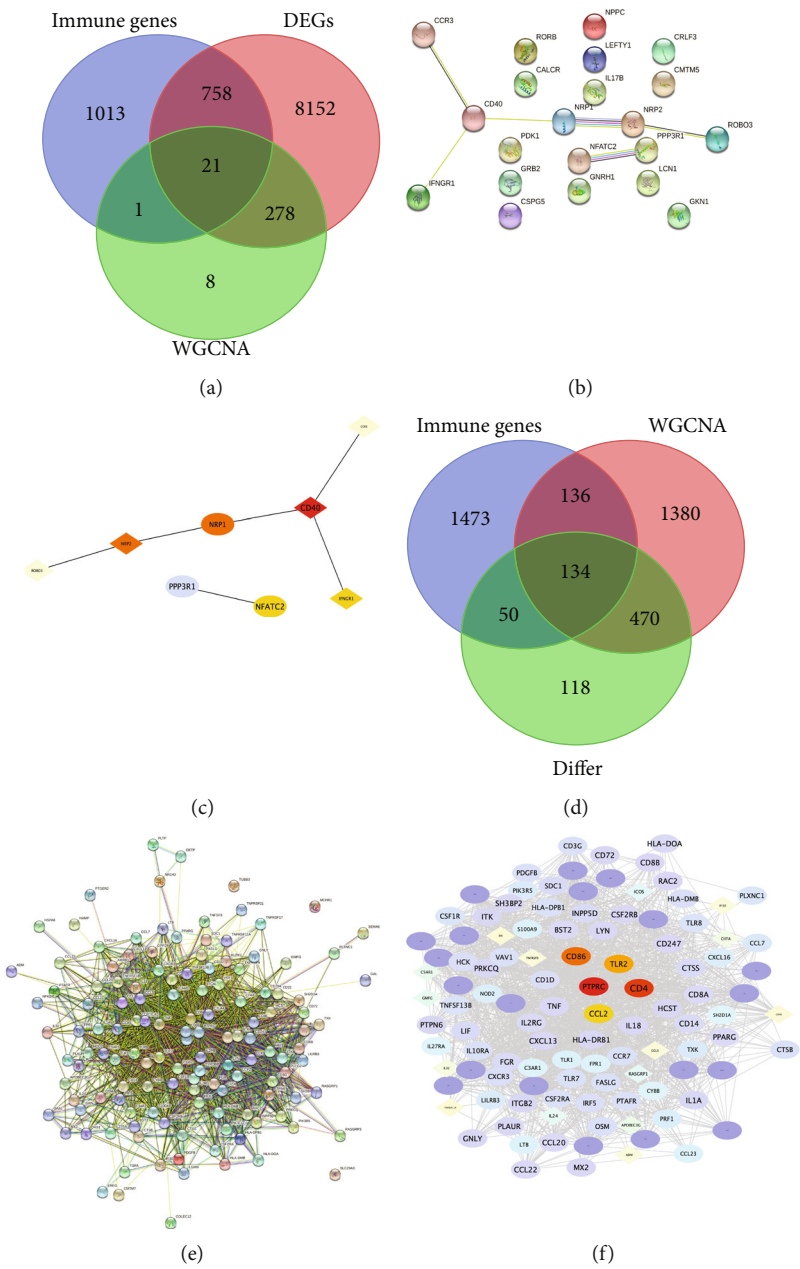

Figure 7: A: Venn diagram of immune-related genes, differentially expressed genes and blue modular genes in carotid artery plaque samples B: Protein-protein interaction network construction using 21 genes from the STRING database in carotid artery plaque samples C: Screening of the top five hub genes (the darker the colour, the higher the gene ranking) in carotid artery plaque samples D: Venn diagram of immune-related genes, differentially expressed genes and turquoise modular genes in peripheral plaque samples E: Protein–protein interaction network construction using 134 genes from the STRING database in peripheral plaque samples F: Screening of the top five hub genes (the darker the colour, the higher the gene ranking) in peripheral plaque samples.

and plaque progression. CCL2 affects carotid atherosclerosis and plaque formation. CCL2 and CCL4 are both pro-inflammatory chemokines in the chemokine family, which attract immune cells to the inflammation site and actively participate in the inflammatory response under the stimulation of IL-1, TNF-α and LPS. Previous studies have shown that CCL2 inhibition alone or in combination with CX3CR1 and CCR5 leads to decreased monocyte recruitment and thus inhibits atherosclerosis occurrence. Winter et al. reported that blocking the CCL2-CCR2 axis can effectively reduce atherosclerosis occurrence. [53, 54]. However, inhibiting CCL4 can reduce MMP-2 and MMP-9 expression, which blocks TNF-α and IL-6 production that is responsible for stimulating macrophage activation and inhibits macrophage and EC activation to reduce atherosclerotic plaque formation and increase plaque stability [55]. Therefore,

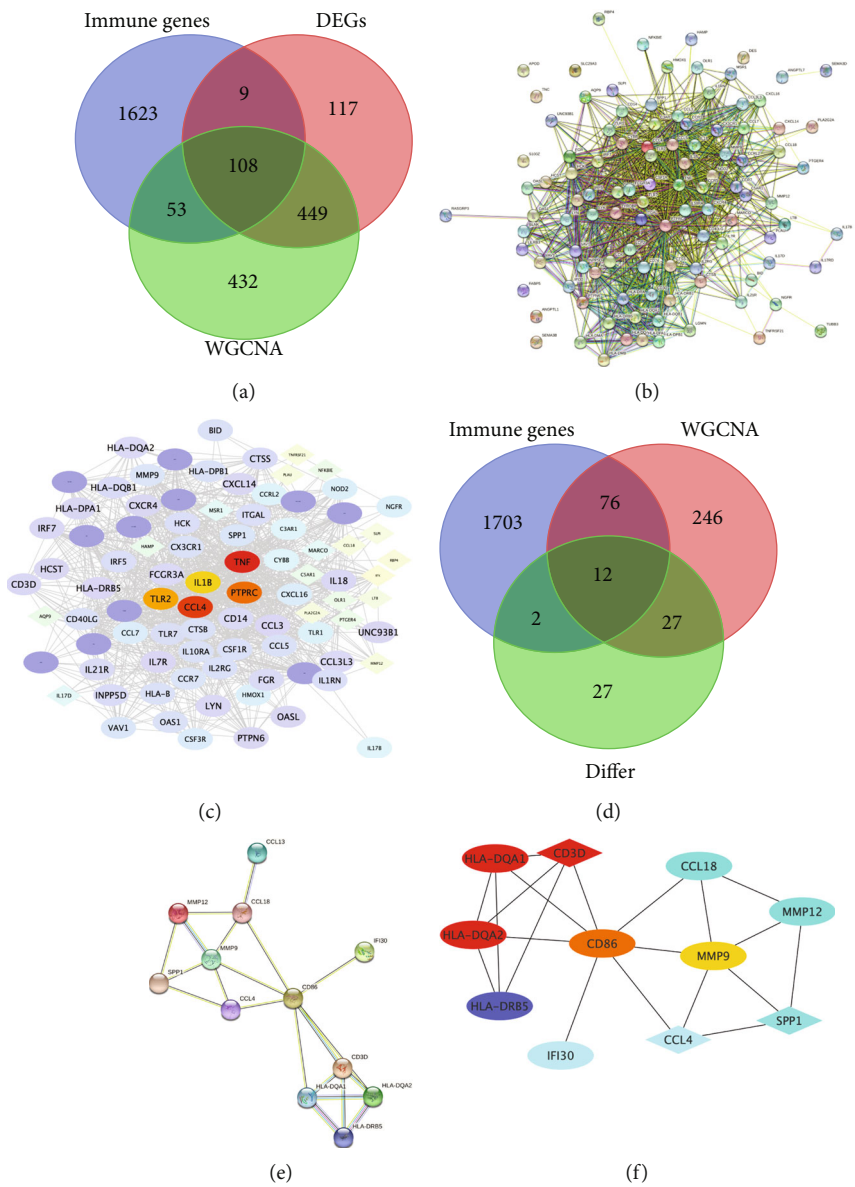

Figure 8: A: Venn diagram of immune-related genes, differentially expressed genes and turquoise modular genes in the carotid atherosclerotic artery samples B: Protein–protein interaction network construction using 108 genes from the STRING database in the carotid atherosclerotic artery samples C: Screening of the top five hub genes (the darker the colour, the higher the gene ranking) in the carotid atherosclerotic artery samples D: Venn diagram of immune-related genes, differentially expressed genes and blue module genes in lower extremity atherosclerotic artery samples E: Protein–protein interaction network construction using 12 genes from the STRING database in lower extremity atherosclerotic artery samples F: Screening of the top five hub genes (the darker the colour, the closer the gene ranking) in lower extremity atherosclerotic artery samples.

CCL2 and CCL4 are novel therapeutic targets for regulating atherosclerosis. Notably, CCL4 has the highest correlation with mast cells in this study. Therefore, exploring the interaction between CCL4 and mast cells may provide new insights into atherosclerosis treatment. As a member of innate immune toll-like receptor (TLR), TLR2 has been proved to play an important role in the innate immune mechanism. Recent studies have indicated that TLR2 is actively involved in atherosclerosis caused by Chlamydia pneumoniae, Porphyromonas gingivalis and Helicobacter pylori [56–58]. Studies have shown that certain drugs blocked TLR2 in ApoE(-/-) mice, which causes the expression of pro-inflammatory cytokines IL-6 and TNF-α to decrease and inactivate NF-KB and STAT3, and thereby greatly reducing plaque area and vascular stenosis [59]. Furthermore, TLR2 can induce chondrogenesis in vascular smooth muscle cells through osteoprotegerin and IL-6-mediated RANKL, leading to vascular calcification and thus promoting atherosclerosis formation [60]. Everett et al. reported a gratifying result by using IL1B inhibitor

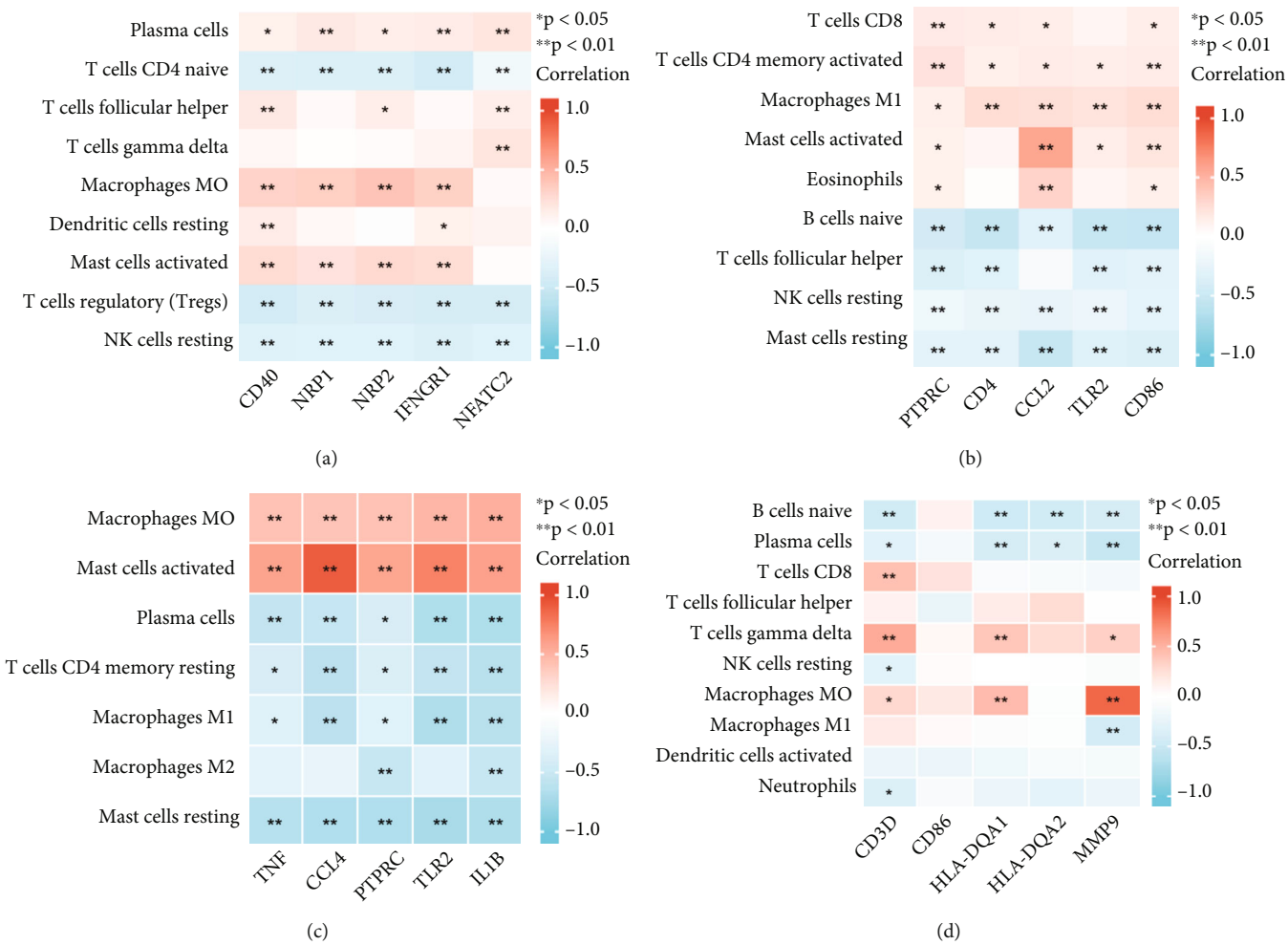

Figure 9: A: Heat map of the correlation between five hub genes and differentially expressed immune cells in carotid artery plaque samples B: Heat map of the correlation between five hub genes and differentially expressed immune cells peripheral plaque samples C: Heat map of the correlation between five hub genes and differentially expressed immune cells in the carotid atherosclerotic artery samples D: Heat map of the correlation between five hub genes and differentially expressed immune cells in lower extremity atherosclerotic artery samples.

canakinumab to effectively inhibit inflammation and improve cardiovascular disease outcomes, suggesting that inflammation is a key factor driving atherosclerosis and targeting immune inflammation. Targeted therapy of related genes has broad prospects regarding atherosclerosis treatment [61]. PTPRC (also known as CD45) is an important leukocyte antigen involved in the immune regulation of T and B cells. It has been identified as a hub gene in several studies on cardiovascular diseases [62–64].

In this study, we found that compared with carotid atherosclerotic plaque samples, the correlation between lower extremity atherosclerosis samples and immune cells was low, and the sensitivity of key genes to lower extremity atherosclerosis immune groups was also reduced. According to previous studies, carotid atherosclerotic plaques show a high incidence and early onset compared with lower extremity arteries [65, 66]. This also indirectly supports the occurrence of carotid atherosclerotic plaque, which may be more closely related to immune inflammation. Therefore, the treatment related to immune inflammation may be more effective for carotid atherosclerosis.

Although previous studies have analysed key genes of atherosclerosis-related diseases [67–70], large sample bioinformatic analyses for different atherosclerosis tissue sources and plaque formation are yet to be reported. This study identified the immune cell infiltration and hub gene in atherosclerosis samples from different tissue sources (plaque, artery) and different sites (carotid plaque, peripheral plaque and lower extremity), which helps to further explain immune cell effects and inflammatory processes on atherosclerosis and the similarities and differences between atherosclerosis samples from different sources. However, this study has some limitations. First, although more than 700 samples were analysed, this study focussed on carotid, peripheral and lower extremity atherosclerotic diseases but did not include coronary atherosclerosis, myocardial infarction and other

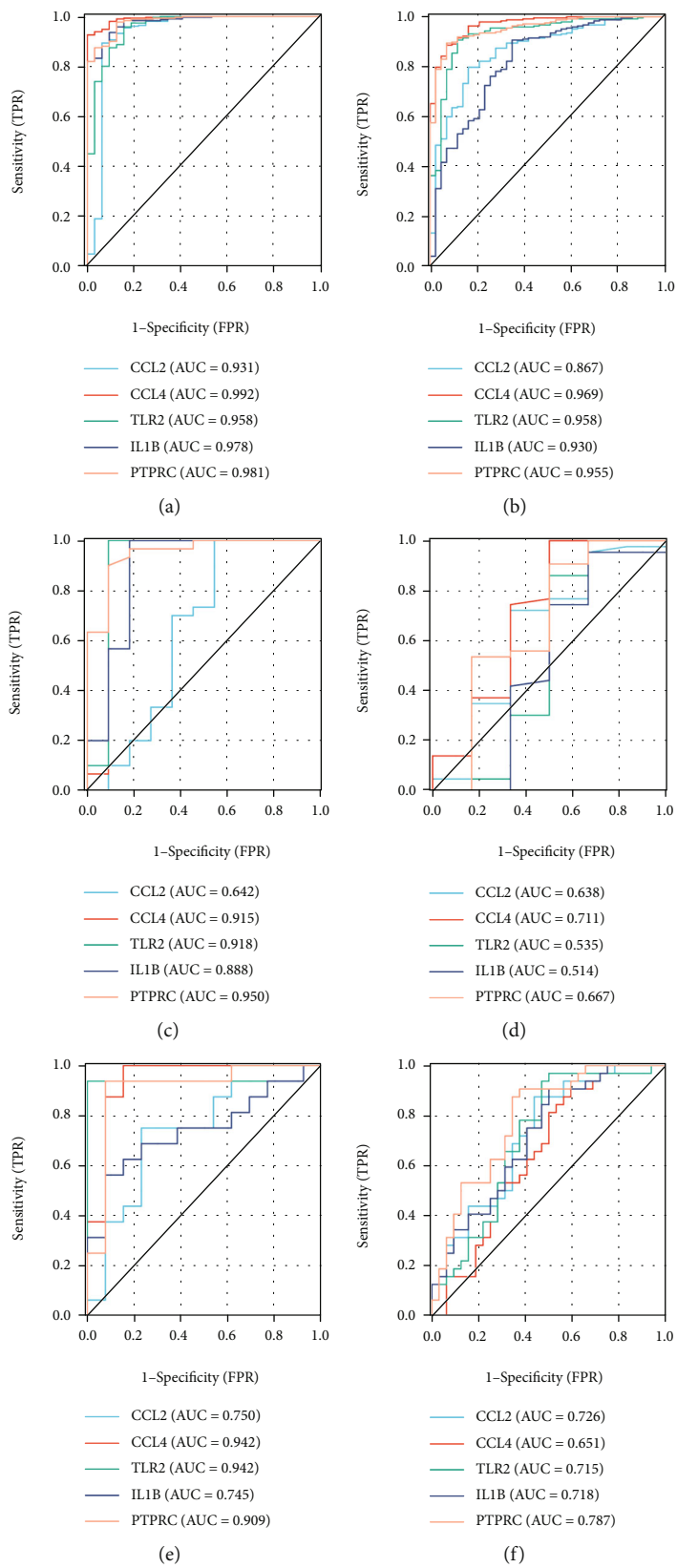

Figure 10: Continued.

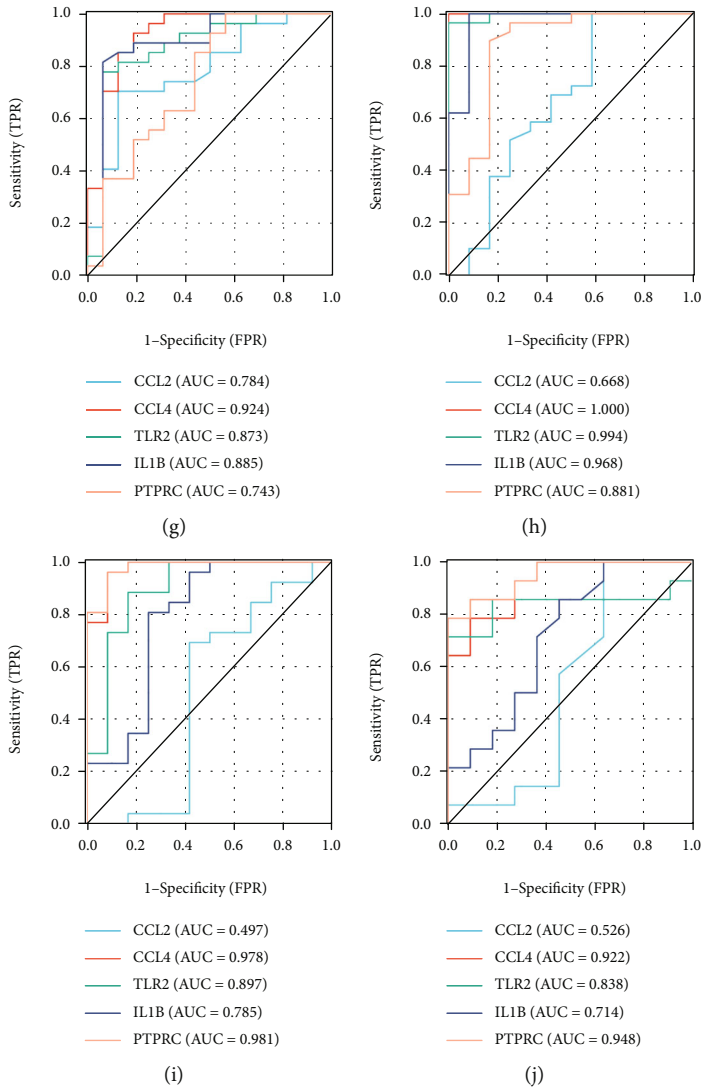

Figure 10: A: ROC analysis of CCL2, CCL4, TLR2, IL1B and PTPRC in the carotid plaque group B: ROC analysis of CCL2, CCL4, TLR2, IL1B and PTPRC in the peripheral plaque group C: ROC analysis of CCL2, CCL4, TLR2, IL1B and PTPRC in the lower extremity atherosclerotic artery group D: ROC analysis of CCL2, CCL4, TLR2, IL1B and PTPRC in the artery group E: ROC analysis of CCL2, CCL4, TLR2, IL1B and PTPRC in GSE28829 (including 16 advanced and 13 early carotid plaques) F: ROC analysis of CCL2, CCL4, TLR2, IL1B and PTPRC in GSE43292 (including 32 carotid plaques and 32 control samples) G: ROC analysis of CCL2, CCL4, TLR2, IL1B and PTPRC in GSE16315 (including 27 intraplaque and 16 non intraplaque haemorrhage samples) H: ROC analysis of CCL2, CCL4, TLR2, IL1B and PTPRC in GSE100927 (including 29 carotid atherosclerotic artery samples and 12 control samples) I: ROC analysis of CCL2, CCL4, TLR2, IL1B and PTPRC in GSE100927 (including 25 femoral atherosclerotic artery samples and 12 control samples) J: ROC analysis of CCL2, CCL4, TLR2, IL1B and PTPRC in GSE100927 (including 14 infra-popliteal atherosclerotic artery samples and 11control samples).

diseases. Second, this is a retrospective study; therefore, a prospective study design or larger sample size can help to further verify the function of hub genes.

5. Conclusion

This study not only presents new ideas regarding atherosclerosis formation and plaque progression but also provides potential therapeutic targets for atherosclerotic arteries and plaques treatment.

Data Availability

The datasets used and/or analyzed during the current study are available from the corresponding author on reasonable request.

Ethical Approval

This article does not contain any studies with patients or animals performed by any of the authors.

Conflicts of Interest

There are no conflicts of interest in this study.

Authors' Contributions

HAN NIE: research design and drafting the manuscript. Chen Yan: help to revise the manuscript. Weimin Zhou: help modify manuscript and collate references. Tao-sheng Li: review and revision of the manuscript. HAN NIE and Chen Yan contributed equally to this work.

Funding

This study was supported by China Scholarship Council (CSC); This study was supported by the National Natural Science Foundation of China (grant no. 81860425), the project of Science and Technology Department of Jiangxi Province (grant no. 20204BCJ23018).

Acknowledgments

Weimin Zhou and Tao-sheng Li are the co-Corresponding authors of this article; Tao-sheng Li is the 1st of the corresponding authors and Weimin Zhou is the 2nd of the corresponding authors. HAN NIE and Chen Yan are the co-first authors of this article; HAN NIE is the 1st of the first authors and Chen Yan is the 2nd of the first authors.

Supplementary Materials

Supplementary Figure1: Analysis flow chart of this work. Supplementary Figure 2. A: The fusion and de-batch effect of five carotid artery plaque data sets B: The fusion and de-batch effect of two lower extremity atherosclerotic artery data sets. Supplementary Figure 3 A: Heatmap of GSE28829 (including 16 advanced and 13 early carotid plaques) obtained using single-sample gene set enrichment analysis (ssGSEA) B: Heatmap of GSE43292 (including 32 carotid plaques and 32 control samples) obtained using ssGSEA C: Heatmap of GSE100927 (including 29 carotid atherosclerotic artery samples and 12 control samples) obtained using ssGSEA D: Principal component analysis (PCA) of GSE28829 (according to ssGSEA score) E: PCA analysis of GSE43292 (according to ssGSEA score) F: PCA analysis of GSE100927 (according to ssGSEA score). Supplementary Figure 4 A: The volcano map of the differences in gene analysis between the high- and low-immune groups in carotid plaque samples B: The volcano map of the differences in gene analysis between the high- and low-immune groups in peripheral plaque samples C: The volcano map of the differences in gene analysis between the high- and low-immune groups in carotid atherosclerotic artery samples D: The volcano map of the differences in gene analysis between the high- and low-immune groups in lower extremity atherosclerotic artery samples. Supplementary Figure 5 A: Proportion of 22 types of immune cell infiltration in GSE28829 (including 16 advanced and 13 early carotid plaques) B: Differential expression of 22 immune cells in GSE28829 (including 16 advanced and 13 early carotid plaques) between the high and low immune groups C: Selection process of the soft threshold using weighted gene co-expression network analysis (WGCNA) in the carotid plaque group D: Selection process of the soft threshold using WGCNA in the peripheral plaque group E: Selection process of the soft threshold using WGCNA in the carotid atherosclerotic artery group F: Selection process of the soft threshold using WGCNA in the lower extremity atherosclerotic artery group. Supplementary Materials Supplementary Table 1: three hundred and eight genes in the blue module in carotid plaque group Supplementary Table 2: two thousand one hundred and twenty genes in the turquoise module in the peripheral plaque group Supplementary Table 3: one thousand and forty-two genes in the turquoise module in the carotid atherosclerotic artery group Supplementary Table 4: three hundred and sixty-one genes in the blue module in the lower extremity atherosclerotic artery group Supplementary Table 5:Correlation analysis between differential immune cells and hub gene in all groups (r value; p value). *(Supplementary Materials)*

References

[1] W. Herrington, B. Lacey, P. Sherliker, J. Armitage, and S. Lewington, "Epidemiology of atherosclerosis and the potential to reduce the global burden of Atherothrombotic disease," *Circulation Research*, vol. 118, no. 4, pp. 535–546, 2016.

[2] World Health Organization, *Media centre, Cardiovascular diseases (CVDs)*, 2013, http://www.who.int/mediacentre/factsheets/fs317/zh/index.html.

[3] P. Libby, "Inflammation in atherosclerosis," *Nature*, vol. 420, no. 6917, pp. 868–874, 2002.

[4] J. E. Kanter, F. Kramer, S. Barnhart et al., "Diabetes promotes an inflammatory macrophage phenotype and atherosclerosis through acyl-CoA synthetase 1," *Proceedings of the National Academy of Sciences*, vol. 109, no. 12, pp. E715–E724, 2012.

[5] I. Tabas, K. J. Williams, and J. Borén, "Subendothelial lipoprotein retention as the initiating process in atherosclerosis: update and therapeutic implications," *Circulation*, vol. 116, no. 16, pp. 1832–1844, 2007.

[6] G. Camejo, F. Lalaguna, F. López, and R. Starosta, "Characterization and properties of a lipoprotein-complexing proteoglycan from human aorta," *Atherosclerosis*, vol. 35, no. 3, pp. 307–320, 1980.

[7] R. Ross, "Atherosclerosis–an inflammatory disease," *The New England Journal of Medicine*, vol. 340, no. 2, pp. 115–126, 1999.

[8] P. Libby, P. M. Ridker, and G. K. Hansson, "Progress and challenges in translating the biology of atherosclerosis," *Nature*, vol. 473, no. 7347, pp. 317–325, 2011.

[9] I. Tabas, G. García-Cardeña, and G. K. Owens, "Recent insights into the cellular biology of atherosclerosis," *The Journal of Cell Biology*, vol. 209, no. 1, pp. 13–22, 2015.

[10] D. A. Chistiakov, A. A. Melnichenko, A. V. Grechko, V. A. Myasoedova, and A. N. Orekhov, "Potential of anti-inflammatory agents for treatment of atherosclerosis," *Experimental and Molecular Pathology*, vol. 104, no. 2, pp. 114–124, 2018.

[11] P. Libby, "Current concepts of the pathogenesis of the acute coronary syndromes," *Circulation*, vol. 104, no. 3, pp. 365–372, 2001.

[12] M. Kaartinen, A. Penttilä, and P. T. Kovanen, "Mast cells of two types differing in neutral protease composition in the human aortic intima. Demonstration of tryptase- and tryptase/chymase-containing mast cells in normal intimas, fatty streaks, and the shoulder region of atheromas," *Arteriosclerosis and Thrombosis*, vol. 14, no. 6, pp. 966–972, 1994.

[13] L. Folkersen, J. Persson, J. Ekstrand et al., "Prediction of ischemic events on the basis of transcriptomic and genomic profiling in patients undergoing carotid endarterectomy," *Molecular Medicine*, vol. 18, no. 4, pp. 669–675, 2012.

[14] O. Puig, J. Yuan, S. Stepaniants et al., "A gene expression signature that classifies human atherosclerotic plaque by relative inflammation status," *Circulation. Cardiovascular Genetics*, vol. 4, no. 6, pp. 595–604, 2011.

[15] Y. Döring, H. D. Manthey, M. Drechsler et al., "Auto-antigenic protein-DNA complexes stimulate plasmacytoid dendritic cells to promote atherosclerosis," *Circulation*, vol. 125, no. 13, pp. 1673–1683, 2012.

[16] H. Jin, P. Goossens, P. Juhasz et al., "Integrative multiomics analysis of human atherosclerosis reveals a serum response factor-driven network associated with intraplaque hemorrhage," *Clinical and Translational Medicine*, vol. 11, no. 6, article e458, 2021.

[17] H. Ayari and G. Bricca, "Identification of two genes potentially associated in iron-heme homeostasis in human carotid plaque using microarray analysis," *Journal of Biosciences*, vol. 38, no. 2, pp. 311–315, 2013.

[18] M. Steenman, O. Espitia, B. Maurel et al., "Identification of genomic differences among peripheral arterial beds in atherosclerotic and healthy arteries," *Scientific Reports*, vol. 8, no. 1, 2018.

[19] J. T. Leek, W. Evan Johnson, H. S. Parker et al., "Sva: surrogate variable analysis," *R package version*, vol. 3, no. 36, 2020.

[20] S. Hänzelmann, R. Castelo, and J. Guinney, "GSVA: gene set variation analysis for microarray and RNA-seq data," *BMC Bioinformatics*, vol. 14, no. 1, 2013.

[21] C. Yue, H. Ma, and Y. Zhou, "Identification of prognostic gene signature associated with microenvironment of lung adenocarcinoma," *PeerJ*, vol. 7, no. 7, article e8128, 2019.

[22] Y. He, Z. Jiang, C. Chen, and X. Wang, "Classification of triple-negative breast cancers based on Immunogenomic profiling," *Journal of Experimental & Clinical Cancer Research*, vol. 37, no. 1, 2018.

[23] K. Yoshihara, M. Shahmoradgoli, E. Martínez et al., "Inferring tumour purity and stromal and immune cell admixture from expression data," *Nature Communications*, vol. 4, no. 1, 2013.

[24] G. Yu, L. G. Wang, Y. Han, and Q. Y. He, "clusterProfiler: an R package for comparing biological themes among gene Clusters," *Omics: a journal of integrative biology*, vol. 16, no. 5, pp. 284–287, 2012.

[25] A. M. Newman, C. L. Liu, M. R. Green et al., "Robust enumeration of cell subsets from tissue expression profiles," *Nature Methods*, vol. 12, no. 5, pp. 453–457, 2015.

[26] P. Langfelder and S. Horvath, "WGCNA: an R package for weighted correlation network analysis," *BMC Bioinformatics*, vol. 9, no. 1, 2008.

[27] C. H. Chin, S. H. Chen, H. H. Wu, C. W. Ho, M. T. Ko, and C. Y. Lin, "cytoHubba: identifying hub objects and sub-networks from complex interactome," *BMC Systems Biology*, vol. 8, no. S4, 2014.

[28] K. J. Moore, F. J. Sheedy, and E. A. Fisher, "Macrophages in atherosclerosis: a dynamic balance," *Nature Reviews Immunology*, vol. 13, no. 10, pp. 709–721, 2013.

[29] F. Ginhoux, J. L. Schultze, P. J. Murray, J. Ochando, and S. K. Biswas, "New insights into the multidimensional concept of macrophage ontogeny, activation and function," *Nature Immunology*, vol. 17, no. 1, pp. 34–40, 2016.

[30] J. Frostegård, A. K. Ulfgren, P. Nyberg et al., "Cytokine expression in advanced human atherosclerotic plaques: dominance of pro-inflammatory (Th1) and macrophage-stimulating cytokines," *Atherosclerosis*, vol. 145, no. 1, pp. 33–43, 1999.

[31] S. C. Huang, B. Everts, Y. Ivanova et al., "Cell-intrinsic lysosomal lipolysis is essential for alternative activation of macrophages," *Nature Immunology*, vol. 15, no. 9, pp. 846–855, 2014.

[32] N. D. Pennock, J. T. White, E. W. Cross, E. E. Cheney, B. A. Tamburini, and R. M. Kedl, "T cell responses: naive to memory and everything in between," *Advances in Physiology Education*, vol. 37, no. 4, pp. 273–283, 2013.

[33] I. Tabas and A. H. Lichtman, "Monocyte-macrophages and T cells in atherosclerosis," *Immunity*, vol. 47, no. 4, pp. 621–634, 2017.

[34] T. Kyaw, A. Winship, C. Tay et al., "Cytotoxic and proinflammatory CD8+ T lymphocytes promote development of vulnerable atherosclerotic plaques in apoE-deficient mice," *Circulation*, vol. 127, no. 9, pp. 1028–1039, 2013.

[35] D. Kolbus, O. H. Ramos, K. E. Berg et al., "CD8+ T cell activation predominate early immune responses to hypercholesterolemia in Apoe^{-}(/)$^{-}$ mice," *BMC Immunology*, vol. 11, no. 1, 2010.

[36] J. van Duijn, J. Kuiper, and B. Slütter, "The many faces of CD8 + T cells in atherosclerosis," *Current Opinion in Lipidology*, vol. 29, no. 5, pp. 411–416, 2018.

[37] K. Tse, H. Tse, J. Sidney, A. Sette, and K. Ley, "T cells in atherosclerosis," *International Immunology*, vol. 25, no. 11, pp. 615–622, 2013.

[38] Z. D. Liu, L. Wang, F. H. Lu et al., "Increased Th17 cell frequency concomitant with decreased Foxp3+ Treg cell frequency in the peripheral circulation of patients with carotid artery plaques," *Inflammation Research*, vol. 61, no. 10, pp. 1155–1165, 2012.

[39] H. Ait-Oufella, B. L. Salomon, S. Potteaux et al., "Natural regulatory T cells control the development of atherosclerosis in mice," *Nature Medicine*, vol. 12, no. 2, pp. 178–180, 2006.

[40] L. Jonasson, J. Holm, O. Skalli, G. Bondjers, and G. K. Hansson, "Regional accumulations of T cells, macrophages, and smooth muscle cells in the human atherosclerotic plaque," *Arteriosclerosis*, vol. 6, no. 2, 1986.

[41] I. Bot, G. P. Shi, and P. T. Kovanen, "Mast cells as effectors in atherosclerosis," *Arteriosclerosis, Thrombosis, and Vascular Biology*, vol. 35, no. 2, pp. 265–271, 2015.

[42] S. K. Kritas, A. Caraffa, P. Antinolfi et al., "IgE generation and mast cell activation," *European Journal of Inflammation*, vol. 12, no. 1, pp. 21–25, 2014.

[43] W. Xiaogang, Z. Dingbiao, Y. Weidong, S. Huaiyin, Z. Xiaoming, and Z. Xiaochen, "Distribution of mast cells in carotid atherosclerotic plaque," *PLA medical journal*, vol. 27, no. 8, pp. 671–673, 2002.

[44] H. Lappalainen, P. Laine, M. O. Pentikäinen, A. Sajantila, and P. T. Kovanen, "Mast cells in neovascularized human coronary

plaques store and secrete basic fibroblast growth factor, a potent angiogenic mediator," *Arteriosclerosis, Thrombosis, and Vascular Biology*, vol. 24, pp. 1880–1885, 2004.

[45] W. K. den Dekker, D. Tempel, I. Bot et al., "Mast cells induce vascular smooth muscle cell apoptosis via a toll-like receptor 4 activation pathway," *Arteriosclerosis, Thrombosis, and Vascular Biology*, vol. 32, no. 8, pp. 1960–1969, 2012.

[46] A. Selathurai, V. Deswaerte, P. Kanellakis et al., "Natural killer (NK) cells augment atherosclerosis by cytotoxic-dependent mechanisms," *Cardiovascular Research*, vol. 102, no. 1, pp. 128–137, 2014.

[47] W. Nour-Eldine, J. Joffre, K. Zibara et al., "Genetic depletion or Hyperresponsiveness of natural killer cells do not affect atherosclerosis development," *Circulation Research*, vol. 122, no. 1, pp. 47–57, 2018.

[48] J. P. Miller and D. Allman, "The decline in B lymphopoiesis in aged mice reflects loss of very early B-lineage precursors," *Journal of Immunology*, vol. 171, no. 5, pp. 2326–2330, 2003.

[49] D. Frasca, A. M. Landin, S. C. Lechner et al., "Aging down-regulates the transcription factor E2A, activation-induced cytidine deaminase, and Ig class switch in human B cells," *Journal of Immunology*, vol. 180, no. 8, pp. 5283–5290, 2008.

[50] G. Caligiuri, A. Nicoletti, B. Poirier, and G. K. Hansson, "Protective immunity against atherosclerosis carried by B cells of hypercholesterolemic mice," *The Journal of Clinical Investigation*, vol. 109, no. 6, pp. 745–753, 2002.

[51] A. S. Major, S. Fazio, and M. F. Linton, "B-lymphocyte deficiency increases atherosclerosis in LDL receptor-null mice," *Arteriosclerosis, Thrombosis, and Vascular Biology*, vol. 22, no. 11, pp. 1892–1898, 2002.

[52] N. Xia, S. Hasselwander, G. Reifenberg et al., "B lymphocyte-deficiency in mice causes vascular dysfunction by inducing neutrophilia," *Biomedicine*, vol. 9, no. 11, 2021.

[53] C. Combadière, S. Potteaux, M. Rodero et al., "Combined inhibition of CCL2, CX3CR1, and CCR5 abrogates Ly6C(hi) and Ly6C(lo) monocytosis and almost abolishes atherosclerosis in hypercholesterolemic mice," *Circulation*, vol. 117, no. 13, pp. 1649–1657, 2008.

[54] C. Winter, C. Silvestre-Roig, A. Ortega-Gomez et al., "Chronopharmacological targeting of the CCL2-CCR2 Axis ameliorates atherosclerosis," *Cell Metabolism*, vol. 28, no. 1, pp. 175–182.e5, 2018.

[55] T. T. Chang, H. Y. Yang, C. Chen, and J. W. Chen, "CCL4 inhibition in atherosclerosis: effects on plaque stability, endothelial cell adhesiveness, and macrophages activation," *International Journal of Molecular Sciences*, vol. 21, no. 18, 2020.

[56] F. Cao, A. Castrillo, P. Tontonoz, F. Re, and G. I. Byrne, "Chlamydia pneumoniae–induced macrophage foam cell formation is mediated by Toll-like receptor 2," *Infection and Immunity*, vol. 75, no. 2, pp. 753–759, 2007.

[57] S. S. Chukkapalli, I. M. Velsko, M. F. Rivera-Kweh, H. Larjava, A. R. Lucas, and L. Kesavalu, "Global TLR2 and 4 deficiency in mice impacts bone resorption, inflammatory markers and atherosclerosis to polymicrobial infection," *Molecular Oral Microbiology*, vol. 32, no. 3, pp. 211–225, 2017.

[58] M. Triantafilou, F. G. Gamper, P. M. Lepper et al., "Lipopolysaccharides from atherosclerosis-associated bacteria antagonize TLR4, induce formation of TLR2/1/CD36 complexes in lipid rafts and trigger TLR2-induced inflammatory responses in human vascular endothelial cells," *Cellular Microbiology*, vol. 9, no. 8, pp. 2030–2039, 2007.

[59] X. X. Wang, X. X. Lv, J. P. Wang et al., "Blocking TLR2 activity diminishes and stabilizes advanced atherosclerotic lesions in apolipoprotein E-deficient mice," *Acta Pharmacologica Sinica*, vol. 34, no. 8, pp. 1025–1035, 2013.

[60] G. L. Lee, C. C. Yeh, J. Y. Wu et al., "TLR2 promotes vascular smooth muscle cell Chondrogenic differentiation and consequent calcification via the concerted actions of Osteoprotegerin suppression and IL-6-mediated RANKL induction," *Arteriosclerosis, Thrombosis, and Vascular Biology*, vol. 39, no. 3, pp. 432–445, 2019.

[61] B. M. Everett, J. G. MacFadyen, T. Thuren, P. Libby, R. J. Glynn, and P. M. Ridker, "Inhibition of interleukin-1β and reduction in Atherothrombotic cardiovascular events in the CANTOS trial," *Journal of the American College of Cardiology*, vol. 76, no. 14, pp. 1660–1670, 2020.

[62] M. Xia, Q. Wu, P. Chen, and C. Qian, "Regulatory T cell-related gene biomarkers in the deterioration of atherosclerosis," *Frontiers in Cardiovascular Medicine*, vol. 8, no. 8, article 661709, 2021.

[63] W. Su, Y. Zhao, Y. Wei, X. Zhang, J. Ji, and S. Yang, "Exploring the pathogenesis of psoriasis complicated with atherosclerosis via microarray data analysis," *Frontiers in Immunology*, vol. 12, no. 12, article 667690, 2021.

[64] Y. Pan, C. Yu, J. Huang, Y. Rong, J. Chen, and M. Chen, "Bioinformatics analysis of vascular RNA-seq data revealed hub genes and pathways in a novel Tibetan minipig atherosclerosis model induced by a high fat/cholesterol diet," *Lipids in Health and Disease*, vol. 19, no. 1, 2020.

[65] R. Clarke, H. Du, O. Kurmi et al., "Burden of carotid artery atherosclerosis in Chinese adults: Implications for future risk of cardiovascular diseases," *European Journal of Preventive Cardiology*, vol. 24, no. 6, pp. 647–656, 2017.

[66] F. G. Fowkes, D. Rudan, I. Rudan et al., "Comparison of global estimates of prevalence and risk factors for peripheral artery disease in 2000 and 2010: a systematic review and analysis," *Lancet*, vol. 382, no. 9901, pp. 1329–13240, 2013.

[67] M. Chen, S. Chen, D. Yang et al., "Weighted gene co-expression network analysis identifies crucial genes mediating progression of carotid plaque," *Frontiers in Physiology*, vol. 12, no. 12, article 601952, 2021.

[68] C. H. Wang, H. H. Shi, L. H. Chen, X. L. Li, G. L. Cao, and X. F. Hu, "Identification of key lncRNAs associated with atherosclerosis progression based on public datasets," *Frontiers in Genetics*, vol. 10, no. 10, 2019.

[69] S. Chen, D. Yang, Z. Liu et al., "Crucial gene identification in carotid atherosclerosis based on peripheral blood mononuclear cell (PBMC) data by weighted (gene) correlation network analysis (WGCNA)," *Medical Science Monitor*, vol. 26, no. 26, article e921692, 2020.

[70] L. Wang, B. Gao, M. Wu, W. Yuan, P. Liang, and J. Huang, "Profiles of immune cell infiltration in carotid artery atherosclerosis based on gene expression data," *Frontiers in Immunology*, vol. 12, no. 12, article 599512, 2021.

Hindawi
Oxidative Medicine and Cellular Longevity
Volume 2022, Article ID 9678625, 9 pages
https://doi.org/10.1155/2022/9678625

Review Article

Inhibiting Ferroptosis: A Novel Approach for Ulcerative Colitis Therapeutics

Jinke Huang,[1] **Jiaqi Zhang**,[1] **Jinxin Ma**,[2] **Jing Ma**,[1] **Jiali Liu**,[1] **Fengyun Wang**,[1] **and Xudong Tang**[1,3]

[1]*Department of Gastroenterology, Xiyuan Hospital of China Academy of Chinese Medical Sciences, Beijing, China*
[2]*Department of Gastroenterology, Peking University Traditional Chinese Medicine Clinical Medical School (Xiyuan), Beijing, China*
[3]*China Academy of Chinese Medical Sciences, Beijing, China*

Correspondence should be addressed to Fengyun Wang; wfy811@163.com and Xudong Tang; txdly@sina.com

Received 27 December 2021; Accepted 14 March 2022; Published 26 March 2022

Academic Editor: Helena Moreira

Ulcerative colitis (UC) is a recurrent and persistent nonspecific inflammatory bowel disease (IBD) that greatly affects human survival and social wealth. Despite the advances in the treatment of UC, there is still a high demand for novel therapeutic strategies for UC patients. Cell death is critical to the development and progression of UC. Understanding how intestinal cells die and how to prevent damage to intestinal cells is of great interest for the diagnosis and early treatment of UC. Ferroptosis, a novel form of regulated cell death (RCD) manifested by iron accumulation, lipid peroxidation, and excessive reactive oxygen species (ROS) production, has been shown to contribute to the development and progression of UC. Inhibitors of ferroptosis have been validated in models of UC. Here, we reviewed the mechanisms of initiation and control of ferroptosis and summarize the therapeutic activity of ferroptosis inhibitors in models of UC. We further discussed the possibility of inhibiting ferroptosis as a novel therapeutic target for UC. These findings revealed novel mechanisms to protect the colonic mucosa and highlighted the importance of ferroptosis in the disease process.

1. Introduction

Ulcerative colitis (UC) is a chronic nonspecific inflammatory bowel disease (IBD) characterized by abdominal pain, diarrhea, blood in the stool, and weight loss [1]. Worldwide, the prevalence of UC continues to rise, and its chronic recurrence and unpredictable nature lead to costly medical treatment, which imposes a huge economic burden on society [2]. The pathophysiological mechanisms of UC are still not well understood, and therefore, the efficacy of existing therapies is limited [3]. Further research on the pathogenesis of UC and the development of novel and effective therapeutic approaches are still urgently needed. Recently, regulated forms of cell death have been observed to be involved in the development and progression of IBD and have the potential to be novel therapeutic targets [4]. The first regulatory cell death modality identified was caspase-dependent apoptosis [5], which has accounted for the vast majority of cell death studies in recent decades. Autophagy, a process in which cells use lysosomes for self-digestion, is observed in both physiological and pathological processes of the organism, but whether it plays a positive or negative role has not been fully elucidated [6]. Ferroptosis is a novel form of programmed cell death mode distinguished from apoptosis, necrosis, and autophagy at the cellular morphology, biochemical characteristics, and genetic level, which is characterized by iron-dependent accumulation of lipid peroxidation to a lethal level [7–9].

As a unique and novel form of cell death, ferroptosis was initially observed in tumor cells [8]. As research has progressed, it has been found that the development and progression of a variety of diseases in addition to tumors are associated with ferroptosis [10–15]. Recent studies have identified ferroptosis as a key regulatory mechanism in intestinal diseases, and inhibition of ferroptosis is expected to be a new direction in the prevention and treatment of

intestinal diseases [16–18]. Extensive ferroptosis has been reported to be observed in UC patients, and recent evidence has found that blocking ferroptosis significantly relieves UC symptoms and promotes intestinal repair [16, 19]. These findings imply a new understanding of the development of therapeutic strategies for UC. Therefore, to synthesize the role of ferroptosis in UC pathology and attempt to elaborate the possibility of targeting ferroptosis in UC therapeutic strategies, we conducted the present review.

2. Ferroptosis and Its Mechanism

Ferroptosis was formally defined in 2012 as nonapoptotic, iron-dependent cell death characterized by lipid peroxidation product accumulation and membrane polyunsaturated fatty acid (PUFA) depletion [9]. As an iron-catalyzed lipid peroxidation process, a large accumulation of reactive oxygen species (ROS) is the most prominent feature of ferroptosis, with sources including excessive production and insufficient scavenging [20, 21]. Details of the process of ferroptosis are shown in Figure 1, and markers that can be used for ferroptosis validation are outline in Table 1.

2.1. Iron Metabolism Pathway. Iron is one of the intrinsic elements of the body, and proper iron levels are essential to maintain normal physiological functions of the body, while once the free iron level exceeds the normal range, it can damage cells. Under physiological conditions, extracellular iron is in dynamic equilibrium with intracellular iron [22, 23]. Extracellular iron is imported into the cell as ferric ions (Fe^{3+}) and is converted to ferrous ions (Fe^{2+}) by intracellular endosomes before being transported to the cell membrane [13, 20]. Once the equilibrium is disrupted, intracellular Fe^{2+} is then in excess, and the excess Fe^{2+} and hydroxyl radicals can be directly catalyzed by Fenton reaction to produce large amounts of ROS, which promotes lipid peroxidation and induces ferroptosis [24, 25].

Intracellular iron overload is central to the stimulation of oxidative damage and iron sagging. Specifically, causes of intracellular iron overload are attributed to increased iron uptake by TfR1, decreased iron excretion by ferroportin, and increased free iron due to ferritin degradation [26]. Iron overload can also induce nonclassical iron uptake pathways causing ferroptosis [27, 28]. For example, CDGSH iron-sulfur structural domain 1 in mitochondrial membranes may contribute to the reduction of iron content and ROS production in mitochondria, thereby inhibiting the development of iron prolapse. However, the role of mitochondria in ferroptosis remains to be clarified [29].

Catalytic iron, namely, ferrous iron, mediates lipid ROS production via Fenton reaction and promote lipid peroxidation directly. Markers like iron content and ROS can be used for ferroptosis validation in this process.

2.2. Lipid Metabolism Pathway. The lipid bilayer structure of the cell membrane directly determines biofilm properties and is essential for maintaining the integrity of membrane function. Increasing evidence suggest that lipid peroxidation is the driving force of ferroptosis [30, 31]. As the key component of cell membranes, polyunsaturated fatty acids (PUFAs), especially arachidonic acid (AA) and epinephrine (AdA), are preferentially oxidized by reactive free radicals [31]. Phospholipids containing PUFAs are lipid precursors for peroxidation reactions, and exposure to exogenous PUFAs can increase ferroptotic sensitivity [31]. Conversely, supplementation with deuterated PUFAs or exogenous MUFAs decelerated the accumulation of lipid peroxides and thus protected cells from ferroptosis [21, 31].

Phosphatidylethanolamine (PE) containing AA or AdA has been reported to be oxidized to phospholipid hydroperoxides (PE-AA/AdA-OOH) via a nonenzymatic reaction, which triggers ferroptosis [31]. In the presence of intracellular ferrous overload, ROS may be converted to hydroxyl radicals ($HO^{\cdot}$), which subsequently affect PUFA on the cell membrane [32]. Free PUFAs are oxidized via the catalytic pathways of lysophosphatidylcholine acyltransferase 3 (LPCAT3), acyl-CoA synthetase long-chain family member 4 (ACSL4), and lipoxygenases (LOXs) [21, 33]. ACSL4 and LPCAT3 have been demonstrated to be key regulators of PUFA-PL biosynthesis [31]. PUFA can be acetylated by ACSL4 to form PUFA-CoA, followed by LPCAT3 insertion of PUFA-CoA into lysophospholipids to form PUFA-PL [34]. Enzymatic lipid peroxidation of ferroptosis is regulated by the LOXs and is predominantly dominated by LOX5 and LOX12/15 [35].

Notably, GPX enzymes inhibit the oxidation of lipids, particularly GPX4, which limits the formation of reactive lipid alkoxides and reduces phospholipid hydroperoxides to lipid alcohols [11].

Lipid peroxide-induced ferroptosis can be summarized in the following three procedures (Figure 1). First, ACSL4 catalyzes the esterification of AA or AdA to PE. Second, LPCAT3 generates PUFA-PE based on PE substrates. Finally, 15-LOX oxidizes AA-PE and AdA-PE to ferroptotic signals (PE-AA-OH and PE-AdA-OOH) [36].

2.3. Amino Acid Metabolism Pathway. As a member of the glutathione peroxidase family, GPX4 catalyzes the conversion of free hydrogen peroxide to water or the reduction of cytotoxic lipid hydroperoxides (L-OOH) to nontoxic lipid alcohols (L-OH), thereby inhibiting the production of lipid ROS [37, 38]. Thiol-containing tripeptide glutathione (GSH) is the major antioxidant in mammalian cells and the primary substrate of GPX4. The conditions leading to glutathione depletion directly affect the activity and stability of GPX4, thus rendering the cells more susceptible to ferroptosis [39]. GSH prevents lipid peroxidation of polyunsaturated fatty acids in cell membranes via GSH-Px, whereas inhibition of the uptake of GSH-generating substrates causes lipid peroxidation to occur [39].

Both the metabolism and synthesis of amino acids are associated with the process of ferroptosis [40]. Glutamine can be converted to glutamate by glutaminases (GLS1 and GLS2) [41]. High extracellular glutamate concentrations promote intracellular cystine depletion and eventually lead to GSH depletion and GPX4 inactivation, with ferroptosis triggered as a result [42] *A*-ketopentanoic acid is a product of glutamine-driven intracellular metabolic pathways and

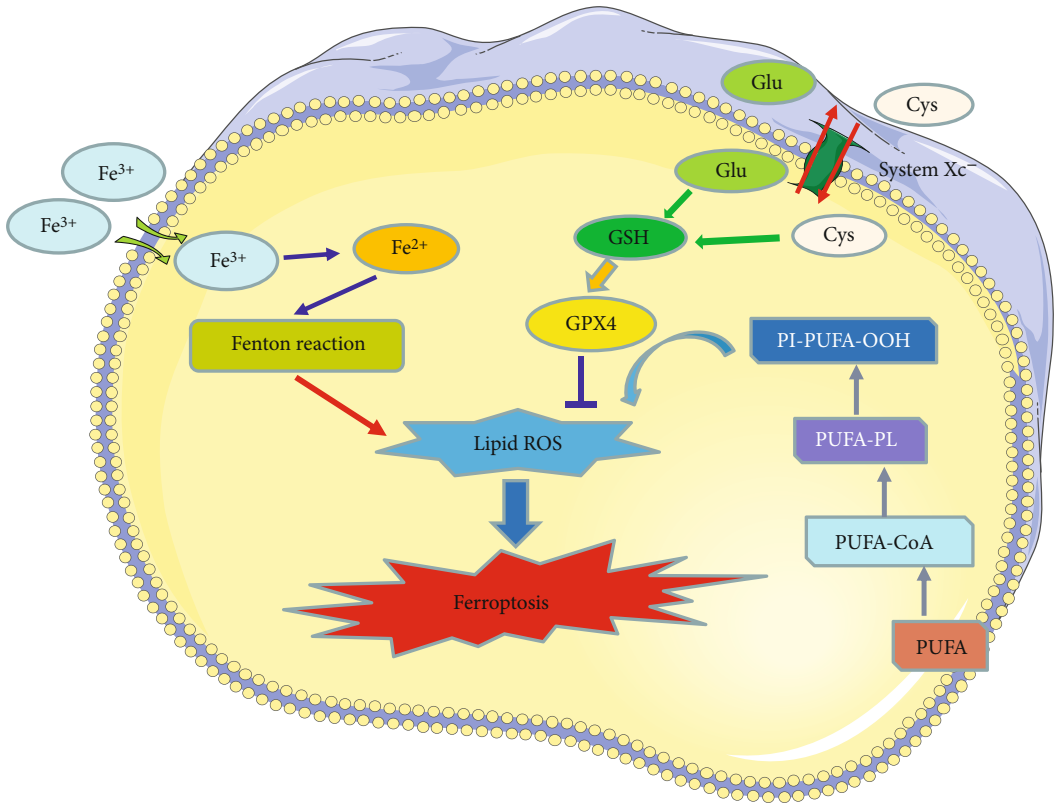

Figure 1: Ferroptosis is characterized by iron accumulation, lipid peroxidation, and excessive ROS production. The ferroptosis process is shown by this figure, including metabolic pathways, amino acid, lipid, and iron pathways which are showed in this figure.

Table 1: Markers that can be used for ferroptosis validation.

Metabolic processes	Markers
Iron metabolism pathway	Fe^{3+}, Fe^{2+}
Oxidative stress	ROS, SOD, OH, H_2O_2
Lipid metabolism pathway	MDA, LPO
Amino acid metabolism pathway	GPX4, GSH, GR, GLU, Cys

can also have a glutamine-like effect when ferroptosis occurs [43]. In addition, the glutaminase GLS2, a transcriptional target of the tumor suppressor p53, can inhibit iron sag by limiting DPP4-mediated lipid peroxidation [44, 45].

3. Ferroptosis in Ulcerative Colitis

The basic features of iron sagging include iron deposition, lipid peroxidation accumulation, GSH depletion, GPX4 inactivation, and LOX upregulation, all of which have been elucidated to be associated with the pathogenesis of UC [16, 46–49]. Iron chelators have been reported to significantly reduce ROS accumulation, improve clinical symptoms, and promote intestinal epithelial cell repair in UC patients [50, 51], and conversely, high dietary iron supplementation can exacerbate UC symptoms [52, 53]. Sensitivity to erastin-induced ferroptosis was found in a UC cell model and could be rescued by a ferroptosis specific inhibitor [16, 46–49]. The ferroptosis phenomenon has also been observed in mouse models of UC and can reduce symptoms by targeted inhibition of ferroptosis [16, 46–49]. These findings further validate that inhibition of ferroptosis may be a novel target for alleviating UC. Details of the role of ferroptosis in UC are shown in Figure 2.

3.1. The Role of Iron in UC. In UC, excessive ROS production by the colorectal mucosa may cause changes in cellular proteins, lipids, and nucleic acids, leading to several cellular dysfunctions that may affect the disease process [54]. Excess-free iron can aggravate oxidative activity within the intestinal epithelium through multiple mechanisms. First, hydrogen peroxide and ferrous ions can generate large amounts of ROS directly through the Fenton reaction. Moreover, superoxide can promote the conversion or release of ferrous ions, which in turn promotes the Fenton reaction [51]. Recessive mutations in the hemochromatosis gene (Hfe) are strongly associated with iron overload [55]. Hfe knockout mice were observed to have increased MDA in colonic tissue [56] and exhibited more severe symptoms of colonic mucosal injury, such as hematochezia and diarrhea [57]. In addition, iron overload not only leads to dysregulated ROS generation and interferes with intestinal bacteria, which in turn aggravates enteritis [58]. While the phenomenon of ferroptosis has been found in UC, accompanied by iron overload, the use of iron chelators can significantly reduce ROS and improve colitis symptoms [16, 46–51]. Therefore, these studies all highlight the pathological role of iron overload in the development of UC; that is, the deposition of iron in the intestine leads to severe

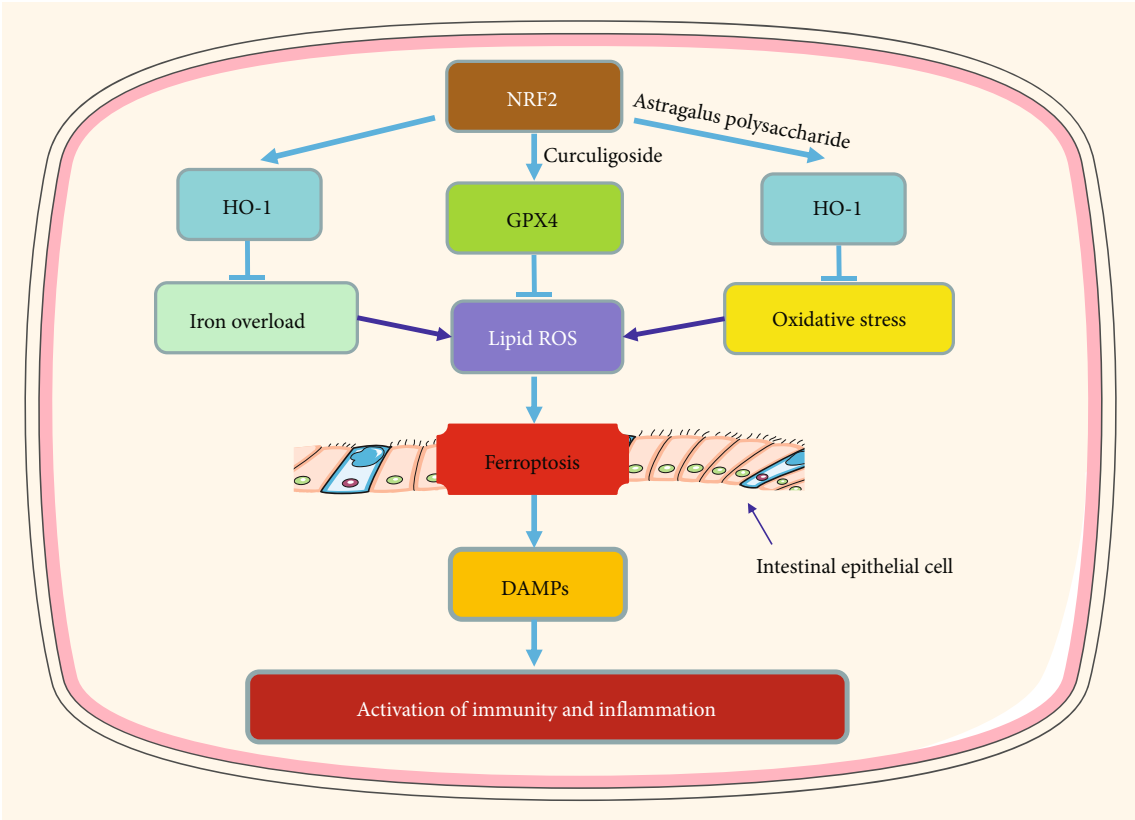

Figure 2: Role of ferroptosis in UC. Ferroptosis promotes the release of damage-associated molecular patterns (DAMPs) from the intestinal epithelium. Subsequently, the immune response is hyperactivated, leading to intestinal inflammation and epithelial damage.

Table 2: Validated ferroptosis regulators in the UC model.

Gene/axis/compound	Mechanism	Function
Ferrostatin-1 [19, 92]	Downregulation of PTGS2 levels, MDA levels, and iron content	Inhibition
Furin [46]	Activation of Nrf2 and upregulation of Gpx4 expression	Inhibition
MELK [48]	Inhibited ferritin formation in intestinal tissues	Inhibition
Lip-1 [19]	Blocking Nrf2/HO-1 and reducing the levels of COX2, ACSL4, FTH1	Inhibition
Deferprone [19]	Blocking Nrf2/HO-1 and reducing the levels of COX2, ACSL4, FTH1	Inhibition
NF-κBp65 [16]	Inhibition of endoplasmic reticulum stress	Inhibition
Curculigoside [47]	Induction of GPX4	Inhibition
Fer-1 [16]	Reduces MDA, iron, and FTH levels	Inhibition
Astragalus polysaccharide [49]	Inhibiting NRF2/HO-1 pathway	Inhibition
RSL3 [16]	Accumulation of ROS	Induction

oxidative stress (OS), promotes the production of ROC through the Fenton reaction, triggers ferroptosis, and then stimulates the release of damage-associated molecular patterns (DAMPs) to cause intestinal immune and inflammatory responses. Iron chelation, on the other hand, may be a promising therapeutic strategy for UC.

3.2. The Role of Oxidative Stress in UC. OS is considered to be a potential driver of UC induction and progression and has been well reported in both patients and animal models of UC [60–63]. A higher OS status is thought to be a cause of altered immune and inflammatory responses that contribute to the development of UC [64, 65]. With the development of UC, the activity of inflammatory cells in the colon is greatly increased, leading to increased production of pro-oxidant molecules [60]. OS is attributed to redox imbalance, which is caused by excessive production of ROS and inadequate response of the antioxidant system to eliminate ROS [66]. Cytokine-induced elevated levels of myeloperoxidase also lead to ROS production [67]. Excessive ROS production leads to changes in cellular proteins, lipids, and nucleic acids, resulting in several cellular dysfunctions

that may affect the course of UC. Colonic epithelial cells contain several antioxidant systems, such as antioxidant enzymes, namely, GSH, GPX4, and LOXs [68], but they are usually dysregulated in UC pathological conditions. As mentioned above, dysregulation of OS function is also observed in iron hypoplasia; it is hard to believe that the broad similarities between UC pathology and aspects of the ferroptosis cell death pathway are merely coincidental.

GSH can directly scavenge ROS and enhance cellular antioxidant capacity [69]. However, higher OS can promote GSH depletion and reduce GSH synthesis [70]. The depletion of GSH is widely observed in UC patients and experimental animal models of UC [71, 72]. Inhibition of the synthesis of GSH has been found to result in intestinal epithelial cell injury, while GSH supplementation significantly improves colonic health [73]. GPX4 is an important antioxidant enzyme that plays an important regulatory role in ferroptosis [74]. Inactivation of GPX4 promotes lipid peroxidation and induces ferroptosis [42]. Studies have reported that Nrf2-Gpx4 signaling pathway can significantly inhibit ferroptosis [75, 76], but Nrf2-Gpx4 signaling pathway is inhibited in UC [16, 46, 77]. Activation of Gpx4 can markedly inhibit ferroptosis and improve UC symptoms [46, 47]. LOXs are able to promote lipid hydroperoxide production and drive ironophilic cell death [31]. Alox15 deletion has been reported to promote inflammation suppression, intestinal barrier integrity maintenance, and colonic injury, while Alox15 overexpression exhibits more severe symptoms of colitis [78]. As a master regulatory molecule of 15-LOX, it was observed that the loss of phosphatidylethanolamine-binding protein 1 (PEBP1) is beneficial to reduce colitis symptoms and accelerate mucosal recovery [79]. Similar effects have been observed with other selective inhibitors acting on 5-LOX [80, 81].

3.3. The Role of Other Ferroptosis Regulators in UC. Nrf2, a major regulator of the antioxidant response, induces the expression of endogenous antioxidant proteins responsible for blocking lipid peroxidation to alleviate OS. Recent studies have demonstrated that Nrf2 can protect UC by inhibiting ferroptosis [19, 46, 49, 77]. Nrf2 has been reported to be involved in the regulation of ferroptosis by controlling the expression of quinone oxidoreductase 1, iron metabolism proteins, GPX4, and GSH production [82, 83]. Nrf2 has been widely demonstrated to be involved in the pathophysiological processes of UC. In NRF2 knockout UC mice, a significant increase in the severity of colitis and risk of colitis-associated colorectal cancer was observed [84, 85]. The regulatory effect of NRF2 on ferroptosis was also observed, with activation of NRF2 inhibiting ferroptosis and knockdown of NRF2 increasing sensitivity to various ferroptosis inducers [86, 87]. Notably, compounds that activate NRF2 inhibit ferroptosis and attenuate colitis-related mucosal damage and colonic inflammation [88]. However, the response of Nrf2 to OS is not specific to ferroptosis, as Nrf2 is also associated with the regulation of pyroptosis [89]. This suggests that the protective effect of Nrf2 on UC may be related to the regulation of multiple forms of cell death.

Mutations in the tumor suppressor P53 have been associated with the development of UC and UC-associated colorectal cancer [90]. Furthermore, P53 transcription inhibits the expression of the cystine/glutamate reverse transporter protein subunit SLC7A11, which in turn disrupts GSH production, thereby sensitizing cells to ferroptosis [73]. It has been observed that P53 is also involved in the regulation of ferroptosis by a mechanism that lies downstream of activation of arginine/arginine N1-acetyltransferase 1 and Alox15 or through transcriptional upregulation of mitochondrial glutaminase 2 [43, 91].

4. Conclusion and Future Perspectives

Patients with UC have a high demand for novel therapeutic strategies. Ferroptosis is a form of RCD characterized by iron overload, lipid peroxidation GPX4 inactivation, and GSH depletion. Based on these features, it is difficult to believe that the broad similarities in UC pathological features and ferroptosis pathways are merely coincidental. Ferroptosis plays an important role in the pathogenesis and progression of UC. The main features of ferroptosis have been widely observed in the colonic tissue of UC patients and animal models. By using UC mouse models, genetic or pharmacological manipulation of ferroptosis-associated genes can improve symptoms and promote recovery from experimental colitis. More specifically, a number of potent ferroptosis regulators (Table 2) can resist lipid oxidation and promote repair of intestinal damage in UC. Targeted inhibition of iron sagging may be a potential novel therapeutic strategy for UC.

Notably, targets involved in the regulation of ferroptosis are continuously being explored. Frataxin protein, which localizes to mitochondria and is involved in the biosynthesis of iron-sulfur clusters, has recently received the attention of investigators. Decreased frataxin expression can lead to iron accumulation at the mitochondrial level, uncontrolled production of reactive oxygen species, and lipid peroxidation [93]. These features are also common to ferroptosis. It has been reported that suppression of frataxin expression specifically activated iron starvation stress, accelerated free iron accumulation, enhanced lipid peroxidation, and resulted in ferroptosis [94–96]. Conversely, enforced expression of frataxin blocked the iron starvation response and erastin-induced ferroptosis [94, 95]. Hence, frataxin is considered to be a key regulator of ferroptosis by modulating iron homeostasis and mitochondrial function. There is a lack of evidence for the role of frataxin in UC. Since frataxin has a key regulatory role on ferroptosis, it may affect UC by regulating ferroptosis, but this hypothesis needs to be further validated by future studies.

Ferroptosis mainly occurs in IE mediating the pathogenesis and development of UC. Based on the currently available evidence, we believe that ferroptosis is a negative regulator of UC, and inhibition of ferroptosis is expected to be a novel approach for UC therapeutics. Although various inhibitors for ferroptosis have been observed to have positive effects in attenuating tissue damage associated with colitis, the underlying molecular mechanisms remain

elusive, and further molecular mechanism studies are important for identifying more selective ferroptosis modulators. Furthermore, it is uncertain whether intestinal immune cells undergo ferroptosis in addition to IECs, and exploring ferroptosis in specific types of epithelial cells and intestinal immune cells will help to comprehensively understand the effects of ferroptosis on UC and provide new evidence for clinical decision-making in UC.

Data Availability

All data obtained or analyzed during this work are included within the article.

Conflicts of Interest

The authors declare that there is no conflict of interest.

Authors' Contributions

Jinke Huang initiated the study design and drafted the manuscript. Jiaqi Zhang, Jinxin Ma, Jing Ma, and Jiali Liu searched the literature. Fengyun Wang and Xudong Tang contributed to review and editing. All authors read and approved the final manuscript.

Acknowledgments

This work was supported by the National Natural Science Foundation of China (No. 81830118), China Academy of Chinese Medical Sciences Innovation Fund (No. CI 2021A01012), China Academy of Chinese Medical Sciences Excellent Young Talent Cultivation Fund (No. ZZ 15-YQ-002), and Administration of Traditional Chinese Medicine Digestive Refractory Disease Inheritance and Innovation Team Project (No. ZYYCXTD-C-C202010).

References

[1] H. S. de Souza and C. Fiocchi, "Immunopathogenesis of IBD: current state of the art," *Nature Reviews Gastroenterology & Hepatology*, vol. 13, no. 1, pp. 13–27, 2016.

[2] S. C. Ng, H. Y. Shi, N. Hamidi et al., "Worldwide incidence and prevalence of inflammatory bowel disease in the 21st century: a systematic review of population-based studies," *Lancet*, vol. 390, no. 10114, pp. 2769–2778, 2017.

[3] C. J. Ooi, I. Hilmi, R. Banerjee et al., "Best practices on immunomodulators and biologic agents for ulcerative colitis and Crohn's disease in Asia," *Journal of Gastroenterology and Hepatology*, vol. 34, no. 8, pp. 1296–1315, 2019.

[4] J. V. Patankar and C. Becker, "Cell death in the gut epithelium and implications for chronic inflammation," *Nature Reviews Gastroenterology & Hepatology*, vol. 17, no. 9, pp. 543–556, 2020.

[5] J. F. Kerr, A. H. Wyllie, and A. R. Currie, "Apoptosis: a basic biological phenomenon with wideranging implications in tissue kinetics," *British Journal of Cancer*, vol. 26, no. 4, pp. 239–257, 1972.

[6] E. L. Eskelinen and P. Saftig, "Autophagy: a lysosomal degradation pathway with a central role in health and disease," *Biochimica et Biophysica Acta*, vol. 1793, no. 4, pp. 664–673, 2009.

[7] L. Galluzzi, I. Vitale, S. A. Aaronson et al., "Molecular mechanisms of cell death: recommendations of the Nomenclature Committee on Cell Death 2018," *Cell Death and Differentiation*, vol. 25, no. 3, pp. 486–541, 2018.

[8] B. R. Stockwell, J. P. Friedmann Angeli, H. Bayir et al., "Ferroptosis: a regulated cell death nexus linking metabolism, redox biology, and disease," *Cell*, vol. 171, no. 2, pp. 273–285, 2017.

[9] S. J. Dixon, K. M. Lemberg, M. R. Lamprecht et al., "Ferroptosis: an iron-dependent form of nonapoptotic cell death," *Cell*, vol. 149, no. 5, pp. 1060–1072, 2012.

[10] C. Liang, X. Zhang, M. Yang, and X. Dong, "Recent progress in ferroptosis inducers for cancer therapy," *Advanced Materials*, vol. 31, no. 51, p. e1904197, 2019.

[11] J. X. Ren, X. Sun, X. L. Yan, Z. N. Guo, and Y. Yang, "Ferroptosis in neurological diseases," *Frontiers in Cellular Neuroscience*, vol. 14, 2020.

[12] H. F. Yan, Q. Z. Tuo, Q. Z. Yin, P. Lei, Department of Neurology and State Key Laboratory of Biotherapy, West China Hospital, Sichuan University, and Collaborative Center for Biotherapy, Chengdu, Sichuan 610041, China, and Chengdu University of Traditional Chinese Medicine, Chengdu, Sichuan 610041, China, "The pathological role of ferroptosis in ischemia/reperfusion-related injury," *Zoological Research*, vol. 41, no. 3, pp. 220–230, 2020.

[13] X. Wu, Y. Li, S. Zhang, and X. Zhou, "Ferroptosis as a novel therapeutic target for cardiovascular disease," *Theranostics*, vol. 11, no. 7, pp. 3052–3059, 2021.

[14] A. Belavgeni, C. Meyer, J. Stumpf, C. Hugo, and A. Linkermann, "Ferroptosis and necroptosis in the kidney," *Cell Chemical Biology*, vol. 27, no. 4, pp. 448–462, 2020.

[15] M. M. Capelletti, H. Manceau, H. Puy, and K. Peoc'h, "Ferroptosis in liver diseases: an overview," *International Journal of Molecular Sciences*, vol. 21, no. 14, p. 4908, 2020.

[16] M. Xu, J. Tao, Y. Yang et al., "Ferroptosis involves in intestinal epithelial cell death in ulcerative colitis," *Cell Death & Disease*, vol. 11, no. 2, p. 86, 2020.

[17] Y. Li, D. Feng, Z. Wang et al., "Ischemia-induced ACSL4 activation contributes to ferroptosis-mediated tissue injury in intestinal ischemia/reperfusion," *Cell Death and Differentiation*, vol. 26, no. 11, pp. 2284–2299, 2019.

[18] Y. Song, H. Yang, R. Lin, K. Jiang, and B. M. Wang, "The role of ferroptosis in digestive system cancer (review)," *Oncology Letters*, vol. 18, pp. 2159–2164, 2019.

[19] Y. Chen, P. Zhang, W. Chen, and G. Chen, "Ferroptosis mediated DSS-induced ulcerative colitis associated with Nrf2/HO-1 signaling pathway," *Immunology Letters*, vol. 225, pp. 9–15, 2020.

[20] Y. Xie, W. Hou, X. Song et al., "Ferroptosis: process and function," *Cell Death and Differentiation*, vol. 23, no. 3, pp. 369–379, 2016.

[21] W. S. Yang, K. J. Kim, M. M. Gaschler, M. Patel, M. S. Shchepinov, and B. R. Stockwell, "Peroxidation of polyunsaturated fatty acids by lipoxygenases drives ferroptosis," *Proceedings of the National Academy of Sciences of the United States of America*, vol. 113, no. 34, pp. E4966–E4975, 2016.

[22] D. J. Lane, A. M. Merlot, M. L. H. Huang et al., "Cellular iron uptake, trafficking and metabolism: key molecules and mechanisms and their roles in disease," *Biochimica et Biophysica Acta*, vol. 1853, no. 5, pp. 1130–1144, 2015.

[23] R. Coffey and T. Ganz, "Iron homeostasis: an anthropocentric perspective," *The Journal of Biological Chemistry*, vol. 292, no. 31, pp. 12727–12734, 2017.

[24] S. J. Dixon and B. R. Stockwell, "The role of iron and reactive oxygen species in cell death," *Nature Chemical Biology*, vol. 10, no. 1, pp. 9–17, 2014.

[25] D. A. Stoyanovsky, Y. Y. Tyurina, I. Shrivastava et al., "Iron catalysis of lipid peroxidation in ferroptosis: regulated enzymatic or random free radical reaction?," *Free Radical Biology & Medicine*, vol. 133, pp. 153–161, 2019.

[26] W. S. Yang and B. R. Stockwell, "Synthetic lethal screening identifies compounds activating iron-dependent, nonapoptotic cell death in oncogenic-RAS-harboring cancer cells," *Chemistry & Biology*, vol. 15, no. 3, pp. 234–245, 2008.

[27] B. Hassannia, B. Wiernicki, I. Ingold et al., "Nano-targeted induction of dual ferroptotic mechanisms eradicates high-risk neuroblastoma," *Journal of Clinical Investigation*, vol. 128, no. 8, pp. 3341–3355, 2018.

[28] Q. Li, X. Han, X. Lan et al., "Inhibition of neuronal ferroptosis protects hemorrhagic brain," *JCI Insight*, vol. 2, no. 7, p. e90777, 2017.

[29] M. Gao, J. Yi, J. Zhu et al., "Role of mitochondria in ferroptosis," *Molecular Cell*, vol. 73, no. 2, pp. 354–363.e3, 2019.

[30] N. Kajarabille and G. O. Latunde-Dada, "Programmed cell-death by ferroptosis: antioxidants as mitigators," *International Journal of Molecular Sciences*, vol. 20, no. 19, p. 4968, 2019.

[31] V. E. Kagan, G. Mao, F. Qu et al., "Oxidized arachidonic and adrenic PEs navigate cells to ferroptosis," *Nature Chemical Biology*, vol. 13, no. 1, pp. 81–90, 2017.

[32] E. L. Berson, B. Rosner, M. A. Sandberg et al., "Further evaluation of docosahexaenoic acid in patients with retinitis pigmentosa receiving vitamin A treatment: subgroup analyses," *Archives of Ophthalmology*, vol. 122, no. 9, pp. 1306–1314, 2004.

[33] S. Doll, B. Proneth, Y. Y. Tyurina et al., "ACSL4 dictates ferroptosis sensitivity by shaping cellular lipid composition," *Nature Chemical Biology*, vol. 13, no. 1, pp. 91–98, 2017.

[34] L. Magtanong, P. J. Ko, and S. J. Dixon, "Emerging roles for lipids in non-apoptotic cell death," *Cell Death and Differentiation*, vol. 23, no. 7, pp. 1099–1109, 2016.

[35] M. M. Gaschler and B. R. Stockwell, "Lipid peroxidation in cell death," *Biochemical and Biophysical Research Communications*, vol. 482, no. 3, pp. 419–425, 2017.

[36] K. D'Herde and D. V. Krysko, "Ferroptosis: oxidized PEs trigger death," *Nature Chemical Biology*, vol. 13, no. 1, pp. 4-5, 2017.

[37] F. Ursini, M. Maiorino, M. Valente, L. Ferri, and C. Gregolin, "Purification from pig liver of a protein which protects liposomes and biomembranes from peroxidative degradation and exhibits glutathione peroxidase activity on phosphatidylcholine hydroperoxides," *Biochimica et Biophysica Acta*, vol. 710, no. 2, pp. 197–211, 1982.

[38] R. Brigelius-Flohé and M. Maiorino, "Glutathione peroxidases," *Biochimica et Biophysica Acta*, vol. 1830, no. 5, pp. 3289–3303, 2013.

[39] H. L. Martin and P. Teismann, "Glutathione—a review on its role and significance in Parkinson's disease," *The FASEB Journal*, vol. 23, no. 10, pp. 3263–3272, 2009.

[40] J. P. F. Angeli, R. Shah, D. A. Pratt, and M. Conrad, "Ferroptosis inhibition: mechanisms and opportunities," *Trends in Pharmacological Sciences*, vol. 38, no. 5, pp. 489–498, 2017.

[41] A. Cassago, A. P. Ferreira, I. M. Ferreira et al., "Mitochondrial localization and structure-based phosphate activation mechanism of glutaminase C with implications for cancer metabolism," *Proceedings of the National Academy of Sciences of the United States of America*, vol. 109, no. 4, pp. 1092–1097, 2012.

[42] W. S. Yang, R. SriRamaratnam, M. E. Welsch et al., "Regulation of ferroptotic cancer cell death by GPX4," *Cell*, vol. 156, no. 1-2, pp. 317–331, 2014.

[43] M. Gao, P. Monian, N. Quadri, R. Ramasamy, and X. Jiang, "Glutaminolysis and transferrin regulate ferroptosis," *Molecular Cell*, vol. 59, no. 2, pp. 298–308, 2015.

[44] Y. Xie, S. Zhu, X. Song et al., "The tumor suppressor p53 limits ferroptosis by blocking DPP4 activity," *Cell Reports*, vol. 20, no. 7, pp. 1692–1704, 2017.

[45] M. Jennis, C. P. Kung, S. Basu et al., "An African-specific polymorphism in the TP53 gene impairs p53 tumor suppressor function in a mouse model," *Genes & Development*, vol. 30, no. 8, pp. 918–930, 2016.

[46] S. Dong, Y. Lu, G. Peng et al., "Furin inhibits epithelial cell injury and alleviates experimental colitis by activating the Nrf2-Gpx4 signaling pathway," *Digestive and Liver Disease*, vol. 53, no. 10, pp. 1276–1285, 2021.

[47] S. Wang, W. Liu, J. Wang, and X. Bai, "Curculigoside inhibits ferroptosis in ulcerative colitis through the induction of GPX4," *Life Sciences*, vol. 259, p. 118356, 2020.

[48] B. Tang, J. Zhu, S. Fang et al., "Pharmacological inhibition of MELK restricts ferroptosis and the inflammatory response in colitis and colitis-propelled carcinogenesis," *Free Radical Biology & Medicine*, vol. 172, pp. 312–329, 2021.

[49] Y. Chen, J. Wang, J. Li et al., "Astragalus polysaccharide prevents ferroptosis in a murine model of experimental colitis and human Caco-2 cells via inhibiting NRF2/HO-1 pathway," *European Journal of Pharmacology*, vol. 911, p. 174518, 2021.

[50] M. Minaiyan, E. Mostaghel, and P. Mahzouni, "Preventive therapy of experimental colitis with selected iron chelators and anti-oxidants," *International Journal of Preventive Medicine*, vol. 3, pp. S162–S169, 2012.

[51] A. D. Millar, D. S. Rampton, and D. R. Blake, "Effects of iron and iron chelation in vitro on mucosal oxidant activity in ulcerative colitis," *Alimentary pharmacology & therapeutics*, vol. 14, no. 9, pp. 1163–1168, 2000.

[52] Y. Kobayashi, S. Ohfuji, K. Kondo et al., "Association between dietary iron and zinc intake and development of ulcerative colitis: a case–control study in Japan," *Journal of Gastroenterology and Hepatology*, vol. 34, no. 10, pp. 1703–1710, 2019.

[53] D. N. Seril, J. Liao, K. L. K. Ho, A. Warsi, C. S. Yang, and G. Y. Yang, "Dietary iron supplementation enhances DSS-induced colitis and associated colorectal carcinoma development in mice," *Digestive Diseases and Sciences*, vol. 47, no. 6, pp. 1266–1278, 2002.

[54] Y. Wan, L. Yang, S. Jiang, D. Qian, and J. Duan, "Excessive Apoptosis in Ulcerative Colitis: Crosstalk Between Apoptosis, ROS, ER Stress, and Intestinal Homeostasis," *Inflammatory bowel diseases*, 2021.

[55] J. N. Feder, A. Gnirke, W. Thomas et al., "A novel MHC class I-like gene is mutated in patients with hereditary haemochromatosis," *Nature Genetics*, vol. 13, no. 4, pp. 399–408, 1996.

[56] R. G. Stevens, J. E. Morris, G. A. Cordis, L. E. Anderson, D. W. Rosenberg, and L. B. Sasser, "Oxidative damage in colon and mammary tissue of the HFE-knockout mouse," *Free Radical Biology and Medicine*, vol. 34, no. 9, pp. 1212–1216, 2003.

[57] S. Sivaprakasam, B. Ristic, N. Mudaliar et al., "Hereditary hemochromatosis promotes colitis and colon cancer and causes bacterial dysbiosis in mice," *Biochemical Journal*, vol. 477, no. 19, pp. 3867–3883, 2020.

[58] M. Constante, G. Fragoso, J. Lupien-Meilleur, A. Calve, and M. M. Santos, "Iron supplements modulate colon microbiota composition and potentiate the protective effects of probiotics in dextran sodium sulfate-induced colitis," *Inflammatory Bowel Diseases*, vol. 23, no. 5, pp. 753–766, 2017.

[59] C. Ettreiki, P. Gadonna-Widehem, I. Mangin, M. Coëffier, C. Delayre-Orthez, and P. M. Anton, "Juvenile ferric iron prevents microbiota dysbiosis and colitis in adult rodents," *World Journal of Gastroenterology: WJG*, vol. 18, no. 21, pp. 2619–2629, 2012.

[60] S. V. Rana, S. Sharma, J. Kaur et al., "Relationship of cytokines, oxidative stress and GI motility with bacterial overgrowth in ulcerative colitis patients," *Journal of Crohn's & Colitis*, vol. 8, no. 8, pp. 859–865, 2014.

[61] S. V. Rana, S. Sharma, K. K. Prasad, S. K. Sinha, and K. Singh, "Role of oxidative stress & antioxidant defence in ulcerative colitis patients from North India," *The Indian Journal of Medical Research*, vol. 139, no. 4, pp. 568–571, 2014.

[62] K. Reissig, A. Silver, R. Hartig et al., "Chk1 promotes DNA damage response bypass following oxidative stress in a model of hydrogen peroxide-associated ulcerative colitis through JNK inactivation and chromatin binding," *Oxidative Medicine and Cellular Longevity*, vol. 2017, Article ID 9303158, 20 pages, 2017.

[63] H. A. A. Elmaksoud, M. H. Motawea, A. A. Desoky, M. G. Elharrif, and A. Ibrahimi, "Hydroxytyrosol alleviate intestinal inflammation, oxidative stress and apoptosis resulted in ulcerative colitis," *Biomedicine & Pharmacotherapy*, vol. 142, p. 112073, 2021.

[64] G. Jena, P. P. Trivedi, and B. Sandala, "Oxidative stress in ulcerative colitis: an old concept but a new concern," *Free Radical Research*, vol. 46, no. 11, pp. 1339–1345, 2012.

[65] Z. Wang, S. Li, Y. Cao et al., "Oxidative stress and carbonyl lesions in ulcerative colitis and associated colorectal cancer," *Oxidative Medicine and Cellular Longevity*, vol. 2016, Article ID 9875298, 15 pages, 2016.

[66] M. Schieber and N. S. Chandel, "ROS function in redox signaling and oxidative stress," *Current Biology*, vol. 24, no. 10, pp. R453–R462, 2014.

[67] C. C. Wu, J. S. Chen, W. M. Wu et al., "Myeloperoxidase serves as a marker of oxidative stress during single haemodialysis session using two different biocompatible dialysis membranes," *Nephrology, Dialysis, Transplantation*, vol. 20, no. 6, pp. 1134–1139, 2005.

[68] E. W. Holmes, S. L. Yong, D. Eiznhamer, and A. Keshavarzian, "Glutathione content of colonic mucosa (evidence for oxidative damage in active ulcerative colitis)," *Digestive Diseases and Sciences*, vol. 43, no. 5, pp. 1088–1095, 1998.

[69] C. J. Kim, J. Kovacs-Nolan, C. Yang, T. Archbold, M. Z. Fan, and Y. Mine, "L-cysteine supplementation attenuates local inflammation and restores gut homeostasis in a porcine model of colitis," *Biochimica et Biophysica Acta (BBA)-Gen- eral Subjects*, vol. 1790, no. 10, pp. 1161–1169, 2009.

[70] B. Sido, V. Hack, A. Hochlehnert, H. Lipps, C. Herfarth, and W. Dröge, "Impairment of intestinal glutathione synthesis in patients with inflammatory bowel disease," *Gut*, vol. 42, no. 4, pp. 485–492, 1998.

[71] G. D. Buffinton and W. F. Doe, "Depleted mucosal antioxidant defences in inflammatory bowel disease," *Free Radical Biology and Medicine*, vol. 19, no. 6, pp. 911–918, 1995.

[72] E. Goldin, E. Ardite, and J. I. Elizaldeetal, "Gastric mucosal damage in experimental diabetes in rats: role of endogenous glutathione," *Gastroenterology*, vol. 112, no. 3, pp. 855–863, 1997.

[73] W. Gao, T. Zhang, and H. Wu, "Emerging pathological engagement of ferroptosis in gut diseases," *Oxidative Medicine and Cellular Longevity*, vol. 2021, Article ID 4246255, 16 pages, 2021.

[74] W. S. Yang and B. R. Stockwell, "Ferroptosis: death by lipid peroxidation," *Trends in Cell Biology*, vol. 26, no. 3, pp. 165–176, 2016.

[75] C. Dai, X. Chen, J. Li, P. Comish, R. Kang, and D. Tang, "Transcription factors in ferroptotic cell death," *Cancer Gene Therapy*, vol. 27, no. 9, pp. 645–656, 2020.

[76] L. W. Xie, S. Cai, T. S. Zhao, M. Li, and Y. Tian, "Green tea derivative (−)-epigallocatechin-3-gallate (EGCG) confers protection against ionizing radiation-induced intestinal epithelial cell death both in vitro and in vivo_," *Free Radical Biology & Medicine*, vol. 161, pp. 175–186, 2020.

[77] Y. Mei, Z. Wang, Y. Zhang et al., "FA-97, a new synthetic caffeic acid phenethyl ester derivative, ameliorates DSS-induced colitis against oxidative stress by activating Nrf2/HO-1 pathway," *Frontiers in Immunology*, vol. 10, p. 2969, 2020.

[78] S. Kroschwald, C. Y. Chiu, D. Heydeck et al., "Female mice carrying a defective *Alox15 gene* are protected from experimental colitis *via* sustained maintenance of the intestinal epithelial barrier function," *Biochimica et Biophysica Acta (BBA)-Molecular and Cell Biology of Lipids*, vol. 1863, no. 8, pp. 866–880, 2018.

[79] W. Lin, C. Ma, F. Su et al., "Raf kinase inhibitor protein mediates intestinal epithelial cell apoptosis and promotes IBDs in humans and mice," *Gut*, vol. 66, no. 4, pp. 597–610, 2017.

[80] L. S. Laursen, J. Naesdal, K. Bukhave, K. Lauritsen, and J. Rask-Madsen, "Selective 5-lipoxygenase inhibition in ulcerative colitis," *Lancet*, vol. 335, no. 8691, pp. 683–685, 1990.

[81] J. Hillingso, J. Kjeldsen, L. S. Laursen et al., "Blockade of leukotriene production by a single oral dose of MK-0591 in active ulcerative colitis," *Clinical Pharmacology & Therapeutics*, vol. 57, no. 3, pp. 335–341, 1995.

[82] S. Kovac, P. R. Angelova, K. M. Holmström, Y. Zhang, A. T. Dinkova-Kostova, and A. Y. Abramov, "Nrf2 regulates ROS production by mitochondria and NADPH oxidase," *Biochimica et Biophysica Acta*, vol. 1850, no. 4, pp. 794–801, 2015.

[83] M. J. Kerins and A. Ooi, "The roles of NRF2 in modulating cellular iron homeostasis," *Antioxidants & Redox Signaling*, vol. 29, no. 17, pp. 1756–1773, 2018.

[84] T. O. Khor, M. T. Huang, K. H. Kwon, J. Y. Chan, B. S. Reddy, and A. N. Kong, "Nrf 2-deficient mice have an increased susceptibility to dextran sulfate sodium-induced colitis," *Cancer Research*, vol. 66, no. 24, pp. 11580–11584, 2006.

[85] T. O. Khor, M. T. Huang, A. Prawan et al., "Increased susceptibility of Nrf2 knockout mice to colitis-associated colorectal cancer," *Cancer Prevention Research*, vol. 1, no. 3, pp. 187–191, 2008.

[86] J. L. Roh, E. H. Kim, H. Jang, and D. Shin, "Nrf 2 inhibition reverses the resistance of cisplatin-resistant head and neck cancer cells to artesunate-induced ferroptosis," *Redox Biology*, vol. 11, pp. 254–262, 2017.

[87] M. Dodson, R. Castro-Portuguez, and D. D. Zhang, "NRF2 plays a critical role in mitigating lipid peroxidation and ferroptosis," *Redox Biology*, vol. 23, p. 101107, 2019.

[88] Y. Yang, X. Cai, J. Yang et al., "Chemoprevention of dietary digitoflavone on colitis-associated colon tumorigenesis through inducing Nrf2 signaling pathway and inhibition of inflammation," *Molecular Cancer*, vol. 13, no. 1, pp. 1–14, 2014.

[89] X. Ran, Z. Yan, Y. Yang et al., "Dioscin improves pyroptosis in LPS-induced mice mastitis by activating AMPK/Nrf2 and inhibiting the NF-κB signaling pathway," *Oxidative Medicine and Cellular Longevity*, vol. 2020, Article ID 8845521, 25 pages, 2020.

[90] X. Lu, Y. Yu, and S. Tan, "p53 expression in patients with ulcerative colitis - associated with dysplasia and carcinoma: a systematic meta-analysis," *BMC Gastroenterology*, vol. 17, no. 1, p. 111, 2017.

[91] Y. Ou, S. J. Wang, D. Li, B. Chu, and W. Gu, "Activation of SAT1engages polyamine metabolism with p53-mediated ferroptotic responses," *Proceedings of the National Academy of Sciences*, vol. 113, no. 44, 2016.

[92] J. Xu, S. Liu, Z. Cui et al., "Ferrostatin-1 alleviated TNBS induced colitis via the inhibition of ferroptosis," *Biochemical and Biophysical Research Communications*, vol. 573, pp. 48–54, 2021.

[93] R. Turchi, R. Faraonio, D. Lettieri-Barbato, and K. Aquilano, "An overview of the ferroptosis hallmarks in Friedreich's ataxia," *Biomolecules*, vol. 10, no. 11, p. 1489, 2020.

[94] J. Du, Y. Zhou, Y. Li et al., "Identification of frataxin as a regulator of ferroptosis," *Redox Biology*, vol. 32, p. 101483, 2020.

[95] J. Liu, H. He, J. Wang et al., "Oxidative stress-dependent frataxin inhibition mediated alcoholic hepatocytotoxicity through ferroptosis," *Toxicology*, vol. 445, p. 152584, 2020.

[96] P. La Rosa, S. Petrillo, R. Turchi et al., "The Nrf2 induction prevents ferroptosis in Friedreich's Ataxia," *Redox Biology*, vol. 38, p. 101791, 2021.